Disulfide-bridging PEGylation of antibody fragments

A thesis submitted by

Hanieh Khalili

for the degree of

Doctor of Philosophy (PhD)

of

University of London

The School of Pharmacy, University of London
29/39 Brunswick Square, London WC1N 1AX, United Kingdom.

March 2012

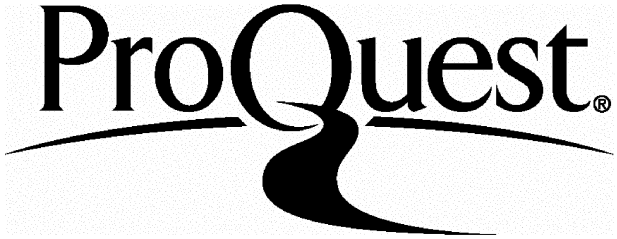

Plagiarism Statement

This thesis describes the research conducted in the School of Pharmacy and PolyTherics Ltd, between 01.10.2008 and 01.03.2012 under the supervision of Professor Steve Brocchini, Dr Rebecca Lever and Dr Antony Godwin. I certify that the research described is original and that any parts of the work that have been conducted in collaboration are clearly indicated. I also certify that the text printed in this thesis is prepared by me and have clearly indicated any part of this thesis that has already appeared in publications.

Hanieh Khalili

Hanieh Khalili _____ _____

(Signature)

ABSTRACT

Monoclonal antibodies are routinely used in the clinic. There are also a small number of antibody fragments (e.g. Fabs) that are clinically used. In many applications where antibody binding is required to antagonise a receptor or simply to bind a ligand, there is no need for the Fc properties that are associated with effector functions. Unfortunately, without the Fc region, antibody fragments rapidly clear from the blood circulation. PEGylation is the most successful and clinically used approach to date for increasing the circulation half-life of therapeutic proteins.

Disulfide bridging PEGylation is an appropriate method to conjugate site-specifically a molecule of PEG at the interchain disulfide of a Fab. Since a PEGylated Fab will be monovalent, it is not possible to exploit the cooperative binding or avidity that is associated with a full IgG which is bivalent. It was hypothesised that site-specific conjugation of a molecule of PEG between the cysteines of the interchain disulfide would allow the monovalent PEGylated Fab to bind effectively to its target. Disulfide bridging PEGylation is accomplished by PEG reagents that undergo bis-alkylation. It was further hypothesised that a PEG reagent with a bis-alkylation functional group at each terminus of the PEG could then be used to conjugate two Fabs one at each end of the PEG molecule, to generate either a homo Fab-PEG-Fab or a hetero Fab-PEG-Fab* conjugate. An important objective of this PhD was to determine the structure-property correlations of a small family of PEGylated-Fabs because it was hypothesised that since the PEGylation is site-specific, the PEG-Fab binding properties would remain constant with increasing PEG molecular weight. It was finally hypothesised that Fab-PEG-Fab conjugates would display comparable binding properties to the full parent IgG.

To test these hypotheses, three Fabs were PEGylated by bis-alkylation at the free thiols that were generated by disulfide reduction. Two clinically used monoclonal antibodies, bevacizumab and trastuzumab were proteolytically digested to provide their respective Fabs, Fab_{beva} and Fab_{trast} for PEGylation. Sourcing the Fabs from an IgG allowed for comparative studies with the parent IgG. The third Fab was also obtained from a clinically used medicine. Ranibizumab is a Fab, so it was PEGylated directly to give PEG-Fab_{rani}. Both Fab_{beva} and Fab_{rani} bind to VEGF and Fab_{trast} binds to HER-2. After treament with DTT to open the interchain disulfide, each Fab

underwent reaction with a PEG mono-sulfone reagent capable of thiol specific, bis-alkylation. PEGylation was accomplished reproducibly at near quantitative conversion with 1-2 equivalents of reagent. A single step ion-exchange purification process was used to obtain purified mono PEG-Fabs. The PEG-Fab conjugates were stable during a 3 month stability study at 4 ^{0}C with no observed de-PEGylation. A PEG_{2x20}-Fab'_{beva} construct was also generated by the conjugation of two molecules of PEG to intrechain disulfide bonds of the Fab'_{beva}. BIAcore and ELISA studies confirmed that compared with the unPEGylated Fabs, the PEGylated Fab_{beva}, Fab_{rani} and Fab_{trast} displayed a 2 fold decrease in binding affinity for their respective ligands. This decrease in binding affinity was much less than had been reported in the literature and was due presumably to the conjugation of PEG far away from the binding reagion of the Fab. PEG-Fab_{beva} conjugates comprising 20, 30 and 40 kDa PEG all displayed similar binding affinities. The binding affinity of the PEG_{2x20}-Fab'_{beva} was decreased compared with mono PEG_{20}-Fab_{beva} as a result of a change in the dissociation rate constant.

The homodimer Fab-PEG-Fab constructs were derived from the 6, 10 and 20 kDa PEG reagents and Fab_{beva}, Fab_{rani} and Fab_{trast}. Both of the homodimers derived from Fab_{beva} and Fab_{trast} maintained binding affinities comparable to their parent IgGs. BIAcore kinetic studies showed there was greater binding affinity and slower dissociation rate for the Fab_{beva}-PEG-Fab_{beva} than the native Fab_{beva}. While a similar binding affinity to bevacizumab was observed for the Fab_{beva}-PEG-Fab_{beva}, the dissociation rates of the the Fab_{beva}-PEG-Fab_{beva} were slower than for bevacizumab. It was also found that using a longer PEG (i.e. Fab_{beva}-PEG_{20}-Fab_{beva}) resulted in slower dissociation. The synthesis of the heterodimer Fab_{beva}-PEG_{20}-Fab^{*}_{trast} could only be achieved one time, but once it was purified it was found to maintain binding to both VEGF and HER-2. An in-vitro angiogenesis assay suggested that the Fab_{beva}-PEG_{20}-Fab_{beva} and Fab_{rani}-PEG_{20}-Fab_{rani} inhibit angiogenesis more effectively than bevacizumab. Using PEG as a linking molecule to conjugate two Fabs would appear to be a way to chemically fuse two Fabs to achieve bivalency that is comparable to a full IgG. These results for Fab-PEG-Fab homodimer are encouraging and together with the results for the Fab-PEG-Fab* suggest a potential hybrid strategy of recombinant protein synthesis and chemical conjugation to develop bivalent and bispecific protein-based medicines.

Research Publications

Original publications

- **H. Khalili**, A. Godwin, R. Lever, S. Brocchini: "Disulfide bridging PEGylation of the antibody fragments derived from bevacizumab", submission to *Bioconjugate Chem.* (in preparation).
- **H. Khalili,** N. Precious, R. Lever, S. Brocchini: "Evaluation of the Stability of Bevacizumab stored in Luor lock syringe for 6 Months." (in preparation).
- **H. Khalili,** A. Godwin, R. Lever, S. Brocchini: "Development of Fab-PEG-Fab and Fab-PEG-Fab* using PEG as a scaffold", (in preparation).
- **H. Khalili,** A. Godwin, S. Brocchini, R. Lever: "Pharmacoketics and biological activity of Fab-PEG-Fab derived from bevacizumab", (in preparation).
- C. Ginn, **H. Khalili**, R. Lever, S. Brocchini; "Recent developments in protein PEGylation and the implications for pharmaceutical design", Submitted.
- G. Badescu, **H. Khalili**, S. Brocchini: Invited book chapter review on "Modification of protein", Submitted.

Selected oral presentations

- **H. Khalili**, A. Godwin, R. Lever, S. Brocchini: " Site specific PEGylation of an antibody fragments". Podium at the School of Pharmacy, University of London, UK. Nov. 2011.
- **H. Khalili**, A. Godwin, R. Lever, S. Brocchini: " Disulfide bridging PEGylation of bevacizumab". Podium in the academy of pharmaceutical science (PharmSci) Annual Meeting, Nottingham, Aug. 2011.
- **H. Khalili**, A. Godwin, R. Lever, S. Brocchini: "Disulfide bridging PEGylation of an antibody fragments derived from bevacizumab". Podium in CRS 37th Annual Meeting, Portland, 2010.

Selected poster presentations

- **H. Khalili**, A. Godwin, R. Lever, S. Brocchini: " Comparative disulfide bridging PEGylation of ranibizumab and bevacizumab-Fab". Poster in AAPS Annual Meeting, Washington. DC, Oct. 2011.
- **H. Khalili**, A. Godwin, R. Lever, S. Brocchini: " Kinetic binding study on site specific PEGylated Fabs derived from bevacizumab". Poster in AAPS Annual Meeting, New Orleans, Nov. 2010.
- **H. Khalili**, A. Godwin, R. Lever, S. Brocchini: "BIAcore binding study of Fab and PEG-Fab". Poster in UKICRS Symposium, Hertfordshire, UK 2010.
- **H. Khalili**, A. Godwin, R. Lever, S. Brocchini: "Antibody PEGylation followed by digestion to generate a PEGylated-Fab". Poster in CRS 36th Annual Meeting, Copenhagen, 2009.

Aknowledgments

Since I would never have started a Ph.D. course, were it not for his support and generosity, my most heart-felt thanks go to Professor Steve Brocchini. With his encouragement, guidance and enthusiasm from the beginning and throughout my PhD, I was able to overcome the hardships I faced during this work. I will never forget his patience and belief in me that helped me not to give up when there was only a small amount of light at the end of tunnel. The last four years have been fantastic, and I have learnt so much, not only about the project, but also about myself. I could not have done it without your priceless support, Steve. Thank you for being such a great supervisor.

I owe my deepest gratitude to Dr Rebecca Lever whose continuous support and invaluable guidance made this project possible. Thank you for all the encouragement and help you have given me.

I would like to thank Dr Antony Godwin, whose guidance and help throughout my time gave me knowledge and understanding of this project.

I would also like to thank Dr Ji-Won Choi for his input and valuable time during this project despite his busy schedule.

My deep thanks to all the academic members of staff at the School of Pharmacy who over the past four years have given me invaluable help. I especially thank Dr Simon Gaisford for all his help with the DSC and ITC experiments and Dr Andy Wilderspin for help with the ELISA experiment. I would also like to thank Berni Widemann in registry and Adrian Rodgers in stores for all the help.

I am grateful to the Dr Tamar Sharif from GE Healthcare for the help with BIAcore.

I am indebted to many colleagues, past and present for their help and also to make my PhD enjoyable and memorable. Special mention must go to the following people; Dr Sibu Balan, Claire Ginn, Sheiliza Carmali, Dr Alastair Lockwood, Negeen Kargar, Dr Hamid Ali Merchant, Alice Parry, Alexandra Bowles, Luis Sousa, Dr Ketan Sharma, Sarfaraj Topia, Sahar Awwad, Wunlapa Mueannoom, Jayanant Lemsam-Arng, Garima Sharma, Fouad Helal, Margarida Carlos, Ning Run, Tan Din and Dr Yuehua Cong.

I would like to express my gratitude to my brothers, Dr Hossein Ali Khalili and Dr Ashkan Khalili for their help and care. My special thanks go to Ashkan whose full support helped me to stand on my own feet, not to mention the nights of chelo kebab dishes during my thesis writing to forget the hardship of writing.

I do not know how to thank my parents, Flora and Mohammad, and express my deepest appreciation for all they have done for me. All of this work would have not happened without their continuous support, love and full trust.

Last but not least, I would like to thank PolyTherics Lt.D and School of Pharmacy for funding my PhD.

Table of Contents

List of Figures

List of Tables

List of Schemes

List of Chemical Equations

List of Abbreviations

ACh	Acetylcholine
ADC	Antibody-drug conjugates
ADCC	Antibody-dependent cellular cytotoxicity
ADCP	Antibody-dependent cell phagocytosis
AKA	A kinase anchoring
AMD	Age macular degeneration
bsMab	Bispecific monoclonal antibodies
BCA	Bicinchoninic acid
BSA	Bovine serum albumin
CDC	Complement-dependent cytotoxicity
C H	Constant heavy
CDR	Antigen binding site
CM5	Carboxymethyl-dextran chip
Db	Diabody
DTT	Dithiothreitol
DTNB	5,5-dithio-bis-(2-nitrobenzoic acid)
EC	Endothelial cell
EDTA	Ethylenediaminetetraacetic acid
EDRF	Endothelium derived relaxing factor
EGF	epidermal growth factor
EGFR	Epidermal growth factor receptor 1
ELISA	Enzyme linked immunosorbent assay
eNOS	Endothelial nitric oxide synthase
FDA	Food and drug administration
$F(ab)_2$	Dimeric F(ab)
Fab	Antigen binding fragment
Fc	Fragment crystalisation
Fv	Variable fragment
FcαR	Fc-alpha receptor
FcγR	Fc-gamma receptors
FcεR	Fc-epsilon receptors
HAMA	Human anti-mouse antibody
HACA	Human anti-chimeric antibodies
HAHA	Human anti-human antibody
HEPS	N-2-Hydroxyethylpiperazine-N-2-ethanesulfonic acid
HER	Epidermal growth factor receptor
HC	Heavy chains
HER2/neu	Epidermal growth factor receptor 2
HIF	Hypoxia-inducible factors
HRP	Horseradish peroxidase
HPLC	High performance liquid chromatography
HUVECs	Human umbilical vein endothelial cells
Ig	Immunoglobulin
ITC	Isothermal titration calorimetry
IEX	Ion exchange chromatography
LC	Light chains

mAb	Monoclonal antibody
MALDI	Matrix assisted laser desorption ionization
2-MEA	2- mercaptoethylamine•HCl
NHS	*N*-hydroxysuccinimide
NK	Natural killer cells
NO	Nitric oxide
NSCL	Non-small-cell lung
PAGE	Polyacrylamide gel electrophoresis
PEG	Poly (ethylene) glycol
PBS	Phosphate buffered saline
PIGF	Placental growth factor
PSA	Polysialic acid
RES	Reticuloendothelial system
PKA	Protein kinase A
RU	Response unit
p-NPP	P-nitrophenol phosphate
Rmax	Maximum capacity of analyte binding
scFvs	Single chain variable fragment
SEC	Size exclusion chromatography
SPHP	Sepharose high performance
SPFF	Sepharose fast flow
SDS	Sodium dodecyl sulphate
SDS-PAGE	Sodium dodecyl sulphate-polyacrylamide gel electrophoresis
SNP	Sodium nitroprusside
SP FF	Sepharose fast flow
SP HP	Sepharose high performance
SPR	Surface plasmon resonance
TACE	TNF-alpha converting enzyme
taDb	Tandem diabodies
TMB	Tetramethyl benzidine
TNF	Tumor necrosis factor
TGF	Transforming growth factor
TCEP	tris(2-carboxyethyl)phosphine
V H	Variable region
VEGF	Vascular endothelium growth factor
VEGFR	Vascular endothelium growth factor receptor

Chapter 1: Introduction

1 Chapter 1: Introduction

1.1 Introduction

There are currently twenty-five antibody based medicines approved for human therapy (Table 1.1) and more than 240 antibodies that are being evaluated clinically [1]. Clinically used antibodies have been developed to bind to targets which are either cell surface receptors or which are circulating ligands [2-4]. Of the twenty-five approved monoclonal antibodies (mAbs) listed in Table 1.1, seven are indicated for cancer treatment and many more are currently being evaluated in clinical trials [1]. Trastuzumab (Herceptin), cetuximab (Erbitux) and bevacizumab (Avastin) are three important antibodies in the clinic for the treatment of solid tumours. Other indications include chronic inflammatory diseases, organ transplantation, cardiovascular diseases, infections and ophthalmological conditions [1, 3].

Mammalian antibodies are produced by plasma cells that are derived from a B-lymphocyte subtype that secrete antibodies as a soluble form. Antibodies are produced specifically to target a foreign extracellular antigen and then to act to trigger an appropriate action from the host immune system. Antibodies are used by the immune system to identify and remove foreign pathogens such as bacteria and viruses. Each antigen binding site is known as an epitope and each B-cell produces its unique antibody. Because some antigens are highly complex, they contain several epitopes, which can be recognised by a number of different B-cells and result in the production of polyclonal antibodies [5]. A monoclonal antibody (mAb) binds to a specific antigen and is derived from a single B-cell population. The interaction between an antibody and its antigen is usually highly specific. This allows the antibody to identify and bind only its unique antigen in the presence of the millions of different molecules that make up the host [6].

Table 1.1 Monoclonal antibodies that are currently approved and marketed for clinical use [1].

Monoclonal Antibody	Molecule type	Indication	Company	Approval
Muromomab	Murine, IgG2a anti-CD3	Organ transplantation	Ortho Biotech	1986 FDA 1987 EMEA
Abciximab	Chimeric Fab fragment, IgG1 IIb/IIIa glycoprotein	Inhibit platelet aggregation	Centocor/Eli Lilly& Co.	1994 FDA
Daclizumab	Humanised, anti-IL-2 receptor	Organ transplantation	Hoffmann-LaRoche	1997 FDA 1999 EMEA
Rituxumab	Chimeric, IgG1k, anti-CD20	Hodgkin's lymphoma	IDEC/Genentech	1997 FDA 1998 EMEA
Basiliximab	Chimeric, anti-IL-2 receptor	Kidney transplant	Novartis	1998 FDA 1998 EMEA
Palivizumab	Humanised, anti-F-protein	Respiratory viral disease	MedImmune	1998 FDA 1999 EMEA
Trastuzumab	Humanised, IgG1k anti-HER-2	HER-2 overexpression breast cancer	Genentech	1998 FDA 2000 EMEA
Infliximab	Chimeric, anti-TNFa	Rheumatoid arthritis, Crohn 's disease	Centocor	1998 FDA 1999 EMEA
Gemtuzumab	Humanised, IgG4k anti-CD33	Relapsed acute myeloid leukemia (AML)	Celltech/Wyeth	2000 FDA
Alemtuzumab	Humanised, IgG1k anti-CD52	Chronic lymphocytic leukemia (CLL)	Millennium	2001 FDA 2001 EMEA
I-131 ch-TNT/ mAb	Chimeric, IgG1k anti-DNA associated antigens, radiolabeled (I-131)	Advanced lung cancer	Shanghai Medipharm biotech	2003(China)
Adalimumab	Human, anti-TNFa	Crohn's disease, Rheumatoid arthritis	Abbott Laboratories	2002 FDA 2003 EMEA
Ibritumomab tiuxetan	Murine, IgG1k, anti-CD20, radiolabeled (Y-90)	Non- Hodgkin's lymphoma, a lymph proliferative disorder	IDEC Pharmaceutical	2002 FDA 2004 EMEA
I-131 tositumomab	Murine, IgG2 aλ anti-CD20, radiolabeled	Non- Hodgkin's lymphoma in rituximab refractory patients	Corixa/GlaxoSmithKline	2003 FDA
Efalizumab	Humanised Ig anti-CD11a	Psoriasis	Genentech/Roche	2003 FDA 2004 EMEA
Cetuximab	Chimeric, IgG1k, anti-EGF receptor	EGFR expression colorectal cancer	Imclone/Bristol-Myers Squibb	2004 FDA 2004 EMEA
Omalizumab	Humanised, IgG1k, anti-IgE Fc	Allergic asthma	Genentech/Novartis	2003 FDA 2005 EMEA
Bevacizumab	Humanised IgG1k, anti-VEGF	Metastatic colorectal cancer	Genentech/Roche	2004 FDA 2005 EMEA
Nimotuzumab	Humanised IgG1, anti-EGF receptor	Advanced head /neck epithelial cancer	YM Biosiences/Biocon	2004 China 2006 India
Natalizumab	Humanised IgG4k, against cellular adhesion a4-integrin	Multiple sclerosis and Crohn's disease	Biogen IDEC	2004 FDA 2006 EMEA
Panitumumab	Human, IgG2k, anti-EGFR1	Metastatic colorectal cancer	Amgen/Abgenix	2006 FDA 2007 EMEA
Ranibizumab	Humanised Fab fragment IgG1k, anti-VEGF	Neovascular age-related macular degeneration	Genentech/Novartis	2006 FDA
Eculizumab	Humanised IgG2k, anti-C5	Chronic orphan blood disorder PNH	Alexion Pharmaceuticals	2007 FDA 2007 EMEA
Certolizumab	PEGylated humanised Fab IgG1k, anti-TNFa	Crohn's disease	UCB Pharma	2008 FDA
Golimumab	Human IgG1, anti-TNFa	Rheumatoid arthritis, active psoriatic arthritis	Centocor	2009 FDA 2009 EMEA

The murine anti-CD3 mAb, muromomab (Orthoclone OKT3), [7] was the first mAb that was approved for human use by the Food and Drug Administration (FDA) in 1986 [8]. Murine mAbs elicit a human anti-mouse antibody (HAMA) reaction [9]. It is reported that 50 % of patients that were treated with OKT3 produce a HAMA after the first dose [10]. Production of HAMA interferes with the binding of OKT3 to T-cells and thus result in reduction of therapeutic efficacy of murine antibody [10]. Murine antibodies were limited because they tended to display a short half-life (less than 20 hours), high immunogenicity and 'suboptimal' effector functions [11].

These problems were solved to a some extent by chimerisation [12, 13]. A chimeric mAb contains the variable regions of a mouse antibody and the constant regions of a human antibody [12]. However chimeric antibodies still induce an immune response known as a human anti-chimeric antibody (HACA) response. Rituximab (Rituxan ^{TM}) was the first chimeric IgG. It is an anti-CD20 mAb that was approved in 1997, for the treatment of some cancers and autoimmune conditions [12]. It is also reported that 61 % of patients treated with infliximab, the chimeric antibody against TNF-α, had a HACA response. This was associated in a shorter half-life of infliximab with an increase risk of infusion reactions [14]. These immunological toxicities, led to development of humanised antibodies. Currently completely human antibodies are being developed [12]. Most of the currently market therapeutic antibodies are humanised mAbs. Recombinant humanised mAbs contain only the complementarity determining regions (CDRs) of a mouse antibody while the remaining structure is human derived [15]. These antibodies can still induce human anti-human antibody (HAHA), however, the incidence of this type of immune response is greatly reduced compared to HAMA and HACA response. Trastuzumab is reported to have 0.1 % HAHA response. While humanised antibodies are less immunogenic than chimeric mAbs, they are not entirely without side effects or complications related to the murine sequences present [1].

Fully-human antibodies have high binding affinity for their antigen and can be made from a single chain variable fragment (scFvs) or antigen binding fragment (Fab) phage display libraries [16]. They also can be obtained from transgenic mice that contain human immunoglobulin genes [16]. Adalimumab (Humira) is an example of a fully-human antibody, approved in 2002 by the FDA for the treatment of rheumatoid arthritis and other inflammatory diseases [16].

1.2 Classes of antibody and antibody fragments

Antibodies are members of the immunoglobulin superfamily of glycoproteins and are found on the surface of lymphocytes as well as in the blood and in extravascular fluids. All immunoglobulins of the class known as Ig are roughly Y-shaped molecules. They are divided into five classes know as: IgA, IgD, IgE, IgM and IgG. The classification is based on their constant regions and valency. While IgG, IgD and IgE are monomers IgAs can be monomeric or dimeric. IgMs are pentameric and hexameric Table 1.2 [10, 13, 17]. The IgG motif is utilised in most therapeutic antibodies. It is the most common naturally occurring immunoglobulin in the blood. The IgG motif has good effector functionality (Table 1.2). IgG is the only class of antibody that is actively transferred from mother to off-spring. This transfer results in passive short-term immunity that is effected through the neonatal Fc receptor (FcRn) [18]. The Fc receptors are located on the surface of certain cells such as natural killer cells (NK), macrophages, neutrophils and endothelial cells. Binding of the IgG antibody to these different Fc receptors occurs at the Fc region on the antibody. Based on the type of antibody, there are different classifications of Fc receptors. Those Fc receptors that bind to the Fc region of IgG are called Fc-gamma receptors (FcγR) and those that bind IgA are Fc-alpha receptor (FcαR). Likewise, the Fc receptors that bind the Fc fragment of IgE are named Fc-epsilon receptors (FcεR).

In general, all antibodies have two main domains, the Fab (fragment of antigen binding) and the Fc (fragment crystallisable). An IgG antibody consists of four polypeptide chains including two identical heavy chains and two identical light chains (Figure 1.1). Each heavy (H) and light chain (L) contains a variable (V) and a constant (C) region (Figure 1.1). The variable regions are responsible for specificity and antigen binding affinity and contain approximately the first 110 amino acids [19] that forms part of fragment antigen-binding (Fab) region. The hyper-variable regions are complementarity determining regions (CDRs) [13, 19] (Figure 1.1).

Table 1.2 Characteristics of the human Ig isotopes [10, 17].

Properties	IgA		IgG				IgM	IgD	IgE
	IgA1	IgA2	IgG1	IgG2	IgG3	IgG4			
Molecular weight (kDa)	160 (m) 400 (d)		150	160	160	150	950 (p) 1150 (h)	175	190
Molecular form	Monomer (m) Dimer (d)		Monomer				Pentamer (p) Hexamer (h)	Monomer	Monomer
Valency	2 or 4		2				10 (p) 12 (h)	2	2
Serum concentration (mg/mL)	1.5 or 2.6		5-12	2-6	0.5-1	0.2-1	0.2-3.1	0.03-0.4	0.001-0.0002
Serum half-life (days)	6		21-24	21-24	7-8	21-24	5-10	2-8	1-5
Functional binding to Fc receptors of phagocytes	-		++	+/-	++	+	Not clear	-	-

The Fc region is a homodimer, which consists of the heavy constant (CH2), and CH3 domains (Figure 1.1). The CH2 and CH3 domains are covalently bound by disulfide bonds in the hinge region [20]. It is thought that the CH2 and CH3 domains are required for IgG catabolism [21]. Binding of Fc to a Fc receptor is pH dependent with binding occurring at acidic pH. Dissociation occurs at neutral or physiological pH [22].

The two Fabs and Fc also connect together by a flexible hinge region. The hinge region is further divided into three sections with total number of 17 amino acids; the upper hinge with 5 amino acids, the core hinge with 4 amino acids that have 8 rotabale bonds which is susceptible to enzymatic or chemical cleavage, and lower hinge with 8 amino acids [23, 24]. The two Fabs in an IgG are able to bind to two identical antigens and provide bivalency (avidity) [13]. The $F(ab)_2$ comprises two Fabs which are linked together through disulfide bonds in the hinge region. The heavy (HC, 50 kDa) and light chains (LC, 25 kDa) are covalently linked together by interchain disulfide bonds in Fab region (Figure 1.2). Additional interchain disulfide bonds link the two HCs together in the hinge region [25].

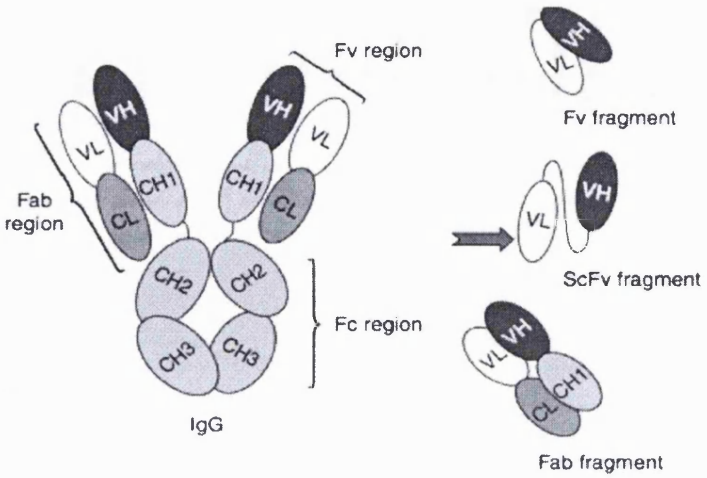

Figure 1.1 Representation of the structure of the IgG motif and related fragments. CH = constant heavy chain; Fab = fragment antigen binding; Fc = fragment crystallizable; Fv = Variable fragment; scFv = single chain Fv, reproduced from [20].

There are several IgG subtypes denoted as IgG1, IgG2, IgG3, IgG4. The light chains can be either κ (kappa), λ (lambda) and σ (sigma), based on differences in the amino acid sequence [26]. Differences in IgG subtypes relate to the number and location of interchain disulfide bonds as well as the length of the hinge region. The interchain disulfide bond linkage between LC and HC involves the last Cys residue (Cys 213) of LC and the Cys residue of HC. The number of Cys residues of the HC depends on the subtype of IgG (Figure 1.2). The Cys 217 of the HC is involved in disulfide bond linkage in IgG1, as opposed to Cys 123 (terminal Cys residue) of HC for IgG2, IgG3 and IgG4.

Different IgG subtypes also have a different number of disulfide bonds between the two HCs in the hinge region. IgG1 and IgG4 have two interchain disulfide bonds in the hinge linking the HCs together, while IgG2 and IgG3 have four and eleven disulfide bonds respectively. All of these Cys residues form interchain disulfide bonds in a correctly folded IgG molecule, meaning that there are no free sulfhydryl groups in native IgG antibodies [25, 27]. Besides interchain disulfide bonds, there are four intrachain disulfide bonds in each domain of the H and L chains in IgG. These intrachain disulfide bonds each link two β-sheets and are required for functional antigen binding and aid in the stability of the antibody structure [19].

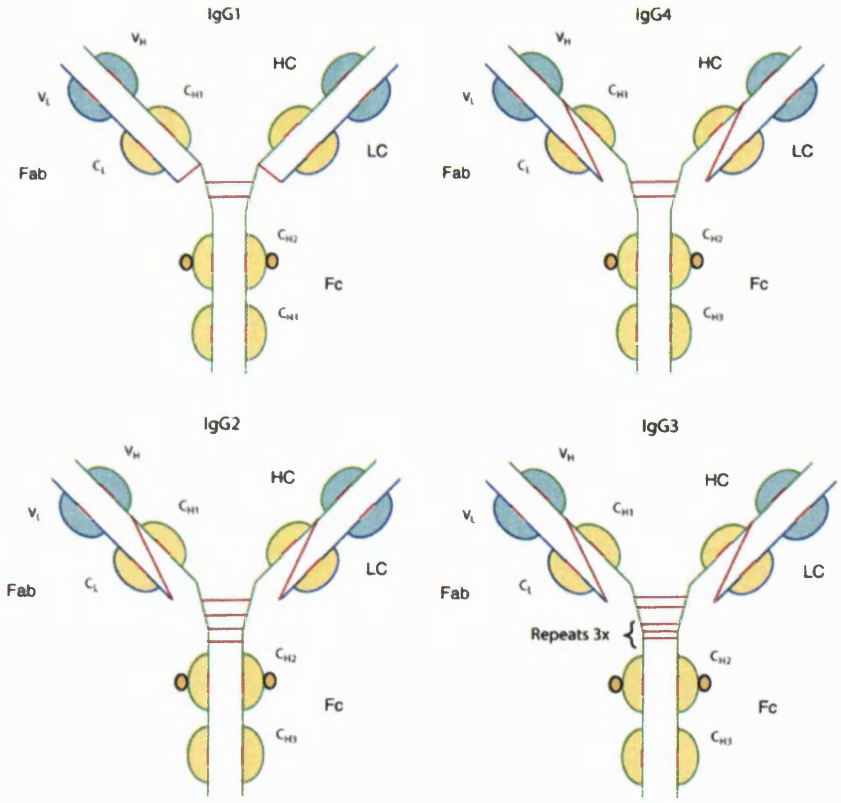

Figure 1.2 Schematic representation of human IgG isotopes and their disulfide bonds, reproduced from [27].

With respect to therapeutic antibodies, the choice of IgG isotype is important during clinical development of the recombinant mAb [4]. IgG1 has been selected as the suitable isotope for oncology diseases. This subclass of IgG has the maximal potential to remove targeted cancer cells through induction of ADCC (antibody-dependent cellular cytotoxicity) /CDC (complement-dependent cytotoxicity) pathways. These effector function pathways often cause apoptosis. Effector function is due to binding affinity that exists between the Fc fragment and a FcR [28]. This effector binding of the Fc to the FcR might not be desired in chronic diseases for which neutralisation of a soluble target is the central objective. Therefore, excessive effector function mediated by Fc-FcR interactions can be detrimental. In this case, IgG1 might not be the ideal choice and other IgG subclasses might be preferred such as IgG2. Most therapeutic antibodies are currently IgG1, although other subclasses are under development. The anti-TNFα agents infliximab and adalimumab are two examples of IgG1 antibodies used for the treatment of rheumatoid arthritis and Crohn's disease. The anti-EGFR (epidermal growth factor receptor) antibody panitumumab is an example of a

therapeutic IgG2 antibody, which is used in the treatment of metastatic colorectal cancer. This IgG subclass has the advantage of less effector function because of the weak interaction between Fc and FcR, while retaining a long serum half-life through the presence of the Fc fragment [4].

All IgGs are glycosylated. There is generally one oligosaccharide group located mostly on the Asn 297 between the CH2 and CH3 domains on the Fc fragment. This glycosylation helps to increase the stability of the antibody structure. Glycosylation also plays an important role in the correct functioning of the IgG, especially Fc function. It has been shown that removal of this oligosaccharide group from IgG results in non-functional IgG that cannot activate the complement system. Hence glycosylation is essential for the induction of effector function, as the IgG conformation is known to be dependent on the presence of the oligosaccharide group [4].

The anti-tumour activities of a therapeutic IgG are mediated by its Fab and Fc fragments. The Fc region in IgG antibodies can elicit an effector function after binding to the antigen. The effector function is manifested by two broad mechanisms: CDC and ADCC/ADCP (antibody-dependent cell phagocytosis) [29]. The Fc induces these effector functions by recruitment of effector cells through Fc-Fc receptor (FcγR) interactions [28]. Binding to FcR mediates ADCC and ADCP to induce endocytosis of the Fc immune complex. This immune complex causes production of antigen and also promotes the release of cytokines. CDC is the complement activation pathway. It can be achieved when C1, the first component of the pathway, binds to the IgG-antigen complex [13, 29]. These two mechanisms of Fc-mediated function are the most prominent in the cytotoxicity of IgG.

The second mechanism that mediates the anti-tumour activity of IgG involves the Fab fragment. A key Fab-mediated activity is the neutralisation of cytokines and angiogenesis factors. There are several immunosuppressive and angiogenic cytokines which are secreted by cancer cells such as TGF-β (transforming growth factor) and VEGF (vascular endothelial growth factor) [13]. Certain therapeutic antibodies, the anti-VEGF agent bevacizumab being an example, work by neutralising soluble factors involved in tumour progression. In addition, delivery of toxins, enzymes and chemical drugs to the cancer cells can be performed by the Fab fragment of an IgG. Therefore, drug delivery is another Fab-mediated activities for which IgG can be used.

For some applications, Fc-mediated effects are not required and are even undesirable. For instance, long serum circulation time in a tissue imaging application is

undesirable because poor image contrast would result, due to difficulty in differentiating between images if the IgG continued to be present in the circulation. Also, inappropriate activation of Fc receptor-expressing cells could result in inappropriate release of cytokines and lead to toxic effects [30].

When only the binding function of an antibody is required, such as blocking biological activity of molecules by either binding to ligand or receptor, or engaging a signalling pathway through cross-linking receptors, it is possible to utilise much smaller proteins known as scaffolds that display high affinity binding properties. There is much interest in developing Fabs and other antibody based fragments (e.g. single chain Fv) as a means to discover highly selective molecules [30]. Currently, many specific fragments (about 19) are being introduced (Figure 1.3) [30].

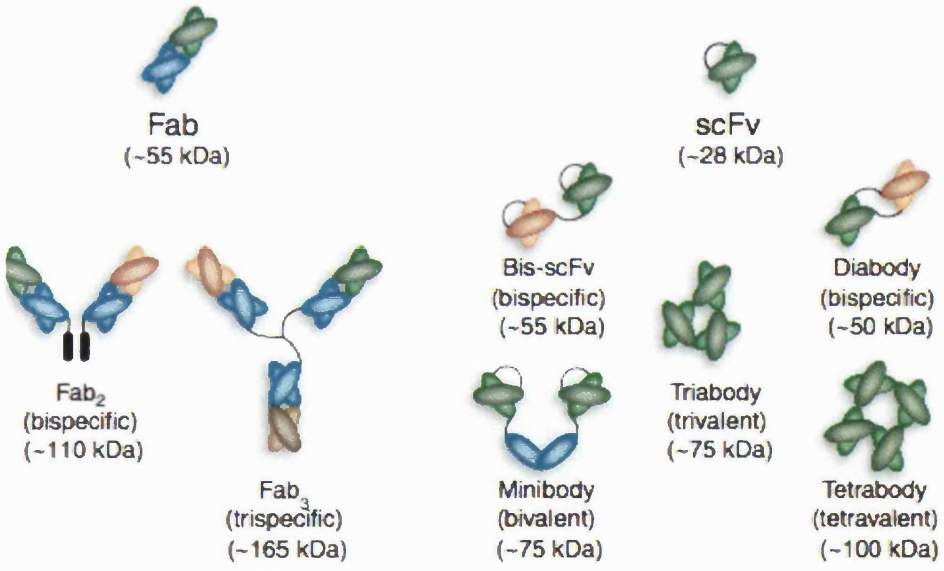

Figure 1.3 Schematic representation of antibody fragments, reproduced from [30].

Table 1.3 A list of antibody fragments currently in clinical and preclinical trial [30].

Fragment type	Specificity/Target antigen	Stage	Indication
Fab/humanised	D-dimer	Phase I	Deep vein thrombosis imaging
Fab/PEGylated humanised	VEGF	Phase I	Cancer (anti-angiogenesis)
Fab/bispecific humanised	HER-2/Neu & CD64 (FcR1)	Phase II	Breast cancer
scFv fused to PEG human	HER-2	Preclinical	Breast cancer
Diabody	HER-2/Neu	Preclinical	Ovarian and breast cancer
Minibody murine-human chimera	HER-2	Preclinical	Ovarian and breast cancer
Bispecific scFv/mouse	CD28 and MAP	Preclinical	Melanoma

It has long been known the Fc can be removed by proteolysis of IgG with enzymes such as papain or pepsin as a means to obtain the Fab or $F(ab)_2$ [31, 32]. The Fab in particular, and $F(ab)_2$ fragments can also be produced by recombinant means [31, 33-35]. One of the potential advantages of the Fab and other binding fragments is that they are smaller than a full IgG. These smaller molecules may penetrate tissue and tumours more effectively [31, 36, 37]. Antibody fragments can be produced in *E. coli,* because of their smaller size and the general lack of glycosylation. Generally, glycosylated antibodies must be produced using a mammalian cell system. It is possible to produce aglycosylated whole antibodies in *E-coli*, however these cannot be used therapeutically because glycosylation is needed to inhibit aggregation, increase physicochemical stability, and to prolong circulation times [19].

The smaller size of antibody fragments results in their rapid clearance from the blood circulation. This rapid clearance can be useful, for example if an antibody is to be used for delivery of cytotoxic radioisotopes or diagnostics [31]. However, this short half-life may be associated with the risk of preventing sufficient accumulation of drug at the desired site.

There are several clinically approved Fab fragments in the market such as ranibizumab (Lucentis, humanised), abciximab (ReoPro, chimeric), crotalidae polyvalent immune Fab (CroFab, Ovine), digoxin-specific Fabs (Digibind and DigiFab, Ovine), and arcitumomab (CEA-scan, murine) and more in clinical trials (Figure 1.3).

Since binding of Fc to FcR results in recycling of the full IgG resulting in half-life up to approximately 20 days, Fab fragments with no Fc display short circulation half-lives of less than a day (19-22 hours). In certain applications, such as the treatment of chronic diseases, this is a disadvantage. Another drawback with antibody fragments is the fact that they tend to aggregate and become less stable in formulation than full IgG because of their smaller size [38]. There are several methods used to increase the half-life and stability of these fragments, such as conjugation to other proteins (e.g albumin) and to polyethylene glycol (PEGylation). In 2007, the PEGylation approach was applied to an anti-TNFα Fab fragment and resulted in the clinically proven agent certozilumab pegol (Cimzia) [39].

1.3 Receptor and ligand binding antibodies

Therapeutic monoclonal antibodies are divided into four groups based on their mode of action; blocking, agonistic, activating and conjugated antibodies. These antibodies differ by both the biology of the target molecule and their clinical indications. Blocking antibodies such as panitumumab (IgG2, anti-EGFR), trastuzumab (IgG1, anti-EGFR), bevacizumab (IgG1, anti-VEGF) and adalimumab (IgG1, anti-TNFα) are all classed as antagonistic mAbs. While bevacizumab and adalimumab bind to soluble ligands, panitumumab and trastuzumab bind to cell surface receptors and block their actions. Agonistic antibodies such as TGN1412 (IgG4, anti-CD28) can bind to cell surface receptors and mimic the action of endogenous ligands. However, TGN1412 caused cytokine storms when adminstarted to the paitent at clinical trials phase I at Northwick park Hospital. The third group is activating antibodies such as rituximab (IgG1, anti-CD20) and alemtuzumab (IgG1, anti-CD52). This group of antibodies is able to recruit the immune system through Fc effector function. The fourth group is conjugated antibodies such as gemtuzumab (IgG4, anti-CD33) and tositumomab-I131 (IgG2, anti-CD20), which are conjugated to a cytotoxic drug and a radionuclide respectively. This group is used for targeted delivery of therapeutic agents [40].

For blocking antibodies that bind to ligands or receptors and acts as antagonists, there may be less need for the Fc portion. For instance, TNFα is a cytokine involved in systemic inflammation and has a primary role in the regulation of immune cell function [41]. TNFα is produced by many immune and non-immune cells such as T-cells, mast cells, smooth muscle cells, fibroblasts and natural killer (NK) cells as a soluble cytokine

(sTNFα). Three 17 kDa monomers form a homotrimer that is released into the serum after cleavage from its cell surface bound precursor (tmTNF, homotrimer of 26 kDa monomers) by the TNF-alpha converting enzyme (TACE) [42]. Both sTNF and tmTNF exert biological activity by interacting with either of two distinct receptors, TNFR1 and TNFR2. These receptors also have to trimerise to allow binding to TNFα and receptor signalling. TNFα as a ligand is a target for at least five clinically used medicines, some of which are bivalent IgG1 monoclonal antibodies (adalimumab, infliximab, golimumab) and one of which is a monovalent Fab fragment covalently conjugated to PEG (2 chains of 20 kDa) and named certolizumab pegol (Cimzia) [41].

Of the clinically approved TNFα antagonists, adalimumab (Humira) and golimumab (Simponi) are fully human monoclonal antibodies. Etanercept (Enbrel) is a soluble TNFR2-Fc fusion protein and infliximab (Remicade) is a chimeric monoclonal antibody. Certozilumab pegol (Cimzia) is a PEGylated humanised Fab

These medicines are used in the treatment of chronic inflammatory diseases including rheumatoid arthritis (RA) and Crohn's disease. The serum half-life of adalimumab is 10-20 days, comparable to that of certozilumab pegol, which is 14 days [41]. Etanercept possesses a serum half-life of four days. Moreover, the TNFα antagonists differ in terms of induction of effector function; infliximab, adalimumab and golimumab are IgG1 that induce effector function through Fc-FcR, however, certolizumab lacks effector function since it has no Fc fragment. Etanercept is a fusion protein consisting of a dimer of the extracellular region of the human TNFR2 fused to the Fc region of human IgG1. The TNFR2 portion in etanercept has four domains and its C-terminal contains 13 glycosylated residues. The Fc region of etanercept has an identical amino acid sequence to that of the other, IgG1-based TNF antagonists. While binding of the Fc to the FcR governs the plasma half-life of etanercept, the plasma half-life is shorter than for the IgG1 mAbs or other Fc fusion proteins. The reason for the shorter half-life of etanercept could be due to differences in the conformation or steric accessibility of the Fc region in etanercept compared with other IgG1 adalimumab and infliximab [41].

All the TNFα antagonists mentioned can bind to either sTNF or tmTNF and thus stop their binding to TNFR. The ligand binding of these antagonists was studied using BIAcore, to measure the on-rate and off-rate of antagonist to ligand [41]. The data showed that all these molecules bind sTNF with high affinity in the nM range, however,

they are different in terms of their kinetic parameters (k_{on} and k_{off}). Infliximab and adalimumab appeared to have slower k_{on} and k_{off} rates than etanercept. It is reported that the on-rate of etanercept is about twice that of infliximab or adalimumab. However, infliximab binds to both monomer (17 kDa) and trimer (51 kDa) sTNF, while etanercept binds only to trimer sTNF. The binding of etanercept to sTNF is through contact of the receptor arm with different faces of the trimer sTNF. Therefore, infliximab and etanercept are different through their binding to different epitopes on sTNF. It has been suggested that infliximab and adalimumab can bind to two sTNF trimers as both are bivalent IgG (slower off-rate), whereas etanercept appears to bind only to single sTNF trimers (hence faster off-rate) [41]. Moreover, the results from studies of the binding of infliximab, adalimumab, etanercept and certolizumab, to cell lines expressing transfected tmTNF, suggest that infliximab and adalimumab have a greater degree of cell-surface binding, up to three fold greater than etanercept and certolizumab [41].

Through not having the Fc region, certolizumab retains the ability to bind to TNFα without the possible cytotoxicity that can be contributed by the Fc. In principle, because certozilumab is a Fab, it is also a lot more economical to produce. After binding to TNFα, antibodies can be cleared from the body through the spleen and liver, followed with degradation in the kidney. The mechanism of clearance can be a combination of Fc receptor dependent in the reticuloendothelial system (RES) in the spleen and liver and then degradation through the kidney.

Another clinically used antibody that binds to a soluble ligand is bevacizumab. As mentioned, bevacizumab is a full IgG1 monoclonal antibody against VEGF which acts as an anti-angiogenesis agent and is used in cancer chemotherapy [43]. Analogous to TNF-a, there is also a clinically used Fab targeted against VEGF. This Fab is called ranibizumab and is available for use only in the eye to treat age related macular degeneration (AMD). Unlike certozilumab pegol, ranibizumab is not PEGylated.

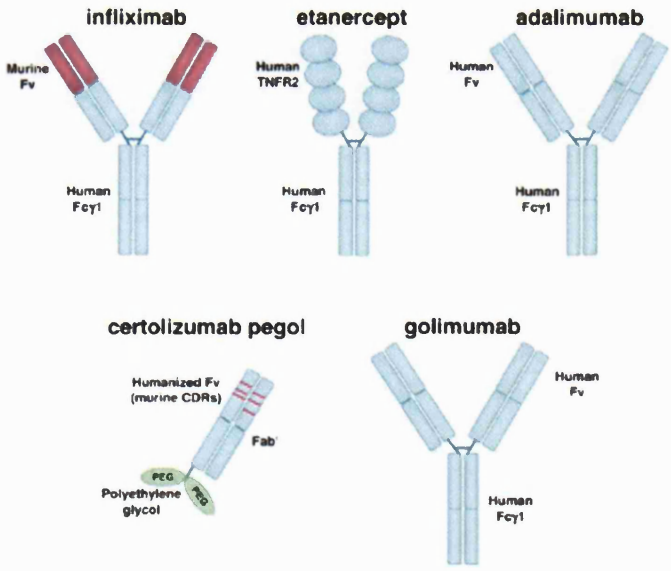

Figure 1.4 Representations of the molecular structures of the five TNF antagonist, reproduced from [41].

1.3.1 Bevacizumab and its mechanisms of action

Angiogenesis is the process of the growth of new blood vessels [44]. The inhibition of angiogenesis was first described by Folkman in 1971 as an effective strategy to treat cancer [45]. Folkman discussed the relationship between inhibition of the angiogenesis and treatment of the cancer. Angiogenesis is also important in several other diseases in addition to cancer, including diabetic retinopathy, psoriasis, rheumatoid arthritis and infection. It also is known to be important in wound healing and embryonic development [46]. As initially discovered by Folkman, angiogenesis is a normal process in the growth and development of blood vessels, it is also a key step in the transition of a tumour from a dormant state to a 'malignant state' [45, 47]. Destruction of tumours by blocking the angiogenic process, to prevent the growth of a tumour blood supply has been discussed for a number of years as a way forward for cancer treatment. Therefore, a number of anti-angiogenesis agents have been then developed and more are in clinical trials (Table 1.4) [46].

Folkman and his colleagues isolated a 'tumour angiogenesis factor' from human and animal tumours [45, 48]. Different factors can induce the angiogenic response, such as epidermal growth factor (EGF), transforming growth factor (TGF)-α, TGF-β, tumour-necrosis factor-α (TNF-α) and angiogenic factors. These factors were shown to induce angiogenesis in functional bioassays, but none of them were found to show

physiological activity. Finally, isolation of vascular endothelial growth factor (VEGF), which is an endothelial-cell-specific mitogen, was reported by Genentech to display activity [48].

VEGF is a heparin-binding homodimeric glycoprotein with approximately 40 kDa molecular weight. It was found that VEGF is a potent endothelial cell mitogen [49] that mediates proliferation, migration and tube formation resulting in angiogenesis. Therefore, VEGF was found to be a key mediator in angiogenesis [46]. In vitro studies have shown that VEGF stimulates angiogenesis causing endothelial cells to proliferate and to migrate [50]. VEGF causes a series of signalling events in endothelial cells. Using specific antibodies in order to block the activity of VEGF to prevent VEGF binding to its receptors, has been suggested as a valid approach to stop tumour growth [50].

The VEGF family includes VEGF-A, VEGF-B, VEGF-C, VEGF-D, VEGF-E, VEGF-F and PlGF (placental growth factor). They bind specifically to three different receptor tyrosine kinases to activate their biological functions. These receptors are VEGFR1 (also called flt-1), VEGFR2 (also called KDR/flk-1), and VEGFR3. The most therapeutically important VEGF is VEGF-A, which plays a key role in angiogenesis.

Human VEGF-A consists of different isoforms based on different number of amino acids, including $VEGF_{121}$, $VEGF_{165}$, $VEGF_{189}$, and $VEGF_{206}$. It is now accepted that $VEGF_{165}$ is vital for angiogenesis and the most biologically important VEGF isoform [48]. Less frequent VEGF isoforms have been reported, including $VEGF_{145}$, $VEGF_{183}$, $VEGF_{162}$.

VEGF-A binds to VEGFR1 and VEGFR2, leading to receptor dimerisation. The function of VEGFR1 is less well defined, but it is established that VEGFR2 is the major mediator of the mitogenic, angiogenic, and permeability enhancing effects of VEGF. VEGF-C and VEGF-D, but not VEGF-A, can bind to a third receptor (VEGFR3), which mediates lymphangiogenesis [51]. Binding to VEGFR2 initiates a tyrosine kinase signalling pathway that stimulates the production of factors that stimulate vessel permeability, proliferation, migration and finally differentiation into mature blood vessels [50]. Figure 1.5 summarises the role of VEGF receptor tyrosine kinases in endothelial cells.

The crystal structure and functional mapping of VEGF has been described [51]. This report showed the receptor binding site of VEGF clearly, whereby two VEGF-monomers form the biologically active dimer. VEGF is composed of two identical

chains that are linked together by disulfide bonds. The dimer has two binding sites for the receptor, which are formed by domains from each monomer [51]. Therefore, dimerisation of VEGF is required for formation of the functional receptor binding site and its biological activity. Receptor dimerisation is also required, as each receptor molecule consists of only one VEGF binding site [51]. Moreover, alanine-scanning analysis of VEGFR1 and VEGFR2 has revealed the binding site on VEGF for its two receptors. This study showed that both receptors bind similar epitopes on VEGF. These epitopes are located on the two opposite parts of the VEGF-homodimer (Figure 1.6).

Another role of VEGF is to induce endothelium-dependent vasorelaxation. Both large and small blood vessels contain endothelial cells to which VEGF can be localised. This localisation of VEGF on endothelial cells will result in cell proliferation and migration and therefore induce an angiogenic response. It has also been found that systemic or intracoronary administration of VEGF leads to a significant depressor response, recognized as VEGF-induced vasodilation, which is known to be NO-dependent [52, 53].

As mentioned above, $VEGF_{165}$ plays a key role in angiogenesis by binding to VEGFR2. In the case of cancer, stopping angiogenesis by blocking VEGF or VEGFR can inhibit tumour growth and consequently kill the tumour. Bevacizumab is a clinically approved monoclonal antibody which shows high affinity binding to human $VEGF_{165}$ [46]. Bevacizumab is a recombinant humanised IgG1k monoclonal antibody (97 % human, 7 % murine sequence) which is produced by humanisation of the murine parent antibody A4.6.1. The approximate molecular weight of bevacizumab is 150 kDa [54]. The combination of bevacizumab with 5-fluorouracil is used for treatment of metastatic colorectal cancer [55].

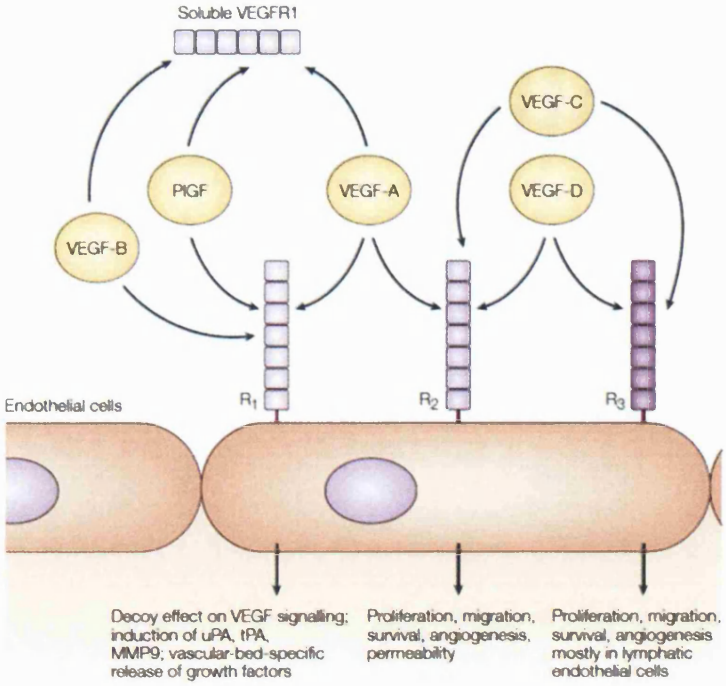

Figure 1.5 Role of the VEGF receptor tyrosine kinase in endothelial cells. VEGFR1 (R1), and VEGFR2 (R2) are located on the surface of vascular endothelial cells. VEGFR3 (R3) is largely limited to lymphatic endothelial cells. VEGF-A binds to both R1 and R2, whereas PlGF and VEGF-B interact only with R1. VEGF-C and VEGF-D bind R3, but they might bind R2 following proteolytic processing, reproduced from [48].

Besides bevacizumab, many other VEGF inhibitors are in clinical trials. Table 1.4 lists some of the most clinically advanced proteins known to inhibit VEGF signalling [48]. Alanine-scanning analyses and the crystal structure of VEGF, in complex with bevacizumab, (Figure 1.6) suggested that the binding epitopes on VEGF for the receptor and for the Fab region in bevacizumab are separate and only partially overlapping. The mechanism of inhibition of receptor binding by bevacizumab is suggested to be steric hindrance [46].

Table 1.4 VEGF inhibitors in development and which have been registered. RTK, receptor tyrosine kinase; VEGF, vascular endothelial growth factor; VEGFR, VEGF receptor [48].

Agent	Description	Company	Development status
Bevacizumab (Avastin)	Humanised Antibody (VEGF-A_{165})	Genentech	FDA approved
Ranibizumab (Lucentis)	Humanised Antibody fragment (VEGF-A_{165})	Genentech	FDA approved
Pegaptanib (Macugen)	PEGylated-aptamer (VEGF-A_{165})	Pfizer	FDA approved
PTK787	RTK inhibitor (VEGFR1, VEGFR2)	Novartis	Phase III
Bay 43-9006	RAF Kinase inhibitor (also several RTKs)	Bayer/Onyx	Phase III
SU11248	RTK inhibitor (several RTKs)	Pfizer	Phase I/III
ZD6474	RTK inhibitor (VEGFR1, VEGFR2)	AstraZeneca	Phase II
AG 013676	RTK inhibitor (several RTKs)	Pfizer	Phase II
VEGF-trap	Soluble receptor	Regeneron	Phase I/III
Anti-VEGFR2	Monoclonal antibody	ImClone	Phase I

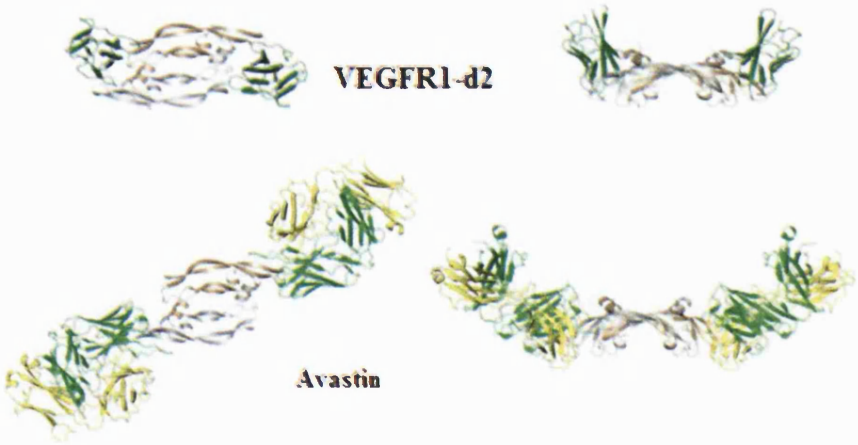

Figure 1.6 Ribbon diagrams of human VEGF in complex with domain-2 of VEGFR1, and bevacizumab (Avastin). The grey and pink colours are VEGF; domain-2 of the VEGFR1 is dark green. The yellow and light green colours are the light and heavy chains of the Fabs, respectively, reproduced from [46].

For treatment of cancers, bevacizumab is administrated intravenously. Intravitreal bevacizumab is also used off label for the treatment of age-related macular degeneration (AMD), and has been administered every 14 days with a vitreous half-life of 4.32 days in rabbit eye [56]. AMD is an eye disease and a major cause of blindness that part of retina called macula damages and results in loss of vision. This damage occurs due to abnormal blood vessel growth in the choriocapilaries and results in blood leakage and blocking below macula [57]. In contrast, ranibizumab is an approved Fab fragment against $VEGF_{165}$, which is administered intravitreally in treatment of AMD and has a short vitreous half-life of 2.88 days in rabbit eye [56]. Ranibizumab is produced in *E-coli* from the insertion of the murine anti VEGF-A CDRs into a consensus human IgG1 framework [58]. Compared with the CDR in bevacizumab, there are some amino acids substituted to increase the binding affinity for VEGF-A ($VEGF_{121}$, $VEGF_{165}$). Ranibizumab contains 214 amino acids in its light chain, which is linked by the disulfide bond at its C-terminus to the N-terminus amino acid residue 231 of the heavy chain. There are 4 intrachain and 1 interchain disulfide bonds in ranibizumab. The molecular weight of ranibizumab is approximately 50 kDa (23 kDa for light chain and 25 kDa for heavy chain) [58]. Since the Fab (ranibizumab) is injected directly into the eye, it does not need to be PEGylated to prolong its residence time. Unlike bevacizumab, it would not be possible to use ranibizumab systemically because it would clear too quickly.

Another therapeutic monoclonal antibody used to treat cancer is trastuzumab, which acts as an antagonist through its blockage of the HER-2 signalling pathway. Unlike bevacizumab that binds to a soluble ligand, trastuzumab binds to a receptor, but both are classified as blocking antibodies.

1.3.2 Trastuzumab and its mechanism of action

The four members of the ErbB family (HER-1, HER-2, HER-3 and HER-4) are epidermal growth factor receptor tyrosine kinases. The HER-1, HER-3 and HER-4 have their specific ligands (EGF or TGFα), which can bind with high affinity, however, HER-2 is the only ErbB receptor without a known high affinity ligand. It has been said that HER-2 is a 'ligand-less' receptor tyrosine kinase [59]. All the ErbB family receptors excluding HER-3 contain an intracellular tyrosine kinase domain and they all contain an extracellular region with 630 amino acids [60]. The extracellular domain is

where ligand binding occurs. Binding of ligand to the extracellular domain of HER-1, HER-3 and HER-4, results in activation and receptor dimerisation. Receptor dimerisation can be either homodimerisation or heterodimerisation, and is required for phosphorylation events and initiation of downstream signalling pathways such as proliferation and cell survival. Therefore, the tyrosine kinase portion of each receptor is activated by dimerisation, which requires ligand binding for initiation. In contrast, HER-2 contains an active tyrosine kinase domain, which is in an 'active' conformation without need for a ligand and is constitutively available for dimerisation. HER-2 is the preferred dimerisation partner for the other HER family members [60]. In breast cancer characterised by HER-2 overexpression it constitutively activates and induces intracellular signalling pathways. This results in stimulation of proliferation, migration, angiogenesis and promotion of tumour cell survival [61].

There are several monoclonal antibodies on the market that target the extracellular domain of the HER-2 receptor in order to inhibit the proliferation of cancer cells [61]. Trastuzumab was approved for the treatment of HER-2 overexpressing breast cancer in 1998. It is a glycosylated with an approximate 150 kDa molecular weight, recombinant monoclonal antibody IgG1. Trastuzumab can bind to the extracellular domain of the HER-2 receptor with high affinity. This antibody is produced by insertion of the CDR amino acids of the murine parent (muAb 4D5) into the framework of a consensus human IgG1 using mammalian chinese hamster ovary cell line [6].

Several mechanisms have been suggested how trastuzumab can decrease HER-2 signalling and Figure 1.7 (panel C, D, E and F) shows some of these possible mechanisms of action. In Figure 1.7 panel A shows the HER family signalling pathway and panel B shows the structure of trastuzumab. The first mechanism suggested is through Fc binding of trastuzumab to the FcR on natural killer cells (NK), to activate the ADCC pathway (panel E in Figure 1.7). However, it was demonstrated that in HER-2 overexpressed breast cancer, the most likely mechanism of action of trastuzumab, is to block the proteolytic cleavage of the HER-2 extracellular domain (panel C, Figure 1.7). It is thought this prevents HER-2 dimerisation and activation of the intracellular tyrosine kinase. Also, physical inhibition of HER-2 dimerisation (panel D, Figure 1.7) could be another mechanism for trastuzumab to inhibit the HER-2 signalling pathway. The forth possible mechanism of action of trastuzumab in HER-2 binding involves an endocytosis effect (panel F, Figure 1.7) [59].

Figure 1.8 shows the ribbon structure of HER-2 (a) and HER-2 in complex with the trastuzumab-Fab (b). Trastuzumab binds HER-2 through its CDR in the Fab fragment. The binding site of HER-2 with trastuzumab-Fab is located on the C-terminal portion of domain IV, including three loops; loops formed by residues 557-561, 570-573, and 593-603. The interaction between the first and third loops with CDRs of trastuzumab is mainly electrostatic, whereas the interaction between second loop and trastuzumab is governed by hydrophobic interactions [60].

Trastuzumab is administrated as a single drug to the patient who receives one or more chemotherapy regiments for their metastatic cancer. Trastuzumab is also administrated in combination with other agent such as paclitaxel and bevacizumab to the patient who has not received any chemotherapy and suffering from chronic cancer [6, 62].

Another human monoclonal antibody against EGFR is pantitumumab. This antibody is an IgG2 and was approved by the FDA for metastatic colorectal cancer in 2006. Panitumumab acts as an anti-cancer agent by inhibiting the growth of cancer cells and inducing apoptosis. Panitumumab is an IgG2 that does not show potent CDC and ADCC pathway due to the weak interaction between the Fc domain to the FcR. It blocks EGF and TGF-α from binding to EGFR1 [63]. Cetuximab (chimeric IgG1k) is also targeted to EGFR and used to treat colorectal cancer and head and neck cancer.

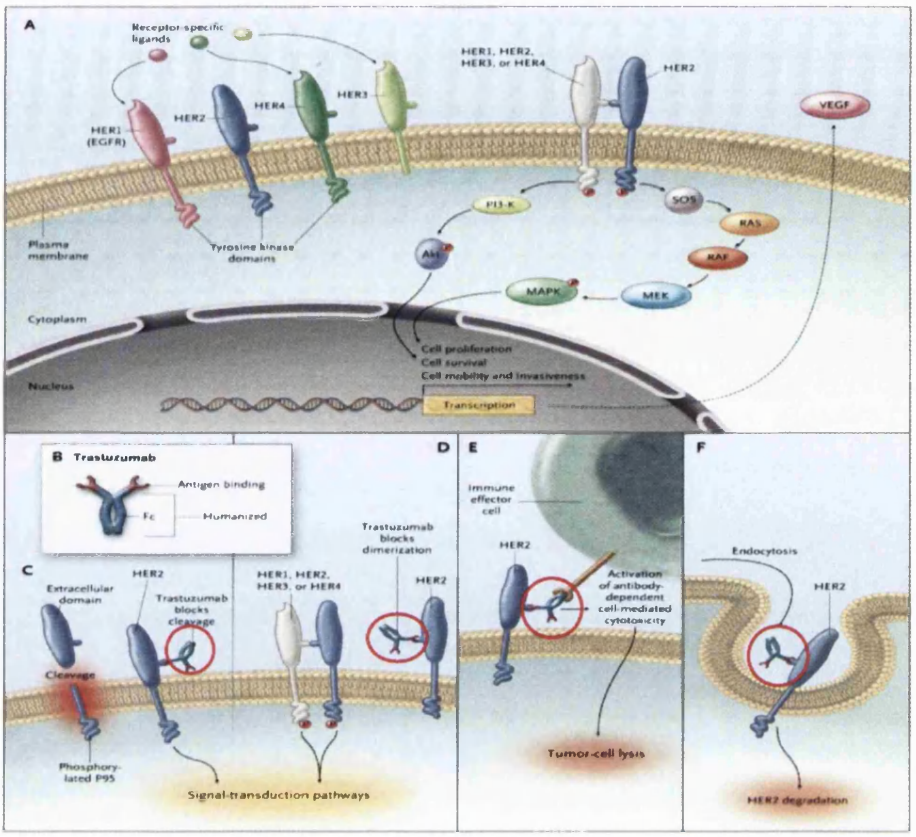

Figure 1.7 Possible mechanisms of action of the anti-HER-2 antibody trastuzumab, **(A)** HER family signalling pathway, **(B)** Trastuzumab, **(C-F)** Trastuzumab mechanism of action after binding to HER-2, reproduced from [59].

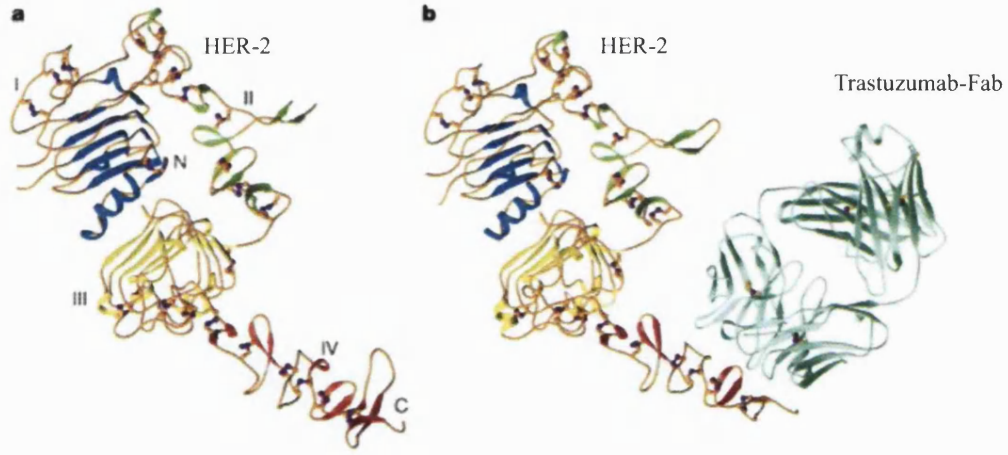

Figure 1.8 The structure of HER-2 and HER-2 bound by Fab-trastuzumab. A; Ribbon diagram of HER-2. Domains I (blue), II (green), III (yellow) and IV (red), and the amino and carboxy termini, are indicated. Disulfide bonds are shown in purple and gold. B; Ribbon diagram of the HER2 (colored as in a) and Fab-trastuzumab (cyan) complex, reproduced from [60].

1.4 Strategies to extend the half-life of therapeutic proteins

The continued development of the protein-based medicines, in particular antibody fragments, is limited to an extent by problems related to their short circulation half-life. Rapidly cleared medicines must be dosed more frequently. While this is inconvenient to the patient and increases the cost of treatment, a suboptimal dosing frequency also increases the risk for immunogenicity and toxicity. Efficacy is also decreased when proteins clear rapidly because a sub-therapeutic plasma concentration exists between doses. Optimise pharmacokinetics are a fundamental requirement for the development protein-based medicines.

There are several strategies that have been suggested to solve the limitation of short serum half-life of therapeutic proteins [64]. These strategies include (i) protein fusion to Fc or to albumin that increase the serum half-life by using the endocytic recycling mechanism [21, 65-72], (ii) PEGylation [73-79] and glycoengineering [80-82] methods which prolong serum half-life of therapeutic protein by increasing the size of the protein molecule in circulation and (iii) using sustained release system such as colloids and pumps to prolong dosing into the blood stream. From these, fusion proteins and protein PEGylation are described in detail in the following sections because clinically proven products using these technologies are currently on the market.

1.4.1 Fusion proteins

One approach to improve the pharmacokinetics of small therapeutic proteins is based on their recombinant fusion with longer circulating serum proteins including Fc and albumin. In Fc fusion proteins, the immunoglobulin Fc fragment is fused genetically to the protein of interest, such as an enzyme, peptide or antibody fragment. The Fc fragment can bind to the FcR to provide longer circulation times in the blood. There are currently five Fc fusion proteins in the clinic and more in clinical trials, Table 1.5 [64]. The first Fc-fused peptide was romiplostim (Nplate), a thrombopoietin conjugate approved for the treatment of chronic immune thrombocytopenia purpura [64]. This drug has an average half-life of four days when administered subcutaneously. Etanercept (Enbrel) is the most successful fusion protein based medicine. It is a dimeric fusion of the soluble 75 kDa TNFα receptor-2 with the Fc fragment of human IgG1 and is a successful example of a Fc-fusion protein that is used relatively widely as a therapeutic drug [83]. Of the fusion approaches, the Fc fusions have been the most

successful clinically.

Another approach that has been evaluated is to fuse a therapeutic protein to albumin. Albumin has been genetically fused to the proteins such as Fab, scFv, cytokines and enzyme [84]. Albumin and IgG are the most abundant proteins in the plasma. They both have a circulation half-life of approximately 20 days [65, 84]. The long serum half-life associated with albumin could be used as a tool to enhance the half-life of a Fab fragment in an albumin-fusion Fab [84]. Several studies have shown that this long serum half-life of albumin is because of its binding to the FcR and a recycling process that is mediated by the FcR, similar to what is observed for IgG molecules, however, no effector function is observed for albumin-FcR binding [65, 85]. The binding of albumin to the FcR is pH-dependent, similar again to binding of the Fc of IgG to FcR.

Table 1.5 Protein based medicines that are fused to Fc which are registered in the clinic and the clinical development [64].

Product	Company	Fusion Partner 1	Fusion Partner 2
Examples of clinically approved fusion proteins			
Amevive (alefacept)	Astellas Pharma US	IgG Fc	LFA-2
Arcalyst (rilonacept)	Regeneron	IgG Fc	IL1Rs
Enbrel (etanercept)	Amgen	IgG Fc	TNFR
Nplate (romiplostim)	Amgen	IgG Fc	TPO-Receptor (c-mpl) binding peptide
Orencia (abatacept)	Bristol-Myers Squibb	IgG Fc	CTLA4
Ontak (denileukin diftitox)	Ligand Pharmaceuticals	Diptheria toxin A & B	IL-2 (Ala1-Thr133)
Examples of fusion proteins in clinical trials (Phase III)			
LEA29Y	BMS	IgG Fc	CTLA4
VEGF Trap	Regeneron	IgG Fc	VEGF
IL13-PE38QQR	NeoPharm	IL-13	Pseudomonas exotoxin PE38
Proximium/ Vicinium	Viventia	Anti-EpCAM FAb	Pseudomonas exotoxin A

The human serum albumin is a single chain protein produced in the liver. This protein has a 67 kDa molecular weight with 585 amino acids and can control the plasma oncotic pressure and pH. The ease of production along with the known structure of albumin has made it an interesting candidate for extending the serum half-life of small proteins [68, 86, 87].

However, there is only one example of an albumin fusion protein, interferon-albumin (Albuferon) which has been evaluated in Phase III trail. The trials were stopped and this fusion protein still remains to be registered for clinical use [70]. Moreover, using the fusion approach, it is possible to fuse two different peptides or antibody fragments together and produce a bispecific construct which is discussed in more detail in section 1.5 of this chapter.

While Fc fusion proteins have been clinically proven to prolong the circulation, this class of proteins is dominated by Entarecept. There are many issues of fusion proteins generally. These have to do with protein production, e.g. ensuring that the fusion protein correctly folds. There have also been many failures, e.g. Albuferon.

1.4.2 Protein PEGylation

Conjugation of polymers (e.g poly(ethylene glycol) (PEG) and polysialic acid (PSA)) to therapeutic proteins is another strategy to extend the circulation half-life. PEGylation or the conjugation of PEG, was described by Davis *et al* [88, 89] in the 1970's and remains one of the most successful and clinically used methods to date to prolong the serum half-life of proteins [90-97]. In PEGylation, PEG is covalently conjugated to the peptide or small protein. The primary reason for PEGylation is to increase the protein circulation half-life, however, enhancement of the stability and immunogenicity are other potential advantages [98, 99].

While there are currently at least 10 PEGylated proteins in clinical use (Table 1.6) [32, 97, 100-102], more than 20 PEGylated proteins are currently in clinical development [76]. It has been shown that the PEGylated proteins are safe in humans and in some cases are used in first line treatments [99]. The PEGylated interferons (IFN- α2a and IFN- α2b) are two clinically used PEGylated proteins used in the treatment of hepatitis C [103-107]. PEGylated Erythropoietin (EPO) and Granulocyte colony-stimulating factor (GCSF) are other examples of clinically used PEGylated protein (Table 1.6).

It is generally recognised that PEG possesses little toxicity when it is used in a wide range of consumer and healthcare products [99]; however, it is a clinically approved excipient in pharmaceuticals including injectable, topical, rectal and nasal formulation. This lack of toxicity is also observed when a PEGylated product is administered parenterally [99, 108]. It has been suggested that parenteral doses of up to 200 mg or more weekly of PEG associated with a PEGylated protein do not have toxicity issues [108-111].

One of the therapeutic advantages of PEGylated proteins is the reduction of the immune-toxicity since the frequency of dosing is decreased for PEGylated products [98, 101, 112, 113]. PEGylation also reduces the propensity for protein aggregation. No other strategy has been developed that is as widely applicable as PEGylation to improve the properties of therapeutic proteins for their use as medicines.

Rapid clearance of many therapeutic proteins is a common limitation and it occurs because of glomerular filtration and proteolytic degradation. PEGylation increases the circulating half-life of proteins by addressing these both issues. In principle PEG is a large molecule and its covalently conjugation to a protein decreases the rate of renal clearance. Also, PEG displays steric shielding effects when it has been conjugated to a protein. These steric shielding effects of PEG act to protect the protein from proteolytic cleavage while in circulation.

In addition, PEGylation can improve the immunogenicity of the therapeutic proteins through steric shielding effect of PEG which reduces the interaction of the protein with the immune system. Some therapeutic proteins induce an immune response when administered to the body since they can be detected as a foreign molecule. PEG can mask the immunogenic sites of protein and hence avoid production of antibodies against the proteins. For instance, asparaginase is a non-human protein and its administration alone will induce immune response. PEGylated L-asparaginase (Pegaspargase) is produced by hyperconjugation of 5 kDa PEG. The surface of this PEGylated protein is fully saturated with PEG molecules. Therefore, the levels of antibodies produced against PEGylated asparaginase are significantly lower in patients when compared with asparaginase alone [99].

Table 1.6 Clinically approved PEGylated protein.

Name (Company)	Mode of action	Indication	Approval
Adagen®, Pegademase Bovine; (Enzon)	Enzyme replacement therapy of adenosine deaminase	Severe combined immunodeficiency disease (SCID)	1990 FDA
Oncaspar®, Pegaspargase; (Enzon)	Asparaginase - part of multi-agent chemotherapy	Leukemia	1994 FDA and EMEA
Pegasys®, PEG-IFN-a2a; (Roche)	Interferon α	HCV	2002 FDA and EMEA
PegIntron®, PEG-IFN-a2b; (Schering/Plough)	Interferon α	HCV	2002 FDA
Somavert® Pegvisomant; (Pharmacia Upjohn)	GH antagonist	Acromegaly	2002 EMEA 2003 FDA
Neulasta®, PEG-GCSF; (Amgen)	Leukocyte growth factor (rh G-CSF)	Neutropenia	2003 EMEA
Macugen®, Pegaptanib (OSI/Pfizer)	VEGF (oligonucleotide)	AMD	2004 FDA 2006 EMEA
Micera®, mPEG-epoetin beta; (Roche)	Erythropoesis stimulating agent	Anemia	2007 EMEA
Cimzia®, Certolizumab Pegol; (UCB)	TNF blocker- rh Fab' fragment with specificity for human TNFα	Crohn's disease	2008 FDA
Krystexxa® ,pegloticase (Savient)	Uricase	Chronic gout	2010 FDA

Although PEGylation does not change the function of the protein, the initial interaction between the protein and target will decrease because of the steric shielding effect of PEG. This means that once the PEGylated protein interacts with its target, the biological outcome is the same as for the non-PEGylated protein. It has been shown that the association constant rate of PEGylated protein to the target is decreased while the dissociation rate constant is found to be little changed from the non-PEGylated protein [114]. The fact that protein-based medicines tend to be highly potent molecules means that clinically, PEGylated proteins can be much better medicines than non-PEGylated proteins. The PEGylated protein often has enough potency to be clinically viable. It is the extension of half-life which helps to ensure a more prolonged exposure of the protein provides clinical efficacy. It is often not possible to predict the clinical efficacy of a PEGylated protein based on *in-vitro* activity alone.

When PEG is conjugated to a protein, the PEGylated protein displays a larger hydrodynamic volume of up to 10 times larger than the native protein [115]. This dramatic change in the hydrodynamic volume of the PEGylated protein causes an increase in the overall size of the molecule to prolong circulation times [116]. The solution size of PEGylated proteins is generally dominated by the PEG rather than the protein. PEGylation can also increase the water solubility of the protein since the PEG moiety is readily water soluble. Thermal and mechanical stability of the therapeutic protein can also be improved by PEGylation [117].

The molecular weights of PEG (5-30 kDa per PEG molecules) that are used for protein PEGylation, are excreted from the kidneys, the major pathway for the elimination of the PEGylated protein, but as PEG size increases clearance rates become slow. Once the PEG solution size approximately matches the size of albumin, the clearance rates do not decrease much further [99]. This is known as the molecular weight threshold.

As mentioned, there are two clinically used PEGylated IFN medicines. They are PEGylated IFN-α2a (Pegasys) or α2b (PegIntron) are now the preferred therapy for hepatitis C in combination with ribavarin. PEGasys is derived from a PEG reagent that has 2 molecules of 20 kDa PEG (total 40 kDa PEG) which increases its circulating half-life from less than one hour for the native IFN to more than two days when administered for the treatment of hepatitis C [112]. Treatment of hepatitis C with IFN-α alone causes severe adverse effects [101] including flu-like symptoms, depression, anxiety and sleep disturbance. The treatment with PEGylated IFN-α causes these sides

effects to occur with less frequency because dosing is much less frequent. Hence patient compliance greatly increases compared to when non-PEGylated IFN is used. Another characteristic that is often under appreciated is that the *in-vitro* activity of PEGylated IFN-α is much less than that of the non-PEGylated IFN while the PEGylated protein is clinically beneficial. In the case of PEGasys, the *in-vitro* activity is approximately 5-10 % of the activity of the native IFN-α. However the clinical efficacy PEGasys is much improved compared to IFN and this is primarily due to the extended half-life of the PEGylated version of the protein.

PEGylation as a method for extending half-life is also being used in other drug delivery systems for a range of different applications, such as PEGylated liposomes (e.g.DOXIL; doxorubicin HCl liposome and PEG-based hydrogel).

1.4.2.1 PEGylation reagents

PEGylation reagents are usually electrophilic. These reagents undergo conjugattion either by alkylation or acylation reactions with the nucleophile group of protein; i.e., often the amino group on lysine [92, 95, 97, 118]. There are often many lysines on a protein so conjugation cannot usually be made to be site-specific. Conjugations by protein thiols rather than amines are often much more selective and efficient. Unfortunately cysteine residues in a protein are usually paired as disulfide bonds. Most proteins with disulfides do not have a free unpaired cysteine because the free thiol would potentially lead to disulfide scrambling, protein misfolding and protein aggregation. There are many examples that have been described where a free cysteine is engineered into a protein by recombinant approaches in an attempt to provide a free cysteine as a site for specific conjugation [119]. However if there is a disulfide present in the protein, these engineered proteins suffer the limitations associated with disulfide scrambling and aggregation. Bis-alkylation PEG reagents have been described that are able to undergo reaction with both of the thiols that make up disulfide bond [117]. Because many proteins consist of amino groups (e.g lysine groups) on their surface, the majority of the PEG reagents were designed to react with protein amino groups.

PEG reagents that are used for clinical products are mono-functionalised at one terminus with the reactive moiety that links the PEG to the protein. The other terminus is usually capped with a methoxy group. The PEG molecule is derived from anionic ring opening polymerisation of ethylene oxide which is often initiated with methoxide anion. The type of polymerisation when conducted under carefully controlled conditions

can result with the PEG being prepared with a narrow molecular weight distribution. Most biomedical synthetic polymers cannot be prepared with a narrow molecular weight distribution. They usually display broad range molecular weights. The ability to make narrow molecular weight distribution PEG is an important advantage for using PEG in protein conjugation. PEG is made in molecular weights for protein conjugation in the range from 1-40 kDa. However, by increasing the size of the PEG, retaining a narrow molecular weight distribution becomes more difficult, therefore, most PEGylated products that have been used in the clinic are made from PEG reagents which comprised of PEG molecules of 30 kDa or less.

For PEGylation on amine residues (e.g lysine) of the protein, amine acylating reagents are used. One such reagent is PEG N-hydroxylsuccinimide. This PEG reagent is not selective. Conjugation occurs on different lysine residues to give a mixture of positional isomers. The conjugation reaction is often difficult to reproduce and the PEG protein conjugate is usually obtained in low yield as a mixture of isomers. Other nucleophilic amino acid residues such as histidine can also undergo conjugation. Each positional PEG-protein isomer usually displays different physiochemical, biological and pharmaceutical properties [92, 97, 120].

Many types of proteins have been PEGylated and are now used clinically (Table 1.6). The first PEGylated proteins to be registered were PEGylated enzymes. These enzymes are hyperPEGylated by the conjugation of many molecules of linear PEG (5.0 kDa). This has been necessary as the enzymes are non-human, so they have to have PEG moieites covering as much of their surface as possible. Such PEGylated proteins are still clinically viable because the substrates the enzymes undergo reaction are small molecules (e.g. asparagine). Examples of hyperPEGylated enzymes include pegaspargase, pegademase and pegvisomant (Table 1.6). Recently pegloticase has been approved for clinical use. This PEGylated uricase is used for the treatment of chronic gout. The tetrameric uricase is conjugated to 36 PEG (10 kDa) molecules through its lysine residues. Uricase is a porcine derived. This hyperPEGylation of uricase serves many purposes including to protect the uricase from proteolytic enzymes to prolong its half life as well as to minimise the immunogenicity of this non-endogenous protein so it can be used to treat a chronic condition.

Proteins that bind other proteins such as cell surface receptors or ligands have been PEGylated with a single large molecule of PEG. The proteins that are currently in the clinic are endogenous replacement proteins (e.g. interferon, erythropoietin).

Increasingly non-endogenous proteins are also being PEGylated with a large PEG molecule and are being clinically evaluated. While these products are mono-PEGylated proteins, PEG reagents are used that are both inefficient and non-selective. PEG aldehyde is designed to undergo reaction with the terminal anime on a protein, but this reaction is inefficient since the first step generates water as a side produce. Once the PEG-aldehyde undergoes reaction with the terminal amine to form an imine, it is locked in place by reduction with a borohydride reagent (e.g. $NaCNBH_3$). This type of PEGylation is known as reductive amination and is used to produce PEGylated GCSF (i.e. Neulasta). Reductive animation is inefficienct and only very narrow conditions can often be found that will tend to result in PEG conjugation at the terminal amine.

Other PEGylation reagents are derived from linear and branched PEG-N-hydroxysuccinimides (PEG-NHS). The products are still mixtures because the conjugation of the PEG occurs at different nucleophilic sites of the protein. All the products in the clinic are heterogeneous. Active ester PEGylation reagents are susceptible to competitive hydrolysis, so conjugation often is inefficient. Because they are inefficient for conjugation, both PEG aldehyde and PEG-NHS reagents have to be used at considerable stoichiometric excess. This means considerable effort is required during downstream processing. Often the cost of the PEG reagent can be as expensive at the protein. While the currently used PEGylated proteins are often described as being mono-PEGylated, these medicines are actually a complex mixture of different PEGylated products (i.e. positional isomers). Each PEG-protein isomer is a mono-PEGylated variant, each with its characteristic property profile (i.e. activity and physicochemical).

It has been recognised for quite some time that there is a need to develop strategies to increase the efficiency and site-specificity of the conjugation of PEG. This need is driven to make more homogenous and efficacious protein-based medicines that are more cost-effective. Thiol based conjugations are often much more efficient and site specific than amine based conjugations at the mild conditions that are appropriate for most proteins. While amines can be derivatised to thiol, it is the thiol group on cysteine that has been considered for site specific PEGylation [119, 121-123]. Most proteins do not have a free cysteine, so much work as been described to add a cysteine recombinantly to a protein for PEGylation [38, 119]. Another approach is to use conjugation reagents capable of conjugating to both cysteines thiols from an existing disulfide in the protein [124, 125]. In addition to cysteine-specific conjugation, other

amino acids (e.g. arginine, glutamic acid) [126-129] and glycosyl moieties [130-133] have also been described as targets for conjugation.

Certolizumab pegol (Cemzia) is the one clinical example of a protein that has had a cysteine added to its structure so that a thiol selective PEGylation can be accomplished. Certolizumab pegol has a 40 kDa branched maleimide PEG (2 x 20 kDa) conjugated to the cysteine residue. While maleimide is the most reactive and most widely used of the mono-thiol based PEGylation reagents, it is hydrolytically unstable and is prone to de-PEGylation by the reverse Michael reaction leading to transfer of PEG to other proteins in the body. Maleimides are prone to ring opening to generate acidic by-products [134]. Certolizumab is an antibody fragment (Fab) that binds to TNFα and is used to treat inflammation caused by rheumatoid arthritis.

Unfortunately certolizumab has native disulfide bonds that are scrambled with the free cysteine that has been added to its structure. The engineered cysteine is on the heavy chain near to the native interchain disulfide of the Fab. This complicate the PEGylation process leading to a heterogeneous mixture with PEG conjugated to different cysteines. For therapeutic proteins that do not have any disulfides, insertion of a single cysteine could be the best approach for site-specific PEGylation. For example, a protein scaffold derived from a fibronectin type III domain does not have a disulfide in its structure, therefore, insertion of free cysteine for PEGylation seems to be appropriate, but again a maleimide reagent has been used. The PEGylated fibronectin type III is currently in clinical trials [135, 136].

To address the limitations of maleimide instability *in-vivo* [134] and the difficulty for engineering a free unpaired cysteine into a protein, new bis-alkylation thiol specific reagents have been developed [137]. These reagents are based on the PEG bis-sulfone **1**. The alpha proton to the ketone is acidic and its deprotonation in mild conditions allows the PEG-bis-sulfone to be converted to the PEG mono-sulfone **2** (Scheme 1.1) which is then capable of undergoing conjugation. The conjugation process is governed by the elimination of a total of 2 molecules of sulfinic acid anion to produce a propenyl group that can undergo reaction at the two terminal carbon atoms. Conjugation leads to two bonds being formed over a three carbon bridge (Figure 1.9).

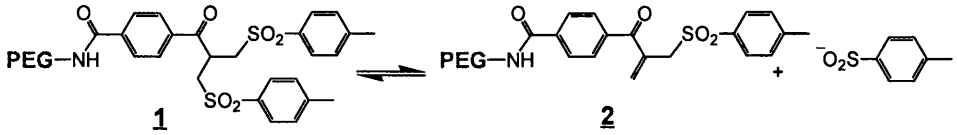

Scheme 1.1 The equilibrium between PEG mono-sulfone (2) and PEG bis-sulfone (1).

These *Bis*-alkylation reagents 1 have been developed in our group to bridge the two sulfurs that form a native disulfide. Since most therapeutic proteins have disulfide bonds, site-specific PEGylation at the natural disulfide bond of the protein is possible [138, 139]. This avoids the need to add a free cysteine to the protein. This disulfide bond can be opened under mild reducing conditions and used as a source of free thiol for conjugation [137].

The PEG mono-sulfone 2 Scheme 1.1, undergoes reaction by a series of addition-elimination reactions with the two sulfure atoms derived from a disulfide bond [117]. The PEG mono-sulfone 2 consists of a substituted propenyl group at the end of the PEG that acts as the conjugating moiety. This conjugation group has a carbonyl group that acts as an electron-withdrawing group, an α,β- unsaturated double bond, and α,β sulphonyl group. The electron-withdrawing group is necessary to initiate thiol addition. The elimination reaction can proceed at a lower pKa of the α-proton. Sequential addition-elimination reactions begins with the conjugated double bond in the PEG mono-sulfone 2 (Figure 1.9) [117]. First a thiolate adds by conjugate addition (i.e. Michael addition) which results in the elimination of a sulfinic acid group. This generates another conjugate double bond at the α,β-position. This second double bond is necessary for addition of a second thiolate. After the two addition conjugation reactions have occurred a three-carbon bridge is formed between the sulfure atoms of the original disulfide [117]. One key advantage of the PEG mono-sulfone 2 reagent is the conjugation product is stable because conjugation of a disulfide in this way is thermodynamically driven. It is thought that the stability of the protein also adds to the stability of this type of conjugation. In cases where the reverse conjugation reaction is observed, the electron withdrawing ketone group can be reduced to hydryoxide. Similar reagents to what are used for reductive amination can be used to reduce this ketone. In this way, the reverse reaction is completely inhibited. The hydrolysis reactions that limit maleimide reagents do not occur for conjugations that have been done with PEG mono-sulfone 2. Also the thiol ether bonds are more stable than the native disulfide which had initially undergone conjugation.

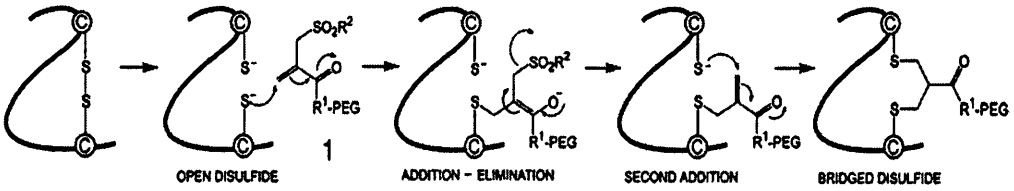

Figure 1.9 Mechanism of action of site specific, disulfide bridging PEGylation of protein.

The use of PEG-bis-sulfone **1** for conjugation can potentially produce a more homogenous PEGylated-protein with higher yield and which is reproducible [137]. However, there is no clinically approved medicine that has been PEGylated using this technique. New PEG reagents have recently been developed in our group to undergo site-specific bis-alkylation PEGylation at each terminus of a PEG molecule. The PEG di(bis-sulfone) reagent **3** and PEG di(mono-sulfone) reagent **4** are shown in Scheme 1.2. The PEG di(mono-sulfone) reagent **4** has two conjugation groups at both ends which can conjugate to two proteins. Each conjugation moiety contains a carbonyl group, an α,β- unsaturated double bond, and α,β sulphonyl group.

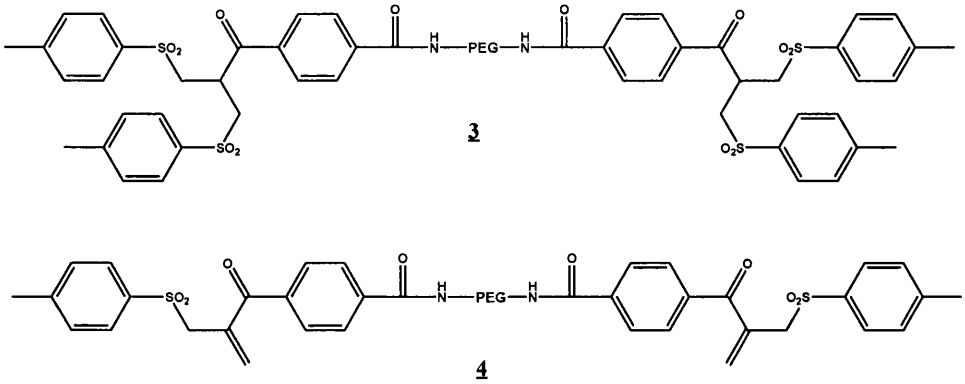

Scheme 1.2 The PEG di(bis-sulfone) reagent **3** and PEG di(mono-sulfone) reagent **4**.

The PEG reagents (**1** and **2**) are also found to undergo site-specific reaction with polyhistidine-tags (His-tag) in proteins [140]. Proteins are often expressed to contain a His-tag on their C- or N-terminus to improve their expression. Inclusion of a His-tag is useful for purification during early studies of a protein and can also increase expression yields [141] and help refolding [142]. A His-tag will not usually compromise the function of the protein [143] and there are several examples of His-tagged proteins being used in the clinic [144-147].

In the context of antibody fragment PEGylation, the most important factors are to maintain an acceptable level of biological activities of the antibody fragments and to improve its serum half-life [38]. These biological activities do not only concern the antigen binding but also relate to the ability of antibody fragment to localise to target tissues. Maintaining sufficient biological activities and binding affinities of PEGylated antibody fragments are dependent on the chemistry of conjugation, the size of PEG used and also the number of PEG molecules attached per protein molecule [38]. Amine-based PEGylation of antibody fragments through their lysine groups result in decreases in the binding activity of the antibody fragment. For instance, the $F(ab)_2$ fragment derived from the A7 murine monoclonal antibody by enzymatic digestion, was PEGylated with 4 PEG (5 kDa) molecules using amine chemistry. This PEGylated $F(ab)_2$ resulted in a 12% loss of a antigen binding activity when compared with the non-PEGylated $F(ab)_2$ [38]. This reduction in the binding activity of antibody fragment after amine PEGylation is probably related to the conjugation site of the PEG. There are several lysine groups on the Fab fragment. Because PEG conjugation may occur at or close to the antigen binding domain, therefore it is likely that PEG causes a steric hindrance to the antigen-antibody interaction. Therefore, applying a site-specific PEGylation method to PEGylate an antibody fragment is required to improve its binding activity. Since cysteine residues are used for PEG attachment in the site specific PEGylation approach, either by insertion in the hinge region or by using the interchain disulfide bond, it causes less interference by the PEG with the antigen-Fab interaction when conjugation is conducted in this reagion of the Fab. Hence, the binding activity of a PEGylated antibody fragment produced in this manner was shown to be improved, compared with those produced by the amine PEGylation method [38]. Study of the binding affinity of a PEGylated antibody fragment prepared by site-specific way using BIAcore demonstrated that the dissociation rate of the antibody fragment from its antigen did not change after its site specific PEGylation, however, the affinity value changed approximate 5 fold because of change in the association constant rate. This reduction in association rate was proposed to be due to steric hindrance effects, smaller though remaining, due to the presence of the PEG [114].

As mentioned earlier, IgGs are bivalent and Fabs are monovalent. The binding affinity and avidity of the Fab are less than for a full IgG towards the target. Also, the IgG and the Fab are both monospecific. Different strategies have been suggested in the literature to address these two aspects of therapeutic Fabs; mono-valency and mono-

specificity.

1.5 Strategies to improve bivalency and specificity of antibody fragments

Polyvalent interactions occur extensively in nature. They involve the simultaneous and often sequential, cooperative binding of ligands to multiple receptors [148]. For example, multiple ligands on the surface of a virus may undergo efficient binding to cell surface receptors. The binding of an IgG antibody is bivalent and so is considered as a molecule that is capable of polyvalent interaction. The binding of multivalent ligands to receptors is much stronger than the analogous binding of the individual, separate ligands [149, 150].

Different methods have been described to generate multivalent binding molecules. These include (i) the synthesis of polymers with multiple copies of sialic acid [151] and multivalent molecules that tightly bind to viruses and bacterial toxins [152, 153] (ii) conjugation of antibodies to micro or nano particles (i.e. quantum dots [154] and liposomes [155] and (iii) conjugation of multiple moieties (i.e small peptides) to polymers. The synthesis of sialic acid displays a multivalent inhibitory effect and has been shown to inhibit the adhesion of influenza virus particles to erythrocytes 10^9 fold greater than the corresponding monovalent sialic acid [151-153, 156, 157].

Conjugation of antibodies to the surface of quantum dots and other colloids are associated with several disadvantageous such as toxicity that may occur due to presence of the metal in the quantum dot cores. It is often very difficult to purify such conjugates to homogeneity [158]. Ultimately the sterilisation and the production of such complex conjugates to GMP specification will require significant effort to achieve. While appropriately functionalised polymers can display multivalent interactions [157, 158], polymers can also be used to conjugate moieties (i.e. small peptides or Fab fragments) at their termini. In the case of a linear polymer this would be two moieties-one on each end of the polymer. The linker used can be a branched polymer with many end groups or a linear polymer to simply link two proteins.

Linking functional group must covalently connect ligands of interest to the polymer while insuring they are separated spatially. A framework should be provided so the ligands can be in conformations that allow cooperative binding. In the case of covalently linking molecules at the termini of a polymer, both the length and flexibility of the overall structure may be important to influence the cooperative binding properties of the conjugate [150, 157, 159, 160].

Intuitively is seems that a dimeric binding molecule would be sensitive to the length and flexibility of the linker used to conjugate the two binding moieties. However this may not always be the case. One example model system is the conjugation of human carbonic anhydrase II (CA). It was found that a binding of the dimer, CA-linker-CA to surface immobilised ligand was not influenced by the length of the linkers used. BIAcore analysis was used and it seems quite a high loading of immobilised ligand was used, so it is possible in this model system that at a much lower immobilisation of ligand that structure-property correlations with linker structure may emerge. Clearly both the polyvalent molecule and the partner target used to measure binding are important. In a related study using CA there was some correlation with binding properties with the size of a oligo(ethylene glycol) linker that was used [161]. Calorimetry was used to show that entropic effects exerted influence on cooperative binding. If the linker was long enough to allow both CA molecules to bind, and if the linker was flexible, then there appeared to be only a weak dependence on binding as linker length increased [161]. Linker flexibility is an important consideration when considering the synthesis of multivalent conjugates. Linker flexibility provides a level of robustness to ensure that cooperative binding can occur within a heterogeneous biological environment where binding distances between targets may vary [157, 160, 162].

Consistent with these observations it has been shown that when using a random coil, rigid rod and a joined rod as a linker between ligands, that the random coil displayed a better effect on avidity [157, 160, 162]. The flexible linker with slightly longer length than the distance between the binding sites of the receptors would provide a better binding affinity to a bivalent molecule. Also, it has been shown that the effective concentration of the multivalent ligands depends on length and flexibility of the linker. A flexible linker with longer length resulted in higher effective molarities [162]. However, if the length of the linker becomes too long, then the effective molarities of the ligand decrease, leading to gradually decrease in binding affinity [157, 162].

While monoclonal IgG antibodies are bivalent, antibody fragment (Fab) is monovalent. When the antigen is a bivalent soluble ligand such as VEGF, then the bivalent IgG has an advantage over monovalent Fab as better binding affinity is expected for the IgG. The same would be true if a receptor is present on a cell surface. Since a monoclonal antibody will recognise one epitope and receptors would generally

not be expected to have multiple copies of an epitope, then receptor denisty on a the cell surface will allow the bivalent character of an IgG antibody to exert cooperative binding. A key aim of this PhD was to use the PEG-di(mono sulfone) **4**, to link two antibody fragments (Fabs) together. It was hoped that binding comparable to the parent IgG of the Fab could be achieved.

Further considering antibody structure and their therapeutic us different approaches have been described including bispecific antibodies (bsMab) and antibody drug conjugates (ADC).

1.5.1 Antibody drug conjugates (ADC)

In ADC, monoclonal antibodies are used for the delivery of anticancer drugs or cytotoxic agents specifically to tumour cells. If cytotoxic drugs distribute to all of the body, it would effects on healthy cells and tissues as well as tumour cells. Conjugation of these drugs to antibody, which has a specific target binding, would reduce this adverse effect on normal tissues as drug can be delivered specifically to the tumour cells. The cytotoxic drugs are released at the tumour cell after internalisation of ADC. When cytotoxic drugs are released, then they becomes activated [163]. In addition, the serum half-life of the cytotoxic drug would be improved by conjugation to IgG [164]. The drug gemtuzumab ozogemicin (Mylotarg, anti-CD33 mAb conjugated to calicheamicin) is an example of an ADC that is approved for the treatment of acute myeloid leukemia and more ADCs are in clinical development.

However, if the conjugation of drug to antibody is not stable, then it is possible to release the drug in the systemic circulation before internalisation to tumour cells. In this situation, therapy with ADC results in some systemic toxicity. Conjugation of drug to antibody can be occurred through lysine groups or the thiols that are derived from reduction of disulfides of the antibody. It has been suggested that conjugation of drug at thiols of antibody can improve the stability of ADCs in some extend. This conjugation performed by mild reduction of interchain disulfide bonds on mAb (in hinge and Fab regions) to provide the sulfhydryl group which can conjugate to cytotoxins drug. This method, however, produces a mixture of one to eight moles of drug per mole of IgG1 because all of the opened interchain disulfide bonds (eight cysteine) could be engaged in conjugation and result in more than 100 different ADC species. To address this heterogeneity issue, the site-specific method has been developed. In this approach a

drug conjugates site-specifically to the antibody through thiols that precisely positioned on the antibody. To achieve this, a peptide substitution with cysteine was suggested to generate an engineered antibody named THIOMAB [165, 166]. In THIOMAB, Ala 114 at the CH1 domain of the antibody was substituted with cysteine to allow thiol conjugation at this site. In this method, one mole of drug could be reliably conjugated to one mole of IgG and thus lead to production of a homogenous product [163, 165, 166].

An example of an ADC is trastuzumab-DM1 which is currently in clinical trial. The efficacy of this drug is being examined for the treatment of patients with trastuzumab resistant HER-2 positive breast cancer [167]. This is a new approach for HER-2 targeted therapy, which uses conjugation of the cytotoxic molecule DM1 (a derivative of maytansine 1) with trastuzumab. Since trastuzumab is an anti-HER-2 monoclonal antibody and DM1 is a microtubule formation inhibitor, it was suggested that this ADC molecule might be a better candidate for treatment of HER-2 positive breast cancer than trastuzumab alone. In this model, the DM1 molecule is delivered to HER-2 overexpressing cells via receptor-mediated endocytosis and then the potent DM1 is released by lysosomal degradation to inhibit microtubule formation and elicit cell death [167].

1.5.2 Bispecific antibodies (bsMab)

Bispecific monoclonal antibodies (bsMab) are another promising approach to enhance the clinical use of antibodies for cancer treatment [168-170]. Such constructs are potential candidates for both diagnostic and therapeutic use. The concept was first introduced by Nisonoff and Rivers 40 years ago [171]. These antibodies have dual specificity in their binding arms, which are able to bind two antigens simultaneously. The simultaneous targeting of a bispecific antibody to two antigens may have an advantage to enhance tumour targeting [172]. Also, using a bispecific antibody might have a potential to avoid from combination therapy that has been suggested for treatment of complex disease. For some chronic diseases combination therapy with two or more therapeutic agents has been suggested to decrease some side effects that may occur with single therapy and to maximise efficacy [173]. The bispecificity properties of bsMab may allow the development of therapeutic strategies that are not possible with mono-specific antibodies [3, 174].

Since native IgGs are mono-specific, a bispecific antibody do not usually occur in nature [174, 175]. There are several bsMabs which are in or have been in clinical trials. A key limitation is the difficulties in producing bsMabs in high yield, purity and construct stability [172, 175]. There are different strategies to produce bispecific antibody constructs; (i) quadroma technology [172, 175], (ii) chemical crosslinking [174, 175] and (iii) recombinant DNA technology [174].

A bispecific IgG can be generated using hybridoma technology by fusing two hybridoma with a B lymphocyte to generate quadromas [174, 175]. Using this method, it is possible to randomly fuse two heavy and light chains and results in more than 10 different antibody species which only one of them is functional bispecific antibody. Because of these side products, the production yield of the desired bispecific antibody is quite low and required many purification steps [176].

Another approach to make bispecific antibodies is through the use of chemical crosslinking methodologies. In this method, a chemical cross-linking reagent is used to covalently conjugate two different antibodies together. An example for this method is random conjugation of 2 molecules of Fab′ by a cross linking reagent (Figure 1.10, b). The conjugation occurs between the free thiols that form from reduction of interchain disulfides of $F(ab)_2$ and the homo-bifunctional cross linking reagent. The major problem with this method is product homogeneity. Similar to what is reported for quadroma technology, the purification of the heterogenious product mixture is required. Complex purification processes were required leading to a lower yield of the bsMab product. Moreover, complex and multiple purification steps can damage proteins since they are prone to misfolding, aggregation and degradation [3, 174].

In recombinant DNA technology is possible to genetically engineered the bispecific antibodies from human in a large scale with high purity. Although using this method involves fewer steps of purification and results in a high yield of bsMab, it is still an expensive and complicated method. While there is many examples of the genetic engineering of bsMab conjugates along with the potential benefits are described in the literature, few of them have reached to clinical development.

In recombinant technology, bispecific antibodies can be produced using a linker or leucine zipper to connect different domains of IgG. Also it is possible to make the bispecific antibodies using an approach called 'knob into hole'. In this approach bsAb constructs can be produced with a very similar structure to human IgG and minimal difference in terms of sequence while no linker is required [174].

Using a linker to generate bsMab has been reported for tendom scFv (tascFv), diabody (Db) and tandem diabodies (taDb) (Figure 1.10, c). In tascFV, two separate scFv linked by linker to produce bivalent and bispecific constructs. The tascFv products are stable, however, they suffered from poor solubility. Therefore, tascFV had to be refolded from inclusion bodies or alternatively would need to be expressed in mammalian cells [3]. In the case of diabody (Db), conjugation of scFv occurs with a shorter linker. When the linker that separates the heavy and light chains of variable domains is shorter, it is not possible to pair these domains together. Hence, these heavy and light chain variable domains would conjugate to the heavy and light chains of a second scFv (Figure 1.10, c). It has been shown that Dbs have a large degree of flexibility, hence two active antigen binding sites at the opposite ends of this molecule are able to approach their targets even if their targets are located on two different cells. Dbs also can be made in large amounts in *E-coli* or yeast, similar to tascFv. The tandem diabodies (taDb), (Figure 1.10, c) is a two diabodies linked together. This molecule can also be expressed in *E-coli* as a monomer while maintains the solubility of the diabody [3, 174].

In the case of bsMab using a leucine zippers, two binding specificities of IgG can be hold together with leucine zipper into a single molecule. An example of this method is shown in (Figure 1.10, e) where two different Fabs are conjugated with interaction between the regulatory subunit of protein kinase A (PKA) and the anchoring domain of A kinase anchoring proteins (AKA). This resulting fusion construct is bispecific and could be trivalent if three Fabs connected [174].

Another example of fusion technology is the fusion of a Fc fragment to Db as a means to increase the circulating half-life of Db (Figure 1.10, d) in Db-Fc and taDb-Fc. In addition, $(scFv)_4$-Fc can be made by incorporation of a first scFv to the CH1-CH2-CH3 domains of an IgG heavy chain and a second scFV to the CL domain of the light chain. This molecule has a similar 'appearance' to IgG and contains a full Fc fragment, however, it is bigger than native IgG (Figure 1.10, d) and four independent binding sites. It is reported that while it is possible to produce homogenous (scFv)4-Fc, the expression yield is not sufficient to allow study in animal models [174].

However, since a linker is a foreign molecule, it may have problems with respect to therapeutic applications. Also, the flexibility properties of the bsAb constructs can have an effect on proteolytic cleavage and stability of the antibody are depended on the length and types of the linker used. In the 'knob into hole' method, two different heavy

chains of different IgGs are conjugated by introducing mutations into the CH3 domains to modify the connection site. This mutation occurs on one heavy chain, which replaces one bulky amino acid with a short side chain amino acid to make a 'hole'. In another heavy chain, an amino acid with a large side chain is included to make a 'knob'. By connecting these two heavy chains, the heterodimer 'knob-hole' can be produced with more than 90 % homogeneity. However, there are some problems associated with this method; such as mispairing leading to production of an inactive bispecific molecule. However, this problem can be solved to some extent by the use of phage display libraries with limited light chain diversity [174].

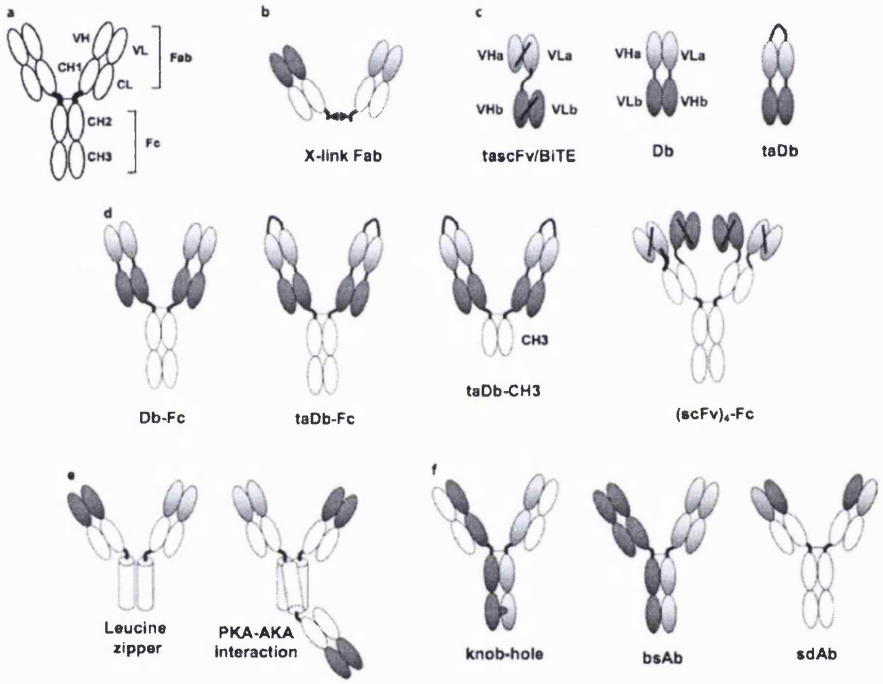

Figure 1.10 The possible structures of bispecific antibody fragments, reproduced from [174].

Another strategy to improve the specificity of antibody-based medicines is to design 'two-in-one' antibodies [177]. In this method, one antibody could bind to two different antigens with high binding affinity. To achieve this, a 'two-in-one' antibody consists of two different antigen-binding sites. One example of such a bispecific antibody that is in development by Genentech is a 'two-in-one' antibody that consists of variants of trastuzumab and bevacizumab using genetic engineering method. This antibody (named bH1) has the ability to bind to HER-2 and VEGF at the same time, which might have significant effects in the treatment of cancer [177].

The rationale for making a bispecific antibody to engage the VEGF ligand and HER-2 receptor simultaneously lies in the interplay between the VEGF and EGFR signalling pathways. Both VEGF and EGFR pathways govern angiogenesis in solid tumours. EGF and TGF-alpha ligands can induce VEGF production by activation of EGFR and, therefore, they both have a pro-angiogenic effect. It is suggested that activation of EGFR and its signalling pathways would stimulate angiogenesis by up-regulation of VEGF. It has also been demonstrated that blockage of EGFR using cetuximab resulted in reduction of pro-angiogenic molecules such as VEGF, and hence reduction in tumour size [178].

Since EGFR inhibition does not completely block VEGF production or signalling, tumour angiogenesis and therefore tumour growth can still progress, however, studies have shown that full inhibition of VEGF signalling is required for elimination of tumour growth [179]. Hence, additional targeting of VEGF would seem to be a more effective way to stop angiogenesis and inhibiting the growth of tumour cells.

In addition, there is a report that some tumour cells in HER-2 overexpression breast cancer may become resistant to anti-EGFR drugs [180, 181]. This resistance to anti-EGFR therapy is a result of over production of VEGF [181]. Over expression of HER-2 results in over expression of VEGF. This problem can eventually be solved by inhibition of VEGF. Combination therapy of bevacizumab and trastuzumab for the patient with HER-2 overexpression breast cancer [55, 177, 182] has already been suggested. It has been demonstrated that combination therapy to target angiogenic pathways, directly by inhibition of VEGF and blocking EGFR, can dramatically reduce size of tumours and therefore improve the efficacy of anti-cancer treatment [180, 183]. These studies show that how dual inhibition of VEGF and EGFR has the benefit of more complete inhibition of growth of a solid tumour than targeting an individual mediator. Dual inhibition of VEGF and EGFR pathways has also been suggested for treatment of patient with non-small cell lung cancer (NSCL) which resulted in reduced tumour endothelial cell proliferation and angiogenesis when compared with single therapy with either bevacizumab or trastuzumab [184].

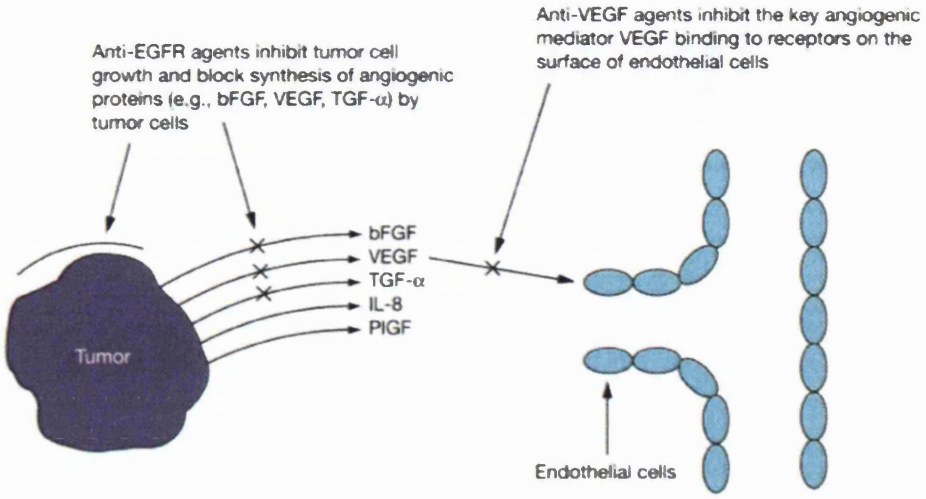

Figure 1.11 Dual blockade occurs with anti-VEGF and anti-EGFR agents to provide a complementary anti-tumour effect, reproduced from [183].

1.6 Hypothesis

For some medical applications where an antibody is used as an antagonist, or to neutralise a soluble ligand, the effector functions of the Fc are not necessary. Side effects caused by the Fc could be avoided completely by removing the Fc fragment. As discussed previously, the isolated Fab has a smaller size and thus can diffuse into the tissue more easily than a full antibody. However, the use of antibody fragments is limited by short circulation half-life, and possibly by monovalency towards bivalent targets.

In this PhD, it was hypothesised that:

1) The starting Fab to be PEGylated can be obtained from a therapeutic monoclonal antibody by proteolytic digestion and that the Fab can be purified and isolated while maintaining its antigen-binding properties.

2) Different Fabs can be PEGylated using the bis-alkylation PEG reagents **2** and **4** after treatment of the Fab with a reducing agent such as DTT to liberate the interchain disulfides. Once PEGylated in this way the PEGylated product will broadly maintain the binding properties of the starting, non-PEGylated Fab.

3) Using PEG di(mono-sulfone) **4** to conjugate one molecule of a Fab to each end of the PEG. In this way, PEG can be used as a scaffold to form a homodimer (Fab-PEG-Fab)

that can display the binding properties of the parent IgG from which the Fab was derived from.

4) The PEG di(mono-sulfone) **4** can be used to conjugate two different Fabs. In this way bispecific construct (Fab-PEG-Fab*) can be obtained that broadly retains the antigen binding properties of the individual Fabs.

The following research aims were formulated to test these hypotheses:

1) In order to obtain the clinically relevant Fabs for PEGylation, enzymatic digestion must be performed on therapeutic antibodies (Figure 1.12). To subject bevacizumab (anti-VEGF) and trastuzumab (anti-HER2) to papain digestion. The antigen-binding properties of these purified Fabs will then be determined using ELISA and BIAcore.

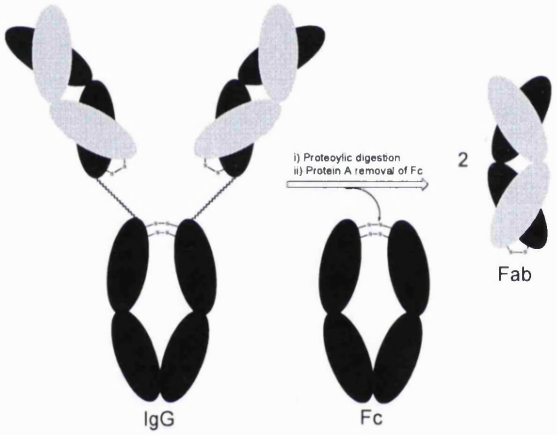

Figure 1.12 Enzymatic digestion of an IgG to obtain a Fab.

2) Use PEG mono-sulfone **2** at molecular weights of 20, 30 and 40 kDa (Scheme 1.1), conduct PEG conjugation reactions with Fab_{beva} and Fab_{trast}. As a third Fab, ranibizumab (Fab_{rani}) will also be PEGylated with this PEG reagent **2**. PEGylation will be conducted after treatment of the Fabs with a reducing agent to reduce the interchain disulfide (Figure 1.13). Following PEGylation, the PEG-Fab conjugates will be purified and then their stability assessed to determine if the PEG remains conjugated to the protein. Contamination of the PEG-Fab product with non PEGylated Fab must be avoided. After confirming the purity and stability of the conjugates, their binding properties will be determined by BIAcore and ELISA to establish structure-property correlations. The starting non-PEGylated Fabs and parent monoclonal antibodies will also be evaluated by BIAcore and ELISA.

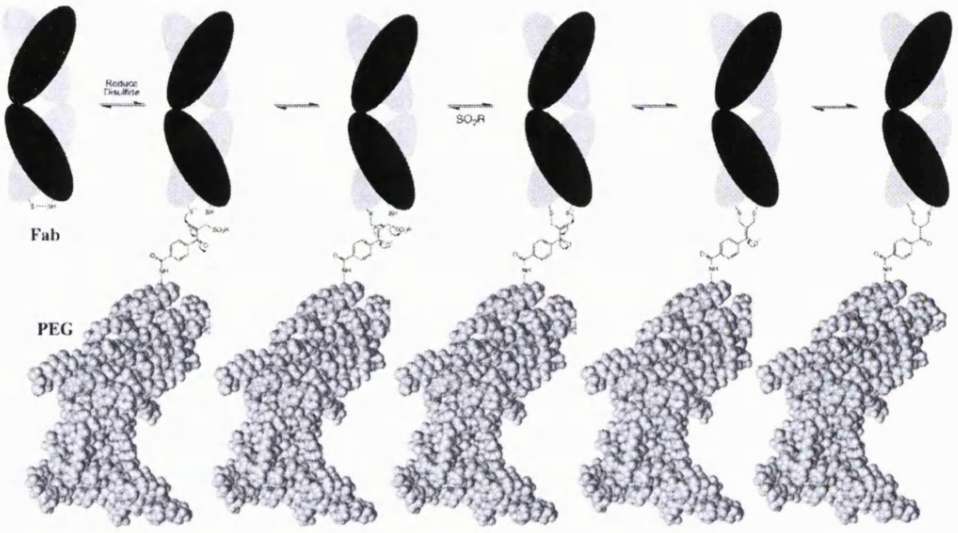

Figure 1.13 Mechanism of disulfide bridging PEGylation of the Fab using bis-alkylation method.

3) The PEG di(mono-sulfone) reagent **4** at molecular weights of 6, 10 and 20 kDa (Scheme 1.2) will be used as a scaffold to conjugate two Fabs together to produce a homodimer Fab-PEG-Fab. This reagent undergoes conjugation by bis-alkylation at each terminus (Figure 1.14). The three Fabs; Fab_{beva}, Fab_{trast} and Fab_{rani} will be PEGylated using PEG reagent **4** and the corresponding Fab-PEG-Fab homodimers will be purified and their stability evaluated. The structure-binding correlations of these homodimers will then be determined using BIAcore and ELISA and compared to their intact Fabs and native IgG.

4) A co-culture anti-angiogenesis assay will be used to evaluate the comparative functional activity of the Fab-PEG-Fab conjugates.

5) The PEG di(mono-sulfone) reagent **4** will also be examined to determine if it is possible to conjugate two different Fabs to make a heterodimer Fab-PEG-Fab* construct (Figure 1.14). Fab_{beva} and Fab_{trast} were selected to be used to make the bispecific Fab-PEG-Fab* construct because of the relevant signalling pathways of HER-2 and VEGF. The binding properties of the bispecific Fab_{beva}-PEG-Fab^*_{trast} will then be studied by BIAcore.

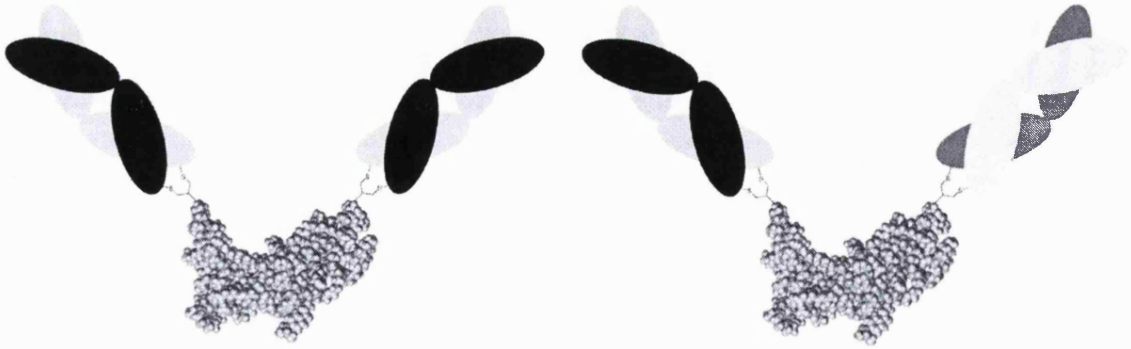

Homodimer (bivalent)

Heterodimer (bispecific)

Figure 1.14 The homodimer (bivalent) and heterodimer (bispecific) using the PEG as a scaffold.

Chapter 2: General Materials and Methods

2 Chapter 2: General materials and methods

2.1 Materials

Bevacizumab (Avastin®, 25 mg/mL, Genentech) and trastuzumab (Herceptin®, 150 mg, Genentech) were purchased from Moorfield Pharmaceuticals (London). Ranibizumab (Lucentis®, 10 mg/mL, Genentech) was obtained from the pooled remains of vials that had been used clinically. The model Fab (ChromoPure human Fab, 2 mg, cat. no. 009-000-007) was purchased from Jackson ImmunoResearch. The model human IgG (50 mg, cat. no. I4506-50MG) was purchased from Sigma-Aldrich.

2.1.1 Protein purification

Desalting columns (PD-10 with cat. no. 17-0851-01, Nap-10 with cat. no. 17-0854-01 and Nap-5 with cat. no. 17-0853-01), cation exchange columns (HiTrap SP FF 1.0 ml with cat. no. 17-5054-01, HiTrap SP HP 1.0 ml with cat. no. 17-1151-01, HiTrap MacroCap SP 1.0 mL with cat. no. 28-9295-91) and a Superdex 200 prep grade size size exclusion column (34.0 μm particle size, cat. no. 17-1069-01) were all purchased from GE Healthcare. Vivaspin 6 centrifugal concentrators with 10 kDa molecular weight cut off (cat. no. VS0612) was purchased from sartorius stedim biotech.

2.1.2 Protein characterisation

Ellman's reagent (5,5-dithio-bis-(2-nitrobenzoic acid)) was purchased from Thermo Fisher (cat. no. 225820). Novex Bis-tris 4-12% gels (cat. no. NP 0321BOX), Sharp Blue standard protein markers (cat. no. LC5800), NuPAGE MOPS running buffer (cat. no. NP0001), NuPAGE LDS sample buffer (cat. no. NP0007) and SilverXpress silver staining kit (cat. no. LC6100) were purchased from Invitrogen. InstantBlue was purchased from Expedeon Ltd. Perchloric acid (0.1 M) and barium chloride (5.0 %) solutions for barium iodide staining were prepared in the lab.

2.1.3 Antibody digestion

Immobilised papain slurry gel (cat. no. 20341) and a NAP protein A plus spin kit (cat. no. 89978), which contained two immobilised protein A spin columns (cat. no. 1860592), two elution immunoPure IgG buffers (0.1 M glycine, pH 2.8, cat. no. 1852020), a neutralization buffer (1.0 M Tris buffer, pH 8.5, cat. no. 1856281) and a binding buffer (1.0 M Tris buffer containing EDTA, pH 8.0, cat. no. 21007) were purchased from Thermo Fisher (Pierce). IdeS enzyme (FabRICATOR® for 5.0 mg IgG,

cat. no. A0-FR1-050) was purchased from Genovis (Sweden). L-cysteine hydrochloride monohydrate (cat. no. 30129), dithiothreitol (DTT, cat. no. 43819), tris (2-carboxyethyl) phosphine (TCEP, cat. no. C4706) and sodium hydroxide (1 N, cat. no. S110411) were purchased from Sigma-Aldrich. The disulfide reducing agent, 2-mercaptoethylamine.HCl (2-MEA, cat. no. 20408) was purchased from Thermo Fisher (Pierce).

2.1.4 PEGylation reagents

The PEG bis-sulfone **1** and mono-sulfone **2** reagents (Scheme 1.1) were donated by PolyTherics Ltd and used for mono PEGylation of antibody fragment. The PEG reagent used for homodimer and heterodimer PEGylation was the PEG di(mono-sulfone) reagent **4** (Scheme 1.2) which was prepared from the PEG di(bis-sulfone) reagent **3** and then donated by PolyTherics Ltd.

2.1.5 BIAcore

All BIAcore consumables were purchased from GE healthcare. These include the amine coupling kit (cat. no. BR-1000-50), *N*-hydroxysuccinimide (NHS), 1-ethyl-3-(3-dimethylaminopropyl)-carbodiimide (EDC), ethanolamine-HCl (1.0 M, pH 8.5), glycine buffer (10 mM, pH range of 1.5 to 2.5, cat. no. 22053613), HBS-EP buffer (including HEPES (0.1 M), NaCl (1.5 M), EDTA (30 mM), 0.5 % V/V surfactant P20, pH 7.4, cat. no. 22-0665-01), and CM3 (cat. no. BR-1005-41) and CM5 (cat. no. BR-1003-99) sensor chips. The test compounds were prepared in an eppendorf tube (1.5 mL). The eppendorf 's (1.5 mL) cap was cut and replaced with the rubber caps (Type 2, cat. no. BR-1004-11).

2.1.6 ELISA assay

The 96 well nune-immunoplates (MAXISORP, cat. no. 442404) were purchased from Thermo Fisher. The washing buffer (PBST) pH 7.3 was prepared in the lab from phosphate buffered saline (PBS, cat. no. BR0014G, from Oxoid) and Tween20 (cat. no. P7949) purchased from Sigma Aldrich. The blocking buffer pH 7.3 was also prepared in the lab from bovine serum albumin (BSA, cat. no. A2153, from Sigma Aldrich), Tween20 and a PBS tablet (cat. no. BR0014G, from Oxoid). The anti-human IgG (Fab specific)-peroxidase (cat. no. A0293), 3,3′,5,5′-Tetramethylbenzidine (TMB, cat. no. T8665) and human vascular endothelial growth factor ($VEGF_{165}$, 10 μg, cat. no. V7259-10UG) were purchased from Sigma Aldrich. The less expensive $VEGF_{165}$ (13 μg, cat.

no. 02/286) was purchased from NIBSC. Recombinant human ErbB2/HER2 (100 μg, cat. no. 10004-H08H) was purchased from Sino Biological Inc.

2.1.7 In-vitro angiogenesis assay

The Angiokit (cat. no. ZHA-1000) is a 24 well plate that was pre-seeded and utilised optimised growth medium. The kit also included anti-CD31-based angiogenesis tubule staining reagents: primary antibody (mouse anti-human CD31), secondary antibody (goat anti-mouse IgG AP conjugate), p-nitrophenol phosphate (p-NPP) tablets, Tris buffer tablets and insoluble substrate BCIP/NBT tablet were purchased from TCS cellworks Ltd.

2.1.8 Ex-vivo *vasodilation assay*

Krebs buffer was freshly made on the day of experiments, consisting of NaCl (6.8 g/L), KCl (0.4 g/L), $MgSO_4.7H_2O$ (0.14 g/L), KH_2PO_4 (0.16 g/L), $NaHCO_3$ (2.1 g/L), glucose (2.0 g/L). $CaCl_2.2H_2O$ (2.5 mM) was added to the final solution after gassing. KCl (3 M), SNP (sodium nitroprusside, 100 mM), ACh (acetylcholine, 100 mM) were prepared in distilled water, from powder stocks. U46619 (10 μM) was prepared by dilution of a stock solution (10 mM in ethanol) in water.

2.2 Instrumentation

A dual beam UV spectrophotometer was used throughout (Hitachi, U-2800A). A size exclusion chromatography (SEC) and ion-exchange chromatography (IEX) system comprised a UV detector (Jasco UV-1570) and HPLC pump (Jasco PU-980 Intelligent) and was used with Azur software. The SDS-PAGE system including tank and power supply was purchased from BDH. A pH meter (HANNA, model pH 211) was used to adjust the pH during the preparation of the buffer. An incubator from Infors (model Minitron) was used to incubate the antibody digestion mixture. A Heraeus centrifuge (model Megafuge 1.0 R) and a BIAcore X-100 from GE healthcare were used throughout. A Malvern dynamic light scattering (DLS) system (Model Zetasizer Nano-ZS) was used to measure the particle size. A pipette (Model eppendorf research) was used to measure volumes. A OHAUS balance (Model Explorer Pro) was used to weigh solids. A PURITE SELECT water purifier (Model ONDEO) used to obtain distilled water (Type 1 quality). The plate reader with 405 nm wavelength filters (Biotek; ELx 800), a class II biological safety cabinet (Heraeus), and the humidified incubator

(Heraeus; 5 % CO_2, 37 ^{0}C) were used. A microscope (Nikon, ECLIPSE FN1) with 4 and 10 times objective attached to digital camera (DXM1200F) was also used. The imaging software of LUCIA (version 4.82) for recording images and the angioSys software (TCS Cellworks Ltd., cat. no. ZHA-1800) for image analysis were used. The multichannel wire myograph (DMT, Model 620 M) connected to a LabChart data acquisition interface (ADInstruments Ltd.) was used.

2.3 Methods

2.3.1 Buffer preparation

Digestion buffer. Sodium phosphate buffer (20 mM, pH 7.4) with EDTA (2 mM) and cysteine-HCl (20 mM) was prepared as follows: To a 500 mL Fisher bottle with a magnetic stir bar was added sodium phosphate monobasic, NaH_2PO_4 (600 mg, Mw= 119.98 g/mol, 5 mmole), EDTA (186 mg, Mw = 372.24 g/mol, 0.5 mmole) and distilled water (250 mL, Type 1, 18 mΩ resistance). The solution was gently stirred until homogeneous. To this buffer (12 mL) was added cysteine-HCl (42 mg) and using a pH meter, the pH was carefully adjusted to 7.0 by the dropwise addition of sodium hydroxide (1 N). The binding buffer (1.0 M Tris buffer with EDTA, pH 8.0), elution buffer (0.1 M glycine pH 2.8) and neutralizing buffer (1.0 M Tris buffer, pH 8.5) were all purchased from Pierce.

PEGylation buffer. Sodium phosphate buffer (20 mM, pH 7.4) with EDTA (10 mM) was prepared as follows: To a 500 mL Fisher bottle with a magnetic stir bar was added sodium phosphate monobasic, NaH_2PO_4 (600 mg, Mw=119.98 g/mol, 5 moles), EDTA (931 mg Mw = 372.24 g/mol, 2.5 mmole) and distilled water (250 mL, Type 1, 18 mΩ resistance). The solution was gently stirred until homogeneous and using a pH meter, the pH was carefully adjusted to 7.4 by the dropwise addition of sodium hydroxide (1 N).

Ion exchange purification buffer. Two buffers were used; buffer A and B. Buffer A was a sodium acetate buffer (100 mM, pH 4.0) that was prepared as follows: To a 500 mL Fisher bottle with a magnetic stir bar was added sodium acetate trihydrate, C_2H_3Na $3H_2O$, (9.34 g, Mw=186.08 g/mol, 50 mmole, Sigma-Aldrich, cat. no. S7670-250G), and distilled water (500 mL, Type 1, 18 mΩ resistance). The solution was gently stirred until homogeneous and using a pH meter, the pH was carefully adjusted to 4.0 by the dropwise addition of hydrochloric acid (1 N). Buffer B was also a sodium acetate buffer (100 mM, pH 4.0) but which contained sodium chloride (1M). This buffer was prepared

as follows: To a 500 mL Fisher bottle with a magnetic stir bar was added sodium acetate trihydrate, $C_2H_3Na\ 3H_2O$, (9.34 g, Mw= 186.08 g/mol, 50 mmole) and sodium chloride (29.0 gr, Mw= 58.44 g/mol, 496 mmol), and distilled water (500 mL, Type 1, 18 mΩ resistance). The solution was gently stirred until homogeneous and using a pH meter, the pH was carefully adjusted to 4.0 by the dropwise addition of hydrochloric acid (1 N). Both buffer A and B solution were filtered using a millipore filter flask with a cellulose nitrate membrane filter (0.45 μm).

Size exclusion purification buffer. Phosphate buffered saline (PBS) contains NaCl (0.16 M), KCl (0.003M), Na_2HPO_4 (0.008M) and KH_2PO_4 (0.001M). PBS was prepared as follows: To a 250 mL Fisher bottle with a magnetic stir bar was added one tablet comprised of the aforementioned salts in the correct proportion to make a 100 mL PBS solution (cat. no. BR0014G, Oxoid) with distilled water (100 mL, Type 1, 18 mΩ resistance). The solution was gently stirred until homogeneous and using a pH meter, a value of 7.3 was measured. The PBS buffer was filtered using a millipore filter flask with a cellulose nitrate membrane filter (0.45 μm) immediately prior to use.

Buffer used in BIAcore. The HBS-ES buffer was prepared as follows: The HBS-EP buffer was purchased from GE healthcare, including HEPES (0.1 M), NaCl (1.5 M), EDTA (30 mM), surfactant P20 (0.5 % v/v), pH 7.4, and then diluted (x10) with distilled water (Type 1, 18 mΩ resistance). The HBS-EP buffer was then filtered using a millipore filter flask with a cellulose nitrate membrane filter (0.45 μm) prior to use.

Buffer used in ELISA. Three buffers were used in ELISA; sample buffer, blocking buffer, and washing buffer.

Sample buffer was prepared as follows: To a 250 mL Fisher bottle with a magnetic stir bar was added one tablet PBS (cat. no. BR0014G, Oxoid) to make a 100 mL sample buffer with distilled water (100 mL, Type 1, 18 mΩ resistance).

Blocking buffer was prepared as follows: To a 250 mL Fisher bottle with a magnetic stir bar was added one tablet PBS (cat. no. BR0014G, Oxoid) to make a 100 mL blocking solution with distilled water (100 mL, Type 1, 18 mΩ resistance), 1 % bovine serum albumin (BSA, 0.1 g) and 0.05 % Tween 20 (0.05 mL).

Washing buffer (PBST) was prepared as follows: To a 250 mL Fisher bottle with a magnetic stir bar was added one tablet PBS (cat. no. BR0014G, Oxoid) to make a 100 mL PBST buffer in distilled water (100 mL, Type 1, 18 mΩ resistance), and 0.05 % Tween 20 (0.05 mL).

2.3.2 Size exclusion chromatography (SEC)

Size exclusion chromatography (SEC) was accomplished with a Superdex 200 prep grade column mounted on a Jasco HPLC system with Azur software. The UV detection wavelength used for the analysis was 280 nm. The flow rate was 1.0 mL/min and the injection volume was varied. The run time for each sample was 100 to 110 min. The mobile phase was the filtered PBS (pH 7.3) and the loop volume was 2.0 mL.

2.3.3 Ion exchange chromatography (IEX)

Ion exchange chromatography (IEX) was performed using the SP HP (1.0 mL, 5.0 mL), SP FF (1.0 mL) and HiTrap MacroCap SP (1.0 mL) columns. The flow rate was 1.0 mL/min and loop volume was 2.0 mL. The loading volume was 1.45 mL.

The optimised linear gradient elution program that was generally used was as follows:

1- Elute buffer A (100 %) for 10 min to ensure void volume is entirely buffer A.
2- Apply a linear elution gradient starting with buffer A (100 %) and running to buffer B (100 %) over a 30 min period.
3- Elute buffer B (100 %) for 5 min to wash the column.
4- Switch to buffer A (100 %) and elute for 10 min to be prepare for next IEX run.

2.3.4 SDS-PAGE analysis

Novex bis-tris 4-12% precast gels were used for PAGE analysis. Samples were prepared with NuPAGE LDS sample buffer. The sample volume was measured with a pipette, 6.0 µl, and LDS sample buffer was 20 µl. The mixture of sample and LDS buffer were then briefly vortexed before loading onto the gel. The sample of 20 µL was loaded onto the 10 well Novex bis-tris gel and 10 µL loaded onto the 15 well Novex bis-tris gel. The running buffer was NuPAGE MOPS SDS (50 mL in 1.0 L distilled water). The voltage applied for analysis was 200 V and the run time was about 1.0 h. The prestained protein molecular weight standards were Sharp blue prestained and 5.0 µL was loaded onto the first well of each gel.

PAGE gel staining methods

2.3.4.1 InstantBlue staining

InstantBlue (is a ready-to-use proprietary Coomassie® stain) was used as follows: approximately 20 mL InstantBlue was used to stain each SDS-PAGE gel. Gels were stained for a minimum of 1 hour and in some cases when only low amounts of protein were present, overnight staining was used. Afterwards, the stained SDS-PAGE gels were de-stained using water (20 mL).

2.3.4.2 Barium iodide staining

Barium iodide staining was used to detect the presence of PEG in the SDS-PAGE gels [185]. In brief, after staining gels with InstantBlue, the gels were then incubated with barium chloride (5 %, 5.0 ml) together with perchloric acid (0.1 M, 5.0 ml) for 10 min. Afterwards an iodine solution (2.0 mL) was added drop-wise and the gel left for approximately 5 min or until the PEG had stained brown sufficiently. The gels were then de-stained using water (20.0 mL) for approximately 5 min.

2.3.4.3 Silver staining

Silver staining was performed to stain the protein in the nano-gram range using a SilverXpress kit (GE healthcare) and used as per the supplied instructions as follows; The Bis-Tris gel (1 mm) was first fixed using a fixing solution (200 mL) which comprised distilled water (90 mL), methanol (100 mL) and acetic acid (20 mL) for 10 min while shaking. The fixing solution was discarded and sensitizing solution (100 mL) which comprised distilled water (105 mL), methanol (100 mL) and sensitizer (included in SilverXpress kit, contains glutaraldehyde, 5 mL) was added onto the gel and shaken for 30 min. After 30 min, the sensitizer solution was discarded and replaced with fresh sensitizer solution (100 mL) for another 30 min while shaking continued. The gel was then washed twice, with distilled water (200 mL) for 10 min each time. Then, the staining solution (100 mL) including stainer A (included in SliverXpress kit, contains silver nitrate, 5 mL), stainer B (included in SliverXpress kit, contains ammonium hydroxide and sodium hydroxide, 5 mL) and distilled water (90 mL) were added and incubated with the gel for 15 min while shaken. After the staining step, the gel was washed twice with distilled water (200 mL) for 5 min each time. Then, the developing solution (100 mL) containing distilled water (95 mL) and developer (included in SilverXpress kit, contains formaldehyde and citric acid, 5 mL) was added and incubated

with the gel for 3 to 15 min. During this step, the brown colour was observed at protein band. The colour development was stopped before the background becomes too dark using stopper solution (included in SilverXpress kit, contains citric acid, 5 mL) for 10 min. Finally, the gel was rinsed with fresh distilled water (200 mL) for three times, each for 10 min.

2.3.5 Digestion of bevacizumab and isolation of Fab_{beva}

The digestion buffer was prepared immediately prior to use. The immobilised 50 % papain slurry (1.0 mL) was equilibrated with the digestion buffer in a centrifuge tube (15 mL) by adding digestion buffer (9.0 mL) into the gel slurry followed by centrifugation (4.0 min, 4000 x g) to separate the gel from the buffer. The buffer supernatant was discarded and this equilibration procedure was repeated. Finally, the gel was resuspended with the digestion buffer (0.4 mL). A solution of bevacizumab (12.5 mg/mL) was prepared by dilution of 0.5 mL of bevacizumab from pharmaceutical vial (25 mg/mL) with 0.5 mL digestion buffer to provide a 1.0 mL solution of 12.5 mg/mL concentration. This bevacizumab solution (12.5 mg/mL) was then added to the equilibrated papain solution and incubated at 37^0 C for 5.5 h while being gently shaken at a speed of 250 x rpm.

Different digestion times were evaluated and an optimal digestion time of 5.5 h was selected. After digestion, the solution was separated from the immobilised papain by centrifugation (4000 x g for 4.0 min). The crude digestion solution (1.4 mL) was transferred to a new tube. For maximum recovery, the immobilised papain was washed once with binding buffer (2.0 mL, Tris buffer with EDTA, pH 8.0). The wash solution was then added to the crude digestion solution to give a total sample volume of 3.4 mL. To separate the Fab from the Fc portion of the antibody, the digestion mixture was eluted over a protein A column which was equilibrated with Tris buffer at pH 8.0. A NAP protein A plus spin kit (Pierce, cat. no. 89978) containing immobilised protein A, elution buffer (0.1 M glycine, pH 2.8), and neutralization buffer (1.0 M tris buffer, pH 8.5) were used to purify the Fab fragment from the Fc fragment from the digested bevacizumab mixture solution.

The protein A column was placed in a centrifuge tube (1.0 mL) and centrifuged (1000 x g, 1.0 min) to remove the storage solution. After this, the protein A column was equilibrated with binding buffer (Tris buffer with EDTA, pH 8.0, 2.0 mL) by addition of the binding buffer (2.0 mL). The column was centrifuged (1.0 min, 1000 x g) to

remove the flow-through. This step was repeated twice. Two protein A columns were used for each digestion experiment because the maximum capacity of each protein A column was 2.0 mL and the total volume of digestion solution at this scale of 12.5 mg digestion was 3.4 mL. The bottom of the column was then capped and the digestion mixture (2.0 mL) was applied to the column. The top of the column was then tightly capped. This same method was applied to the second protein A column which had 1.4 mL of the digestion mixture. After this, the columns were incubated at ambient temperature with end-over-end mixing for 10 min. After 10 min, the columns were placed in a new centrifuge tube (15.0 ml) and the bottom cap and top cap were removed. The columns were centrifuged (1.0 min, 1000 x g) and the flow-through solutions were saved and labelled as the first fraction (F1, 3.4 mL from both columns). The columns were transferred to a new centrifuge tube (15.0 ml) and binding buffer (2.0 ml) was added to the columns to allow any further non-binding Fab to elute. Centrifugation (1.0 min, 1000 x g) was again used to separate the solution from the column. The column flow-through for this wash step was collected and labelled as the second fraction (F2, 4.0 mL from both columns). This washing step was then repeated twice. A total of 4 fractions were collected (F1-F4). The elution buffer (2.0 ml) was then added to the columns to dissociate the Fc fragment. The columns were centrifuged (1.0 min, 1000 x g) and fractions were collected (F5 to F7, each 2.0 ml). The low pH of the elution buffer (0.1 M glycine, pH 2.8) can affect the stability of the Fc fragment, so a neutralisation buffer (Tris buffer, pH 8.5, 100 μL) was added into each of the elution fractions to provide neutral pH for longer term storage.

To maintain the column during storage for re-use, the elution buffer (0.1 M glycine, 3.0 mL) was added into each column once more and the columns were centrifuged (1.0 min, 1000 x g). This was then repeated with sodium phosphate buffer (pH 7.6, 3.0 ml) to remove the elution buffer. Finally, a storage solution (0.02 % sodium azide, 3.0 ml) was added and the columns were capped and stored at 4^0C.

The Fab fragments of the F1 and F2 fractions after the protein A column were then buffer exchanged to sodium phosphate buffer (20.0 mM, pH 7.6) with EDTA (10 mM) or PBS (pH 7.4) using a PD-10 column to remove the cysteine present in the digestion buffer. The PD-10 column was first equilibrated with sodium phosphate buffer (20.0 mM, pH 7.6, 25 mL) with EDTA (10 mM). 2.5 mL of a Fab solution was loaded onto the column and discarded. Then, 3.5 mL of sodium phosphate buffer (20.0 mM, pH 7.6) with EDTA (10 mM) was eluted onto PD-10 column and collected. Three

PD-10 columns were used to buffer exchange F1 and F2. The F1 and F2 solutions after PD-10 columns and F3 and F4 were then pooled and concentrated using viva-spin (4000 x g, 10 min) in a 1.0 mL solution and considered as pure Fab_{beva}. The yield of approximate 70 % was calculated for the purified Fab_{beva} when 12.5 mg bevacizumab was digested.

2.3.6 Digestion of bevacizumab and isolation of F(ab)$_2$

To obtain $F(ab)_2$ much of the initial work focused on the use of pepsin for proteolytic digestion. However it was subsequently found that IdeS enzyme was much more effective. Bevacizumab (5.0 mg/mL, 1.0 mL) was digested using IdeS enzyme (FabRICATORE, 75 µL) at 37 ^{0}C for 30 min. The $F(ab)_2$ was purified from the enzyme and Fc fragments by SEC (Superdex 200 prep grade; UV detection at 280 nm) using a mobile phase of PBS (pH 7.3) at a flow rate of 1.0 mL/min. Injection volume was 0.96 mL and the run time was 100 min. The purified $F(ab)_2$ was then analysed by SDS-PAGE. The cleavage site of IgG by immobilised papain and IdeS enzyme is shown in Figure 2.1.

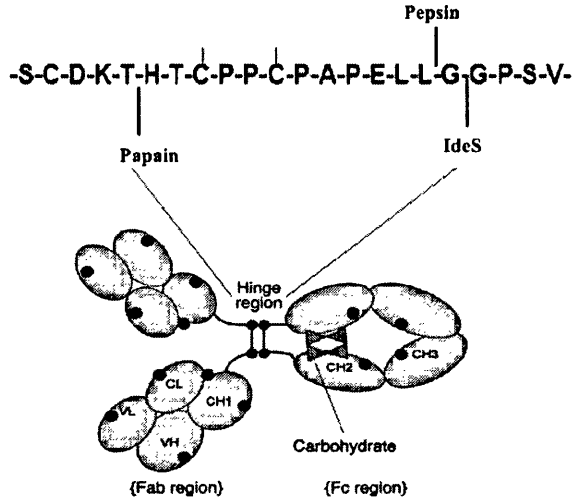

Figure 2.1 Cleavage sites of papain, pepsin and IdeS [186].

2.3.7 Digestion of trastuzumab and isolation of Fab_{trast}

The method for trastuzumab digestion was taken initially from [187] and was further modified as described here. The digestion buffer was prepared immediately prior to use. The immobilised 50 % papain slurry (1.0 mL) was equilibrated with the digestion buffer by adding the digestion buffer (9.0 mL) into the gel slurry followed by centrifugation (4.0 min, 4000 x g) to separate the gel from the buffer. The buffer was discarded and this wash procedure was repeated once more. The papain gel was then resuspended with

the digestion buffer (0.4 mL). A solution of trastuzumab (6.5 mg/mL) was prepared by dilution of 0.5 mL of trastuzumab (12.9 mg/mL) with 0.5 mL of digestion buffer. This solution of trastuzumab was then added to pre-equilibrated papain and the reaction mixture was incubated at 37^0 C for 20.0 h while being gently shaken.

The crude Fab was then purified from the digestion mixture by SEC using PBS (pH 7.3) as the mobile phase. Digestion mixture (1.95 mL) was loaded onto the SEC column with 100 min run time. The Fab_{trast} were eluted (1.0 mL/min) from the SEC (Superdex 200 prep grade size) column at 86-90 min, the Fc fragments were eluted at 82-84 min and undigested trastuzumab had a retention time of 71 min. Fab fractions were then pooled (total volume of the pooled fractions was 3.0 mL) and concentrated to a 1.0 mL solution using a vivaspin column (5 min, 4000 x g). The concentration of the purified Fab was then calculated by UV at 280 nm. A yield of 26 % was calculated for the purified Fab_{trast}.

2.3.8 Representative Fab PEGylation to produce PEG-Fab

In an eppendorf (1.5 mL) containing DTT (1.0 mg) was added a solution of Fab (1.0 mg, 1.0 mL in the PEGylation buffer) and then incubated at ambient temperature without shaking for 30 min. The final concentration of DTT was 6 mM when 1.0 mg was added into 1.0 mL Fab solution. DTT was removed by PD-10 column by first buffer exchanging into a sodium phosphate buffer (20 mM, pH 7.6) with EDTA (10 mM). A representative procedure to remove the DTT from a volume of 1.0 mL of reaction mixture using a PD-10 column was as follows: first a PD-10 column was equilibrated by allowing solutions of sodium phosphate buffer (20 mM, pH 7.6, 25 mL) with EDTA (10 mM) to elute through the column. Then, the protein solution with DTT (1.0 mL) was loaded onto the equilibrated PD-10 column, and allowed the protein solution to elute from the PD-10 column. After this, 1.5 mL sodium phosphate buffer (20 mM, pH 7.6) with EDTA (10 mM) was added to the PD-10 column and allowed to elute. Finally, the protein solution was recovered by addition of a 3.3 mL sodium phosphate buffer (20 mM, pH 7.6) with EDTA (10 mM) to the PD-10 column.

The PEG mono-sulfone **2** (3.0 mg) was dissolved into distilled water (1.0 mL) prior to PEGylation. An aliquot of the 2 equivalents PEG reagent **2** (0.26 mL, 3.0 mg/mL in distilled water, 20 kDa) was added to the solution containing the reduced Fab (3.3 mL, 0.3 mg/mL, 1 equivalent). The PEG mono-sulfone reagent **2** was added at either 1.0 or 2.0 equivalents. Different molecular weights of the PEG mono-sulfone

reagent **2** (20, 30 and 40 kDa) were used. The PEGylation solution was incubated at ambient temperature for 3.0 h without shaking. The PEG-Fabs were then purified from other non PEGylated Fab and non-conjugated PEG using a single step IEX chromatography with a SPHP column (1.0 mL, 1.0 mL/min).

2.3.9 Preparation of PEG_2-Fab'_{beva}

Into the solution of $F(ab)_2$ (1.0 mg/mL, 1.0 mL of PBS pH 7.3) was added DTT (1.0 mg) and the solution was allowed to incubate for 30 min at ambient temperature without shaking. The DTT was removed by a PD-10 column using the method described in section 2.3.8. The reduced-$F(ab)_2$ (3.3 mL, 0.3 mg/mL) was then added the 4 equivalents of PEG mono-sulfone reagent **2** (0.08 mL, 10 mg/mL, 20 kDa). The PEGylation mixtures were then purified from other PEG species by IEX chromatography using an SPHP column (1.0 mL, 1.0 mL/min).

2.3.10 PEGylation of bevacizumab

Bevacizumab (1.25 mg/mL, 1.0 mL PBS pH 7.3) was reduced using DDT (1.0 mg, 6.0 mM) over a 30 min period at ambient temperature. The excess DTT was removed using a PD-10 buffer exchange column as already described. To a solution of the reduced-bevacizumab (3.3 mL, 0.38 mg/mL) was added 4 equivalents the PEG mono-sulfone reagent **2** (0.11 mL of 3.0 mg/mL PEG solution, 10 kDa) and incubated for 3 h at ambient temperature. Different isomers of PEG-bevacizumab were observed in the PEGylation reaction mixture. Mono PEG-bevacizumab was then purified from the other multi-PEGylated isomers and PEG species by SEC and then by IEX. For SEC purification, PBS (pH 7.4) was used as a mobile phase. A run time of 100 min and flow rate of 1.0 mL/min were applied. IEX using a SPHP column (1.0 mL, 1.0 mL/min) was performed to further purify the mono PEG-bevacizumab.

2.3.11 PEGylation of trastuzumab

Trastuzumab (1.25 mg/mL, 1.0 mL solution) was also PEGylated on its interchain disulfide bonds using different equivalents (1, 2, 3 and 4) of PEG mono-sulfone reagent **2** (10 kDa). Trastuzumab solution (1.25 mg/mL, 1.0 mL in PEGylation buffer) was first treated with DTT (1.0 mg, 6 mM) and incubated for 30 min at ambient temperature. The excess DTT was then removed by the PD-10 column. Into a solution (3.3 mL, 1 equivalent, 0.38 mg/mL) of reduced trastuzumab, 4 equivalents of PEG reagent **2** (0.11

mL, 3.0 mg/mL in distilled water, 10 kDa) were added. The mono PEG-trastuzumab was then purified using SEC purification.

2.3.12 Representative Fab PEGylation to produce Fab-PEG-Fab

Fab_{beva}, Fab_{rani} and Fab_{trast} were used for homodimer PEGylation. A typical procedure for homodimer PEGylation is described as follows: Into an eppendorf containing DTT (1.0 mg), a solution of Fab (1.0 mg, 1.0 mL) in PEGylation buffer was added and then incubated at ambient temperature without shaking for 30 min. DTT was then removed by a PD-10 column by buffer exchanging into a sodium phosphate buffer (20 mM, pH 7.6) with EDTA (10 mM).

The PEG di(mono-sulfone) reagent **4** (0.06 mL, 3.0 mg/mL in distilled water, 20 kDa) was added to an aqueous solution of the reduced-Fab (3.3 mL, 0.3 mg/mL) to produce 0.5 equivalent PEG to 1.0 equivalent Fab. Different molecular weights of PEG (6, 10 and 20 kDa) were used. Different equivalents of PEG reagent **4** (0.5, 1.0, 2.0 and 5.0 equivalent PEG to 1.0 equivalent Fab) were also used. The PEGylation solution was then incubated at ambient temperature approximately 3 h without shaking. The homodimer Fab-PEG-Fab was then purified from mono PEG-Fab and unreacted Fab using IEX-SPHP (1.0 mL, 1.0 mL/min) followed by SEC.

*2.3.13 Representative Fab PEGylation to produce Fab-PEG-Fab**

To obtain the heterodimer Fab_{beva}-PEG-Fab^*_{trast} construct, stepwise PEGylation using PEG di(mono-sulfone) reagent **4** (20 kDa) was performed. Fab_{beva} (1.0 mg/mL, 1.0 mL in PEGylation buffer) was first treated with DTT (6 mM, 1.0 mg/mL) and incubated for 30 min at ambient temperature. After removal of DTT using PD-10, 5.0 equivalent of PEG di(mono-sulfone) reagent **4** (0.66 mL, 3.0 mg/mL in distilled water, 20 kDa) was added and incubated for 3.0 h at ambient temperature without shaking. Following this, the mono PEG-Fab_{beva} was purified from the Fab_{beva}-PEG_{20}-Fab_{beva} using a IEX-SPHP (1.0 mL, 1.0 mL/min) column. The IEX fractions of the mono PEG-Fab_{beva} were pooled and then concentrated to 1.0 mL solution using vivaspin (5 min, 4000 x g). To estimate an approximate concentration of this solution, UV spectroscopy was used at 280 nm. Then, in separate eppendorf tube, Fab_{trast} was treated with DTT (6 mM, 1.0 mg/mL). The excess DTT was removed after 30 min incubation by PD-10. The buffer that used for PD-10 purification was sodium phosphate (50 mM), EDTA (10 mM, pH 7.4). Into reduced-Fab_{trast} (3.3 mL), 1.0 mL IEX purified PEG-Fab_{beva} (1.0 mL in 20 mL sodium

acetate buffer pH 4.0) was added and incubated for 3.0 h at ambient temperature and then overnight at 4 ^{0}C. For purification of heterodimer Fab_{beva}-PEG-Fab^{*}_{trast}, IEX-SPHP column was first used. To further purify the heterodimer Fab-PEG-Fab* from unreacted Fabs, SEC performed on the IEX fractions.

2.3.14 Micro BCA assay for determination of protein concentration

Bicinchoninic acid (BCA) assay is a well known method for protein quantitation which is conducted in alkaline condition [76]. The peptide bonds present in a protein convert Cu^{+2} to Cu^{+} under alkaline conditions, a reaction widely known as the Biuret reaction. Cu+ forms a complex with the bicinchoninic acid to form an intense, purple coloured solution. The complex has an absorbance maximum at 562 nm. The standard BCA assay has a protein concentration sensitivity of 0.1-1.0 mg/mL and micro BCA assay has a sensitivity of 0.5-10 µg/mL. Micro BCA was used throughout this study since the isolated conjugate typically had a concentration range of 10-1000 µg/mL.

2.3.15 Ellman's assay

The reaction buffer was sodium phosphate buffer (20 mM), containing EDTA (1.0 mM) pH 8.0. To make Ellman's reagent solution, Ellman's reagent (4.0 mg) was dissolved in reaction buffer (1.0 mL). A set of cysteine standards were prepared by dissolving cysteine hydrochloride monohydrate at the 0.0, 0.25, 0.5, 0.75, 1.0, 1.25 and 1.5 mM, concentrations in reaction buffer. After this, another set of tubes were prepared which contained a mixture of Ellman's reagent solution (50 µL) and of reaction buffer (2.5 mL). Standard (cysteine known concentration (250 µL) and unknown samples (250 µL)) were added into each test tube to a mixture of Ellman's reagent and reaction buffer. The solutions were mixed and incubated for 15 min at ambient temperature. The absorbance of each solution was measured at 412 nm relative to a blank as a control. The value obtained was used for the calculation of number of free thiols using the molar extinction coefficient of TNB (14150 M^{-1} cm^{-1}). Firstly concentration of thiols in the sample solution (0.2 mL) was calculated. Then, the value was divided by the concentration of protein in the sample solution to obtain the number of thiols in the solution.

2.3.16 MALDI-TOF analysis

Mass spectrometry analysis was performed on an Applied Biosystem Voyager DE Pro. Samples were prepared by mixing with 2,5-dihydroxybenzoic acid (10 mg/mL in 50:50 acetonitrile/water + 0.1 % trifluoroacetic acid) and spotting 1.0 µL on to a MALDI

target plate. The spotted samples were analysed in linear positive mode with an accelerating voltage of 25000 V and an extraction delay time of 750 nsec. A total of 50 laser shots were accumulated and the laser was varied accordingly on a sample-to-sample basis.

2.3.17 BIAcore assay

BIAcore X-100 (BIAcore, GE healthcare LTD Amersham) was used for binding affinity studies of the purified PEGylated conjugates (analyte). A $hVEGF_{165}$ (38 kDa Mw) was immobilised on CM5 and CM3 chips whereas a CM3 chip was immobilised with an extracellular domain of recombinant human HER-2 (110 kDa Mw).

Three steps involved in chip preparation; pre-concentration, immobilisation and regeneration.

(1) Pre-concentration step or pH scouting:

To perform the pre-concentration assay, VEGF (10 µg/mL, 55 µL) was dissolved in sodium acetate (10 mM) buffer at pH (4.0, 4.5, 5.0 and 5.5, 6.0 and 6.7) and run into flow channel 2 (Fc=2). Contact time of 180 sec was applied. Sodium hydroxide (50 mM) was injected over the sensor surface to remove the VEGF and regenerate the surface. It was found that VEGF (10 µg/mL) in sodium acetate buffer (10 mM, pH 5.5) provided a better electrostatic interaction with dextran chip. A solution of HER-2 (10 µg/mL) in sodium acetate buffer (10 mM, pH 5.0) was found to show better electrostatic interaction between HER-2 and dextran chip.

(2) Immobilisation procedure:

Amine coupling chemistry performed for immobilization. Three immobilized chips were successfully prepared; two CM3 chips were immobilized with VEGF (Mw 38 kDa, 0.2 µg/mL) to provide low immobilization level (61 and 57 RU) and one CM3 chip with HER-2 (110 kDa, 0.2 µg/mL) to provide immobilization level of 51 RU. To immobilise the chip, the first thing was to dock the CM3 chip inside the BIAcore and start manual run on flow channel 2 (Fc=2) with 5 µl/min flow rate. Using manual run, allow controlling the activation time and also ligand contact time. The protocol used to immobilise CM3 with 61 and 57 RU immobilisation level is as follows:

1. Wash the chip with NaOH (50 mM) for 60 sec.
2. Activate the surface by injection of reagent (NHS (300 µl) / EDC (300 µl)) for 200 sec.
3. Allow the HBS-ES buffer to run over the chip surface for 200 sec.
4. Inject the VEGF solution (1.0 µL of 0.1 mg/mL into 500 µL sodium acetate buffer pH 5.5 to make 0.2 µg/mL solution) for 140 sec to achieve 57 RU and 200 sec to achieve 61 RU immobilisation level.
5. Inject ethanolamine-HCl (126 µl, 1.0 M) to deactivate remaining active group on the surface and remove non-covalent bound ligand for 180 sec.

(3) Regeneration step:

After ligand immobilization, the analyte was injected over the prepared surface to test the chip. To regenerate the chip for next experiment and remove bound analyte, regeneration buffer was used. Different regeneration buffers were applied (10 mM glycine–HCl pH 2.5, pH 2.0 and if necessary pH 1.5) for 1200 sec. Because harsh regeneration buffer can damage the ligand on the chip, 10 mM glycine–HCl buffer with higher pH tested first. It was found that using a glycine–HCl (10 mM, pH 2.0) the baseline was achieved. The glycine–HCl (10 mM pH 2.0) was also used for regeneration buffer of the chip prepared with HER2.

All of the test compounds were prepared in the HBS-EP running buffer (10 mM HEPES, pH 7.4, 150 mm NaCl, 3.0 mM EDTA, 0.005% surfactant P20) before run into the BIAcore. All kinetic measurements were conducted at 25 ^{0}C at a flow rate of 30 µL/min with an association time of 180 sec and dissociation constant rate of 1200 sec. Double-referencing was performed to account for bulk effects caused by changes in the buffer composition or nonspecific binding [188]. Data were evaluated with BIAevaluation software (version 2.1) and the best fit (lowest Chi^2) was obtained using a 1:1 binding model. The sensogram was fitted globally over the association and dissociation phases. Equilibrium dissociation constants (affinity) were calculated from the rate constants ($K_D = k_{off}/k_{on}$). The kinetic assay was performed 4 times for bevacizumab and Fab_{beva}, and 3 times for $F(ab)_2$, 2 times for trastuzumab and once for other constructs (PEG-Fab_{beva}, Fab_{beva}-PEG_{20}-Fab_{beva}, Fab_{trast}, PEG-Fab_{trast}, Fab_{trast}-PEG_{20}-Fab_{trast}). Therefore, it was not possible to calculate standard deviation for the affinity value of the constructs that the BIAcore performed less than 3 times. However, standard error (SE) was calculated by software for each kinetic rate constant (k_a and k_d)

which suggested the significant of the value.

2.3.18 ELISA assay

The ELISA plate was coated with $VEGF_{165}$ (0.1 μg/mL, 100 μL from 1.0 μg/mL solution) and for the molecules derived from trastuzumab; the plate was coated with HER-2 (0.25 μg/mL, 100 μL from 2.5 μg/mL solution). A typical ELISA procedure when VEGF was coated on the plate is as follow: The $VEGF_{165}$ (0.1 μg/mL) was coated in each well of a 96 well plates for overnight incubation at 4 ^{0}C. The next day, the VEGF solutions were removed and without washing, blocking buffer (300 μL, PBS tablet + 1 % B.S.A + 0.05 % Tween20 buffer) was added into each well and incubated at ambient temperature for 2.0 h. After this, the blocking buffers were removed and plate was washed with washing buffer (PBST, 300 μL, PBS tablet + 0.05% Tween20) once and then test compounds, which were prepared in PBS at a range of concentrations, were added into each well. The plate was incubated for 2.0 h at ambient temperature. After 2.0 h incubation, the protein solutions were removed and wells washed with washing buffer (PBST, 300 μL) three times. Then, anti-human IgG (Fab specific)-peroxidase (100 μL, 1/5000 dilution, cat. no. A0293 from Sigma Aldrich) was added into each well and incubated for 1.0 h at ambient temperature. The solutions were then removed and plate was washed off with washing buffer (PBST, 300 μL) for three times. TMB (100 μL) was then added and development of the blue colour was monitored. After approximately 5 min, when the blue colour was visible enough for each well, HCl (50 μL, 1.0 M) solution was added to produce a constant yellow colour. The plate was then read using a plate reader at 450 nm wavelengths. Similar procedures were applied to determine the affinity value of the molecules derived from trastuzumab. The 96 well plate was coated with HER-2 (2.5 μg/mL, 100 μL) overnight at 4 ^{0}C. In the following days, the same protocol as described for VEGF was performed.

2.3.19 In-vitro angiogenesis using AngioKit

On the day that the Angiokit was received (day 1), test compounds were sterilised by passage through a 0.22 μm filter before being diluted to their final required concentration in optimised growth medium, which was then allowed to equilibrate in a humidified incubator (37°C, 5% CO_2) The growth medium of the Angiokit plate was then gently replaced from the side of the well with the growth medium (0.5 mL per well) containing the test compounds, using a plastic pipette. The plate was then placed

in the incubator.

On days 4, 7 and 9 the plate was examined for cell morphology and signs of growth using an inverted microscope and the growth medium was replaced with freshly prepared medium containing the test compounds. On day 10, cells in the plate were fixed and stained to assess tubule development and angiogenesis.

2.3.19.1 Fixing and staining procedure:

For culture fixation, two buffers were prepared and kept at room temperature; wash buffer (PBS) and blocking buffer which consisted of wash buffer supplemented with 1% BSA. To fix the cells, the medium was removed very carefully and then cells were rinsed with the wash buffer (0.5 mL). Then, ice-cold fixative solution (70% ethanol; 0.5 mL) was added to each well and incubated at room temperature for 30 min. Then, the fixative solutions were removed and each well was washed with blocking buffer (0.5 mL) three times. After the final wash, the blocking buffer was removed and primary antibody solution was added to each well.

2.3.19.2 Staining for CD31 (PECAM-1):

The primary antibody (mouse anti-human CD31) was diluted first in the blocking buffer (1:400, 35 µL of antibody in 14 mL of blocking buffer and 0.5 mL was added to each well and incubated for 60 min at 37 ^{0}C. Following this period, the primary antibody was removed and wells were washed three times with blocking buffer (0.5 mL) for 5 minutes per wash. The secondary antibody (goat anti-mouse IgG, conjugated to alkaline phosphatise (AP)) was added to each well (1:500 dilution; 0.5 mL). The plate was again incubated for 60 min at 37 ^{0}C. Then, the secondary antibody was removed and wells were washed three times with distilled water.

2.3.19.3 ELISA readout

To assess the extent of endothelial cell proliferation by ELISA, the soluble AP substrate p-nitrophenol phosphate (p-NPP) was used. One p-NPP tablet and one Tris buffer tablet were dissolved in 20 mL distilled water and 0.3 mL was added to each well. The plate was incubated at 37 ^{0}C for exactly 20 minutes, after which, two aliquots (100 µL) were removed from each well of the Angiokit plate and transferred to separate wells of a 96 well plate, which already contained 25 µL NaOH (3 M) per well. Two blank control wells on the 96 well plate received substrate that had not been in contact with cells, to provide a background absorbance. The 96 well plate was then read at 405 nm

wavelength. The Angiokit plate was then fully washed three times with distilled water (0.5 mL) for three times before further use.

2.3.19.4 Tubular staining

To permanently stain the tubules, the insoluble AP substrate 5-bromo-4-chloro-3-indolylphosphate/nitroblue-tetrazolium salt (BCIP/NBT) was used. Two BCIP/NBT tablets were dissolved in distilled water (20 mL) and passed through a 0.22 μm filter. 0.5 mL was added to each well and the plate was incubated at ambient temperature until dark purple colour developed in positive control wells (approximately 3 to 10 min). After this, each well was washed carefully three times with distilled water (0.5 mL). The plate was then left to air dry. Photomicrographs were then taken from each well using an upright microscope with 4 times objective attached to a digital camera. The images were later analysed using Angiosys software to calculate the number of junctions and tubules formed in each well.

2.3.20 Ex-vivo vasodilation assay

Male Wistar rats (200-250g) were purchased and housed in the School of Pharmacy animal care facility. The temperature, humidity and dark:light cycles (12:12) were carefully controlled at all times. All procedures involving animals, in terms of housing and killing, were carried out in accordance with the Home Office animal care guidelines and the Animals (Scientific Procedures) Act of 1986. Rats were killed by CO_2 asphyxiation, using an airtight chamber connected to a CO_2 cylinder. Rats inhaled CO_2 for approximately 10 minutes while CO_2 concentration was elevating inside the chamber. A midline incision was made to the abdomen and a loop of ileum, with supplying vasculature intact, was removed into cold Krebs buffer. Then, the third branch of the superior mesenteric artery was isolated and cleaned of all fat and connective tissue under light microscopy by micro-dissection. 2 mm sections of this artery were then mounted onto the myograph. A four channel wire myograph was used. For mounting, a wire (approximately 2.5 cm in length) was cut and then attached to one jaw of the myograph. Two wires were required for mounting the vessel. The first wire was attached to the force transducer jaw from one end and then tightened around the first screw. The vessel was then transferred from a Petri dish and mounted onto the wire. After this, the vessel was moved along the wire and positioned between the jaws. Once the vessel was correctly situated, the loose end of the wire was then secured

around the second jaw screw. The second wire was passed through the lumen of the vessel carefully and then secured around the screws on the micrometer jaw at both ends, (Figure 2.2). The wire connected to the transducer in Figure 2.2 was to measure force development while the second wire attached to the micrometer was to allow initial vessel diameter to be manually set.

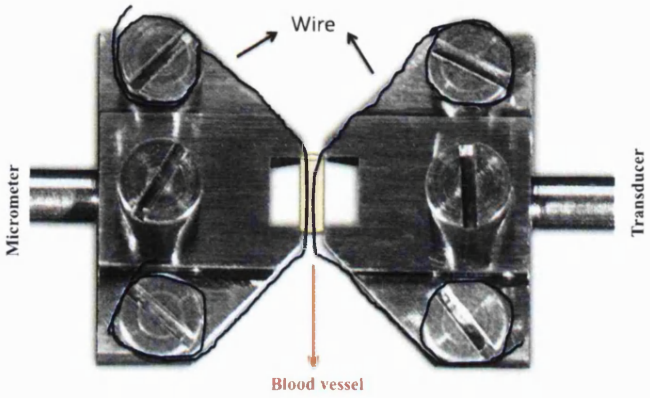

Figure 2.2 Schematic representation of a blood vessel mounted onto a wire myograph.

Once the vessels were mounted onto the myograph, they were maintained in individual chambers containing oxygenated (95% O_2/5% CO_2) Krebs buffer (5 mL) at 37 ^{0}C. When all four chambers were equilibrated, normalisation was performed. This step was performed to stretch the blood vessels to a specific normalised internal circumference (IC1). This is defined as a set fraction of the internal circumference (IC_{100}) that a fully relaxed artery would have had at a specific transmural pressure (e.g 100 mmHg for systemic arteries, as in this case). For normalisation, the vessels are stretched manually in a stepwise manner by changing the distance between the two wires inside the vessel (using the micrometer), and measurement of the force generated. These data are converted into values of IC (μm) and wall tension T (mN/mm) by an integrated module (NORM) within the LabChart software. According to LaPlace's law which describes the relationship between the transmural pressure difference and wall tension, radius and thickness, the vessel wall tension is proportional to intraluminal pressure. High transmural pressure results in more wall tension, however, thicker wall results in less tension. The exponential curve is plotted for wall tension generated against internal circumference applied, Figure 2.3. By then overlaying the isobar line corresponding to 100 mmHg, the IC_{100} can be calculated from the point of intersection using the Laplace relationship shown in Figure 2.3. IC_{100} is the internal diameter of the vessels which would have had *in-vivo* under basal conditions and a transmural pressure

of 100 mmHg [189]. The IC1 is then calculated by multiplying the IC_{100} x 0.9 for rat arteries by convention, and whereby the sensitivity of the vessels to agonist is maximal.

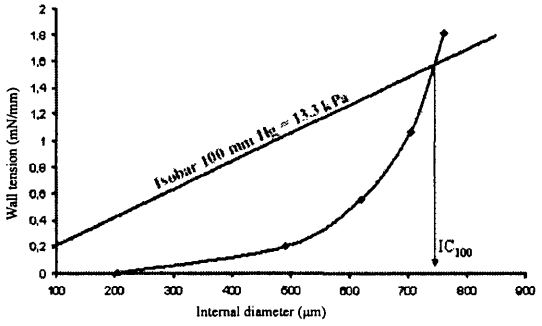

Figure 2.3 The exponential curve fitting and determination of IC100

After the vessels had been set to the calculated IC1 and allowed to equilibrate, KCl (120 mM) was added to each chamber to obtain a large contraction of the arteries due to full membrane depolarization. The KCl response was determined as a reference and to confirm tissue viability. Then, the vessels were washed three times (5 mL) and then maintained in Krebs buffer (5 mL). The vessel tone was monitored until it returned to a steady baseline. Then, the thromboxane A2 mimetic and vasoconstrictor agent U46619 (10-30 nM) was added into each chamber and vessel tone was monitored. When a stable 10-20 % of KCl tone was achieved for each vessel segment, the vasodilator agent (VEGF) with or without pre-incubation with bevacizumab was added in cumulatively increasing concentration. The anti-VEGF agents were mixed with the VEGF prior to addition and incubated for 2 hour at 37 ^{0}C. The experiment was then ended by addition of ACh (10 μM) and SNP (100 μM) in sequence. ACh is a muscarinic and nicotinic receptor agonist and induces endothelium-dependent vasodilation via muscarinic receptors through nitric oxide generation. SNP is spontaneous nitric oxide donor, which works directly on the smooth muscle and causes dilation of blood vessels. At this high concentration, the response to SNP can be assumed to be the maximum relaxation of a vessel that can be mediated through the NO pathway. At the end of experiment, the blood vessels were washed and removed from the wire.

2.3.20.1 Data analysis

The LabChart (version 8) program was used for collection of data and later off-line analysis. The relaxation responses for each vessel were calculated by subtracting the

active tone remaining after vasodilator treatment from the initial active tone induced by the pressor agent (U46619), then dividing the result by the active tone due to U46619 minus the active tone remaining after the addition of SNP. This relaxation was expressed as a percentage and was then plotted against log [VEGF] as a log-dose response curve, using Prism software.

Chapter 3: Preparation of PEGylated Antibody Fragments

3 Chapter 3: Preparation of PEGylated Antibody Fragments

Bis-alkylation PEG sulfone reagents **2** and **4** were utilised to prepare a small family of PEG-Fab and Fab-PEG-Fab products to determine their structure property correlations. It was necessary to source therapeutically relevant Fabs. To accomplish this, clinically used antibodies were obtained and then proteolytically digested to obtain the Fabs. Optimisation of the digestion process was first necessary. Once the Fabs were obtained and their purification confirmed, small-scale PEGylation reaction were conducted to learn the PEGylation process and to optimise conditions for the PEGylation reaction. Larger scale PEGylations were then conducted to isolate suitable amounts of the PEGylated products. It was necessary to ensure that the PEGylated products were completely pure without any contamination of the starting Fab. Once pure PEGylated products were obtained, it was necessary to evaluate their stability to ensure that no de-PEGylation occurred. Once purity and stability were confirmed, it then became possible to evaluate the binding properties of the PEGylated products. The key for the evaluation of any PEGylated protein is to ensure that it is not contaminated by the starting protein and that the conjugate is stable so that characterisation reflects the properties of the conjugate only.

3.1 PEGylation of Fabs to produce PEG-Fab conjugates

The PEGylation reagents used were PEG bis-sulfone reagent **1** and PEG mono-sulfone reagent **2** (Scheme 1.1). Since Fabs have one interchain disulfide bond between the light and heavy chain, it was thought that this disulfide bond could be selectively opened to provide two free sulfhydryl groups for conjugation to the PEG mono-sulfone reagent **2** so the resulting three-carbon bridge PEGylated Fab (Figure 3.1) could then be produced.

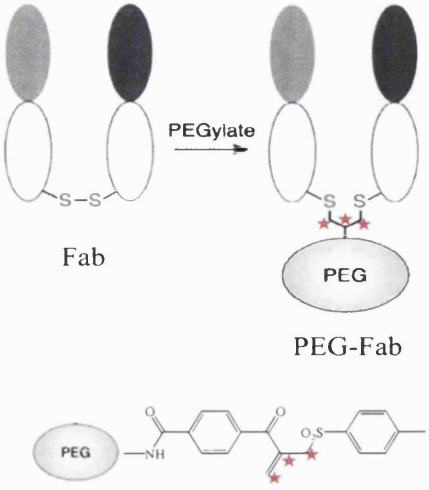

PEG mono-sulfone reagent **2**

Figure 3.1 The disulfide bridging PEGylation of the Fab.

The PEG bis-sulfone reagent **1** must undergo elimination of one equivalent of toluene sulfinic carboxylate to give the PEG mono-sulfone **2** (Scheme 1.1). Elimination is necessary to generate the α,β-unsaturated double bond so that the conjugation reaction can occur. The PEG mono-sulfone reagent **2** is reactive towards nucleophiles because of the conjugated double bond that is present. The PEG mono-sulfone reagent **2** is thus susceptible to hydrolysis. The PEG mono-sulfone reagent **2** is considered the 'active form' of the PEG bis-sulfone reagent **1** and it is the form of the reagent that undergoes the first alkylation in the reaction pathway.

Formation of the PEG mono-sulfone reagent **2** can be accomplished in both organic [125] and aqueous [137] solutions. While using a dry organic solvent is certainly a good approach as a means to isolate the activated reagent by minimising the risk for hydrolysis of the mono-sulfone, we still typically used an entirely aqueous system to activate the reagent. This allowed simple lyophilisation to be used to isolate the activated reagent without need to worry about residual organic solvent residues.

The activation of the PEG bis-sulfone reagent **1** can be performed *in-situ* with sodium phosphate buffer (20 mM, pH 7.8) in the presence of the reduced-protein [138]. Since it was anticipated that the free thiols from reduction of Fab disulfide would be quite reactive, little work was done to optimise the *in-situ* activation PEGylation. Instead the PEG mono-sulfone reagent **2** was generally used as a preformed reagent. One method was to dissolve the PEG bis-sulfone reagent **1** overnight in sodium phosphate buffer (20 mM, pH 7.8) at 37 ^{0}C in the presence of hydroquinone prior to its addition to the reduced protein [138]. Hydroquinone behaves as radical inhibitor and

was added to prevent competitive polymerisation of the conjugated double bond and thiol derived transfer reaction in the PEG mono-sulfone reagent **2**. The limitation for this approach is that exposure of the PEG mono-sulfone **2** to an aqueous environment during the incubation period increases the propensity for the addition of water to the double bond, leading to hydrolysis of the reagent. This would cause the reagent to be susceptible to mono-thiol conjugation only, essentially consuming the reagent because under the conditions of the protein conjugation reaction, it was not expected that thiolate would be able to displace the hydroxide. Another way to produce the PEG mono-sulfone reagent **2** was from activation of the PEG bis-sulfone **1** in a basic environment and then lyophilisation to a solid form. This allowed the practical formation of the PEG mono-sulfone reagent **2** in aqueous solution with high purity (approximately 90 %, H-NMR in Appendix I, A). The PEG mono-sulfone reagent **2** was stored at -20 ^{0}C as a solid.

At the time of PEGylation, the PEG mono-sulfone reagent **2** was dissolved in freshly distilled water and then this solution was added to a solution of the reduced-Fab. The activated PEG mono-sulfone reagent **2** was used to PEGylate the Fab fragment throughout this project. It was found in early experiments that this PEG mono-sulfone reagent **2** gave higher PEGylation conversion (>%90) compared to that observed from the activation of PEG bis-sulfone reagent **1** in sodium phosphate buffer (pH 7.8) for overnight. Different molecular weights of PEG mono-sulfone reagent **2** ranging from 10-40 kDa were used to PEGylate a Fab to compare the structure-properties of the different sizes of the PEG-Fabs.

To compare PEG-Fab analogues with the corresponding full antibody, it was necessary to obtain the purified Fab by the enzymatic digestion of the full antibody. Proteolytic digestion is a well-known method for cleaving full antibodies into their Fab and Fc portions [190, 191]. Proteolytic antibody digestion was originally developed to study the structure of different antibody fragments [32, 190]. An enzyme such as papain was found to produce the Fab fragment from IgG1 antibody [191]. Other enzymes, such as pepsin, were found to cleave the hinge region differently so that $F(ab)_2$ and Fab′ could be obtained [192]. However, not all the fragments obtained by enzymatic digestion retain their antigen binding [192]. It was reported that antigen binding properties of antibody fragments obtained from full antibody by enzymatic digestion was lost [192] probably due to unfolding and denaturation during incubation with enzyme. It was a key that the Fab fragments from bevacizumab and trastuzumab would

retain their antigen binding after proteolytic digestion.

Ranibizumab is a clinically used Fab and it is essentially the Fab of bevacizumab. There are few numbers of amino acid substitutions within the CDR region of ranibizumab compared to bevacizumab [58, 193]. Ranibizumab has a better binding affinity to $VEGF_{165}$ compared to the Fab_{beva} [58, 193]. This Fab was also PEGylated in this work and used as a model to compare with the PEGylated Fab_{beva}.

Once these Fabs were PEGylated and the PEG-Fab products were produced, it was thought that the PEG di(mono-sulfone) reagent **4** could be used to make homodimer PEG Fabs (i.e. Fab-PEG-Fab). The homodimer Fab-PEG-Fab constructs were then produced from the Fab_{beva}, Fab_{rani} and Fab_{trast} using the PEG reagent **4** at 6, 10 and 20 kDa molecular weights. The challenges involved with the homodimer Fab PEGylation are further discussed in section 3.2 of this chapter.

The following nomenclature was used to identify the different Fabs and their PEGylated products: Fab_{beva}, Fab_{trast} and Fab_{rani} denote the Fabs from bevacizumab, trastuzumab and ranibizumab respectively. The PEGylated variants are correspondingly denoted: PEG-Fab_{beva}, PEG-Fab_{trast} and PEG-Fab_{rani}. Since different molecular weights of the PEG mono-sulfone reagents **2** were used, this information will be conveyed using this nomenclature as follows with the example of a 20 kDa PEG reagent: PEG_{20}-Fab_{beva}, PEG_{20}-Fab_{trast} and PEG_{20}-Fab_{rani}. Analogously the nomenclature for dimeric conjugates derived from the PEG di(mono-sulfone) reagent **4** will be as follows using Fab_{beva} and 20 kDa PEG as an example: Fab_{beva}-PEG_{20}-Fab_{beva}.

3.1.1 Preparation of PEG-Fab_{beva}

Bevacizumab is supplied as a solution in a vial for use in oncology clinics. Each vial contains 16 mL of bevacizumab solution at a concentration of 25 mg/mL in antibody. Bevacizumab is formulated with sodium phosphate buffer (pH 6.6, 51 mM), α,α trehalose dehydrate (60 mg/mL) and polysorbate20 (0.04 %). Initially bevacizumab was obtained from vials that had been used in the clinic. There was after un-used solution that still remained in the vial after the patient was treated. This allowed initial digestion experiments to be conducted on a small scale (2.5 mg) of bevacizumab using immobilise papain. We were eventually able to purchase a vial of bevacizumab and this allowed us to conduct the digestion on a larger scale of about 12.5 mg of bevacizumab. Digestion conditions were then optimised at this larger scale of 12.5 mg of

bevacizumab.

Proteolytic digestion of IgG is traditionally conducted with papain which generates two separate monovalent Fabs and an intact Fc fragment by cleavage of a peptide bond above the hinge region [192, 194, 195]. Papain has a molecular weight of 23 kDa and was originally isolated from crude papaya (carica papaya) latex obtained from the unripe papaya fruit [194]. Papain is immobilised onto beaded agarose resin and is used as a slurry. This aids purification because after digestion the only protein species in solution are those derived from the antibody. The resin-linked papain is easily removed by filtration.

Papain is thiol-endopeptidase with 212 amino acids that stabilised with three disulfide bonds [195]. It has a sulphydryl group in the active site, which must be in the reduced form for papain to be proteolytically activated. Therefore, cysteine-HCl was added to the papain preparation to cause the activation of the enzyme. The phosphate buffer used for papain digestion also contains 20 mM cysteine hydrochloride with EDTA. EDTA was used to chelate with metals such as copper that can catalyse reoxidation of the papain. The pH of the digestion buffer was adjusted to 7.0 since the optimal pH for the enzymatic activity of papain about this value at 37 ^{0}C [192, 195].

It was necessary to optimise the digestion conditions to ensure the antibody would be completely digested to produce the Fab and Fc fragments while ensuring the binding sites of the Fab were not damaged [196]. Different monoclonal antibodies behave differently during enzymatic digestion, so the digestion protocol should be optimised for each antibody. To optimise the digestion of bevacizumab using immobilised papain, a solution of 12.5 mg/mL (1.0 mL) of bevacizumab was prepared by diluting a 0.5 mL aliquot of pharmaceutical grade bevacizumab with 1.0 mL digestion buffer. This solution was then transferred to a vial containing pre-incubated immobilised papain. Immobilised papain was first incubated with digestion buffer so that it could be activated by the cysteine hydrochloride in digestion buffer.

The bevacizumab digestion solution was gently shaken and incubated at 37 ^{0}C. Different amounts of immobilised papain 0.4, 0.6 and 1.0 mL were examined for an incubation period of 5.5 h. It was found that 1.0 mL of immobilised papain produced more intact Fab_{beva} (Figure 3.2, Lane 2). Digestion time was then optimised using 1.0 mL immobilise papain using 4.0, 4.5, 5.5, 6.0, and 8.0 hours. Bevacizumab was found to be completely digested after 8.0 h digestion time (Figure 3.2, Lane 3). Using SDS-PAGE it was clear that the interchain disulfide had undergone reduction to give the

dissociated heavy and light chain fragments when digestion was conducted for 8 h. Using a shorter digestion time (4.0-4.5 h), more bevacizumab remained undigested compared to the 5.5 and 6 h digestion time. When the digestion time of 5.5 h was used, bevacizumab appeared to be fully digested and produced more intact Fab (Figure 3.2, Lane 2). It is possible that using 8.0 h digestion time, the Fab would remain associated in solution and could be reoxidised, but it was decided to use the shorter digestion time as it was hoped this would provide a higher yield of the intact Fab and functionally active.

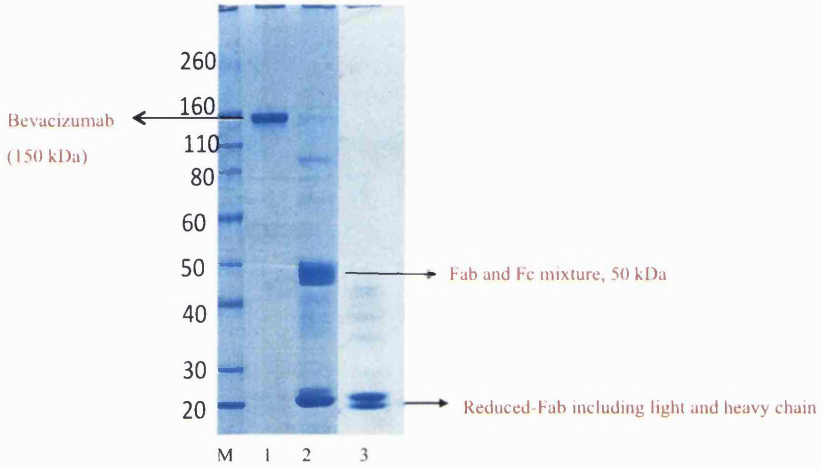

Figure 3.2 SDS-PAGE gel of digestion of bevacizumab, Novex Bis-Tris 4-12% gel stained with colloidal blue (Lanes M-3). *Lane M:* Protein standard marker, *Lane 1:* Bevacizumab, *Lane 2:* Bevacizumab digestion mixture after 5.5 h digestion time with 1.0 mL papain. *Lane 3:* Bevacizumab digestion mixture after 8.0 h digestion time and 1.0 mL papain.

The digestion mixture purified by passing it over an immobilised protein A column. Protein A, G and L are different bacterial proteins that bind with high specificity to mammalian immunoglobulin [190]. Immobilised forms of these proteins are used to purify antibodies from serum or hybridoma culture supernatant samples. Depending on the IgG, different type of these immobilised proteins are preferred. Protein A binds human and rabbit IgG specifically. In contrast, protein G has better binding capacity for a range of mouse IgG. Protein L binds to certain immunoglobulin kappa light chains [190].

Protein A was initially discovered during studies of the bacterial cell wall of *staphylococcus aureus* [197, 198]. Later, protein A was purified and isolated from other proteins present in the cell wall. Forsgren was the first to show the actual binding site of antibodies to the protein A was located in the Fc region of the antibody [197]. Protein A has four high-affinity (K_a = 108/mole) binding sites; however, only two of them are used at a time. The second and third constant regions (Fc) of the IgG heavy-chains, bind to protein A. This means that there are at least two binding sites on any antibody molecule for protein A. Binding occurs by hydrophobic interactions [190]. Optimal binding occurs at pH 8.0, although binding is also good at neutral or physiological conditions [199]. The Fc fragment can then be dissociated from protein A using pH 2.8 where the protein-protein interactions can be disrupted to release the Fc. In this way it is possible to purify a Fab obtained by the proteolytic digestion of an antibody. Protein A is expressed in *E. coli* with a mass of 42 kDa and then covalently immobilised onto cross linking beaded agarose resin column with high density. The digestion mixture is eluted over the column. The Fab eludes while the Fc binds to the protein A. Once the Fab is completely eluded, then the Fc can be isolated by changing the pH of the eluding media. The advantages of using an immobilised protein A column are: (i) fast separation and (ii) higher yield of the Fab after separation.

Figure 3.3 shows the fractions obtained by passing the digestion mixture over a protein A column. Once the Fab has eluted, the Fc can be dissociated from the column by using what is termed the "elution buffer". The elution buffer (1.5 M glycine, pH 2.8) is an effective buffer to disrupt the interaction between the bound Fc and protein A.

In Figure 3.3, Lanes 1-4 show the Fab fragment (50 kDa), which was eluted through the protein A column. The first fraction (F1) contained the majority of the Fab and was essentially a first solution that was recovered from the column after adding the digestion mixture in its buffer (2.0 mL, pH 7.0) to the protein A column. More Fab fragment was eluted from the column when the binding buffer (2.0 ml, tris buffer, pH 8.0) was applied. This step was repeated for three more times and the collected fractions were labelled F1-F4.

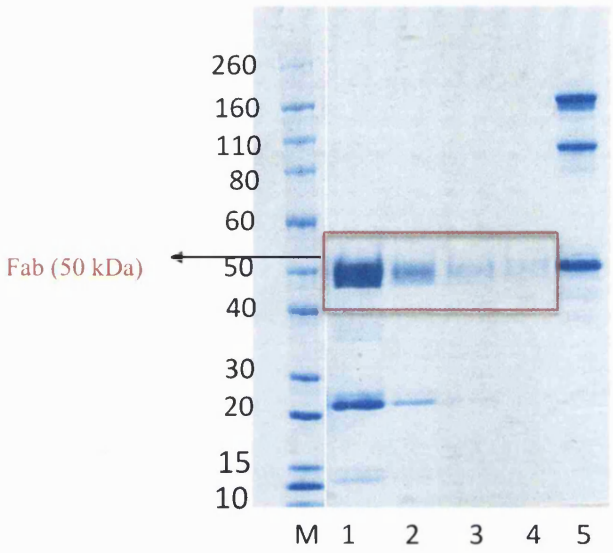

Figure 3.3 SDS-PAGE gel of purification of digestion mixture by protein A column, Novex Bis-Tris 4-12% gel stained with colloidal blue (Lanes M-5) for the five fractions that were isolated. *Lane M:* Protein standard marker, *Lanes 1-4:* The first to forth fractions after protein A columns (Fabs). *Lane 5:* Vivaspin concentrated of fifth to seventh fraction (Fc and undigested antibody).

The Fc fragment and undigested IgG were eluted from the column when the elution buffer (2.0 ml) was applied. Three fractions containing the Fc (labelled F5-F7) were pooled and concentrated using a vivaspin column (4 min, 4000 x g) (Figure 3.3, Lane 5). Since cysteine was used during the digestion, some of the Fab interchain disulfide was reduced. This resulted in some degree of heavy and light dissociation as observed by SDS-PAGE to give a band at 25 kDa. The reason for the dissociation of the light and heavy chain at the 25 kDa band (Figure 3.3, Lane 1) was due to presence of sodium dodecyl sulphate (SDS) used for sample preparation prior to loading into the gel. SDS is an anionic surfactant and can break the hydrophobic interactions between the light and heavy chains in the Fab [200].

A vivaspin column is a centrifugal concentrator column with a polycarbonate filter on its membrane. Using vivaspin (6 mL) with 10 kDa molecular weigh cut off, it can be possible to concentrate the Fab or Fc solution with more than 90 % recovery [201]. The vivaspin process can be performed using either a swing bucket (4000 x g) or fixed angle (10000 x g) centrifuge. The centrifuge time depends on the volume of solution desired and could be between 1 to 30 min. In a single step, the protein solution can be concentrated up to 100 fold using vivaspin [201]. The vivaspin membrane is

designed to be in vertical position, which helps to concentrate the solution very fast. The vivaspin column was used throughout this work as a tool to concentrate protein solutions with a molecular weight above 10 kDa. The solution remaining above the vivaspin membrane was the concentrated protein. The solution in the bottom of vivaspin was also recovered and the protein concentration was measured by UV spectroscopy to evaluate the recovery of the protein solution after vivaspin

Cysteine that was present in the digestion buffer was eluted from the protein A column in the fractions containing Fab and could interfere with readout in UV spectroscopy to estimate protein concentration (Table 3.2). Therefore further purification was thought necessary to remove cysteine from the fractions by using a PD-10 column prior to determining the concentration of the Fab (Table 3.2).

PD-10 columns are disposable columns pre-packed with Sephadex G-25 DNA grade resin. PD-10 columns are used by allowing elution to occur by gravity over the resin which separates molecules by size. This is known as size exclusion chromatography (SEC). Molecules larger than the largest pores in the matrix are eluted first. PD-10 columns are routinely used for desalting and to exchange buffer. The PD-10 column that was used is suitable for a protein solution with a volume in the range of 1.0-2.5 mL.

The protein concentration for each fraction after protein A and PD-10 column purification was obtained by measuring the UV absorbance at 280 nm. Many proteins absorb ultraviolet radiation with an absorbance maxima at 200 and 280 nm [202, 203]. Amino acids with aromatic rings (tryptophan, tyrosine and phenylalanine) and disulfide bonds in proteins structures are the main sources for the absorbance at 280 nm [202-204]. Protein concentration was calculated based on Beers Law and the accepted value often used for the extinction coefficient of human IgG. IgG with concentration of 1.0 mg/mL displays an approximate absorbance of 1.30 at 280 nm with an extinction coefficient (210,000 M^{-1}. cm^{-1}) and the Fab fragment with concentration of 1.0 mg/mL has an absorbance of approximate 1.40 at 280 nm with the extinction coefficient of 216,000 M^{-1}. cm^{-1} [205-209]. It has been suggested the absorbance of 1.35 at 280 nm is appropriate to be used for 1.0 mg/mL human IgG1 [210]. For the work present here, an absorbance of 1.40 at 280 nm was used for 1.0 mg/mL Fabs. This value was tested with a solution of 1.0 mg/mL of Fab_{rani} that was prepared from the vial used in the clinic. In this case Fab_{rani} was a solution (10 mg/mL) in a pharmaceutical formulation. Fab_{rani} displayed an absorbance of 1.4 at 280 nm. The excipients were not removed prior to UV

measurement as there was concern that Fab_{rani} would aggregate if the excipients had been removed. Ranibizumab is formulated with 10 mM histidine HCl, 10% α, α-trehalose dihydrate, 0.01% polysorbate 20. The calibration curve made with bevacizumab (in its excipients) and Fab_{rani} displayed an approximate similar absorbance value when the same concentration of bevacizumab and Fab_{rani} were evaluated (Figure 3.4, Table 3.1). This result suggested that presence of histidine in excipients of Fab_{rani} did not make a difference in absorbance of Fab_{rani} compared to bevacizumab that contains no histidine in its excipients. While it was expected to observe a non-linear calibration curve for absorbance above 1 unit, the r^2 of 0.99 and 0.98 were measured for the calibration curves for bevacizumab and Fab_{rani} respectively.

Table 3.1 The average absorbance at 280 nm for bevacizumab and Fab_{rani}. Average was taken from two measurments.

Concentration (mg/mL)	Absorbance at 280 nm Bevacizumab	Absorbance at 280 nm Fab_{rani}
0.078	0.116	0.102
0.150	0.249	0.266
0.312	0.495	0.523
0.625	0.929	0.992
1.25	1.625	1.650

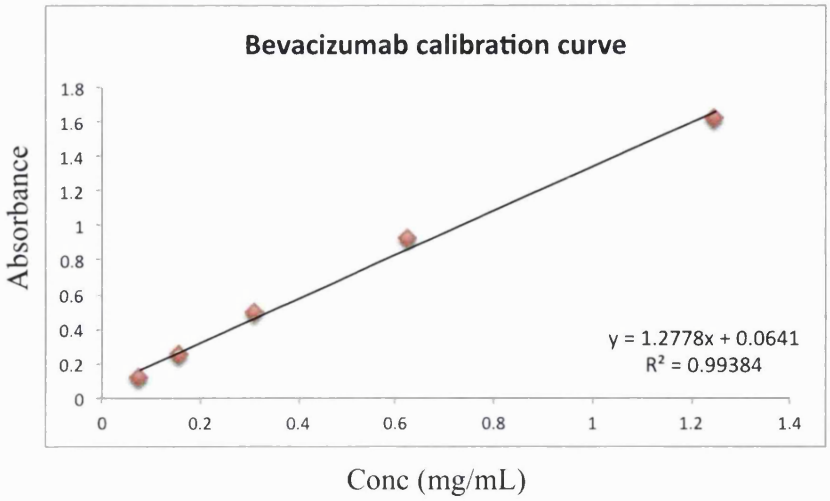

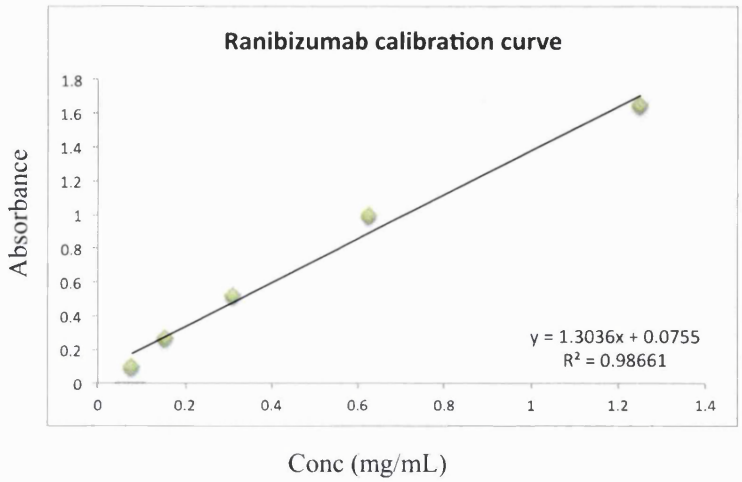

Figure 3.4 Calibration curve made with bevacizumab and Fab_{rani} at 280 nm wavelenght in their formulation buffer.

A representative example is described for how the concentration of the Fab_{beva} was determined after being obtained by digestion of bevacizumab. The solution of 2.5 mL of F1 fraction after protein A and before PD-10 column had an absorbance of 1.633 at 280 nm (Table 3.2). After this fraction was eluted over a PD-10 column, an absorbance of 0.984 was observed for a total volume of 3.5 mL (Scheme 3.1, Table 3.2) indicating 2.46 mg of Fab (0.984 absorbance / 1.40 absorbance = 0.70 mg/mL x 3.5 mL = 2.46 mg). The difference between the absorbance value for the F1 fraction before and after PD-10 was due to presence of cysteine in the solution before PD-10 column. A similar PD-10 method was applied on 2.5 mL solution of F2 and F3 fractions after protein A column to remove trace of cysteine (Scheme 3.1, Table 3.2).

While the total volume of the F1 fraction after protein A column was 3.4 mL at large scale of digestion, the total volume of the F2, F3 and F4 after protein A column was 4.0 mL (Scheme 3.1). To purify the remaining 0.9 mL solution of the F1, and 1.5 mL solution of the F2 and the F3, these solutions were pooled and two more PD-10 columns were used (Scheme 3.1). An absorbance of 0.368 was observed for a total volume of 7.0 mL that corresponded to 1.84 mg Fab. Since the absorbance of the third fraction after PD-10 did not change (Table 3.2) from the absorbance before the PD-10 column, other fractions were considered to be pure from cysteine. It was also decided to perform PD-10 purification only on the F1 and the F2 fractions for other digestion experiments. All the solutions after PD-10 column (F1-F3) and F4 fraction were pooled and viva-spin (4000 x g, 10 min) to a solution of 1.0 mL.

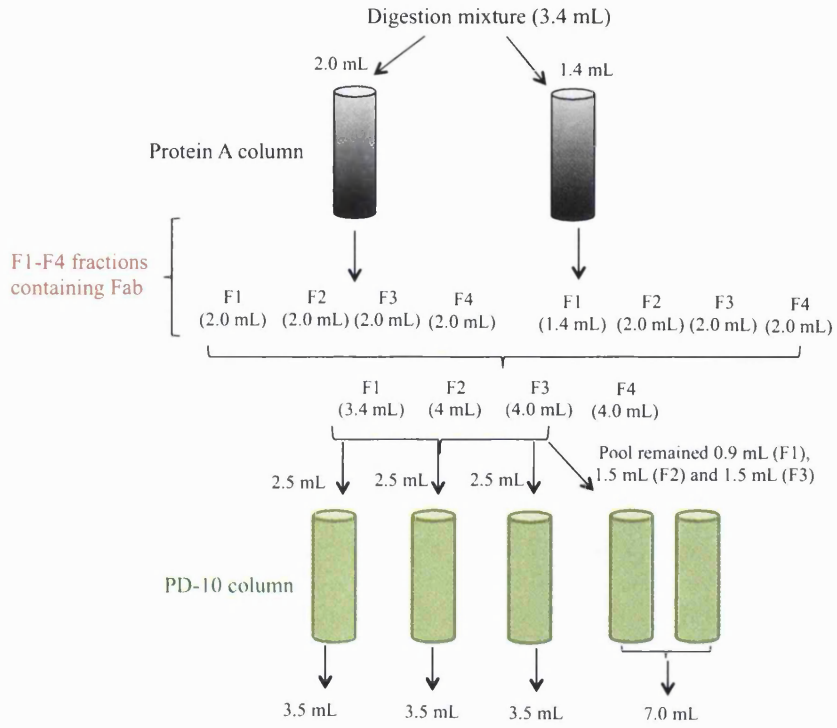

Scheme 3.1 A represention of purification of Fab using protein A and PD-10 column. The Digestion scale is 12.5 mg bevacizumab and 1.0 mL papain.

Table 3.2 Absorbance of fractions (F1-F7) after protein A column. ND; Not determined.

Fractions after protein A	Absorbance before PD-10	Absorbance after PD-10
F1	1.633 (2.5 mL)	0.984 (3.5 mL)
F2	0.535 (2.5 mL)	0.329 (3.5 mL)
F3	0.139 (2.5 mL)	0.111 (3.5 mL)
F4	0.052 (4.0 mL)	ND
F5	1.107 (4 mL)	ND
F6	0.657 (4 mL)	ND
F7	0.210 (4 mL)	ND

The total amount of Fab (fractions 1-4) isolated after purification was 5.548 mg (2.46 mg (F1) + 0.823 mg (F2) + 0.277 mg (F3) + 0.148 mg (F4) + 1.84 mg (from remained F1-F3) = 5.548 mg) based on determination by UV spectroscopy. This

amount compared well with the initial IgG (12.5 mg). Since the total Fab content is 2/3 of the whole IgG, an approximate 65 % yield was achieved from digestion of 12.5 mg bevacizumab.

A slightly better yield of Fab_{beva} was obtained (approximate 73.0 %) when the digestion was conducted during exploratory reactions at smaller scale of 2.5 mg in bevacizumab with 0.4 mL immobilised papain over a 5.5 h digestion time. Throughout the duration of this PhD project, the proteolytic digestion of bevacizumab at a scale of 12.5 mg was performed more than 15 times, 4 individual digestions at each time to provide a larger amount of Fab_{beva} for PEGylation. The isolated yield of Fab_{beva} was in the range of 50 to 70 %. The 4 batches of digestion of 12.5 mg bevacizumab (total amount of IgG 50 mg) were pooled after protein A and PD-10 chromatography to give 20 mg Fab_{beva} which was concentrated to 1.0 mL solution using a viva-spin column. An aliquot of 0.05 mL (1.0 mg) of this solution was kept in the freezer. This aliquot was then used at the time of PEGylation after dissolving in 0.95 mL PEGylation buffer to give a 1.0 mg in 1.0 mL solution. The concentration was checked routinely before conducting an experiment by UV spectroscopy to ensure the protein concentration did not change during the freeze and thawing process.

Since accurate knowledge about protein concentration was important, micro BCA was also performed on the Fab fragment after the protein A and PD-10 purification steps to compare with the results obtained by UV spectroscopy. The bicinchoninic acid (BCA) assay is a well-known method to determine protein concentration [32, 211]. The peptide bonds of the protein convert Cu^{+2} to Cu^{+1} under alkaline condition. This reaction is known as Biuret reaction. The produced-Cu^{+1} complexes with bicinchoninic acid and results in a solution with an intense purple colour after 1.0 h incubation at 37 ^{0}C. The complex has an absorbance maximum at 562 nm. The protein concentration sensitivity is in the range of 0.1-1.0 mg/mL for standard BCA assay and 0.5-10 μg/mL for micro BCA assay [211]. The micro BCA assay was used throughout this research. The buffer used in the BCA assay was PBS with no EDTA. Small amounts of EDTA (0.5 mM) can interfere with the BCA reagent as it can make a complex with Cu^{+2}. In the micro BCA assay standard curve should be first made with known concentrations of a protein. The protein required to make a standard curve should have a similar structure to the protein for which a concentration is to be determined. For instance, to measure the concentration of Fab_{beva}, a model Fab (ChromoPure human Fab) which was purchased from *Jackson ImmunoResearch* was

used to make a standard curve. The ChromoPure human Fab (2.0 mg) was reconstituted using distilled water and the series of concentrations were made for standard curve.

Table 3.3 Micro BCA assay using a Chromopure model Fab at 562 nm.

Sample (μg/mL)	Average absorbance	Av abs-blank
0 (blank)	0.28	0
6.25	0.286	0.006
12.5	0.295	0.015
50	0.446	0.166
100	0.615	0.335
Fab_{beva}	0.588	0.308

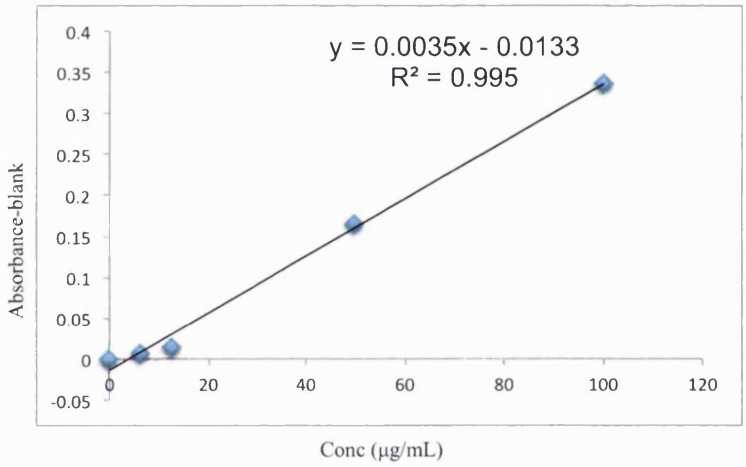

Figure 3.5 Micro BCA assay using ChromoPure model Fab standard curve at 562 nm.

To compare protein concentration as determined by UV at 280 nm with the concentration as determined by micro BCA assay for Fab_{beva}, a solution of 1.0 mL Fab_{beva} was evaluated by both techniques. The purified Fab_{beva} displayed an absorbance of 0.135 at 280 nm by UV spectroscopy. Based on calculation of 1.0 mg/mL Fab has absorbance approximately 1.40, a Fab_{beva} solution with absorbance of 0.135 corresponds to 0.093 mg/mL concentration. In the micro BCA assay, the standard curve was made using a model Fab (Figure 3.5) and the purified Fab_{beva} was then examined (Table 3.3). Based on the standard curve in Figure 3.5, a concentration of 0.092 mg/mL was calculated for the Fab_{beva} by micro BCA assay. Since the concentration calculated for

Fab_{beva} by UV spectroscopy (0.093 mg/mL) and BCA assay (0.092 mg/mL) was similar, it was then decided to use UV spectroscopy at 280 nm throughout this work to calculate the Fab concentration.

The purified Fab_{beva} was pooled and concentrated to a 1.0 mL solution volume using a vivaspin column (4 min, 4000 x g). This solution was characterised using an IEX-SPHP (1.0 mL) column. Since band at 25 kDa was observed in SDS-PAGE gel (Figure 3.3, Lane 1) for the purified Fab after protein A column, it was thought that using IEX chromatography it would be possible to characterise this Fab. If the band at 25 kDa corresponded to the dissociated light and heavy chain due to SDS, then these chains should be associated in solution and elute from IEX column at the same time as the intact Fab with the band at 50 kDa. However, if the light and heavy chains were dissociated in solution, then separate fractions should be obtained by IEX.

To establish the initial conditions for IEX chromatography, the pI value (7.8) of bevacizumab and its Fab fragment was considered [212]. The isoelectric point (pI) of a protein is the pH value at which it has no net charge. A protein has a positive charge when it is in a buffer with pH below its pI value, for instance pH 4.0. A key advantage of IEX compared to SEC is that there is less dilution during purification. IEX allows selective electrostatic binding and subsequent release of species to a stationary phase. IEX is based on the ionic binding of a charged protein to an oppositely charged moiety that has been immobilised to an insoluble matrix. Cation exchange columns bind to positively charged molecules, while un-charged molecules elute without binding to the column. Since the Fab pI was 7.8, it was decided to use a cation exchange column. The cation exchange column used was a SPHP (SP Sepharose high performance). This column has 34-μm beads which results in a better purification than the cation exchange column with larger particle size such as SPFF (SP Sepharose fast flow, 45-165 μm bead size).

To ensure the Fab fragment was positively charged prior to loading onto the IEX-SPHP column, the purified Fab (1.0 mL, 1.0 mg/mL) was buffer exchanged with sodium acetate pH 4.0 using Nap-10 column. The Nap-10 column is another buffer exchanged column with sephadex G-25 DNA grade resin. This column is suitable to buffer exchange solutions with a volume in the range of 0.75 mL-1.0 mL. The Nap-10 column was pre-equilibrated with sodium acetate buffer (pH 4.0, 7 mL) and then 1.0 mL of Fab solution was eluted by gravity. The sodium acetate buffer (pH 4.0, 1.5 mL) was again loaded and collected. This 1.5 mL fraction contains a Fab in the sodium

acetate pH 4.0.

Prior to adding the Fab solution to the SPHP-IEX column, the SPHP column was equilibrated with sodium acetate buffer (pH 4.0) by a series of washing steps. The SPHP column was first washed with sodium acetate buffer A (100 mM, pH 4.0) with a flow rate of 1.0 mL/min for 10 min and then washed with sodium acetate buffer B (100 mM, 1.0 M NaCl, pH 4.0) for another 10 min and washed again with sodium acetate buffer A (100 mM, pH 4.0) for a further 10 min. After eluting from the Nap-10 column (1.5 mL), the Fab solution was loaded onto a SPHP-IEX column that had been pre-equilibrated at pH 4.0.

Different elution gradient programs including linear and stepwise gradients were evaluated. A linear gradient program was found to be efficient for purification and was used. In this program, the column was first washed with 100 % buffer A for 10 min and then a linear gradient started with buffer B including 1.0 M sodium chloride. The second buffer (B) was added in increasing proportion until after 30 min the eluting solution contained 1.0 M sodium chloride. Sodium chloride was present in the second buffer to act as a positive ion (Na^+), to exchange with positively the charged Fab that was bound to the column. If the binding of Fab species is strong, a higher concentration of salt (Na^+) is required. The retention time in IEX chromatography is based on the gradient program that is applied. The Fab_{beva} eluted from the IEX-SPHP column (Figure 3.6, A) at 22 min as indicated by the band observed by SDS-PAGE at about the 50 kDa molecular weight marker (Figure 3.6, B, Lane 1). For the linear elution gradient that was applied, a retention time between 20 to 25 min indicates there is approximately 35-40% of buffer B (0.35-0.40 M NaCL) in the eluting medium.

The single IEX peak for the Fab_{beva} suggested that the band at 25 kDa (Figure 3.3, Lane 1) resulted from the dissociation of the light and heavy chains of the reduced Fab during SDS-PAGE. The IEX behaviour suggested the heavy and light chains had remained associated while the Fab was in the solution. The purified IEX Fab_{beva} was then analysed by MALDI-TOF mass spectroscopy (Figure 3.7, B). A molecular weight of 48 kDa was observed for Fab_{beva}. The small shoulder at 47 kDa for Fab_{beva} (Figure 3.6, C) was thought to be due to miscleavage or excess proteolysis by papain. No effort was made to determine the proportion of different Fab molecules that might be present, but as described in Chapter 4, it was observed that binding of Fab_{beva} to VEGF was maintained. In order to evaluate Fc fragment, SEC was performed to separate the Fc fragment from un-digested bevacizumab in fractions (F5-F7). A protein with a

molecular weight of 52 kDa (Figure 3.7, C) was observed and thought to be the Fc fragment. Bevacizumab displayed a molecular weight of 150 kDa by MALDI-TOF mass spectral analysis (Figure 3.7, A).

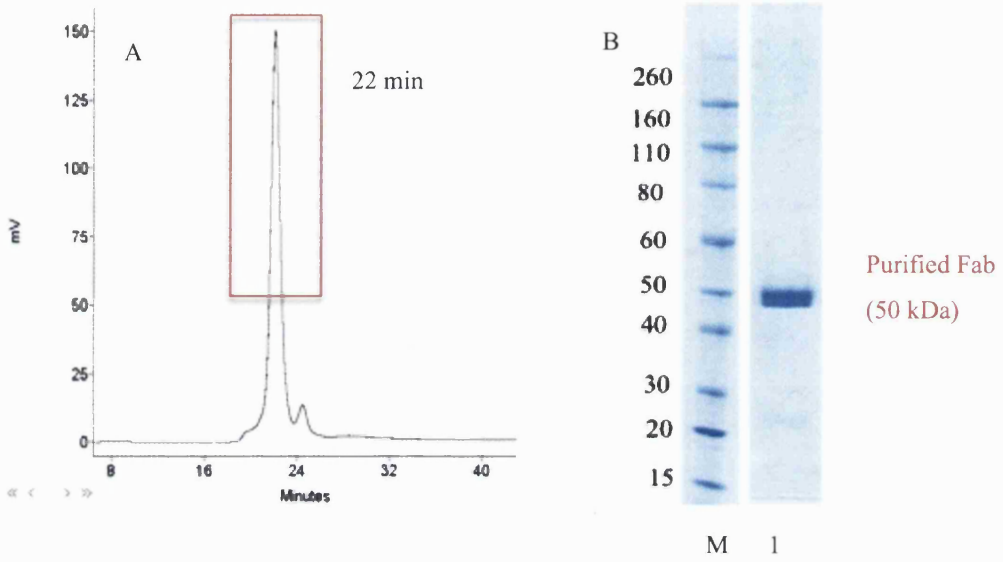

Figure 3.6 (A) The IEX-SPHP chromatogram of the Fab after protein A and PD-10 column, **(B)** The SDS-PAGE gel of the IEX fraction at 22 min shows the purified Fab (*Lane 1*, 50 kDa).

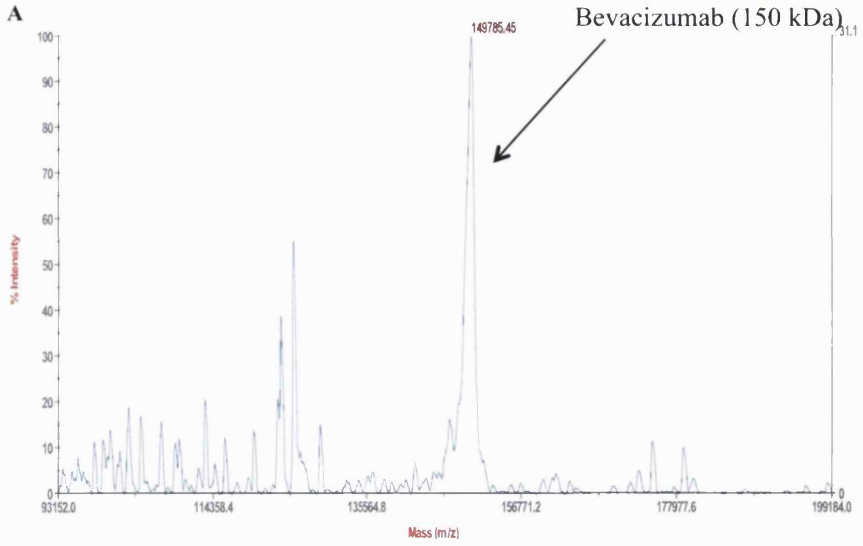

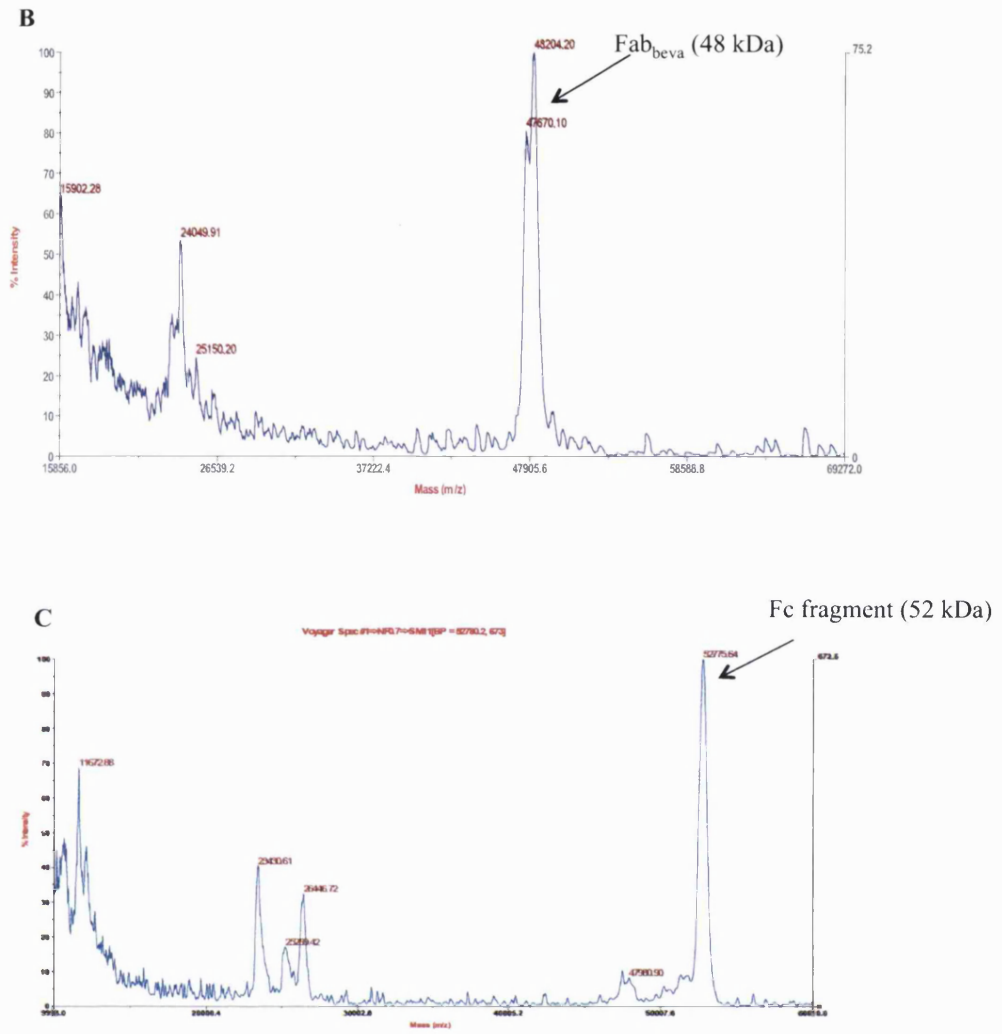

Figure 3.7 MALDI-TOF spectra of **(A)** Bevacizumab, **(B)** Fab$_{beva}$, **(C)** Fc fragment.

Size exclusion chromatography (SEC) was also used to characterise the purified Fab$_{beva}$. SEC was performed to evaluate the size and purity of this Fab in the solution. SEC separates molecules based on their size. It takes longer for the smaller molecules to elute from the column as they diffuse into the pores that are in each of the cross-linked resin particles used to pack the column. Large molecules elute from the column more quickly because they do not diffuse into the pores as readily as the smaller molecules in the mixture. A peak that has a lower retention time is related to larger molecules while a peak that has higher retention time is related to smaller sized molecules within the eluting solution. The SEC mobile phase was PBS (pH 7.4) and bevacizumab was eluted with a retention time of 72 min (Figure 3.8, A) and Fab$_{beva}$ was eluted at 89 min (Figure 3.8, B). To control, a model Fab was eluted at 89 min (Figure 3.8, C) which was similar

to the Fab_{beva}. To determine the origin of the peak at 114 min in these chromatograms (Figure 3.8, B and C), sodium phosphate buffer (20 mM) with EDTA (10 mM) was loaded onto the column in a separate experiment and a peak at 114 min (Figure 3.8, D) was observed. The chromatogram of bevacizumab was run for only 100 min.

The Fab chromatogram (Figure 3.8, B) indicates that there was no aggregation in this sample and protein A and PD-10 purification step were sufficient to obtain the Fab in high enough purity for PEGylation. The absence of aggregation was a key observation because of the propensity of Fabs to aggregate, especially in the absence of formulation excipients. The model Fab was also observed to elute at the same time as our Fab fragment (89 min). The spectral response (Y-axis) for both Fab_{beva} and model Fab was similar when the same concentration of both Fabs were loaded to SEC column. This suggested that both Fab eluted and could be isolated with a similar recovery.

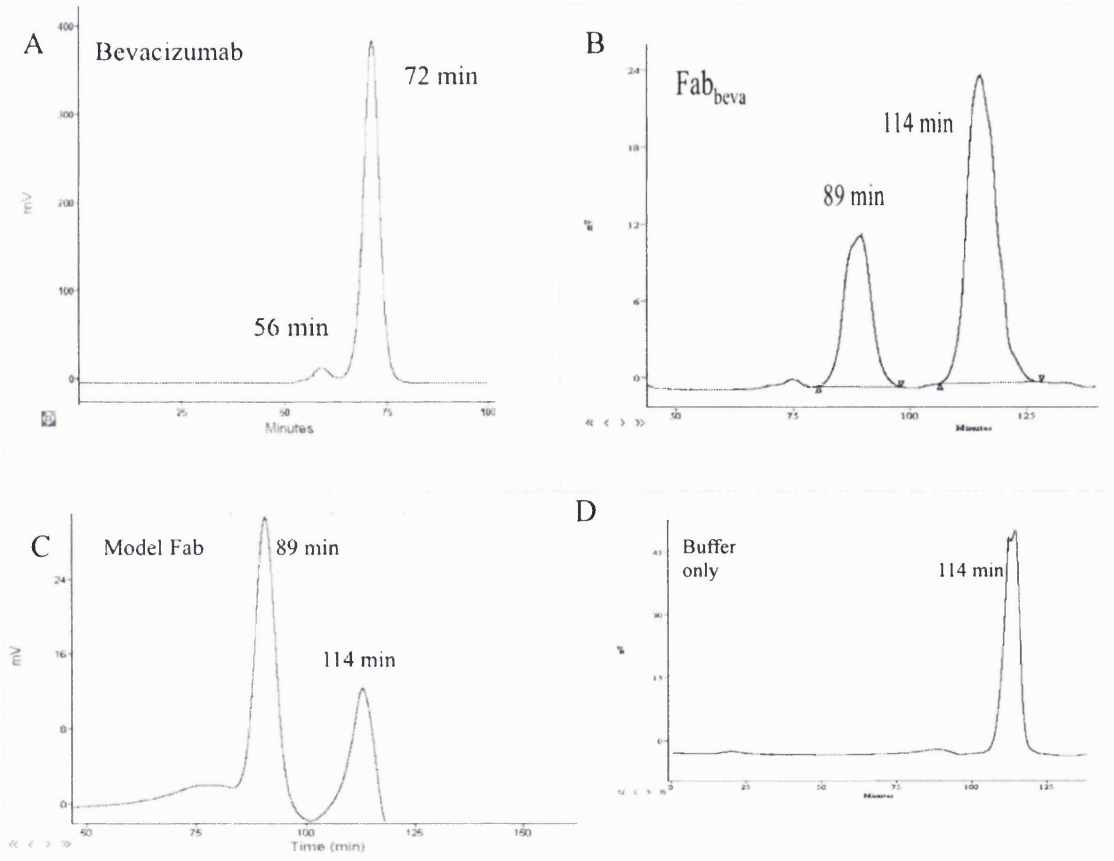

Figure 3.8 SEC chromatogram of bevacizumab (1.25 mg/ml) and its digestion fractions. **(A)** Pharmaceutical bevacizumab, the peak at 72 min was for bevacizumab, **(B)** The first fraction after protein A (indicated as Fab), obtained peak at 89 min, **(C)** The model Fab at 89 min, **(D)** Sodium phosphate buffer (20 mM) with 10 mM EDTA pH 7.0), obtained peak at 114 min.

Before attempting to PEGylate the Fab_{beva}, the number of free thiols in bevacizumab and its Fab fragment were calculated. It was necessary to ensure that the purified Fab_{beva} had no free thiols or any remaining cysteine in the solution. There are different methods to measure the number of free thiols in a protein. These include fluorimetric and electrochemical assays which can be very sensitive and accurate methods but the incubation time is very long (2 hour) [213, 214]. Using a chromene derivative in a calorimetric detection assay is also claimed to have high sensitivity (nM) for thiol detection [213, 215]. Although spectrophotometric thiol assays such as the Ellman's assay are less sensitive (mM), they are rapid and simple [214].

The reagent used for Ellman's assay is 5,5'-dithio-bis-(2-nitrobenzoic acid) (DTNB) which is water-soluble. It was first introduced in 1959 [216] (reagent 5 in Figure 3.9). DTNB undergoes a reaction with a free thiol by disulfide exchange to generate one equivalent of 5-thiol-2-nitrobenzic acid 7. This yellow coloured substance 7 has a high molar extinction coefficient of 14,150 $M^{-1}cm^{-1}$ at 412 nm [217, 218]. The Ellman's assay is useful to measure free sulfhydryl groups at neutral pH in the range of 0.1-1.0 mM [219].

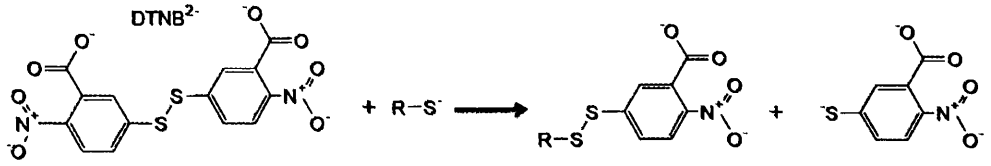

Ellman's reagent 5 Mixed disulfide, 6 TNB^{2-}, 7

Figure 3.9 Reduction of Ellman's reagent.

An Ellman's assay was conducted in a buffer of sodium phosphate (0.1 M) and EDTA (1mM) pH 8.0. DTNB reagent (4 mg) was dissolved in reaction buffer (1.0 mL). Cysteine hydrochloride monohydrate was used as a standard at the following concentration; 0.0, 0.25, 0.5, 0.75, 1.0, 1.25 and 1.5 mM. The incubation time of the sample with DTNB was 15 min at ambient temperature. The absorbance was then read at 412 nm (Table 3.4). No free thiol was observed with the purified Fab_{beva} or starting bevacizumab (Table 3.4).

Table 3.4 Ellman's result at 412 nm for Fab_{beva} and bevacizumab.

Samples	Absorbance
Cysteine 0.0 mM (blank)	0.005
Cysteine 0.25 mM	0.30
Cysteine 0.5 mM	0.55
Cysteine 0.75 mM	0.76
Cysteine 1.0 mM	0.97
Cysteine 1.25 mM	1.20
Cysteine 1.5 mM	1.32
Bevacizumab	0.004
Purified Fab_{beva}	0.005

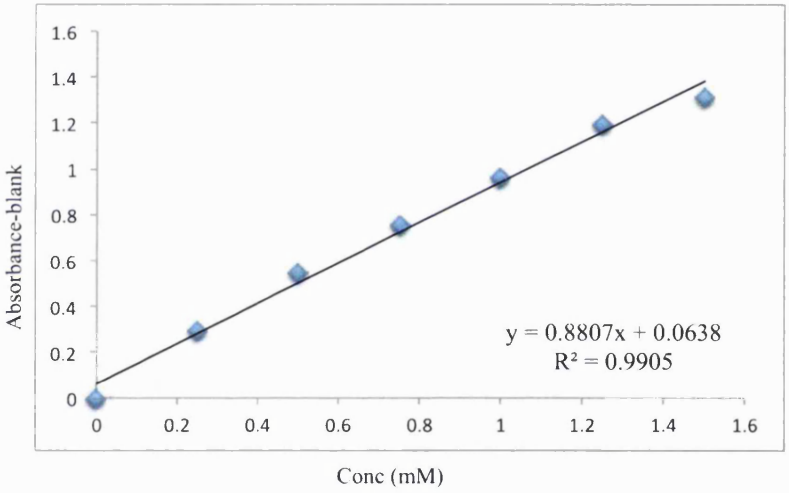

Figure 3.10 The calibration curve made from cysteine standard solution for Ellman's test at 412 nm.

To PEGylate the Fab_{beva} with a thiol specific bis-alkylation reagent such as PEG mono-sulfone reagent **2**, it was first necessary to reduce the interchain disulfide bond to liberate the two cysteine thiols. It has [124] also been described the reduction of native disulfide bond to free thiols for reaction with a bis-alkylation PEG reagent. In addition, it has been recently published the 3-carbon bridging bioconjugation of somatostatin on its disulfide bond using the iodo- and ethynyl agent containing bis-alkylation mono-sulfone linker [125]. The single disulfide bond of somatostatin had to be reduced prior to conjugation. It has been shown in this paper that the biological activity and 3D structure of the modified somatostatin was retained [125].

There is a wide range of reducing agents and techniques that can be used to reduce protein disulfide bonds [137, 220-222]. A protein disulfide can be reduced using thiol based reagents such as 2-mercaptoethylamine (2-MA), 2-mercaptoethanol (2-ME), 2-mercaptoethylamine.HCl (2-MEA), dithiothreitol (DTT), glutathione and cysteine [221]. Phosphorous based agents such as *tris*(2-carboxyethyl) phosphine (TCEP) and *tris*(butyl) phosphine (TBP) can also be used.

The thiol based reducing agents form mixed disulfide that are then reduced to give free thiols of disulfide by the presence of excess reagent (Equation 3.1). Excess reagent is necessary to complete the reduction. Of the thiol reagents, DTT undergoes cyclisation so that a low concentration can be used (Figure 3.11) [220, 222]. Since thiol based reagents can compete with a thiol specific alkylation reagent, the reducing agent must be removed prior to PEGylation.

$$R'S^- + RSSR \longrightarrow RSSR' + RS^-$$

$$R'S^- + RSSR' \longrightarrow R'SSR' + RS^-$$

$R'S^-$ (thiolated anion): DTT and 2-ME

Equation 3.1 The mechanism of disulfide reduction by exchanging thiolate anion.

If there is excess reducing agent in the presence of the reduced antibody, then the PEG reagent would be consumed without the opportunity to undergo reaction with the freed thiols on the antibody. There are also large molecule effects where it may be a case that even a small excess of reducing agent could be enough to preclude reaction of our PEG reagent with the thiols of antibody disulfide. The small molecule thiols may be much more reactive with the PEG end groups than the thiols from the antibody. Hence it was important to ensure no reducing agent was present during PEGylation.

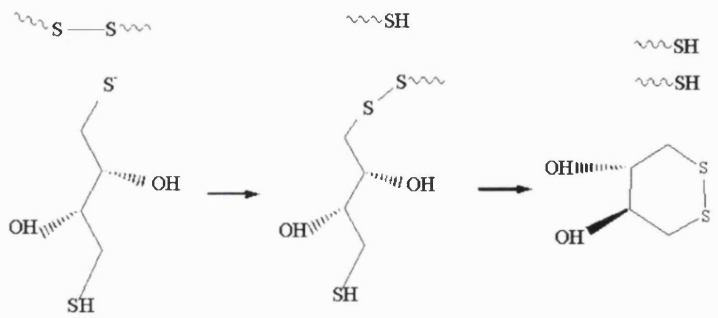

Figure 3.11 DTT reduction mechanism.

As with the mono-thiol reducing agents, phosphorous based agents form an analogous mixed disulfide intermediate (Equation 3.2). This intermediate then undergoes reaction with water leading to the oxidised phosphine and to the production of two free thiols from each disulfide (Equation 3.2). Analogous to free thiol reducing agents, free phosphine can also undergo conjugation reactions with our PEGylation reagents. If phosphine is not removed after incubation with the protein, it is necessary to ensure an excess of the PEG mono-sulfone **2** is added during the PEGylation reaction. So that competing reactions with any unreacted phosphine results in the consumption of the PEG reagent prior to conjugation with the protein thiols. Of the phosphorous based agents, TCEP is a strong reducing agent that irreversibly reduce disulfide bonds in stoichiometry to protein at lower pH (e.g pH 5.0) [223]:

$$(CH_2CH_2COOH)_3P: + RSSR \longrightarrow (CH_2CH_2COOH)_3P{-}SR + RSH + H_2O \longrightarrow (CH_2CH_2COOH)_3P{=}O + 2RSH$$

Equation 3.2 The mechanism to disulfide reduction by phosphine.

It has been suggested that TCEP is a stronger and more stable reducing agent than DTT [223, 224]. Often an excess amount of DTT is required to ensure the reduction is complete, whereas TCEP can be used at lower stoichiometry. The reduction of a disulfide bond with TCEP is often faster than with DTT [223]. TCEP can be used at a wide range of pH, from 1.5-8.0 whereas DTT is often used at a pH value of 7 to 8 [223].

The effect of interchain disulfides on the stability of Fab′ has been studied [221, 225]. It has been shown that if the LC and HC of the Fab′ are non-covalently associated, there would be no significant difference in its in-vitro stability during purification process compare to the native Fab′ [225]. This observation was further studied and it was suggested that the Fab′ with no interchain disulfide bond displayed similar in-vivo stability and half-life as the intact Fab′ [221]. It was found that the interchain disulfide can be removed with little effect on the solution structure of the Fab′. So that, it was suggested that using strong reducing agent to reduce the interchain disulfide in the Fab′, would not disturb the Fab′ properties [221].

During initial work [117] in our group, an interchain disulfide of an anti-CD40 Fab was reduced with DTT and after removal of DTT, the PEGylation was accomplished with PEG mono-sulfone reagent **2**. It was reported that anti-HIV-1

activity of an anti-CD40 Fab was retained after PEGylation [117]. DTT was also used to PEGylate IFN-a2 [138] with PEG mono-sulfone where it was found that excess DTT readily reduced the two disulfides in this protein. It was reported that the DTT could be readily removed from the protein solution using a PD-10 column while maintaining the protein in a folded state and without reoxidation of the disulfides [138]. PEGylation of the reduced IFN-α2 was efficient with slightly more than 1 equivalent of the bis-alkylation PEG leading to almost quantitative PEGylation of the IFN [138]. DTT (1.0 mg/mL, 6 mM) was therefore used to reduce interchain disulfide bond of Fab_{beva} in this PhD. Since the Fab has four buried intrachain disulfides in addition to the interchain disulfide, it was necessary to be aware that these disulfides could in principle be reduced and effect on Fab stability properties. Other work in our group [139, 140] has shown that in many buried disulfides were not readily reduced by DTT alone and addition of a denaturant (e.g. RNAse) is required.

Excess DTT was removed after incubation with Fab_{beva} by carefully passing the reaction mixture over a PD-10 column. DTT in solution has a strong thiol smell and while not quantitative as an analytical method, the reduced Fab_{beva} solution did not have smell of DTT once eluted from a PD-10. The method to use a PD-10 column to remove DTT was the same as the method that was used to remove the cysteine during the purification of the Fab after papain digestion.

An Ellmans assay was then conducted to confirm that only one disulfide in Fab_{beva} was reduced using the cysteine standard curve in Figure 3.10 and Table 3.4. After removal of DTT, Fab_{beva} (0.009 mM) in the presence of DTNB displayed an absorbance of 0.026 at 412 nm. By subtracting this number from blank absorbance (0.005), an absorbance of 0.021 was obtained for the reduced-Fab_{beva}. To calculate the sulfhydryl concentration in μmoles per mL of the reduced-Fab_{beva}, the extinction coefficient (ε) of 14150 $M^{-1}cm^{-1}$ for TNB was used. Taking Beer's Law ($A= \varepsilon. b. c$) and using 1 cm path length for b, the c (mole/lit) was calculated as 1.48×10^{-6} M (0.021/ 14150). This value represented the concentration of the solution in the cuvette. To calculate the number of free thiols in the solution of 0.25 mL of reduced-Fab_{beva}, it was necessary to consider the dilution factor that was used. The dilution factor was 2.8 mL as 2.5 mL reaction buffer was mixed with 0.25 mL of sample and 0.05 mL DTNB. Calculation of the number of free thiols in the solution was as follows;

(1) 1.48 x 10^{-6} x 2.8 mL x 1 L/1000 mL = 4.15 x 10^{-9} number of sulfhydryl moles in the 0.25 mL solution.

(2) 4.15 x 10^{-9} mole/0.25 mL x 1000 mL = 1.66 x 10^{-5} M (concentration of sulfhydryl in 0.25 mL solution.

(3) To calculate the number of free thiols, the concentration of sulfhydryl was divided by the concentration of the protein 1.66 x 10^{-5} / 0.9 x 10^{-5} = 1.85 number of free thiols.

This number was an approximate number for two free thiols produced from one interchain disulfide bond. This data suggested that only interchain disulfide bond reduced in the Fab_{beva} using DTT (1.0 mg/mL) and intrachain disulfide bond remain intact.

The reduction of the Fab (1.0 mg in 1.0 mL) by DTT (1.0 mg/mL, 6 mM) is shown in Figure 3.12 (Lane 2) where under the conditions of SDS-PAGE both the heavy and light chains appeared to be completely dissociated. A solution of the PEG reagent **2** was then added to the reduced-Fab_{beva} solution after it had been passed over a PD-10 column (Figure 3.13, Lanes 3-5). While 1.0 equivalent of the PEG reagent **2** gave a good apparent conversion of the PEGylated Fab (Figure 3.13, Lanes 3-5), it was thought that 2.0 equivalents of the reagent would ensure quantitative conversion.

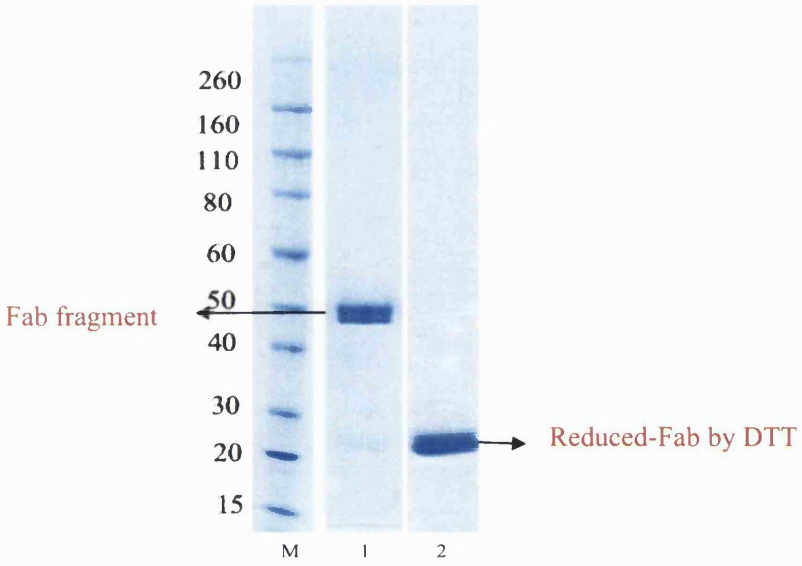

Figure 3.12 SDS-PAGE gel of the reduction of the Fab fraction, Novex Bis-Tris 4-12% gel stained with colloidal blue (Lanes M-2). *Lane M:* protein standard, *Lane 1:* Fab fragment before reduction, *Lane 2:* reduced-Fab fragment by DTT (6 mM).

No effort was made to determine if only slight excess of the PEG reagent could have been used in these reactions. It was clear from the published IFN PEGylation work [138] and from other PEGylation work that is ongoing in our group (unpublished results) that only a slight excess would have been enough. However using **2** equivalents of the PEG mono-sulfone **2** gave a near quantitative conversion for the PEGylation to give the mono PEG-Fab_{beva} (Figure 3.13, Lanes 6, 7).

However in these conditions, a trace amount of what was thought to be the di PEG-Fab_{beva} was observed in the PEGylation reaction (Figure 3.13, Lanes 6 and 7). The di PEG-Fab_{beva} may have been produced as a result of the conjugation of two PEG molecules to the Fab_{beva}. It is possible that two PEG mono-sulfone **2** molecules conjugate to the two free thiols in the single Fab separately without bridging. This may be more probable as the reaction proceeds and there is a high relative concentration of the PEG reagent compared to Fab, especially if some of the PEG reagent has undergone a hydrolysis reaction.

PEGylation reactions can often be effectively monitored by SDS-PAGE to monitor consumption of the starting protein and formation of the PEG conjugate. It is often possible to monitor formation of products with increasing numbers of PEG molecules that are conjugated to the protein. The protein can usually be detected on the gel in SDS-PAGE by using InstantBlue colloidal stain [185]. This staining method is easy to use to detect protein species including Fab, reduced-Fab and the PEGylated-Fab. InstantBlue is a colloidal reagent, which specifically binds to proteins [185]. Protein detection is often displayed as a blue band on the polyacrylamide gel. Since non-glycosylated pure proteins are mono-disperse with a defined molecular weight and the migration of the protein in the gel is based on its size, detection of the protein is generally observed as a narrow blue band.

The blue colloidal stains used to detect proteins do not efficiently detect PEG. So while different protein bands of increasing molecular weight can be observed after a PEGylation reaction using a colloidal blue stain, there is no colour specific indication that the bands are also caused by PEG being conjugated to the protein. Iodide binds to PEG without generally binding to protein and a barium iodide stain has been developed to use in SDS-PAGE to detect PEG species. This stain is based on the formation of a barium iodide complex with PEG, which shows as a brown colour on the SDS-PAGE gel. If a PEG is conjugated to a protein, the colour of the band will be a combination of the blue for the protein and brown for the PEG (Figure 3.13, Lane 7). In this way by

using both a colloidal blue stain for protein and barium iodide for PEG it becomes possible to detect PEGylated proteins from free PEG and free protein species.

In addition to the detection offered by the use of both colloidal blue and barium iodide stains, we often observe that PEG migrates at twice its molecular weight when compared to protein standards in SDS-PAGE. PEG is a random coil molecule and is more flexible than the protein, so it appears larger in solution [115, 226]. Hence much can be deduced by SDS-PAGE analysis of PEGylation reactions. For example an intact, oxidised Fab will migrate to about the 50 kDa protein sharp blue standard marker. If an intact Fab is conjugated to a PEG molecule of 20 kDa, then the conjugate would be expected to migrate to about the 90 kDa marker; 50 kDa for the Fab and 2 × 20 kDa for the 20 kDa PEG. Further confirmation of the 90 kDa band being a 20 kDa PEG conjugated to the Fab will be that the band will be a blue-brown colour due to the complexation of both stains to different parts of the molecule (i.e. colloidal blue to protein and iodide to PEG).

Another important fact of SDS-PAGE is that molecules primarily migrate according to their size. Many polymers have been conjugated to proteins. While PEG is widely used in healthcare, one of its advantages is that it can be made to have a narrow molecular weight distribution. Hence PEG-protein conjugates are also expected to display narrow bands when detected by SDS-PAGE. This is not possible for most polymer-protein conjugates simply because most polymers are not made with such a narrow molecular weight distribution as it possible with PEG. In these cases, the SDS-PAGE analysis will show a broad, diffused band for the polymer protein conjugate [227].

To examine whether PEGylation occurred by conjugation of PEG had resulted from disulfide reduction, control reactions were conducted under the same PEGylation conditions but without prior treatment of the Fab with DTT. The conditions such as buffer and pH, incubation time, concentration of the Fab and the PEG reagent were exactly the same to the conditions used for the PEGylation reaction. No PEGylation was observed when conducted with Fab_{beva} that had not previously been incubated with DTT (Figure 3.13, Lanes 8 and 9). The only protein species observed was the unPEGylated Fab_{beva} at the expected 50 kDa band (Figure 3.13, Lanes 8 and 9). These control reactions indicated that the amine groups (e.g lysine) of the proteins do not tend to react with the PEG mono-sulfone reagent **2** under the reaction conditions (pH 7.4) that we

used for conjugation. Presumably the majority of free amines were protonated.

Different molecular weights (10, 20, 30 and 40 kDa) of the PEG mono-sulfone **2** were used to prepare the corresponding PEG-Fab_{beva} conjugates for comparative study. Using higher molecular weights of PEG [117, 228] can, up to a molecular weight threshold, extend the half-life of the PEGylated-protein in the circulation. The presence of the PEG moiety in a PEGylated-protein usually interferes with the binding of the PEGylated-protein. Often the extent of interference depends on the site of PEG conjugation. This interference is often due to the steric shielding effects of PEG. Earlier studies in our group have shown that PEGylated asparaginases with 5, 10 and 20 kDa bis-alkylation PEG on their disulfide bonds retained their enzymatic binding activity irrespective of the size of PEG conjugated [138]. It was hoped that the binding affinity of PEG-Fab_{beva} would remain broadly the same for each of the different molecular weights of the PEG mono-sulfone **2** (20, 30 and 40 kDa) that were used.

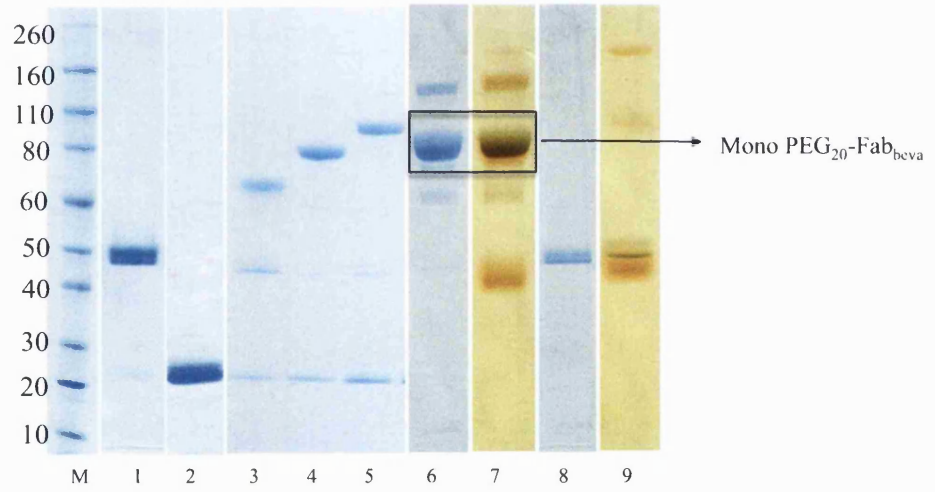

Figure 3.13 SDS-PAGE gel of the reduction of the Fab and PEGylation using (10, 20 and 30 kDa) PEG. SDS-PAGE analysis of reduced-Fab, Novex Bis-Tris 4-12% gel stained with colloidal blue (Lanes M-6 and 8) and barium iodide (Lanes 7, 9). *Lane M:* Protein standard, *Lane 1:* Fab fragment before reduction, *Lane 2:* Reduced-Fab fragment by DTT (1.0 mg/ml), *Lane 3:* PEGylated-Fab reaction mixture using 1.0 eq PEG (10 kDa), *Lane 4:* PEGylated-Fab reaction mixture using 1.0 eq PEG (20 kDa), *Lane 5:* PEGylated-Fab reaction mixture using 1.0 eq PEG (30 kDa), *Lanes 6, 7:* PEGylated-Fab reaction mixture using 2.0 eq PEG (20 kDa), *Lanes 8, 9:* Control reaction, 2.0 eq PEG (20 kDa) on non-reduced Fab.

The PEGylation reaction mixture was then purified from the non-conjugated PEG and the small amount of what was tentatively identified as the di PEG-Fab_{beva}. Purification of the mono PEG_{20}-Fab_{beva} was accomplished by ion exchange (IEX) using an IEX-SPHP (1.0 mL). Two cation exchange columns were initially evaluated. The

SPFF column was considered first. While this column is routinely used in protein purification, the purification of the PEG_{20}-Fab from the non-conjugated PEG and di PEG-Fab_{beva} using SPFF column was not as successful as which SPHP column. This could be due to a smaller particle size (34 μm) in SPHP column, which aid purification. It has also been shown [221] that SPHP-IEX purification was efficient to purify the PEG-Fab′ from unreacted Fab′ using a shallow NaCl gradient.

PEG is not a charged molecule, when PEG-Fab and Fab molecules will bind to the column in a buffer with pH below their pI value. Hence, the protein species will be bound to the column while the non-conjugated PEG will be expected to elute without binding to the column. While disulfide bridging PEGylation does not change the charge of the Fab, there is a difference in the binding characteristics between the Fab and the PEG-Fab. The PEG-Fab interacted with the cation exchange column more weakly than the non-PEGylated Fab. This weaker interaction occurred due to the steric shielding effects of the PEG moiety in the PEG-Fab. The PEGylated-Fab eluted more quickly than the non-PEGylated Fab from the cation exchange column resulting in separation of these two species. Moreover, di PEG-Fab eluted before mono PEG-Fab from IEX column as di PEG-Fab_{beva} has a weaker interaction to the IEX column than mono-PEG-Fab_{beva}.

Anion exchange column (e.g QFF) binds to negatively charged molecules. Non-charged molecules also do not bind. In order to confer a negative charge to a molecule, it is necessary to use a buffer with a pH higher than the pI value of the protein prior to loading on a column. Initial work that was conduced using anion exchange columns for purification did not show a high degree of purification or yield of the PEG-Fab. Since the pI value of bevacizumab is 7.8 [212], Tris buffer pH 8.0 was used to prepare the sample for anion exchange chromatography. It is possible in these conditions that the protein did not have enough negative charge to bind effectively to the anion exchange column. Therefore, the PEGylated-Fab eluted with the un-conjugated PEG in the first 10 min and could not be separated. It is possible in principle to use an anion-exchanged column if a higher pH Tris buffer (pH 10) is considered. There are risks for using such a high pH including protein racemisation and hydrolysis, so it was thought that it is better to use cation IEX. Using sodium acetate buffer at pH 4.0 in cation exchange chromatography was good enough to bind the Fab species to the column.

Prior to loading the PEGylated-Fab onto the column, the mixture must be prepared in an appropriate buffer so that the protein species will bind to the column. To achieve this, the reaction mixture was buffer exchanged either with an exchange column or by diluting (approximately 10 times volume) with the appropriate buffer. Therefore, the PEGylated-Fab mixture (1.0 mL) was buffer exchanged using a Nap-10 column with sodium acetate buffer (pH 4.0). The resulting 1.5 mL solution after treatment with the Nap-10 column was then added to the IEX column. Figure 3.14 (A) shows the IEX chromatogram of the PEG_{20}-Fab_{beva} and (B) the SDS-PAGE gel of the IEX fractions which were collected around the maximum of the peak, from 19 to 21 min, 1.0 mL fraction.

IEX fractions at 19-21 min appeared as a band, which migrated slightly above the 80 kDa protein marker band in SDS-PAGE gel (Figure 3.14, B, Lanes 5-7) and corresponded to the mono PEG_{20}-Fab_{beva}. A small shoulder at 18 min was thought to be di PEG-Fab_{beva} (Figure 3.14, B, Lanes 3, 4). The IEX peak at 3 min, appeared to be unreacted PEG (Figure 3.14, B, Lane 2) since no interaction occurred between uncharged-PEG with the IEX column. It was observed that by using a single step IEX that the mono PEG-Fab_{beva} could be purified (Figure 3.14, B, Lanes 5-7).

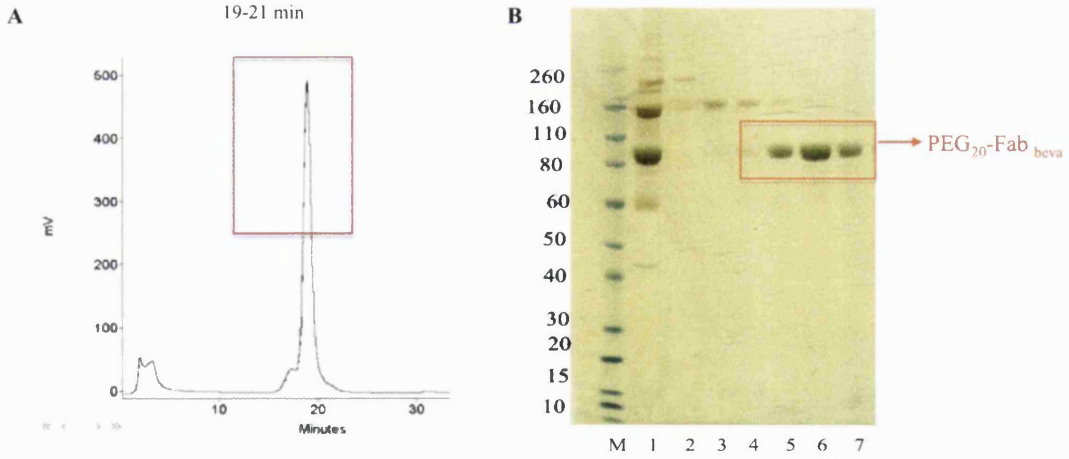

Figure 3.14 (A) IEX-SPHP chromatogram, **(B)** SDS-PAGE gel of IEX fractions of PEG_{20}-Fab_{beva}, Novex Bis-Tris 4-12% gel stained with barium iodide (Lanes M- 7). *Lane M:* Standard protein marker, *Lane 1:* The PEGylation Fab (20 kDa, 2.0 eq PEG reagent 2) mixture before IEX, *Lane 2:* IEX fraction at 5 min, *Lanes 3, 4:* IEX fractions at 17 and 18 min (di PEG-Fab_{beva}), *Lanes 5-7:* IEX fractions at 19-21 min (mono PEG-Fab_{beva}).

The mono PEG-Fab_{beva} fractions from 19 min to 21 min were pooled and concentrated using a vivaspin column (4 min, 4000 x g) to 1.0 mL solution. This solution was then buffer exchanged to PBS (pH 7.4) using Nap-10 column for long term storage at 4 ^{0}C. Different PEGylated Fabs using 20, 30 and 40 kDa of the PEG reagent **2** were also purified (Figure 3.15, Lanes 2-4) following this step IEX chromatography process.

Silver staining was performed on the pooled purified PEG-Fab_{beva} (Figure 3.15, Lanes 8-10) products to determine if there was any non-PEGylated protein after IEX purification. The presence of non-PEGylated protein would distort the binding experiments. Silver staining is a very sensitive staining method, which can detect protein species at the nano gram per mL concentration level. The detection with the silver stain is 100-fold more sensitive than colloidal blue staining [229].

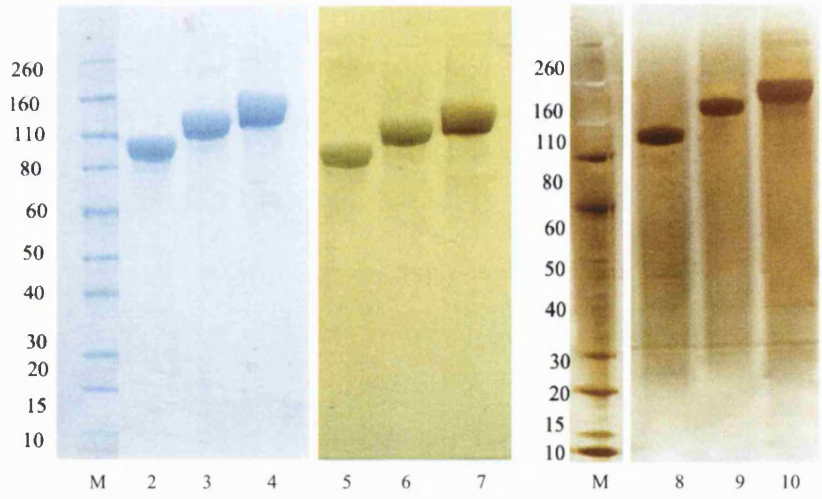

Figure 3.15 SDS-PAGE gel of the IEX-purified PEG-Fab_{beva} (20, 30, 40 kDa), Novex Bis-Tris 4-12% gel stained with colloidal blue (Lanes M-4), barium iodide (Lanes 5-7) and silver staining (Lanes 8-10), *Lane M:* Protein standards, *Lanes 2, 5, 8:* The PEG_{20}-Fab_{beva}, *Lanes 3, 6, 9:* The PEG_{30}-Fab_{beva}, *Lanes 4, 7, 10:* The PEG_{40}-Fab_{beva}.

No evidence of the un-conjugated Fab or other protein impurity was observed after silver staining of the IEX-purified 20, 30 and 40 kDa PEG-Fab_{beva} conjugates. This observation in the silver staining was important to evaluate the purity of the PEGylated-Fab_{beva}. It is rare that silver stain is used to confirm the purity of PEGylated proteins. It was gratifying that by using a single step IEX purification process that purified PEG-Fab_{beva} conjugates using 3 different PEG mono sulfones **2** at 20, 30 and 40 kDa molecular weights were obtained with a high yield.

Table 3.5 Micro BCA absorbance at 562 nm for PEG_{20}-Fab_{beva}.

Sample (µg/mL)	Average absorbance - blank
0 (blank)	0
4.68	0.056
9.37	0.079
18.79	0.178
37.5	0.288
75	0.481
150	0.858
PEG_{20}-Fab_{beva}	0.225

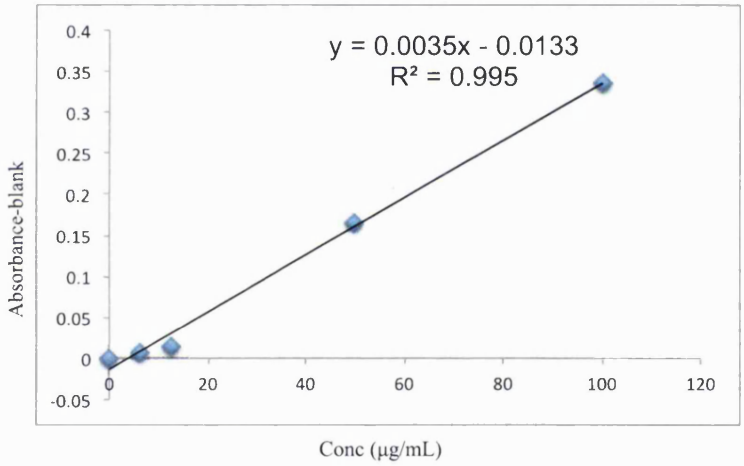

Figure 3.16 Micro BCA Fab_{beva} standard curve at 562 nm.

The concentration of the PEG_{20}-Fab_{beva} in PBS was calculated using two methods, UV spectroscopy at 280 nm and micro BCA assay. Fab_{beva} was selected to make a standard curve in micro BCA assay (Figure 3.16). The concentration of 0.42 mg/mL was calculated for PEG-Fab_{beva} using UV spectroscopy at 280 nm (based on absorbance of 1.4 for 1.0 mg/mL Fab), whereas the concentration of 0.33 mg/mL was calculated using micro BCA assay. These two methods gave two significant different concentrations for PEG-Fab conjugate. Micro BCA assay measurement is based on protein quantity only and PEG reagents do not have absorbance in BCA assay based on the work conducted in PolyTherics. However, the presence of the PEG linker in a

PEGylated Fab could influence the UV reading at 280 nm. Therefore, it was decided to rely on the micro BCA assay result to calculate the concentration of PEGylated Fab conjugates throughout this work.

From a starting amount of 1.0 mg Fab_{beva}, it was found that 0.66 mg PEG_{20}-Fab_{beva} was purified giving an isolated yield of 66 % for the conjugate. The PEGylation of the Fab_{beva} using 20 kDa PEG reagent **2** and purification of PEG_{20}-Fab_{beva} was performed more than 10 times with the isolation yield of 60-66%. The PEG_{30}-Fab_{beva} and PEG_{40}-Fab_{beva} were produced for three times and the similar yield as PEG_{20}-Fab_{beva} was obtained.

MALDI-TOF was performed on the PEG_{20}-Fab_{beva} to determine the exact molecular mass of the PEG-Fab (Figure 3.17). Peak at 68 kDa was detected for the PEG_{20}-Fab (48 kDa Fab + 20 kDa PEG = 68 kDa). The peak for PEG_{20}-Fab_{beva} was not as sharp as a MALDI peak for Fab_{beva} due to the polydispersity of the PEG polymer.

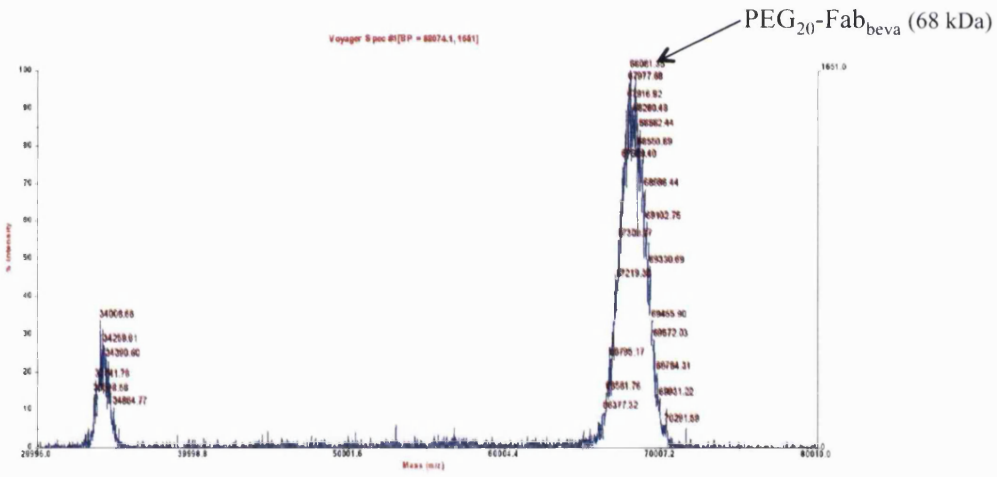

Figure 3.17 MALDI-TOF spectrum of the PEG_{20}-Fab_{beva}.

3.1.2 Stability study of Fab_{beva} and PEG-Fab_{beva}

Fab is a smaller molecule than the full antibody and it is not often glycosylated. Fab tends to aggregate when it is not formulated. Since most protein-based medicines are administered parentally, formulation options are limited in terms of the excipients that are used. Protein aggregation can make it difficult to achieve dose reproducibility and may also increase the risk of immunogenicity [230-232]. For instance, ranibizumab (Fab) is formulated in 10 mM histidine HCl, 10% α, α-trehalose dihydrate, 0.01%

polysorbate 20, pH 5.5 [58]. Using these additives in formulation was necessary to stabilise Fab_{rani} to avoid the aggregation [233]. It has been shown that histidine in solution would increase stability of the antibody during lyophilisation process and results in less aggregate [233]. Besides formulation to avoid aggregation, PEGylation was also thought to be an approach, which can decrease the susceptibility for proteins to aggregate in solution. It was also necessary to study the stability of the PEGylated Fab to investigate if there was a de-PEGylation during storage in the PEG-Fab solution. If de-PEGylation occurred a free Fab would be expected to be observed. The presence of free Fab would interfere with the binding studies.

Since the Fab_{beva} prepared in this work was stored in PBS (pH 7.4) at 4 ^{0}C without any additive, it was necessary to study its stability. A three month stability study was conducted with Fab_{beva} and the PEG_{20}-Fab_{beva} stored in PBS (pH 7.4) at 4 ^{0}C. One sample of the PEG_{20}-Fab_{beva} was also examined after 8 months storage at 4 ^{0}C to see if there would be any de-PEGylation occurs during storage.

SEC analyses were performed on the Fab_{beva} (0.2 mg/mL) and PEG-Fab_{beva} (0.1 mg/mL) at the time for the start of storage (T0) and after 3 months storage (T3) (Figure 3.18). The peak at 89 min (Figure 3.18, A) corresponded to the Fab_{beva} with 50 kDa molecular weight size and peak at 75 min corresponded to the high molecular weight species (e.g aggregate). The peak at 75 min appeared to increase after three months storage (Figure 3.18, B). The PEG-Fab_{beva} was also examined using SEC at T0 (Figure 3.18, C) and T3 (Figure 3.18, D). The retention time for PEG-Fab_{beva} was 63 min, where small peak at 54 min was also observed. However, no significant difference in the area under peak at 54 min was observed for the PEG-Fab_{beva} after three months storage. When higher concentration of PEG-Fab_{beva} (0.4 mg/mL) applied, the peak at 54 min became even smaller (Figure 3.18, E) compared to the PEG-Fab (0.1 mg/mL) at T0. No peak at 89 min was observed for free Fab_{beva} in the PEG_{20}-Fab_{beva} solution at T3 as suggested no de-PEGylation.

A; SEC of Fab_{beva} (0.2 mg/mL) at T0

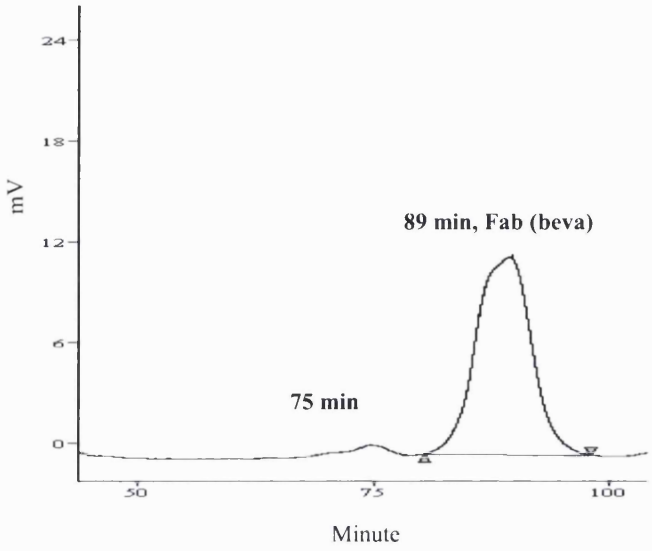

B; Fab_{beva} (0.2 mg/mL) at T3

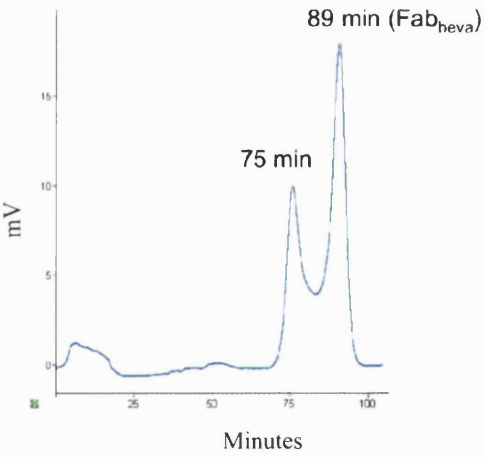

C; SEC of the PEG_{20}-Fab_{beva} (0.1 mg/mL) at T0

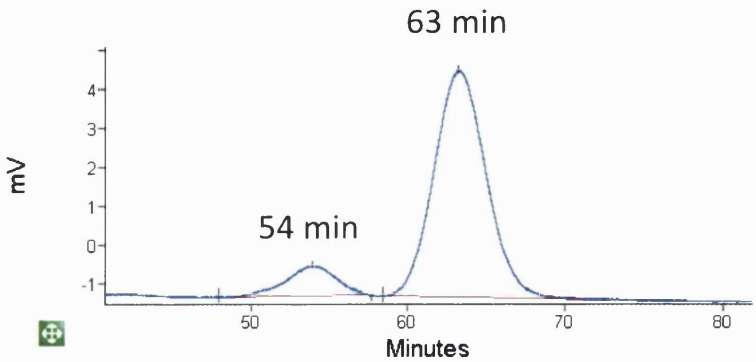

D; SEC of PEG_{20}-Fab_{beva} (0.1 mg/mL) at T3.

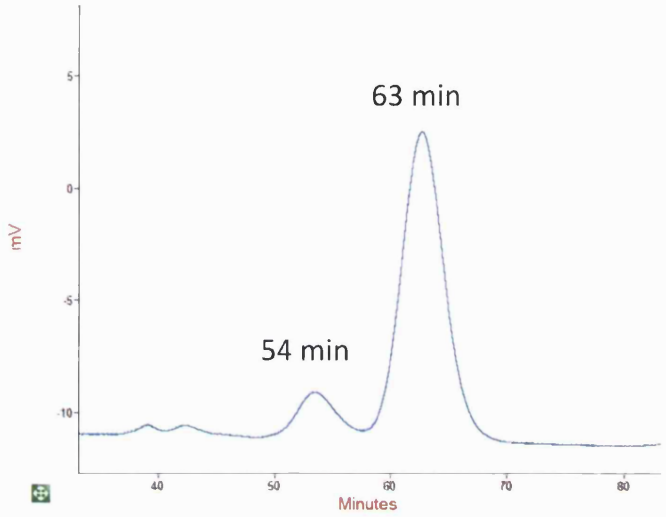

E; SEC of PEG_{20}-Fab_{beva} (0.4 mg/mL) at T0

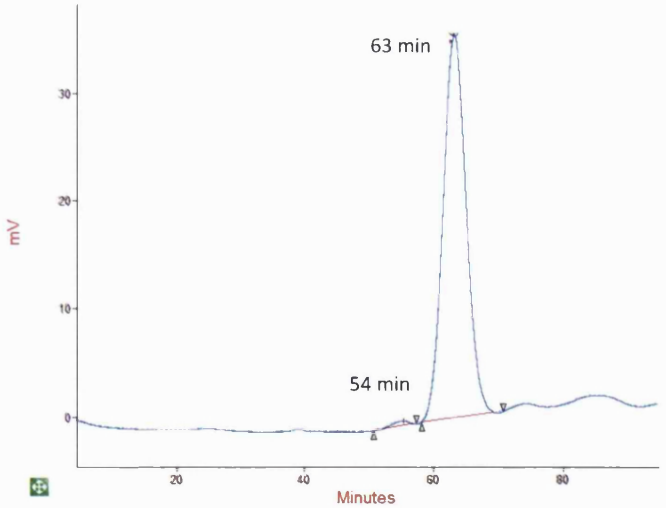

Figure 3.18 SEC chromatograms of Fab_{beva} at T0 **(A)**, and T3 **(B)**, the PEG_{20}-Fab_{beva} at T0 **(C, E)**, and T3 **(D)**.

To further study the possible aggregation of the Fab_{beva} during storage, dynamic light scattering (DLS) analysis was also performed. DLS can measure the size of molecules or particles in the submicron range. A typical application of DLS is the measurement of the diameter and size distribution of particles dissolved in a solution. The diameter that is measured in DLS is called the hydrodynamic diameter and refers to

how a particle diffuses within a fluid [234]. DLS is one of the established techniques to investigate protein aggregation phenomena in solution. In DLS there is a term called the polydispersity index (PdI) that is a measure of the distribution of molecular mass in a given sample. If the size distribution for a molecule of interest is high, the PdI increases (above 1.0) suggesting non-homogenous solution. Contaminating particles such as dust in a solution can be detected in DLS and cause interference; so all solutions must be carefully filtered (0.2 μm).

DLS analysis was performed on the Fab_{beva} at T0 and T3. The particle size in Table 3.6 is an average of three DLS analysis for Fab_{beva} at T0 and T3 and an average of two for PEG-Fab_{beva} at T0, T3 and T8. The average particle size of 9.02 nm was measured for Fab_{beva} at T0 while the average particle size of 14.18 nm was observed at T3 (Figure 3.19, A and B). The DLS data together with the SEC data for the Fab_{beva} suggested that aggregation occurred to some extend during storage over a three-month period. The PEG_{20}-Fab_{beva} (0.4 mg/mL) showed one peak in DLS analysis at T0 and T3 (Figure 3.19, C) with an average particle size of 21.0 nm. As it was mentioned, one sample of the PEG_{20}-Fab_{beva} was studied after 8 months storage using DLS. It appeared that the PEG_{20}-Fab_{beva} was aggregated since two peaks were observed (Figure 3.19, D) with an average particle size of 48 nm and PdI also increased to 1.0. However further work is required to be conducted to study the stability of the PEG-Fab_{beva} from 3 months to 8 months period to find out at what time point the PEG-Fab starts to aggregate.

SDS-PAGE analysis was also conducted on the Fab_{beva} at T0 and T3 and PEG-Fab_{beva} (with 20, 30 and 40 kDa PEG) at T0, T3 and PEG_{20}-Fab_{beva} at T8 (Figure 3.20). Some aggregates can be missed in SDS-PAGE analysis as SDS can denature and dissociate an aggregate in the protein solution, however, it is possible to see de-PEGylation using SDS-PAGE. Fab_{beva} at T3 did not show any aggregate even when silver staining performed (Figure 3.20, A). No de-PEGylation was observed in PEG_{20}-Fab_{beva}, PEG_{30}-Fab_{beva} and PEG_{40}-Fab_{beva} over a 3-month period (Figure 3.20, C) and in PEG_{20}-Fab_{beva} over an 8-month period (Figure 3.20, B) as no free Fab_{beva} at 50 kDa band was appeared in SDS-PAGE gel. These results suggested that PEGylation could increase stability of the Fab_{beva} in a solution and PEG-Fab conjugate was stable during storage time, however, some aggregates could be observed in PEG-Fab_{beva} after 8 months.

A; Fab_{beva} at T0

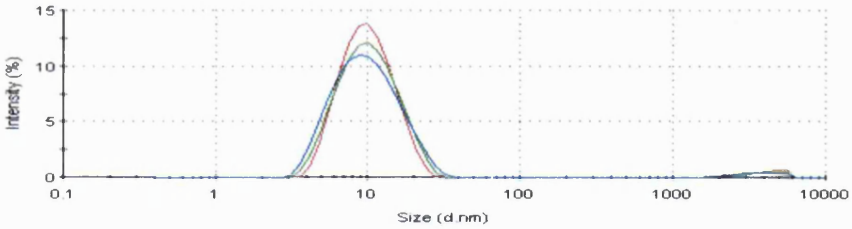

B; Fab_{beva} at T3

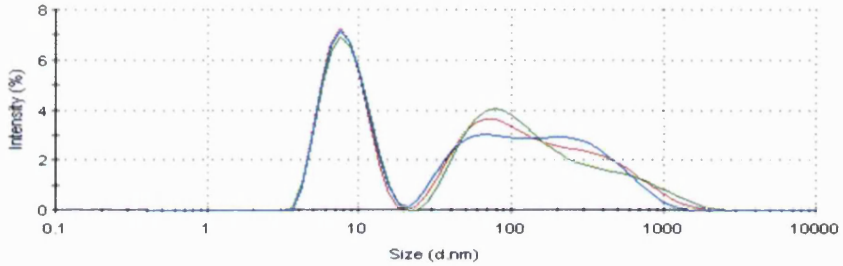

C; PEG-Fab_{beva} at T0 and T3

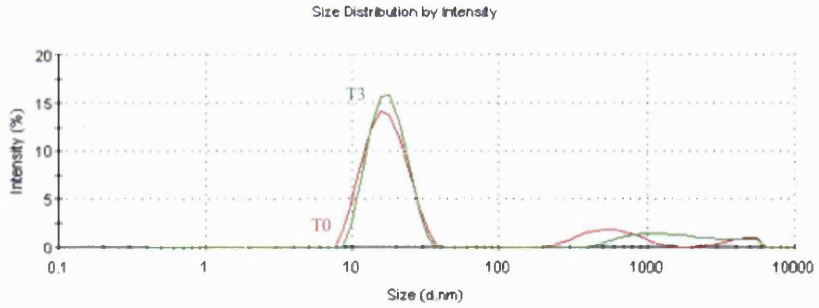

D; PEG-Fab_{beva} at T8

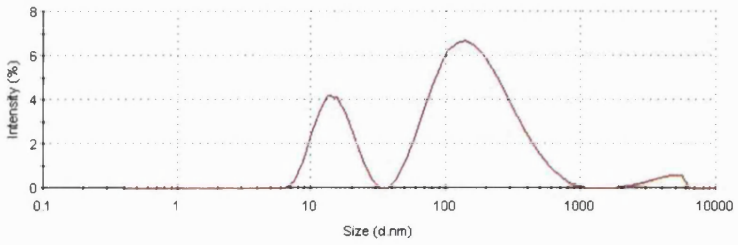

Figure 3.19 DLS analysis of the Fab_{beva} at T0 **(A)**, at T3 **(B)**, and PEG-Fab_{beva} at T0 and T3 **(C)**, and at T8 **(D)**.

Table 3.6 DLS analysis of Fab_{beva} and PEG-Fab_{beva} at T0-T3.

Sample	Z-average size (d. Nm)	PdI
Fab_{beva} at T0	9.02 ± 0.07	0.21± 0.005
Fab_{beva} at T3	14.18 ± 0.09	0.52 ± 0.010
PEG-Fab_{beva} at T0	21.02	0.35
PEG-Fab_{beva} at T3	23.20	0.33
PEG-Fab_{beva} at T8	48.04	1.0

A; The Fab_{beva} in T0 and T3.

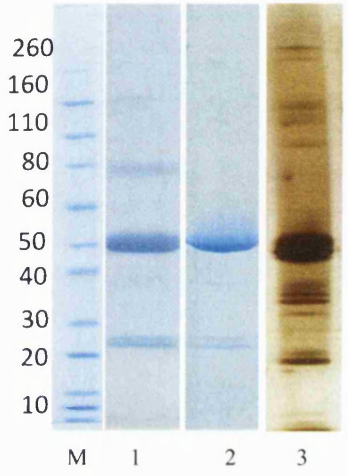

B; The PEG_{20}-Fab_{beva} at T0 -T3 and T8.

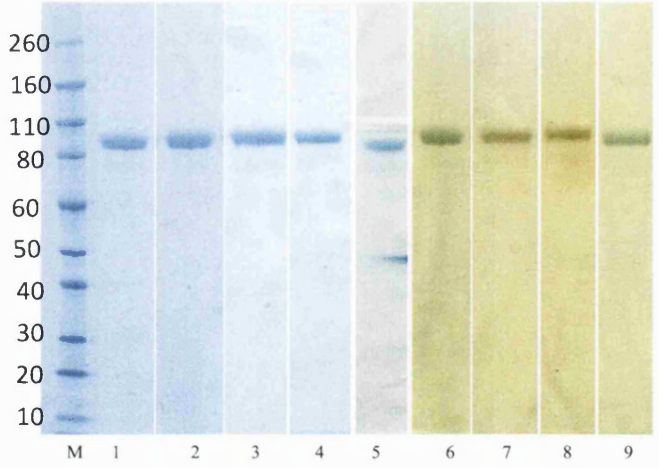

C; The 20, 30 and 40 kDa PEG-Fab_{beva} at T3.

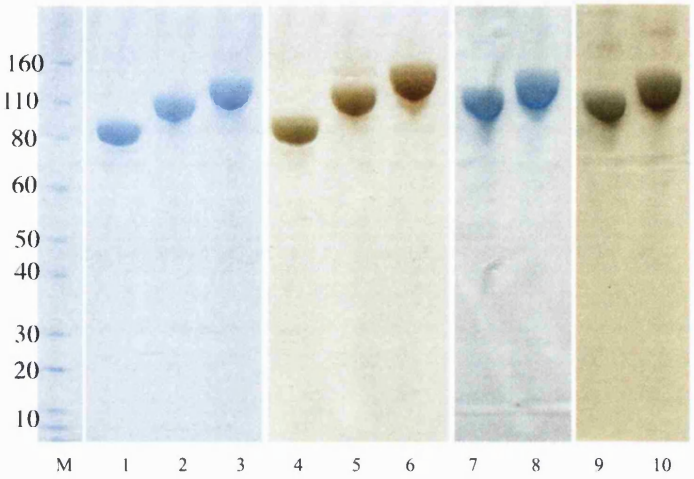

Figure 3.20 SDS-PAGE gel of the PEG-Fab_{beva} over 3 months (T0-T3) and after 2 years at 4 ^{0}C in PBS buffer, Novex Bis-Tris 4-12% gels were stained with colloidal blue in A (Lanes M-2), B (Lanes M-4) and C (Lanes M-3 and 7-8), barium iodide staining in B (Lanes 6-9), C (Lanes 4-6 and 9-10) and silver staining in A (Lane 3). **(A)** The Fab_{beva} at T0 and T3, *Lane M:* Protein standards, *Lane 1:* The Fab_{beva} at T0, *Lanes 2, 3:* The Fab_{beva} at T3, **(B)** The PEG_{20}-Fab_{beva}, *Lane M:* Protein standards, *Lanes 1, 6:* The PEG_{20}-Fab_{beva} at T0, *Lanes 2, 7:* The PEG_{20}-Fab_{beva} at T1, *Lanes 3, 8:* The PEG_{20}-Fab_{beva} at T2, *Lanes 4, 9:* The PEG_{20}-Fab_{beva} at T3, *Lane 5:* The PEG_{20}-Fab_{beva} at T8. **(C)** The 20, 30 and 40 kDa PEG-Fab_{beva} at T3 and 2 years, *Lane M:* Protein standards, *Lanes 1, 4:* The PEG_{20}-Fab_{beva} at T3, *Lanes 2, 5:* The PEG_{30}-Fab_{beva} at T3, *Lanes 3, 6:* The PEG_{40}-Fab_{beva} at T3, *Lanes 7, 9:* The PEG_{30}-Fab_{beva} after 2 years, *Lanes 8, 10:* The PEG_{40}-Fab_{beva} after 2 years.

During stability studies of the PEGylated Fab that were made, we were contacted by Moorfields Pharmaceuticals to conduct a related stability study on bevacizumab stored on luer-lock syringes. A collaborative project between Moorfields Pharmaceuticals and our group in the School of Pharmacy was conducted for comparative stability study during 9 months. This collaboration provided good sources of bevacizumab for our PEGylation studies. The bevacizumab stability studies are described in Appendix II.

3.1.3 Preparation of PEG_2-Fab'_{beva}

$F(ab)_2$ with about 100 kDa molecular weight comprises two Fabs that covalently linked at the hinge region through at least 2 disulfide bonds depending on the IgG subtype [25]. $F(ab)_2$ can be produced by enzymatic digestion of parent antibody or it can be made recombinantly in E-coli [235]. Using the IdeS enzyme to generate $F(ab)_2$, the hope was that there would be 2 disulfides remaining in the hinge sequence linking the heavy chains from each Fab. Reduction of the hinge disulfides was expected to generate two equivalents of Fab′ for each $F(ab)_2$ molecule (Figure 3.21). A Fab′ is

essentially a Fab with a heavy chain sequence leading into the hinge region. If the Fab′ is derived from a full antibody as it was in this study, then the number of hinge cysteines will depend on the number present in the precursor antibody and the type of digestion enzyme used.

Once the purified $F(ab)_2$ from bevacizumab was produced, scouting reduction studies were conducted to see if selective, partial disulfide reduction was possible. Initially we had wanted to PEGylate the $F(ab)_2$ but this was not possible as the reduction studies indicated that the interchain disulfides all underwent reduction. So it was decided to determine if it was possible to conjugate 2 PEG molecules to the Fab'_{beva}. This would require two cysteines in the hinge region. If only one cysteine was present in each heavy chain in the hinge region then we would have expected to observe PEGylated $F(ab)_2$ products. If there were 3 cysteines in the hinge we would expected multi-PEGylated, large molecular weight $F(ab)_2$ derived products. It was possible to isolate pure a PEGylate product consistent with conjugating two PEG molecules to the Fab'_{beva}. This result indicate that one PEG molecule was conjugated to the two cysteines derived from the Fab heavy-light interchain disulfide and the other PEG was conjugated to 2 cysteines on the heavy chain in the hinge region.

To obtain the $F(ab)_2$ fragment, enzymatic digestion of bevacizumab using immobilised pepsin was first conducted. Pepsin cleaves the full antibody in the hinge region between the hinge disulfides and the Fc to produce a $F(ab)_2$ fragment. Papain proteolytically cleaves the heavy chain after the hinge disulfides and closer to the Fab resulting in giving two Fab molecules. Pepsin requires different conditions for proteolytic cleavage than were used for papain. While pepsin was also immobilised to aid its removal after reaction it is activated at acidic pH. In contrast to papain which is a papaya derived cysteine protease that requires the presence of cysteine, pepsin is one of the key proteolytic enzymes in the human digestive system and is produced in the stomach. So pepsin requires an acidic pH when used to digest an antibody. This enzyme denatures at neutral pH.

Bevacizumab (5.0 mg/mL in 1.0 mL digestion buffer) was digested with 300 μL immobilised pepsin. The digestion buffer that was used is sodium acetate trihydrate (20 mM) at pH 4.5. Three digestion times were evaluated (4.0, 5.0 and 6.0 h) and purification was performed using a Nap protein A column. It was found that the yield of purified $F(ab)_2$ using immobilise pepsin was very low (less than 10 %) at any of above conditions as calculated by UV spectroscopy.

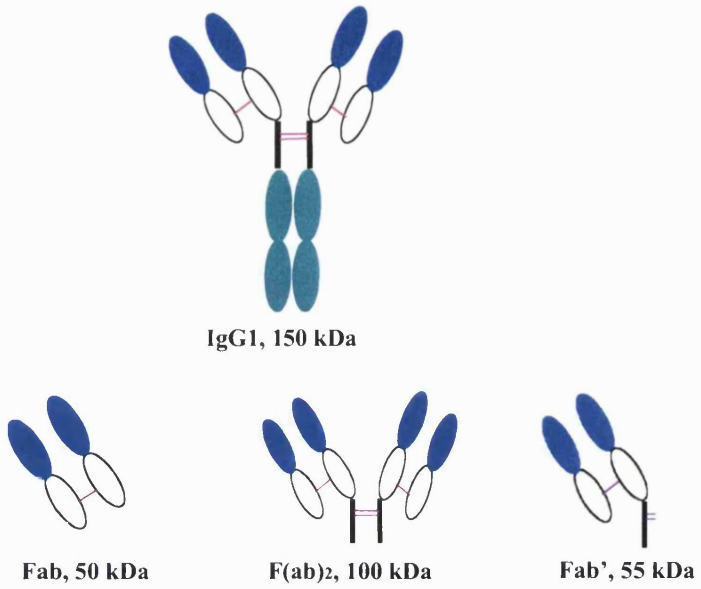

Figure 3.21 Structure of $F(ab)_2$, Fab and Fab´ in comparison with IgG.

Since bevacizumab is an engineered antibody registered for therapeutic use, it was decided to investigate the use of other proteolytic enzymes to obtain the $F(ab)_2$. There was some concern that the bevacizumab structure could have been engineered to be more stable or less susceptible to pepsin proteolysis. An IdeS enzyme was identified as a possible replacement of pepsin that could be used to digest an IgG to produce $F(ab)_2$ in high yield [236]. This enzyme cleaves IgG in the hinge region below the two thiol bridges before Gly236, leaving an intact $F(ab)_2$ and residual Fc fragments [186].

The human pathogen streptococcus pyogenes produces various surface proteins in order to avoid the host immune defense systems [186, 237]. Two of these proteins, EndoS (IgGZERO^{TM}) and IdeS (FabRICATOR^{TM}), have been shown to be very useful as tools in antibody engineering [236]. IdeS is a cysteine protease that cleaves the IgG molecule at a unique site in the hinge region [237].

The protocol from the manufacturer was followed to digest the bevacizumab with IdeS (FabRICATORE) [238]. According to the manufacturers, 5000 units of the IdeS enzyme can digest up to 5.0 mg of IgG. This amount of IdeS enzyme was reconstituted with distilled water (75 µL) and then incubated with 5.0 mg bevacizumab for 30 min incubation at 37 ^{0}C. The buffer solution of sodium phosphate (50 mM) with

NaCl (150 mM) at pH 6.6 was used for this digestion. Different digestion times (10, 15, 20 and 25 min) were examined and it was found that a 30 min digestion time was necessary to achieve near complete digestion of bevacizumab (Figure 3.22, Lane 1). Using IdeS enzyme to digest bevacizumab was faster and resulted in a higher yield of $F(ab)_2$ compared to immobilised pepsin.

The digestion mixture was then purified by SEC to purify the $F(ab)_2$ (100 kDa) from small fragments. In contrast to the digestion with pepsin, purification was conducted by SEC instead of using a protein A column. Using SEC could result in dilution of the $F(ab)_2$ when it is collected, but was less complicated and faster than using a protein A column. The IdeS enzyme has a molecular weight of 36 kDa and can be separated from $F(ab)_2$ (MW; 100 kDa) and small fragments of Fc (MW; 50 kDa). The digestion of bevacizumab using IdeS enzyme and purified $F(ab)_2$ after SEC purification is shown (Figure 3.22).

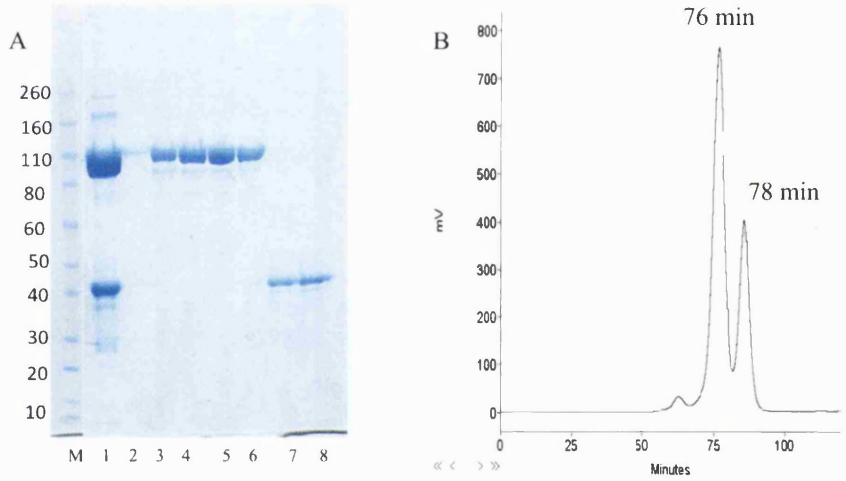

Figure 3.22 Digestion of bevacizumab using IdeS followed by SEC purification. **(A)** SDS-PAGE gel of digestion of bevacizumab, Novex Bis-Tris 4-12% gel stained with colloidal blue (Lanes M-8). *Lane M:* Protein standards, *Lane 1:* Digestion mixture (1.0 mg IgG) before SEC, *Lanes 2-6:* Purified $F(ab)_2$ fractions (SEC fractions at 72-76 min), *Lanes 7 and 8:* IdeS enzyme and Fc fragment (SEC fractions at 78-79 min). **(B)** SEC chromatogram of the digested bevacizumab after 30 min incubation in IdeS enzyme.

SEC fractions collected from 73 to 76 min corresponded the purified $F(ab)_2$ with about 100 kDa molecular mass (Figure 3.22, Lanes 3-6). The fractions collected at 78 and 79 min were smaller proteins in the digestion mixture and along with the IdeS enzyme (Figure 3.22, Lanes 7 and 8). The yield of the $F(ab)_2$ as determined by UV spectroscopy (280 nm) was in the range of 86 %. From 5 mg (3.3×10^{-5} mmole) of

bevacizumab, 2.84 mg of $F(ab)_2$ (2.84×10^{-5} mmole) was obtained. The bevacizumab digestion using IdeS enzyme was performed for 5 times with an approximate similar range of yield.

Before attempting to PEGylate the $F(ab)_2$ an Ellman's assay was conducted to confirm that there were no free cysteines present in the purified $F(ab)_2$. The assay was conducted as described for Fab_{beva} and bevacizumab using the same cysteine standard curve Figure 3.10 and Table 3.4. An absorbance of 0.004 was measured for the purified $F(ab)_2$ indicating that there was no free thiol present in the purified $F(ab)_2$. This result suggested there were no free cysteines in the hinge. PEGylation would help to determine how many disulfides held the hinge together.

The reduction of the $F(ab)_2$ was then studied prior to attempting a PEGylation reaction. The $F(ab)_2$ has the 2 interchain disulfide bonds between the heavy and light chain. It was also anticipated that there were 2 disulfides between the heavy chains in the hinge region and the possible reduction products are shown in Scheme 3.2. Reduction studies were conducted using TCEP and DTT.

Different stoichiometries of TCEP (1.0-6.0 eq) were examined. These TCEP reductions were conducted in the presence of selenocystamine (Se), which has been identified as a catalyst for TCEP reduction [239]. Most of the $F(ab)_2$ remained intact when treated with TCEP at these reaction conditions that were evaluated. Of the two bands at about 25 kDa (Figure 3.23), the higher molecular weight band was thought to be the free heavy chain and the lower molecular weight band was thought to be the free light chain (Scheme 3.2, D, E). Of the two bands at about 50 kDa, the lower one was thought to be the Fab′ [240] (Scheme 3.2, C). The second band at slightly higher molecular weight was thought to be fragment B in Scheme 3.2. Increasing the amount of TCEP to 8.0 and 10.0 equivalents appeared to reduce $F(ab)_2$ to give more of the free heavy and light chains (fragments D and E, Scheme 3.2). Using TCEP in these conditions did not appear to lead to selective reduction to generate fragments such as A, B or C, Scheme 3.2. These experiments indicated that once reduction was initiated, that susceptibility to reduction increased leading to complete reduction of the interchain disulfides between the heavy-light and heavy-heavy chains.

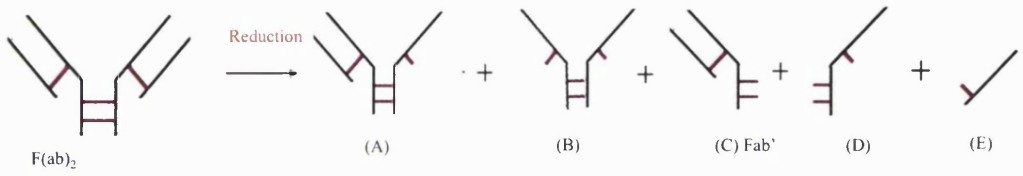

Scheme 3.2 The possible peptide fragments which can be produced by partial reduction of $F(ab)_2$.

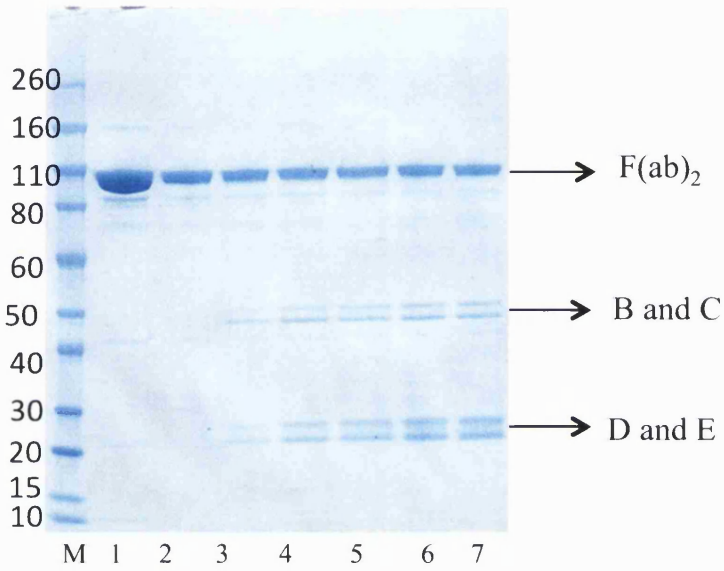

Figure 3.23 SDS-PAGE gel of a reduction of $F(ab)_2$ using TCEP, Novex Bis-Tris 4-12% gel stained with colloidal blue (Lanes M-7), *Lane M:* Protein standards, *Lane 1:* The purified $F(ab)_2$, *Lane 2:* Reduced $F(ab)_2$ with 1.0 eq TCEP and 0.1 eq Se. *Lane 3:* Reduced $F(ab)_2$ with 2.0 eq TCEP and 0.2 eq Se. *Lane 4:* Reduced $F(ab)_2$ with 3.0 eq TCEP and 0.3 eq Se. *Lane 5:* Reduced $F(ab)_2$ with 4.0 eq TCEP and 0.4 eq Se. *Lane 6:* Reduced $F(ab)_2$ with 5.0 eq TCEP and 0.5 eq Se. *Lane 7:* Reduced $F(ab)_2$ with 6.0 eq TCEP and 0.6 eq Se.

Based on our experience with the PEGylation of Fabs in this and other projects [117], it was anticipated that upon reduction, the heavy and light chains would remain associated in solution. Once TCEP has reduced a disulfide, the oxidised product is not reactive toward the PEG mono-sulfone **2**. PEGylation was then conducted after the $F(ab)_2$ was treated with TCEP (8 and 10 equivalents), without removal of the TCEP from the solution. After the $F(ab)_2$ was allowed to undergo reaction with TCEP for 10 min, 4 equivalents of the PEG mono-sulfone reagent **2** (20 kDa, 3.0 mg/mL) was added. The PEGylation process was evaluated after 3.0 h incubation time at ambient temperature by SDS-PAGE (Figure 3.24, Lanes 3 and 4). Two new products appeared

to have formed. The major product appeared to be a new band that appeared just under the starting $F(ab)_2$. A second band at about same molecular weight as bevacizumab was also present.

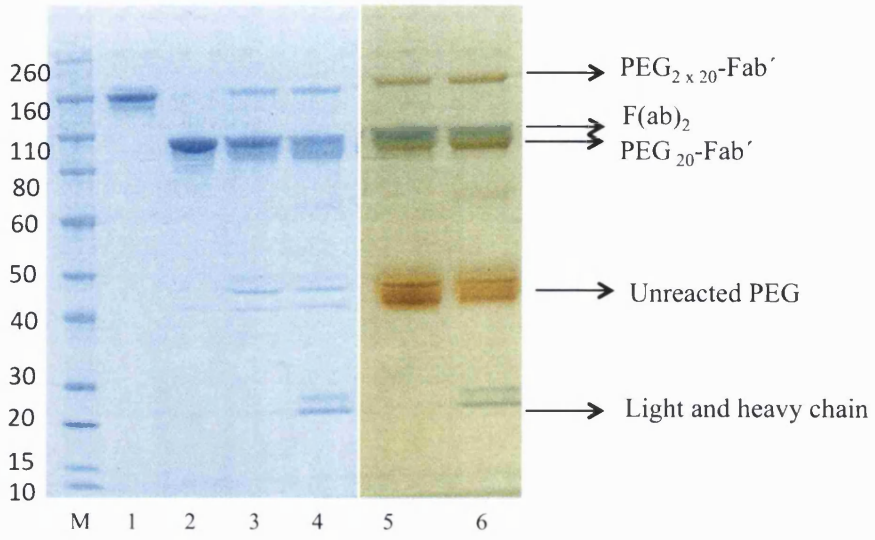

Figure 3.24 SDS-PAGE gel of PEGylation of $F(ab)_2$ after TCEP reduction. Novex Bis-Tris 4-12% gel stained with colloidal blue (Lanes M-4), barium iodide (Lanes 5, 6), *Lane M:* Protein standards, *Lanes 1:* Bevacizumab, *Lane 2:* Purified $F(ab)_2$, *Lanes 3, 5:* PEGylation reaction mixture of $F(ab)_2$ after TCEP/Se (8 equivalents TCEP and 0.8 eq Se), *Lanes 4, 6:* PEGylation reaction mixture of $F(ab)_2$ after TCEP/Se (10 equivalents TCEP and 1.0 eq Se).

Considering the results of both the preliminary TCEP reduction and PEGylation experiments, it was apparent more effort was necessary to examine the reduction step. The TCEP experiments were conducted in the hope of mono PEGylating $F(ab)_2$. The presence of the major PEG product at a molecular weight just under the molecular weight of the starting $F(ab)_2$ suggested that a Fab´ adduct had been PEGylated. While immobilised TCEP could have been examined, these observations suggested that it was going to be difficult to reduce and PEGylate one of the disulfides in $F(ab)_2$. Producing PEGylated Fab´ products were desired as a means to compare multiple PEGylated molecules being conjugated site-specifically to a monovalent Fab derivative, however we also wished to examine if it would be possible to make a PEGylated $F(ab)_2$. If such a product could be prepared it could be compared to PEG-bevacizumab and could help to establish a more complete profile of the structure property correlations for the PEGylated fragments.

Since it appeared that a Fab′ PEG conjugate could be obtained, it was decided to use DTT (6.0 mM, 1.0 mg/ml) as before with Fab_{beva} and to reduce all the interchain disulfides. In this way DTT would completely reduce these disulfides and the heavy and light chains would remain associated as the DTT was removed. Once DTT was removed, PEGylation would occur at the cysteines that had formed the disulfide between the heavy and light chain. PEGylation would also occur with the hinge cysteines (Figure 3.25). In this case PEGylation was expected to occur in a way that depended on the number of disulfides actually present in the hinge between the two heavy chains. If there were 2 disulfides between the heavy chains, then the PEG_2-Fab′ would be an expected product (Figure 3.25).

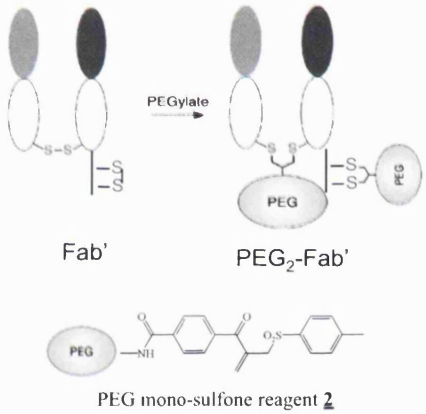

Figure 3.25 Fab′ and disulfide bridging diPEGylation.

After the DTT was removed by passing the reaction mixture over a PD10 column, PEGylation scouting experiments were conducted using different stoichiometric amounts of the PEG reagent **2** (1, 3 and 4 equivalents, 20 kDa). Since all the disulfide bonds were reduced, PEGylation occurred at all the available free thiols. It appeared that one PEG product was formed when 3 and 4 equivalents of PEG mono-sulfone **2** was used (Figure 3.26, Lanes 4 and 5). Multiple PEGylated products and starting light chain was observed when 1 equivalent of the PEG reagent was used (Figure 3.26, Lane 3). A control reaction was conducted using the same PEGylation conditions and 4 equivalents of the PEG mono-sulfone **2** without prior treatment of the $F(ab)_2$ with DTT (Figure 3.26, Lanes 9 and 10). No PEGylated product was observed.

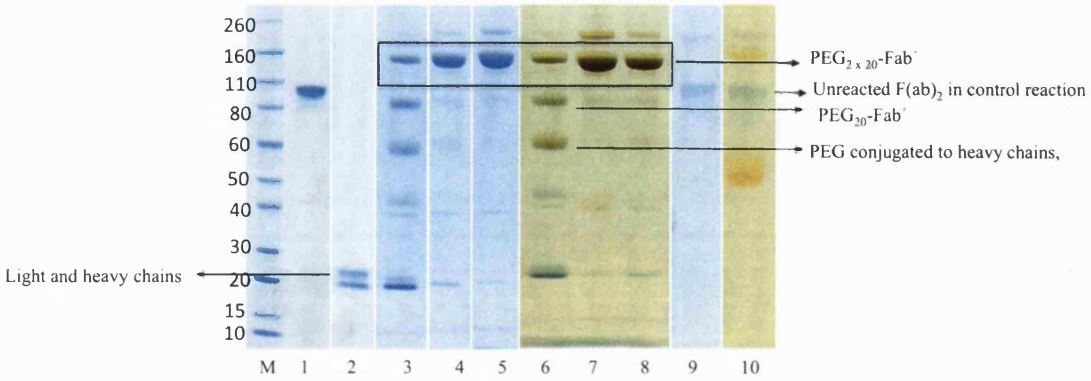

Figure 3.26 SDS-PAGE gel of PEGylation of $F(ab)_2$ after DTT reduction. Novex Bis-Tris 4-12% gel stained with colloidal blue (Lanes M-5 and 9), barium iodide (Lanes 6-8 and 10), *Lane M:* Protein standard, *Lane 1:* $F(ab)_2$, *Lane 2:* $F(ab)_2$ after DTT treatment, *Lanes 3, 6:* Reaction mixture of PEGylation of $F(ab)_2$ (1 eq, 20 kDa PEG), *Lanes 4, 8:* Reaction mixture of PEGylation of $F(ab)_2$ (3 eq, 20 kDa PEG), *Lanes 5, 7:* Reaction mixture of PEGylation of $F(ab)_2$ (4 eq, 20 kDa PEG), *Lanes 9, 10:* Control reaction, PEG with non-reduced $F(ab)_2$.

It did appear that 3 equivalents of the PEG reagent resulted in one product being produced in high conversion that was detected by the new band at about 140 kDa. While an experiment could have been conducted with 2 equivalents of the PEG mono-sulfone **2** it did appear that 2 molecules of PEG was conjugated to the Fab′. Since a 20 kDa PEG reagent **2** was used and the PEG essentially migrates twice its molecular weight in a SDS-PAGE gel, the new band at about 140 kDa could constitute a PEG_2-Fab′ product. The Fab′ contributes about 55 kDa to the molecular weight of this band. If there were 2 PEG molecules conjugated, they would contribute an apparent molecular weight of 80 kDa to this band (i.e. 2 × 40 kDa apparent molecular weight). The molecular weight of a PEG_2-Fab′ conjugate would have an apparent molecular weight on a SDS-PAGE gel of about 135 kDa. Since the resolution of the gel is not good at molecular weights above about 80 kDa, this band was consistent with this structure.

In principle it is possible that this band for the PEG-conjugate (Figure 3.26, Lanes 7 and 8) could have been due to a PEG-$F(ab)_2$ product. In this case the one PEG molecule would contributed an apparent molecular weight of 40 kDa to the gel and the $F(ab)_2$ part of such a conjugate would have contributed about 105-110 kDa. While the actual band for the PEG conjugate that was formed seemed to be less than what would be expected for this product on the gel, the experiment using 1 equivalent of PEG did not really support the formation of a PEG-$F(ab)_2$.

The multiple PEG products that were formed when only 1 equivalent of the PEG mono-sulfone **2** was used suggested multiple conjugation reactions having occurred

(Figure 3.26, Lanes 3 and 6). There was evidence for the conjugation to one PEG molecule to give a mono PEG-Fab′$_{beva}$ with the band at approximately 95 kDa (Figure 3.26, Lanes 3 and 6). Another PEG conjugate appeared to be a conjugate derived from the PEGylation of a single heavy chain, probably on two cysteines in the hinge region. This may explain the band at about 65-70 kDa (Figure 3.26, Lanes 3 and 6). In this case the PEG would contribute an apparent molecular weight of 40 kDa and the heavy chain would contribute a molecular weight of 25-30 kDa. Also since there appeared to be a significant amount of the light chain still present (Figure 3.26, Lanes 3 and 6), this implied that re-oxidation of the disulfides was slower in these conditions than conjugation. Hence in the presence of excess PEG reagent, conjugation of cysteines derived from multiple disulfides occurred faster than re-oxidation. If this was the case and if there was one heavy-light chain disulfide and one heavy-heavy chain disulfide, the PEG product formed in Lanes 4 and 5 was PEG$_2$-Fab′. Since excess PEG reagent seems to drive the reaction to this single product, no effort was made to purify the intermediate conjugates that were formed when one equivalent of PEG mono-sulfone **2** was used.

In addition, PEGylation of F(ab)$_2$ was conducted using 4 equivalents of the 30 kDa PEG mono-sulfone reagent **2** to produce the PEG$_{2x30}$-Fab′$_{beva}$. The 20 and 30 kDa PEG$_2$-Fab′$_{beva}$ were purified using a IEX-SPHP column as was performed for PEG-Fab$_{beva}$. Using a single step IEX chromatography (Figure 3.27, A and B), it was possible to purify PEG$_{2x20}$-Fab′$_{beva}$ and PEG$_{2x30}$-Fab′$_{beva}$ (Figure 3.27, C, Lanes 3-4 and 6-7). In the case of PEG$_{2x30}$-Fab′$_{beva}$, 2 PEG molecules would contribute to give an apparent molecular weight of 120 kDa on the gel (i.e. 2 × 60 kDa apparent molecular weight) and the Fab′ contributes about 55 kDa to the molecular weight of the band above 160 kDa molecular weight marker, about 175 kDa (Figure 3.27, Lanes 6 and 7). The IEX fractions at 17 and 18 min were pooled (2.0 mL) and vivaspin (2 min, 4000 x g) to 1.0 mL solution (Figure 3.28, Lanes 2 and 4) and labelled as pure PEG$_{2x20}$-Fab′$_{beva}$ and PEG$_{2x30}$-Fab′$_{beva}$ respectively. These solutions were buffer exchanged with PBS buffer using Nap-10 column to store at 4 ^{0}C. The concentration was then calculated by micro BCA assay using F(ab)$_2$ to make a standard curve. From a starting amount of 0.5 mg F(ab)$_2$, it was found that 0.1 mg PEG$_{2x20}$-Fab′$_{beva}$ was purified giving an isolated yield of 36 % for the conjugate.

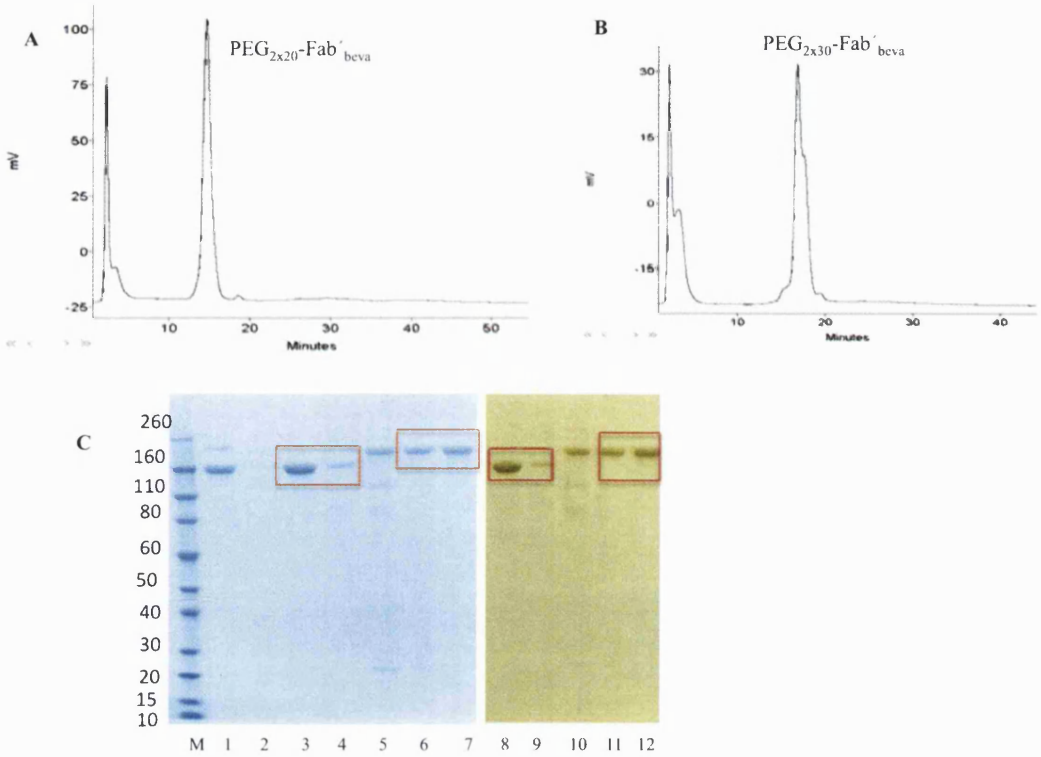

Figure 3.27 IEX-SPHP chromatogram (A, B) and SDS-PAGE (C) of IEX fractions of 20 and 30 kDa PEG-Fab´$_{beva}$, Novex Bis-Tris 4-12% gel stained with colloidal blue (C, Lanes M-7) and barium iodide (C, Lanes 8-12). *Lane M:* Standard protein marker, *Lane 1:* The reaction mixture of PEGylation of F(ab)$_2$ (20 kDa, 4 equivalents PEG) before IEX, *Lane 2:* IEX fraction at 5 min, Lanes 3, 4, 8, 9: IEX fractions at 17-18 min (PEG$_{2x20}$-Fab´$_{beva}$), *Lanes 5 and 10:* The reaction mixture of PEGylation of F(ab)$_2$ (30 kDa, 4 equivalents PEG) before IEX, *Lanes 6, 7, 11, 12:* IEX fractions at 17-18 min (PEG$_{2x30}$-Fab´$_{beva}$).

To evaluate the conjugation of two PEG molecules on hinge and Fab interchain disulfide in the PEG$_{2x20}$-Fab´$_{beva}$ construct, the purified PEG$_{2x20}$-Fab´$_{beva}$ was treated with DTT and then heated to 80 ^{0}C for 10 min. If the PEG reagent **2** was not conjugated to the interchain disulfide bonds in the Fab and hinge, DTT would have reduced these and produced light and heavy chains (25 and 30 kDa) that could be observed by SDS-PAGE. Heating the PEG$_{2x20}$-Fab´$_{beva}$ construct was to evaluate the stability of the conjugation site. If the PEG conjugation to the free thiols was not stable, the light and heavy chains would have been appeared in SDS-PAGE gel. Figure 3.28, Lane 6 and 7 show the PEG$_{2x20}$-Fab´$_{beva}$ treated with DTT and heat. No free light and heavy chains were observed at 25 and 30 kDa molecular weight mass (Figure 3.28, Lanes 6 and 7). These results suggested that the 2 PEG reagents **2** were conjugated to the interchain free thiols in Fab and hinge region of the Fab´$_{beva}$.

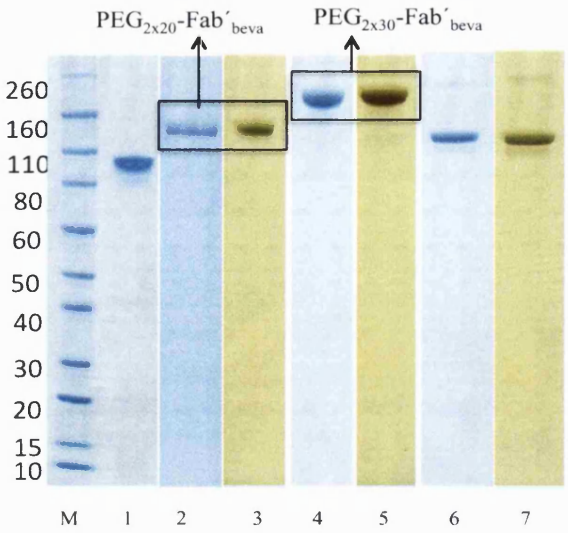

Figure 3.28 SDS-PAGE gel of the purified PEG_2-Fab´$_{beva}$, 20 and 30 kDa PEG. Novex Bis-Tris 4-12% gel stained with colloidal blue (Lanes M-2, 4 and 6), barium iodide (Lanes 3, 5, 7), *Lane M:* Protein standard, *Lane 1:* $F(ab)_2$, *Lanes 2, 3:* The purified PEG_{2x20}-Fab´$_{beva}$, *Lanes 4, 6:* The purified PEG_{2x30}-Fab´$_{beva}$, *Lanes 6, 7:* DTT and heat (10 min, 80 ^{0}C) on the purified PEG_{2x20}-Fab´$_{beva}$.

Since it was a challenge to partially and selectively reduce only one interchain disulfide bond at either Fab or hinge region of $F(ab)_2$ and therefore able to produce PEG-$F(ab)_2$, another technical approach was considered to possibly obtain PEG-$F(ab)_2$ by PEGylating bevacizumab first and then using IdeS enzyme to digest mono PEG-bevacizumab. This approach is described in more details in section related to bevacizumab PEGylation.

3.1.4 Preparation of PEG-Fab$_{trast}$

Trastuzumab is supplied in a vial (150 mg or 440 mg) as a lyophilised powder. A vial of 150 mg contains 150 mg trastuzumab, and the excipients such as L-histidine hydrochloride (3.3 mg), L-histidine (2.1 mg), α, α-trehalose dehydrate (133 mg) and polysorbate 20 (0.6 mg). Reconstitution of this lyophilised solid with water for injection (7.2 mL) that is provided gives a 21 mg/mL solution of trastuzumab at pH 6.0. The water for solution contains benzyl alcohol (1.1%) as preservative. The total weight of the lyophilised solid is thus approximately 290 mg of which 150 mg of this is trastuzumab. To conduct the digestion, 50 mg of the lyophilised solid was weighed and then dissolved into 2.0 mL of distilled water to give a 12.9 mg/mL solution of trastuzumab. The 0.5 mL of this solution was then diluted with 0.5 mL of digestion buffer to provide 1.0 mL solution of 6.45 mg/mL of trastuzumab which was then

digested enzymatically using immobilised papain to produce Fab_{trast} fragment.

A digestion time of 5.5 h was initially examined using 1.0 mL immobilised papain with 20 mM cysteine in the digestion buffer. These digestion conditions were found to be optimal for bevacizumab. Unfortunately, most of the trastuzumab remained undigested when the digestion was conducted for 5.5 h. A longer digestion time (20.0 h) was then examined with 1.0 mL immobilised papain [187] (Figure 3.29, A, Lane 1). Increasing the digestion time to 20.0 h appeared to be enough to digest trastuzumab. While 20 h digestion time and 20 mL immobilised papain were used to fully digest 12.5 mg trastuzumab (0.6 mL) in [187], it was not possible to have 20 mL papain in this PhD. Two different amounts of immobilised papain (1.0 mL and 3.0 mL) were possible to be examined in the presence of cysteine (20 mM) over 20 h digestion time (Figure 3.29, A, Lanes 2 and 3). It was found that 1.0 mL of immobilised papain was enough to produce intact Fab_{trast} to conduct PEGylation, however, the Fc fragment was also remained intact.

Two concentrations of cysteine (20 and 40 mM) in the digestion buffer were also examined. Cysteine concentration was evaluated using 1.0 mL of immobilised papain and a 20 h digestion time period. Using cysteine (40.0 mM) in the digestion buffer resulted in excessive reduction of the Fab, therefore, it was decided to use 20.0 mM cysteine (Figure 3.29, A, Lane 4).

Purification of Fab_{trast} was conducted in a similar way as for Fab_{beva}. The digestion mixture was first eluted over a Nap protein A column to remove Fc. Surprisingly, it appeared that most of the Fab remained bound to the protein A column. In contrast with the purification used for Fab_{beva}, the first, second and third fractions from the protein A column did not appear to contain any Fab_{trast} (Figure 3.29, B, Lanes 3-5). Elution was continued and the Fab_{trast} was eluted from the column along with Fc fragment in the forth and fifth fractions (Figure 3.29, B, Lanes 6-8). Purification using a Nap protein A column was repeated three more times to see if there was an experimental error, however, it was still not possible to separate the Fab_{trast}.

It had been suggested in the literature that an amicon centrifuge tube with a 30 kDa cut off could be used [187] to separate Fab_{trast} from the smaller fragments of the Fc below 30 kDa. In this study [187] using 20 mL papain and long (20 h) incubation time digest Fc fragment into peptide fragments that could be separated from the intact Fab by a centrifuge tube. Since 1.0 mL papain was used, the Fab and Fc fragments were both produced, hence no purification was occurred using the 30 kDa amicon centrifuge tube

(Figure 3.29, B, Lane 2) and all the fragments remained above the centrifuge tube. Then, it was thought that SEC could be used to separate the Fab_{trast} from the Fc (Figure 3.30, B). Figure 3.30, A shows a SDS-PAGE gel of the fractions obtained by SEC. While some of the Fc may have been digested into smaller fragments, intact Fc was still expected to be present. Utilising SEC to separate Fab (50 kDa) from Fc (52 kDa) with no contamination from each other was not going to be efficient. Resolution of molecules so close in molecular weights by SEC is not usually possible. A broad SEC peak from 78-95 min was observed (Figure 3.30) and purified Fab_{trast} could be obtained at the highest part of this peak at 87-90 min (Figure 3.30, A, Lanes 10-14).

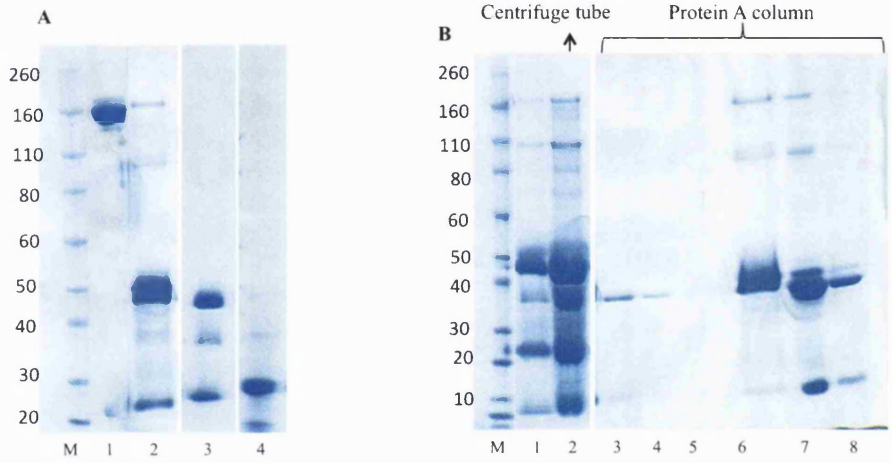

Figure 3.29 Digestion and purification of trastuzumab (12.5 mg/mL) at different conditions. Novex Bis-Tris 4-12% gel stained with colloidal blue (Lanes M-8, A and B). **(A)** *Lane M:* Protein standard, *Lane 1:* Trastuzumab (1.25 mg/mL), *Lane 2:* Trastuzumab digestion mixture with 1.0 mL papain, 20 mM cysteine and 20 h digestion time, *Lane 3:* Trastuzumab digestion mixture with 3.0 mL papain, 20 mM cysteine and 20 h digestion time, *Lane 4:* Trastuzumab digestion mixture with 1.0 mL papain, 40 mM cysteine and 20 h digestion time, **(B)** *Lane M:* Protein standard, *Lane 1:* Trastuzumab digestion mixture with 1.0 mL papain, 20 mM cysteine and 20 h digestion time, *Lane 2:* Purification trastuzumab digestion mixture with amicon centrifuge 30 kDa cut off, *Lanes 3-5:* First-third fractions after protein A column of digested trastuzumab, *Lanes 6-8:* Forth-sixth fractions after protein A column.

The SEC fraction collected at 69 min (Figure 3.30, B) migrated to a molecular weight of 100 kDa in the SDS-PAGE gel (Figure 3.30, A, Lanes 3-5). The 100 kDa molecular weight was correlated with the molecular weight of $F(ab)_2$ fragment that appeared in trace amounts after IgG papain digestion. The fractions collected at 78 min and at 80-82 min at the peak shoulder gave SDS-PAGE band above 50 kDa molecular weight marker (Figure 3.30, A, Lanes 6-9) and was thought it could be corresponded to

the Fc fragment. Fractions collected at peak at 87-90 min, in Figure 3.30, B, were consistent for the Fab fragment, which was observed below 50 kDa molecular weight markers in SDS-PAGE (Figure 3.30, A, Lanes 10-14). It was then confirmed by MALDI-TOF analysis that the fractions at 89 mins were Fab_{trast} with 48 kDa mass (Figure 3.31, B).

The SEC fractions from 87 to 90 min were pooled and concentrated from 3 mL to 1.0 mL using vivaspin (4 min, 4000 x g). The concentration of the Fab_{trast} was then calculated using UV spectroscopy at 280 nm. The absorbance of 1.61 was observed for 1.0 mL of this purified Fab_{trast} solution which represented a 1.12 mg/mL concentration based on the knowledge that 1.0 mg/mL Fab has an absorbance of 1.40 at 280 nm. From an initial amount of 6.45 mg of trastuzumab it was possible to obtain 1.12 mg Fab_{trast} which was enough for PEGylation. The yield to produce the purified Fab_{trast} from trastuzumab digestion was lower (approximately 26 %) than that observed to produce Fab_{beva} (approximately 80 %) from bevacizumab. Although the incubation time for the trastuzumab digestion was longer from (20 h) than for bevacizumab (5.5 h), the reason for the lower yield of Fab_{trast} was probably due to lack of complete separation of the Fab_{trast} by SEC and possible aggregation of trastuzumab [241]. The trastuzumab digestion was performed a total of 7 times and the yield was in the range of 20 to 26 %. When used in the clinic, trastuzumab should be diluted in sodium chloride (0.9 %) and its dilution in dextran (5 %) should be prohibited. There was a report that presence of dextran (5 %) appears to cause aggregation of trastuzumab [62].

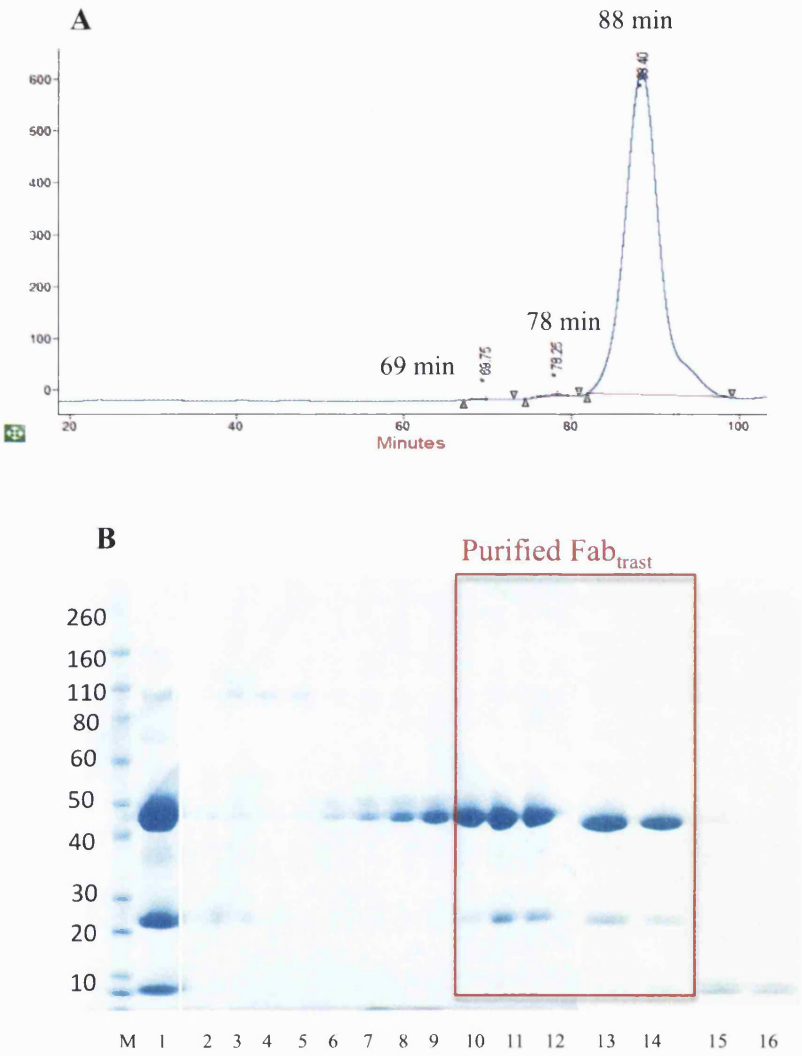

Figure 3.30 Digestion of trastuzumab (12.5 mg/mL) using immobilised papain (1.0 mL) in 20 h and purification by SEC. **(A)** SEC chromatogram, **(B)** SDS-PAGE gel of trastuzumab digestion fractions, Novex Bis-Tris 4-12% gel stained with colloidal blue (Lanes M-16), *Lane M:* Protein standards, *Lane 1:* Trastuzumab digestion mixture before SEC, *Lane 2:* The SEC fraction at 71 min, *Lanes 3-5:* The SEC fractions at 77, 78 and 79 min, *Lanes 6-9:* The SEC fractions at 82, 83, 84, 85 min, *Lanes 10-14:* The SEC fractions at 86, 87, 88, 89 and 90 min, *Lanes 15, 16:* The SEC fractions at 94 and 95 min.

A linear calibration curve was made for trastuzumab (Figure 3.32). The average absorbance for trastuzumab that was reconstituted in PBS and stored at 4 ^{0}C for three months, was much less than absorbance observed for bevacizumab prepared from pharmaceutical vial at the same concentration and same storage time (Table 3.7). This result indicated the possible aggregation for trastuzumab. This experiment was

performed along with Fab_{rani} and the calibration curve of bevacizumab and Fab_{rani} with their absorbance value are presented in (Figure 3.4).

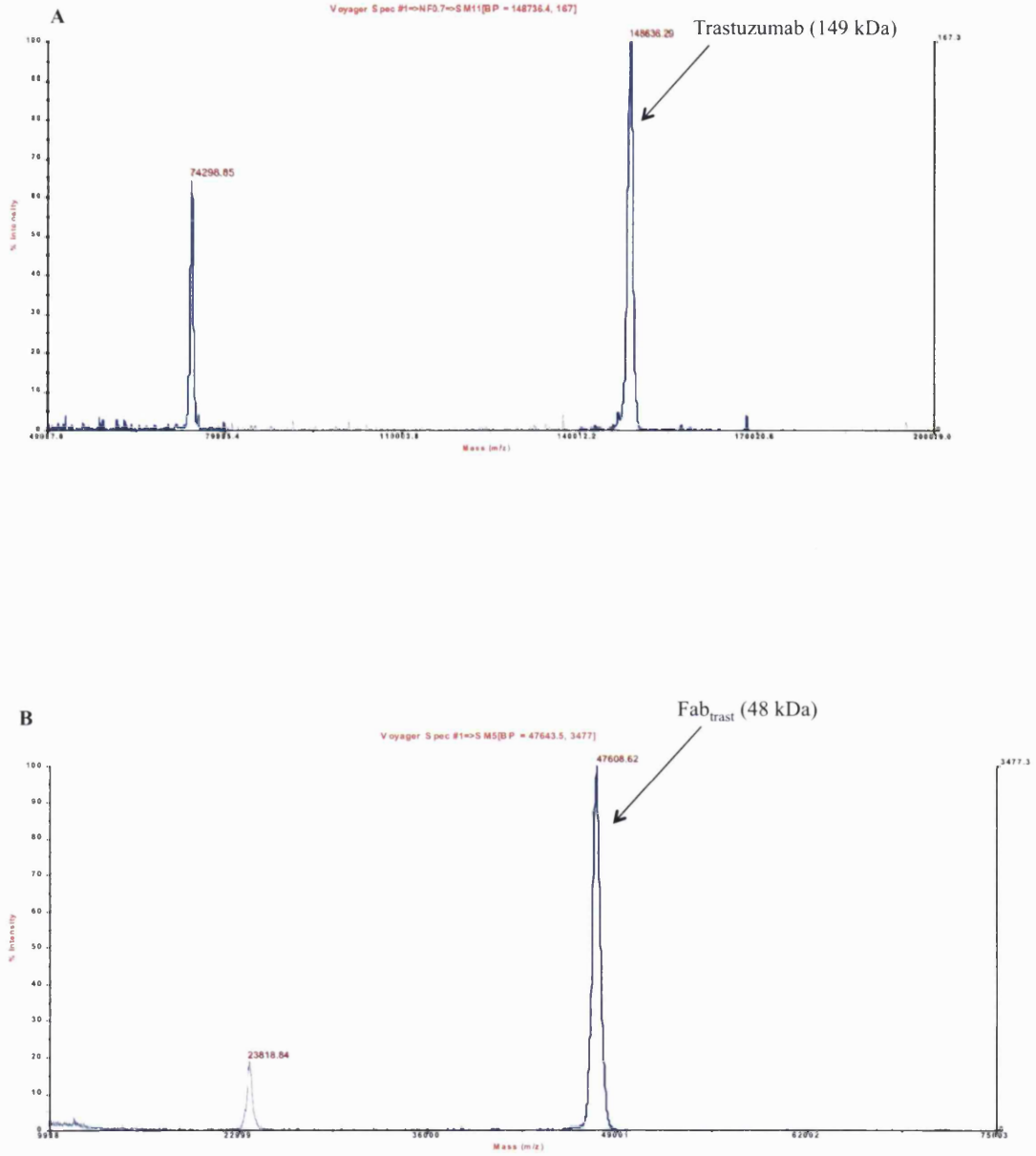

Figure 3.31 MALDI-TOF spectrum of **(A)** Trastuzumab, **(B)** Fab_{trast}.

Table 3.7 The average absorbance at 280 nm for bevacizumab and trastuzumab.

Concentration (mg/mL)	Absorbance at 280 nm Bevacizumab	Absorbance at 280 nm Trastuzumab
0.078	0.116	0.007
0.150	0.249	0.068
0.312	0.495	0.177
0.625	0.929	0.378
1.25	1.625	0.779

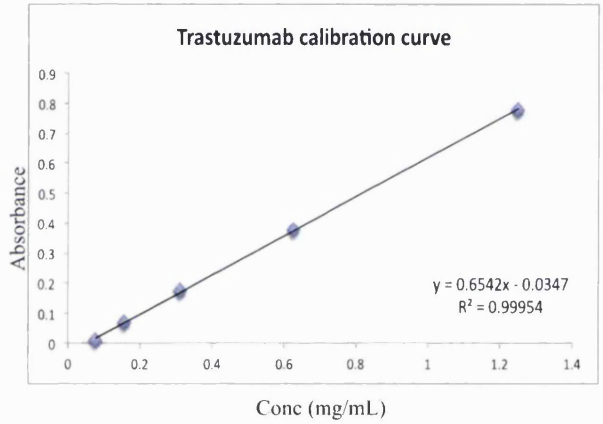

Figure 3.32 Calibration curve made with trastuzumab at 280 nm in trastuzumab formulation buffer.

PEGylation of Fab_{trast} was conducted in a similar way as was the PEGylation of Fab_{beva}. The interchain disulfide of Fab_{trast} (0.1 mg/mL) was again reduced with DTT (6 mM). Scouting experiments were conducted using PEG mono-sulfone reagent **2** (20 kDa) using 1 and 2 equivalents to 1 equivalent Fab_{trast}. Figure 3.33, Lanes 4 and 5, shows the PEGylation reactions when 1.0 and 2.0 equivalents of the PEG reagent **2** (20 kDa) were used. The PEGylation conversion of reduced-Fab_{trast} to mono PEG-Fab appeared to be better when 2.0 equivalents of the PEG reagent **2** was used (Figure 3.33, Lane 5) similar to the PEGylated Fab_{beva}.

PEG_{20}-Fab_{trast} was purified by an IEX chromatography step in the same way as was PEG-Fab_{beva}. Fractions of IEX purification (Figure 3.34, A) were collected at their highest peak (18 and 19 min) and then loaded onto SDS-PAGE gel, Figure 3.34, B, Lanes 3 and 4.

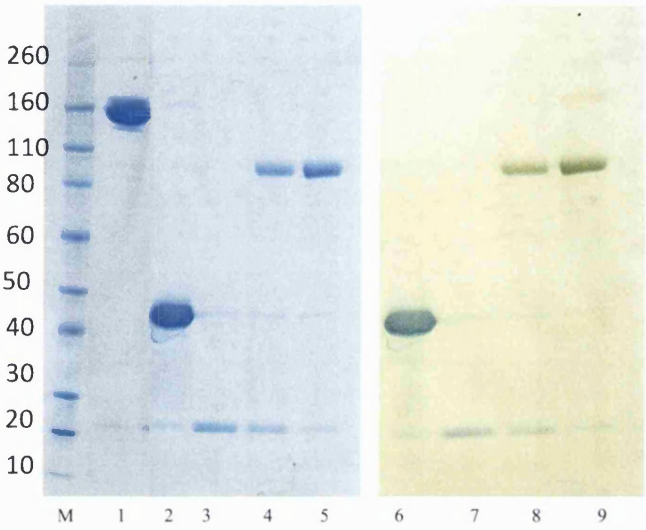

Figure 3.33 SDS-PAGE gel of PEGylation of Fab_{trast} with 1.0 and 2.0 equivalent mono-sulfone PEG (20 kDa), Novex Bis-Tris 4-12% gel stained with colloidal blue (Lanes M-5) and barium iodide (Lanes 6-9). *Lane M:* Protein standard, *Lane 1:* Trastuzumab (1.25 mg/mL), *Lanes 2, 6:* Fab_{trast} (0.1 mg/mL), *Lanes 3, 7:* Reduced-Fab fragment by DTT (1.0 mg/ml), *Lanes 4, 8:* PEGylated-Fab_{trast} reaction mixture using 1.0 eq PEG (20 kDa), *Lanes 5, 9:* PEGylated-Fab_{trast} reaction mixture using 2.0 eq PEG (20 kDa).

As with PEG_{20}-Fab_{beva}, the PEG_{20}-Fab_{trast} migrated to slightly above the 80 kDa molecular weight marker in SDS-PAGE (Figure 3.34, B, Lanes 3-5). A trace amount of unreacted Fab in the PEGylation reaction mixture was observed as a band at 50 kDa (Lanes 1 and 2, Figure 3.34). As expected unPEGylated Fab was eluted from the IEX column after the PEG-Fab_{trast}.

The buffer was replaced with PBS (pH 7.4) for storage and the concentration of purified PEG_{20}-Fab_{trast} was then calculated by micro BCA assay using Fab_{trast} to make a standard curve. For instance, from a starting amount of 0.1 mg Fab_{trast}, it was found that 0.065 mg of PEG_{20}-Fab_{trast} was purified giving an isolated yield of 65 % for the conjugate. PEGylation of Fab_{trast} and purification of PEG_{20}-Fab_{trast} was performed about 5 times with the range of 60-65 % yield.

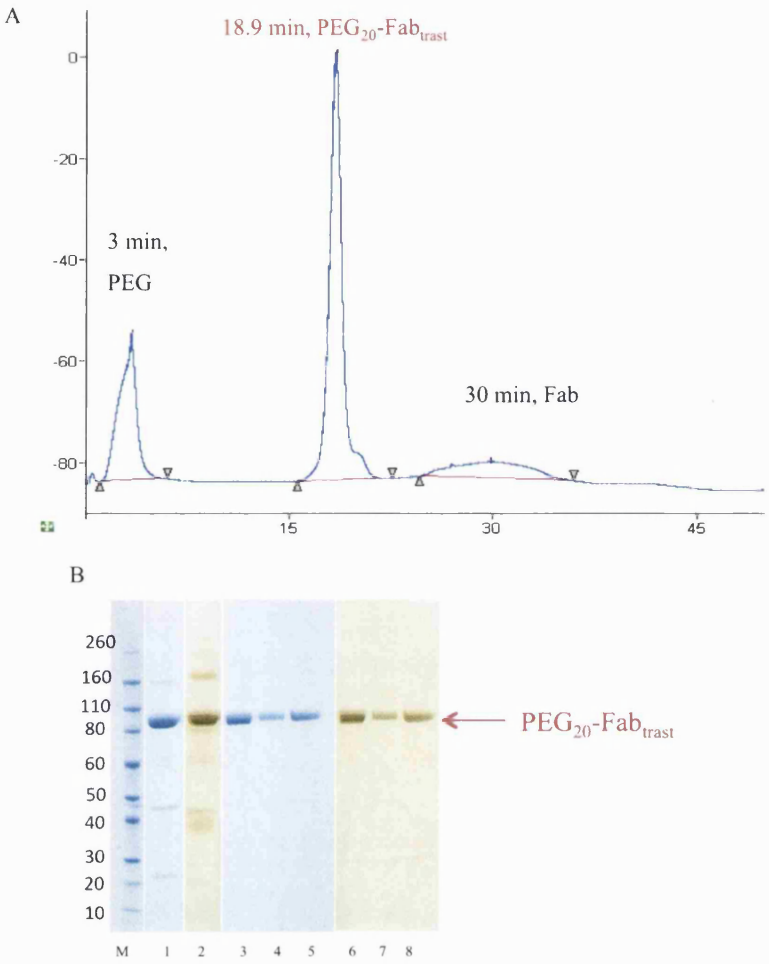

Figure 3.34 IEX-SPHP chromatogram **(A)** and SDS-PAGE **(B)** of IEX fractions of 20 kDa PEG-Fab_{trast}, Novex Bis-Tris 4-12% gel stained with colloidal blue (Lanes M-1, 3-5) and barium iodide (Lanes 2, 6-8). *Lane M:* Standard protein marker, *Lanes 1, 2:* The PEGylation of Fab_{trast} (20 kDa, 2.0 eq PEG) reaction mixture before IEX, *Lanes 3, 6:* IEX fraction at 19 min, *Lanes 4, 7:* IEX fractions at 18 min, *Lanes 5-8:* combined IEX fractions of 18 and 19 min.

3.1.5 PEGylation of Fab_{rani}

Ranibizumab is supplied in vials at a concentration of 10 mg/mL in a total volume of 0.23 mL. To compare the PEGylation of Fabs derived from monoclonal antibodies (bevacizumab and trastuzumab) and their PEGylation conversion, this clinically used Fab_{rani} was also PEGylated. Since the binding affinity of Fab_{rani} to VEGF was reported to be improved compare to Fab-bevacizumab, it was important to study the difference between binding affinity of the PEGylated Fab_{rani} and PEGylated Fab_{beva}. It was important to determine what was the relative loss of binding affinity for these two Fabs. It was expected that each Fab would show the same relative decrease in binding affinity

after PEGylation. The PEG mono-sulfone reagent **2** (20 kDa) was again used. Since Fab_{rani} is administered to the back of the eye by intravitreal injection, each dose is very small (0.05 mL). Each vial of Fab_{rani} contains 2.3 mg Fab_{rani} with the average cost of 1026 £ in the U.K. [242]. For this study, Fab_{rani} was donated from Moorfields eye hospital which was a collection of the left over ranibizumab in the void volume of the needle after injection to the patient. The void volume in the needle was approximately 0.02 mL and the left over solution was approximately 0.1 mL in the vial. So that many needles and left over solution in the vial had to be collected in order to have enough ranibizumab to conduct PEGylation. We eventually collected approximately 15 mL ranibizumab for this study from left over solution and needle.

Ranibizumab which for the sake of consistency will be called Fab_{rani} was PEGylated by the same process as the two Fabs from the digested antibodies. To prepare a 1 mL volume Fab_{rani} at a concentration of 1.0 mg/mL, a 0.1 mL aliquot of the collected Fab_{rani} (10 mg/mL) was added to 0.9 mL of PBS. To verify the concentration, an absorbance of 1.4 was calculated by UV at 280 nm for this solution which corresponded to 1.0 mg/mL Fab solution. Next the interchain disulfide was reduced with DTT, which was then removed by PD-10 column and then 2 equivalents of the PEG mono-sulfone **2** (3.0 mg/mL, 20 kDa) was used. The PEGylation reaction mixture was then incubated for 3.0 h at ambient temperature and the course of the conjugation was followed by SDS-PAGE (Figure 3.35, A, Lanes 3 and 4). The PEGylation conversion of Fab_{rani} was again similar to the PEGylation conversion of Fab_{beva} and Fab_{trast} based on observation in SDS-PAGE (Figure 3.35, A, Lanes 3 and 4). The mono PEG-Fab_{rani} was then purified using a single IEX-SPHP chromatography step as was done to purify PEG-Fab_{beva} and PEG-Fab_{trast}. Figure 3.35, B shows the IEX chromatogram for the purification of PEG_{20}-Fab_{rani}. IEX peak at 21 min appeared at 90 kDa molecular weight band in SDS-PAGE (Figure 3.35, A, Lanes 5 and 6). IEX fractions from 19-21 min were pooled (Figure 3.35, A, Lanes 5, 6,) and concentrated using vivaspin (4 min, 4000 x g) to 1.0 mL solution.

The PEG-Fab_{rani} was then buffer exchanged to PBS using Nap-10 column to be stored at 4 ^{0}C. The concentration of PEG_{20}-Fab_{rani} was then calculated using micro BCA assay with Fab_{rani} used to make a standard curve. A total of 0.67 mg of PEG_{20}-Fab_{rani} was purified from PEGylation of 1.0 mg Fab_{rani}. This resulted in 67 % isolation yield for PEG-Fab_{rani}. This yield of isolation for PEG_{20}-Fab_{rani} (67 %) was similar to the yields obtained for PEG-Fab_{trast} (65 %) and PEG-Fab_{beva} (66 %). The PEGylation of Fab_{rani}

and purification of PEG_{20}-Fab_{rani} was performed 7 times resulting in an approximate similar yield for all the reactions.

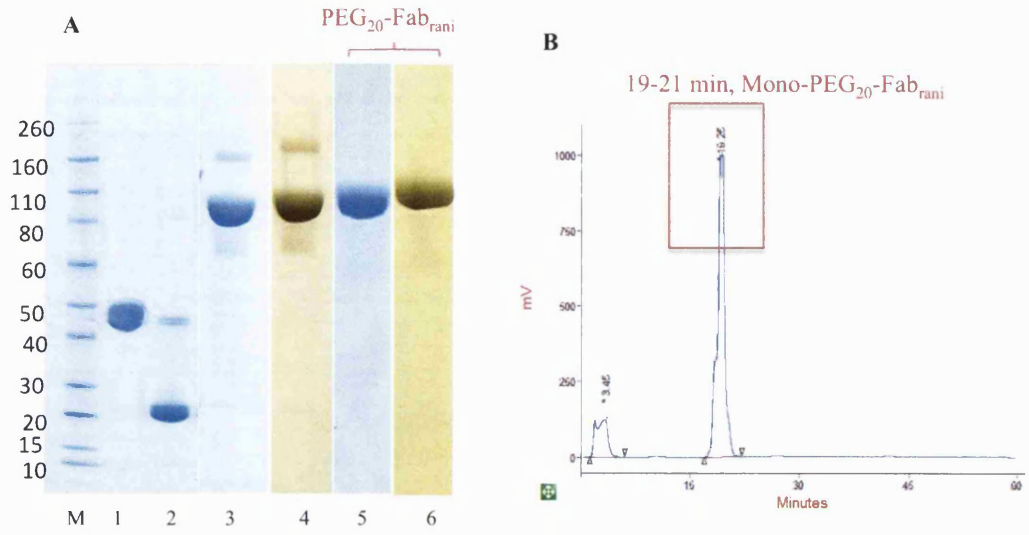

Figure 3.35 SDS-PAGE gel of PEGylation of Fab_{rani} and IEX purification of PEG_{20}-Fab_{rani}, Novex Bis-Tris 4-12% gel stained with colloidal blue (Lanes M-3, 4), barium iodide (Lanes 4, 6). **(A)** *Lane M:* Protein standard, *Lane 1:* Fab_{rani} (1.0 mg/mL). *Lane 2:* Fab_{rani} treated with DTT (1.0 mg/mL). *Lanes 3, 4:* Reaction mixture of PEGylated-Fab (2.0 eq, 20 kDa PEG). *Lanes 5, 6:* The IEX purified PEG_{20}-Fab_{rani}, **(B)** IEX chromatogram of PEGylated Fab_{rani} using SPHP-IEX (1.0 mL) column.

3.1.6 PEGylation of bevacizumab

It was thought that PEG-$F(ab)_2$ could be made by first PEGylating the full antibody, bevacizumab followed by proteolytic digestion with the IdeS enzyme. It would also be interesting to determine if the PEG-Fab_{beva} could also be analogously produced by proteolytic digestion of PEG-bevacizumab using papain. This experiment approach would allow a comparison of the different steps in (i) PEGylation, (ii) digestion and (iii) purification.

Generally IgG1 antibodies have 4 interchain and 12 intrachain disulfide bonds that are associated with 12 individual domains [13]. The presence of the intrachain disulfide bonds are critical for stability and biological activity of the IgG [243]. The interchain disulfide bonds are more accessible than 12 intrachain disulfide and they are more susceptible to reduction [243]. Moreover, this susceptibility of the disulfide bonds to reduction is different for IgG1κ compared to IgG1λ [243]. Bevacizumab is IgG1κ. It has been suggested that the Fab interchain disulfide bond in IgG1λ is more susceptible to reduction than the interchain hinge disulfide bonds, and the upper disulfide bond

located in hinge region is more susceptible to reduction than the lower one of the hinge [243]. This difference between the susceptibility of the Fab interchain disulfide bond and the hinge interchain disulfide bond to reduction, however, was not suggested for IgG1κ and a random reduction of the interchain disulfide bonds may result in IgG1κ.

To evaluate the potential for selective reduction and examine the susceptibility of the four interchain disulfide bonds in bevacizumab, TCEP, 2-MEA and DTT were used to reduce interchain disulfide bonds. It was thought that by using small amounts of different reducing agents of varying strengths, it would be possible to reduce one of the disulfide bonds and then mono PEGylated bevacizumab.

Bevacizumab was first treated with different stoichiometries of TCEP (1-24 eq) in the presence of selenocystamine. TCEP reduction was evaluated at two time points (15 min and 12 h) at two temperatures (ambient and 4 ^{0}C). It was first thought to incubate bevacizumab with TCEP for only 15 min at ambient temperature would be enough to reduce the accessible disulfide [244]. However, most of the bevacizumab remained intact when treated with TCEP (1-10 eq) at ambient temperature (Figure 3.36) for 15 min. Two main bands appeared at about 25 kDa and 100 kDa molecular weight marker in Figure 3.36. The band at 25 kDa was thought to be the free light chain (Scheme 3.3, E). The second band at about 100 kDa (Figure 3.36) was thought to be a heavy-heavy chains that were connected by the hinge disulfide bonds (Scheme 3.3, B) while the interchain disulfide bond between light and heavy chains were both reduced. Since there was not a good reduction after 15 min incubation with TCEP (1-10 eq), it was then decided to incubate for a longer period at 4 ^{0}C to examine whether disulfide reduction could be increased (Figure 3.37). Increasing the reduction time between bevacizumab and TCEP appeared to reduce bevacizumab to give more of the light chains (25 kDa) and heavy-heavy chain (100 kDa). The new band at 75 kDa appeared when TCEP (4-6 eq) with longer reduction time applied (Figure 3.37, Lanes 5-8). This band was thought to be a fragment C in Scheme 3.3 which reduction of the hinge interchain disulfide bonds in bevacizumab. These results suggested that to reduce the hinge interchain disulfide bonds of bevacizumab, longer incubation times with TCEP (4-6 eq) or applying greater amount of TCEP was required (Figure 3.38, Lanes 4 and 5). The Fab interchain disulfide bond was first reduced with 3 equivalent of TCEP in 15 min before hinge disulfides (Figure 3.37, Lane 4).

The presence of selenocystamine during reduction did not appear to influence on the reduction process (Figure 3.36, Lanes 7-11). Therefore, it was decided not to use selenocystamine for TCEP based reductions of bevacizumab. Increasing the amount of TCEP to 12 and 24 equivalents at ambient temperature in 15 min appeared to reduce more of bevacizumab to give more of the band at 75 kDa molecular weigh marker (Figure 3.38, Lanes 4 and 5).

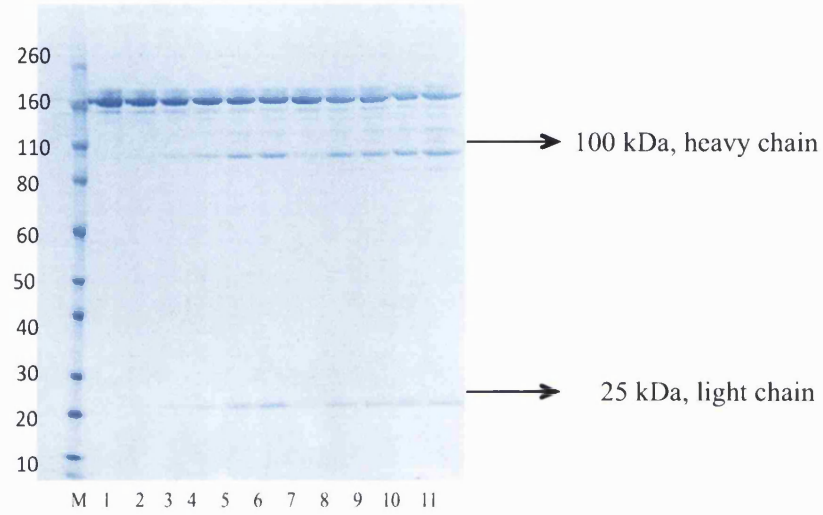

Figure 3.36 SDS-PAGE gel of a reduction of bevacizumab using TCEP after 15 min incubation at ambient temperature, Novex Bis-Tris 4-12% gel stained with colloidal blue (Lanes M-11), *Lane M:* Protein standards, *Lane 1:* bevacizumab, *Lane 2:* Reduced-bevacizumab with 1.0 eq TCEP, no Se. *Lane 3:* Reduced-bevacizumab with 2.0 eq TCEP, no Se. *Lane 4:* Reduced-bevacizumab with 4.0 eq TCEP, no Se. *Lane 5:* Reduced-bevacizumab with 8.0 eq TCEP, no Se. *Lane 6:* Reduced-bevacizumab with 10.0 eq TCEP, no Se. *Lane 7:* Reduced-bevacizumab with 1.0 eq TCEP, 0.1 eq Se. *Lane 8:* Reduced-bevacizumab with 2.0 eq TCEP, 0.2 eq Se. *Lane 9:* Reduced-bevacizumab with 4.0 eq TCEP, 0.4 eq Se. *Lane 10:* Reduced-bevacizumab with 8.0 eq TCEP, 0.8 eq Se. *Lane 11:* Reduced-bevacizumab with 10.0 eq TCEP, 1.0 eq Se.

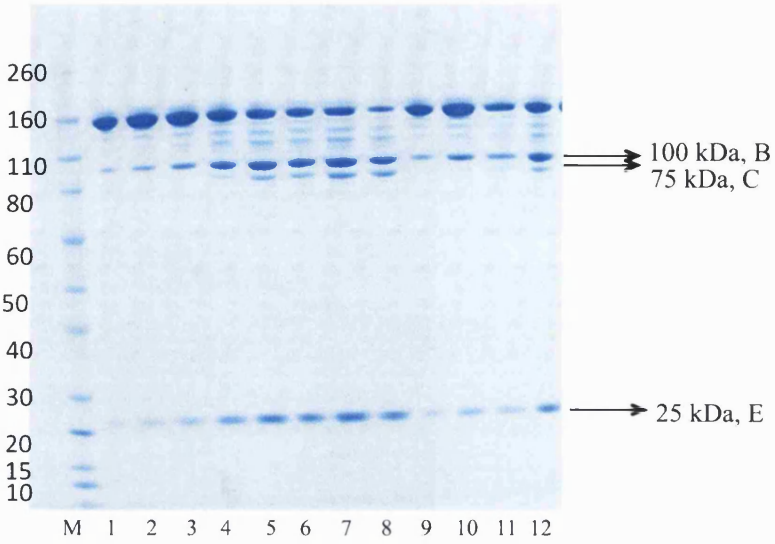

Figure 3.37 SDS-PAGE gel of a reduction of bevacizumab using TCEP after 12 h incubation at 4 ^{0}C, Novex Bis-Tris 4-12% gel stained with colloidal blue (Lanes M-12), *Lane M:* Protein standards, *Lane 1:* Reduced-bevacizumab with 1.0 eq TCEP, *Lane 2:* Reduced-bevacizumab with 1.5 eq TCEP, no Se. *Lane 3:* Reduced-bevacizumab with 2.0 eq TCEP, no Se. *Lane 4:* Reduced-bevacizumab with 3.0 eq TCEP, no Se. *Lane 5:* Reduced-bevacizumab with 4.0 eq TCEP, no Se. *Lane 6:* Reduced-bevacizumab with 4.5 eq TCEP, no Se. *Lane 7:* Reduced-bevacizumab with 5.0 eq TCEP, no Se. *Lane 8:* Reduced-bevacizumab with 6.0 eq TCEP, no Se. *Lane 9:* Reduced-bevacizumab with 1.0 eq TCEP, 0.1 Se. *Lane 10:* Reduced-bevacizumab with 2.0 eq TCEP, 0.2 eq Se. *Lane 11:* Reduced-bevacizumab with 4.0 eq TCEP, 0.4 eq Se. *Lane 12:* Reduced-bevacizumab with 5.0 eq TCEP, 0.5 eq Se.

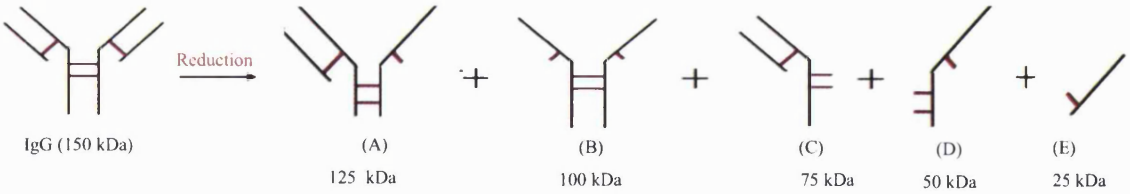

Scheme 3.3 The possible peptide fragments after reduction of interchain disulfide bonds of bevacizumab.

While addition of 24 equivalents of TCEP resulted in more reduction of hinge interchain disulfide bonds, no selective reduction was observed to generate fragments such as A, B or C Scheme 3.3. These experiments suggested that interchain disulfide bond of the Fab in bevacizumab is more susceptible to reduction than hinge interchain disulfide bond. But it was difficult to control the reduction to only a single interchain disulfide bond at the Fab or hinge disulfide bond. This proposed that as the first disulfide is reduced in bevacizumab, the antibody becomes more susceptible to

reduction. The reduction of the second disulfide may be faster than the first disulfide. This may be due to an increase in conformational mobility as disulfides are reduced.

While presence of TCEP could compete with PEGylation of thiols with the PEG mono-sulfone reagent **2**, PEGylation was conducted after treatment of bevacizumab with TCEP (6, 12 and 24 equivalents). After the bevacizumab was allowed to undergo reaction with TCEP for 15 min, 4 equivalents of the PEG mono-sulfone reagent **2** (10 kDa, 3.0 mg/mL) was added. The PEGylation process was evaluated after 3.0 h incubation time at ambient temperature by SDS-PAGE (Figure 3.39, Lanes 6-8). While two new products appeared to have formed, most of reduced bevacizumab was re-oxidised as a result of consumption of most of the PEG reagent by TCEP. The major product appeared to be just above the starting bevacizumab. A second band appeared at above the product band. The band above the bevacizumab in SDS-PAGE gel (Figure 3.39, Lanes 6-8) was thought to be mono PEGylated bevacizumab with an apparent molecular weight of 170 kDa. When one PEG molecule (10 kDa) conjugated to bevacizumab with 150 kDa, it would contribute an apparent molecular weight of 20 kDa (i.e. 2 × 10 kDa apparent molecular weight) to the 170 kDa band. This one molecule of PEG reagent **2** could be conjugated to either free thiols in the Fab region or free thiols in hinge region, since fragments B, C and E (Scheme 3.3 and Scheme 3.4) were present in the reduced-bevacizumab solution. If PEG molecule conjugate to free thiols in hinge region of one heavy chain a band at 95 kDa was expected to appear in SDS-PAGE gel (Scheme 3.4). However, no band at about 95 kDa was observed. There is also a possibility for the PEG reagent **2** to conjugate to one cysteine from one heavy chain in the hinge region and then bridge with another free cysteine of the second heavy chain and results in 170 kDa band in SDS-PAGE (Scheme 3.4). While mono PEGylated bevacizumab was produced, the PEGylation conversion was not good because of the presence of unreacted TCEP in the solution which compete with PEGylation.

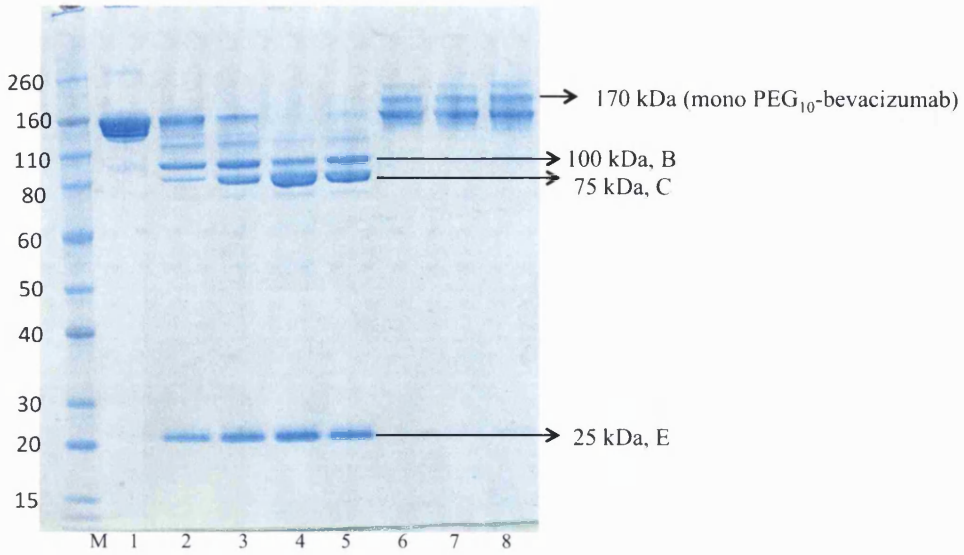

Figure 3.38 SDS-PAGE gel of reduction and PEGylation of bevacizumab using TCEP (3, 6, 12 and 24 eq) without selenocystamine and 10 kDa PEG reagent 2 (4 eq), Novex Bis-Tris 4-12% gel stained with colloidal blue (Lanes M-8). *Lane M:* protein standards, *Lane 1:* Bevacizumab 0.25 mg/ml, *Lane 2:* Reduced-bevacizumab with 3 eq TCEP, *Lane 3:* Reduced-bevacizumab with 6 eq TCEP, *Lane 4:* Reduced-bevacizumab with 12 eq TCEP, *Lane 5:* Reduced-bevacizumab with 24 eq TCEP, *Lane 6:* PEGylation reaction of bevacizumab after 6 eq TCEP with PEG molecule (10 kDa, 4eq), *Lane 7:* PEGylation reaction of bevacizumab after 12 eq TCEP with PEG molecule (10 kDa, 4eq), *Lane 8:* PEGylation reaction of bevacizumab after 24 eq TCEP with PEG molecule (10 kDa, 4eq).

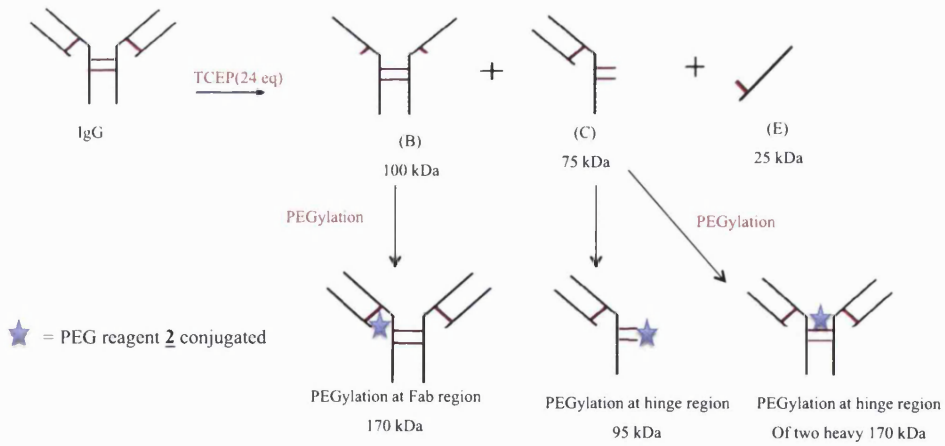

Scheme 3.4 The possible mono PEGylated peptide fragment of bevacizumab using 10 kDa PEG mono-sulfone reagent **2**.

It was suggested [245] that 2-MEA would selectively reduce the hinge disulfide bond of IgG1 and produce only 75 kDa reduced-fragment (Scheme 3.5). Incubation times of 30, 60 and 90 mins at 37 ^{0}C were examined using an excess of 2-MEA (6.0 mg) with 1.0 mg of bevacizumab (1.0 mL). While the hope was to reduce the hinge disulfides, no reduction was observed at hinge disulfides under these conditions (Figure

3.39, Lanes 1-3).

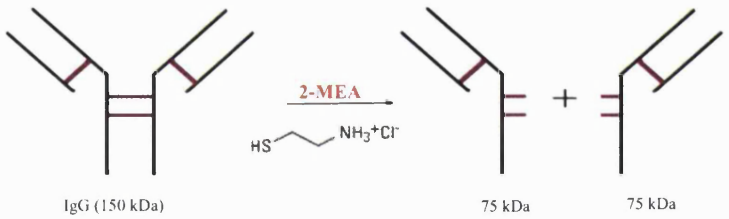

Scheme 3.5 Proposed selective reduction of interchain disulfide bonds in the hinge of IgG with 2-MEA.

Instead, the interchain disulfide bond between light and heavy chain was reduced and resulted in two main bands at about 25 kDa and 100 kDa (Figure 3.39, Lanes 1-3). The band at 100 kDa, was thought to be fragment B in Scheme 3.3.

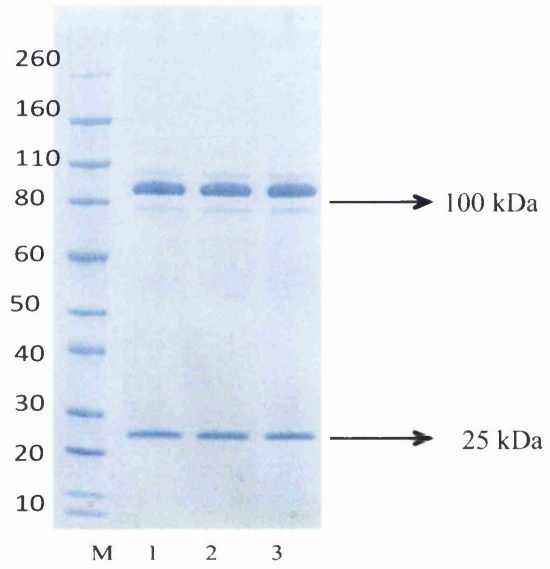

Figure 3.39 SDS-PAGE gel of reduction of bevacizumab using 2-MEA at 30, 60 and 90 min, Novex Bis-Tris 4-12% gel stained with colloidal blue (Lanes M-3), *Lane M:* Protein standards, *Lane 1:* Reduced-bevacizumab with 2-MEA after 30 min at 37 ^{0}C, *Lane 2:* Reduced-bevacizumab with 2-MEA after 60 min at 37 ^{0}C. *Lane 3:* Reduced-bevacizumab with 2-MEA after 90 min at 37 ^{0}C.

After elution over a PD-10 column to remove 2-MEA, 4 equivalents of 10 kDa PEG mono-sulfone reagent **2** was added. No PEGylation was observed and bevacizumab remained in reduced form in the gel. One explanation is that 2-MEA was not removed by PD-10. It may have been possible that the light and heavy chains of the reduced bevacizumab were dissociated from each other as a result of the need to conduct the reduction at 37 ^{0}C. While PD-10 in principle should remove 2-MEA in a

similar way as DTT, other desalting column such as Zeba desalt spin column was also examined. However, no PEGylation was observed using Zeba desalting column. It was thought that probably the light and heavy chains of bevacizumab were dissociated during reduction with 2-MEA at 37 ^{0}C. It was then decided to use DTT to partially reduce interchain disulfide bonds as was used for Fab_{beva} and $F(ab)_2$.

Bevacizumab (1.25 mg/mL) was then decided to treat with DTT. Once DTT was removed by PD-10 column, PEGylation scouting experiments were conducted using different stoichiometric amounts of the PEG reagent **2** (1, 2 and 4 equivalents, 10 kDa). It was possible to reduce interchain disulfide bond in the Fab and hinge region by DTT similar to what was observed with $F(ab)_2$ treated with DTT. Hence, PEGylation can occur at the Fabs free thiols and the hinge thiols leading to different isomers of PEGylated bevacizumab. To purify a mono PEGylated bevacizumab from other isomers of PEG-bevacizumab SEC followed IEX purification was performed. In contrast with purification of PEG-Fabs, the purification of mono PEG-bevacizumab was first conducted by SEC as a means to separate high molecular weight PEG-bevacizumab isomers (tetra, tri) from di and mono PEG-bevacizumab. Using IEX on SEC purified fraction allowed separation of mono from di PEG-bevacizumab.

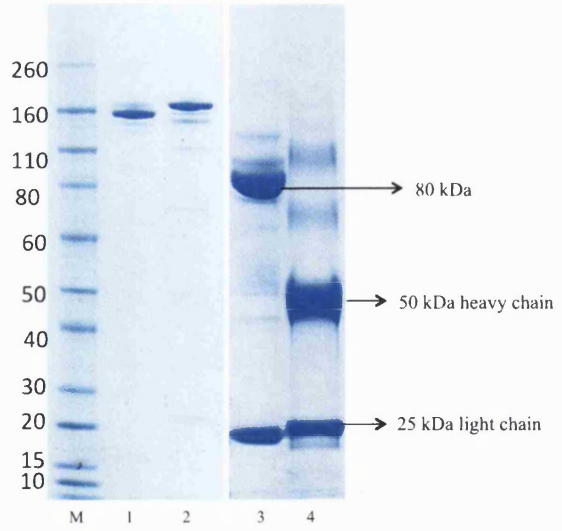

Figure 3.40 SDS-PAGE gel of DTT reduction of bevacizumab. Novex Bis-Tris 4-12% gel stained with colloidal blue (Lanes M-4), *Lane M:* Protein standards, *Lane 1:* Bevacizumab, *Lane 2:* Bevacizumab treated with SDS and heated for 10 min at 80 ^{0}C, *Lane 3:* Bevacizumab treated with DTT, *Lane 4:* Bevacizumab treated with DTT and then treated with SDS and heated for 10 min at 80 ^{0}C.

Complete reduction of interchain disulfide bonds of bevacizumab was expected to result in two heavy and two light chains, each 50 kDa and 25 kDa respectively (Scheme 3.6). However, result in Figure 3.40, Lane 3 indicates two bands at approximate 80 kDa and 25 kDa molecular weight marker for bevacizumab treated with DTT. The band at about 80 kDa could not be any reduce peptide fragment in Scheme 3.3 apart from fragments C or D.

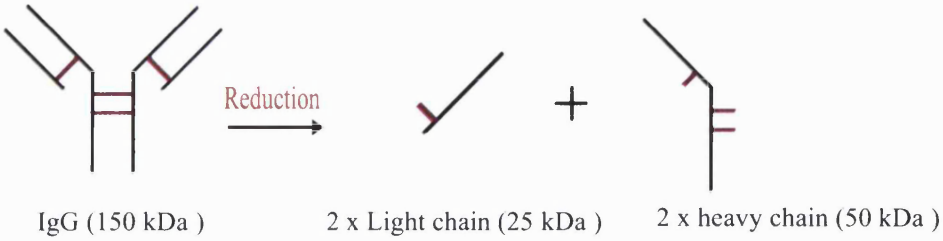

Scheme 3.6 Complete reduction of bevacizumab using DTT.

To evaluate which fragment was generated from bevacizumab by DTT, it was thought to treat the reduced-bevacizumab with SDS and heat at 80 ^{0}C for 10 min. It would be possible the disulfide bonds in the hinge are in reduced form, but heavy-heavy chains do not dissociate in SDS-PAGE due to their strong hydrophobic interaction and appeared at about 80-100 kDa band in SDS-PAGE. Applying heat to the reduced-bevacizumab in the presence of SDS ensured that the hydrophobic interactions were disrupted. This resulted in two separate heavy chains at 50 kDa (Figure 3.40, Lane 4). As a control, non-reduced bevacizumab was also treated with SDS and heated at 80 ^{0}C for 10 min (Figure 3.40, Lane 2). Because the interchain disulfide bonds were not in reduced, no 50 and 25 kDa band were observed and only hydrophobic interaction between heavy-heavy and heavy-light chains cleaved and caused in a slight decrease in migration of bevacizumab to a higher molecular weight (Figure 3.40, Lane 2).

Addition of 1, 2 and 4 equivalents of the PEG mono-sulfone reagent **2** resulted in different multiple PEGylated species after 3 h incubation at ambient temperature (Figure 3.41, Lanes 3-5).

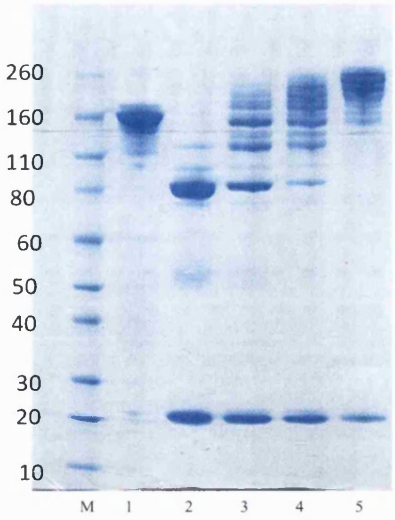

Figure 3.41 SDS-PAGE gel of PEGylation of bevacizumab after treatment with DTT (6 mM). Novex Bis-Tris 4-12% gel stained with colloidal blue (Lanes M-6), *Lane M:* Protein standards, *Lane 1:* Bevacizumab, *Lane 2:* Reduced-bevacizumab using DTT, *Lane 3:* The PEGylation reaction mixture of bevacizumab using 1 equivalent PEG, *Lane 4:* The PEGylation reaction mixture of bevacizumab using 2 equivalents PEG, *Lane 5:* The PEGylation reaction mixture of bevacizumab using 4 equivalents PEG.

Using 4 equivalents of the PEG reagent **2** appeared to give more multiple PEGylated species. This PEGylation reaction mixture was then purified by SEC (Figure 3.42) followed by IEX chromatography. SEC fractions (58-60 min) appeared at the band about 170-180 kDa molecular weight marker (Figure 3.43, Lanes 10-12) was thought to be di and mono PEGylated bevacizumab. SEC fractions at 48-52 min was thought to be a higher isomer of PEGylation of bevacizumab as three or four PEG molecules were conjugated and eluded earlier from SEC column (Figure 3.43, Lanes 2-8). To separate mono from di PEGylated bevacizumab, IEX was performed on the purified SEC fractions (58-60 min). Before loading to IEX, these SEC fractions were concentrated by viva-spin (3 min, 4000 x g) to 1.0 mL solution in order to be applicable to buffer exchanged with IEX-buffer A (pH 4.0) using Nap-10 column. The 1.5 mL solution after Nap-10 column was then loaded onto SPHP-IEX column (Figure 3.44, A).

The IEX peak at 21 min was thought to be a mono PEG_{10}-bevacizumab as it appeared as a band at about 170 kDa, slightly above bevacizumab band in SDS-PAGE (Figure 3.44, B, Lane 5). The di PEG-bevacizumab appeared at the band slightly above the mono PEG-bevacizumab (Figure 3.44, B, Lane 4). As expected, di PEG-bevacizumab eluted with a lower concentration of salt in buffer B than mono PEG-

bevacizumab.

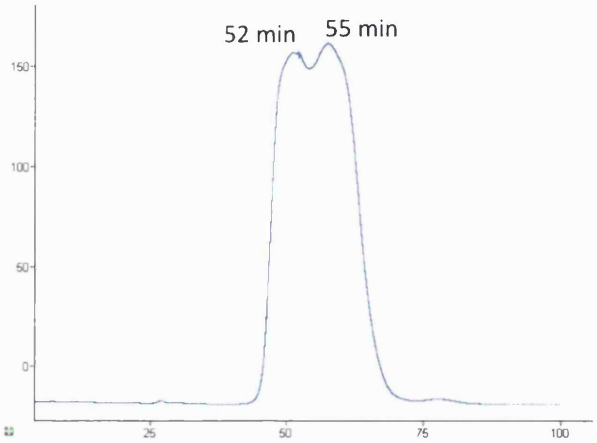

Figure 3.42 SEC chromatogram of PEGylated bevacizumab.

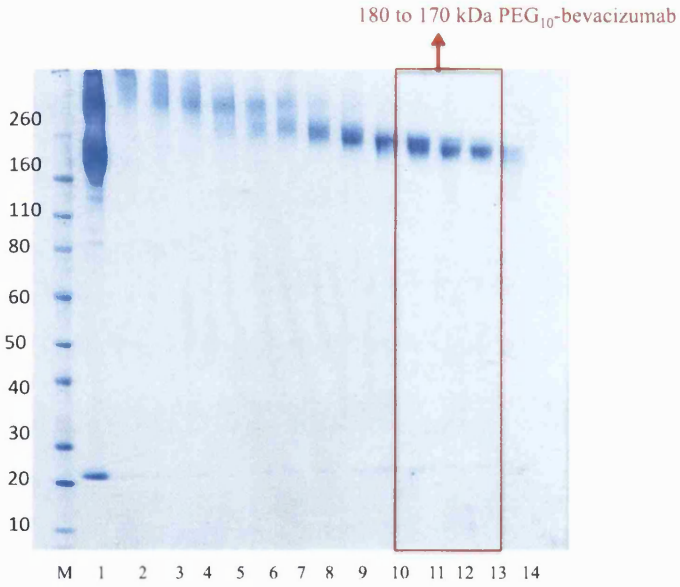

Figure 3.43 SDS-PAGE gel of SEC fractions of PEGylation of bevacizumab. Novex Bis-Tris 4-12% gel stained with colloidal blue (Lanes M-14), *Lane M:* Protein standards, *Lane 1:* The PEGylation of bevacizumab reaction mixture (4eq, 10 kDa PEG) before SEC, *Lane 2*: SEC fraction at 48 min, *Lane 3:* SEC fraction at 49 min, *Lane 4:* SEC fraction at 50 min, *Lane 5:* SEC fraction at 51 min, *Lane 6:* SEC fraction at 52 min, *Lane 7:* SEC fraction at 53 min, *Lane 8:* SEC fraction at 54 min, *Lane 9:* SEC fraction at 55 min, *Lane 10:* SEC fraction at 57 min, *Lane 11:* SEC fraction at 58 min, *Lane 12*: SEC fraction at 60 min, *Lane 13:* SEC fraction at 61 min, *Lane 14:* SEC fraction at 65 min.

The IEX fraction at 21 min was then considered as a mono PEG_{10}-bevacizumab. The silver staining performed on this IEX fraction (Figure 3.44, C, Lane 4) suggested that a pure mono PEG_{10}-bevacizumab had been isolated. The purified PEG-

bevacizumab was buffer exchanged to PBS (pH 7.4) using Nap-10 column for long-term storage at 4 ^{0}C. Using micro-BCA assay, the concentration of the purified PEG_{10}-bevacizumab was then calculated. Bevacizumab was used as a standard to make a calibration curve and a concentration of 0.193 mg/mL (1.0 mL) was obtained for PEG_{10}-bevacizumab. The isolation yield for mono PEG_{10}-bevacizumab was about 15.4 % as 0.193 mg PEG_{10}-bevacizumab was obtained from starting 1.25 mg bevacizumab. The lower yield of PEG_{10}-bevacizumab was primarily due to the need to use two purification steps and the fact that multiple PEGylation products could be produced. The PEGylation and purification of bevacizumab using these conditions was performed 5 times with similar yields being obtained.

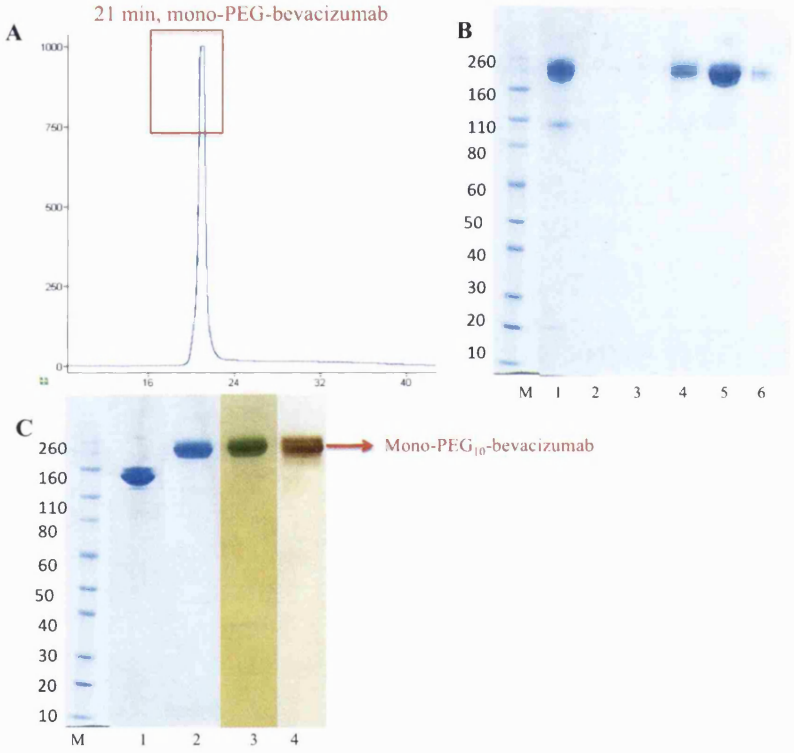

Figure 3.44 (A) IEX-SPHP purification on SEC fractions of PEGylated bevacizumab, **(B)** and **(C)** SDS-PAGE gel of IEX fractions of PEGylated bevacizumab. **(B)** Novex Bis-Tris 4-12% gel stained with colloidal blue (Lanes M-6), barium iodide **(C,** Lane 3**)** and silver staining **(C,** Lane 4**)**. **(B)** *Lane M:* Protein standards, *Lane 1:* Pooled SEC fraction of PEGylated bevacizumab before IEX, *Lane 2:* IEX fraction at 18.5 min, *Lane 3:* IEX fraction at 19 min, *Lane 4:* IEX fraction at 20 min, *Lane 5:* IEX fraction at 21 min, *Lane 6:* IEX fraction at 21.5 min. **(C)** *Lane 1:* Bevacizumab, *Lanes 2, 3 and 4:* The purified PEG_{10}-bevacizumab.

To proteolytically digest PEG-bevacizumab, it was incubated with the IdeS enzyme. In a first attempt, the digestion was performed on PEG-bevacizumab, using 1.77 µL of IdeS enzyme to 0.118 mg in 1.0 mL PEG-bevacizumab and 30 min incubation at 37 ^{0}C. The digestion mixture was then evaluated using SDS-PAGE. Results in SDS-PAGE gel showed no band related to PEG-F(ab)$_2$, however, the F(ab)$_2$ itself could be obtained. It was then thought that the conjugation of PEG mono-sulfone reagent **2** to bevacizumab might not be stable enough at this condition and during digestion with IdeS enzyme it was dissociated. It was then decided to treat the PEG$_{10}$-bevacizumab with sodium triacetoxyborohydride (which is less toxic than $NaBH_4$) before digestion. In principle, sodium borohydride ($NaBH_4$) converts selectively aldehyde and ketone group to alcohol group [246]. It has no influence on ester and amide moieties in a molecule. So, it acts as a source of hydride to reduce the ketone group on the PEG linker conjugated to protein and convert a ketone to an alcohol which is more stable in the basic environment. So that, this reagent can be used to stabilize the conjugation of PEG reagent **2** to the protein. The PEG$_{10}$-bevacizumab (0.2 mg/mL) was treated with sodium triacetoxyborohydride (25 mM) and incubated for 1.0 h at 4 ^{0}C. Then, this sultion was buffer exchanged to sodium phosphate buffer (20 mM) EDTA (10 mM), pH 7.4 using Nap-10 desalting column to remove an excess $NaBH_4$. Then, 1.8 µL IdeS enzyme was added and incubated at 37 ^{0}C for 30 min. The digestion solution was then evaluated by SDS-PAGE (Figure 3.45). Results showed that the digestion did not occur and even no F(ab)$_2$ fragment produced. While a small amount of bevacizumab was observed at 150 kDa molecular weight marker in SDS-PAGE (Figure 3.45, Lanes 2 and 3), the majority of PEG-bevacizumab remained intact. The reason could be the interference of the conjugated-PEG which might prevent interaction of the IdeS at the proteolytic site in bevacizumab.

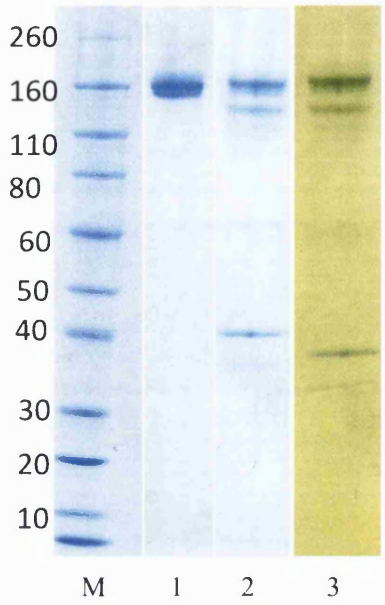

Figure 3.45 SDS-PAGE analysis of digestion of the purified PEG_{10}-bevacizumab after $NaBH_4$ treatment using IdeS enzyme. Novex Bis-Tris 4-12% gel stained with colloidal blue (Lanes M-2) and barium iodide staining (Lane 3), *Lane M:* Protein standards, *Lane 1:* The purified PEG_{10}-bevacizumab after $NaBH_4$ treatment, *Lanes 2 and 3:* The digestion mixture of PEG-bevacizumab using IdeS enzyme.

Immobilised papain was also examined to determine if PEG-bevacizumab could be proteolytically digested. Limitation for this approach included decrease proteolysis and the potential to produce multiple PEGylated species along with un-PEGylated fragments. SDS-PAGE analysis on papain digestion mixture of PEG_{10}-bevacizumab (Figure 3.46, Lane 2) suggested that PEG-Fab could be obtained by this method, however, the yield appeared to be low. The protein A column was used to purify the PEG-Fab_{beva} from digestion mixture. But a mixture of the Fab_{beva} and the PEG-Fab_{beva} were eluted from a protein A column (Figure 3.46, Lane 3). The yield of the purified PEG-Fab_{beva} was quite low (less than 10 %) based on observation on SDS-PAGE, compared with the directly PEGylation of Fab_{beva}.

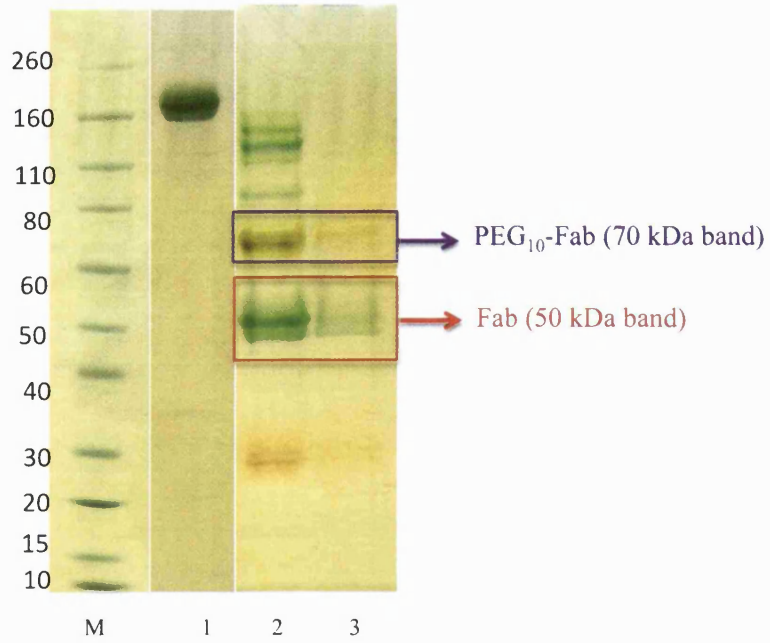

Figure 3.46 SDS-PAGE gel of digestion and purification of PEG_{10}-bevacizumab using immobilised papain. Novex Bis-Tris 4-12% gel stained with barium iodide staining (Lanes M-3), *Lane M:* Protein standards, *Lane 1:* The purified PEG_{10}-bevacizumab, *Lane 2:* The digestion mixture of PEG-bevacizumab using immobilised papain before protein A purification, *Lane 3:* The first fraction of digested PEG-bevacizumab after protein A purification.

3.1.7 PEGylation of trastuzumab

Exploratory experiments were also conducted to PEGylate trastuzumab using PEG mono-sulfone reagent **2**. Trastuzumab (1.25 mg/mL) first treated with DTT (6 mM, 1.0 mg/mL) again to accomplish the full interchain disulfide reduction. Excess DTT was again removed using a PD-10 column. Scouting PEGylation reactions of trastuzumab were then conducted using PEG mono-sulfone reagent **2** (1, 2 and 4 eq, 10 kDa). Reactions were incubated for 3 h at ambient temperature. The PEGylation reaction was then evaluated by SDS-PAGE (Figure 3.47, Lanes 3-5).

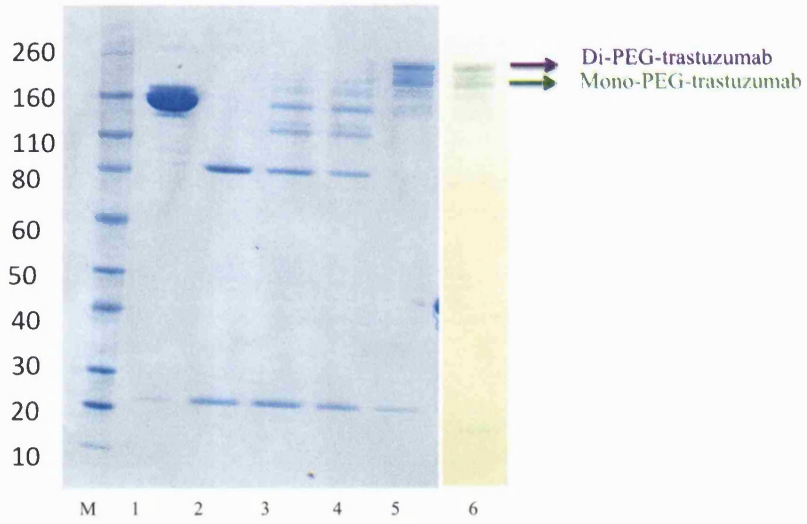

Figure 3.47 SDS-PAGE gel of PEGylation of trastuzumab. Novex Bis-Tris 4-12% gel stained with colloidal blue (Lanes M-5) and barium iodide staining (Lane 6), *Lane M:* Protein standards, *Lane 1:* Trastuzumab (1.25 mg/mL), *Lane 2:* Trastuzumab treated with DTT (6 mM), *Lane 3:* The PEGylation reaction mixture of trastuzumab (1.0 equivalent of PEG 10 kDa), *Lane 4:* The PEGylation reaction mixture of trastuzumab (2.0 equivalents of PEG 10 kDa), *Lanes 5, 6:* The PEGylation reaction mixture of trastuzumab (4.0 equivalents of PEG 10 kDa).

Using 4 equivalents of PEG reagent **2**, (Figure 3.36, Lanes 5 and 6) suggested that most of the reduced trastuzumab was PEGylated to give mono and di PEG-trastuzumab. Only trace trastuzumab was observed. These observations were consistent for the PEGylation of bevacizumab using the same conditions. However only the di and mono PEG-trastuzumab conjugates were observed. The mono PEG-trastuzumab was then purified from the reaction mixture by IEX chromatography.

3.2 PEGylation of Fabs to produce Fab-PEG-Fab homodimers

Since molecules with lower valence have lower binding affinity towards their targets [157] there was a need to prepare bivalent PEG-Fab conjugates. To address the monovalency limitation of the PEGylated Fabs that had been produced, we used the new bis-alkylation PEG reagent **4** (Figure 3.48). This reagent **4** is similar to the PEG mono-sulfone reagent **2** except there is a conjugations moiety at each end of the PEG molecules. The PEG di(mono-sulfone) reagent **4** is the 'active form' of PEG di(bis-sulfone) reagent **3**. Hence it is susceptible to hydrolysis. The PEG di(mono-sulfone) reagent **4** was prepared to undergo bis alkylation with two reduced-Fabs and generate the Fab-PEG-Fab conjugate (Figure 3.48).

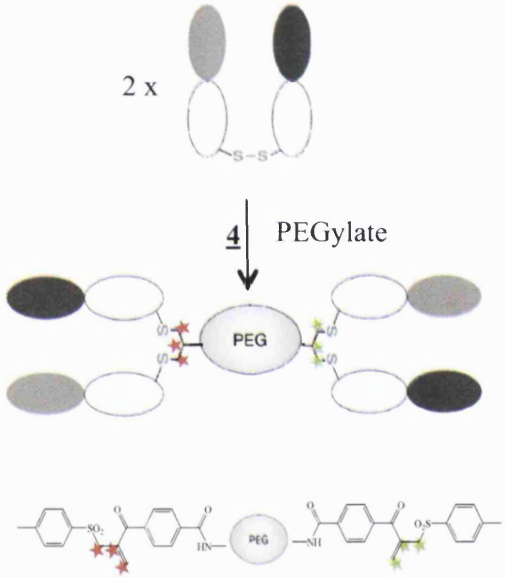

PEG di(mono-sulfone) reagent **4**

Figure 3.48 Homodimer PEGylation of Fab using PEG di(mono-sulfone) reagent **4**.

The pre-activated PEG di(mono-sulfone) reagent **4** was used in an effort to make Fab-PEG-Fab which was provided by PolyTherics company. This PEG reagent was stored as a solid at -20 ^{0}C and dissolved in distilled water at the time of PEGylation, similar to PEG mono-sulfone reagent **2**. The purity of this PEG reagent **4** in solution was approximately 90 % at the time of its synthesis with the remaining amount of material being the PEG di(bis-sulfone) reagent **3** (H-NMR in Appendix I, B). However, it was found that the PEG di(mono-sulfone) **4** further decreased in impurity during storage at -20 ^{0}C and it hydrolysed after some period of time opposite of PEG mono-

sulfone reagent **2**. Therefore there was a variation between PEGylation conversion and isolation yield for preparation of Fab-PEG-Fab. To evaluate structure-property correlations 6, 10 and 20 kDa PEG di(mono-sulfone) reagent **4** was used to make the Fab-PEG-Fab using Fab_{beva} and Fab_{rani}. The 20 kDa reagent **4** was used to make the analogous homodimer from Fab_{trast}.

3.2.1 Preparation of PEG homodimer, Fab-PEG-Fab

The PEGylation was conducted with PEG di(mono-sulfone) reagent **4** in the same way as with PEG mono-sulfone reagent **2**. It was hoped that Fab homodimer PEGylation would be similar to Fab mono-PEGylation, however, there were some concerns. Cyclisation and hydrolysis were the main concerns regarding the PEG di(mono-sulfone) reagent **4**.

The Fab_{beva} (1.0 mg in 1.0 mL) was first treated with DTT (1.0 mg/mL) and excess DTT was removed by PD-10 column (Figure 3.49, Lane 2) as described for mono PEGylation of Fab_{beva}. Theoretically, 0.5 equivalent of PEG di(mono-sulfone) reagent **4** should be enough to conjugate to two Fabs and produce only Fab-PEG-Fab. However, both mono PEG-Fab and the derived homodimer Fab-PEG-Fab were observed (Figure 3.49, Lane 3). The reason for this could be the purity of the PEG reagent **4** that was made and/or because some of the PEG di(mono-sulfone) reagent **4** may have undergone hydrolysis and therefore won't have the active groups at both ends. Also, this reagent could have cyclised after its conjugation to the first Fab_{beva}. This cyclisation prevents conjugation of the second Fab and results in mono PEG-Fab_{beva}. Although, adding 1.0 equivalent of PEG can improve this conversion and produce more of the Fab_{beva}-PEG-Fab_{beva} (Figure 3.49, Lane 4) but still some mono PEG-Fab_{beva} was formed. The band at about 120 kDa in SDS-PAGE gel in Figure 3.49 corresponds to two Fabs conjugated to one PEG (10 kDa). PEG contributes 20 kDa into 120 kDa molecular weight band. Increasing the amount of the PEG reagent **4** (e.g 2.0 equivalents) led to the formation of more of the mono PEG-Fab_{beva} (Figure 3.49, Lane 5). Similar range of PEGylation conversion to Fab-PEG-Fab conjugation was observed when smaller scale of PEGylation conducted with 0.1 mg/mL Fab_{beva}.

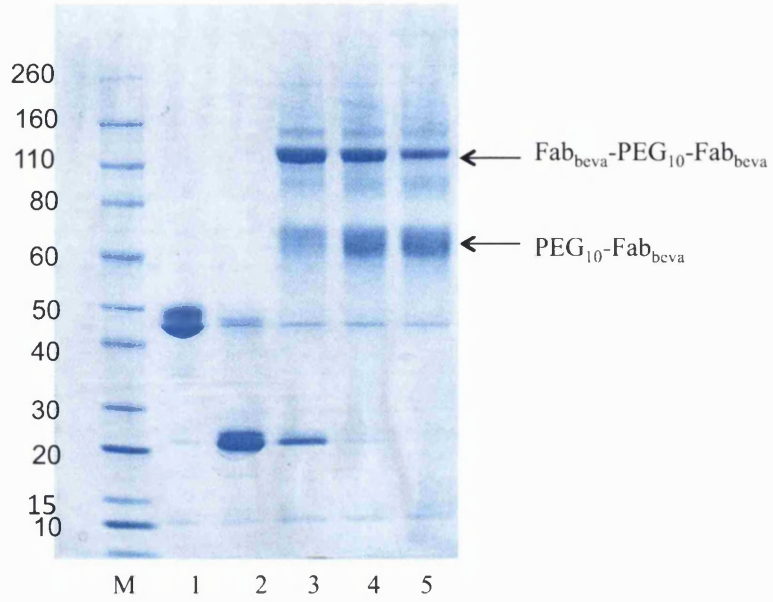

Figure 3.49 SDS-PAGE gel of PEGylation of Fab$_{beva}$ (1.0 mg/mL) using 10 kDa PEG di(mono-sulfone) reagent **4**, Novex Bis-Tris 4-12% gel stained with colloidal blue (Lanes M-5) *Lane M:* Protein standard, *Lane 1:* Fab$_{beva}$. *Lane 2:* Fab$_{beva}$ treated with DTT, *Lane 3:* PEGylation reaction mixture of Fab$_{beva}$ with 10 kDa PEG reagent **4** (0.5 eq), L*ane 4:* PEGylation reaction mixture of Fab$_{beva}$ with 10 kDa PEG reagent **4** (1.0 eq). *Lane 5:* PEGylation reaction mixture of Fab$_{beva}$ with 10 kDa PEG reagent **4** (2.0 eq).

Since 1.0 equivalent of PEG di(mono-sulfone) reagent **4** displayed better PEGylation conversion to Fab-PEG-Fab construct, different molecular weights of PEG reagents **4** (6 and 20 kDa) were examined with 1.0 equivalent of PEG (Figure 3.50, Lanes 3 and 4).

The band at about 140 kDa molecular weight marker in SDS-PAGE (Figure 3.50, Lane 5) corresponds to Fab$_{beva}$-PEG$_{20}$-Fab$_{beva}$ (2 x 50 (Fabs) + 2 x 20 (PEG) = 140 kDa), as the PEG reagent appears as twice its molecular weight in an SDS-PAGE gel. Similarly, the band at about 120 kDa (Figure 3.50, Lane 4) represents the Fab$_{beva}$-PEG$_{10}$-Fab$_{beva}$ and the band at about 112 kDa represents the Fab$_{beva}$-PEG$_{6}$-Fab$_{beva}$ (Figure 3.50, Lane 3). In addition, bands at lower molecular weight at 60, 70 and 90 kDa are consistent with the formation of the mono PEG-Fab adducts (Figure 3.50, Lanes 3, 4 and 5). It appeared that using 6.0 and 20 kDa PEG di(mono-sulfone) reagent **4** resulted in a higher PEGylation conversion than the 10 kDa PEG di(mono-sulfone) reagent **4**. This could be due to differences in the purity of the PEG reagents **4**.

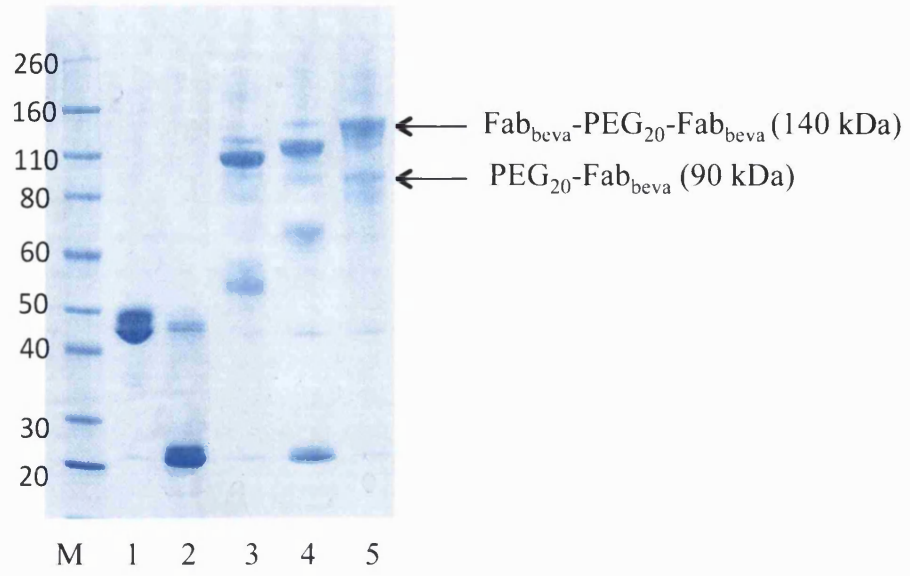

Figure 3.50 SDS-PAGE gel of PEGylation of Fab_{beva} using PEG di(mono-sulfone) reagent **4**, Novex Bis-Tris 4-12% gel stained with colloidal blue (Lanes M-5) *Lane M:* Protein standard, *Lane 1:* Fab_{beva}, *Lane 2:* Fab_{beva} treated with DTT, *Lane 3:* PEGylation reaction mixture of Fab_{beva} with 6 kDa PEG reagent **4** (1.0 eq), *Lane 4:* PEGylation reaction mixture of Fab_{beva} with 10 kDa PEG reagent **4** (1.0 eq), *Lane 5:* PEGylation reaction mixture of Fab_{beva} with 20 kDa PEG reagent **4** (1.0 eq).

Fab_{rani} was then PEGylated with 1.0 equivalent of 6.0, 10.0 and 20 kDa PEG di(mono-sulfone) reagent **4**. The reaction mixture from the PEGylation of Fab_{rani} with the 20 kDa PEG reagent **4** is shown (Figure 3.51, Lane 3). As was hoped, the homodimer PEGylation conversion of Fab_{rani} was similar to what was observed with Fab_{beva} since mono PEGylation conversion of Fab_{rani} was similar to Fab_{beva} .

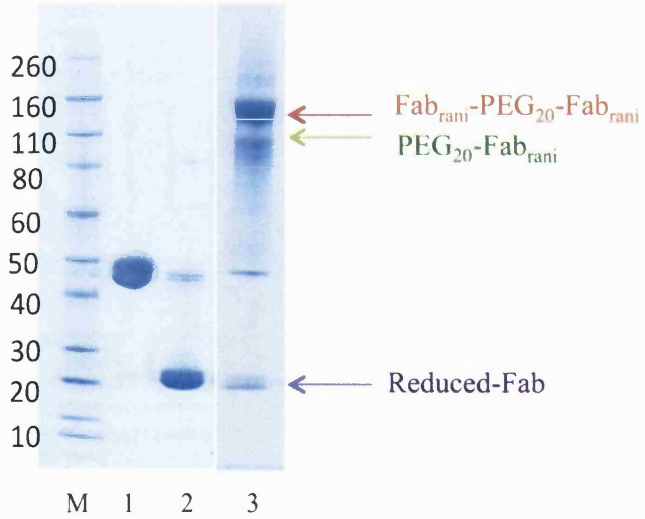

Figure 3.51 SDS-PAGE gel of PEGylation of Fab_{rani} using PEG di(mono-sulfone) reagent **4**, Novex Bis-Tris 4-12% gel stained with colloidal blue (Lanes M-3). Lane M: Protein standard, *Lane 1:* Fab_{rani}, *Lane 2:* Fab_{rani} treated with DTT, *Lane 3:* PEGylation reaction mixture of Fab_{rani} using 20 kDa PEG reagent **4** (1.0 eq).

The PEGylation reaction mixtures of Fab_{beva} and Fab_{rani} were then purified using a SPHP-IEX (1.0 mL) column followed by SEC chromatography. Since the PEGylation conversion to Fab-PEG-Fab appeared to be less than mono PEGylation of Fabs, two purification steps were required. The IEX purification method was similar to that used for the mono PEGylated-Fab. All the homodimers that were prepared were purified using the same methods.

The purification of Fab_{beva}-PEG_{20}-Fab_{beva} is explained in details for an example. The PEGylation reaction mixture (1.0 mL) was buffer exchanged with IEX buffer A (pH 4.0) using Nap-10 column prior to purification. The IEX-SPHP (1.0 mL) column was prepared with IEX buffer A (10 min) and then IEX buffer B (10 min) and buffer A for the final 10 min. The linear elution gradient was used as described for the PEG-Fab_{beva}. The PEGylation reaction mixture (1.5 mL in buffer A) was then loaded onto the IEX-SPHP column.

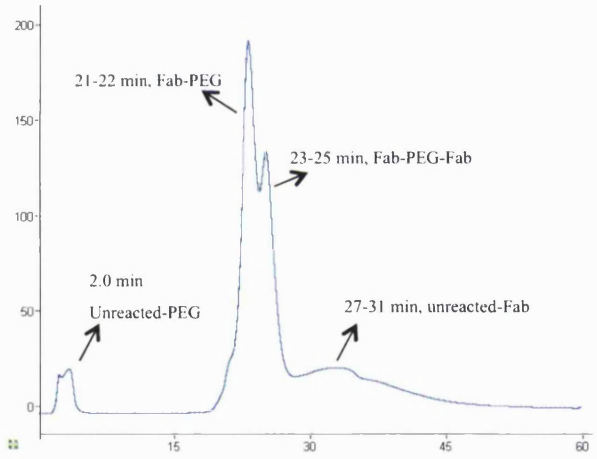

Figure 3.52 IEX chromatogram of reaction mixture of Fab_{beva}-PEG_{20}-Fab_{beva}. Peak at 2 min represent the unreacted PEG, peak at 21-22 min represents mono PEG-Fab_{beva} and peak at 23-25 min represents homodimer Fab_{beva}-PEG_{20}-Fab_{beva}. Peak at 27-31 min indicates unreacted Fab_{beva}.

IEX fractions at 21-22 min were evaluated by SDS-PAGE and there was a band at about 90 kDa molecular weight marker that corresponded to the mono PEG_{20}-Fab_{beva} (Figure 3.53, Lanes 3 and 4). The SDS-PAGE of IEX fractions at 23-25 min that displayed the band about 140 kDa molecular weight marker (Figure 3.53, Lanes 5 and 6) suggested the Fab_{beva}-PEG_{20}-Fab_{beva} product. The IEX fractions at 26-31 min was thought to be non-PEGylated Fab_{beva} as observed in 50 kDa molecular weight marker (Figure 3.53, Lane 7). As expected, the mono PEG-Fab_{beva} eluted from the SPHP-IEX

column before the Fab_{beva}-PEG-Fab_{beva} with lower sodium chloride concentration due to a weaker interaction with the cation exchange column. The homodimer Fab-PEG-Fab with two Fabs has a tighter interaction with the IEX column and so required a higher salt concentration to elute from IEX column.

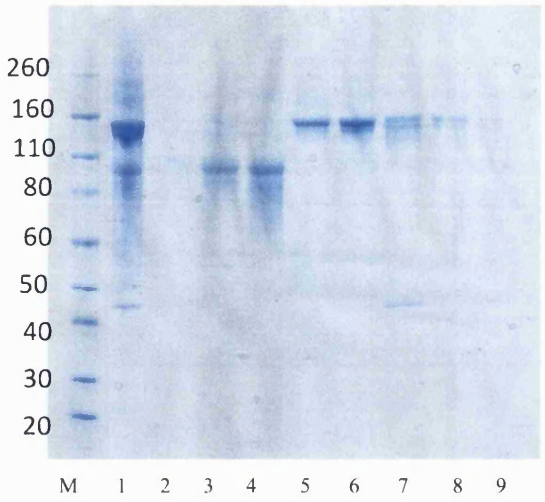

Figure 3.53 SDS-PAGE gel of IEX fractions of Fab_{beva}-PEG_{20}-Fab_{beva}, Novex Bis-Tris 4-12% gel stained with colloidal blue (Lanes M-10). *Lane M:* Standard protein marker, *Lane 1:* The PEGylation reaction mixture of Fab_{beva}, (20 kDa, 1.0 eq) before IEX, *Lane 2:* IEX fraction at 2 min, *Lanes 3, 4:* IEX fractions at 21 and 22 min (mono PEG-Fab), *Lanes 5-7:* IEX fractions at 23-25 min (20 kDa Fab-PEG-Fab), *Lanes 8, 9:* IEX fractions at 27 and 31 min (Unreacted Fab).

To ensure the Fab_{beva}-PEG_{20}-Fab_{beva} was completely purified from non-PEGylated Fab_{beva}, the IEX fractions at 23 to 25 min were pooled (3.0 mL) and concentrated using vivaspin (2 min, 4000 x g) to 2.0 mL. This solution (2.0 mL) was then loaded onto a SEC column to further purify the Fab_{beva}-PEG_{20}-Fab_{beva} (Figure 3.54, A).

The SEC fractions were then collected at the peak which appeared at 60 mins. This material was consistent with being the Fab_{beva}-PEG_{20}-Fab_{beva} (Figure 3.54, B, Lane 2). The SDS-PAGE was stained with silver stain to detect any trace of impurity in the solution. The silver staining of SEC fraction at 60 min, did not show any impurity in the Fab_{beva}-PEG_{20}-Fab_{beva}, (Figure 3.54, B, Lane 2). The peak at 53 min that appeared as a shoulder to the peak at 60 min, was thought to be a trace di Fab_{beva}-PEG_{20}-Fab_{beva} (Figure 3.54, B, Lane 1) at a band above 160 kDa. The SEC fraction at 89 min was non-conjugated Fab_{beva} as expected.

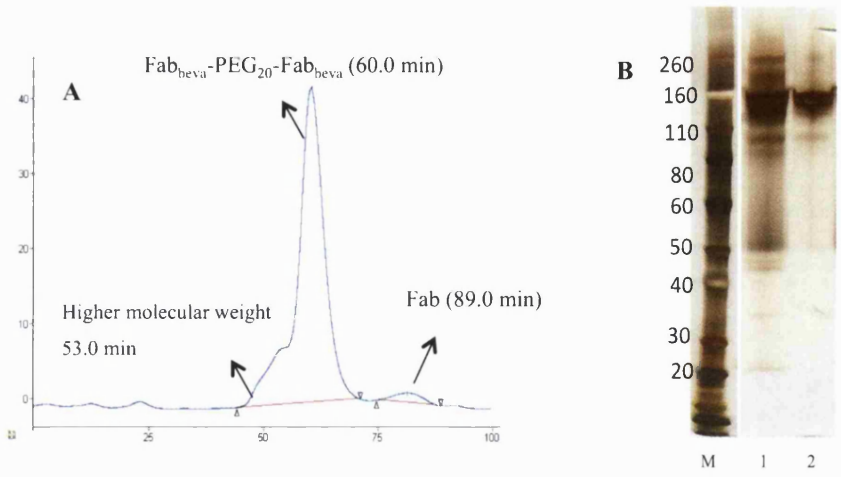

Figure 3.54 SEC chromatogram **(A)**, and **(B)** SDS-PAGE of SEC fractions of 20 kDa Fab-PEG-Fab, Novex Bis-Tris 4-12% gel stained with silver-staining (Lanes M-2). *Lane M:* Standard protein marker, *Lane 1:* Pooled IEX fractions (23-25 min) of mixture of Fab-PEG-Fab (20 kDa) before SEC, *Lane 2:* SEC fraction at 60 min represents pure Fab$_{beva}$-PEG$_{20}$-Fab$_{beva}$.

The SEC fractions from 59 min to 63 min representing the Fab$_{beva}$-PEG$_{20}$-Fab$_{beva}$ were pooled (4 mL) and concentrated with vivaspin (4 min, 4000 x g) to give a 1.0 mL solution in the SEC buffer which was stored at 4 ^{0}C. Using the same method of PEGylation and purification, the 6 and 10 kDa Fab$_{beva}$-PEG-Fab$_{beva}$ were also prepared (Figure 3.56, Lanes 2 and 3). The silver staining (Figure 3.56, Lanes 7-9) for the purified 6, 10 and 20 kDa Fab$_{beva}$-PEG-Fab$_{beva}$ suggested that the purification methods were efficient and there were no traces of impurities in the Fab$_{beva}$-PEG-Fab$_{beva}$ products.

It was necessary to calculate an accurate concentration of each construct to determine their binding affinity and biological activity. The concentration of the Fab$_{beva}$-PEG$_{20}$-Fab$_{beva}$ was then calculated using the micro BCA assay. Fab$_{beva}$ was used as a standard to produce a calibration curve (Figure 3.55). A concentration of 0.227 mg/mL was calculated for purified Fab$_{beva}$-PEG$_{20}$-Fab$_{beva}$ using micro BCA assay (Table 3.8). From a starting amount of 1.0 mg Fab$_{beva}$, it was found that 0.227 mg Fab$_{beva}$-PEG$_{20}$-Fab$_{beva}$ was purified giving an isolated yield of 22.7 % for the conjugate. The PEGylation reaction to make Fab$_{beva}$-PEG$_{6}$-Fab$_{beva}$ and Fab$_{beva}$-PEG$_{20}$-Fab$_{beva}$ was conducted about 12 times and isolated yield tended to be in the range of 5-20%. Yield was dependent on the purity PEG di(mono-sulfone) **4** that was supplied. The Fab$_{beva}$-PEG$_{10}$-Fab$_{beva}$ which was prepared about 10 times tended to be isolated at a lower yield (5-10%) compared to the other two Fab-PEG-Fab homodimers.

Table 3.8 Micro BCA assay absorbance at 562 nm for Fab-PEG-Fab.

Sample (μg/mL)	Average abs-blank
0	0
6.25	0.097
12.5	0.173
25	0.323
50	0.618
100	1.049
200	1.723
1:2 diluted Fab_{beva}-PEG-Fab_{beva}	1.069

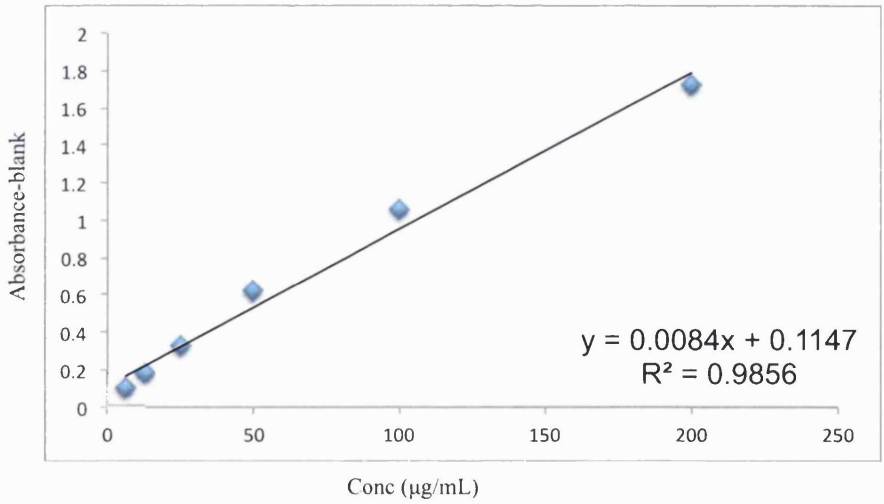

Figure 3.55 Micro BCA assay using Fab_{beva} standard curve for Fab_{beva}-PEG-Fab_{beva} at 562 nm.

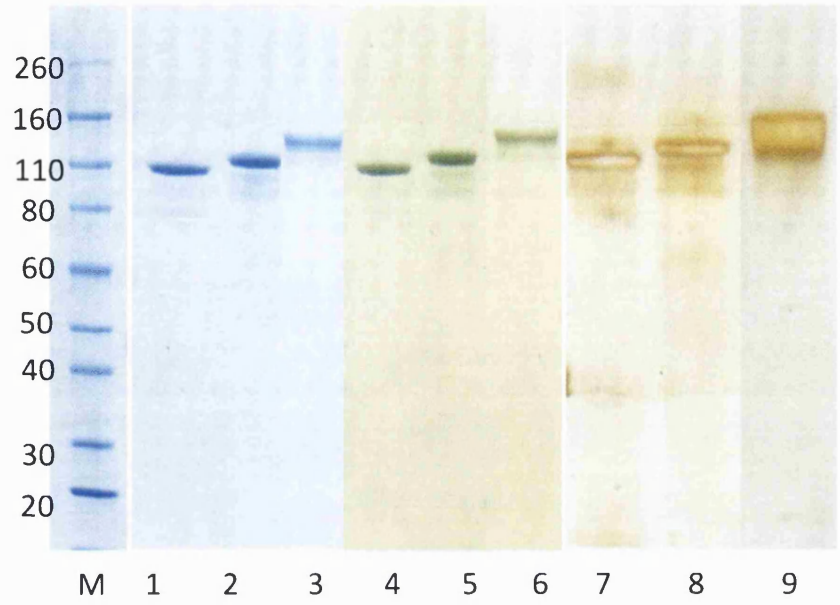

Figure 3.56 SDS-PAGE gel of the purified Fab_{beva}-PEG-Fab_{beva} (6, 10, 20 kDa), Novex Bis-Tris 4-12% gel stained with colloidal blue (Lanes M-3), barium iodide (Lanes 4-6) and silver staining (Lanes 7-9), *Lane M:* Protein standards, *Lanes 1, 4, 7:* The purified Fab_{beva}-PEG_6-Fab_{beva}. *Lanes 2, 5, 8:* The purified Fab_{beva}-PEG_{10}-Fab_{beva}. *Lanes 3, 6, 9:* The purified Fab_{beva}-PEG_{20}-Fab_{beva}.

The 6, 10 and 20 kDa Fab_{rani}-PEG-Fab_{rani} conjugates were also prepared using PEG di(mono-sulfone) reagent **4**. These homodimer conjugates were purified using the same methods as described for purification of Fab_{beva}-PEG_{20}-Fab_{beva} homodimers. Figure 3.57 shows the purified 6, 10 and 20 kDa Fab_{rani}-PEG-Fab_{rani} (Lanes 1-3). Silver stain detection after SDS-PAGE (Figure 3.57, Lanes 7 and 8) indicated there were no impurities observed in these conjugates and no initial Fab remained in the purified samples. PEGylation of Fab_{rani} with PEG reagent **4** was conducted at least 5 times for each of the three molecular weights that were studied. A similar isolated yield was in the range of 7-20% was obtained for the Fab_{rani}-PEG-Fab_{rani} conjugates.

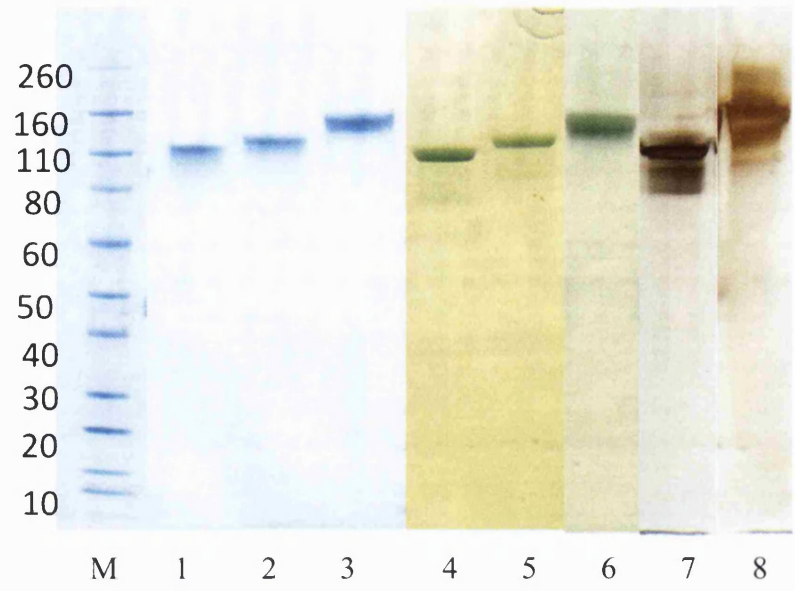

Figure 3.57 SDS-PAGE gel of the purified Fab_{rani}-PEG-Fab_{rani} (6, 10, 20 kDa), Novex Bis-Tris 4-12% gel stained with colloidal blue (Lanes M-3), barium iodide (Lanes 4-6) and silver staining (Lanes 7-8), *Lane M:* Protein standards, *Lanes 1, 4, 7:* The purified Fab_{rani}-PEG_6-Fab_{rani}. *Lanes 2, 5:* The purified Fab_{rani}-PEG_{10}-Fab_{rani}, *Lanes 3, 6, 8:* The purified Fab_{rani}-PEG_{20}-Fab_{rani}.

To homodimer PEGylate the Fab_{trast}, the 20 kDa PEG di(mono-sulfone) reagent **4** was used with the same method as for Fab_{beva} and Fab_{rani}. To PEGylate, the Fab_{trast} (0.650 mg/mL) was first reduced with DTT (1.0 mg/mL) as before and excess DTT was then removed by PD-10 column. Into reduced-Fab_{trast} was added 1.0 equivalent of 20 kDa PEG di(mono-sulfone) reagent **4** and incubated for 3.0 h at ambient temperature. After 3.0 h incubation, the reaction mixture was evaluated by SDS-PAGE and purified using IEX-SPHP (1.0 mL, 1.0 mL/min) column. Prior to loading the IEX column, the reaction mixture (1.0 mL) was again buffer exchanged with IEX buffer A (pH 4.0) using Nap-10 column. The reaction mixture (1.5 mL in buffer A) was then loaded onto the IEX column (Figure 3.58, A).

The IEX fraction at 19 min migrates in SDS-PAGE to a band at 140 kDa (Figure 3.58, B, Lanes 6 and 14) which is consistent with the expected molecular weight of Fab_{trast}-PEG_{20}-Fab_{trast}. The IEX fractions from 16.5-18 min appeared at 90 kDa molecular mass marker in SDS-PAGE (Figure 3.58, B, Lanes 4 and 5) corresponded to mono PEG_{20}-Fab_{trast}. The IEX peak at 22 min, was thought to be non-conjugated Fab_{trast}, however, it was too diluted to appear in SDS-PAGE stained with colloidal blue.

The IEX fraction at 19 min appeared to be essentially pure Fab_{trast}-PEG-Fab_{trast} as could be ascertained by SDS-PAGE (colloidal blue and barium iodide detection). This fraction was then buffer exchanged to PBS (pH 7.4) using a Nap-10 column for long

term storage at 4 ^{0}C. The concentration of the purifed Fab_{trast}-PEG_{20}-Fab_{trast} was then calculated using micro BCA assay. From a starting amount of 1.0 mg Fab_{trast}, it was found that 0.1 mg Fab_{trast}-PEG_{20}-Fab_{trast} was purified giving an isolated yield of 10 % for the conjugate. This yield was lower than that for Fab_{beva}-PEG_{20}-Fab_{beva} (20%) because only IEX fraction at 19 min was selected as a pure product. The PEGylation of Fab_{trast} to make the Fab homodimer was conducted 5 times at a 1.0 mg scale and the isolated yield was in the range of 5-10%.

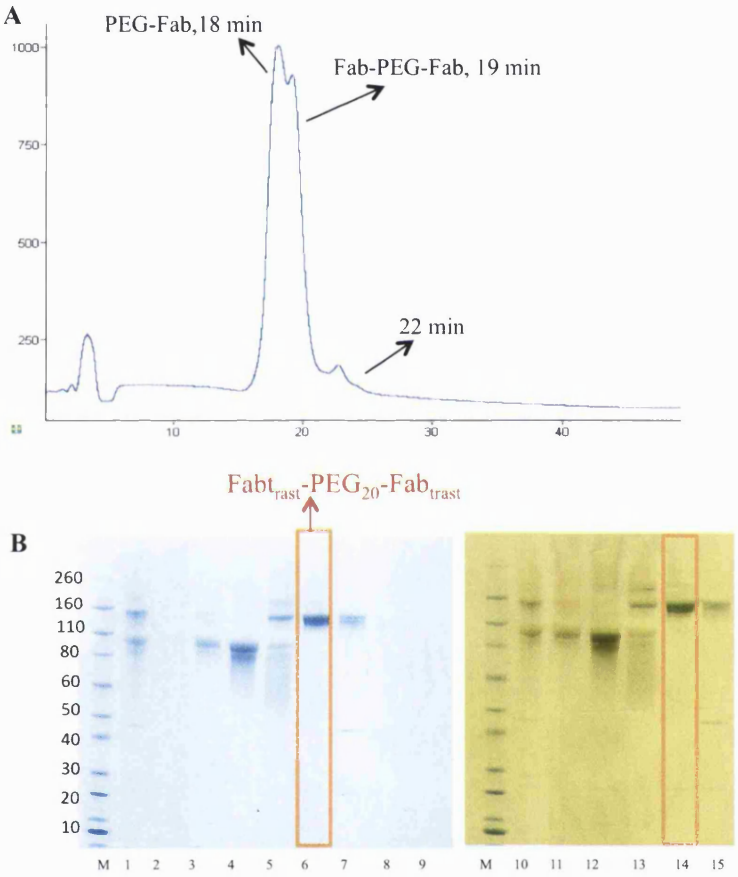

Figure 3.58 IEX-SPHP chromatogram **(A)**, and **(B)** SDS-PAGE of IEX fractions of Fab_{trast}-PEG_{20}-Fab_{trast}, Novex Bis-Tris 4-12% gel stained with colloidal blue (Lanes M-9) and barium iodide (Lanes 10-15). *Lane M:* Standard protein marker, *Lanes 1, 10:* The PEGylation Fabtrast (20 kDa, 1.0 eq PEG) reaction mixture before IEX, *Lane 2:* IEX fraction at 14.8 min, *Lanes 3, 11:* IEX fractions at 15.8 min, *Lanes 4-12:* IEX fractions at 16.8 min, *Lanes 5-13:* IEX fractions at 18.5 min, *Lanes 6-14:* IEX fractions at 19.0 min, *Lanes 7-15:* IEX fractions at 19.5 min, *Lane 8:* IEX fractions at 20.5 min, *Lane 9:* IEX fractions at 21.5 min.

DLS analysis was conducted on freshly purified Fab_{beva}-PEG_{20}-Fab_{beva}. The solution was first filtered using a 0.2 μm filter to remove small particles which may interfere with the DLS measurment (Figure 3.59, B). DLS measurments were also obtained for bevacizumab (Figure 3.59, A). A particle size of 12.66 nm was measured for the Fab_{beva}-PEG_{20}-Fab_{beva} (Table 3.9), whereas an avarage particle size of 11.37 nm was measured for bevacizumab (Table 3.9) and 9.02 nm for Fab_{beva} (Table 3.6). Since DLS analysis calculates the hydrodynamic diameter of a spherical particle, the similarity of the Fab_{beva}-PEG_{20}-Fab_{beva} (12.66 nm) particle size to bevacizumab's particle size (11.37 nm) suggested a similar spherical particle shape structure for the Fab_{beva}-PEG_{20}-Fab_{beva} and bevacizumab. This observation helped to understand the relative binding affinity between homodimer Fab-PEG-Fab and bevacizumab that is discussed in Chapter 4.

A; Bevacizumab

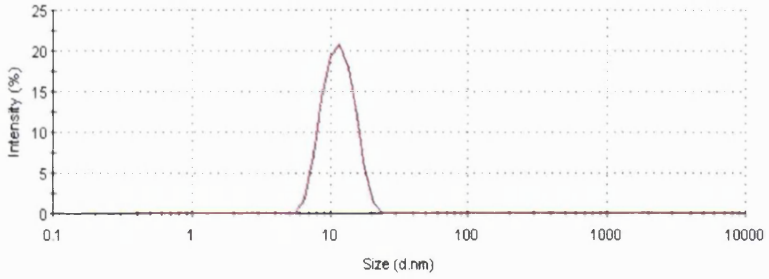

B; Fab_{beva}-PEG_{20}-Fab_{beva}

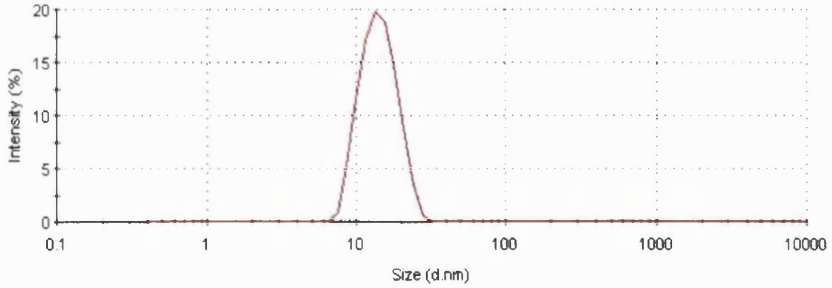

Figure 3.59 DLS analysis of **(A)** bevacizumab, **(B)** Fab_{beva}-PEG_{20}-Fab_{beva}.

Table 3.9 An average DLS analysis on bevacizumab and Fab_{beva}-PEG_{20}-Fab_{beva} from two analysis.

Sample	Particle size (d. nm)	PdI
Bevacizumab	11.37	0.09
Fab_{beva}-PEG_{20}-Fab_{beva}	12.66	0.17

3.2.2 Stability study on Fab_{beva}-PEG-Fab_{beva}

To investigate the stability of the conjugation of the PEG di(mono-sulfone) reagent **4** with two Fabs under harsh conditions and also understand whether PEG reagent **4** was conjugated to the Fabs via the interchain disulfide bond, the purified Fab_{beva}-PEG_{20}-Fab_{beva} was treated with DTT (1.0 mg/mL, 30 min) and then heated (80 ^{0}C for 10 min). If the conjugation site of the PEG molecules to the Fab_{beva} was not on the interchain disulfide bond, then the intact disulfide bond could be reduced when exposed to DTT. The Fab_{beva}-PEG_{20}-Fab_{beva} treated with DTT only (Figure 3.60, A, Lane 2), showed no reduction and no light and heavy chains at 25 kDa in SDS-PAGE gel. This suggested that there was no intact interchain disulfide bond in the Fab_{beva}-PEG_{20}-Fab_{beva} construct to be reduced in the presence of DTT. However, the light and heavy chains were observed at 25 kDa molecular mass marker (Figure 3.60, A, Lane 3) when the Fab_{beva}-PEG_{20}-Fab_{beva} treated with DTT and then heated. This observation (Figure 3.60, A, Lane 3) suggested that conjugation of the PEG reagent **4** to the Fabs was not stable under heat at 80 ^{0}C, in contrast with the PEG mono-sulfone reagent **2** conjugation to the Fabs. However, the Fab-PEG-Fab conjugates were stable during storage in PBS (pH 7.3) at 4 ^{0}C for an approximate 3 month as no de-PEGylation was occurred based on observation by SDS-PAGE gel.

To stabilize the conjugation of the PEG di(mono-sulfone) reagent **4** to the Fabs under harsh conditions at 80 ^{0}C, $NaBH_4$ treatment was examined. As described before, $NaBH_4$ treatment sometimes is required in order to stabilize the PEG reagent conjugation to proteins when harsh conditions are used, however, it was not a case for the PEG mono-sulfone reagent **2** conjugations to the Fabs under conditions at 80 ^{0}C. It was thought that the ketone group in PEG di(mono-sulfone) reagent **4** might be hydrolyzed under heating and then become dissociated from its conjugation site. It was found that the Fab_{beva}-PEG_{20}-Fab_{beva} treated with $NaBH_4$ became stable with DTT and heating (Figure 3.60, B, Lanes 7 and 8) and no de-PEGylation observed.

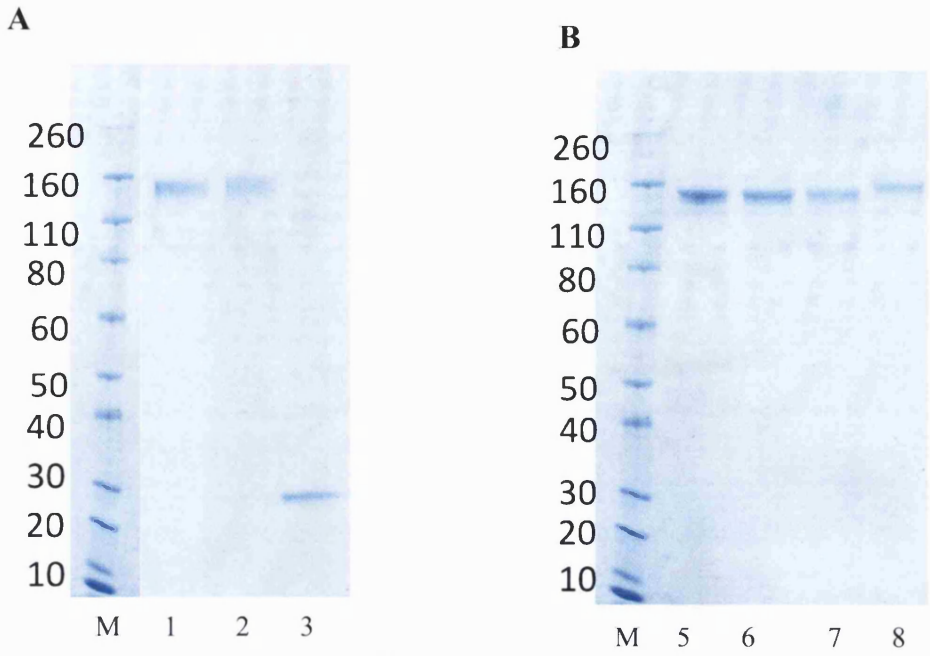

Figure 3.60 SDS-PAGE analysis of the DTT and heat over Fab_{beva}-PEG_{20}-Fab_{beva}. Novex Bis-Tris 4-12% gel stained with colloidal blue (Lanes M-8), A and B; *Lane M:* Protein standards, *Lanes 1 and 5:* The purified Fab_{beva}-PEG_{20}-Fab_{beva} without any treatment. *Lane 2:* The DTT treated Fab_{beva}-PEG_{20}-Fab_{beva}, without heat, *Lane 3:* The DTT and heat-treated Fab_{beva}-PEG_{20}-Fab_{beva}, *Lane 6:* The Fab_{beva}-PEG_{20}-Fab_{beva} after $NaBH_4$ treatment, *Lane 7:* The DTT treated Fab_{beva}-PEG_{20}-Fab_{beva} after $NaBH_4$ treatment without heat, *Lane 8:* The DTT and heat-treated Fab_{beva}-PEG_{20}-Fab_{beva} after $NaBH_4$ treatment.

3.3 PEGylation of Fab_{beva} and Fab^*_{trast} to produce Fab_{beva}-PEG-Fab^*_{trast}

Beside monovalency of the Fab fragment, mono specificity of the Fab needed to be investigated. To prepare the bispecific antibody fragment (Fab-PEG-Fab*) with two clinically relevant Fabs, the Fab_{beva} and Fab_{trast} were selected since VEGF and HER-2 signalling pathways are related together [247].

The approach used in this work, was to use PEG di(mono-sulfone) reagent **4** to conjugate two different Fab fragments in a stepwise PEGylation. It was thought that by using 5 equivalents of the PEG di(mono-sulfone) reagent **4** to PEGylate the Fab_{beva}, the majority of the Fab_{beva} would be PEGylated to mono PEG-Fab_{beva} rather than Fab_{beva}-PEG-Fab_{beva}. By separating the mono PEG-Fab_{beva} from the reaction mixture, it would be possible to conjugate this to the free thiols available in reduced-Fab^*_{trast} and produce Fab_{beva}-PEG-Fab^*_{trast}. However, the concern over hydrolysis and cyclisation of the PEG di(mono-sulfone) reagent **4** still remained.

3.3.1 Preparation of PEG heterodimer Fab_{beva}-PEG-Fab^*_{trast}

The Fab_{beva} (1.0 mg/mL, 1.0 mL) was first reduced with DTT (1.0 mg/mL) during 30 min incubation and then excess DTT was removed from the solution using a PD-10 column. Into 1.0 equivalent of reduced-Fab_{beva}, 5 equivalents of PEG di(mono-sulfone) reagent **4** (20 kDa, 5 equivalent) was added and incubated for 3 h at ambient temperature (Figure 3.61, Lane 1). The PEGylation reaction mixture was then purified using SPHP-IEX column applying similar elution gradient and buffers as explained previously (Figure 3.61, A). The IEX fractions were collected (1.0 mL at each min) and then loaded onto SDS-PAGE (Figure 3.61, B). The IEX fraction at 19 and 20 min indicated the most purified mono PEG_{20}-Fab_{beva} as it showed a band at about 90 kDa molecular weight in SDS-PAGE (Figure 3.61, B, Lanes 6 and 7). These IEX fractions (19 and 20 min) were then pooled and concentrated using vivaspin (4000 x g, 3 min) to 1.0 mL solution. The approximate concentration of this solution was estimated using UV at 280 nm, however, using UV did not give an accurate value for PEGylated fragments. An approximate concentration of 0.23 mg/mL was considered for mono PEG-Fab_{beva} (1.0 mL). The Fab^*_{trast} (0.2 mg/mL) was then reduced with DTT (1.0 mg/mL) and after removal of DTT with PD-10 column, was added (3.3 mL) to the mono PEG-Fab_{beva} (1.0 mL) solution and incubated for 3 h at ambient temperature and then 12 h at 4 ^{0}C.

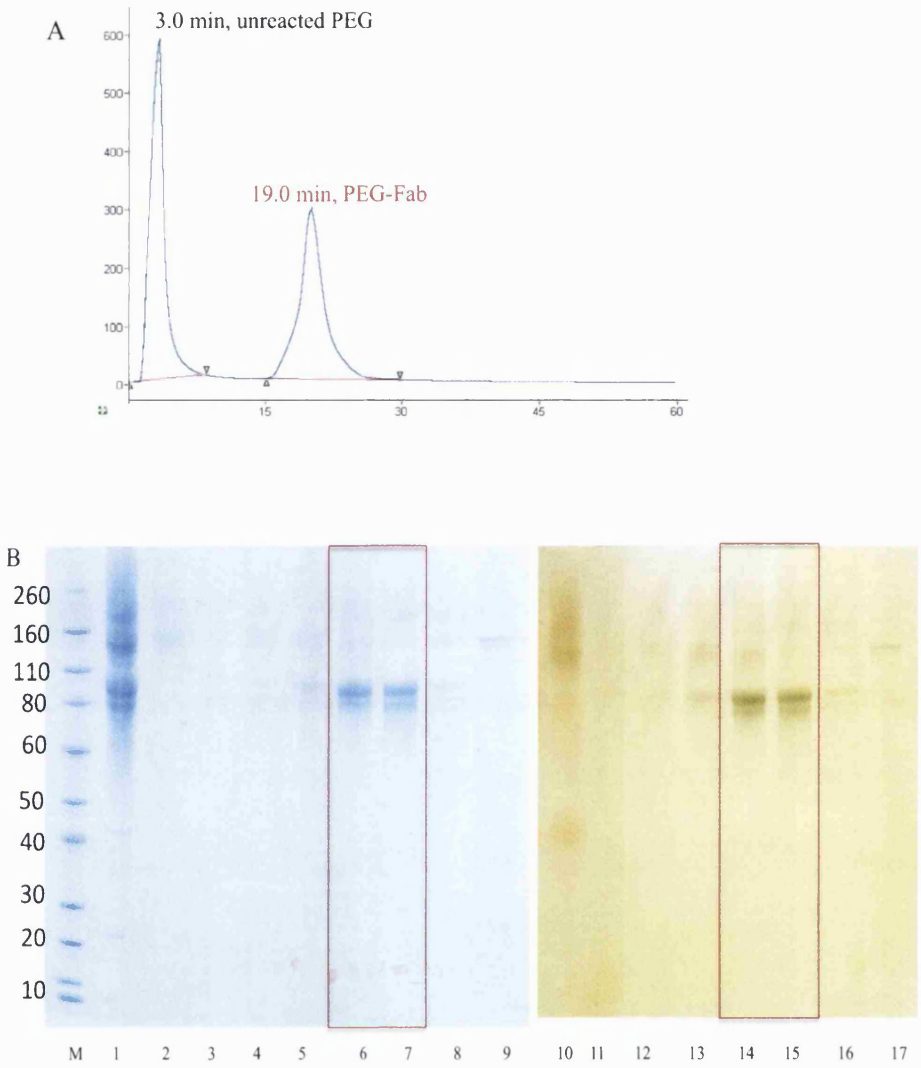

Figure 3.61 IEX-SPHP chromatogram **(A)**, and **(B)** SDS-PAGE of IEX fractions of PEGylation of Fab_{beva} (5.0 eq PEG reagent **4**), Novex Bis-Tris 4-12% gel stained with colloidal blue (Lanes M-9) and barium iodide (Lanes 10-17). *Lane M:* Standard protein marker, *Lane 1:* The reaction mixture of PEGylation of Fab_{beva} (20 kDa, 5 eq PEG) before IEX, *Lanes 2, 10:* IEX fraction at 3.0 min, *Lanes 3, 11:* IEX fractions at 16.2 min, *Lanes 4-12:* IEX fractions at 17.0 min, *Lanes 5-13:* IEX fractions at 18.0 min, *Lanes 6-14:* IEX fractions at 19.0 min, *Lanes 7-15:* IEX fractions at 20.0 min, *Lanes 8, 16:* IEX fractions at 21.0 min, *Lanes 9, 17:* IEX fractions at 22.5 min.

The heterodimer reaction mixture (Figure 3.62, B, Lane 1) was then purified using SPHP-IEX column followed by SEC column. Using IEX (Figure 3.62, A) was thought to be useful to separate heterodimer from non-reacted mono PEG-Fab, however, non-reacted Fab* could be eluted with the Fab-PEG-Fab*. Using SEC (Figure 3.62) on the collected IEX fractions was used to remove the remaining non-reacted Fab*. The IEX fractions (Figure 3.62, B) were evaluated by SDS-PAGE. The IEX fractions at 19.7 and 20.5 min migrate to about 140 kDa molecular mass marker in

SDS-PAGE (Figure 3.62, B, Lanes 4 and 5) and corresponds to the Fab_{beva}-PEG_{20}-Fab^*_{trast} construct, similar to what was observed for homodimer Fab-PEG_{20}-Fab conjugate. The IEX fraction at 18 min migrates to above 90 kDa molecular weight marker (Figure 3.62, B, Lane 2) and represents mono PEG_{20}-Fab_{beva} that remained non-reacted in the solution. Most of the reduced-Fab^*_{trast} were remained non-reacted in the reaction solution as observed in SDS-PAGE (Figure 3.62, B, Lanes 6 and 14). SEC purification was performed on the IEX fractions (19.7 + 20.5 min), to remove non-reacted Fab^*_{trast} (Figure 3.63, A).

SEC fractions were collected (1.0 mL at each min) and evaluated by SDS-PAGE (Figure 3.63, B). SDS-PAGE was stained by silver staining to detect small traces of protein. The SEC fraction at 59 min (Figure 3.63, A) appeared at about 140 kDa molecular weight in SDS-PAGE (Figure 3.63, B, Lanes 9 and 18) indicated the Fab_{beva}-PEG_{20}-Fab^*_{trast}. The SEC retention time for the heterodimer (59 min) was similar to the retention time observed for purified homodimer Fab-PEG-Fab, at 60 min. In addition, SEC fraction at 89 min (Figure 3.63, A) indicates the non-reacted Fab^*_{trast}.

The amount and volume of purified Fab_{beva}-PEG-Fab^*_{trast} was not enough to conduct a micro BCA assay to calculate the concentration and yield. Based on observation in SDS-PAGE gel (Figure 3.62, Lane 1), it appeared that this amount was very low. The silver-staining, however, did not show impurities in the Fab_{beva}-PEG-Fab^*_{trast}. While synthesis of the heterodimer Fab_{beva}-PEG_{20}-Fab^*_{trast} could only be achieved one time out of 6 attempts, it was possible to make the heterodimer Fab-PEG-Fab* conjugate that preserve binding to HER-2 and VEGF (Chapter 4). Several efforts were made to reproduce and improve heterodimer PEGylation using PEG di(mono-sulfone) **4** by changing conditions such as pH, increasing PEGylation time to 3 days at 4 ^{0}C and decreasing the volume of PEGylation reaction. Unfortunately, none of these efforts worked because the PEG di(mono-sulfone) reagent **4** underwent cyclisation after first PEGylation and avoid conjugation to the second Fab*. Certainly there is a need to improve the chemistry and purity of this PEG reagent for further work to make a bispecific antibody fragments.

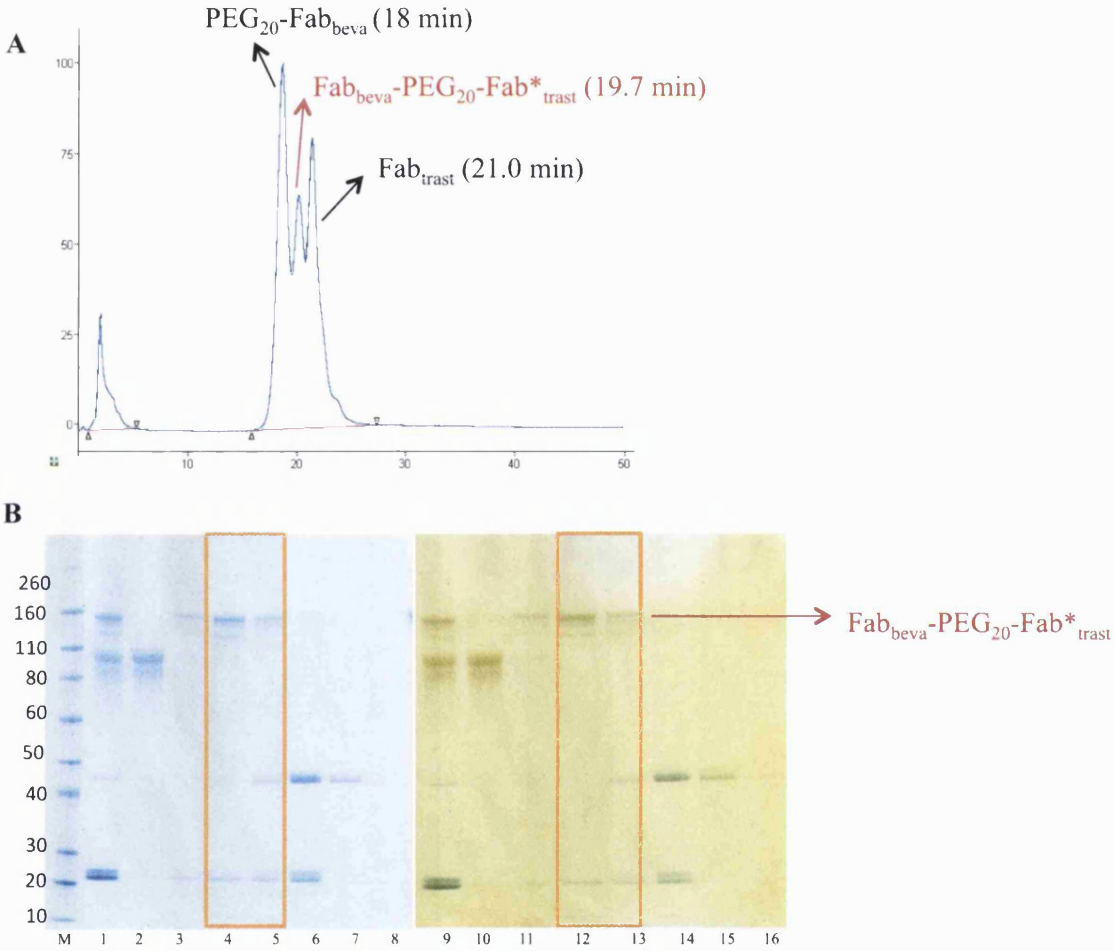

Figure 3.62 IEX-SPHP chromatogram **(A)**, and **(B)** SDS-PAGE of IEX fractions of Fab_{beva}-PEG-Fab^*_{trast}, Novex Bis-Tris 4-12% gel stained with colloidal blue (Lanes M-8) and barium iodide (Lanes 9-16). *Lane M:* Standard protein marker, *Lanes 1, 9:* The reaction mixture of Fab_{beva}-PEG-Fab^*_{trast} (20 kDa PEG) before IEX, *Lanes 2, 10:* IEX fraction at 18.0 min, *Lanes 3, 11:* IEX fractions at 19.0 min, *Lanes 4-12:* IEX fractions at 19.7 min, *Lanes 5-13:* IEX fractions at 20.5 min, *Lanes 6-14:* IEX fractions at 21.0 min, *Lanes 7-15:* IEX fractions at 22.0 min, *Lanes 8, 16:* IEX fractions at 23.8 min.

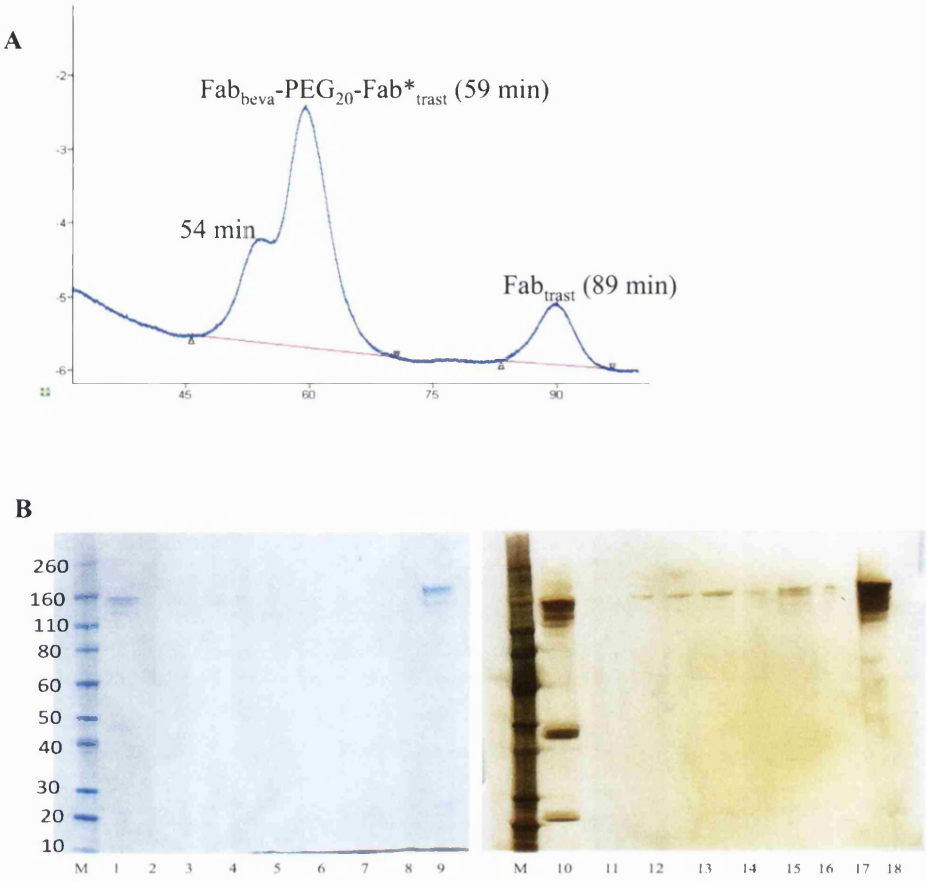

Figure 3.63 SEC chromatogram **(A)** and **(B)** SDS-PAGE of SEC fractions of Fab$_{beva}$-PEG-Fab*$_{trast}$ mixture, Novex Bis-Tris 4-12% gel stained with colloidal blue (Lanes M-9) and silver staining (Lanes 10-18). *Lane M:* Standard protein marker, *Lanes 1, 10:* The pooled IEX fractions at 19.7 and 20.5 min before SEC, *Lanes 2, 11:* SEC fraction at 53.5 min, *Lanes 3, 12:* SEC fractions at 56.5 min, *Lanes 4-13:* SEC fractions at 57.5 min, *Lanes 5-14:* SEC fractions at 58.5 min, *Lanes 6-15:* SEC fractions at 59.5 min, *Lanes 7-16:* SEC fractions at 60.5 min, *Lanes 8, 17:* SEC fractions at 61.5 min, *Lanes 9, 18:* Combined and concentrated SEC fractions from 56.5-61.7 min.

3.4 Summary

Bis-alkylation PEG reagents **2** and **4** were used to conjugate PEG to Fabs at their interchain disulfide bond. Several PEG-Fab conjugates were prepared in an effort to determine structure-property correlations related to the binding properties of the conjugate. To compare binding with an IgG and with the unconjugated Fab, it was necessary to obtain the Fabs by the proteolytic digestion of their parent IgGs. Bevacizumab and trastuzumab were digested with immobilized papain to obtain their respective Fabs. Ranibizumab is a clinically used Fab and was thus the direct source of Fab$_{rani}$, which was also PEGylated. Using 2 equivalents of the PEG mono-sulfone **2**

gave a near quantitative conversion for the PEGylation to give the mono PEG-Fabs. Control reaction conducted on non-reduced native Fab with 2 equivalents PEG mono-sulfone **2** did not show any PEGylation. The PEG-Fabs were purified using a single IEX chromatographic step. A silver staining indicated no impurities in the purified PEG-Fab solutions. The isolated yields for PEG-Fab_{beva}, PEG-Fab_{rani} and PEG-Fab_{trast} were all about 65% (Table 3.10). A $F(ab)_2$ fragment was also prepared from bevacizumab by proteolytic digestion using IdeS. Using $F(ab)_2$ it was possible to prepare the PEG_2-Fab′ conjugate. Two PEG molecules were conjugated on the Fab′, one on the thiols at the interchain disulfide and the other at the two cysteines on the heavy chain in hinge region. The PEG-Fab conjugates were stable during a 3 months stability study at 4 ^{0}C with no de-PEGylation.

PEGylation of the full IgGs was also examined. There are at least 4 interchain disulfide bonds in each IgG so it was clear that many potential products could be generated. After some exploratory experiments to evaluate reduction conditions, both bevacizumab and trastuzumab were treated with DTT and then incubated with PEG mono-sulfone **2** (4 eq). As expected, multiple PEGylated products were observed by SDS-PAGE and purification of the mono PEG-IgG conjugate required two purification steps (SEC followed by IEX) to achieve some semblance of purity. Some effort was made to proteolytically digest the PEGylated bevacizumab in the hope to obtain PEG-$F(ab)_2$, but this was not possible.

Homodimer Fab-PEG-Fab conjugates were also prepared. These molecules were made by the conjugation of two Fab molecules, one to each end of a PEG molecule using PEG reagent **4**. Different molecular weight of 6, 10 and 20 kDa of the PEG di(mono-sulfone) reagent **4** were used. Purification of the conjugates was achieved using two purification steps (IEX followed by SEC). A silver staining on the purified Fab-PEG-Fab homodimer did not show trace of impurities. For comparative binding studies, three homodimer molecules were obtained using Fab_{beva} (Fab-PEG-Fab 6, 10 and 20 kDa PEG). The analogous conjugates were also made using Fab_{rani}. The 20 kDa Fab_{trast}-PEG_{20}-Fab_{trast} was also prepared. The isolated yields for these homodimer PEG conjugates were in the range of 5-20% (Table 3.10) for the conjugates derived from Fab_{rani} and Fab_{beva}, and about, 5-10 % for Fab_{trast}-PEG_{20}-Fab_{trast}.

Using stepwise PEGylation, the Fab_{beva}-PEG_{20}-Fab^*_{trast} was prepared by conjugation of the PEG di(mono-sulfone) reagent **4** to the Fab interchain disulfide bond. This heterodimer Fab-PEG-Fab* was then purified using IEX followed by SEC. While

the amount and volume of purified Fab-PEG-Fab* was not enough to use micro BCA assay, it was possible to use PEG reagent **4** to conjugate two different Fabs. However, further improvement in the chemistry and purity of the PEG reagent **4** is required to increase the production of the heterodimer Fab-PEG-Fab*.

Table 3.10 Summary of the PEGylated products that were prepared. (★ = from digestion).

Construct	Number of replicate (≅)	%Yield of purified product
PEG_{10}-bevacizumab	5	15
Fab_{beva}	≥50	70★
PEG_{20}-Fab_{beva}	≥10	65
PEG_{30}-Fab_{beva}	3	65
PEG_{40}-Fab_{beva}	3	65
PEG_{20}-Fab_{rani}	7	65
PEG_{2x20}-Fab'_{beva}	4	36
PEG_{2x30}-Fab'_{beva}	4	36
Fab_{beva}-PEG_6-Fab_{beva}	12	5-20
Fab_{beva}-PEG_{10}-Fab_{beva}	10	5-10
Fab_{beva}-PEG_{20}-Fab_{beva}	12	5-20
Fab_{rani}-PEG_6-Fab_{rani}	7	7-20
Fab_{rani}-PEG_{10}-Fab_{rani}	5	5-20
Fab_{rani}-PEG_{20}-Fab_{rani}	7	7-20
Fab_{trast}	7	25★
PEG_{20}-Fab_{trast}	5	65
Fab_{trast}-PEG_{20}-Fab_{trast}	5	5-10
PEG_{10}-trastuzumab	2	ND
Fab_{beva}-PEG_{20}-Fab^*_{trast}	6 attempts (Once worked)	ND

Chapter 4: Binding Affinity and Functional Activity Studies

Part A: Binding Affinity Studies

4 Binding Affinity and Functional Activity Studies

4.1 Introduction to part A

The affinity of a mAb with its antigen has a major effect on the biological activity of the antibody [248, 249]. The terms affinity and avidity are two important parameters that are used to describe the binding properties of mAbs. These terms are related but can be easily confused. Affinity is a thermodynamic term that donates the strength of the binding interaction between a single region of a mAbs and a single antigen [248]. It is related to the extent of the formation of the complex (AB) between interacting proteins, in this case a mAb (A) and its antigen (B) (Figure 4.1). Affinity is often expressed as K_D or the equilibrium dissociation constant. It can also be calculated as K_A or equilibrium association constant. K_A and K_D are both thermodynamic parameters (Figure 4.1) [250, 251]. Affinity can be influenced by pH, temperature and solution composition [251]. The affinity of IgG antibodies can be in the micormolar to subnanomolar range [251].

$$A + B \underset{k_d}{\overset{k_a}{\rightleftharpoons}} AB$$

$$K_A = k_a / k_d = \frac{[AB]}{[A].[B]}$$

$$K_D = k_d / k_a = \frac{[A].[B]}{[AB]}$$

Figure 4.1 Affinity can be expressed as K_D or K_A [252, 253].

Avidity is related to binding cooperativity and is related to the valency of a binding molecule and it is also related to the sum of binding of two molecules to one another at multiple sites. Avidity is mainly referred to the stability of the interaction between antibody and antigen as a whole molecule. It can be measured by the functional activity of a bivalent antibody bound to a multivalent antigen and is called 'functional affinity' [248, 251]. The functional affinity was first called 'apparent affinity' by Karush in 1978 [254, 255]. It was proposed that functional affinity could be calculated with the same methods as used for intrinsic affinity by measuring the bound and free antibody at a series of antibody concentrations [254]. In contrast, it has been reported that when an IgG binds to an antigen which is located on the cell surface, the functional affinity may not adequately describe the interactions between the IgG and its antigen because the dissociation rate of antibody from antigen could be heterogenic. Some antibodies (minority) could bind monovalently and therefore dissociate relatively faster

compared to the majority of antibodies that bound bivalently and dissociate more slowly. In addition, it was found that the functional affinity could be different for these monovalently binding IgGs at different experimental conditions depending on the volume of incubation [255, 256]. It was sometimes not possible to determine a single functional affinity value for these antibodies.

A Fab is monovalent and the binding of an IgG antibody is bivalent. The hinge region in the IgG is flexible. After one Fab in an IgG is bound to an antigen, the binding of the second Fab will be enhanced if another available antigen is nearby. The Fab-PEG-Fab homodimers were prepared to examine if binding could be increased compared to the PEG-Fab conjugates. These Fab-PEG-Fab homodimers had a random coil, flexible PEG molecule between each Fab molecule. These conjugates were prepared using the PEG di(mono-sulfone) reagent **4**. It was thought that it might be possible that conjugation of a Fab to each terminus of a PEG molecule would allow the Fab moieties to interact cooperatively during binding. The end groups in polymers are thought to often be close together in solution and move more frequently than the other parts of a polymer [159, 257]. To determine the structure-property correlations of the homodimer Fab-PEG-Fabs, it was necessary to determine their binding affinities and their dissociation and association rates compare to the full IgG. There are different methods to determine protein-protein interactions and the binding affinity of an antibody including ELISA (enzyme linked immunosorbent assay) [258], SPR techniques (surface plasmon resonance) [259], affinity chromatography [258], isothermal titration calorimetry (ITC) [260] and fluorescence correlation spectroscopy [261].

ITC measures the heat change that occurs during complex formation of an antibody and ligand in solution at constant temperature [260, 262]. ITC is considered the only method that can directly measure the binding equilibrium and thermodynamic properties of protein-protein interactions in the solution. Heat is measured when one binding partner is titrated with the other binding partner in solution. With the ITC experiment, the association binding constant (K_A), the stoichiometry (n) of binding and the enthalpy (ΔH) can be directly calculated from one experiment [262, 263]. However, the ITC experiment requires a very high concentration of the protein compared to methods such as ELISA and SPR [263]. For instance, the binding affinity of human single chain Fv fragment to human fibroblast growth factor 2 (FGF-2) was determined by ITC. The hFGF-2 (30-40 μM) was titrated with scFv (400-600 μM) at 25 ^{0}C [264]

and binding affinity, ΔH, ΔG and ΔS of the interaction were determined. Some effort to conduct an ITC experiment was made to measure the binding equilibrium properties of some the PEGylated products with VEGF. Starting with bevacizumab as control it quickly became apparent that the amount of VEGF needed was going to be excessive and very expensive. In an initial experiment VEGF (0.18 μM in sample cell, 1.4 mL) was titrated with bevacizumab (8.3 μM, 5 μL injection for 20 times) at 25 ^{0}C. However, it was found that even this amount of VEGF was too low to obtain an adequate signal when allowed to interact with bevacizumab and a minimum of 3.0 μM VEGF was required. Sourcing this much VEGF was not at all possible.

SPR is a non-labeling technique that allows measurement of protein-protein interactions such as antibody-antigen interactions in real time. One of the interacting molecules is immobilised onto a sensor chip and the other molecule is allowed to flow over the functionalised sensor chip. The sensor chip is made up with glass and covered with an approximately a 50 nm thick layer of gold that causes conductivity. The light source is a light-emitting diode (LED) at 760 nm with a bandwidth of approximately 15 nm [265]. The free electrons at the surface of the sensor chip can absorb the incident photons during the SPR phenomenon [265] and conducts the signal to the detector (Figure 4.2) [253, 265].

BIAcore (Biomolecular Interaction Analysis) is a commercial SPR instrument used to measure the molecular interactions between two molecules [253, 266]. The sensor chip is at the centre of the BIAcore system which provides the physical conditions necessary to generate the SPR signal (Figure 4.2) [267]. The glass of the sensor chip and the sample solution together make the media in the BIAcore [268].

Carboxymethylated (CM) dextran coated gold chips are widely used to immobilise one of the interacting molecules. Immobilisation is accomplished by carbodiimide coupling to forms an amide bond between a dextran carboxylate and an amine from the molecule of interest. The carboxymethylated dextran is a flexible unbranched carbohydrate polymer that form a thin layer of approximately 100 nm above the sensor surface and 0.2 % of the height of the flow chamber [252, 269].

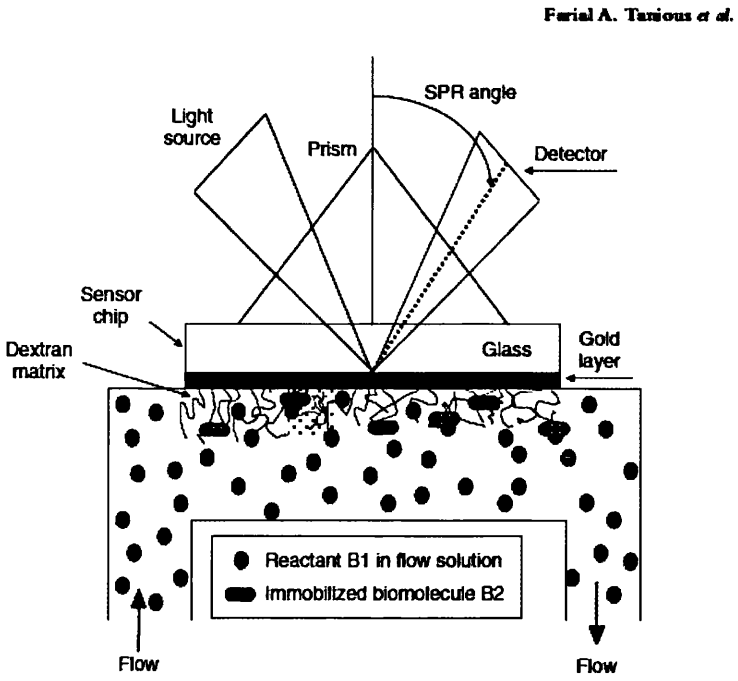

Figure 4.2 Production of the SPR signal, reproduced from [268].

The term 'analyte' is applied to the interaction partner that is in the solution that flows over the chip surface that has been immobilised with the 'ligand'. The analyte binds directly to the ligand [253]. A binding response is therefore generated from binding of analyte to the immobilised ligand. Two major parameters are involved in the binding measurement; the transport of analyte from solution to the dextran layer and transport of analyte within the dextran layer [269].

The binding response is related to the mass changes on the chip surface which results in changes in the measured intensity of the refractive index [253, 265]. This response can be detected to a few picograms per square millimetre on the sensor surface. This small surface area is proportional to the concentrations of the immobilised ligand in the range of pico to nanomolar. The resulting plot is known as a sensogram and it involves three different steps (Figure 4.3), association, dissociation and regeneration. The period during which analyte is being injected into the media flowing over the sensor chip is called the 'association phase' and the period where there is no analyte present in the media flowing over the sensor chip and only buffer is running over is called 'dissociation phase' [253] (Figure 4.3). The dissociation phase allows the complex to dissociate. The regeneration step allows removal of remaining bound analyte from the chip surface without causing any damage to the immobilised ligand. The regeneration step also prepares the chip for a new analysis cycle. Using BIAcore

allows kinetic parameters for association and dissociation rates of antibody-antigen interaction to be measured [253, 269-271].

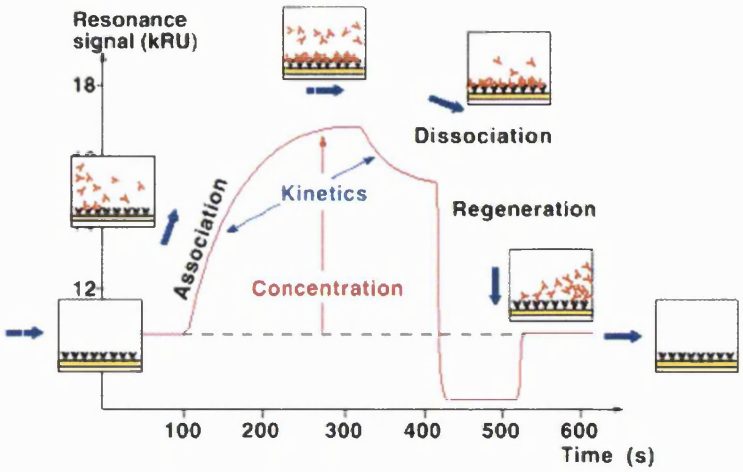

Figure 4.3 Typical BIAcore sensogram, reproduced from [272].

ELISA is another widely used technique that can be used to determine antibody affinity. It is a relatively fast and simple method that only requires small quantities of the proteins of interest (e.g. antibody and ligand) [273, 274]. However, there are some disadvantages associated with ELISA when compared with BIAcore. ELISA is an end-point technique, which means that the results of an ELISA assay can be seen only after the final step. Results in BIAcore can be monitored at each step during binding, which allows calculating association and dissociation constant rates. ELISA also requires an additional step of using a secondary reagent to measure the amount of antibody that is bound to antigen, whereas no labelling is required in BIAcore [275]. ELISA is used with relatively high affinity antibodies because antibody-antigen complex needs to be maintained during both the incubation and washing steps [258], whereas BIAcore can detect low affinity molecules as well as high affinity antibodies [276].

ELISA and BIAcore were used as two methods to measure the binding affinities of the purified molecules whose preparation is described in Chapter 3. In much of this project, VEGF (the ligand) was immobilised onto the chip surface for BIAcore measurement or coated on the plate for ELISA measurement while measuring the binding of bevacizumab and its PEGylated analogues as an analyte.

As was described in Chapter 3, Fab_{beva} and Fab_{trast} were obtained by proteolytically digesting bevacizumab and trastuzumab. Their purified fragments are shown in Figure 4.4, A. Lanes 3 and 10. It was necessary to determine the binding

affinity of these Fabs to understand if their antigen-binding properties were retained after the digestion and purification processes. Afterwards, these Fabs along with Fab_{rani} were PEGylated at their interchain disulfide bond. The purified PEG-Fab_{beva} derived with three different molecular weights of PEG mono-sulfone **2** (20, 30 and 40 kDa) are shown in Figure 4.4, A. Lanes 4-6. The purified PEG_{20}-Fab_{rani} and PEG_{20}-Fab_{trast} are also shown in Figure 4.4, A. Lanes 9 and 11. The aim was to determine the binding affinity and kinetic constant rates of these purified PEG-Fab conjugates to study the effect of disulfide bridging PEGylation on binding strength of the parent Fab. In addition, Fab'_{beva} was also PEGylated with two PEG reagents **2** (20 kDa) (Figure 4.4, A. Lane 7) to compare its binding kinetics with the mono PEG_{20}-Fab_{beva}. Bevacizumab and trastuzumab were also PEGylated and the binding affinity of PEG_{10}-bevacizumab (Figure 4.4, A, Lane 2) was studied in BIAcore to evaluate the effect of PEGylation on the binding of bevacizumab.

The homodimer of Fab_{beva}-PEG-Fab_{beva} (Figure 4.4, B, Lanes 1, 2 and 3) and Fab_{rani}-PEG-Fab_{rani} (Figure 4.4, B, Lanes 4, 5 and 6) were prepared with three molecular weights of the PEG di(mono-sulfone) reagent **4**, 6, 10 and 20 kDa, and Fab_{trast}-PEG-Fab_{trast} with 20 kDa PEG di(mono-sulfone) reagent **4**, was prepared (Figure 4.4, B, Lane 7). The structure-property correlations between different molecular weights of the homodimer Fab-PEG-Fabs were compared with the full IgG using BIAcore and ELISA. It was hoped that the homodimer Fab-PEG-Fabs display binding properties comparable to the full IgG. It was also thought that using different molecular weights of the PEG reagent **4** in the homodimer construct may display different binding properties.

In addition, the heterodimer Fab_{beva}-PEG_{20}-Fab^*_{trast} was prepared (Figure 4.4, B, Lane 8) from the Fab_{beva} and Fab_{trast} using the PEG di(mono-sulfone) reagent **4**. It was hoped that using BIAcore, the binding of this heterodimer could be determined and preserved with its perspective ligands. Table 4.1 is a summery table of all the constructs, which were prepared in Chapter 3 and their binding affinity determined in this chapter either by ELISA or BIAcore.

Table 4.1 List of the molecules and the purified PEGylated constructs that were used in BIAcore and ELISA binding studies.

Antibody	PEG-antibody	Fab	PEG-Fab	Fab-PEG-Fab	Fab-PEG-Fab*
Bevacizumab	PEG_{10}-bevacizumab	Fab_{beva}	PEG_{20}-Fab_{beva}	Fab_{beva}-PEG_6-Fab_{beva}	Fab_{beva}-PEG_{20}-Fab^*_{trast}
			PEG_{30}-Fab_{beva}		
			PEG_{40}-Fab_{beva}	Fab_{beva}-PEG_{10}-Fab_{beva}	
			PEG_{2x20}-Fab'_{beva}	Fab_{beva}-PEG_{20}-Fab_{beva}	
Trastuzumab		Fab_{trast}	PEG_{20}-Fab_{trast}	Fab_{trast}-PEG_{20}-Fab_{trast}	
	Ranibizumab		PEG_{20}-Fab_{rani}	Fab_{rani}-PEG_6-Fab_{rani}	
				Fab_{rani}-PEG_{10}-Fab_{rani}	

A

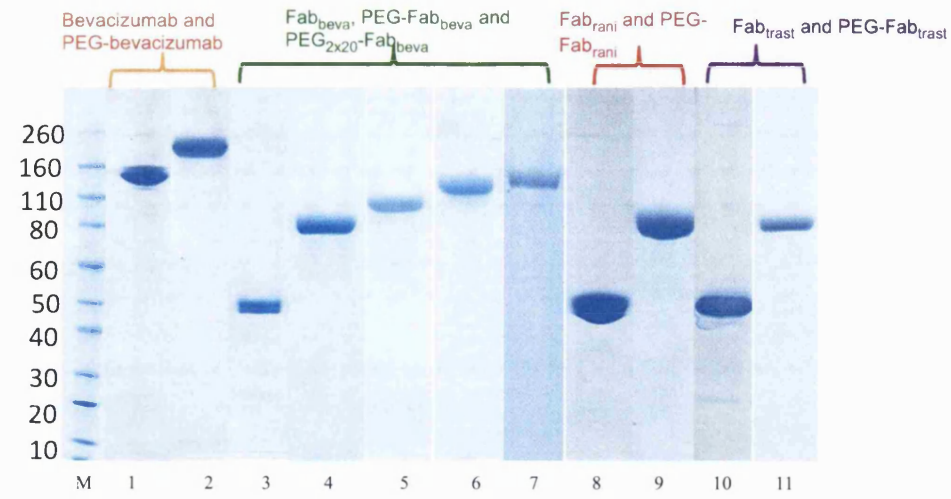

B

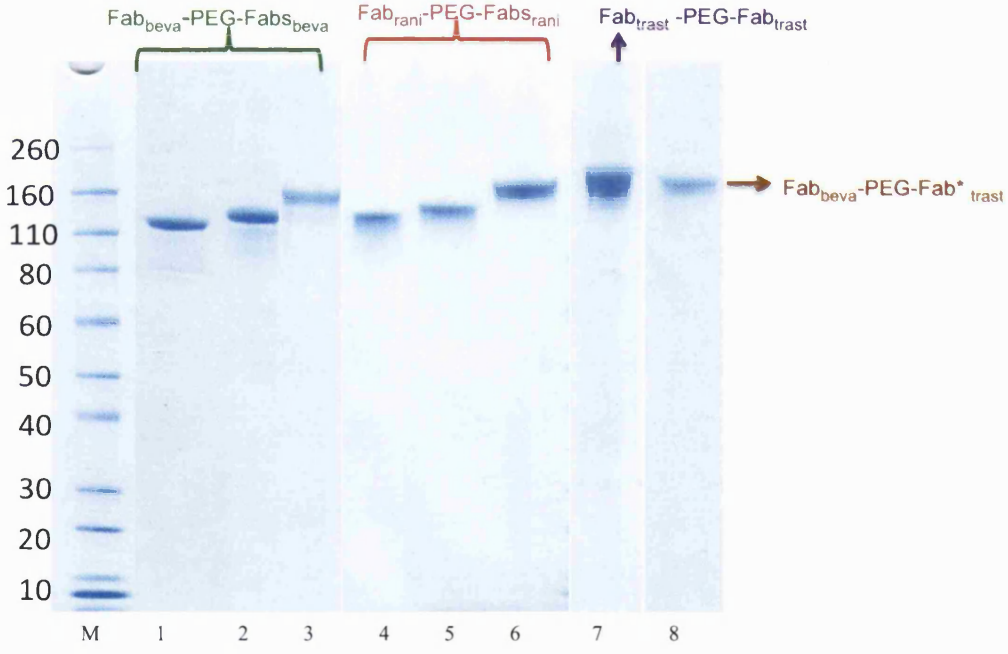

Figure 4.4 SDS-PAGE analysis of the purified constructs listed in Table 4.1, Novex Bis-Tris 4-12% gel stained with colloidal blue (Lanes M-11 (A) and M-8 (B)). **(A)** *Lane M:* Protein standard, *Lane 1:* Bevacizumab, *Lane 2:* The purified PEG_{10}-bevacizumab, *Lane 3:* Fab_{beva}, *Lanes 4-6:* The purified 20, 30 and 40 kDa PEG-Fab_{beva}, *Lane 7:* The purified PEG_{2x20}-Fab'_{beva}, *Lane 8:* Fab_{rani}, *Lane 9:* The purified PEG_{20}-Fab_{rani}, *Lane 10:* Fab_{trast}, *Lane 11:* The purified PEG_{20}-Fab_{trast}. **(B)** *Lane M:* Protein standard, *Lanes 1-3:* The purified 6, 10 and 20 kDa Fab_{beva}-PEG-Fab_{beva}, *Lanes 4-6:* The purified 6, 10 and 20 kDa Fab_{rani}-PEG-Fab_{rani}, *Lane 7:* The purified Fab_{trast}-PEG_{20}-Fab_{trast}, *Lane 8:* The purified Fab_{beva}-PEG_{20}-Fab^*_{trast}.

4.2 Kinetic affinity using BIAcore

The SPR response is directly related to the mass concentration of material at the sensor surface [188, 265]. A key consideration is how much ligand should be immobilised to the chip [265]. The amount of ligand to use depends on the relative molecular weights of the ligand and analyte, and on the stoichiometry of interaction between the analyte and ligand [266]. The theoretical binding capacity (R_{max}) of a sensor surface with an analyte is related to the amount of immobilised ligand as follows [272]:

$$R_{max} = \text{MW analyte / MW ligand} \times S_m \times R_L$$

R_{max} is the maximum capacity of analyte binding and R_L is the actual level or amount of immobilised ligand on the surface. S_m is the binding stoichiometry and is the stoichiometry of binding between ligand and analyte. The immobilisation level is calculated based on the amount of ligand remaining on the surface at the end of the immobilisation procedure after the deactivation step [272]. Not all of the immobilised ligand on the sensor surface are available and active for binding to analyte because during immobilisation the ligand binding sites are likely to be damaged or hindered within the dextran layer. Therefore, the theoretical R_{max} is often higher than experimental R_{max}.

In this project, the sensor surface was prepared based on VEGF as a ligand and the Fab as an analyte. A binding stoichiometry of 2 was used since the immobilised VEGF ligand was bound as a dimer to two Fabs. Two VEGF-monomers form a biologically active ligand. The dimer has two binding sites for the analyte and each binding site is formed by domains from both monomers [277, 278]. It was proposed that two anti-VEGF Fabs are required to bind to VEGF dimer to make a Fab-VEGF complex [278]. In addition, it was reported that one molecule of bevacizumab binds to one molecule of VEGF and the binding epitopes of VEGF interact with bevacizumab do not overlap with the binding epitopes of VEGF to VEGFR and the neutralising effect occurs due to the steric shielding of bevacizumab binding to VEGF [46, 278].

The carboxymethylated (CM) dextran matrix on the sensor chip surface is hydrophilic, flexible and has a high binding capacity. The dextran layer is present in all sensor chips except sensor chip C1, HPA and underivatised Au chips. The carboxylic acids on the dextran are easily functionalised to active esters for covalent coupling, which are then exposed to the protein, or molecule of interest, that is to be immobilised. A wide range of molecules such as small organic molecules, proteins, nucleic acids, and carbohydrates can be immobilised. In the case of a protein, amines will non-selectively

undergo reaction to form an amide with the active ester moieties on the dextran. If amine groups are too near or concentrated to the binding site of protein of interest, other chip immobilisation strategies are available including thiol and aldehyde coupling, and streptoavidin-biotin capture [272].

The CM chip can be purchased with different amounts of dextran bound to the surface. This allows for different amounts, or densities of the immobilised molecule to be conjugated to the chip. These chips are known as CM5, CM4, and CM3 chips (Figure 4.5). The CM5 chip has a highest amount of carboxymethylated cellulose on its surface and provides the high surface capacity for immobilisation. The high binding capacity of the CM5 chip is an advantage for capture assays and work with small molecules [272]. Also, the CM5 chip provides high surface stability and can result in more accurate and precise analysis. The CM4 chip has a lower amount of carboxymethylation (approximately 30 % of that of CM5) on the surface compared to the CM5 chip, which results in the reduction of the immobilisation capacity and surface charge density in the CM4 chip. The lower charge on the surface of CM4 chip causes reduction of non-specific binding that may occurs between positively charge molecule and the surface. Therefore, this chip is appropriate when the ligand is to be extracted from a mixture that the analyte may also be present such as cell extract and culture media. In addition, because of its lower immobilisation capacity, the CM4 chip might be advantageous to conduct kinetic assays where low immobilisation level is required.

The CM3 chip contains the same relative molar carboxymethylation level as the CM5 chip, but the dextran chains in the matrix are shortened compared to the CM5 chip. This shorter dextran chain can help to reduce steric effects that occur when a large molecules such as antibodies, viruses and whole cells are used. In addition, the change in dextran length allows a closer interaction between the surface and the ligand and helps to improve sensitivity. Similar to CM4 chip, the immobilisation capacity of the CM3 chip is about 30 % of the CM5 chip and this can again be an advantage for conducting kinetic assays [272].

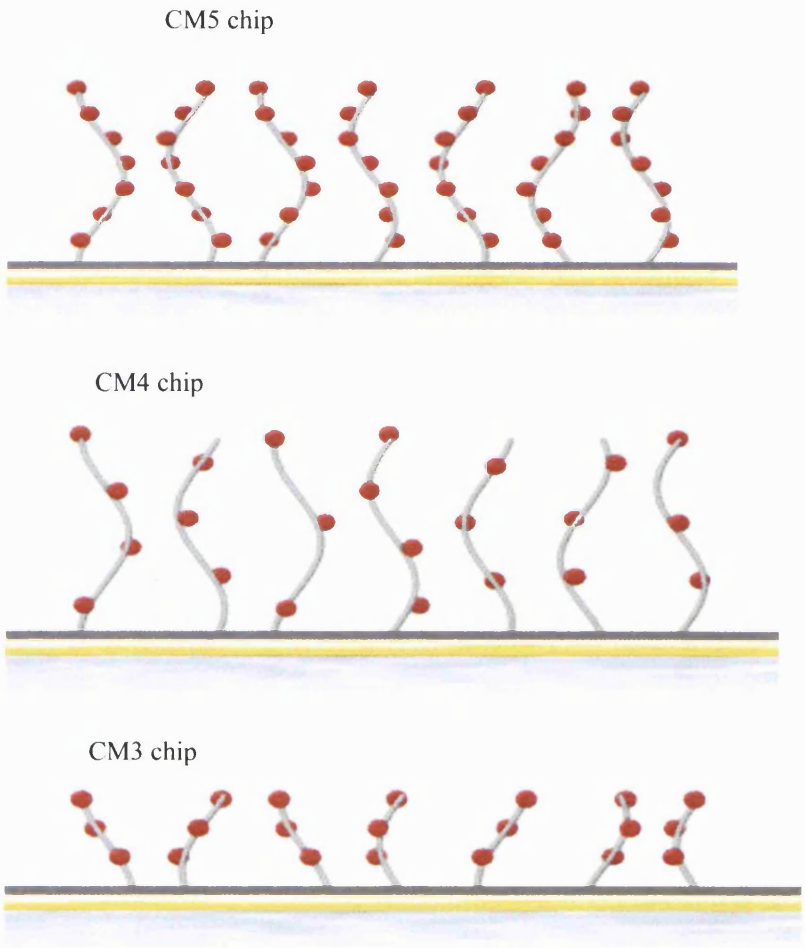

Figure 4.5 Carboxymethylated dextran chip. CM5 chip with high amount of carboxymethylate group, CM4 chip with a lower degree of carboxymethylation, CM3 chip with shorter dextran chain. Dextran matrix covered with carboxyl groups (red circles), reproduced from [272].

Three different experiments can generally be designed when evaluating antibody-ligand interactions by BIAcore; (i) binding, (ii) active concentration and (iii) binding kinetics. Interactions between analyte and ligand can be detected in a binding assay. This experiment is used to determine whether there is any binding between the analyte and ligand or not. This assay can provide some indication about the specificity of an analyte of interest with the immobilised molecule. For instance, it was studied the difference in binding of human VEGF and mouse VEGF to bevacizumab in the situation where, bevacizumab was immobilized on the CM5 with a 1000 RU immobilization level using binding assay [279]. They found that no binding was measured between mVEGF and bevacizumab, whereas strong binding was detected between hVEGF and bevacizumab [279].

In a concentration assay, the active protein concentration in the analyte is determined. This experiment can be conducted either with or without a calibration curve. When using calibration curve, the concentration assay is a direct binding experiment that measures the analyte that is bound to the immobilised ligand on the sensor surface. The concentration of an unknown sample can be calculated based on the binding response correlated to the calibration curve. When a calibration curve is used, the surface density of the ligand immobilised on the sensor chip should be high enough to ensure the mass transfer effect occurs. The 'mass transfer effect' is referred to the situation where the rate at which analyte binds to ligand exceed the rate at which analyte transfer from bulk to sensor surface [280]. This effect and its limitation are discussed further in the following section.

In the calibration free concentration assay (CFCA) no calibration curve is used. CFCA is based on the relationship between the diffusion or mass transport properties of the analyte from the bulk flowing solution to the sensor surface. The interactions of the analyte can be evaluated with short sample injections using at least two different flow rates. One flow rate should be low (e.g. 5 µl/min) and the other flow rate should be high (e.g. 100 µl/min). A high concentration of ligand should be immobilised on the chip so that mass transport effects can occur. The CM5 chip is therefore most often used in the CFCA experiment.

There are some limitations with conducting CFCA. Proteins with molecular mass above 5000 Da can only be applied for this method. Also analyte-ligand interactions that have a slow association constant rate (below 5 x 10^4 $M^{-1}s^{-1}$) and low affinity value (K_D higher than 10^{-6} M) cannot be used. More importantly, not all proteins have a known diffusion coefficient and are not suitable for CFCA assay. The CFCA assay, however, was recently introduced by the GE Healthcare BIAcore group and few studies have been published using this assay.

Determination of the rates of association and dissociation can be accomplished by a kinetic assay using BIAcore. Determination of these kinetics parameters is an important characteristic of SPR where it is possible to determine the binding rates between analyte and ligand at real time. The kinetic experiment provides information regarding how fast the analyte-immobilised ligand complex associates and is formed (k_a) and dissociates leading to its decay (k_d) [6]. This experiment provides a method to determine the affinity and strength of the binding between an analyte and its ligand because the equilibrium constant (K_D) is derived from the ratio of the dissociation and

association constant rates (k_d/k_a) (Figure 4.1). The kinetic data are analysed mainly by BIAevaluation software. The background response that occurred in the control flow cell needs to be subtracted from the total binding response and then by applying the right kinetic model, the kinetic parameters can be calculated [253]. Different fitting models can be applied depending on the nature of interaction between the analyte and ligand, however, in the most cases of antibody-antigen interaction, the simple 1:1 Langmuir binding model is recommended [281, 282]. For example, a k_a value of 7.9 x 10^4 $M^{-1}.S^{-1}$, k_d of 1.23 x 10^{-4} s^{-1} and the K_D value of 1.55 nM were calculated for bevacizumab in the situation where $VEGF_{165}$ was immobilized on a CM5 chip applying 1:1 binding model at 25 ^{0}C [283]. In another study, the kinetic assay was performed on bevacizumab and bevacizumab-Fab (called Fab-12) where $VEGF_{165}$ was immobilized on the CM5 chip with 60 RU immobilization level at 37 ^{0}C applying 1:1 binding model. The Fab-12 was a Fab portion of bevacizumab that was engineered in E-coli. The k_a value of 9.2 x 10^4 $M^{-1}.S^{-1}$and k_d value of 2.0 x 10^{-4} s^{-1} and the K_D value of 2.2 nM were calculated for bevacizumab whereas the k_a value of 7.5 x 10^4 $M^{-1}.S^{-1}$ and k_d value of 6.4 x 10^{-4} s^{-1} and the K_D value of 8.5 nM were calculated for Fab-12 [284]. The binding affinity and kinetic rate constant of Fab-12 were also studied by another group where VEGF was immobilized on a CM5 chip with 190 RU immobilization level at 37 ^{0}C applying 1:1 binding model [285]. The k_a value of 5.5 x 10^4 $M^{-1}.S^{-1}$ and k_d value of 11 x 10^{-4} s^{-1} and the K_D value of 20 ± 3.8 nM were calculated for Fab-12 in this study [285].

For kinetic assays a low Rmax is often required (less than 100 RU) [252, 253]. The reason a low Rmax value is required is to minimise mass transfer and rebinding limitations that are associated with high Rmax value. This is discussed in more details in the following section. The way to achieve a low Rmax value is to ensure a small relative amount of ligand is immobilised on the surface of the sensor chip.

4.2.1 Kinetics assay

The association constant rate (k_a or k_{on}) is the rate of complex formation, i.e. the number of AB complexes formed per second in a 1 molar solution of A and B. The main factors affecting the association constant rate are (i) the concentration of analyte (A) near to the immobilised ligand, (ii) the amount of the immobilised ligand (B) [252] and (iii) the contact time between flowing analyte and the immobilised ligand. If there is a high density of ligand present on the sensor chip (high immobilisation level), then the rate at

which the analyte binds to the ligand can exceed the rate at which the analyte can be delivered to the surface. This is referred to as the mass transport effect. In this situation, binding is limited by mass transport effects and the association rate will yield an *apparent* k_a or *apparent* k_{on}. In this condition the observed k_{on} will be slower than the true k_{on} [252, 253]. It is not possible to determine k_{on} in this situation and experimental conditions must be optimised to minimise the mass transport limitation.

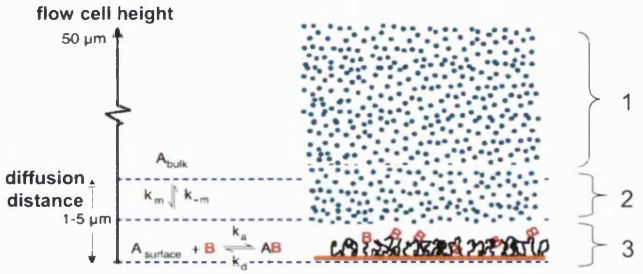

1. Analyte supplied by convection (continuous flow)
2. Diffusion becomes increasingly important as the flow rate reduces closer to the surface
3. Biomolecular interaction processes at the ligand/analyte interface

Figure 4.6 Different ways that analyte transfer from bulk to the sensor surface, reproduced from [272].

In general, the analyte can be transferred from the bulk towards the ligand by both convection and diffusion (Figure 4.6). Convection transport is controlled by the flow rate of the analyte solution over the sensor chip. Higher flow rates will result in greater convection transport. This will help to minimise the mass transport limitation because more analyte can be delivered from bulk to sensor surface (step 1 in Figure 4.6). However, the mass transport can still be limiting, even at maximal flow rates because of an unstirred 'diffusion layer' (step 2 in Figure 4.6) that is close to the sensor surface. The transport of analyte through this layer is primarily controlled by diffusion processes. In this case, mass transport limits can only be minimised by decreasing the surface density of the immobilised ligand to increase the diffusion process [267].

The key parameter that affects the dissociation constant rate (k_d or k_{off}) is the time allowed for dissociation to occur. The dissociation constant rate defines the stability of the complex once it is formed. It denotes the fraction of complex that decays per second (Scheme 4.1). The main factors that influence analyte dissociation are the surface density of the bound analyte, the dissociation rate constant (k_{off}) and also whether the dissociated analyte can re-bind to immobilised ligand before leaving the sensor surface (re-binding effect). The dissociation constant rate can be limited by such

re-binding effects [253]. Although, increasing the flow rate will increase the convection rate and may decrease re-binding effects, re-binding can still occurred due to the unstirred diffusion layer. The only way to minimise re-binding effects is by decreasing the level of the ligand immobilised on the surface. Together both the mass transport limitation and re-binding can lead to an underestimation of the true kinetics (k_{on} and k_{off}). Often these effects can be minimised and avoided by lowering the amount of immobilised ligand and to some degree by increasing the flow rate.

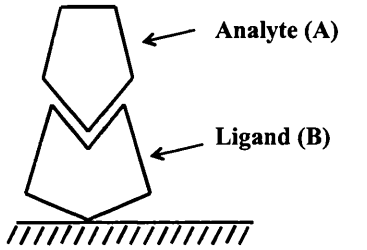

$$A + B \underset{k_d}{\overset{k_a}{\rightleftharpoons}} AB$$

$d[AB]/dt = k_a . [A] . [B]$

$- d[AB]/dt = k_d . [AB]$

k_a: Association constant rate $[M^{-1}S^{-1}]$

k_d: Dissociation constant rate $[S^{-1}]$

$K_D = k_d / k_a$ = Equilibrium dissociation constant $[M] = [A] . [B] / [AB]$

$K_A = k_a / k_d$ = Equilibrium association constant $[M^{-1}] = [AB] / [A] . [B]$

Scheme 4.1 The diagram of association and dissociation constant rate.

The K_A constant is an equilibrium constant and is a ratio of the forward rate over the reverse rate. K_D is the reciprocal of K_A. The K_D is described as a dissociation tendency and it is in units of molar concentration and is defined as a ratio of the dissociation constant rate to the association constant rate (k_d / k_a). Often for antibody-ligand binding, this ratio is also defined as k_{off} / k_{on}, to represent the ratio of the off rate to the on rate. The typical range of k_{off} which is acceptable in BIAcore is 1×10^{-1} to 1×10^{-6} s^{-1}. The acceptance range of 1×10^{3} to 1×10^{7} $M^{-1}.s^{-1}$ is for k_{on} and 1×10^{-5} to 1×10^{-12} M for K_D [253].

Measurement of K_D by BIAcore involves injecting a series of analyte concentrations to flow over the immobilised ligand on the chip and measuring the binding level at equilibrium to determine k_{off} and k_{on} (Scheme 4.1). The relationship between the binding and analyte concentration allows the calculation of K_D. The higher a relative K_D number, the lower is the affinity between the analyte in solution and the immobilised ligand. Higher relative K_D values indicate that the analyte-ligand complex will have the tendency to dissociate more readily than complexes with lower K_D values. Smaller relative K_D values means that there is a higher affinity and thus, stronger

interaction between an analyte and ligand.

In addition to re-binding effects and mass transport limitations, there may be other effects that occur when a relatively high level of ligand is immobilised onto the sensor chip. In principle it is possible that at a threshold immobilisation concentration that a cross-linking effect could also occur (Figure 4.7). If a high amount of the VEGF ligand were to be immobilised on the chip, a bivalent analyte (e.g full IgG, homodimer Fab-PEG-Fab construct) can bind to two different ligand molecules (Figure 4.7, A). It would be difficult to estimate the kinetic fitting model if this type of binding occurs. A low level of ligand immobilisation would be expected to minimise such cross-linking from occurring (Figure 4.7, B). A single monovalent analyte (e.g Fab) can bind to one homodimer ligand with 1:1 binding model, when a low amount of ligand is immobilised (Figure 4.7, C).

Selecting the right model in the kinetics assay is important [253]. It is recommended by the manufacturer to use the simplest model that best fits the data. As the complexity of the model increases, more fitting parameters are required. This results in more degrees of freedom which can give a better fit but not necessarily lead to more relevant or accurate results [286]. The 1:1 binding model is considered the simplest model because less fitting parameters are involved than more complex models which are often used with heterogeneous analyte. The nature of the interaction between ligand and the analyte should also be considered to find the optimal kinetic model. When one molecule of analyte binds to one molecule of ligand based on Langmuir model, the nature of interaction is one to one binding.

Several steps are required to determine which kinetic model should be used. The initial step is to seek agreement between experimental data and a fitted curve by evaluating residual plots and by assessing Chi^2. The Chi^2 is the sum of the squared error between the fitted curve and experimental curve. This number should be as small as possible (less than 2 and even less than 1). The shape of the residual plot that is obtained from the difference between the experimental and calculated curve is important to validate the fit. The ideal fit has a residual plot scattered around zero, which means there is no difference between the experimental sensogram and the fitted (calculated) curve. There are other parameters such as the T-value, U-value and tc value which help to assess the fitting model. These values are embedded in the software used in the calculation of the kinetic model. The T-value is calculated by dividing the kinetic rate constants by the standard error (value/SE) and indicates the significance of the

kinetic parameters. The T-value should be greater than 100 or even higher which results in lower standard error. In addition, the standard error (SE) of association and dissociation rate constant can be calculated by BIAevaluation software and considered as fitting parameters, which show the precision and significance of the kinetic rate constant. Generally, the SE of the k_a and k_d should not be greater than two degrees of the magnitude of the value of k_a and k_d. The parameter which represents the effect of mass transport limitation is tc. If the tc value is between 10^7 to 10^9, then there is a mass transport limitation.

Sensor chips used in this project were prepared with low levels of immobilised ligand. Kinetic data for all the samples were evaluated using BIAevaluation software (version 2.0.1 plus package) applying a simple 1:1 binding model. The data were double-referenced to subtract the bulk effect that occurs due to the changes in the buffer composition or non-specific binding. A flow rate of 30 μL/min was selected to run the kinetic assays, and an association time of 180 sec and dissociation time of 1200 sec were used. The flow rate of 30 μL/min was the highest flow rate that could be used in the BIAcore X-100 that was used. An association time of 180 sec and dissociation time of 600 sec were applied in [114] to determine the binding affinity between anti-$p185^{HER-2}$ antibody single chain (scFv) to an immobilised antigen anti-$p185^{HER-2}$ [114]. Applying longer dissociation time (1200 sec) would ensure that most of the analytes were dissociated from the ligand before regeneration step and it would help to evaluate and compare the dissociation profiles of different constructs. The kinetic assay was performed at a temperature of 25 ^{0}C as the BIAcore X-100 that was available can only be used at this temperature. All these parameters were kept constant during the kinetics assays for all the test compounds.

A; High amount of ligand on the chip, cross-linking occurs.

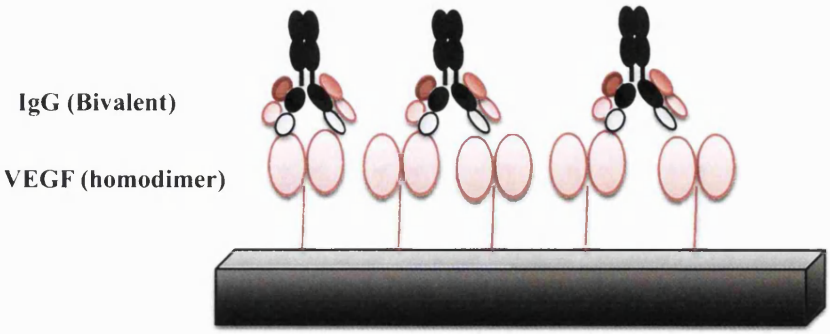

B; Low amount of ligand on the chip, no cross-linking.

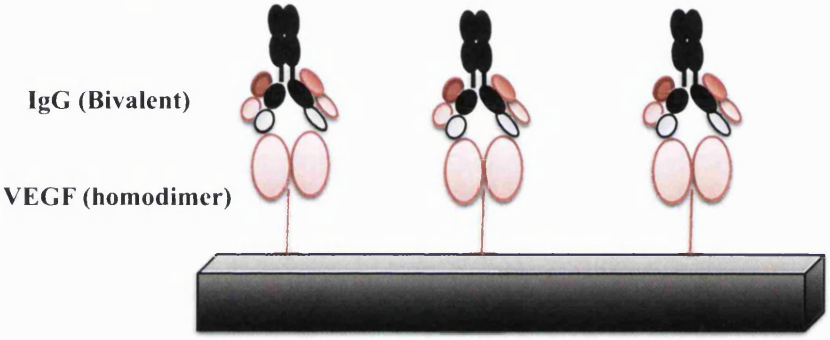

C; Low amount of ligand on the chip, 1:1 binding model with the Fab.

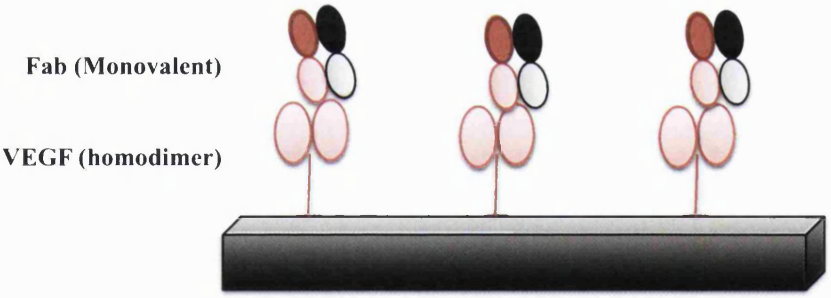

Figure 4.7 1:1 binding model of bivalent antibody (A, B) and (C) monovalent antibody fragment. **(A)** High amount of ligand on the chip cause cross-linking, **(B)** Low amount of ligand immobilised on the chip, less cross linking, **(C)** Binding of the Fab to ligand with low immobilisation level (1:1 binding).

The majority of work described herein was accomplished with immobilised $VEGF_{165}$, but both this ligand and HER-2 were bound to CM3 chips at a low immobilisation concentration on the surface. This meant that after the dextran carboxylate were activated by the carbodiimide reagent, this was followed by an injection of a small amount of the ligand followed by the injection of ethanolamine which was used to conjugate the remaining activated dextran carboxylic acid moieties.

While CM3 chips were prepared for kinetic assays with low immobilisation level, initial attempts were also performed to immobilise CM5 chips. However, it was not possible to achieve a low immobilisation level using CM5 chip because of high amount of the carboxymethylated groups on the sensor surface.

4.2.2 CM3 chip preparation:

There are three steps to immobilise a ligand onto a sensor chip:

1. Ligand pre-concentration (electrostatic attraction between ligand and dextran surface).
2. Immobilisation step.
3. Regeneration step.

Pre-concentration assay:

Electrostatic interactions between the ligand and the sensor surface are used to aid the localisation of the ligand at the sensor surface. This is known as the pre-concentration step. If the ligand has good electrostatic interactions with the dextran surface, then there will be more effective control of the covalent conjugation with the carboxylic acid group on the dextran. The sensor chip surface carries a net negative charge at pH above 3.5 (pI value of dextran is 3.5). Therefore, to achieve an efficient pre-concentration, the pH of the ligand buffer solution should be above 3.5 and lower than the pI of the ligand. Human $VEGF_{165}$ (38.2 kDa molecular weight) has a pI value of 8.6 [287]. The HER-2 (110 kDa molecular weight) used was the extracellular domain of the receptor and it has a pI value of 5.58. Many proteins tend to aggregate or precipitate at low pH, it is also necessary to determine an optimum pH which is a compromise between efficient pre-concentration and not precipitating the ligand. This is accomplished by conducting scouting experiments which can determine which pH appears to give the best interaction between the ligand and the sensor chip.

Figure 4.8 shows pH scouting assay performed for $VEGF_{165}$ (10 μg/mL) in sodium acetate (10 mM) buffer at different pH values (4.0, 4.5, 5.0, 5.5, 6.0, 6.7). A contact time of 180 sec was set to perform this pH scouting assay.

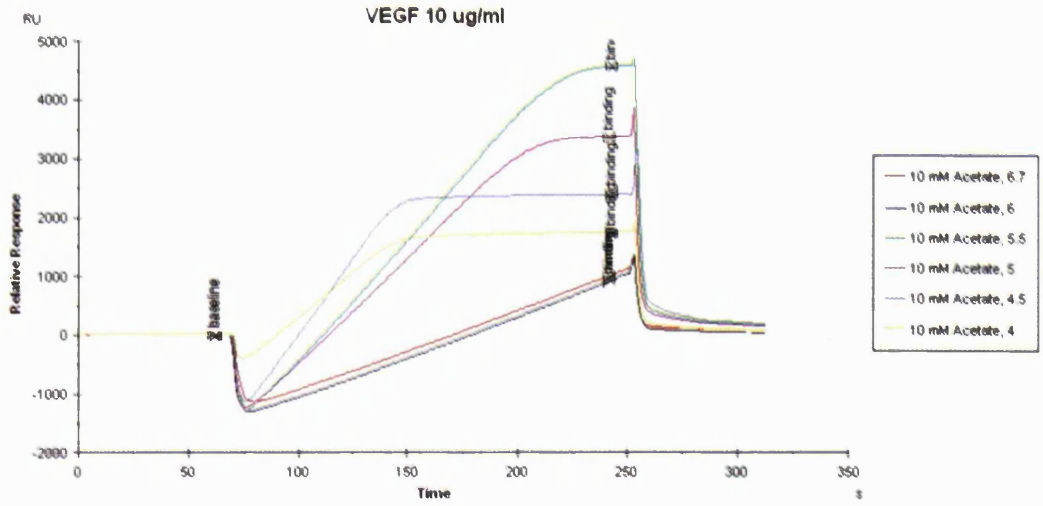

Figure 4.8 pH scouting assay using VEGF (10 µg/mL) in sodium acetate buffer.

At pH 4.0 and 4.5, VEGF (Figure 4.8, yellow and dark blue lines) displayed a low binding response and appeared to be degraded after 40 sec. This could be a result VEGF degradation and precipitation in acidic pH. At higher pH (Figure 4.8, pH 6.0 and 6.7, red and black lines respectively), the slope of binding appeared to be very low suggesting that the interactions between the ligand and dextran were not good. In contrast, there appeared to be a high binding response at pH 5.0 or 5.5 with a good binding slope (Figure 4.8, green and purple lines). The response at pH 5.5 displayed a better binding level (Figure 4.8, green line) which indicated a higher degree of non-covalent interaction between the ligand and the dextran surface. Since the response was correlated with pH, it was thought that it was driven primarily by electrostatic interactions. After these scouting experiments, sodium acetate (10 mM) pH 5.5 was selected as the solution to immobilise $VEGF_{165}$ to the sensor chip surface. Removal of the VEGF from the sensor surface after its contact period had elapsed, was achieved with sodium hydroxide (50 mM, 60 sec). The NaOH was injected over the sensor chip surface to disrupt the electrostatic interactions between the VEGF ligand and carboxylic acid moieties on the dextran. Exposure to NaOH was necessary to regenerate a clean dextran layer ready for immobilisation step.

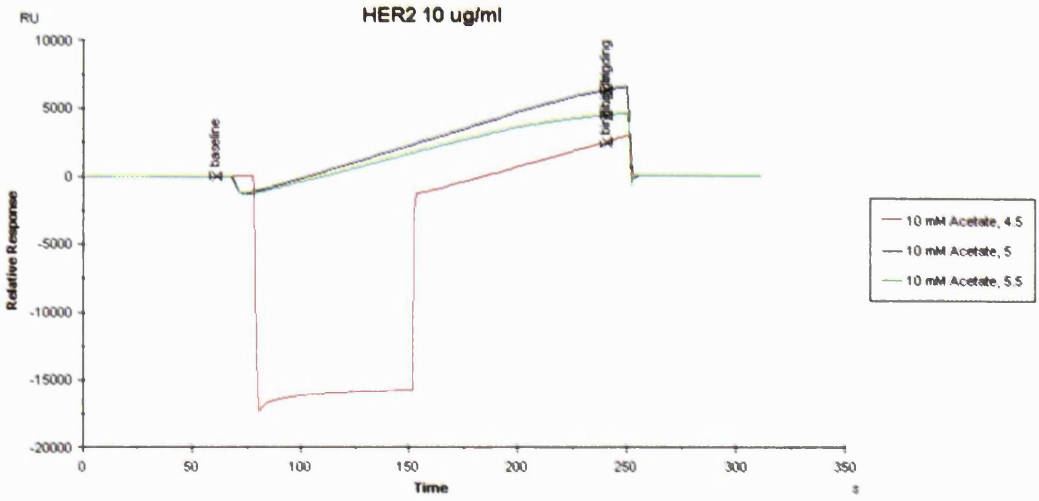

Figure 4.9 pH scouting assay using HER-2 (10 μg/mL) in sodium acetate buffer.

Figure 4.9 shows the analogous pH-scouting experiment that was performed for the HER-2 ligand. In this assay, HER-2 (10 μg/mL) was dissolved in sodium acetate (10 mM) pH 4.5, 5.0 and 5.5. The HER-2 appeared to be degraded at pH 4.5 (Figure 4.9, red line) similar to VEGF. The binding response for the HER-2 solution at pH 5.0 (Figure 4.9, black line) appeared to be higher than pH 5.5 (Figure 4.9, green line) and a higher binding slope. Since HER-2 at pH 5.0 displayed a better binding level, it was selected for the immobilisation step. Sodium hydroxide was again used to regenerate a clean dextran surface on the sensor chip ready for the immobilisation step.

Ligand immobilisation:

The general method involve in immobilisation of the ligand on CM3/CM5 chip using amine-coupling method. This consists of three basic steps:

1- Activation: The sensor surface has to be activated first with a mixture of 1-ethyl-3-(3-dimethylaminopropyl)-carbodiimide (EDC) and N-hydroxysuccinimide (NHS) to produce reactive succinimide ester (Scheme 4.2). This activation is necessary because the carboxymethyl group on the dextran surface is not very reactive by itself, however, succinimide ester is a very good reactive group since ester is a good leaving group.

2- Coupling: The ligand was then injected over the activated surface until the sufficient amount of ligand is bound (Scheme 4.2). In amine chemistry, the covalent conjugation occurs between the activated dextran and primary amine group of the ligand (Scheme 4.2). Other coupling (thiol, aldehyde) can also perform for chip preparation suing thiol and aldehyde groups of the ligand.

3- Deactivation: By injecting a blocking solution such as ethanolamine, a remaining activated site can be quenched. Ethanolamine is a primary amine which can conjugate to non-bound but activated dextran carboxylic acid moieties and therefore avoid a non-specific binding.

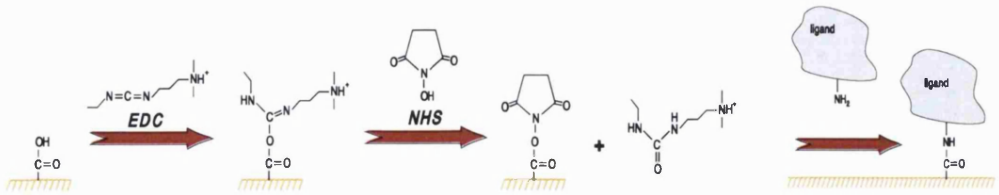

Scheme 4.2 Activation (EDC/NHS) and coupling mechanism.

In a first attempt, a wizard program on the BIAcore instrument was followed for the immobilisation of VEGF onto a CM5 sensor chip as it is a more commonly used chip and method for immobilisation that recommended by GE Healthcare BIAcore group. Using this method, the requested Rmax (e.g 100 RU) is entered into the software and the actual parameters such as contact time between ECD/NHS solution and dextran surface and between the ligand and activated surface are all set by the software program. Using the wizard programme, it is not possible to change the contact time for surface activation from 500 sec. Less activation time could result lower number of activation sites on the sensor surface. Besides the lack of being able to control the individual steps during the immobilisation process, the CM5 chip also contains a higher amount of dextran bound to the surface. To achieve the theoretical R_{max} of 100 RU with VEGF as a ligand and Fab_{beva} as an analyte, the immobilisation level (R_L) of 38.5 RU was required (100 RU = 50000/38000 x 2 x R_L). However, it was not possible to immobilise this low density to give a R_{max} about 100 RU, using the CM5 chip. Instead, 534 RU level of VEGF (Figure 4.10) which corresponded to the R_{max} of 1405 RU was immobilised (Figure 4.10). A VEGF concentration of 10 µg/mL in sodium acetate buffer (10 mM, pH 5.5) was applied for this immobilisation. Using a lower concentration of VEGF (2.0 µg/mL) and again wizard program, the new CM5 chip was immobilised with immobilisation level of 208 RU. While the immobilisation level of this CM5 chip was too high for kinetic assay, it was thought that this chip would be useful for binding assay. The binding assay was necessary to be conducted to measure the binding of the purified Fab_{beva} and $F(ab)_2$ after bevacizumab enzymatic digestion.

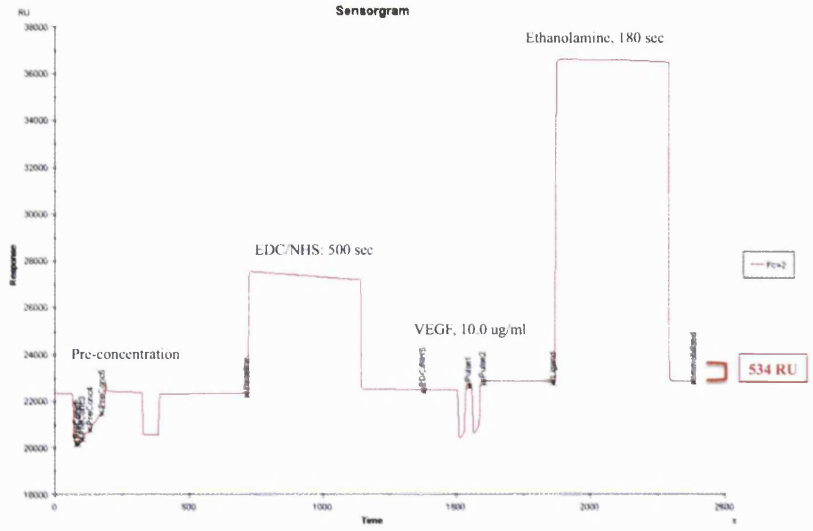

Figure 4.10 Wizard immobilisation of CM5 chip with VEGF (10 µg/mL). The immobilisation level of 534 RU achieved.

To prepare an appropriate chip for kinetic assay, it was then decided to change the CM5 chip to CM3 chip that contains shorter dextran chains with less immobilisation capacity. This means that there are less carboxylic acid moieties available for activation and subsequent lower ligand immobilisation level. It was also decided to use a manual program to conduct immobilisation. Using manual method, it was possible to control all the parameters involve and optimise the conditions to achieve the desired level of immobilisation.

Following manual control, a CM3 chip was then immobilised with VEGF. Different concentrations of VEGF (from 10 µg/mL to 0.2 µg/mL) were applied to find the best conditions to immobilise CM3 with the Rmax about 100 RU. Different activation times (500 sec to 200 sec) for EDC/NHS exposure and different contact times of the ligand with the activated surface (200 sec and 140 sec) were also examined. After these experiments, it was found that using 0.2 µg/mL of VEGF in sodium acetate at pH 5.5 with a CM3 that had been exposed to EDC/NHS with an activation time of 200 sec, that it was possible to immobilise VEGF with 57 RU.A 140 sec contact time of the VEGF was used to achieve this low level of response (Figure 4.11, A). The 57 RU immobilisation level of VEGF corresponded to theoretical Rmax of 150 RU and was appropriate for kinetic assay. CM3 chip with 61 RU was also prepared when 200 sec contact times performed with 0.2 µg/mL VEGF (Figure 4.11, B).

A; CM3 chip immobilised with VEGF, 57 RU immobilisation level.

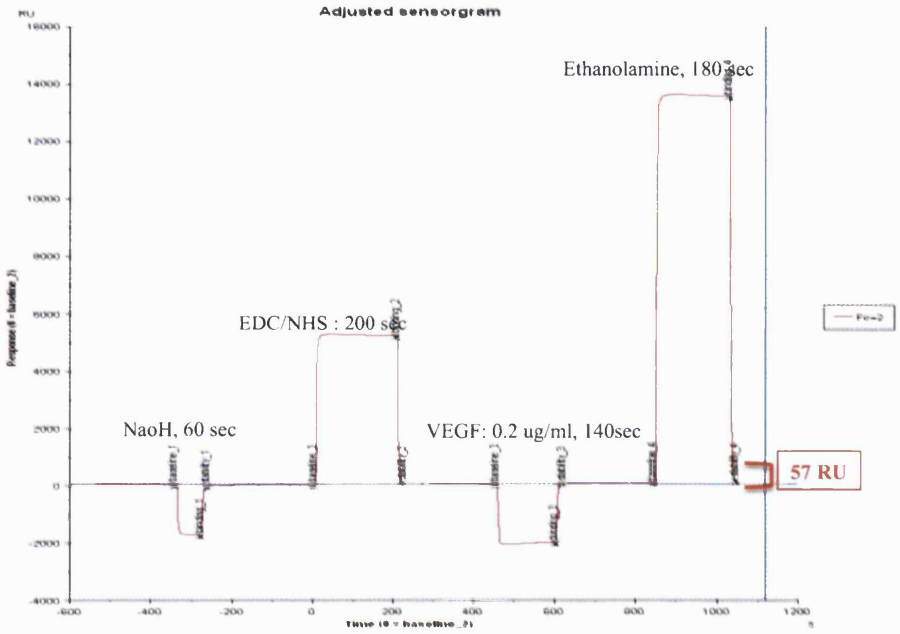

B; CM3 chip immobilised with VEGF, 61 RU immobilisation level.

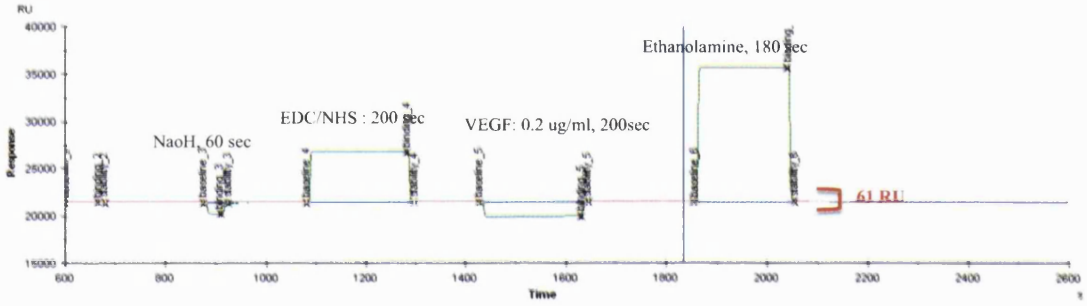

Figure 4.11 Manual immobilisation of two CM3 chips with VEGF, **(A)** The VEGF contact time was 140 sec and 57 RU immobilisation level achieved, **(B)** The VEGF contact time was 200 sec and 61 RU immobilisation level.

A CM3 chip was also immobilised with the HER-2 ligand using a similar procedure. In the case of HER-2 (MW; 110000) as a ligand and Fab_{trast} as an analyte, the binding stoichiometry of 1 was selected between Fab_{trast} and HER-2 monomer. To achieve the theoretical Rmax of 100 RU, the immobilisation level (R_L) of 222 RU was required (100 RU = 50000/110000 x 1 x R_L). Figure 4.12 shows the immobilisation sensogram of the CM3 chip with 0.2 µg/mL of HER-2 with 51 RU immobilisation level when activation time of 200 sec and contact time of 140 sec performed. The 51 RU immobilisation level of HER-2 corresponded to theoretical Rmax of 23.2 RU.

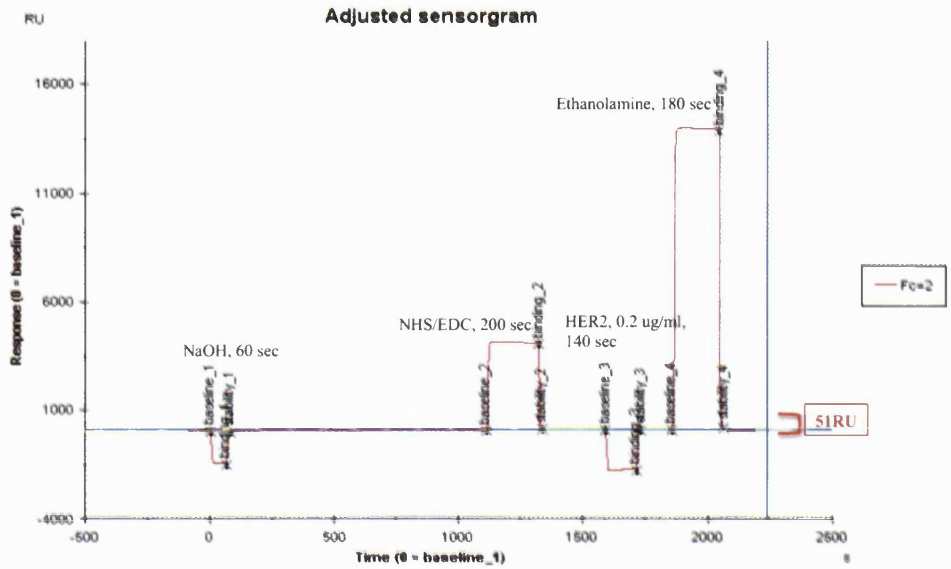

Figure 4.12 Manual immobilisation of CM3 chip with HER-2. The HER-2 contact time was 140 sec and 51 RU immobilisation level.

These chips were then used for all the kinetic assays performed on the prepared constructs derived from bevacizumab and trastuzumab.

Regeneration steps:

The regeneration buffer was then optimised. Regeneration is the process to remove bound analyte from the immobilised ligand and to prepare the chip for the next analysis. The number of times that each chip can be regenerated depends on the nature of attached ligand. The choice of regeneration buffer is an important for preserving the immobilised ligand. Repeated exposure of the immobilised ligand to a buffer designed to disrupt non-covalent interactions between the analyte-ligand can also destroy the immobilised ligand. Common solutions used to regenerate the sensor chip surface include dilute HCl, glycine-HCl, and NaOH solutions [272]. Other solutions for more difficult to separate analyte-ligand pairs include higher ionic strength solutions (1-2 M NaCl or 4 M $MgCl_2$) and solutions that also contain a low concentration of SDS (0.05 %). It was hoped that with VEGF immobilised at a low Rmax that glycine-HCl would be enough to regenerate the sensor chip after each run. Scouting experiments were conducted glycine-HCl (10 mM) at pH values of 1.5, 2.0 and 2.5. Figure 4.13 shows regeneration conditions using glycine-HCl (pH 2.5 and 2.0) after Fab_{beva} (300 µg/mL) had been exposed to a functionalised CM3 chip (57 RU, VEGF).

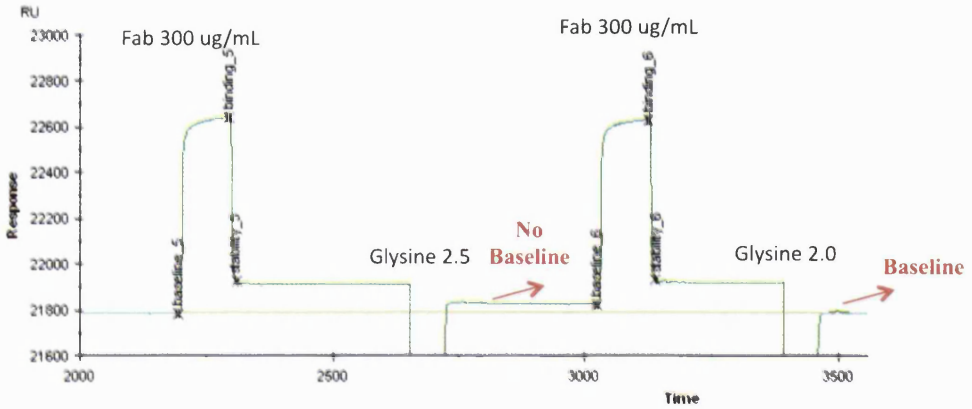

Figure 4.13 Regeneration conditions on CM3 (57 RU, VEGF).

The sensogram in Figure 4.16 indicates that when using glycine at pH 2.5 for regeneration that some of the Fab_{beva} was still in bound with VEGF as the baseline could not be re-established. However, glycine at pH 2.0 appeared to dissociate all the bound Fab_{beva} from the immobilised VEGF and the baseline was successfully regenerated. The Fab_{beva} binding response was again examined after regeneration with glycine pH 2.0 and it was found that the VEGF was still fully active and no damage occurred on VEGF during regeneration. The same result was observed for CM3 chip immobilized with HER-2 (51 RU), where using glycine-HCl (10 mM, pH 2.0) baseline could be regenerated.

4.2.3 Binding study of Fab_{beva} and $F(ab)_2$

The binding of the Fab_{beva} that was prepared by papain digestion of bevacizumab was first examined using the CM5 chip immobilised with 208 RU VEGF. The series of concentrations (0.18–2.88 μM) of the Fab_{beva} after protein A and PD-10 columns purification were prepared with HBS-EP buffer and then loaded onto the BIAcore. The binding sensograms of Fab_{beva} at different concentrations are shown in Figure 4.14 and involved association, dissociation and regeneration phases. These binding sensograms suggested that the binding of the Fab_{beva} was maintained to VEGF with concentration dependent manner. Higher concentrations of the Fab_{beva} appeared to have higher binding response and the solution with zero concentration of the Fab_{beva} (buffer only) appeared to have no binding response (Figure 4.14). In addition, the sensograms shown in Figure 4.14 demonstrated that baseline was achieved when glycine pH 2.0 was applied for regeneration buffer indicating that all Fab_{beva} had been dissociated from the chip surface.

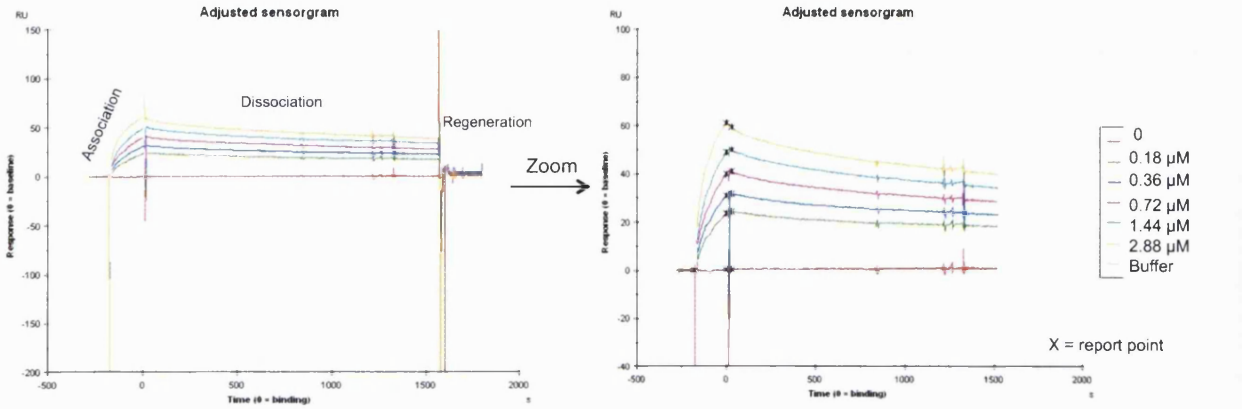

Figure 4.14 Binding sensograms of the Fab_{beva} using CM5 chip with 208 RU.

The binding of the $F(ab)_2$ fragment derived from bevacizumab by IdeS enzyme was also determined. The binding assay was again performed using the CM5 chip with 208 RU VEGF. The series of concentrations (0.07-1.25 µM) of $F(ab)_2$ were prepared with the HBS-EP buffer and then loaded onto the BIAcore. The binding sensograms of $F(ab)_2$ at different concentrations are shown in Figure 4.15. Again, the binding sensograms showing all three phases suggested that the binding of the $F(ab)_2$ fragments were retained to VEGF in a concentration dependent manner and that higher concentrations led to a higher binding response. Again, the baseline was achieved when glycine pH 2.0 was applied for the regeneration buffer.

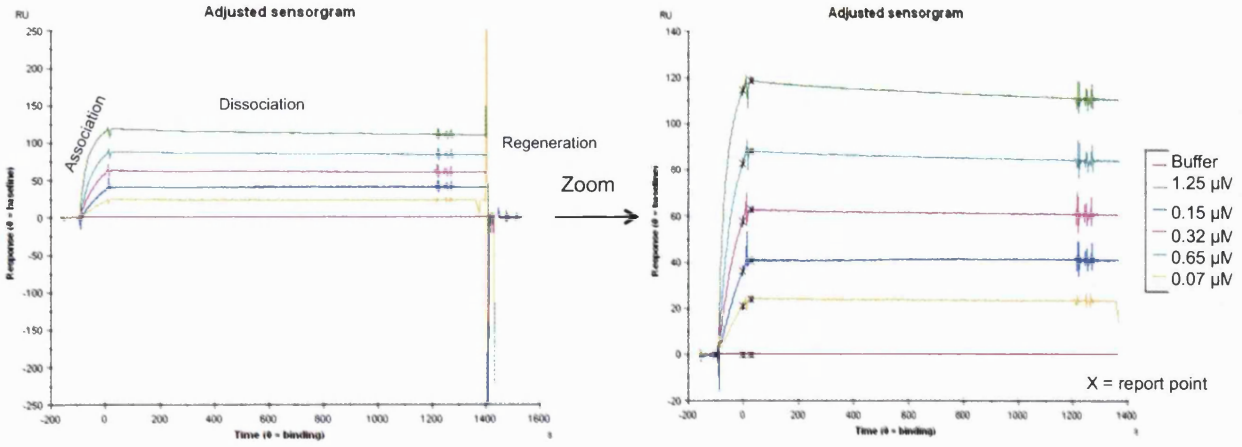

Figure 4.15 Binding sensograms of the $F(ab)_2$ using CM5 chip with 208 RU.

4.2.4 Kinetic assays of Fabs and PEG-Fabs

After study of the binding of the Fab and $F(ab)_2$, it was important to study the binding affinity of these fragments after PEGylation to examine the kinetic and affinity of interaction between the antibody and its antigen [38]. The binding affinity of antibody and antibody fragments after conjugation to PEG depends on the chemistry of PEGylation, the site, size of the PEG molecule used and the number of the PEG molecules that are conjugated per each molecule of antibody fragment [38]. It has been reported that if the PEG conjugation site is close or at the binding site of protein, it would result in the loss of binding affinity. In the case of antibodies, this loss of binding affinity is most likely due to steric hindrance of PEG with the antigen-antibody interaction [38]. When site-specific PEGylation was performed on a cysteine residue of an antibody fragment that is far from its antigen binding site, the binding affinity was decreased five fold [114] compared to the unPEGylated fragments.

Beside study of binding affinity of PEGylated antibody fragment, the study of kinetic rate constants (k_a and k_d) is important to understand the effect of the PEG conjugation site. Kinetic rate constants and the binding affinity of bevacizumab were first determined by applying different concentrations of bevacizumab (range of 0.04 μM to 0.60 μM) over the CM3 chip (VEGF, 61 RU) (Figure 4.16, A). In addition, Fab_{beva} and the 20, 30 and 40 kDa PEG-Fab_{beva} conjugate (range of 0.07 μM to 2.0 μM) were evaluated with this chip to determine their kinetic constants (Figure 4.16, B and D). The PEG_{10}-bevacizumab (range of 0.03 μM to 0.7 μM) and PEG_{2x20}-Fab'_{beva} (range of 0.05 μM to 2 μM) were also examined to calculate their kinetic constant. The concentration of the PEGylated antibody and antibody fragments were calculated by micro BCA assay with respective to protein molecular weight. The kinetic constants of the $F(ab)_2$ were also examined (Figure 4.16, C) using a similar range of concentration as bevacizumab. The kinetic fitting curve and residual plot of bevacizumab, Fab_{beva}, $F(ab)_2$ and PEG_{20}-Fab_{beva} using a 1:1 binding model are shown in Figure 4.16 as an example. The fitting parameters were also determined to ensure that the value of the kinetic rate constants and affinity were significant (Table 4.2).

A; Bevacizumab

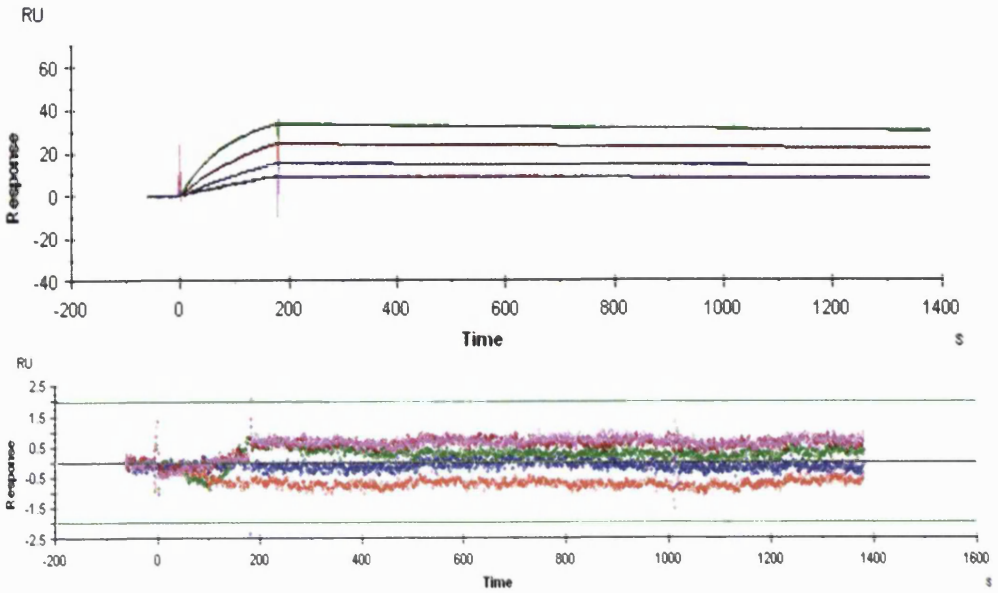

B; Fab_{beva}

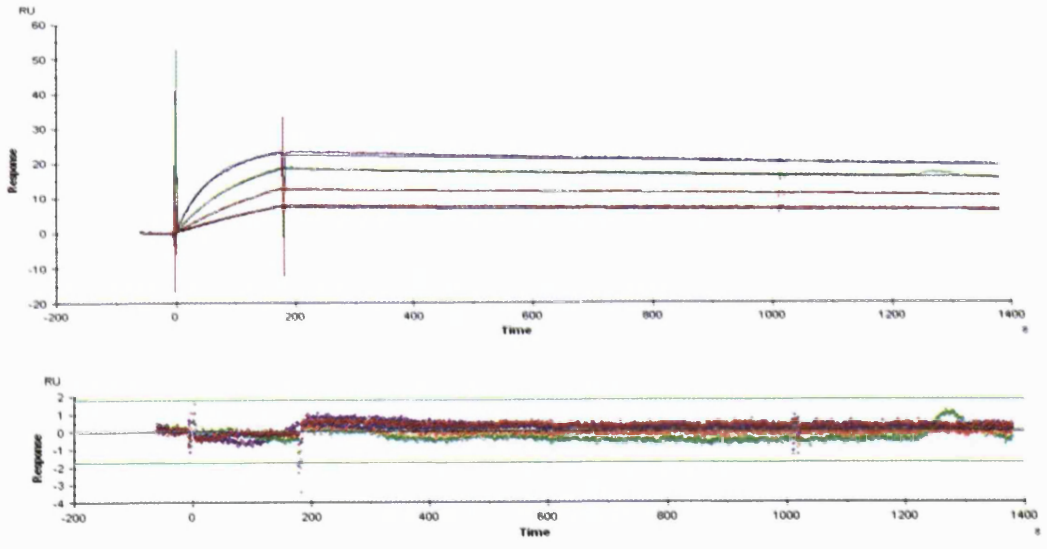

C; $F(ab)_2$-beva

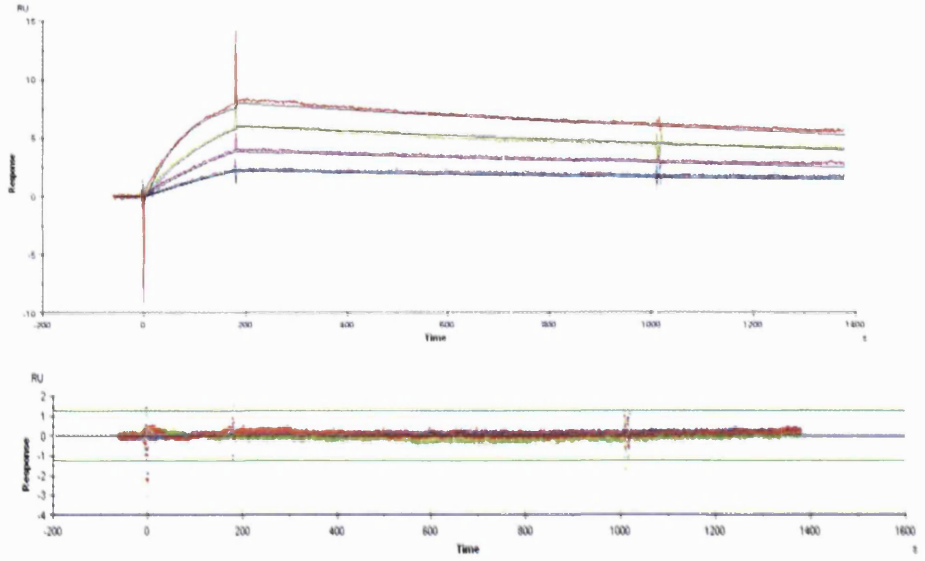

D; PEG_{20}-Fab_{beva}

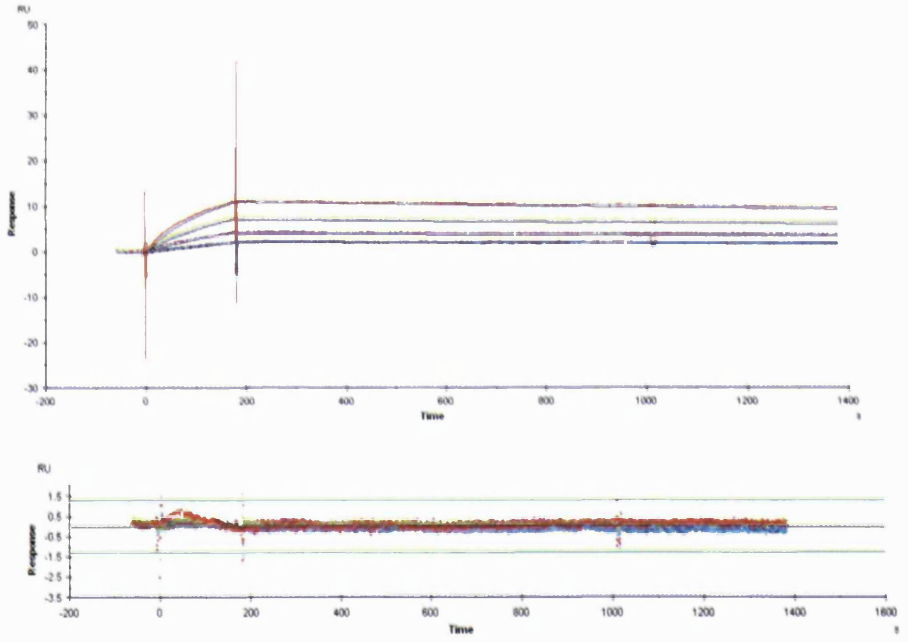

Figure 4.16 The fitting curve and residual plot of the constructs derived from bevacizumab, applying 1:1 fitting model. **(A)** Bevacizumab, **(B)** Fab_{beva}, **(C)** $F(ab)_2$, **(D)** PEG_{20}-Fab_{beva}.

The residual plots (Figure 4.16, A-D) suggested that there was no difference between the experimental curve (colour curves) and the fitted curve (black curve) when applying a 1:1 binding model as it was scattered around zero. The Chi^2 values that were less than 1 suggested a good fit. The SE value of k_a and k_d for bevacizumab, Fab_{beva} and

their PEGylated derivatives were less than two orders of magnitude the k_a and k_d value (Table 4.2). The experimental Rmax in Table 4.2 appeared to be lower than the theoretical R_{max} (150 RU) when using the chip with 61 RU immobilisation level. A larger value in experimental R_{max} suggests that either the binding model is not 1:1 or that there are impurities in the analyte solution. The tc values were also more than 10^9 which indicate there was no mass transfer limitation. Since, the fitting parameters including Chi^2, SE, Rmax and tc, were in acceptable ranges, this suggested that using a 1:1 binding model the kinetic constants (k_{on}, k_{off} and K_D) could be calculated. The kinetic assay was performed four times for bevacizumab, Fab_{beva}, three times for $F(ab)_2$ and two times for PEG_{20}-Fab_{beva} using two CM3 chips (57 RU and 61 RU levels). The kinetic assay was performed once for PEG_{30}-Fab_{beva}, PEG_{40}-Fab_{beva}, PEG_{2x20}-Fab'_{beva} and PEG_{10}-bevacizumab. Table 4.3 is a summary of the kinetic constants of these constructs and the average was taken for the samples where kinetic assays were conducted more than once.

Table 4.2 Kinetic constants and parameters of the bevacizumab and its derivatives using chip with 61 RU VEGF.

Constructs	k_a ($M^{-1}s^{-1}$)	SE (ka)	k_d (s^{-1})	SE (kd)	K_D nM	Rmax	SE (Rmax)	Chi^2	tc
Bevacizumab	6.93×10^4	2.70×10^2	9.04×10^{-5}	2.02×10^{-6}	1.30	38.3	0.092	0.21	1.04×10^{19}
$F(ab)_2$	5.19×10^4	1.90×10^2	9.19×10^{-5}	2.70×10^{-6}	1.77	28.5	0.06	0.40	1.03×10^{22}
Fab_{beva}	2.98×10^4	67	1.34×10^{-4}	1.26×10^{-6}	4.2	19.1	0.024	0.16	2.5×10^{13}
PEG_{20}-Fab_{beva}	1.0×10^4	55	1.35×10^{-4}	2.10×10^{-6}	13.0	17.57	0.058	0.03	9.1×10^{17}
PEG_{30}-Fab_{beva}	8.12×10^3	17	1.0×10^{-4}	1.10×10^{-6}	12.30	17.8	0.024	0.03	2.3×10^{13}
PEG_{40}-Fab_{beva}	1.10×10^4	34	1.19×10^{-4}	1.0×10^{-6}	10.79	11.88	0.026	0.02	2.08×10^{15}
PEG_{2x20}-Fab'_{beva}	1.13×10^4	26	1.09×10^{-4}	1.20×10^{-6}	9.59	13.46	0.031	0.02	1.7×10^{15}
PEG_{10}-bevacizumab	1.51×10^4	73	8.20×10^{-5}	2.70×10^{-7}	5.49	16.6	0.051	0.13	2.08×10^{14}

Since k_d represents the strength of interaction between antibody and antigen, its comparison between the antibody fragment and its PEGylated derivatives is important to evaluate the effect of PEGylation. A smaller k_d value is related to a slower dissociation rate and results in stronger binding interaction between the analyte and

ligand in the formed complex. A smaller k_a value is related to a slower association rate and can lead to less binding tendency between analyte and ligand.

Table 4.3 The average of kinetic constants and affinity value of bevacizumab and its derivatives using chip with 57 and 61 RU VEGF. N=4 for bevacizumab and Fab_{beva} and N=3 for $F(ab)_2$, N=2 for PEG_{20}-Fab_{beva}, PEG_{30}-Fab_{beva}, PEG_{40}-Fab_{beva}, and N=1 for PEG_{2x20}-Fab'_{beva} and PEG_{10}-bevacizumab. The analysis of PEG_{2x20}-Fab'_{beva} was performed with 53 RU VEGF chip.

Constructs	$k_a(\times 10^4)\ M^{-1}s^{-1}$	$k_d(\times 10^{-5})\ s^{-1}$	$K_D\ (k_d/k_a)$ nM
Bevacizumab	6.12	8.16	1.33 ± 0.34
$F(ab)_2$	5.49	6.39	1.16 ± 0.87
Fab_{beva}	2.01	13.40	6.66 ± 1.52
PEG_{20}-Fab_{beva}	0.96	12.1	12.0
PEG_{30}-Fab_{beva}	0.88	9.67	10.98
PEG_{40}-Fab_{beva}	1.31	12.90	9.84
PEG_{2x20}-Fab'_{beva}	1.13	10.90	9.59
PEG_{10}-bevacizumab	1.51	8.2	5.49

The Fab_{beva} displayed a faster dissociation rate than bevacizumab (Table 4.3). An average k_d value of 13.40 x 10^{-5} s^{-1} was measured for the Fab_{beva}, whereas an average k_d value of 8.16 x 10^{-5} s^{-1} was observed for bevacizumab and k_d of 6.39 x 10^{-5} s^{-1} for $F(ab)_2$. This faster dissociation rate for the Fab_{beva} was thought to be due to its monovalent binding to VEGF. No difference between the k_d value of bevacizumab and $F(ab)_2$ was observed as both have similar binding strength towards VEGF. These results suggested that there was no loss of binding properties due to the proteolytic digestion of the full antibody to obtain Fab and $F(ab)_2$.

This loss of bivalency in the Fab_{beva} was also reflected in its association rate constant (Table 4.3). A k_a value of 2.01 x 10^4 $M^{-1}.s^{-1}$ was calculated for the Fab_{beva}, while a k_a value of 6.12 x 10^4 and 5.49 x 10^4 $M^{-1}.s^{-1}$ were calculated for bevacizumab and $F(ab)_2$ respectively. While Fab_{beva} is smaller than the full IgG and can diffuse from bulk to the sensor surface faster, its k_a was slower. This slower association rate in the Fab_{beva} was thought to be due to the monovalency properties of the Fab_{beva} which can effect its overall binding tendency towards VEGF.

In the PEG-Fab_{beva} conjugates, the dissociation constant rates did not change between the 20, 30 and 40 kDa PEG-Fab_{beva} (Table 4.3) and they were all in an approximate similar range (10-12 x 10^{-5} s^{-1}) to the dissociation constant rates of the Fab_{beva} (13.4 x 10^{-5} s^{-1}). This result implies that the strength of binding of the Fab_{beva} to VEGF did not change by the interchain disulfide PEGylation and that once bound, the PEG-Fab_{beva} binds to VEGF at a similar strength as the Fab_{beva}. Using different sizes of the PEG mono-sulfone reagent **2** (20, 30 and 40 kDa PEG) in PEG-Fab_{beva} resulted in an approximately similar k_d value. This means that the size of the PEG where conjugated site-specifically at the interchain disulfide did not vary the binding of PEG-Fab to VEGF. If PEGylation had not been site-specific or had been close to the binding region, then more variation in the binding properties would have been expected.

The association constant rate appeared to be slower for the PEG-Fab_{beva} (e.g. 0.96 x 10^4 $M^{-1}.s^{-1}$for PEG_{20}-Fab_{beva}) compared to the Fab_{beva} (2.01 x 10^4 $M^{-1}.s^{-1}$). This slower association rate constant of the PEG-Fab_{beva} may be due to the molecular mass effect and also steric shielding effect of the PEG. PEG-Fab_{beva} would diffuse form bulk to sensor surface slower as a result of increase the molecular mass. However, it has been suggested [114] that the more likely reason of slower k_a of a PEGylated anti-$p185^{HER-2}$ antibody fragment to its target was due to the steric shielding effect of the PEG. It has been shown that PEGylation of anti-$p185^{HER-2}$ antibody fragments on an inserted thiol group at the hinge region, displayed slower association rate constant. It was proposed that this reduction was not because of a diffusion limitation, but it was due to a blocking mechanism of the PEG molecule to block the binding interface. More studies [288, 289] were also demonstrated a slower association constant rate as much as 10 fold decrease for PEGylated single chain antibody fragment using site specific PEGylation on an inserted cysteine residue. It was also observed no difference in the k_d value of these antibody fragments after the PEGylation [114, 288, 289]. Interestingly, the affinity value of the PEGylated anti-$p185^{HER-2}$ antibody fragment decreased by 5 fold [114] and in the case of PEGylated single chain antibody, the affinity value decrease by 10 fold [288, 289]. In contrast, the affinity value of the PEG-Fab_{beva} decreased about two fold compared to non-PEGylated Fab_{beva}. This decrease was due to a slower association constant rate in the PEG-Fab_{beva}, whereas the dissociation constant rate did not change. It was thought that the reason for the improvement in binding affinity value from 5 or 10 fold in [114, 288, 289] to 2 fold in this work, was related to the site of PEGylation and also the stability of 3-carbon disulfide bridging PEGylated conjugates. The PEG

maleimide that was used for conjugation to cysteine residue of the antibody fragment [114, 288, 289] may hydrolyse. Also a free cysteine when engineered with these other fragments, it is possible there was disulfide scrambling leading to multiple PEGylated species.

To further demonstrate the effect of disulfide PEGylation, the binding affinity of PEG_{10}-bevacizumab was also studied in BIAcore. The dissociation rate constant of bevacizumab (8.16×10^{-5} s^{-1}) appeared to be close in value to the dissociation rate constant of the PEG_{10}-bevacizumab (8.2×10^{-5} s^{-1}) whereas the association rate constant became slower in the PEG_{10}-bevacizumab (1.51×10^{4} $M^{-1}.s^{-1}$).

For the PEG_{2x20}-Fab'_{beva} ($k_d = 10.90 \times 10^{-5}$ s^{-1}), the dissociation rate constant was in the range of k_d of the Fab_{beva} ($k_d = 13.40 \times 10^{-5}$ s^{-1}) and mono PEG_{40}-Fab_{beva} ($k_d = 12.90 \times 10^{-5}$ s^{-1}). Also, no change in the association rate constant between PEG_{2x20}-Fab'_{beva} ($k_a = 1.13 \times 10^{4}$ $M^{-1}.s^{-1}$) and PEG_{40}-Fab_{beva} ($k_a = 1.01 \times 10^{4}$ $M^{-1}.s^{-1}$) was observed. Since both of these PEG conjugated constructs possess a similar molecular mass, it was thought that the similar association rate constants might suggest the threshold for shielding hindrance as the conjugation of the second PEG molecules did not cause more shielding hindrance. The similar dissociation rate constant in PEG_{2x20}-Fab'_{beva} was in agreement with what was thought to be a reason for similar k_d between PEG-Fab_{beva} and Fab_{beva}.

To further study the difference in dissociation rate constants between bevacizumab and the PEGylated derivatives, the dissociation profile was produced. This dissociation profile is obtained by overlaying all of the sensograms. The sensograms were adjusted based on binding level and concentration differences [286]. For example 0.3 μM of bevacizumab displayed similar binding RU to 2 μM of Fab_{beva} and 1.7 μM of PEG_{20}-Fab_{beva}. The sensograms of these three samples were superpositioned and followed by adjustment of the baseline to zero and a dissociation phase to 100 RU. The resulting sensogram was named a dissociation profile (Figure 4.17). This method helped to compare dissociation profile of different samples. The dissociation profile of the Fab_{beva} was faster than bevacizumab, whereas $F(ab)_2$ showed the same dissociation profile as full antibody (Figure 4.17, A). The dissociation profile of Fab and the 20, 30 and 40 kDa PEG-Fab_{beva} were also superimposed (Figure 4.17, B) and no difference observed in their dissociation profiles.

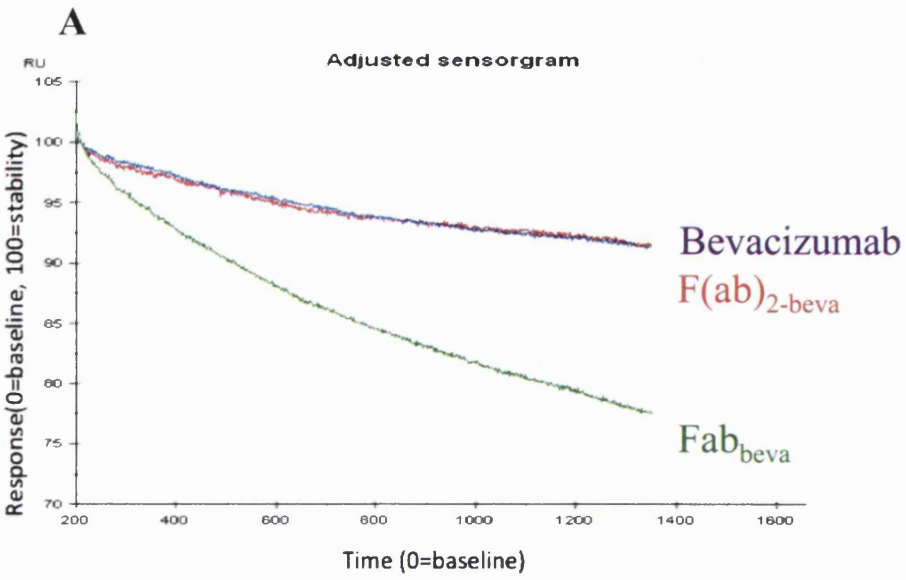

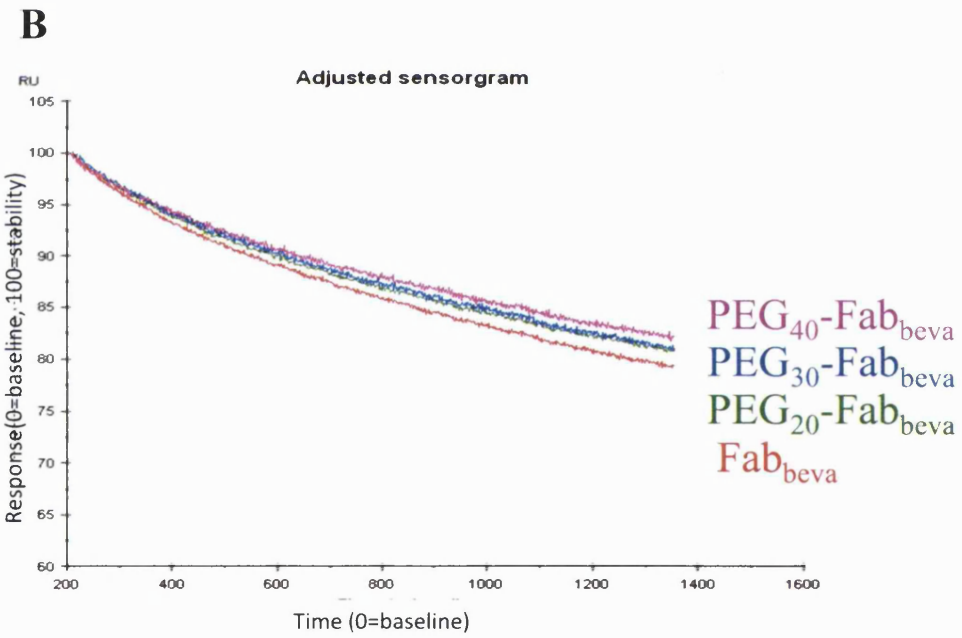

Figure 4.17 (A) The dissociation rate profile of Fab, $F(ab)_2$ and bevacizumab, **(B)** The dissociation rate profile of the Fab and PEG-Fabs. The concentrations of the all samples were normalized against their molecular weight and their binding.

The kinetic assay was also conducted with the Fab_{rani} and the PEG_{20}-Fab_{rani} using the same conditions and the CM3 chip with 61 RU VEGF. The Fab_{rani} was first buffer exchanged into HBS-EP buffer to exclude the effects of excipients. The kinetic fitting curve and residual plot of Fab_{rani} and PEG_{20}-Fab_{rani} using 1:1 binding model are

shown in Figure 4.18. The residual plot and Chi^2 indicated a good fit with a 1:1 binding model. The association rate constants of 3.6 x 10^4 $M^{-1}.s^{-1}$ and 1.74 x 10^4 $M^{-1}.s^{-1}$ were calculated for Fab_{rani} and PEG_{20}-Fab_{rani} respectively (Table 4.4). The k_a value of Fab_{rani} was slower than the k_a of bevacizumab (6.93 x 10^4 $M^{-1}.s^{-1}$) presumably as a result of the monovalency of the Fab_{rani} towards VEGF. The slower association rate constant that was observed for PEG_{20}-Fab_{rani} was thought to be due to the steric shielding effect of the PEG molecule. However, the attempt to calculate the dissociation rate constants for Fab_{rani} and PEG-Fab_{rani} was failed. There is a limited range of the dissociation rate constants (1 x 10^{-1} to 1 x 10^{-6} s^{-1}) which can be calculated in the BIAcore at 25 ^{0}C. This meant that the K_D value could not be accurately calculated.

The binding affinity of ranibizumab to $VEGF_{121}$, $VEGF_{165}$ and $VEGF_{110}$ was studied [290] using BIAcore 3000. This BIAcore instrument has four flow cells, hence each of these three forms of VEGF-A could be immobilised to one of four flow cells on the CM5 chip with varied immobilisation levels of 50-200 RU. Applying a 1:1 binding model, the association rate constant of 5.6 x 10^4 $M^{-1}.s^{-1}$ was calculated for ranibizumab to $VEGF_{165}$ [290]. However, these researchers experienced the same issue with calculation of dissociation rate constants of ranibizumab at 25 ^{0}C which was observed to be very slow. A similar result was observed [285] when the binding affinity of the mutant Fab-12 was studied in BIAcore at 25 ^{0}C. They substituted some amino acids in CDR region of Fab-12 (Fab-bevacizumab) to improve the binding affinity to $VEGF_{165}$ and the affinity values of these different mutants were compared. The dissociation rate constant of one of the highest affinity mutant Fab-12 named Y0317 was very slow and exceeded the BIAcore 2000 limit at 25 ^{0}C, however, it was possible to calculate k_d when the kinetic assay temperature in the BIAcore was increased to 37 ^{0}C. The Fab Y0317 was later known as ranibizumab [193].

A; Fab_{rani}

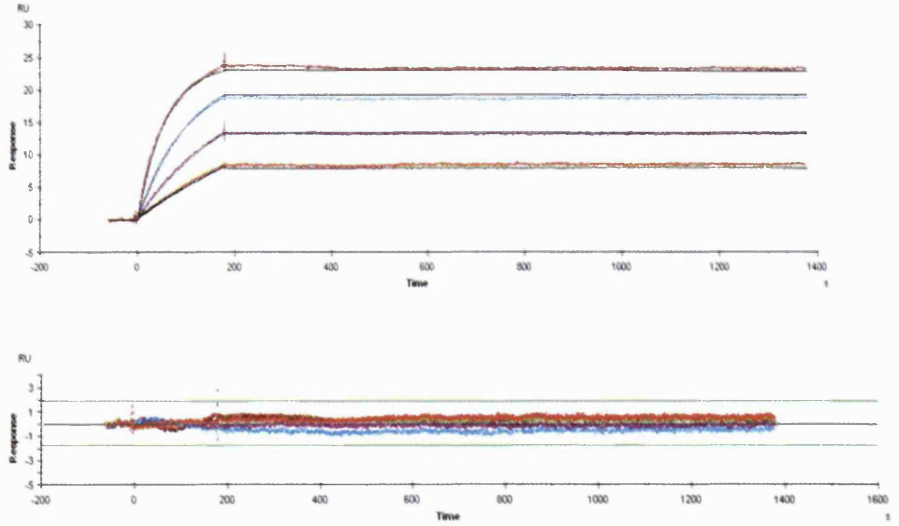

B; PEG_{20}-Fab_{rani}

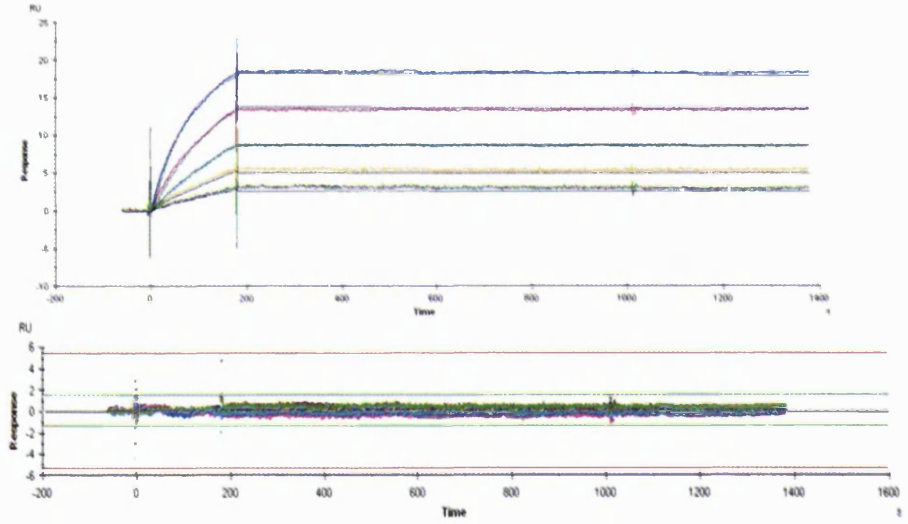

Figure 4.18 The fitting curve and residual plot of **(A)** Fab_{rani}, and **(B)** PEG_{20}-Fab_{rani} applying 1:1 binding model.

Table 4.4 Kinetic constants and parameters of Fab_{rani} and PEG_{20}-Fab_{rani} using chip with 61 RU VEGF. N=2 for Fab_{rani} and PEG_{20}-Fab_{rani}. * NAD: not accurately determined

Constructs	k_a ($M^{-1}s^{-1}$)	SE (ka)	k_d (s^{-1})	K_D (k_d/k_a) nM	Rmax	Chi^2	tc
Fab_{rani}	3.65×10^4	49	$\leq 10^{-6}$	NAD*	23.96	0.19	2.30×10^{16}
PEG_{20}-Fab_{rani}	1.74×10^4	46	$\leq 10^{-6}$	NAD*	20.39	0.23	8.17×10^{19}

To study the binding affinity of the Fab_{trast} and PEG_{20}-Fab_{trast}, the CM3 chip was immobilised with HER-2 (RU=51). The kinetic assay was conducted over a range of concentration for trastuzumab (0.03 μM to 0.6 μM) and for both Fab_{trast} and PEG_{20}-Fab_{trast} (0.08 μM to 2.0 μM). The 1:1 binding model was also used to calculate the kinetic constants. Figure 4.19 shows the fitting curve and residual plot of trastuzumab and PEG_{20}-Fab_{trast}. The residual plots were in agreement with a 1:1 binding model since the residual plot was scattered around zero. The kinetic parameters are summarised in Table 4.5. The experimental R_{max} in Table 4.5 was again slower than the theoretical R_{max} (23 RU). Also, the Chi^2 values were less than 1 which suggested a good fit. The SE value for k_a and k_d were less than two orders of magnitude of the k_a and k_d value. Therefore, the kinetic constant rates and affinity value were significant and could uniquely be calculated. The kinetic assay was performed two times for trastuzumab and Fab_{trast}, and once for the PEG-Fab_{trast}. The average values are summarised in Table 4.6.

Table 4.5 Kinetic constants and parameters of trastuzumab, Fab_{trast} and PEG-Fab_{trast} using chip with 51 RU HER-2.

Constructs	k_a ($M^{-1}s^{-1}$)	SE (ka)	k_d (s^{-1})	SE (kd)	K_D	Rmax	SE (Rmax)	Chi^2	tc
Trastuzumab	3.4×10^5	1.30×10^3	3.6×10^{-5}	1.70×10^{-6}	0.10	6.4	0.008	0.03	1.2×10^{10}
Fab_{trast}	1.01×10^6	2.1×10^4	1.15×10^{-4}	2.10×10^{-6}	0.13	2.67	0.003	0.02	6.8×10^{19}
PEG_{20}-Fab_{trast}	2.6×10^5	1.10×10^3	1.30×10^{-4}	2.90×10^{-6}	0.49	2.59	0.006	0.02	2.4×10^{19}

A; Trastuzumab.

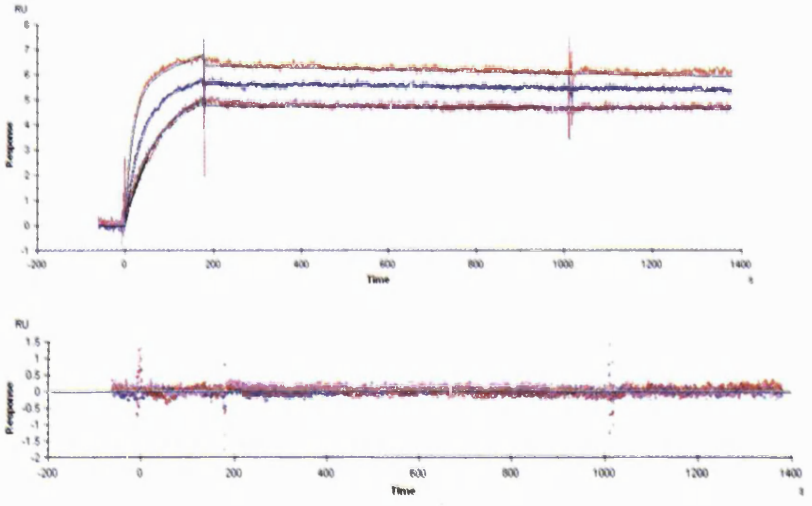

B; PEG_{20}-Fab_{trast}.

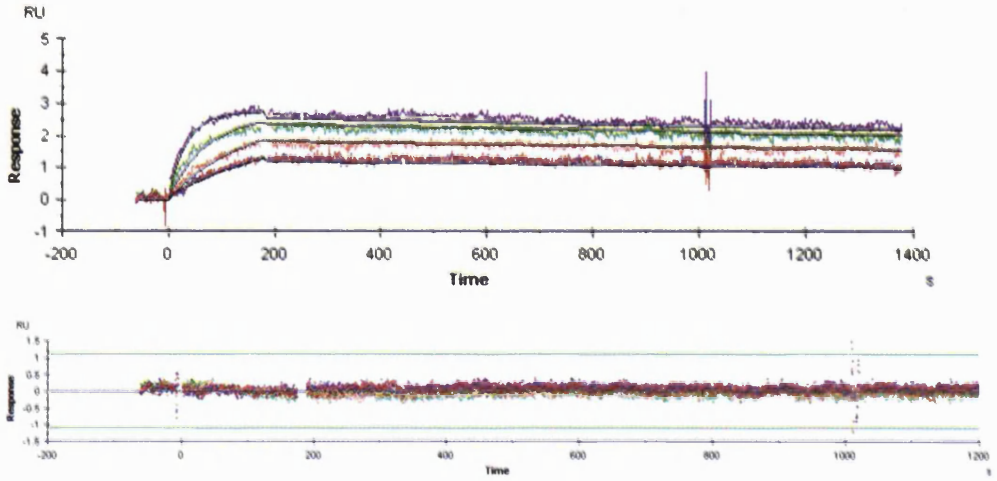

Figure 4.19 The fitting curve and residual plot of **(A)** trastuzumab, **(B)** and the PEG_{20}-Fab_{trast} applying 1:1 binding model.

Table 4.6 The average kinetic constant rates of trastuzumab and its PEGylated Fab using chip with 51 RU HER-2. N=2 for Fab_{trast} and trastuzumab and N=1 for PEG_{20}-Fab_{trast}.

Constructs	$k_a(\times 10^6)$ $M^{-1}s^{-1}$	$k_d(\times 10^{-4})$ s^{-1}	K_D (k_d/k_a) nM
Trastuzumab	0.38	0.42	0.11
Fab_{trast}	1.02	1.15	0.13
PEG_{20}-Fab_{trast}	0.26	1.31	0.49

A K_D value of 0.5 nM was reported for trastuzumab [291] applying a 1:1 binding model at 30 ^{0}C when HER-2 was immobilised on a CM5 chip (150 RU) in [291]. A K_D value of 0.11 nM at 25 ^{0}C was calculated for trastuzumab in this study when HER-2 was coated on CM3 chip (51 RU).

The affinity value of Fab_{trast} (K_D = 0.13 nM) appeared to be about the same as trastuzumab (K_D = 0.11 nM). Interestingly, it was found that the dissociation and association rate constants of Fab_{trast} (k_d = 1.15 x 10^{-4} s^{-1}, k_a = 1.02 x 10^6 $M^{-1}.s^{-1}$) were faster than dissociation and association rate constants of trastuzumab (k_d = 0.42 x 10^{-4} s^{-1}, k_a = 0.38 x 10^6 $M^{-1}.s^{-1}$). It was thought that since the CM3 chip was immobilised with the monomer HER-2 in low immobilisation level, binding of trastuzumab occurs

through one of its Fab portions, leading to one Fab interaction with HER-2. Hence, the affinity for trastuzumab and Fab_{trast} was thought to result from monovalent binding to the immobilised HER-2. The association rate constant was faster for Fab_{trast} and this was thought to be due to the mass difference between Fab_{trast} and trastuzumab. The Fab can diffuse from the bulk to the sensor surface faster than the full antibody. The slower dissociation rate constant of trastuzumab was thought to be due to more stable binding of full IgG because of the hinge flexible region.

The dissociation rate constant of Fab_{trast} appeared to be similar to dissociation rate constant of the PEG_{20}-Fab_{trast} as was observed for the PEG_{20}-Fab_{beva} conjugates. Again the association rate constant was decreased for PEG_{20}-Fab_{trast} most probably due to the steric shielding effect of the PEG. The affinity of the Fab_{trast} was after PEGylation less than a two fold as a result of changes in association rate constant, where dissociation rate constant remained unchanged.

4.2.5 Kinetic assays of the Fab-PEG-Fabs

To evaluate the binding valency and determine the structure-property correlations of the Fab-PEG-Fab constructs, kinetic assays were performed. The binding affinity and kinetic rate constants for the 6, 10 and 20 kDa Fab_{beva}-PEG-Fab_{beva} conjugates were determined and compared to bevacizumab and PEG-Fab_{beva}. A CM3 chip (VEGF, 57 RU) was used to evaluate the Fab-PEG-Fab conjugates derived from Fab_{beva} and Fab_{rani}. The kinetic rate constant parameters for the purified Fab_{trast}-PEG_{20}-Fab_{trast} were determined using CM3 chip immobilised with HER-2 (51 RU). The 1:1 fitting model was again selected as the best fit to obtain the binding affinity of these homodimer constructs.

The fitting curve and residual plot of the 6, 10 and 20 kDa Fab_{beva}-PEG-Fab_{beva} are shown in Figure 4.20 using a 1:1 binding model. A range of concentrations (0.02 μM to 0.8 μM) for the Fab_{beva}-PEG-Fab_{beva} were used for kinetics assay. The fitting parameters are listed in the Table 4.7. The kinetic assay was performed twice for Fab_{beva}-PEG_6-Fab_{beva} and Fab_{beva}-PEG_{10}-Fab_{beva} and once for Fab_{beva}-PEG_{20}-Fab_{beva}. The average was then taken for these two constructs and are listed in Table 4.8 along with kinetic constants of Fab_{beva}-PEG_{20}-Fab_{beva}.

The residual plot of the Fab_{beva}-PEG-Fab_{beva} (Figure 4.20, A-C) using 1:1 fitting model suggested that there was no difference between the fitting curve and the experimental curve as the residual plot was scattered around zero. The Chi^2 value also was less than 1 for each homodimer constructs (Table 4.7) which suggested there was a good fit of the data. The SE values of k_a and k_d were less then a two order of magnitude of k_a and k_d value indicating that values of the kinetic rate constants were significant. As was expected, no mass transport limitation was observed in any of experiments conducted as the tc value was above 10^9 (Table 4.7). These fitting parameters supported using a 1:1 fitting model to calculate the kinetic rate constants and affinity value for the Fab_{beva}-PEG-Fab_{beva} homodimer.

A; Fab_{beva}-PEG_6-Fab_{beva}.

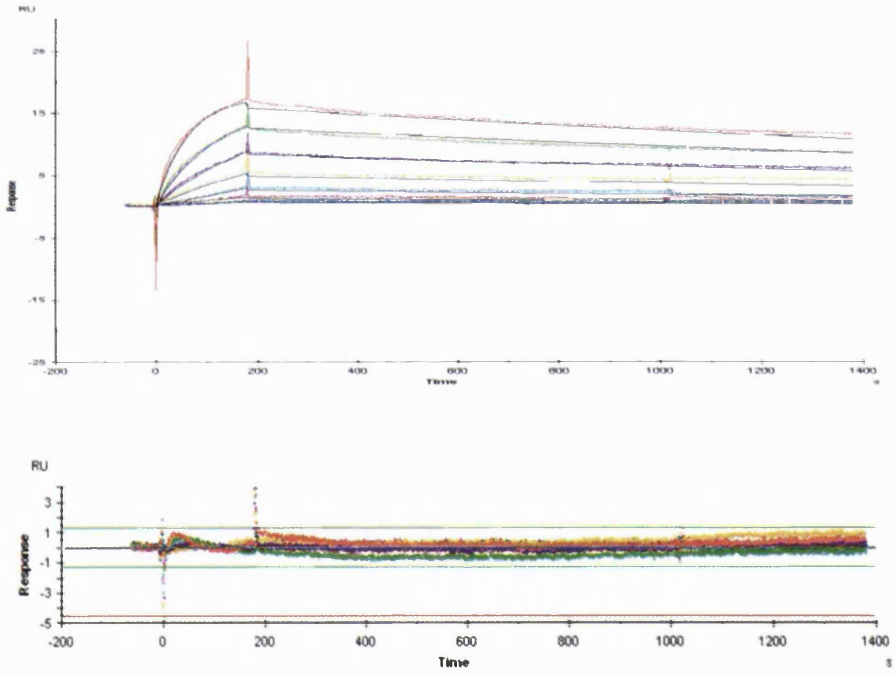

B; Fab_{beva}-PEG_{10}-Fab_{beva}.

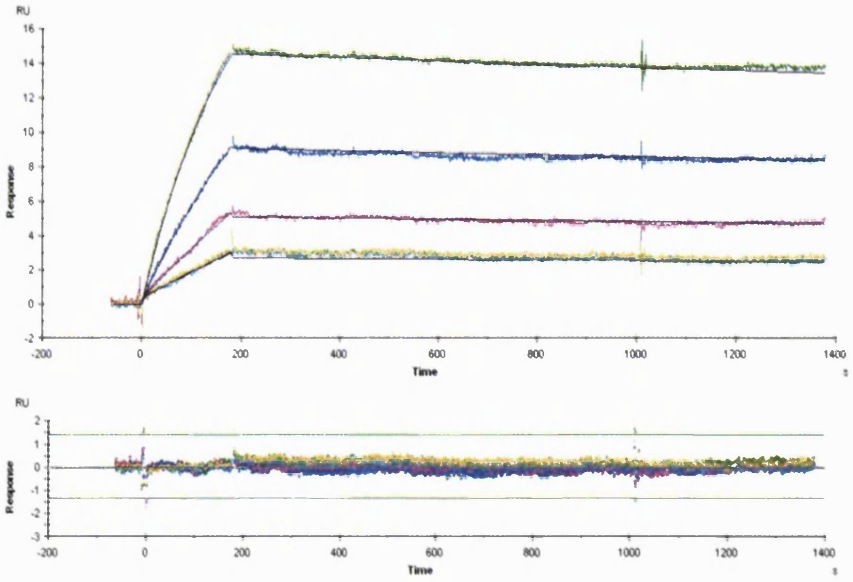

C; Fab_{beva}-PEG_{20}-Fab_{beva}.

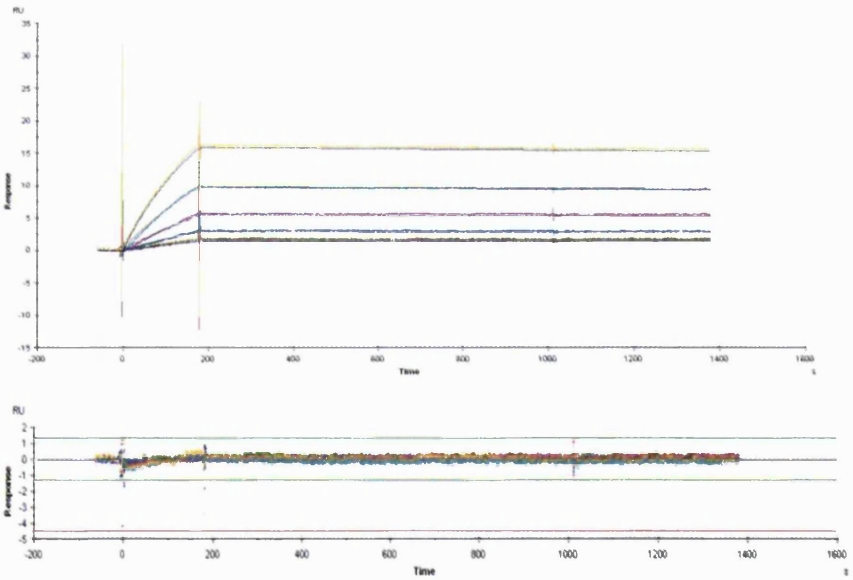

Figure 4.20 Fitting curve and residual plot of **(A)** Fab_{beva}-PEG_6-Fab_{beva}, **(B)** Fab_{beva}-PEG_{10}-Fab_{beva}, **(C)** Fab_{beva}-PEG_{20}-Fab_{beva}.

Table 4.7 Kinetic constants and parameters of Fab_{beva}-PEG-Fab_{beva} using chip with 57 RU VEGF.

Constructs	k_a ($M^{-1}s^{-1}$)	SE (ka)	k_d (s^{-1})	SE (kd)	K_D (nM)	Rmax	SE (Rmax)	Chi^2	tc
Fab_{beva}-PEG_6-Fab_{beva}	2.2×10^4	31	3.49×10^{-5}	7.0×10^{-7}	1.57	28.45	0.079	0.07	1.08×10^{13}
Fab_{beva}-PEG_{10}-Fab_{beva}	3.18×10^4	99	4.67×10^{-5}	1.60×10^{-6}	1.46	27.70	0.05	0.09	1.17×10^{20}
Fab_{beva}-PEG_{20}-Fab_{beva}	1.96×10^4	1.17×10^2	3.02×10^{-5}	2.80×10^{-6}	1.53	26.1	0.017	0.07	1.70×10^{16}

Table 4.8 The average kinetic rate constants and affinity value of Fab_{beva}-PEG-Fab_{beva} using chip with 57 RU VEGF. N=2 for Fab_{beva}-PEG_6-Fab_{beva} and Fab_{beva}-PEG_{10}-Fab_{beva} and N=1 for Fab_{beva}-PEG_{20}-Fab_{beva}.

Constructs	$k_a(\times 10^4)$ $M^{-1}s^{-1}$	$k_d(\times 10^{-5})$ s^{-1}	K_D (k_d/k_a) nM
Fab_{beva}-PEG_6-Fab_{beva}	3.43	5.29	1.54
Fab_{beva}-PEG_{10}-Fab_{beva}	4.46	5.65	1.27
Fab_{beva}-PEG_{20}-Fab_{beva}	1.96	3.02	1.53

The average dissociation rate constants of the homodimer Fab_{beva}-PEG-Fab_{beva} constructs appeared to be slower than the average dissociation rate constant of the Fab_{beva} (k_d = 13.40 x 10^{-5} s^{-1}) and PEG_{20}-Fab_{beva} (k_d = 12.10 x 10^{-5} s^{-1}). The dramatic decrease in k_d for the homodimer constructs was due to the tighter interaction between the construct and its target. This was thought to be a reflection of the bivalency properties in the homodimer construct compare to monovalent Fab_{beva} and mono PEG-Fab_{beva} to VEGF. These observations suggest that conjugation of a second Fab_{beva} to the PEG-Fab_{beva} caused cooperative binding of the two Fabs in homodimer to VEGF. The homodimer displayed bivalency properties that lead to better binding affinity. Therefore, using PEG reagent **4** as a scaffold to link two Fabs, it was possible to make a homodimer conjugate with bivalent properties. Surprisingly, the dissociation rate constants of the homodimer constructs were found to be even slower than bevacizumab (k_d = 8.16 x 10^{-5} s^{-1}). This tighter interaction between Fab_{beva}-PEG-Fab_{beva} to VEGF was thought to be due to the effect of flexible linker (PEG) in the conjugation structure. While the hinge region in bevacizumab was responsible for flexibility of the antibody for bivalent binding, it was thought that PEG provided better flexibility in the homodimer structure leading to better binding properties. Many groups have studied the

effect of length and flexibility of a linker used to conjugate the two molecules [150, 157, 160-162]. It has been proposed that the flexibility and length of the linker can both have a major effect on the properties of the resulting conjugate. The length of the linker was thought to have a primary effect [157]. It was also found that a flexible linker with a slightly longer length could lead to greater binding affinity [157, 160]. In addition, it has been reported that effective molarities (M_{eff}) of a bivalent molecule to it ligand will depend on the length and flexibility of the linker used in this molecule [162]. The value of M_{eff} can be used to predict the avidity of the bivalent molecule and is related to the properties of linker. When the linker is a flexible polymer, the end groups spend much time being close to each other. The end groups are conformationally mobile in flexible polymers. This effect would increase the local concentration of the binding groups translating to a degree of cooperativity between the binding groups (e.g. Fabs in our case) and thus enhance the effective molarities. It was shown that if the length of linker may need to be optimised, as if it is too short, a smaller value of M_{eff} was observed, which indicated in that study that there was less binding interactions between the ligand (*p*- substituted benzenesulfonamides) and a bivalent binding molecule of human carbonic anhydrase II. The linker with longer length resulted in a higher M_{eff} [162].

It was observed in our studies that the dissociation rate constant of the Fab_{beva}-PEG_{20}-Fab_{beva} (3.02×10^{-5} s^{-1}) was slower than the dissociation rate constant of Fab_{beva}-PEG_{10}-Fab_{beva} (5.65×10^{-5} s^{-1}) and Fab_{beva}-PEG_6-Fab_{beva} (5.29×10^{-5} s^{-1}). This suggested that conjugation of two Fab_{beva} with longer the PEG reagent **4** (20 kDa) resulted in a better binding as a consequence of a better flexibility in homodimer structure for bivalent binding. It is thought that when two Fabs are linked together in a molecule has flexibility in its structure then it is possible that the two Fabs can tightly bind to their target resulting in a slower dissociation rate constant.

The average association rate constants of the 6 and 10 kDa Fab_{beva}-PEG-Fab_{beva} constructs were faster than Fab_{beva} ($k_a = 2.01 \times 10^4$ $M^{-1}.s^{-1}$). This faster association rate constant in these homodimer constructs were again due to bivalency properties of these molecules. However, the association rate constant of the Fab_{beva}-PEG_{20}-Fab_{beva} was found to be close in value to the association rate constant of Fab_{beva}. The slower association constant rate for Fab_{beva}-PEG_{20}-Fab_{beva} was probably due to the mass difference between these three constructs, which effects the diffusion rate of the conjugate from the bulk to the sensor surface. Also steric shielding effects of the 20 kDa PEG may have been greater than that for the 6 and 10 kDa PEG molecules in these

conjugates.

In addition, the association rate constants of the Fab_{beva}-PEG-Fab_{beva} constructs were slower than the association rate constant of bevacizumab ($k_a = 6.12 \times 10^4\ M^{-1}.s^{-1}$). This slower k_a was due to the possible shielding hindrance effect of the PEG molecule present in the homodimer construct. Association and dissociation rate constants of the homodimer Fab_{beva}-PEG-Fab_{beva} were slower than bevacizumab, but the affinity values appeared to be similar.

To further evaluate the difference in dissociation rate constant of the homodimer constructs compared to bevacizumab and Fab_{beva}, the dissociation profiles were obtained by overlaying all of the sensograms (Figure 4.8). The sensograms were adjusted based on binding level and concentration differences. For example Fab_{beva} (2.0 μM) displayed a similar binding RU to 0.6 μM of Fab_{beva}-PEG-Fab_{beva} and 0.5 μM bevacizumab. The sensograms of these three samples were superpositioned and followed by adjustment of the baseline to zero and a dissociation phase to 100 RU. Figure 4.21, shows an example of the normalisation sensogram for these three conjugates showing the similar binding that was observed.

A; Overlay of the 6 and 20 kDa Fab_{beva}-PEG-Fab_{beva} with the Fab_{beva}.

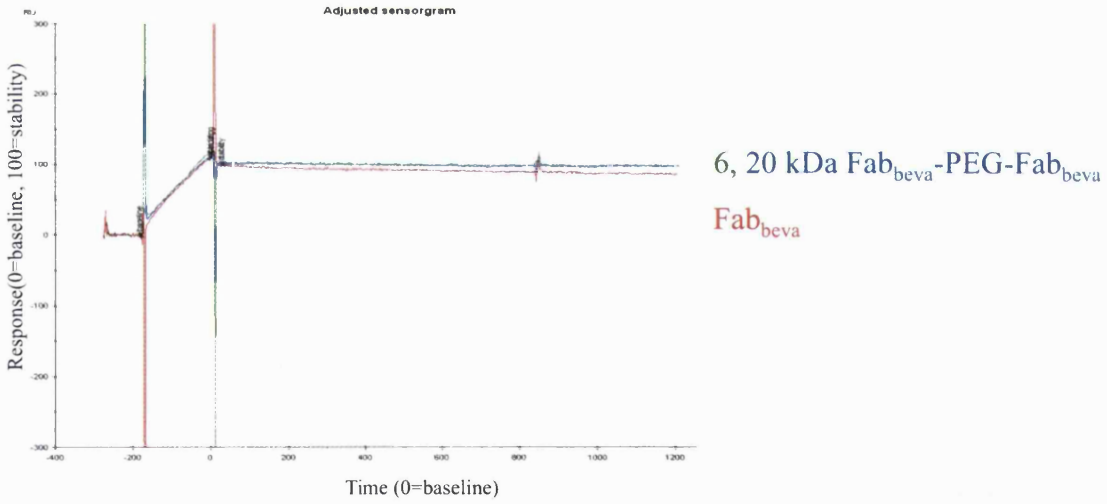

B; Dissociation profile of the 6 and 20 kDa Fab_{beva}-PEG-Fab_{beva} with the Fab_{beva}.

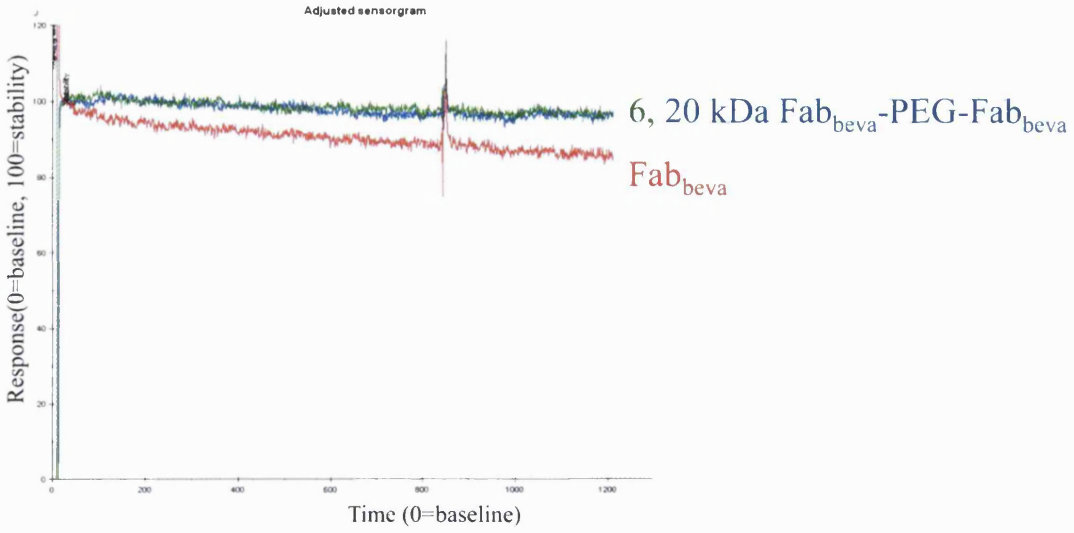

C; Dissociation profile of the Fab_{beva}-PEG_6-Fab_{beva} with Fab_{beva} and PEG_{20}-Fab_{beva}.

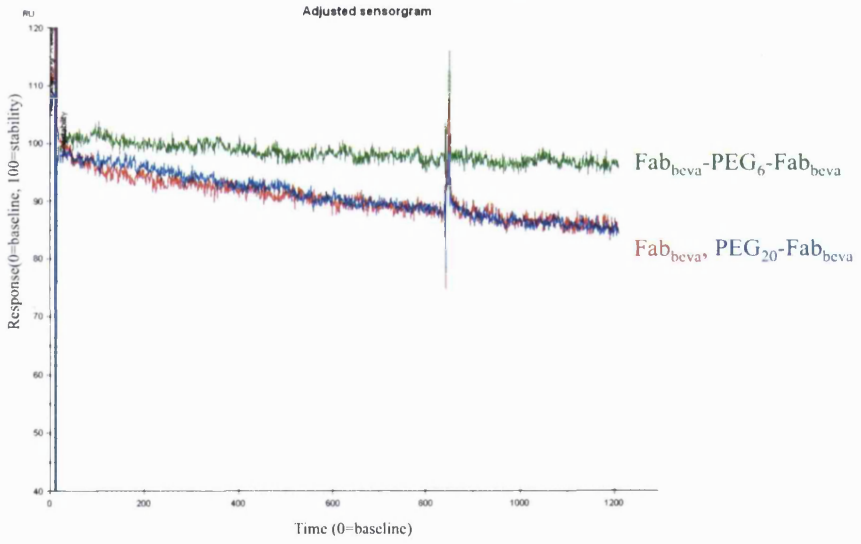

D; Dissociation profile of Fab_{beva}-PEG-Fab_{beva} (6, 10 and 20 kDa) with bevacizumab.

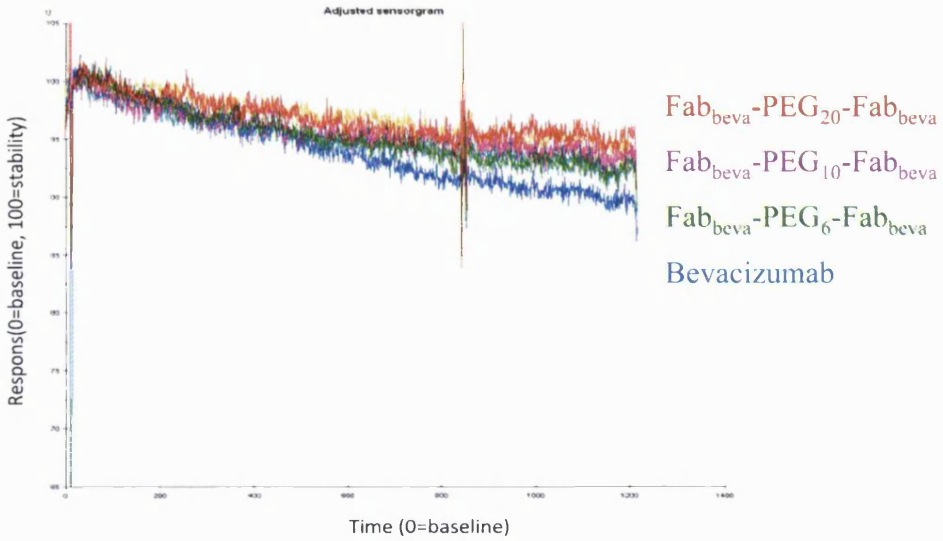

Figure 4.21 The dissociation profiles of Fab_{beva}-PEG-Fab_{beva} compared to Fab_{beva}, **(A)** Overlay graph of 6 and 20 kDa Fab_{beva}-PEG-Fab_{beva} with Fab_{beva}, **(B)** The dissociation rate profile of 6 and 20 kDa Fab_{beva}-PEG-Fab_{beva} with Fab_{beva}, **(C)** The dissociation profile of the Fab_{beva}-PEG_6-Fab_{beva} with Fab_{beva} and PEG_{20}-Fab_{beva}, **(D)** The dissociation profile of 6, 10 and 20 kDa Fab_{beva}-PEG-Fab_{beva} with bevacizumab.

The dissociation profile for 6 and 20 kDa Fab_{beva}-PEG-Fab_{beva} appeared to be slower than the Fab_{beva} and mono PEG-Fab_{beva} (Figure 4.21, B and C). This was correlated with their dissociation rate constants. As already described, the dissociation profile of the homodimer Fab_{beva}-PEG-Fab_{beva} at either size of the PEG reagent **4**, were slower than bevacizumab (Figure 4.21, D).

A similar study was conducted with Fab_{rani}-PEG_6-Fab_{rani} using the CM3 chip with 57 RU VEGF and using a 1:1 binding model. The kinetic fitting curve and residual plot of Fab_{rani}-PEG_6-Fab_{rani} is shown in Figure 4.22. The residual plot and Chi^2 (0.76) indicated a good fit. The association rate constant of 3.8×10^4 $M^{-1}.s^{-1}$ was calculated for Fab_{rani}-PEG_6-Fab_{rani} with an acceptable SE value for k_a. Again the dissociation rate constant exceeded the capabilities of the BIAcore instrument. Therefore, the K_D value could not be accurately calculated.

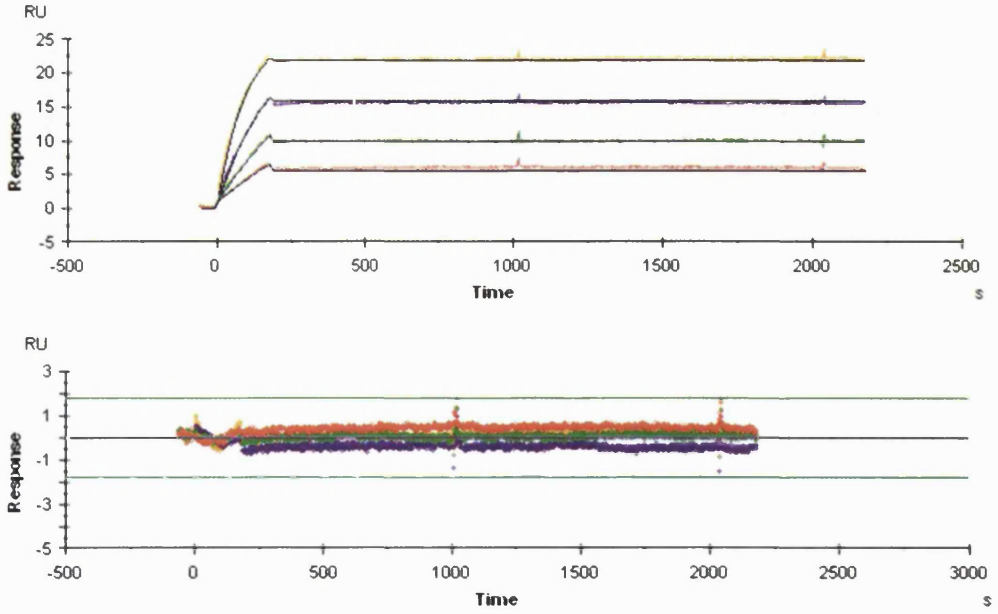

Figure 4.22 The fitting curve and residual plot of Fab_{rani}-PEG_6-Fab_{rani} applying 1:1 binding model.

While it was not possible to determine the dissociation rate constant, a association rate constant of 3.80 x 10^4 $M^{-1}.s^{-1}$ was calculated for Fab_{rani}-PEG_6-Fab_{rani} and was similar to the average association rate constant of Fab_{beva}-PEG_6-Fab_{beva} (k_a = 3.43 x 10^4 $M^{-1}.s^{-1}$).

Table 4.9 Kinetic constants and parameters of Fab_{rani}-PEG_6-Fab_{rani} using chip with 57 RU VEGF. N=1 for Fab_{rani}-PEG_6-Fab_{rani}.* NAD: not accurately determined.

Constructs	k_a ($M^{-1}s^{-1}$)	SE (ka)	k_d (s^{-1})	K_D (k_d/k_a) nM	Rmax	Chi^2	tc
Fab_{rani}-PEG_6-Fab_{rani}	3.80 $\times 10^4$	80	$\leq 10^{-6}$	NAD*	31.10	0.76	5.01$\times 10^{16}$

The same studies were performed with the Fab_{trast}-PEG_{20}-Fab_{trast} using CM3 chip (51 RU, HER-2). Concentration of Fab_{trast}-PEG_{20}-Fab_{trast} in the range of 0.02-0.2 μM was applied. A 1:1 fitting model was again applied and the fitting parameters were assessed. Figure 4.23 shows the fitting curve and the residual plot for Fab_{trast}-PEG_{20}-Fab_{trast}.

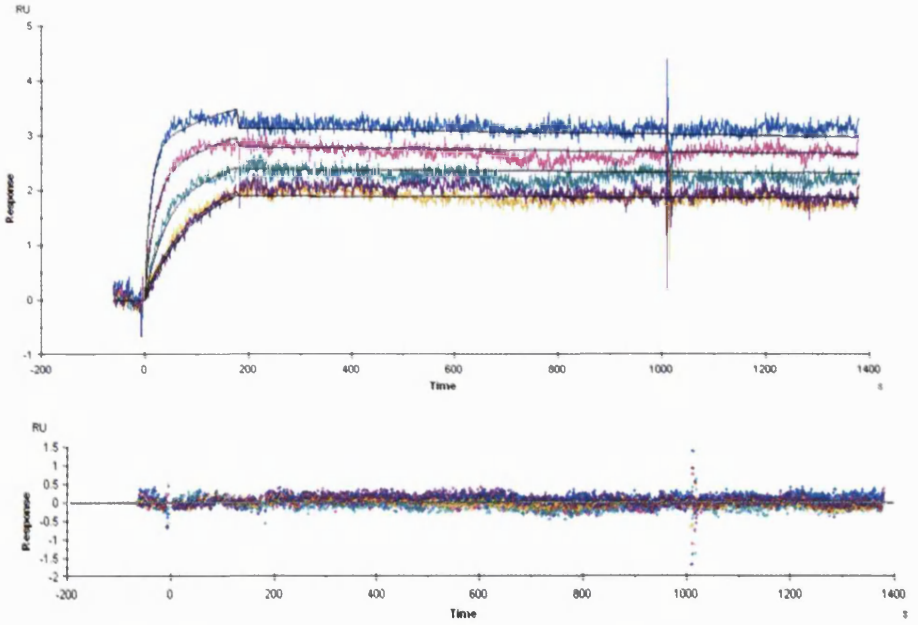

Figure 4.23 The fitting curve and residual plot of Fab_{trast}-PEG_{20}-Fab_{trast} applying 1:1 binding model.

Looking at the residual plot for Fab_{trast}-PEG_{20}-Fab_{trast}, there was no difference between the fitting curves and the experimental curve that obtained when a 1:1 binding model was applied. The fitting parameters and kinetic rate constant for Fab_{trast}-PEG_{20}-Fab_{trast} are listed in Table 4.10. The SE values for k_a and k_d were in acceptable range as well as the Chi^2 value (0.04) (Table 4.10)

The affinity value of the Fab_{trast}-PEG_{20}-Fab_{trast} (K_D = 0.13 nM) did not change compared to affinity value for trastuzumab (K_D = 0.11 nM) and the Fab_{trast} (K_D = 0.13 nM). While Fab_{trast} and Fab_{trast}-PEG_{20}-Fab_{trast} had similar binding affinities as trastuzumab, the dissociation rate constant was slower in the Fab_{trast}-PEG_{20}-Fab_{trast} (k_d = 0.56 x 10^{-4} s^{-1}) than the Fab_{trast} (k_d = 1.15 x 10^{-4} s^{-1}). The k_d of Fab_{trast}-PEG-Fab_{trast} was similar to trastuzumab (k_d = 0.42 x 10^{-4} s^{-1}). This result indicated that binding interaction of Fab_{trast}-PEG_{20}-Fab_{trast} with the HER-2 ligand was tighter than single Fab_{trast} and similar to full IgG presumably due to the flexibility effect of the PEG linker in Fab_{trast}-PEG_{20}-Fab_{trast}. The association rate constant of the Fab_{trast}-PEG_{20}-Fab_{trast} (k_a = 0.42 x 10^6 $M^{-1}.s^{-1}$) was slower than the Fab_{trast} (k_a = 1.02 x 10^6 $M^{-1}.s^{-1}$) and again similar to the association rate constant of trastuzumab (k_a = 0.38 x 10^6 $M^{-1}.s^{-1}$). Since it is likely to have similar binding tendency towards the monomer HER-2 between Fab_{tarst} and the Fab_{trast}-PEG_{20}-Fab_{trast} and trastuzumab, it was thought that the molecular mass influenced the difference in k_a value. The molecular mass of homodimer Fab_{trast}-PEG_{20}-

Fab_{trast} was more than Fab and almost in the same range of trastuzumab. Therefore, k_a value of Fab_{trast}-PEG_{20}-Fab_{trast} was slower than Fab_{trast} and almost similar to trastuzumab.

Table 4.10 The kinetic constant rates and parameters of Fab_{trast}-PEG_{20}-Fab_{trast}. CM3 chip with 51 RU HER-2 was used. N=1 for Fab_{trast}-PEG_{20}-Fab_{trast}.

Constructs	k_a ($M^{-1}s^{-1}$)	SE (ka)	k_d (s^{-1})	SE (kd)	K_D (k_d/k_a) nM	Rmax	SE (Rmax)	Chi^2	tc
Fab_{trast}-PEG_{20}-Fab_{trast}	0.42×10^6	2.1×10^4	0.56×10^{-4}	3.20×10^{-5}	0.13	3.0	0.007	0.04	3.56×10^{20}

This observation that the k_d value for Fab_{trast}-PEG_{20}-Fab_{trast} is slower to that of Fab_{trast} was further investigated by graphing the dissociation profile. A similar method was used to make the dissociation profile for Fab_{trast}-PEG_{20}-Fab_{trast} and Fab_{trast} (Figure 4.24). The dissociation profiles for Fab_{trast} and Fab_{trast}-PEG_{20}-Fab_{trast} were correlated to the dissociation rate constants that were calculated.

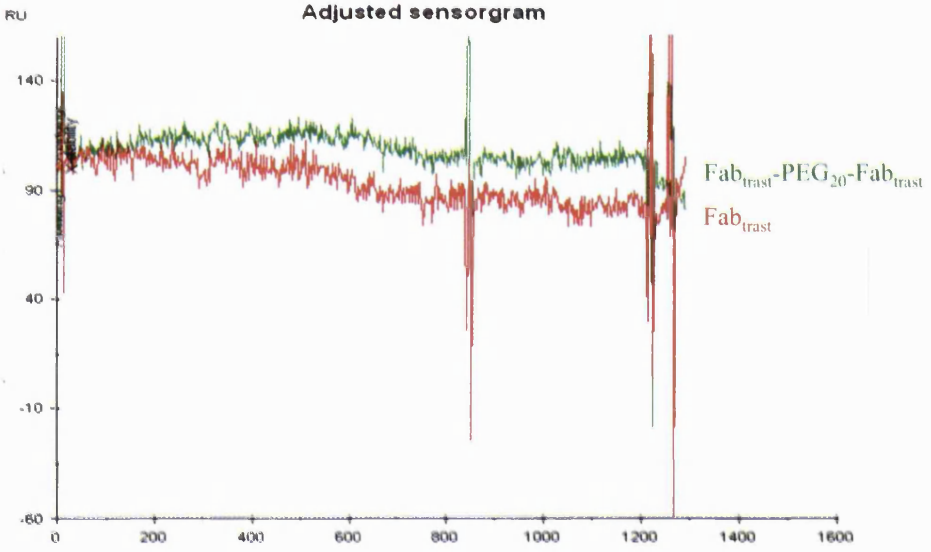

Figure 4.24 Dissociation profile of Fab_{trast} and Fab_{trast}-PEG_{20}-Fab_{trast}.

4.2.6 Binding study of the Fab_{beva}-PEG_{20}-Fab^*_{trast}

The binding of the heterodimer Fab_{beva}-PEG_{20}-Fab^*_{trast} was then examined. The hope was that binding of the Fab_{beva} and Fab_{trast} moieties would be retained in the Fab_{beva}-PEG_{20}-Fab^*_{trast} conjugate. The binding of the Fab_{beva}-PEG_{20}-Fab^*_{trast} was first studied using a CM3 chip immobilised with HER-2 (RU=51) to evaluate the binding of the

Fab_{trast} and then in another experiment binding of this heterodimer was examined using a CM3 chip immobilised with VEGF (RU=57) to evaluate the binding of the Fab_{beva}.

The binding of the Fab_{beva}-PEG_{20}-Fab^*_{trast} was first evaluated (Figure 4.25, A) at three different concentrations using the CM3 with immobilised HER-2. The binding of the homodimer Fab_{beva}-PEG-Fab_{beva} and Fab_{trast}-PEG-Fab_{trast} were also studied (Figure 4.25, B) using this chip and used as a control. Only a small amount of the purified heterodimer conjugate, Fab_{beva}-PEG_{20}-Fab^*_{trast} could be prepared and it was only purified in 1 out of 6 attempts. Since the amount of the heterodimer was so small, a BIAcore binding assay was conducted with a series serial concentrations for Fab_{beva}-PEG_{20}-Fab_{trast}*. Three dilutions of the Fab_{beva}-PEG_{20}-Fab^*_{trast} were prepared as follows: an aliquot of the starting was diluted 1:2 and 1:4 using HEPES buffer (Figure 4.25, A and B). Results showed that binding of the heterodimer constructs were preserved towards HER-2 with a concentration dependent response (Figure 4.25, A). This binding corresponded to the presence of the Fab_{trast} in the heterodimer Fab_{beva}-PEG_{20}-Fab^*_{trast} conjugate. The Fab_{beva}-PEG-Fab_{beva} did not display any binding to the HER-2 (Figure 4.25, B) which suggested the specificity of the binding assay performed. The Fab_{trast}-PEG-Fab_{trast} displayed binding to the HER-2 as was expected. However, using this binding assay, these results were not quantitative and they only corresponded towards establishing whether or not binding had occurred.

Binding of the heterodimer Fab_{beva}-PEG_{20}-Fab^*_{trast} was also examined using a chip with VEGF (Figure 4.26, A). A similar concentration range of the Fab_{beva}-PEG_{20}-Fab^*_{trast} were studied and the binding sensograms displayed the concentration dependent binding response (Figure 4.26, A). The Fab_{trast}-PEG_{20}-Fab_{trast} was used as a control and no binding to VEGF was observed (Figure 4.26, B) which suggested no non-specific binding. The homodimer Fab_{beva}-PEG-Fab_{beva} was retained its binding to VEGF (Figure 4.26, B).

An approximate similar concentration of the Fab_{beva}-PEG_{20}-Fab_{beva} (Figure 4.28, Lane 1) and Fab_{trast}-PEG_{20}-Fab_{trast} (Figure 4.28, Lane 2) and Fab_{beva}-PEG_{20}-Fab^*_{trast} were used in the binding assays (Figure 4.27). This concentration was estimated by the density of the bands for the heterodimer that were observed by SDS-PAGE. The intensity of the bands for Fab_{trast}-PEG_{20}-Fab_{trast}, Fab_{beva}-PEG_{20}-Fab_{beva} and Fab_{beva}-PEG_{20}-Fab^*_{trast} in the gel appeared to be similar. Equivalent loading volumes were used to try to set these concentrations. The Fab_{trast}-PEG_{20}-Fab_{trast} did not display any evidence of binding to VEGF (Figure 4.27). The binding of Fab_{beva}-PEG_{20}-Fab_{beva}

appeared to be better than the binding level of Fab_{beva}-PEG_{20}-Fab^*_{trast} (Figure 4.27). This was due to presence of two Fab_{beva} in the Fab_{beva}-PEG_{20}-Fab_{beva} which lead to higher binding level.

A; Binding sensogram of Fab_{beva}-PEG_{20}-Fab^*_{trast} using CM3 chip with HER-2.

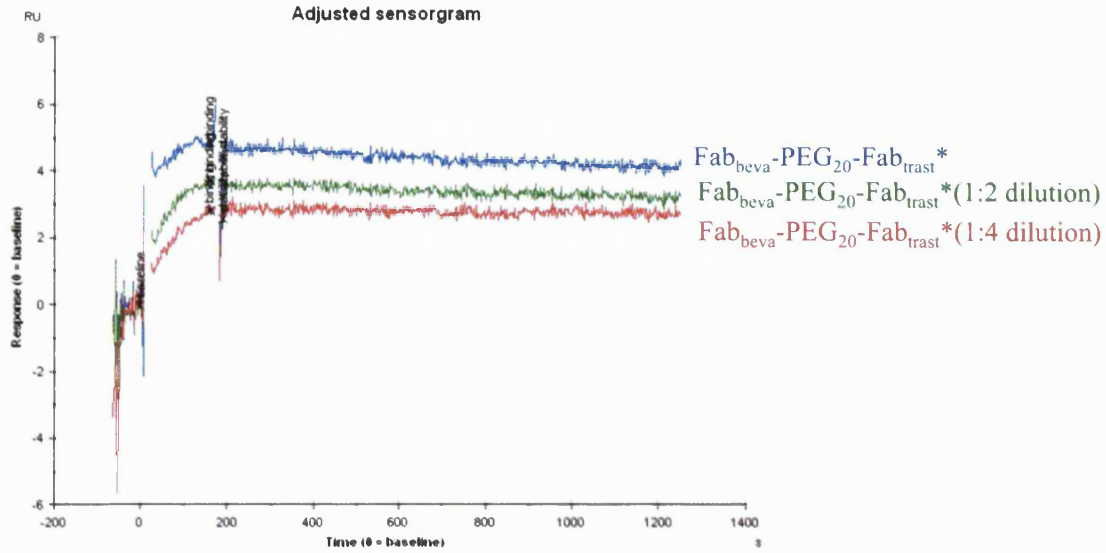

B; Binding chart of Fab_{beva}-PEG_{20}-Fab^*_{trast} and control using CM3 chip with HER-2.

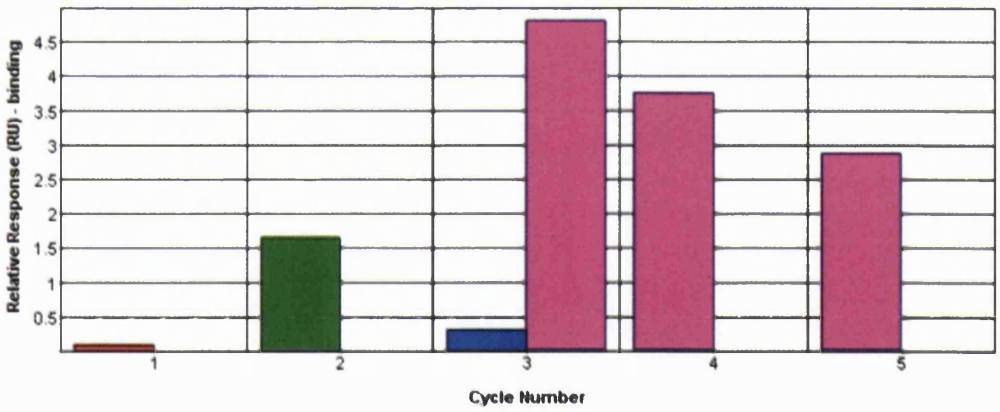

Figure 4.25 Binding sensogram **(A)** of Fab_{beva}-PEG_{20}-Fab^*_{trast} using CM3 chip with HER-2, **(B)** Binding chart with relative response unit of Fab_{beva}-PEG_{20}-Fab^*_{trast} and homodimer Fab_{trast}-PEG_{20}-Fab_{trast} and Fab_{beva}-PEG_{20}-Fab_{beva}. Cycle 1; Running buffer, Cycle 2; Fab_{trast}-PEG_{20}-Fab_{trast}, Cycle 3; Fab_{beva}-PEG_{20}-Fab_{beva}, Cycle 3; Fab_{beva}-PEG_{20}-Fab^*_{trast}, Cycle 4; 1:2 dilution of Fab_{beva}-PEG_{20}-Fab^*_{trast}, Cycle 5; 1:4 dilution of Fab_{beva}-PEG_{20}-Fab^*_{trast}.

A; Binding sensogram of Fab_{beva}-PEG_{20}-Fab^*_{trast} using CM3 chip with VEGF.

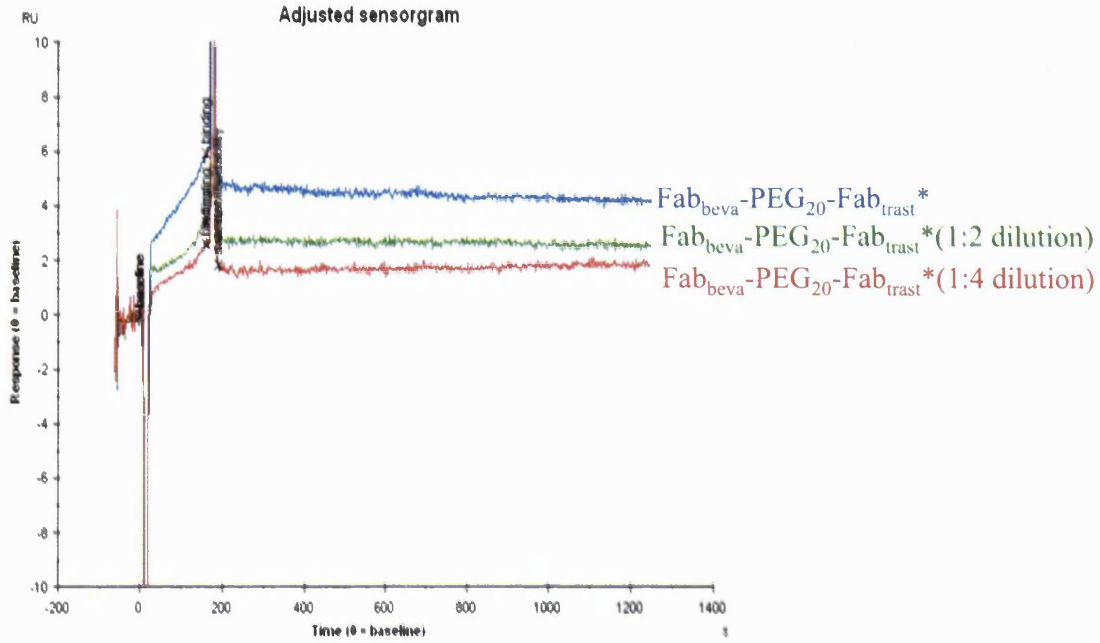

B; Binding chart of Fab_{beva}-PEG_{20}-Fab^*_{trast} and control using CM3 chip with VEGF.

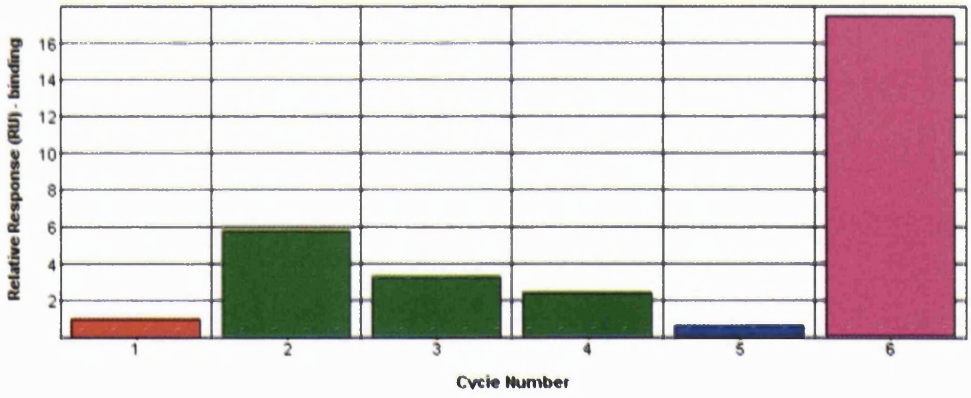

Figure 4.26 Binding sensogram **(A)** of Fab_{beva}-PEG_{20}-Fab^*_{trast} using CM3 chip with VEGF, **(B)** Binding chart with relative response unit of Fab_{beva}-PEG_{20}-Fab^*_{trast} and homodimer Fab_{trast}-PEG_{20}-Fab_{trast} and Fab_{beva}-PEG_{20}-Fab_{beva} using VEGF chip. Cycle 1; Running buffer, Cycle 2; Fab_{beva}-PEG_{20}-Fab^*_{trast}, Cycle 3; 1:2 dilution of Fab_{beva}-PEG_{20}-Fab^*_{trast}, Cycle 4; 1:4 dilution of Fab_{beva}-PEG_{20}-Fab^*_{trast}, Cycle 5; Fab_{trast}-PEG_{20}-Fab_{trast}, Cycle 6; Fab_{beva}-PEG_{20}-Fab_{beva}.

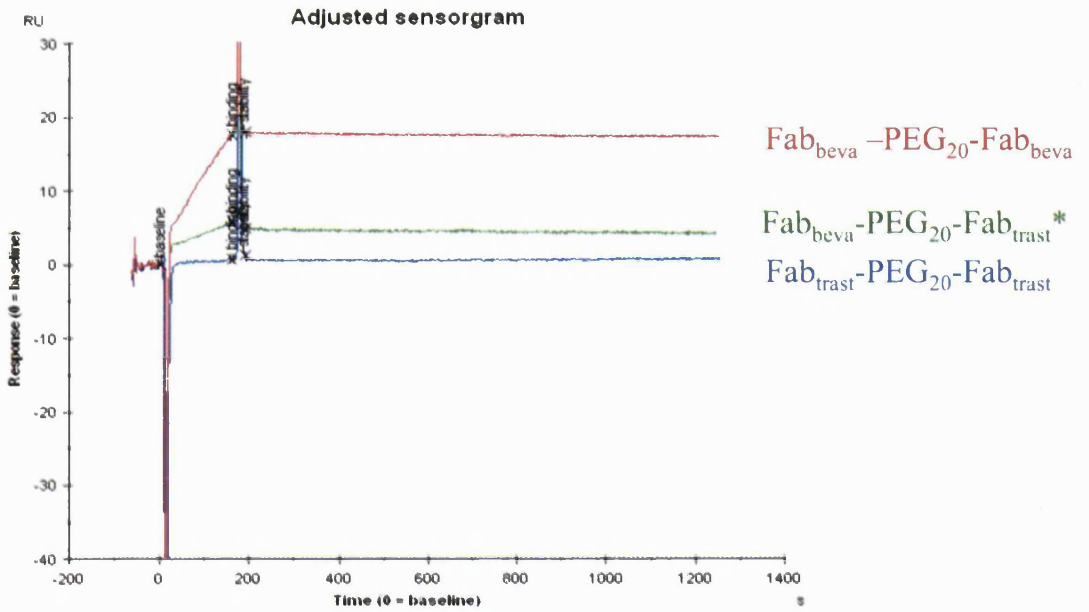

Figure 4.27 Binding sensogram of Fab$_{beva}$-PEG$_{20}$-Fab*$_{trast}$, homodimer Fab$_{beva}$-PEG$_{20}$-Fab$_{beva}$ and Fab$_{trast}$-PEG$_{20}$-Fab$_{trast}$ when same concentration applied, using CM3 chip with VEGF.

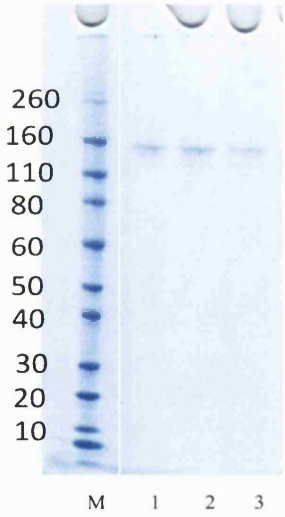

Figure 4.28 SDS-PAGE gel of the purified homo and heterodimer constructs used in the binding assay, Novex Bis-Tris 4-12% gel stained with colloidal blue (Lanes M-3) *Lane M:* Protein standard, *Lane 1:* The purified Fab$_{beva}$-PEG$_{20}$-Fab$_{beva}$, *Lane 2:* The purified Fab$_{trast}$-PEG$_{20}$-Fab$_{trast}$, *Lane 3:* The purified Fab$_{beva}$-PEG$_{20}$-Fab*$_{trast}$.

It was thought that it might be possible to immobilise both ligands on one chip and hence evaluate the binding of the heterodimer in one experiment without a need to change the chip over. Also, the aim was to compare the binding properties and kinetic parameters of heterodimer Fab-PEG-Fab* conjugates to homodimer Fab-PEG-Fab conjugates using a single chip. A new method was designed to immobilise the chip

stepwise with VEGF and then the HER-2 ligand. As far as we can determine, the immobilisation of two ligands on a single chip to evaluate a heterofunctional molecule has not been described in the literature. A single CM3 chip was immobilised with VEGF first and then HER-2 using stepwise immobilisation (Figure 4.29). A low immobilisation level for both ligands was used to minimise rebinding and cross link interaction. Manual immobilisation was selected to allow control of the injection of the ligands and activation time. The sensor surface was first activated with EDC/NHS (200 sec), and the ligand (VEGF, 0.1 μg/mL) was then injected for a 140 sec contact time. After this, the second ligand (HER-2, 0.1 μg/mL) was injected also for a 140 sec contact time. Ethanolamine (1.0 M) was then injected to block all the remaining active sites. The immobilisation level was monitored for each ligand during the contact with the chip. The immobilisation level of 55 RU and 64 RU were achieved for VEGF and HER-2 respectively (Figure 4.29).

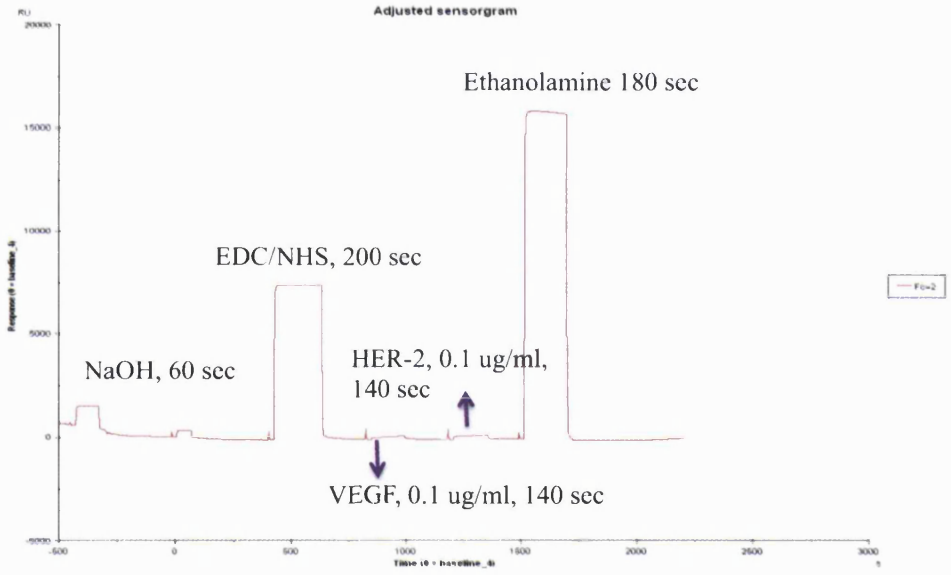

Figure 4.29 Manual immobilisation of CM3 chip with VEGF (0.1 μg/mL) and HER-2 (0.1 μg/mL). The 140 sec contact time performed for each ligand.

To determine whether both ligands were functionally active, bevacizumab (0.4 μM) and trastuzumab (0.4 μM) were loaded onto the chip. The binding of these two antibodies to their respective ligands was then observed (Figure 4.30). The sensograms of bevacizumab and trastuzumab were overlaid (Figure 4.30) and the baseline was adjusted to zero. At the same concentrations, bevacizumab and trastuzumab appeared to have similar binding, however, different dissociation profile. Bevacizumab displayed a slower dissociation profile than trastuzumab. This observation could be due to the fact

that bevacizumab has bivalency towards VEGF whereas trastuzumab has monovalent binding toward HER-2.

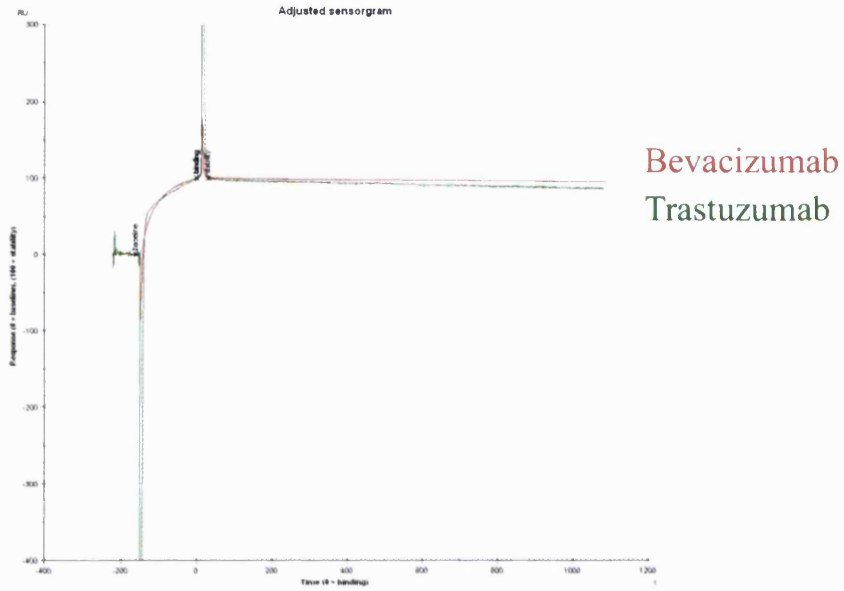

Figure 4.30 The binding sensogram of bevacizumab and trastuzumab using CM3 chip immobilised with HER-2 and VEGF.

To examine this chip further to see if the binding of Fab_{beva} to VEGF was similar to what was observed for the chip with VEGF only, the binding of bevacizumab (0.4 μM) and the Fab_{beva} (1.0 μM) were evaluated (Figure 4.31). The dissociation profile of the Fab_{beva} was faster than bevacizumab as was expected (Figure 4.31).

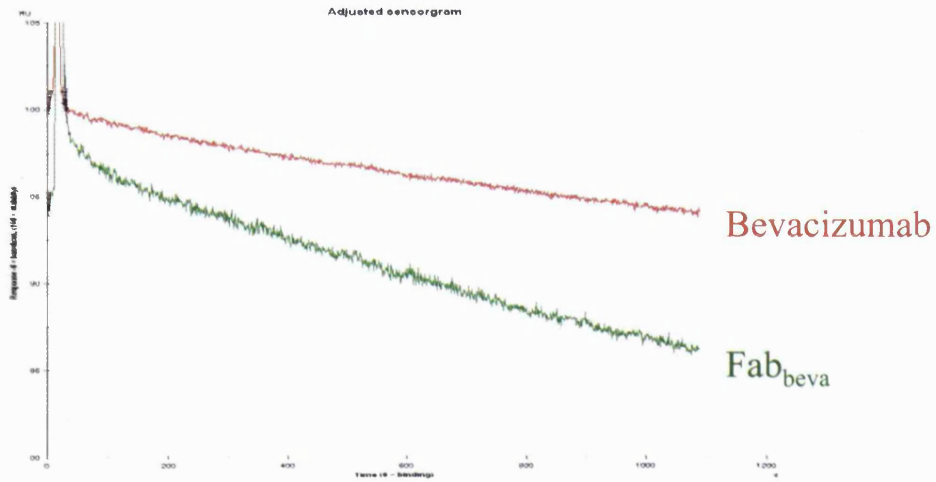

Figure 4.31 The dissociation profile of bevacizumab (0.4 μM) and Fab_{beva} (1.0 μM), using CM3 chip with VEGF and HER-2.

The binding of the heterodimer Fab_{beva}-PEG_{20}-Fab^*_{trast} was then studied using this chip (Figure 4.32) applying different concentrations. This result suggested that the heterodimer molecule maintained its binding to VEGF and HER-2 at the same time, with concentration dependent manner.

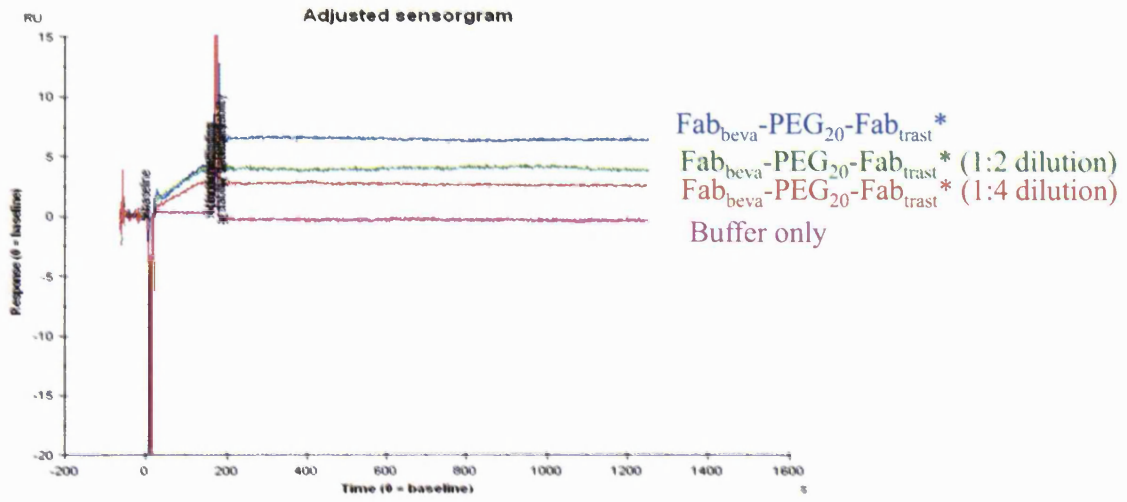

Figure 4.32 Binding sensogram of the heterodimer Fab_{beva}-PEG_{20}-Fab^*_{trast} using CM3 chip immobilised with both VEGF and HER-2.

4.3 Kinetic affinity using ELISA

ELISA is a widely used technique to determine antibody affinity [274, 275]. Direct ELISA (Scheme 4.3) can be a useful method to measure the concentration of a PEGylated antibody in a serum sample [292]. In direct ELISA the antigen is coated in the wells of the plate with a fixed concentration. The binding affinity is then estimated by applying different concentrations of the antibody of interest. For example, the binding affinity of cerolizumab pegol (PEGylated anti-TNFα Fab) with recombinant human TNFα [293] was determined by direct ELISA. TNFα was coated onto the surface of the wells on the plate. Once exposed to the cerolizumab pegol, binding was then detected with a secondary goat anti-human antibody targeted to the cerolizumab pegol.

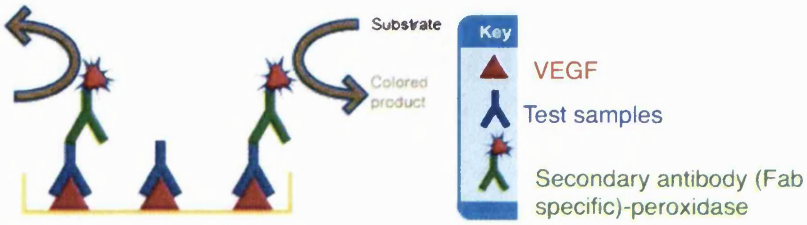

Scheme 4.3 ELISA design when VEGF applied as a ligand.

The secondary was conjugated to horseradish peroxidase (HRP). Once the secondary antibody was washed from the wells, tetramethyl benzidine (TMB), which undergoes reaction with HRP was added. TMB is a chromogenic substrate and can be used in staining procedures. It binds to HRP and produces the blue colour. The resulting colour can be measured by UV-visible spectroscopy at 370 or 655 nm. However, to stop the reaction between TMB and HRP, strong acid such as HCL (50 µL, 1.0 N) was used and yellow colour resulted which can be read at 450 nm.

There are some limitations to use ELISA to determine binding affinity values because equilibria might not be achieved as a result of the several washing steps that are often used. Also cross-linking of the antibody with the antigen can occur when using extra ligand to coat the individual wells. However it was important to evaluate the binding by ELISA to determine if the relative binding correlations of the different PEGylated products as determined by BIAcore analysis was maintained. Direct ELISA was also performed to evaluate the binding affinity of the PEGylated Fabs that were prepared from Fab_{beva}, Fab_{rani} and Fab_{trast}. The associated ligand, e.g. VEGF or HER2, was coated onto the surface of the wells on the assay plate. For binding affinity of all the constructs derived from bevacizumab and also Fab_{rani}, the ELISA plate was coated with VEGF (0.1 µg/mL in well concentration, add 100 µL per well from 1.0 µg/mL) and for the test compounds derived from trastuzumab, the plate wells were coated with HER-2 (0.25 µg/mL in well concentration, 100 µL per well from 2.5 µg/mL).

Generally direct ELISA is conducted using a flat-bottom plate with 96 small wells. The plate is generally made from polystyrene and has advantages over other plates, such as a low background absorbance, uniform optical surface and also high capacity to absorb protein and peptides [251].

Buffers that are used in the assay are also important. Often there are several buffers including a coating buffer, a blocking buffer and a washing buffer. The first step in ELISA is a coating or immobilisation of the ligand on the plate. This coating occurs non-covalently associated the molecule of interest onto the surface of the wells [251]. Proteins often display maximum hydrophobicity near to their pI value. Therefore, the pH of the coating buffer with the dissolved ligand should be at about the pI value of the protein to be absorbed. Since the pI value of VEGF is 8.6, the coating buffer of PBS (pH 7.4) was selected to coat VEGF on the plate. The same coating buffer (PBS pH 7.4) was chosen to prepare the HER-2 solution. Overnight incubation at 4 ^{0}C was found to be an appropriate time to allow coating of the ligand. Coating of the plate is a nonspecific process and depends on the concentration of the coating material. Generally the surface of the well is not saturated with the absorbed protein of interest. Since exposed surface sites can cause non-specific binding of the analyte to be assayed [251], a blocking buffer with a protein such as bovine serum albumin (BSA) is used to ensure the surface of the plastic is completely covered. The blocking buffer may also contain a detergent (e.g. Tween20) which can temporarily bind to the exposed surface sites in the wells. The protein in the blocking buffer binds to any exposed plastic surface in the well and is considered as a permanent blocker.

For the ELISAs described herein, 1 % BSA was used in blocking buffer. The nonionic detergent, Tween 20 (0.05%) was also used in both the blocking and washing buffers. A blocking step of 2 hours at ambient temperature was found to be effective to minimise non-specific binding. After the blocking solution was removed and the wells were washed, the analyte was then added. For each PEG-Fab construct that was evaluated, a replicate of two wells were evaluated. A contact time of 2 hours at ambient temperature between the analyte and absorbed ligand in the wells was used. The wells were then washed three times and the amount of the bound analyte was determined by incubating (1 h) a HRP conjugated secondary antibody that binds to Fab. The secondary antibody was removed by three washing steps then TMB was added and the absorbance read at 450 nm.

4.3.1 ELISA of Fabs and PEG-Fab conjugates

The ELISA experiment was conducted using bevacizumab, Fab_{beva}, Fab_{rani}, and the PEG_{20}-Fab_{beva} and PEG_{20}-Fab_{rani} conjugates to determine their binding affinity to VEGF. Separately, ELISA was also performed on trastuzumab, Fab_{trast} and PEG_{20}-Fab_{trast} using HER-2. The relative binding affinity between the Fabs and their PEGylated derivatives obtained by ELISA were then compared to the relative binding affinities that had been determined by BIAcore.

A Scatchard plot can be used to linearise data from a binding saturation curve to determine the binding affinity. The Scatchard plot was suggested in 1949 as a graphic tool to calculate the equilibrium dissociation constant of the small proteins [294]. Prism is often used for evaluating biological data and within this programme, there is a function called one-site binding with Hill slope that calculates a non-linear regression to calculate the binding affinity (K_D) and maximum binding (B_{max}) [274].

The Scatchard plot can be obtained by plotting the bound/free concentration against bound analyte [295] and by superimposing the line between the best estimate of K_D and B_{max}. A linear Scatchard plot indicates that the data can be fitted with a 1:1 binding model. A non-linear Scatchard plot means that the data do not fit a 1:1 binding model [280] which could be a consequence of heterogeneous ligand or multivalent analyte [280]. The limitation of the Scatchard plot in the binding determination of drug-protein is that it is only suitable for 1:1 binding interaction between protein and ligand and if the sample contains more than one binding sites the binding can not be accurately estimated [296].

An ELISA was first conducted with bevacizumab and shows the appearance of the plate at the end of assay (Figure 4.33). The first 20 wells were coated overnight with VEGF. All of wells in the plate were treated with blocking buffer to block any non-specific binding of the bevacizumab to the plastic. These wells were then treated with bevacizumab in the range of 6×10^{-9} to 6×10^{-13} M. The negative control was human IgG at two concentrations 1×10^{-8} and 5×10^{-9} M. The wells, which were not coated with VEGF, were also exposed to bevacizumab and human IgG to test any non-specific binding. A concentration dependent response was observed for the wells coated with VEGF after exposure to the secondary antibody and TMB (Figure 4.33. A). No colour changes occurred for the wells coated with VEGF and treated with human IgG. This observation suggested that binding of VEGF to bevacizumab was specific as there was

no binding observed between VEGF and control human IgG. Additionally the wells that were not pre-coated with VEGF did not produce any colour (Figure 4.33. A) indicating that there was minimal non-specific binding of the bevacizumab.

A, ELISA plate appearance

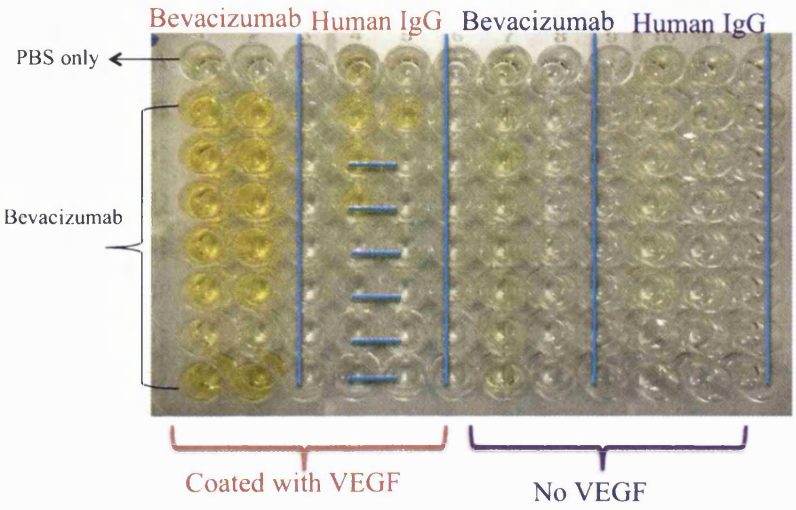

B; Bevacizumab.

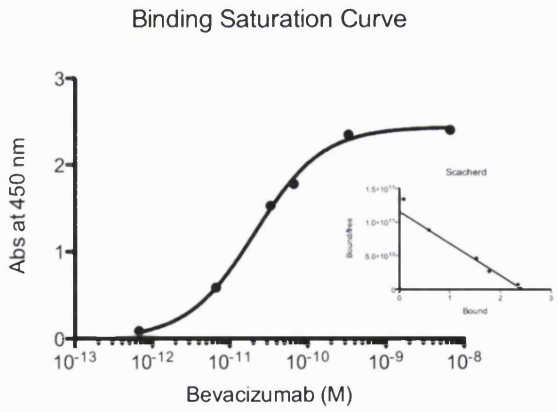

C; $F(ab)_2$

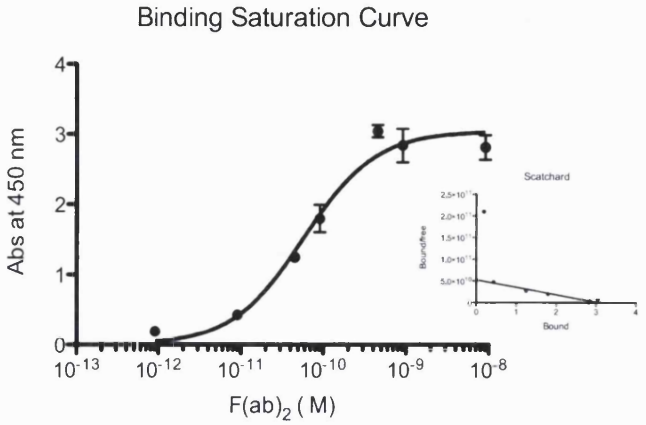

D; Fab_{beva}

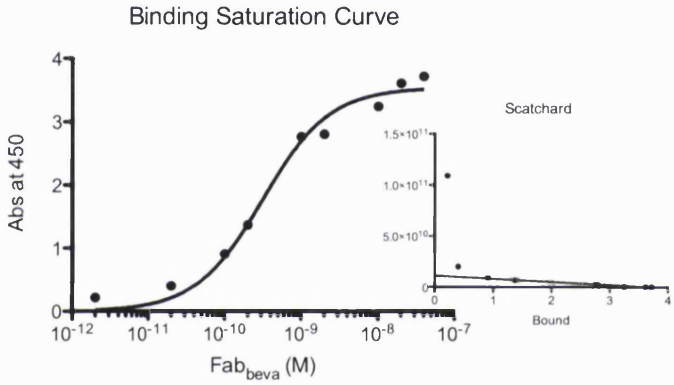

E; PEG_{20}-Fab_{beva}

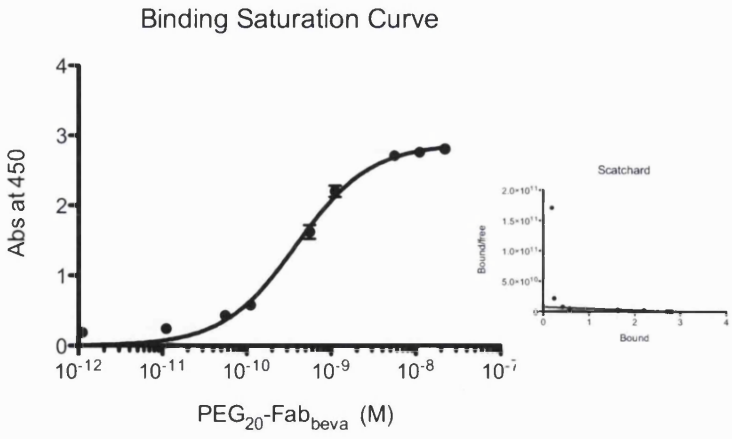

Figure 4.33 (A) ELISA plate coated with and without VEGF and treated with bevacizumab and human IgG, **(B)** Binding saturation curve and Scatchard plot of bevacizumab, **(C)** Binding saturation curve and Scatchard plot of $F(ab)_2$, **(D)** Binding saturation curve and Scatchard plot of Fab_{beva}, **(E)** Binding saturation curve and Scatchard plot of the PEG_{20}-Fab_{beva}.

Similar ELISA experiments were conducted with the digested Fabs and their PEGylated products. Saturation binding curves were then made for bevacizumab, $F(ab)_2$, Fab_{beva} and PEG_{20}-Fab_{beva} (Figure 4.33). The corresponding Scatchard plots are also shown (Figure 4.33). Actual concentrations ranged from 6×10^{-13} to 6×10^{-9} M for bevacizumab, from 9×10^{-13} to 9×10^{-9} M for $F(ab)_2$, from 4×10^{-12} to 2×10^{-8} M for Fab_{beva} and from $2 \times 10^{-12} - 2 \times 10^{-8}$ M for PEG_{20}-Fab_{beva}. The Scatchard plot was used to examine the validity of the 1:1 binding model that was used in the BIAcore kinetics assays. Non-linear regression was used to generate the binding saturation curves. The Scatchard plot was then drawn as bound (ELISA readout) versus bound/free (ELISA readout divided by concentration of test compound at each time points). The Y and X-axis intercepts then in principle give the K_D and B_{max} values. Determination of these values by non-linear regression was accomplished by constructing a new table manually in the Prism with the content of X=0, $Y=B_{max}/K_D$ in one row and the Y=0, $X=B_{max}$ in another row. This table contained two points marking the Y and X intercepts (B_{max}/K_D and B_{max}) was then combined with the first Scatchard of saturation binding data graph. The line was then drawn between data points connecting the X and Y-axis intercepts. A linear line resulted in the Scatchard plots of bevacizumab, $F(ab)_2$, Fab_{beva} and the PEG-Fabs were consistent with the 1:1 binding model used in BIAcore.

The ELISA was performed four times for bevacizumab, Fab_{beva} and the PEG_{20}-Fab_{beva} and two times for $F(ab)_2$. Figure 4.34 shows the binding saturation curves for bevacizumab, Fab_{beva} and $F(ab)_2$ that were superimposed. The minimum (0%) and saturation/maximum binding (B_{max}) were achieved for bevacizumab, $F(ab)_2$, Fab_{beva} and PEG_{20}-Fab_{beva} (Figure 4.34 and Figure 4.35). The calculated binding affinity of Fab_{beva} (0.32 nM ± 0.03) was lower than bevacizumab (0.08 nM ± 0.013) and $F(ab)_2$ (0.07 nM). The lower binding affinity of Fab_{beva} compared to bevacizumab was similar to what was observed in BIAcore kinetic assay. The similar binding affinity observed for $F(ab)_2$ and bevacizumab was a consequence of the bivalent binding capacity of these two molecules.

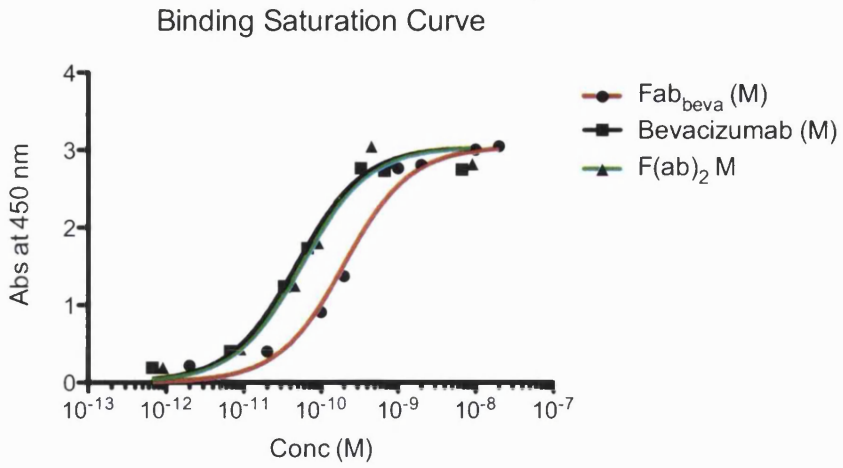

Figure 4.34 Superimposed binding saturation curves of bevacizumab, Fab_{beva} and $F(ab)_2$.

In the case of Fab_{beva} and PEG_{20}-Fab_{beva}, a lower B_{max} was observed for PEG_{20}-Fab_{beva} compare to Fab_{beva} (Figure 4.35). A series of binding events are involved to produce a colour at the end of assay; binding between secondary antibody and Fab_{beva} or PEG-Fab_{beva} and then VEGF. Since ELISA was run with same conditions for Fab_{beva} and PEG-Fab_{beva}, theoretically similar B_{max} should have been observed. In principle, a lower B_{max} in PEG-Fab_{beva} could be a result of (i) a lower VEGF coated on the well as less target leads to less total binding and hence less total absorbance, (ii) a lower binding affinity of PEG-Fab_{beva} to VEGF but the same binding affinity of secondary antibody to PEG-Fab_{beva}, (iii) same binding affinity of PEG-Fab_{beva} but lower binding affinity of secondary or (iv) lower binding affinity of PEG-Fab_{beva} and lower binding affinity of secondary antibody. While scenario (i) was unlikely to be a reason because similar coating conditions and VEGF concentration were used to conduct ELISA for Fab_{beva} and PEG-Fab_{beva}, scenario (ii), (iii) and (iv) were possible. However, it was less possible for scenario (ii) to be a reason because of the position of the PEG was closer to the recognition site of secondary antibody and probably caused steric shielding effect leading to lower binding affinity for secondary antibody. It was more likely that scenario (iii) and (iv) happened because no matter how much PEG-Fab_{beva} was added, it was certain that absorbance could not be suppressed. This indicated that there was a detection limitation. Scenario (iv) was also possible because slower association rate constant was observed for PEG-Fab_{beva} in BIAcore as a consequence of steric shielding effect of the PEG with binding of Fab_{beva} to VEGF. In addition, it might be possible to observe a lower B_{max} as a result of heterogeneous and mixed population of PEGylated

protein, however, it was not the case for PEG-Fab_{beva} since the single IEX peak and silver staining demonstrated the pure and homogenous solution for PEG-Fab_{beva}.

To compare binding affinity of Fab_{beva} to PEGylated Fab_{beva} while B_{max} was achieved for both but in different level, it was thought that to express B_{max} as 100% for both situations and converting the changes in absorbance into percentage. This would result in 100 % binding curve. This procedure was applied for the PEGylated Fab and non-PEGylated Fab in order to be able to compare the data and to superimpose the curve. The 100 % binding curve was therefore made throughout this work where the PEGylated construct were applied in ELISA. Figure 4.36 is a 100 % binding curve of the Fab_{beva} and PEG_{20}-Fab_{beva} that were superimposed.

As expected and consistent with what was observed by BIAcore, the binding of the PEG_{20}-Fab_{beva} was less than that for Fab_{beva} (Figure 4.36). Presumably the steric shielding of the PEG interferes both in the interaction of the PEG-Fab with the absorbed VEGF and the interaction of the secondary antibody used for detection. So reduced Bmax for PEG_{20}-Fab_{beva} compare to Fab_{beva} caused by the steric shielding of PEG [292] that can impact more than one step in the ELISA. Polymer conjugation often negatively influences *in-vitro* data that is collected during the preclinical development. This has been observed over a wide range of polymer-drug and polymer protein conjugates and basically is related to different features of steric crowding and shielding that can be imparted by the polymer that is conjugated to the biologically active moiety [297].

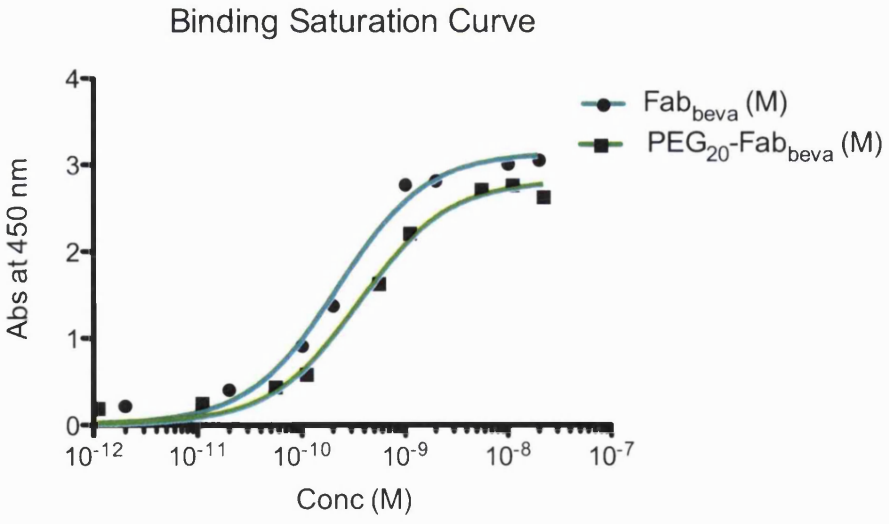

Figure 4.35 Superimposed binding saturation curves of Fab_{beva} and PEG_{20}-Fab_{beva}.

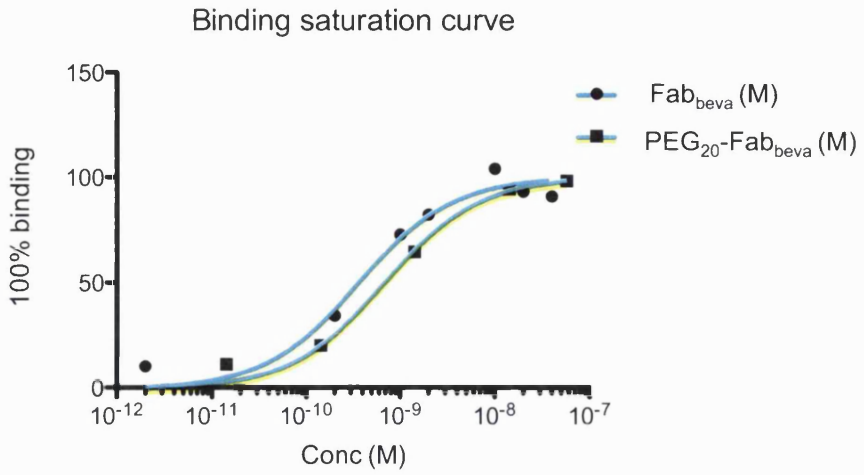

Figure 4.36 Superimposed binding saturation curves of Fab_{beva} and PEG_{20}-Fab_{beva}.

Average K_D values of 0.32 ± 0.03 nM and of 0.61 ± 0.08 nM was obtained for Fab_{beva} and PEG_{20}-Fab_{beva} respectively. The ELISA results showed that PEG_{20}-Fab_{beva} displayed a K_D value that was about half of that which for Fab_{beva}. This relative difference was the same as that observed by BIAcore, however the BIAcore derived values indicated that K_D was about one order of magnitude higher (i.e. K_D value of 6.66 nM for Fab_{beva} and 12.0 nM for PEG_{20}-Fab_{beva}). The reason for the difference in an absolute value between BIAcore and ELISA could be due to the difference in a nature of the experiment. In the ELISA an antibody is incubated with antigen under stationary conditions for 2 h, where in the BIAcore antibody is constantly flowing over an antigen. Also, it is possible in ELISA to have cross linking of antibody with antigen resulting in a higher apparent binding affinity value compared with the value calculated in BIAcore. ELISA wells are often coated with excess antigen to ensure enough material remains after several washing steps for binding to an antibody.

Fab_{rani} and PEG_{20}-Fab_{rani} were then examined by ELISA. Since ELISAs are appropriate to evaluate strongly interacting molecules and since the dissociation rate constant of Fab_{rani} was too slow to obtain by BIAcore at 25 ^{0}C, it was thought that ELISA would be useful to determine the relative binding affinity of Fab_{rani} and its PEGylated construct. The Fab_{rani} and PEG_{20}-Fab_{rani} were evaluated using the following concentration ranges respectively ($4 \times 10^{-12} - 2 \times 10^{-8}$ M) and ($2 \times 10^{-12} - 2 \times 10^{-8}$ M). Figure 4.37 shows the superimposed binding saturation curves for Fab_{rani} and PEG_{20}-Fab_{rani}. Average K_D values of 0.11 nM and 0.22 nM for Fab_{rani} and PEG_{20}-Fab_{rani} were

obtained. Similar to Fab_{beva} and PEG_{20}-Fab_{beva}, this result for Fab_{rani} and PEG_{20}-Fab_{rani} indicated that the unconjugated Fab had about double the binding affinity compared to its PEGylated conjugate.

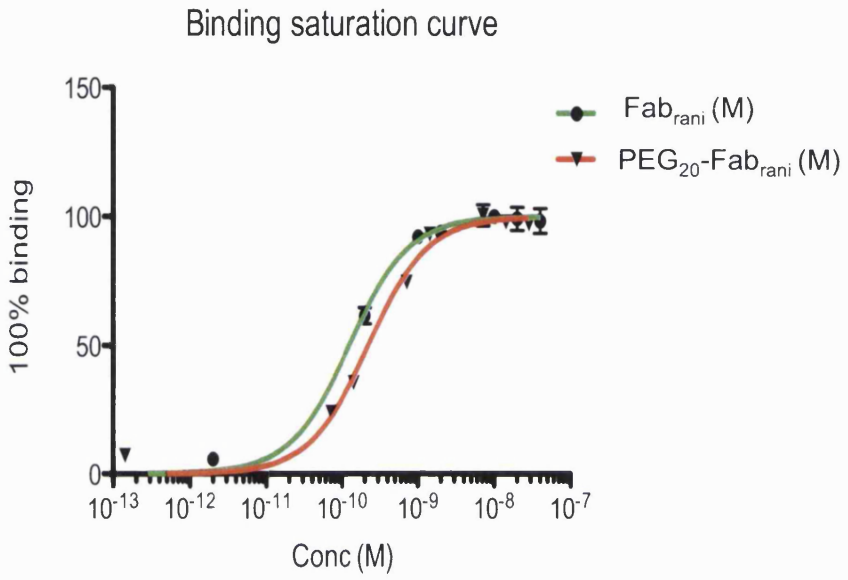

Figure 4.37 Superimposed binding saturation curves of the Fab_{rani} and PEG_{20}-Fab_{rani}.

As it was mentioned, the affinity of the Fab_{rani} is suggested by European Medicine Agency (EMEA) in 2007 [58] to be similar to the bevacizumab and greater than bevacizumab-Fab [193]. This similar binding affinity was observed in this work using ELISA (Figure 4.38). The affinity value of the Fab_{beva}, however, was slower than Fab_{rani}. Figure 4.39 is a superimposed binding saturation curve of the Fab_{rani} with Fab_{beva} in similar range of concentration, from 4×10^{-12} to 2×10^{-8} M.

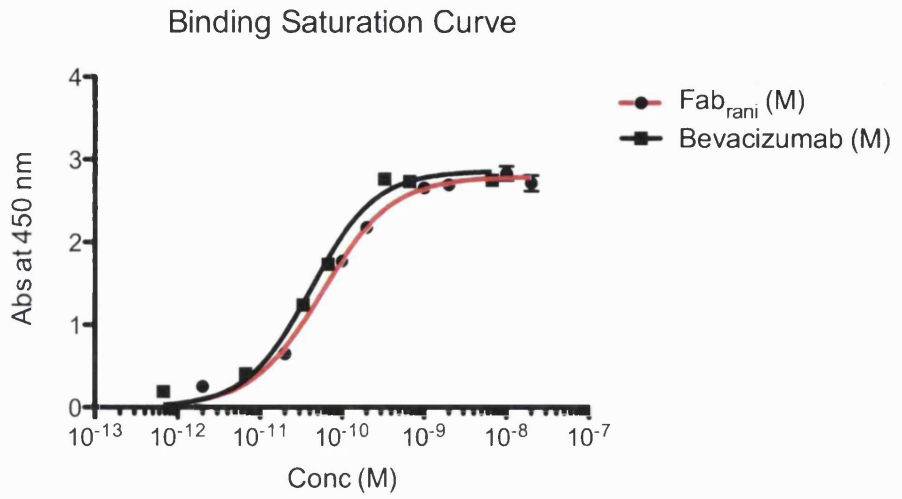

Figure 4.38 Superimposed binding saturation curves of Fab_{rani} and bevacizumab.

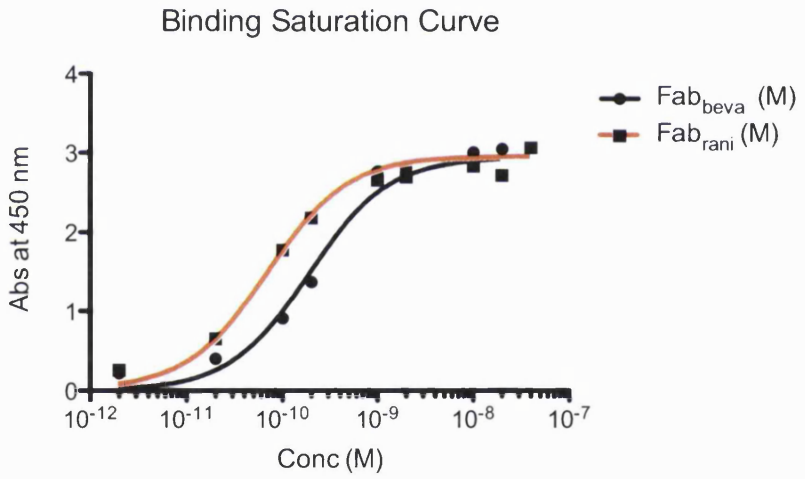

Figure 4.39 Superimposed binding saturation curves of Fab_{rani} and Fab_{beva}.

Using HER-2, an ELISA was conducted with Fab_{trast} and PEG_{20}-Fab_{trast}. The amount of HER-2 used to coat the each well was 100 µL at a concentration of 2.5 µg/mL. This solution was allowed to incubate in the wells overnight at 4 ^{0}C. The ELISA was then conducted as before. Concentrations ranging over 2-3 orders of magnitude for trastuzumab ($5 \times 10^{-12} - 5 \times 10^{-9}$ M), Fab_{trast} ($1.0 \times 10^{-11} - 2 \times 10^{-8}$ M) and PEG_{20}-Fab_{trast} ($7 \times 10^{-11} - 2 \times 10^{-9}$ M) were applied in the ELISA plate and the ELISA was performed once.

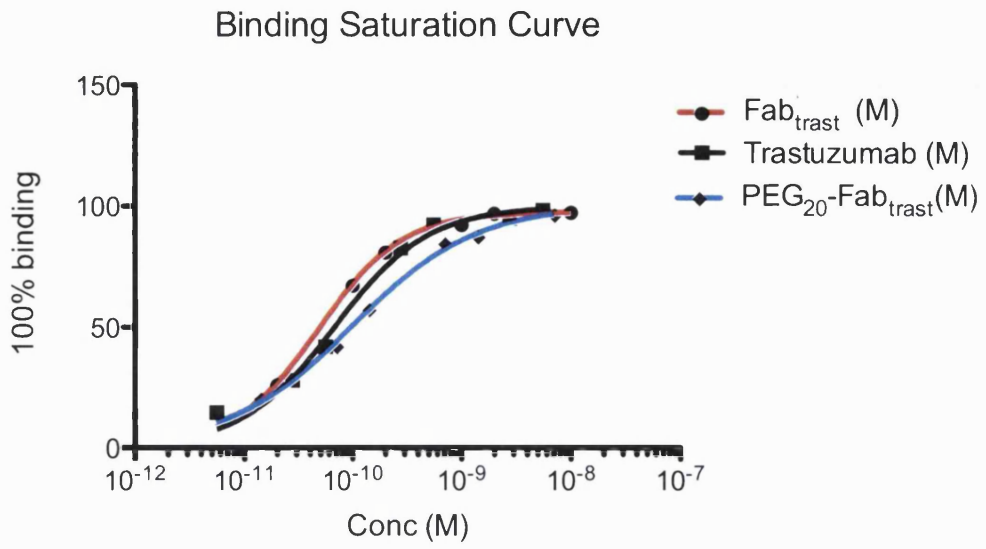

Figure 4.40 Superimposed binding saturation curves of trastuzumab, Fab_{trast} and PEG_{20}-Fab_{trast}.

K_D value calculated for trastuzumab was 0.06 nM and for the Fab_{trast} was 0.05 nM. This closeness in binding affinity value of trastuzumab and the Fab_{trast} was comparable to the binding affinity values that calculated in kinetic assay by BIAcore. This result was again corresponded to the binding properties of trastuzumab and its Fab to HER-2 as both have similar binding tendency towards HER-2 monomer. The affinity value of the PEG_{20}-Fab_{trast}, however, decreased about a two fold (K_D = 0.09 nM). This change in relative binding affinity value between Fab_{trast} and PEG_{20}-Fab_{trast} was similar to the BIAcore data. Table 4.11 is a summary of average binding affinity value of the Fabs and the 20 kDa PEG-Fabs calculated by ELISA.

Table 4.11 Average binding affinity value of the Fabs and their the PEG-Fabs in ELISA and BIAcore. ND; Not determined.

Constructs	K_D (nM) ELISA	K_D (nM) BIAcore
Bevacizumab	0.08	1.33
$F(ab)_2$	0.07	1.16
Fab_{beva}	0.32	6.66
PEG_{20}-Fab_{beva}	0.61	12.0
Fab_{rani}	0.11	ND
PEG_{20}-Fab_{rani}	0.22	ND
Trastuzumab	0.06	0.11
Fab_{trast}	0.05	0.13
PEG_{20}-Fab_{trast}	0.09	0.49

4.3.2 ELISA of Fab-PEG-Fab conjugates

The binding affinity of the 6, 10 and 20 kDa Fab_{beva}-PEG-Fab_{beva} were calculated using ELISA and their structure-properties were correlated with Fab_{beva} and bevacizumab. Two independent assays were performed for 6 and 20 kDa Fab_{beva}-PEG-Fab_{beva}, while one ELISA was performed for Fab_{beva}-PEG_{10}-Fab_{beva}. The range of concentrations of 2 x 10^{-8} – 9 x 10^{-13} M for 6, 10 and 20 kDa Fab_{beva}-PEG-Fab_{beva} were applied in ELISA plate coated with VEGF (0.1 µg/mL in well concentration). The average K_D values of 0.11 nM, 0.14 nM and 0.17 nM were calculated for the 6, 10 and 20 kDa Fab_{beva}-PEG-Fab_{beva} respectively (Figure 4.41, A and B).

The binding affinity of the 6, 10 and 20 kDa Fab_{beva}-PEG-Fab_{beva} were appeared to be similar to binding affinity of bevacizumab in ELISA. This similar in relative binding affinity between Fab_{beva}-PEG-Fab_{beva} and bevacizumab was comparable to what was determined in BIAcore for these homodimer contsructs. This result was again suggested the similarity in binding properties between homodimer Fab_{beva}-PEG-Fab_{beva} and bevacizumab (Figure 4.41).

A; 6 and 10 kDa Fab_{beva}-PEG-Fab_{beva} with Fab_{beva} and bevacizumab.

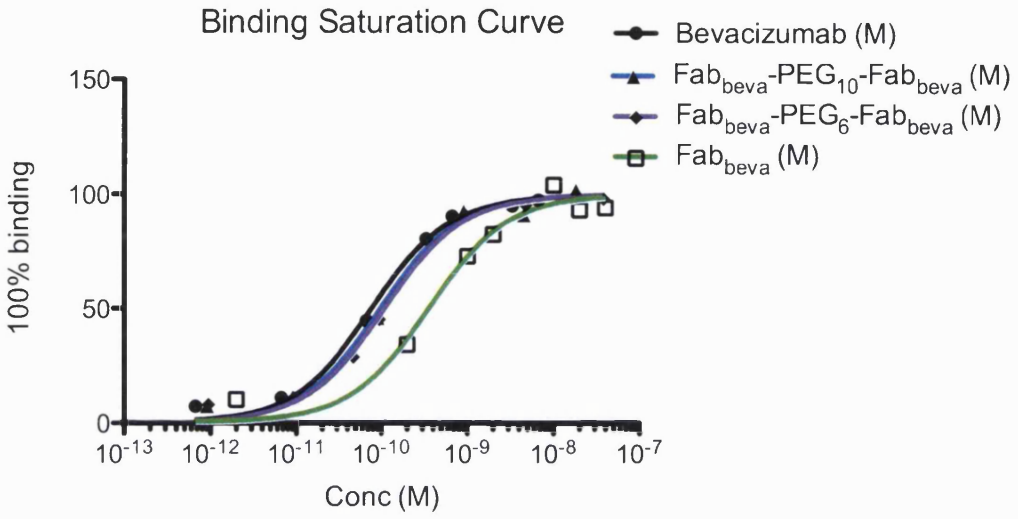

B; 10 and 20 kDa Fab_{beva}-PEG-Fab_{beva} with Fab_{beva}.

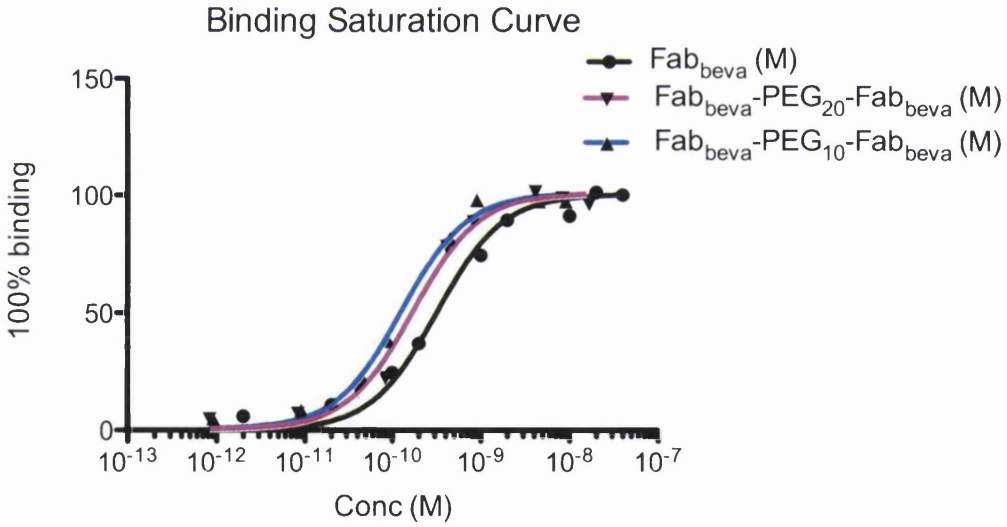

Figure 4.41 Superimposed binding saturation curves of the 6, 10 and 20 kDa Fab_{beva}-PEG-Fab_{beva} with the Fab_{beva} and bevacizumab.

In the case of Fab_{rani} and Fab_{rani}-PEG-Fab_{rani}, only 6 and 10 kDa PEGylated homodimer constructs were examined once in ELISA and compared to bevacizumab. In this experiment, the Fab_{trast}-PEG_{20}-Fab_{trast} (range from 1.3×10^{-10} to 6.6×10^{-8} M) was used as a control on the plate coated with VEGF.

A; Binding saturation curve of the Fab_{rani} and Fab_{trast}-PEG_{20}-Fab_{trast} on VEGF plate.

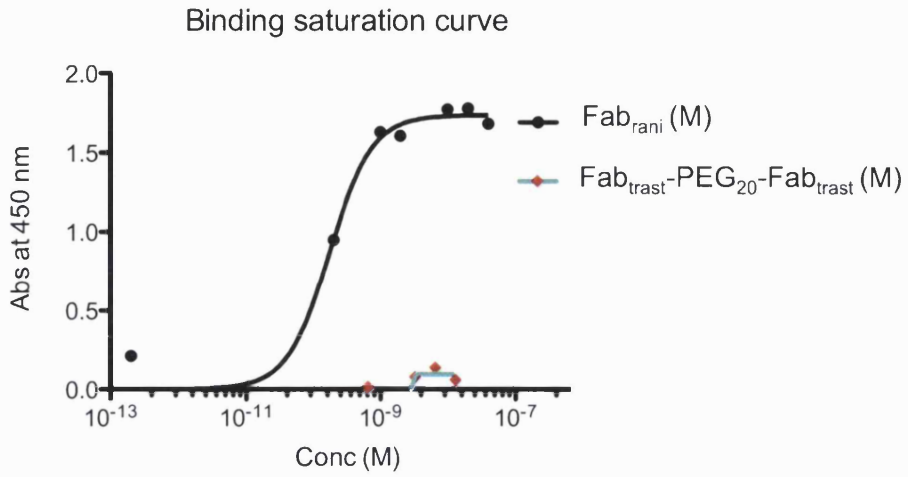

B; Superimposed binding curve of the Fab_{rani} and the Fab_{rani}-PEG_{10}-Fab_{rani} with bevacizumab.

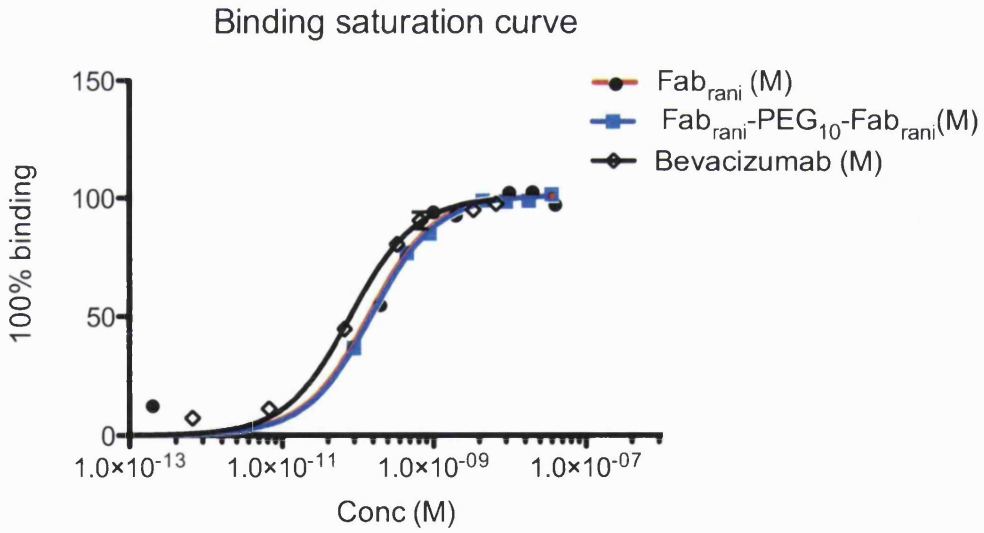

C; Superimposed binding saturation curves of the Fab_{rani} and the Fab_{rani}-PEG_6-Fab_{rani} with bevacizumab.

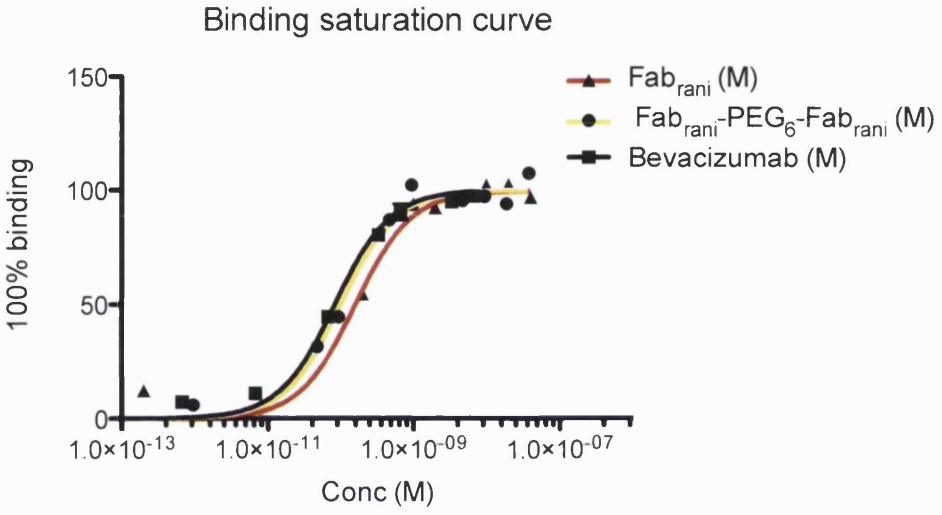

Figure 4.42 Superimposed binding saturation curves of the Fab_{rani}-PEG-Fab_{rani} with bevacizumab and Fab_{rani}.

Using Fab_{trast}-PEG_{20}-Fab_{trast} in the plate coated with VEGF, was to evaluate the specificity of interaction between Fab_{rani}-PEG-Fab_{rani} and VEGF. The result suggested no binding for Fab_{trast}-PEG_{20}-Fab_{trast} to VEGF. The relative binding affinity of the 6 and 10 kDa Fab_{rani}-PEG-Fab_{rani} with K_D value of 0.10 nM and 0.15 nM, respectively, were compared to the K_D value of Fab_{rani} (0.11 nM) and bevacizumab (0.08 nM). They all displayed similar binding affinity related to each other. The reason for the similar binding affinity between the Fab_{rani} and its homodimer constructs could be due to a better binding affinity of Fab_{rani} itself that is similar to bevacizumab. However, there might be a difference between the dissociation constant rate of the Fab_{rani} and the Fab_{rani}-PEG-Fab_{rani}, if we were able to study them in the BIAcore. Further comparison between different molecular weights of Fab_{rani}-PEG-Fab_{rani} was performed using functional assay which is described in part B of this Chapter.

The affinity values of the homodimer constructs 6, 10 and 20 kDa Fab_{beva}-PEG-Fab_{beva} and the 6 and 10 kDa Fab_{rani}-PEG-Fab_{rani} calculated by ELISA are summerised in Table 4.12.

Table 4.12 Average binding affinity value of Fabs and homodimer Fab-PEG-Fabs calculated by ELISA and BIAcore. ND; Not determined.

Constructs	K_D (nM) ELISA	K_D (nM) BIAcore
Bevacizumab	0.08	0.08
Fab_{beva}	0.32	0.32
Fab_{beva}-PEG_6-Fab_{beva}	0.11	1.54
Fab_{beva}-PEG_{10}-Fab_{beva}	0.14	1.27
Fab_{beva}-PEG_{20}-Fab_{beva}	0.17	1.53
Fab_{rani}	0.11	ND
Fab_{rani}-PEG_6-Fab_{rani}	0.10	ND
Fab_{rani}-PEG_{10}-Fab_{rani}	0.15	ND

Part B: Functional Activity Studies

4.4 Introduction to part B

In addition to its important role in the growth and development of new blood vessels (angiogenesis), VEGF is also involved in promoting vascular permeability and in systemic vasodilation. Binding of VEGF-A to VEGFR2 (Figure 4.43) on endothelial cell mediates increases in vascular permeability, cell survival, cell migration, cell proliferation and nitric oxide production [298]. Production of nitric oxide by endothelial cells results in vasodilation, through relaxation of adjacent smooth muscle cells, and it has been shown that the vasodilatory effect of VEGF is endothelium dependent [52].

As discussed previously, angiogenesis is another consequence of VEGF/VEGFR signaling that plays a critical role in cancer, inflammatory and vascular disease [298]. The angiogenesis process mainly occurs when the proliferation or metabolic rate of a tissue exceeds the nutrient and oxygen supply. So, the cellular responses to lack of oxygen result in stimulation of VEGF production and hence angiogenesis, to promote the growth of more blood vessels and dilation of existing blood vessels, to allow better delivery of blood and hence oxygen [299]. The key regulators of this cellular response to reduced oxygen tension, leading to VEGF production, are known as the hypoxia-inducible factors (HIF) [299].

As a general concept, angiogenesis is the multistep process whereby new blood vessels develop from the pre-existing vasculature. It involves proteolytic degradation of the extracellular matrix as the first step, followed by migration of endothelial cells. At the next stage, the endothelial cells proliferate and start making a new extracellular matrix. The later stages of angiogenesis involve tubule formation and anastomosis of the newly formed vessels. In tumours, angiogenesis provides adequate blood supply to allow growth and maintenance. Therefore, targeting angiogenesis has been validated as a promising method for cancer treatment. Stopping angiogenesis could be achieved by inhibiting VEGF signalling. To block the VEGF-mediated effects, different strategies have been suggested such as neutralising VEGF itself or blocking VEGFR signalling [298]. Bevacizumab and ranibizumab are both anti-$VEGF_{165}$ agents and act to inhibit angiogenesis in cancer and AMD, respectively. Their functional activities are through binding and neutralisation of $VEGF_{165}$.

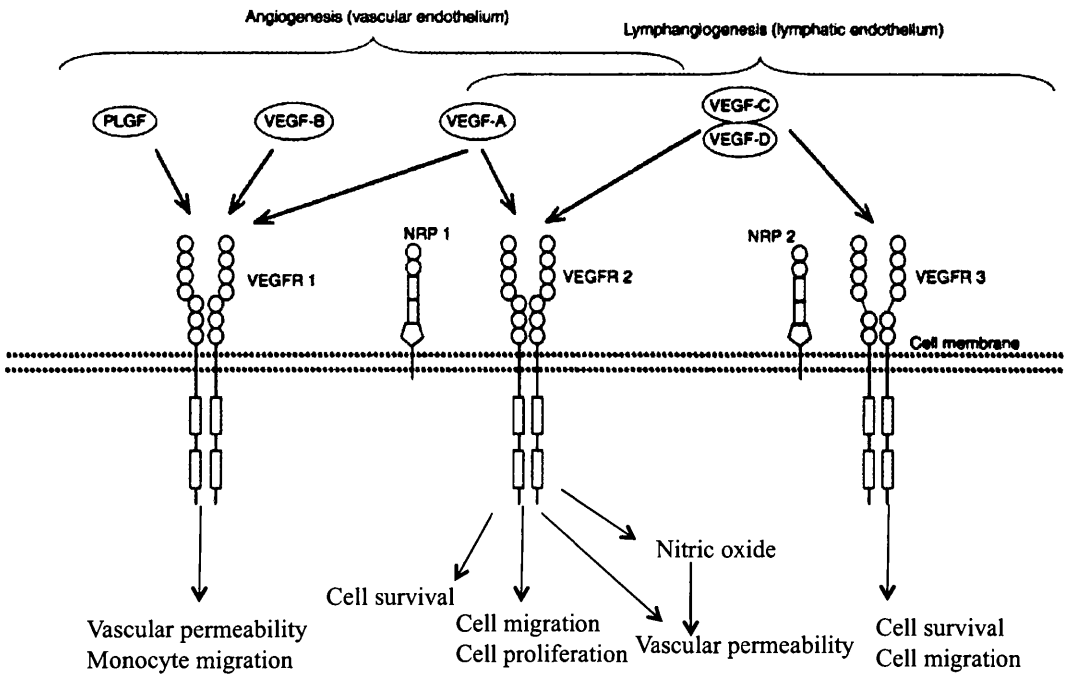

Figure 4.43 The signalling pathways of VEGFR [298].

4.4.1 In-vitro angiogenesis assay

The *in-vitro* anti-angiogenesis effect of anti-VEGF molecules that were prepared and purified in Chapter 3 is examined in this section. In angiogenesis assay, the functional activity of bevacizumab, the purified Fab_{beva}, and homodimer 6 and 20 kDa Fab_{beva}-PEG-Fab_{beva} along with Fab_{rani}, the homodimer 6 and 20 kDa Fab_{rani}-PEG-Fab_{rani} were studied.

The proprietary Angiokit assay consisted of a 24 well pre-seeded tissue culture plate and a bottle of an optimised growth medium. The plate contained an early stage co-culture of human umbilical vein endothelial cells (HUVECs) with interstitial cells (e.g fibroblasts). The number of cells initially seeded in the plate and the precise contents of the growth medium were not provided with this kit because of company confidentiality. Once placed in culture, the HUVECs began to make small islands within the culture matrix and then started to proliferate and entered a migration phase. At this stage they can move through the culture matrix and form threadlike tubule structures. These tubules can progress to join up at day 8 up to day 11 to form an anastomosing network.

Fibroblasts provide soluble pro-angiogenesis factors, which promote endothelial sprouting and tube formation. However, fibroblasts can form structures which are not actually tubes, as they lack a lumen, but which can look similar to the tubes formed by endothelial cells by eye. It is difficult to differentiate between genuine tubes and these fibroblast structures under a microscope. Therefore, fixation and staining procedures were necessary to differentiate HUVECs from fibroblasts at the end of the experiment. In this study, CD31 was used as an endothelial marker.

The constructs selected for testing in this assay were bevacizumab, Fab_{beva}, 6 and 20 kDa Fab_{beva}-PEG-Fab_{beva}, Fab_{rani}, 6 and 20 kDa Fab_{rani}-PEG-Fab_{rani} in three different concentrations. Human IgG was also used as a negative control. All the test compounds were pre-mixed with $VEGF_{165}$. Selection of the most appropriate VEGF concentration, incubation time and temperature with test compounds, as well as the ratio of VEGF to test compounds, required some consideration. It was decided to follow the conditions described by Wang and co workers in 2004, in studying the biological properties of bevacizumab. It was reported in this paper that full inhibition of VEGF-induced HUVEC proliferation was achieved by adding a 2.6:1 molar ratio of bevacizumab to homodimeric $hVEGF_{165}$ and incubating for 2 h at 37 ^{0}C, before the addition of the mixture to the cells [300]. Based on this paper, the ratio of 3 molar equivalents of bevacizumab to $VEGF_{165}$ and 2 h prior incubation at 37 ^{0}C was selected. Also, three different ratios of test compound to VEGF were assessed. For bevacizumab and its homodimer 6 and 20 kDa Fab_{beva}-PEG-Fab_{beva} and 6 and 20 kDa Fab_{rani}-PEG-Fab_{rani}, 3, 1:5 and 0.5 equivalents were mixed per mole of $VEGF_{165}$. The fixed final concentration of $VEGF_{165}$ used was 10 ng/mL in wells and the concentrations of PEGylated constructs were normalised for their protein molecular weights. For example, for ratios of 3:1, 1.5:1 and 0.5:1 of test compound:VEGF, concentrations of 0.12, 0.06 and 0.02 μg/mL bevacizumab and 0.08, 0.04 and 0.13 μg/mL homodimer Fab-PEG-Fab were required, respectively. Solutions of 100 times the final concentration required in wells were prepared, and 5 μL of each were added to the optimised growth medium (0.5 mL) plus VEGF (5 μL of a 1 μg/mL solution) to prepare the required mixture and then incubated for 2 h at 37 ^{0}C. Only one concentration of Fab_{beva} and Fab_{rani} was applied, giving a final well concentration of 0.04 μg/mL which provided a molar ratio of 3 equivalents per mole of VEGF. This same ratio (3:1) was used for control human IgG, to provide a negative control for the effects of anti-VEGF antibodies. For a baseline and positive control, respectively, a

set of wells was treated with medium only (no VEGF) and another set of wells was treated with VEGF (10 ng/mL) only. Duplicate wells were prepared for each test compound. Figure 4.44 shows the plate design for bevacizumab and the homodimer Fab-PEG-Fab constructs. Two Angiokit plates were used for this study.

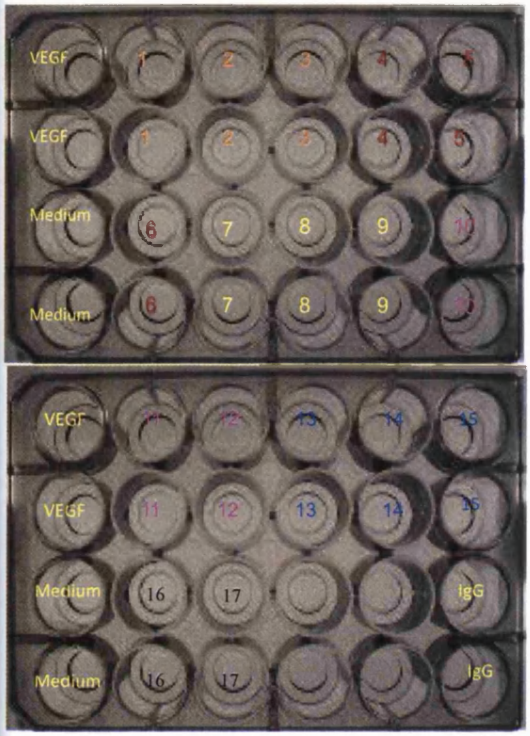

Test compounds	Concentration in well (µg/ml)
Bevacizumab	0.12
Bevacizumab	0.06
Bevacizumab	0.02
Fab_{beva}	0.04
Fab_{rani}	0.04
Fab_{beva}-PEG_6-Fab_{beva}	0.08
Fab_{beva}-PEG_6-Fab_{beva}	0.04
Fab_{beva}-PEG_6-Fab_{beva}	0.013
Fab_{beva}-PEG_{20}-Fab_{beva}	0.08
Fab_{beva}-PEG_{20}-Fab_{beva}	0.04
Fab_{beva}-PEG_{20}-Fab_{beva}	0.013
Fab_{rani}-PEG_6-Fab_{rani}	0.08
Fab_{rani}-PEG_6-Fab_{rani}	0.04
Fab_{rani}-PEG_6-Fab_{rani}	0.013
Fab_{rani}-PEG_{20}-Fab_{rani}	0.08
Fab_{rani}-PEG_{20}-Fab_{rani}	0.04
Fab_{rani}-PEG_{20}-Fab_{rani}	0.013

Figure 4.44 The plate design for bevacizumab and homodimer Fab-PEG-Fabs.

The Angiokit plates were examined using an inverted microscope with camera on days 1, 3, 6 and 8. Figure 4.45 shows images of a well, which was treated with VEGF only, at these time points. The red arrow on the image at day 8 indicates a possible tubule formed by HUVECs, likely to be such because of the networking observed. At day 10, all of the cells were fixed with ethanol and then stained. The tubules made by HUVECs were immediately observed as a dark purple precipitate in the plate, while no colour was observed for any structures made by fibroblasts, since CD31 is an endothelium-specific marker. Similarly, because the tubule formation was stimulated by the addition of VEGF, where VEGF signalling had been blocked to some extent by its inhibitors, less purple colour was apparent in the relevant wells.

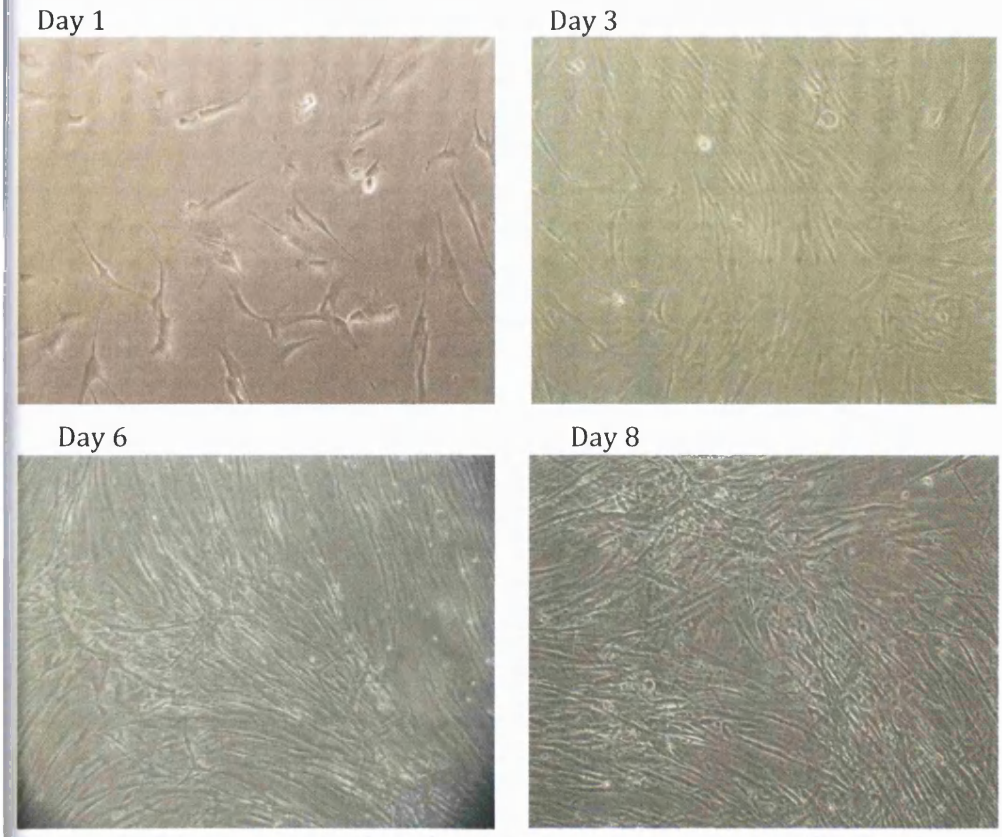

Figure 4.45 Images at day 1, 3, 6 and 8 of a well treated with VEGF only.

Figure 4.46 shows the gross appearance of the plate after fixation and staining. An inverted microscope with camera was used to take an image (x 10 objective) from each well at day 10. Figure 4.47 shows these images, which were taken from each set of wells treated with test compounds.

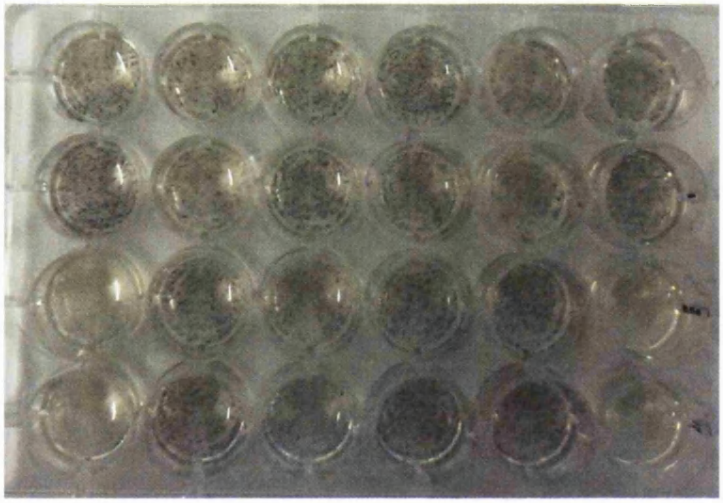

Figure 4.46 The Angiokit plate appearance after staining at day 10.

A; Bevacizumab

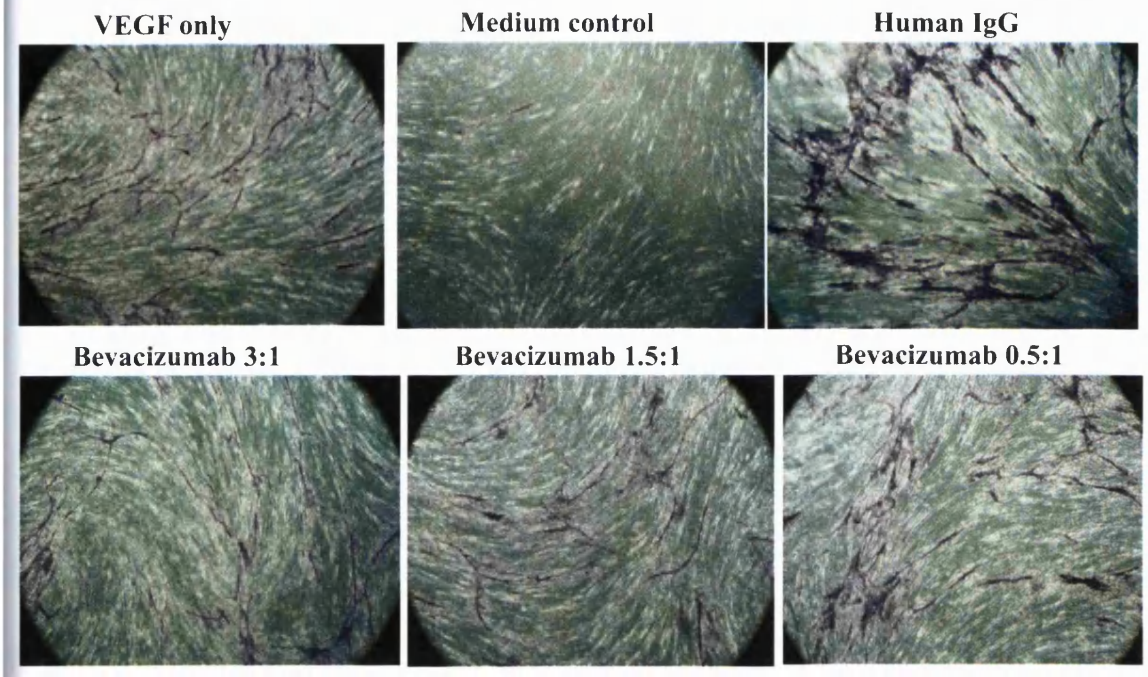

B; 6 and 20 kDa Fab_{beva}-PEG-Fab_{beva}

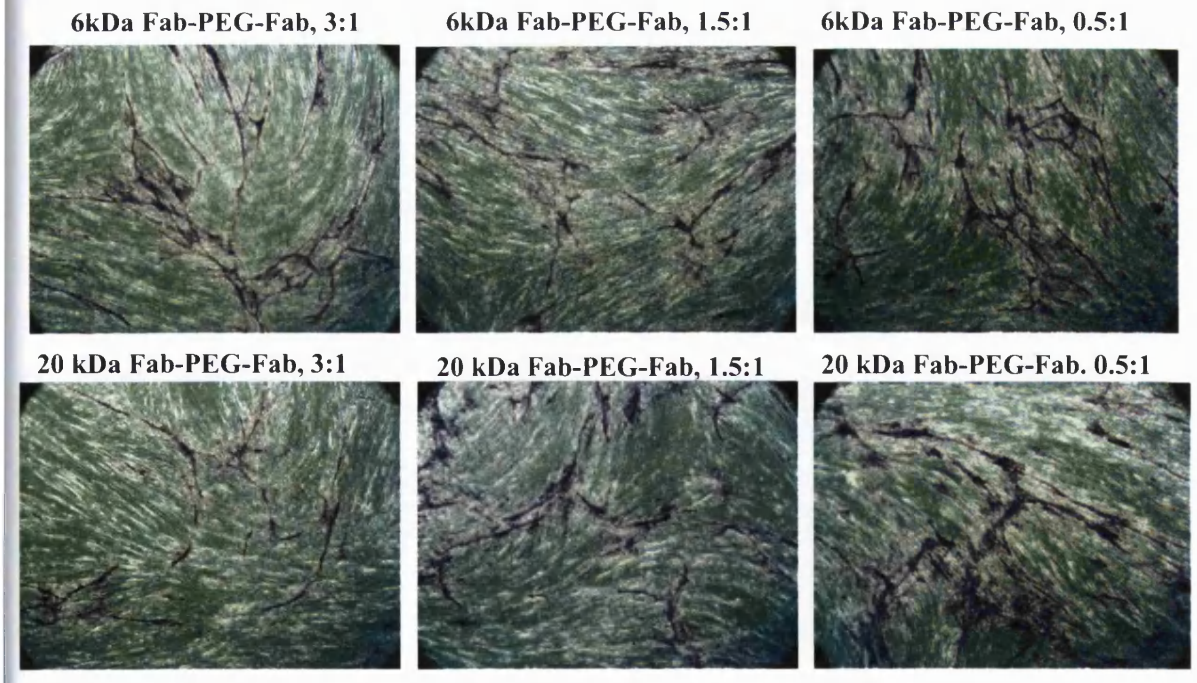

C; 6 and 20 kDa Fab_{rani}-PEG-Fab_{rani}

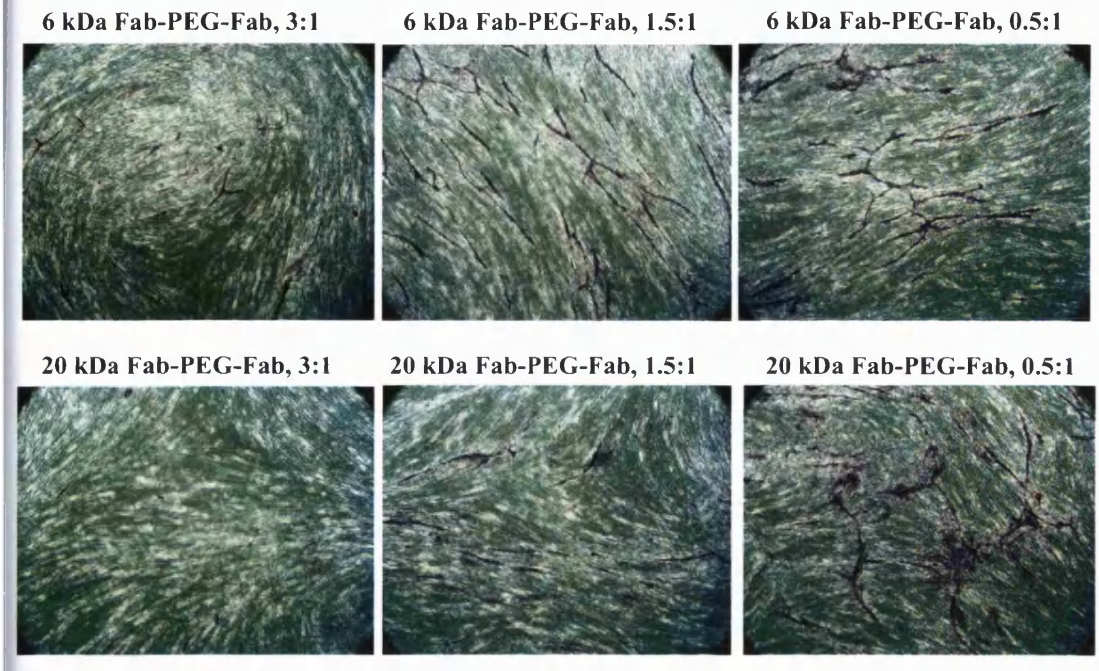

Figure 4.47 Images of wells treated with **(A)** Bevacizumab, **(B)** 6 and 20 kDa Fab_{beva}-PEG-Fab_{beva}, **(C)** 6 and 20 kDa Fab_{rani}-PEG-Fab_{rani}.

The images for control human IgG, medium only and VEGF only are shown in Figure 4.47, A. Results suggested that angiogenesis occurred in wells treated with VEGF. Also, when no VEGF was applied, little or no angiogenesis was observed. For human IgG with no anti-VEGF effect, no interference with VEGF function was observed, as the level of angiogenesis was retained, based on the images in Figure 4.47, A.

For the cells treated with the higher molar ratio of bevacizumab to VEGF (3:1) less angiogenesis was observed based on qualitative image analysis. Moreover, in Figure 4.47, B the homodimer Fab_{beva}-PEG-Fab_{beva} also appeared to stop angiogenesis in a concentration-dependent manner. A similar trend was observed from the images in Figure 4.47, C for the homodimer Fab_{rani}-PEG-Fab_{rani}. Looking at the images in Figure 4.47, B and C, it would appear that the 20 kDa Fab-PEG-Fab construct from either Fab_{beva} or Fab_{rani} resulted in more inhibition of angiogenesis than the 6 kDa Fab-PEG-Fab construct. Also, they all appeared to produce a greater inhibition than bevacizumab at the same molar concentration. Fab_{rani}-PEG-Fab_{rani} seemed to show a greater anti-angiogenesis effect than Fab_{beva}-PEG-Fab_{beva} in general. The reason for this may lie in the nature of the Fab used for homodimer preparation; Fab_{rani} has been reported to have better binding affinity for VEGF than Fab_{beva} [193], as was also

observed in ELISA. Therefore, a better functional activity of the Fab_{rani}-PEG-Fab_{rani} was to be expected.

For better comparison between bevacizumab and the homodimer constructs, Figure 4.48 was prepared from the images taken of the 3 molar equivalents of test compounds to 1 VEGF. From the images in Figure 4.48, it appears that Fab_{rani}-PEG_{20}-Fab_{rani} completely stopped the formation of tubules. Moreover, it was clear that Fab-PEG_{20}-Fab constructs were more inhibitory than Fab-PEG_6-Fab.

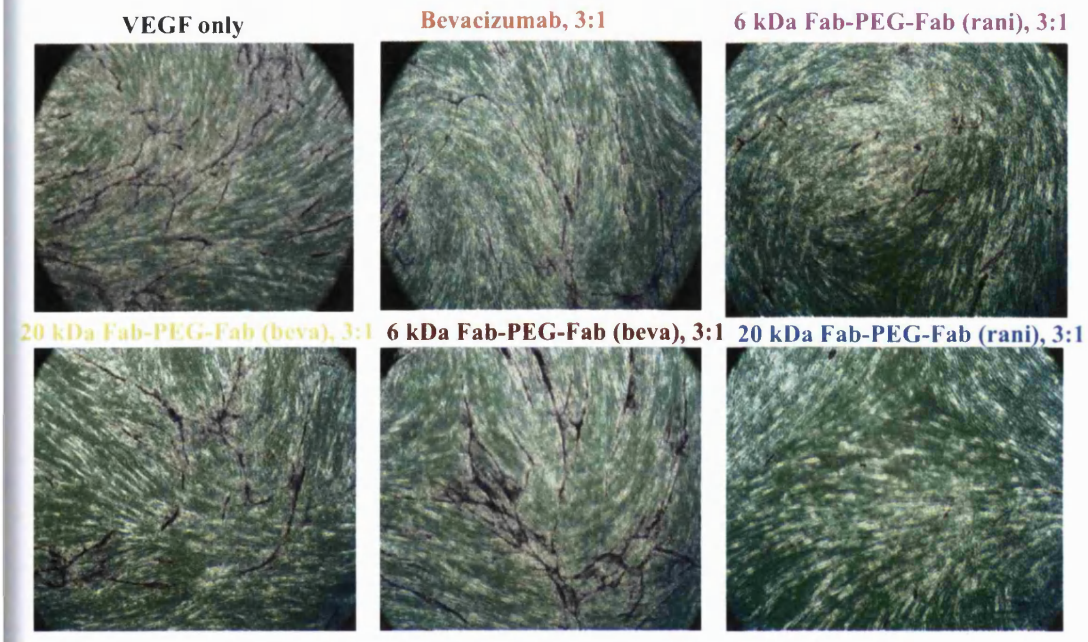

Figure 4.48 Images of wells treated with bevacizumab and the 6 and 20 kDa Fab_{beva}-PEG-Fab_{beva} and Fab_{rani}-PEG-Fab_{rani} at a 3 to 1 VEGF molar ratio.

ELISA was also performed as a semi-quantitive approach. The ELISA readout was based on the number of endothelial cells present, regardless of tubular and anastomosing network formation. It was based simply on the presence of CD31 on the endothelial cell surface, which could react with the anti-CD31 primary antibody and then be detected with the secondary antibody conjugated with AP. However, it did allow a quantitative measurement of the effect of VEGF on endothelial cell proliferation, and the effects of bevacizumab and other inhibitors on this.

Figure 4.49 shows the ELISA results for bevacizumab and the homodimer molecules. The mean absorbance was calculated for each test compound and then corrected for absorbance from the wells treated with medium alone (background). Data were then expressed as % of VEGF control. The number located on each bar in

Figure 4.49, represents the % of VEGF (control) proliferation and reflects the number of endothelial cells present after 10 days treatment. Results in Figure 4.49 show that bevacizumab at its highest concentration (3 to 1 VEGF) reduced proliferation to 13 % of control (or produced 83 % inhibition). The degree of inhibition decreases with reducing concentrations of bevacizumab.

A; VEGF-induced proliferation in the absence and presence of bevacizumab (3, 1.5 and 0.5 equivalent to 1 VEGF).

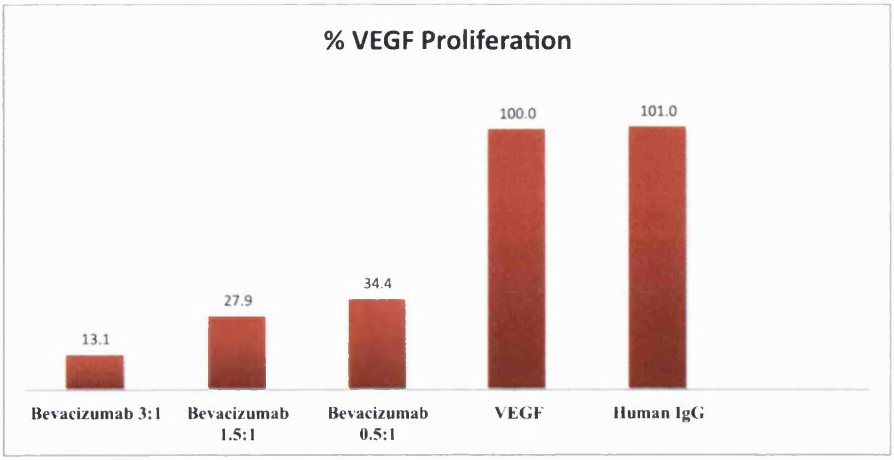

B; VEGF-induced proliferation in the absence and presence of bevacizumab and the Fab-PEG-Fabs (3 to 1 VEGF).

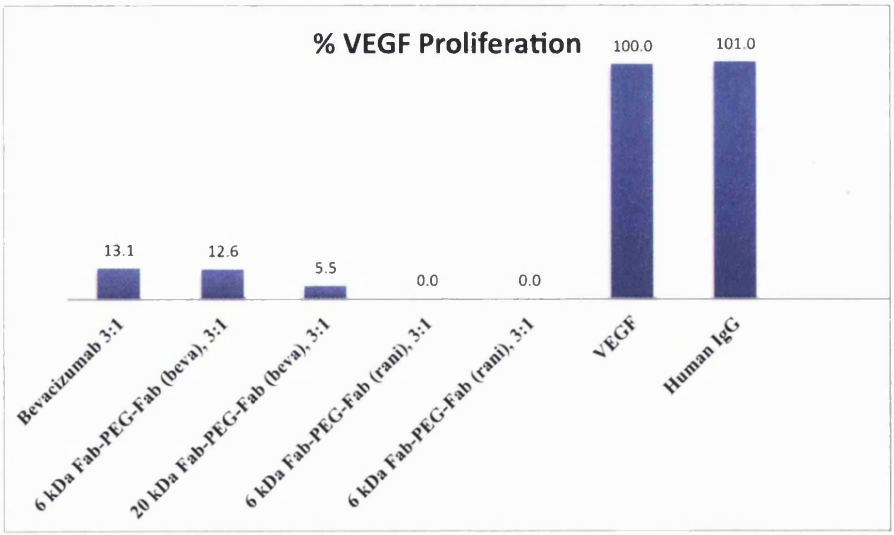

Figure 4.49 Anti- CD31 ELISA data. **(A)** VEGF-induced proliferation in the absence and presence of bevacizumab at 3, 1.5 and 0.5 equivalents to 1 VEGF, **(B)** VEGF-induced proliferation in the absence and presence of bevacizumab and the Fab-PEG-Fab (beva and rani, 6 and 20 kDa at 3 equivalents to 1 VEGF.

Similar results were observed for the Fab-PEG-Fab constructs, whereby higher concentrations of the homodimer resulted in greater inhibition of proliferation. Results demonstrated that the homodimer Fab-PEG-Fabs in general, inhibited VEGF induced proliferation better than bevacizumab. Also, 20 kDa Fab-PEG-Fab constructs resulted in better VEGF inhibition than 6 kDa Fab-PEG-Fab homodimer, either from Fab_{beva} or Fab_{rani}. However, the Fab_{rani}-PEG-Fab_{rani} showed better inhibition than Fab_{beva}-PEG-Fab_{beva}. Moreover, human IgG was also examined in ELISA and 100 % of control proliferation was observed, suggesting no non-specific inhibitory effect on VEGF function and a specific interaction between the bevacizumab and homodimer constructs and VEGF.

However, these results from ELISA provide an indication of only part of the angiogenesis process (proliferation). Since this was an angiogenesis assay, it was more important to evaluate the angiogenesis effect in terms of the number of tubules and junctions between tubules made.

Therefore, analysis was performed using angiogenesis-specific software (AngioSys). Using this software, it was possible to quantify the angiogenesis effect of VEGF and its inhibition by bevacizumab and related molecules. The number of tubules and junctions present provides a more physiologically relevant way to evaluate angiogenesis effects.

Figure 4.50 shows a screen shot of the AngioSys analysis for bevacizumab and the homodimer constructs. The images were taken using an upright microscope with 40 x magnification. Junctions are made when the tubules start branching and then making an anastomosing capillary-like network. Anastomosis is a connection between two blood vessels and happens at the later stages of angiogenesis *in-vivo* and *in-vitro*. Therefore, the number of junctions indicates the degree of angiogenesis that has occurred. For instance, in the wells treated with VEGF only 830 junctions and 1933 tubules were observed. By comparison, 382 junctions were counted in the bevacizumab-treated wells, with 172 and 109 for the Fab_{beva}-PEG_6-Fab_{beva} and Fab_{beva}-PEG_{20}-Fab_{beva} treated wells, respectively (3 equivalents to 1 VEGF in all cases). Table 4.13 provides a summary of the AngioSys analysis data for each test compound.

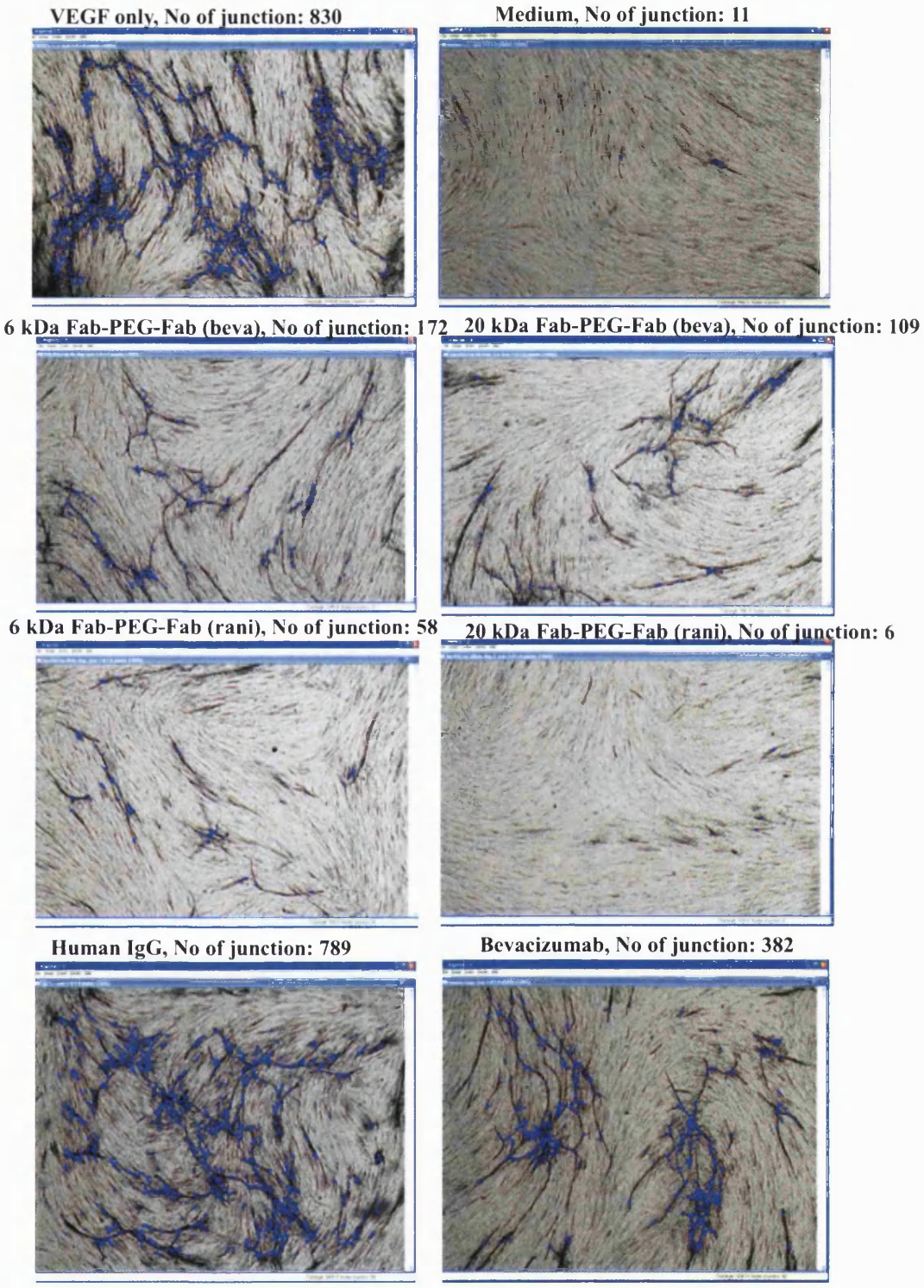

Figure 4.50 A screen shot of the AngioSys analysis. Bevacizumab and the Fab-PEG-Fab (6 and 20 kDa) either from Fab_{beva} and Fab_{rani} were at the same concentration, 3 equivalents to 1 VEGF.

Table 4.13 The average number of junctions and tubules calculated for each test compound using the AngioSys software.

Test compounds	Number of junction	Number of tubules
Medium	11	283
VEGF	830	1933
Human IgG	784	1854
Bevacizumab (0.5:1)	733	1910
Bevacizumab (1.5:1)	617	1310
Bevacizumab (3:1)	382	964
Fab_{beva} (3:1)	403	1083
Fab_{rani} (3:1)	233	635
Fab_{beva}-PEG_6-Fab_{beva} (0.5:1)	601	1454
Fab_{beva}-PEG_6-Fab_{beva} (1.5:1)	375	951
Fab_{beva}-PEG_6-Fab_{beva} (3:1)	172	536
Fab_{beva}-PEG_{20}-Fab_{beva} (0.5:1)	473	1116
Fab_{beva}-PEG_{20}-Fab_{beva} (1.5:1)	448	1080
Fab_{beva}-PEG_{20}-Fab_{beva} (3:1)	109	334
Fab_{rani}-PEG_6-Fab_{rani} (0.5:1)	301	764
Fab_{rani}-PEG_6-Fab_{rani} (1.5:1)	230	703
Fab_{rani}-PEG_6-Fab_{rani} (3:1)	58	318
Fab_{rani}-PEG_{20}-Fab_{rani} (0.5:1)	308	854
Fab_{rani}-PEG_{20}-Fab_{rani} (1.5:1)	99	517
Fab_{rani}-PEG_{20}-Fab_{rani} (3:1)	6	67

Figure 4.51 shows the number of junctions in wells treated with A; bevacizumab at three molar ratios to VEGF and Fab_{beva} and Fab_{rani} at one concentration (3 equivalent Fabs to 1 VEGF) and B; the Fab_{beva}-PEG-Fab_{beva} (6 and 20 kDa) at three concentrations and C; the Fab_{rani}-PEG-Fab_{rani} (6 and 20 kDa) at three concentrations. In Figure 4.51, D the number of junctions made in the presence of bevacizumab was compared with the number of junctions made in the presence of the Fab_{beva}-PEG-Fab_{beva} and Fab_{rani}-PEG-Fab_{rani} (6 and 20 kDa) at the same concentration.

A; Number of junctions formed in wells treated with bevacizumab, Fab_{beva} and Fab_{rani}

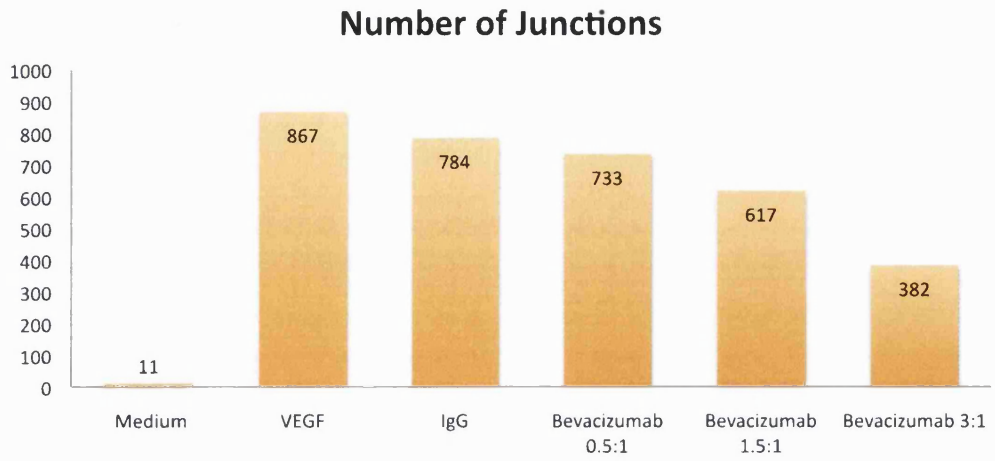

B; Number of junctions formed in wells treated with 6 and 20 kDa Fab_{beva}-PEG-Fab_{beva}

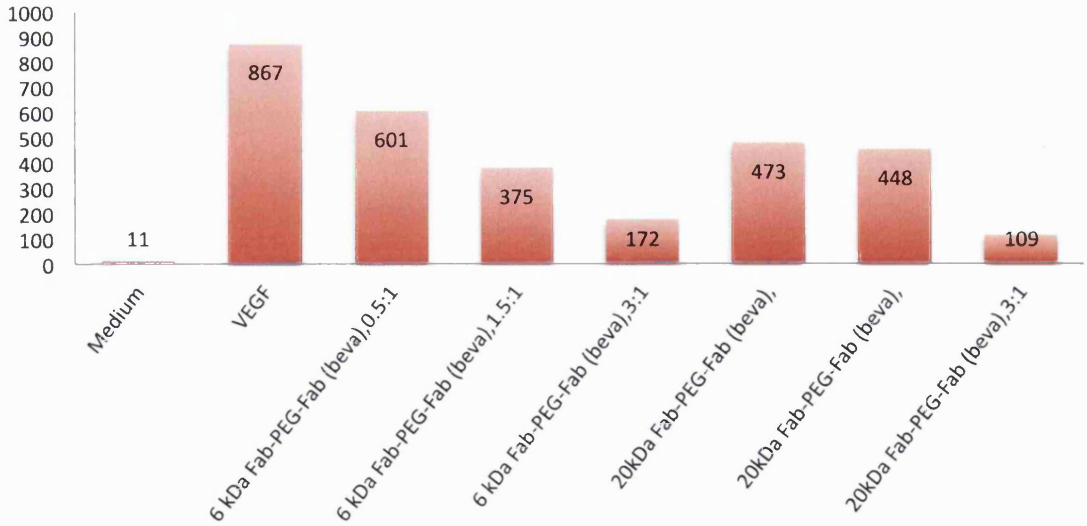

C; Number of junctions formed in wells treated with 6 and 20 kDa Fab_{rani}-PEG-Fab_{rani}.

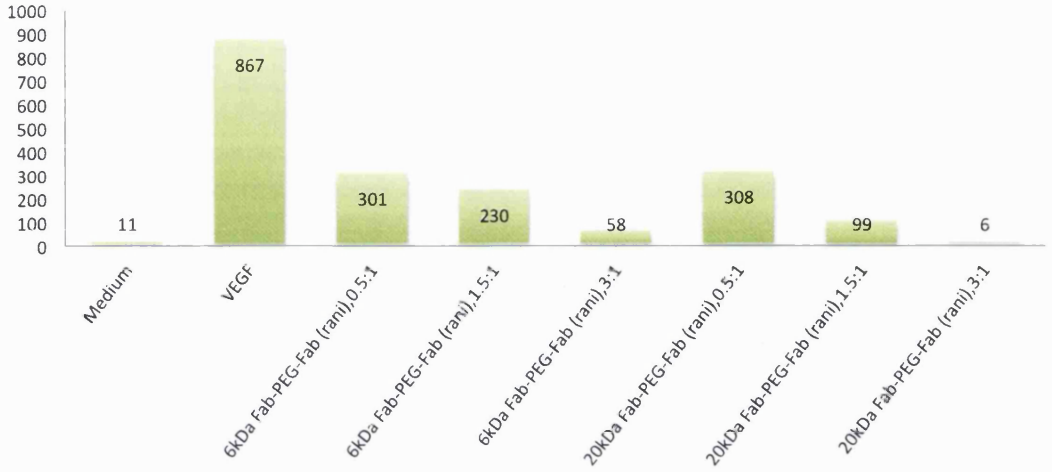

D; Number of junctions formed in wells treated with the Fab_{beva}-PEG-Fab_{beva} Fab_{rani}-PEG-Fab_{rani} compared with bevacizumab.

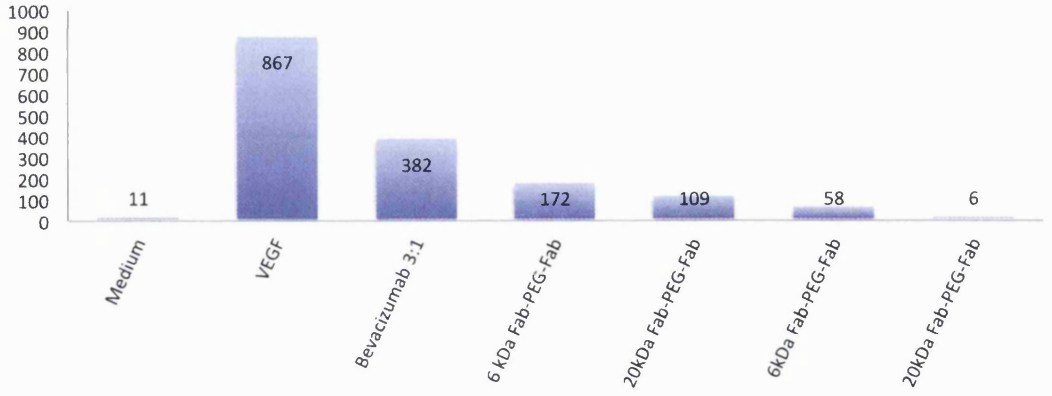

Figure 4.51 The number of junctions made in the absence and presence of the test compounds.

Figure 4.51, A shows a concentration response relationship for bevacizumab. Applying higher concentrations of bevacizumab resulted in fewer junctions formed and hence greater VEGF inhibition. Also, in this chart, the number of junctions made in wells treated with control human IgG is compared with that for bevacizumab at the same concentration, relative to VEGF. The control IgG wells were similar to the wells treated with VEGF only. Figure 4.51, B shows a concentration response relationship for Fab-PEG-Fab (beva, 6 and 20 kDa) similar to that seen for bevacizumab.

However, the results for the Fab_{beva}-PEG_{20}-Fab_{beva} indicate fewer junctions compared with the Fab_{beva}-PEG_6-Fab_{beva} and, furthermore, both resulted in fewer junctions compared with bevacizumab treated wells. Figure 4.51, C shows an identical pattern of inhibition for the 6 and 20 kDa Fab_{rani}-PEG-Fab_{rani} but with the fewest tubules present out of all the treatments tested. Figure 4.51, D provides a comparison of the number of junctions made in the presence of bevacizumab and the Fab_{beva}-PEG-Fab_{beva} and Fab_{rani}-PEG-Fab_{rani} (6 and 20 kDa) at the same concentration. These results suggest again that the homodimer Fab-PEG-Fab either from Fab_{rani} or Fab_{beva} inhibit angiogenesis more effectively than bevacizumab. For wells treated with the Fab_{rani}-PEG_{20}-Fab_{rani} the number of junctions was the same as in the wells treated with medium alone. This suggests that the Fab_{rani}-PEG_{20}-Fab_{rani} inhibited VEGF signalling completely.

Using the AngioSys software, it was also possible to measure the number of individual tubules formed by the HUVECs. Figure 4.52 shows the number of tubules made for each test compound (these data can also be found in Table 1.1). As expected, these data mirror those seen for the number junctions formed. While it is important to quantify both of these phenomena, it is clear that junctions and anastomosis between tubes in this assay form from tubes that have been newly generated. Hence, a greater number of junctions is likely to reflect a greater number of tubules formed.

A; Number of tubules formed in wells treated with bevacizumab, Fab_{beva} and Fab_{rani}.

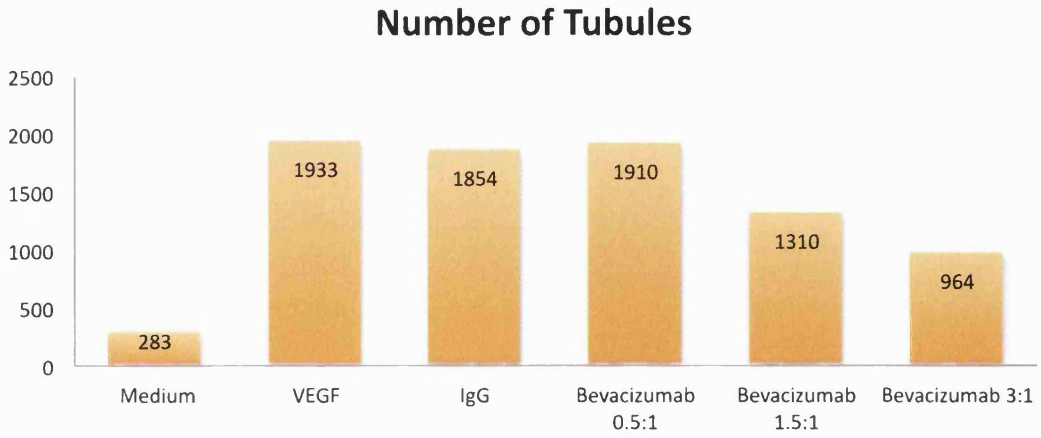

B; Number of tubules formed in wells treated with the 6 and 20 kDa Fab_{beva}-PEG-Fab_{beva}.

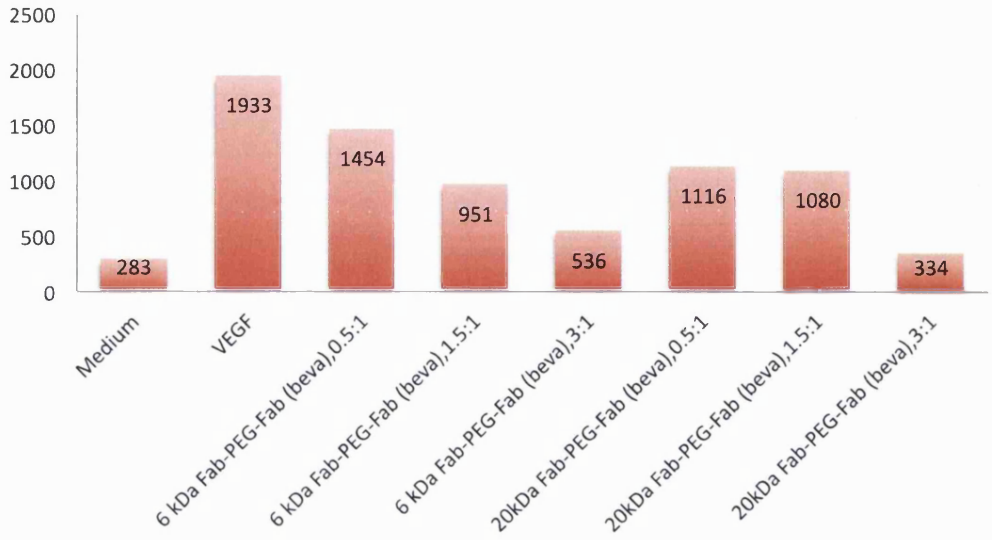

C; Number of tubules formed in wells treated with the 6 and 20 kDa Fab_{rani}-PEG-Fab_{rani}.

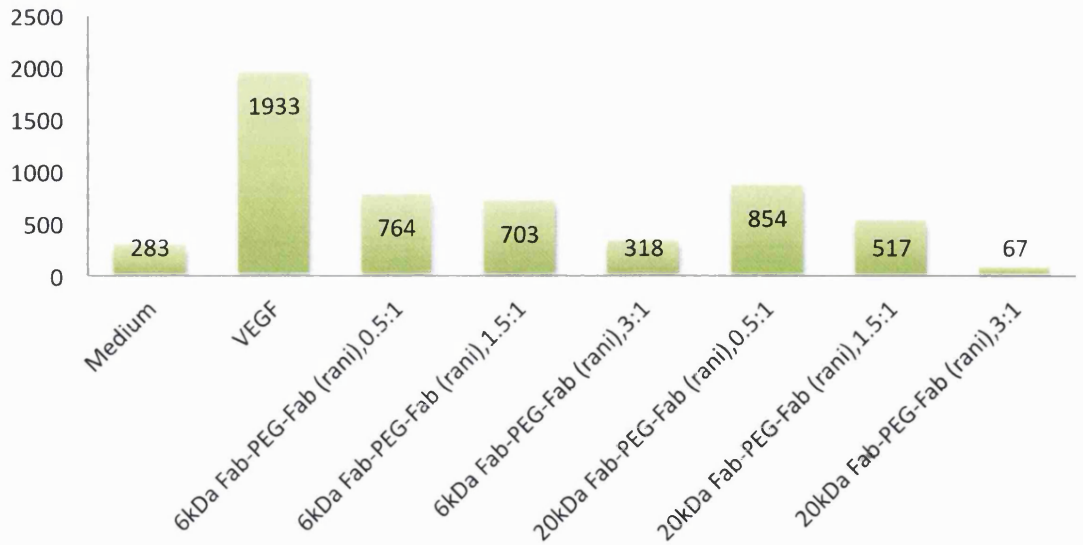

D; Number of tubules formed in wells treated with the Fab_{beva}-PEG-Fab_{beva} and Fab_{rani}-PEG-Fab_{rani} compare to bevacizumab.

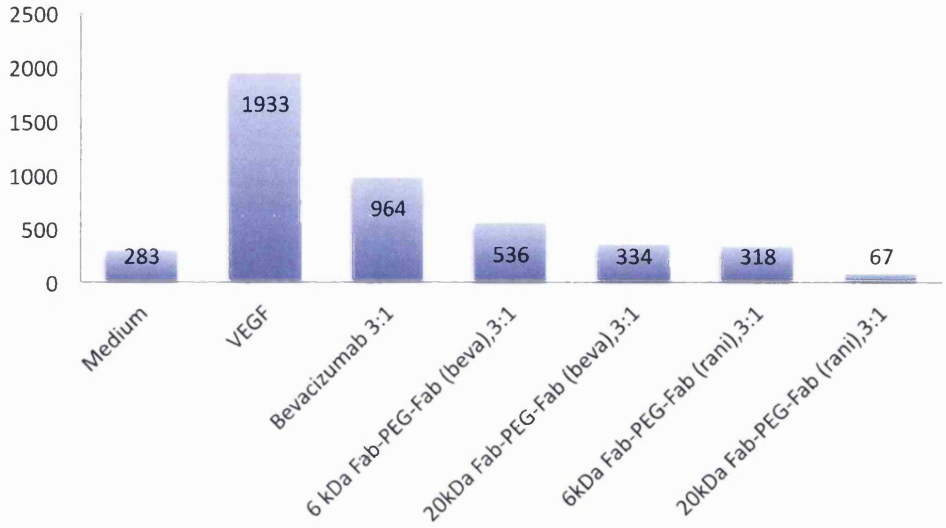

Figure 4.52 The number of tubules made in the absence and presence of the test compounds.

4.4.2 Ex-vivo Vasodilation assay

To establish an *ex-vivo* experiment to allow study of the binding VEGF with anti-VEGF molecules in the solution with a much faster readout (minutes less than day), preliminarily work was conducted to study the anti-vasodilation functional activity of bevacizumab. It was hoped that after optimisation of conditions with bevacizumab, the activity of other anti-VEGF molecules such as Fab-PEG-Fab could be examined in this model and compared with the results obtained from the angiogenesis assay. In the present work, the optimisation of the *ex-vivo* vasodilation assay with bevacizumab is discussed.

The vasodilation assay is an endothelium dependent assay that based on relaxation of smooth muscle. The vasodilation effect of VEGF is one of the well-known biological pathways of VEGF-VEGFR2 signalling. VEGFR2 is located on endothelial cells and one of its key signalling pathways is production of nitric oxide, which causes smooth muscle relaxation. Nitric oxide is an important vasodilator and the main endothelium derived relaxing factor (EDRF), synthesized in this context by endothelial nitric oxide synthase (eNOS) [301]. EDRF was first discovered by Furchgott and Zawadzki in 1980, when relaxation of arteries in response to

acetylcholine (ACh) was shown to occur only in the presence of an intact endothelial layer. The endothelial synthesis of NO can be induced by a range of agonists, including acetylcholine (ACh) which does this by binding to muscarinic (M3) cholinergic receptors on endothelial cells. Once NO is produced, it can diffuse to the adjacent smooth muscle cells and stimulate soluble guanylate cyclase. Guanylate cyclase is an enzyme that leads to the formation of cyclic 3',5'-guanosine monophosphate (cGMP) from guanosine-5'-triphosphate, which results in activation of the cGMP-dependent protein kinase G. The activation of protein kinase G ultimately leads to a reduction in the intracellular [Ca^{2+}], activation of myosin light chain phosphatase and inactivation of myosin light chain kinase, therefore, dephosphorylation of the regulatory myosin light chain occurs, causing relaxation of smooth muscle. The vasodilation effect of NO has an important role in the regulation of blood flow and hence blood pressure [302]. While VEGF and ACh are both endothelium-dependent vasodilator agents, SNP (sodium nitroprusside) is an endothelium-independent agent. SNP is a potent vasodilator agent in arteries and veins and donates NO regardless of the presence of endothelial cells. This NO likewise results in smooth muscle relaxation and vasodilation.

In this work, rat blood vessels were contracted with U46619 (10-30 nM) until the active tone reached 10-20 % of the response to 120 mM K^+. Then, the contracted blood vessels were treated with $VEGF_{165}$ in cumulatively increasing concentrations (1 pM to 3 nM) to study the relaxation of the arteries. In some experiments, the effect of bevacizumab on this response was studied. To assess the maximum achievable endothelium-dependent relaxation of blood vessels, ACh (10 μM) was added at the end of each VEGF concentration response series. In order to examine the specificity of the smooth muscle relaxation response to the endothelium-dependent agents, and to confirm further the integrity of the endothelium, SNP (100 μM) was also added. SNP produces nitric oxide chemically, and at this high concentration causes a nominal maximum relaxation. If blood vessels relaxed in the presence of SNP, but neither VEGF nor ACh, this would indicates that the endothelium was damaged or dysfunctional and the results for these vessels should be discarded.

U46619 is a thromboxane A2 analogue and potent TP prostanoid receptor agonist and hence vasoconstrictor. Very small amounts of this reagent were required to contract blood vessels to 10-20% of the KCl response. Artificially increasing extracellular [K^+] to levels similar to those found inside cells (by the addition of 120

mM KCl) resulted in a rapid and robust contraction of the arterial smooth muscle due to the disrupting effect on the concentration driven and electrical driven potassium equilibrium across the membrane. Voltage gated calcium channels located on the cells can open once the electrochemical gradient to K^+ is lost and the membrane depolarises, allowing Ca^{2+} to enter the cells. This results in contraction of smooth muscle and is used to confirm vessel function and provide a reference contractile potential. After this step, the vessels had to be washed thoroughly with Krebs buffer to restore resting ionic conditions before contracting with U46619. When the contractile response to U46619 was steady, VEGF was added cumulatively. Figure 4.53 shows the relaxation response of the blood vessels with increasing VEGF concentration. This graph shows the results of 5 independent experiments using tissues from 5 different rats.

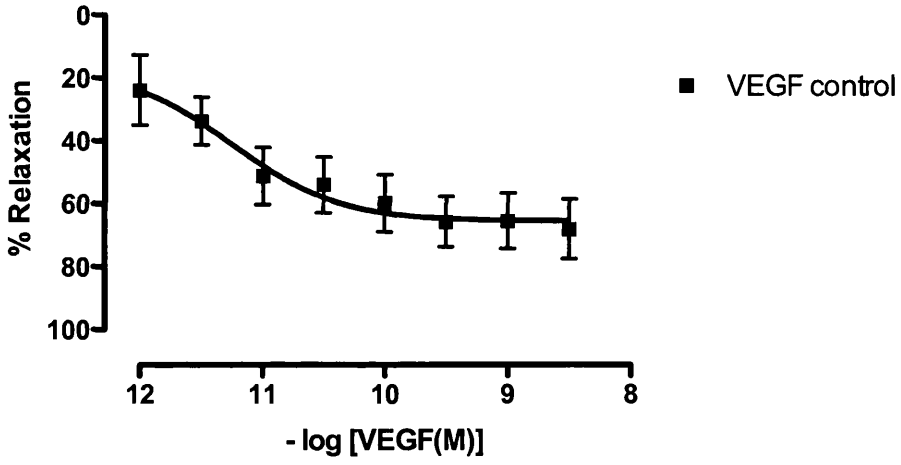

Figure 4.53 The endothelium-dependent relaxation in response to VEGF. Data are expressed as mean ± s.e.(n=5).

The results in Figure 4.53 show that VEGF induced a concentration-dependent vasodilation. A maximum relaxation was observed with between 300 pM and 3 nM VEGF. 100 % endothelium-dependent relaxation was achieved when ACh (10 μM) was added. Any further relaxation observed after addition of SNP was endothelium independent. The maximum relaxation achieved in response to VEGF was typically 80-90 % of that induced by ACh (10 μM).

The effect of bevacizumab as an anti-VEGF agent was studied when 1.5, 0.75 and 0.375 molar equivalents of bevacizumab were mixed with VEGF (3 nM) and incubated for 2 h prior to experimentation as before. Figure 4.54 shows the

endothelium-dependent relaxation response of the blood vessels in response to Ach, following the different treatments. These results suggest that the endothelium was intact and its function was not adversely affected by the presence of bevacizumab. Therefore, we can conclude that the inhibitory effects of bevacizumab were due to VEGF neutralisation rather than due to a non-specific effect on the tissue.

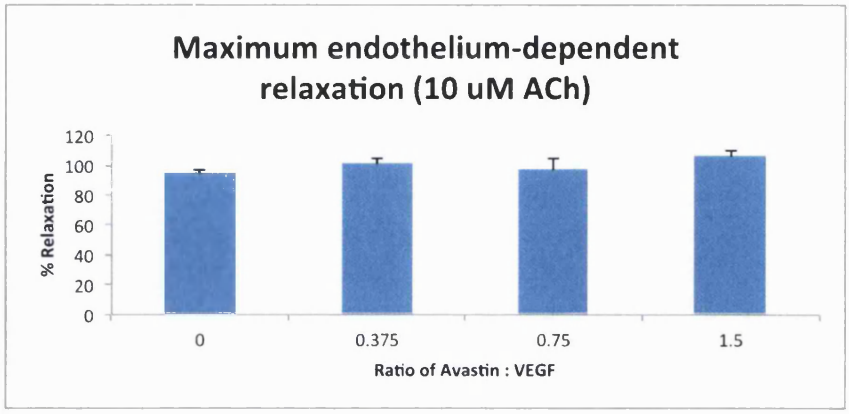

Figure 4.54 The maximum endothelium-dependent relaxation to ACh. Expressed as a percentage of the response to SNP, mean ± s.e. (n=5).

Figure 4.56 and Figure 4.57 show the percentage relaxation of arteries in response to VEGF, in the absence and presence of bevacizumab at the different concentrations tested. These results demonstrated a concentration-dependent effect of bevacizumab on VEGF-induced vasodilation. These data were obtained from 4 independent experiments using tissue from 4 different rats.

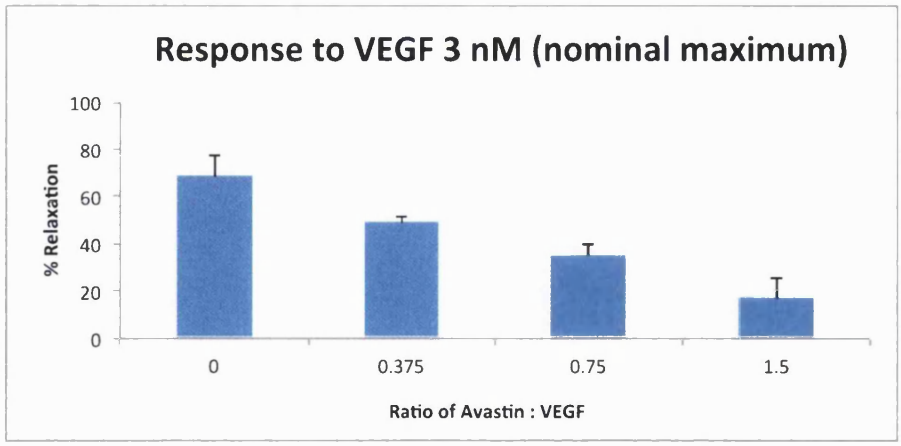

Figure 4.55 The maximum relaxation response to VEGF in the absence and presence of bevacizumab. Expressed as a percentage of the response to SNP, mean ± s.e. (n=4).

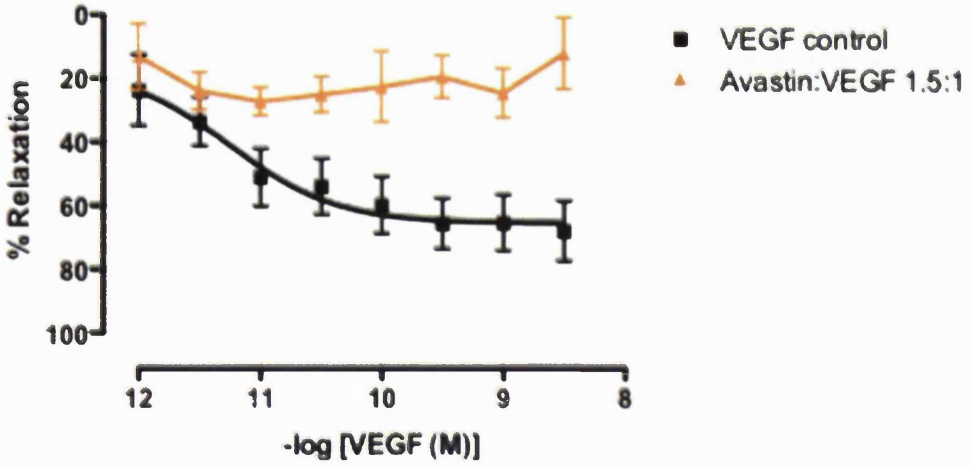

Figure 4.56 VEGF-induced arterial relaxation in the absence and presence of bevacizumab (1.5 : 1 molar equivalent). Expressed as a percentage of the response to SNP, mean ± s.e. (n=4).

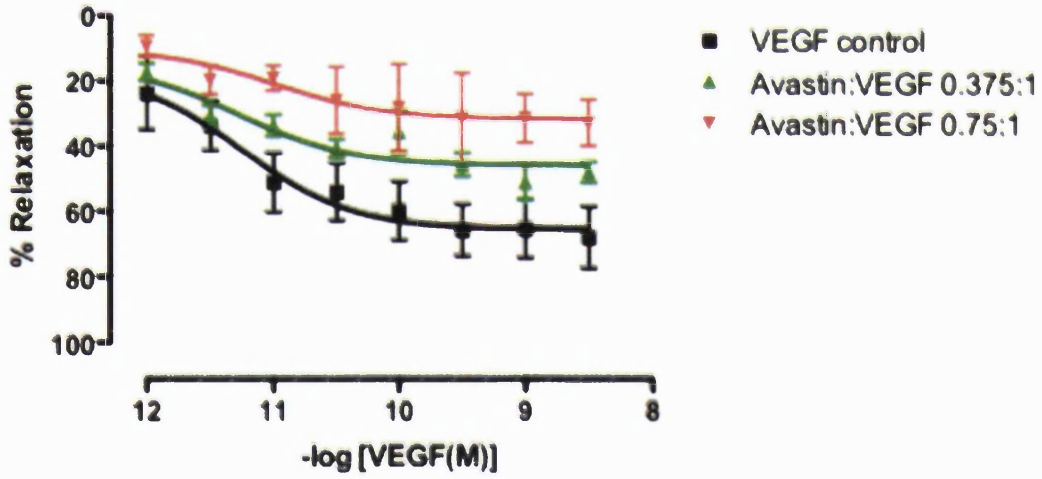

Figure 4.57 VEGF-induced arterial relaxation in the absence and presence of bevacizumab (0.375 and 0.75 : 1 molar equivalents). Expressed as a percentage of the response to SNP, mean ± s.e. (n=4).

Comparison of the graphs in Figure 4.57 shows that bevacizumab at the lowest concentration tested (0.375 molar ratio: 1 VEGF) was sufficient to inhibit VEGF function and thus inhibit vasodilation. Bevacizumab at the highest concentration

tested (1.5:1 molar equivalent to VEGF) completely inhibited the vasodilation response. Based on this work on bevacizumab, the anti-vasodilation functional activity of the Fab_{rani} and homodimer Fab_{rani}-PEG_{20}-Fab_{rani} will be examined in future work.

4.5 Summary

The structure properties correlation between Fab, mono PEG-Fab and homodimer Fab-PEG-Fab were studied and determined in BIAcore and ELISA. Three different Fabs were used for these studies. The binding affinity of the PEGylated constructs was calculated using BIAcore and ELISA assays. The kinetic rate constants, association and dissociation, were also determined using BIAcore.

The binding of the Fab fragment derived from enzymatic digestion of full IgG, bevacizumab and trastuzumab, were first determined. The results observed in BIAcore suggested that the binding of these Fabs (Fab_{beva}, Fab_{trast}) to their targets were maintained. The binding affinity of the Fab_{beva} was lower than bevacizumab, whereas the binding affinity of the Fab_{trast} was similar to that of trastuzumab using BIAcore and ELISA. This was thought to be due to the multivalent ligand (VEGF) involved in the bevacizumab interaction versus monovalent HER-2 in the trastuzumab interaction.

The binding of the PEGylated Fab fragments prepared from Fab_{beva}, Fab_{trast} and Fab_{rani}, to their respective ligands was preserved in both BIAcore and ELISA assays. The binding affinity calculated by these two methods suggested that the affinity value of the PEGylated Fabs decreased about two fold compared with their corresponding native Fabs. BIAcore data suggested that this decrease in affinity value of PEG-Fab was due to change in association rate constants while and their dissociation rate constant remained unchanged. While most works described in the literature suggested that the binding affinity of the PEGylated Fab fragments decreases by 5 fold [114] and even in single chain fragments by 10 fold [288] when the PEGylation occurred on inserted cysteine, using disulfide bridging PEGylation on the interchain disulfide bond of the Fab appeared to decrease the binding affinity of the Fabs by about 2 fold. In addition, the effect of different molecular weights of the PEG conjugated in the PEG-Fab structure on its binding affinity and dissociation rate constant were studied in BIAcore. It was shown that using 20, 30 and 40 kDa PEG in the PEG-Fab structure, the binding affinity appeared to be similar with the same

dissociation and association rate constant. However, the dissociation rate appeared to be much faster when two molecules of PEG (20 kDa) were conjugated to the Fab derivatives. This construct (PEG_{2x20}-Fab′) displayed a similar association rate constant to PEG_{40}-Fab and suggested the possible presence of a threshold for steric shielding effects of the PEG.

The homodimer Fab-PEG-Fab constructs (Fab_{beva}-PEG-Fab_{beva}, Fab_{rani}-PEG-Fab_{rani}, Fab_{trast}-PEG-Fab_{trast}) displayed similar binding affinities to their respective full IgGs in BIAcore and ELISA. The dissociation rates of the Fab_{beva}-PEG-Fab_{beva} appeared to be slower than for bevacizumab, which suggested a tighter binding to its target. Differences in dissociation rate constants for the 6, 10 and 20 kDa Fab_{beva}-PEG-Fab_{beva} were observed in BIAcore, however, they appeared to have similar binding affinity values in BIAcore and ELISA.

The binding affinities of bispecific antibody fragments Fab_{beva}-PEG-Fab_{trast}* construct were also examined in BIAcore. The CM3 chip was immobilised with two ligands and appeared to be functionally active to bind to two analytes. Using this chip and also the chip with the respective single ligands, it was shown that the binding of the heterodimer Fab_{beva}-PEG-Fab_{trast}* to VEGF and HER-2 respectively was preserved.

From angiogenesis assays it can be concluded that the functional activity of the homodimer constructs is preserved, and may even be improved, when compared with the individual Fabs and the parent IgG, where relevant. These findings correlate very well with the bivalent properties and binding affinities associated with the homodimer constructs, as discussed earlier. Also, with respect to the individual homodimer constructs, the length of the PEG used to make the homodimer influenced the functional activity, whereby the 20 kDa PEG in the Fab-PEG-Fab resulted in better inhibition of angiogenesis than 6 kDa Fab-PEG-Fab. As shown in binding affinity studies in part A, the binding affinities of the homodimer Fab-PEG-Fabs were improved as their dissociation rates became slower.

Chapter 5: Conclusions

The main objective of this PhD project was to determine the structure-property correlations of a small family of PEGylated Fab conjugates. A PEGylation approach was used such that the conjugation of the PEG molecule would be far from the binding region of the Fab while conjugation was site-specific. The PEG bis-alkylation reagents **2** and **4** can selectively undergo conjugation with the free thiols from a reduced disulfide bond (Scheme 1.1). In this approach the Fab does not need to be re-engineered to insert free cysteine for conjugation. Many approaches to doing this have been described particularly inserting a free cysteine at the hinge region [38] or in the case of monoclonal antibodies within the Fab. Instead the conjugation using our PEG bis-alkylation reagents occurs at the two thiols derived from the reduction of the interchain disulfide bond. In this way it was hoped a general approach could be developed for the PEGylation of Fabs. We thought it is important that to PEGylate the free thiols from a disulfide, that PEGylation should yield a stable conjugate with both thiols linked to the conjugated PEG. Often disulfides in antibodies are reduced and conjugated with maleimide reagents but these reagents undergo hydrolysis and dePEGylation reactions leading to acidic by products [134]. Critically maleimide based conjugations undergo exchange reactions with other proteins *in-vivo* [134].

The PEG bis-alkylation reagents **2** and **4** are designed to undergo reaction in a sequential manner leading to site-specific reaction with the two thiols derived from a disulfide bond, even in proteins with multiple disulfide bonds that have been reduced [117]. The ability of these reagents to accomplish this type of conjugation relies on the thermodynamic nature of the addition-elimination reactions that occur during conjugation. The fact that both alkylation conjugation reactions occur utilising the same ketone electronic withdrawing group allows there to be an interaction between the bonds being formed. The mechanism for conjugate addition (Figure 1.9) allows for reversibility so that in the presence of multiple reduced disulfides it becomes possible that the thermodynamics of the protein (e.g. hydrophobic effects) are able to help direct the conjugation to thiols that pair up naturally. The PEG mono-sulfone **2** can be used to conjugate one Fab selectively at the thiols of its interchain disulfide while the PEG di(mono-sulfone) **4** is functionalised on each PEG terminus to conjugate two Fabs, one Fab at each end of PEG. The purpose of PEG di(mono-sulfone) **4** is to provide a means to make Fab-PEG-Fab homodimer conjugates (Scheme 1.2). It was hypothesised that it would be possible to make examples of Fab-

PEG-Fab conjugates with different molecular weight PEGs, some of which could display comparable binding properties to the parent IgG.

In the work described here, PEGylation was conducted using Fabs derived from the proteolytic digestion of two clinically used monoclonal antibodies, bevacizumab and trastuzumab. Using PEG reagent **2** to conjugate to the single Fab obtained from these antibodies resulted in a small family of mono PEG-Fab constructs that could be compared to the full parent antibody and its unconjugated Fab. Likewise, dimeric Fab-PEG-Fab conjugates were also prepared for comparative study. As the Fab-PEG-Fab was designed to be an alternative molecule to mimic the bivalent binding of a full IgG, it was necessary to have the full parent IgG available for comparison.

Preliminary work with PEG reagent **4** was also conducted in an effort to prepare a heterodimer, Fab-PEG-Fab*. Since the PEG reagent **4** was predominantly activated as its di(mono-sulfone) form, the risk from hydrolysis after the first conjugation and during purification of the first Fab was always a concern. However we recognised that there is much ongoing work to develop bispecific proteins. Much of this work is based solely on recombinant technologies [174] and we wished to consider chemical fusion as a possible alternative to prepare bispecific molecules. We also wanted to examine if a Fab-PEG-Fab* construct would have dual binding properties and whether the two different antigens could bind simultaneously. A key question was whether the binding properties for each binding Fab could be maintained. Clearly there is a need to optimise our ability to make heterodimeric Fab-PEG-Fab* type molecules, but the preliminary results presented here are encouraging in that binding for each Fab can be maintained.

After sourcing bevacizumab from vials after their use in clinics, the antibody was proteolytically digested with papain. This allowed generation of a clinically relevant Fab that can be considered as a model Fab for VEGF. An early challenge in this work was to both optimise the digestion of bevacizumab and to ensure that Fab binding properties were maintained. Fabs tend to be prone to aggregation [231, 304] and there was some concern that there could be some problems with Fab purification and maintenance of its structural fidelity. We did not unequivocally determine the amount of mis-folded Fab that could have potentially been present. This is an important consideration for the future, but we were able to establish that the digestion

could be accomplished reproducibly and that the binding properties of the Fab could be maintain to an expected level.

To further aid in our effort for comparative study and to help ensure that Fab activity could be maintained, a clinically used Fab (ranibizumab) was also PEGylated and was used for comparison with Fab_{beva}. Since ranibizumab is used only in the eye, its dose is a small volume (50 μL) and each dose is extremely expensive (~£1,000 /dose). So it was necessary to collect many used syringes from clinics at Moorfields Hospital to be able to have enough material for PEGylation. These sourcing challenges could have been much more problematic if the formulations had undergone aggregation or protein degradation.

In the case of bevacizumab, it was eventually possible to purchase a dose of this monoclonal antibody giving us 400 mg of material to work with. By the end of the project we were able to source a good supply of both bevacizumab and ranibizumab. Vials of bevacizumab was donated by Moorfields Pharmaceuticals during a collaboration to evaluate the stability of bevacizumab that been transferred from the vial to a syringe for use in ocular medicine.

Both Fab_{beva} and Fab_{rani} were used to prepare and to evaluate Fab-PEG-Fab conjugates and to determine if there were any structure property correlations with PEG molecular weight. Clearly many different types of PEG could have been used such as multi-arm PEG molecules, but we were most interested in evaluating a bivalent conjugate that could mimic the binding properties of an IgG.

A Fab from a different biological target was also studied. Trastuzumab is a monoclonal antibody that is targeted against HER-2 and is used to treat breast cancer. The proteolytic digestion of trastuzumab with immobilised papain allowed generation of the Fab_{trast} for PEGylation. Unlike bevacizumab, which comes as a solution (25 mg/mL), trastuzumab is obtained as a lyophilised cake that is reconstituted. Upon reconstitution of trastuzumab, the manufacturer stipulates the solution (21 mg/mL trastuzumab) should be used within 28 days [62]. The advantage of VEGF in the BIAcore experiments was that it could be easily sourced and immobilised for binding studies. It is a circulating ligand rather than a cell surface receptor, which made it easier to source. While several antibodies were considered as a second antibody for study in this PhD project, we eventually decided to study trastuzumab because we could purchase HER-2 from a commercial source. One antibody of note that we considered was panitumumab which binds to the HER-1 receptor. We thought we

could also prepare heterodimers using the Fab of this antibody and the Fab from trastuzumab. Unfortunately we were unable to source panitumumab. Study of a heterodimer using trastuzumab and panitumumab would have also faced the challenge for obtaining the two receptors (HER-1 and HER-2) for evaluation. It was a challenge to obtain HER-2, at least compared to the relative ease for obtaining VEGF. Fortunately, research had been described in the literature describing the potential for a VEGF-HER2 based bispecific antibody [183]. Once PEG-Fab_{trast} could be prepared and characterised, Fab_{trast} would then be used to make both the homo- and heterodimers, Fab-PEG-Fab and Fab-PEG-Fab* respectively. The heterodimeric material would be Fab_{beva}-PEG-Fab^*_{trast}.

We were concerned about the differences between trastuzumab and bevacizumab for the proteolytic digestion step. After some experimentation with conditions it was found that trastuzumab could be digested, but a longer time was required to ensure the Fc portion of the antibody could be proteolytically cleaved into smaller peptide fragments. It had appeared that the Fab_{trast} during purification would bind to the protein A column along with the Fc. This made it difficult to purify Fab_{trast} in good yield. This problem had been described in the literature and a relatively large amount of papain was used in the digestion [187] to address this issue of Fab/Fc competitive binding on protein A. The amount of papain used was prohibitively expensive, so we increased the digestion period (with 1.0 mL papain) and were then able to use SEC to isolate Fab_{trast} from the reaction mixture after removal of the immobilised papain. While some Fc still remained in solution, it was possible to sample the peaks from the SEC eluent to obtain some of the purified Fab_{trast}. This effort required careful collection of the fractions that only contained material at about 48 kDa rather than material at above 50 kDa. The fractions were pooled and they displayed a narrow band by SDS-PAGE. This effort while producing Fab_{trast}, resulted in lower yield of approximately 30% compared to the yield obtained for the preparation of Fab_{beva} (70 %). MALDI-TOF mass spectral analysis indicated that the material identified as Fab_{trast} had a molecular mass of 48 kDa. The binding affinity of both of these Fabs was maintained to their respective targets as determined by BIAcore and ELISA.

A K_D value of 6.66 nM was determined for Fab_{beva} by BIAcore analysis at 25 ^{0}C. This was comparable to a reported K_D value of 8.5 nM that was obtained at 37 ^{0}C by BIAcore for a similar VEGF binding Fab that was called Fab-12 [284]. An affinity

value of 2.2 nM was also reported for bevacizumab at 37 ^{0}C [284], whereas a value of 1.33 nM was determined at 25 ^{0}C in this study. Since K_D is the thermodynamic parameters, difference in K_D value in different temperature is expected. Using BIAcore X-100 with BIAevaluation software (version 2.1) it was not possible to change the temperature from 25 ^{0}C.

The binding affinity of Fab_{beva} appeared to be lower than the binding affinity of bevacizumab. This was due to slower association and faster dissociation rate constants observed for Fab_{beva}. These differences between association and dissociation rate constants of Fab_{beva} and bevacizumab were similar to what was reported for Fab-12 and bevacizumab [284, 285]. It is thought that the slower association rate constant for Fab_{beva} was due to its monovalent binding. Bevacizumab is bivalent. Even with the low amount of immobilised VEGF on the chip, since the VEGF has two epitope sites it was expected that the full antibody would display a better binding affinity compared to the Fab. The faster dissociation rate constant for Fab_{beva} further suggested a weaker interaction between the monovalent Fab_{beva} to VEGF compare to that observed for bivalent IgG. While it was not possible to calculate the dissociation rate constant and hence K_D value for Fab_{rani} at 25 ^{0}C, the calculated association rate constant (3.65 x 10^4 $M^{-1}.s^{-1}$) was similar to that reported in literature (5.6 x 10^4 $M^{-1}s^{-1}$) for ranibizumab at 25 ^{0}C [290]. Fab_{rani} also had a slower k_a value than that observed for bevacizumab.

The binding affinity of Fab_{trast} (K_D = 0.13 nM) was similar to binding affinity of trastuzumab (K_D = 0.11 nM) at the low amounts of immobilised HER-2 that used. HER-2 has one epitope site and at the low immobilisation loading where crosslinking would not be expected, the similar affinity values for trastuzumab and its Fab were consistent. The association and dissociation rate constants were both faster in Fab_{trast}. A similar binding affinity between Fab_{trast} and trastuzumab in both ELISA and BIAcore experiments indicated that they both have similar binding affinity towards monomer HER-2. A faster association rate observed in Fab_{trast} suggested that binding tendency between Fab_{trast} and trastuzumab to bind HER-2 were similar, however, Fab_{trast} could diffuse faster from bulk to sensor surface as its smaller than full IgG. A faster dissociation rate constant in Fab_{trast} indicated a weaker interaction between Fab_{trast} and HER-2 compare to full IgG. It was thought that IgG which has flexible hinge region in its structure, is able to bind to antigen in a tighter manner than single Fab.

All three Fabs that were examined (Fab_{beva}, Fab_{trast} and Fab_{rani}) underwent efficient conjugation with PEG mono-sulfone reagent **2**. A single interchain disulfide bond from each of these Fabs was reduced with DTT. An Ellmans assay on the Fab_{beva} after treatment with DTT indicated that there were only 2 free thiols. Small stoichiometries (1-2 eq) of the PEG reagent **2** were then sufficient to give at near quantitative PEGylation conversion to mono the respective PEG-Fabs. A control reaction with the non-DTT treated, and therefore non-reduced Fab_{beva} using 2 equivalents of PEG mono-sulfone **2** did not show any evidence of PEGylation (Figure 3.13). While it is possible that the PEG reagents can undergo hydrolysis and other addition reactions, such as with amino moieties on the protein, it was necessary to determine if the PEG reagent **2** conjugated to the thiols of the Fabs in the conditions that were actually used for PEGylation.

To conduct comparative studies of the PEG-Fab conjugates, different molecular weights of PEG mono-sulfone **2** (20, 30 and 40 kDa) were used to conjugate with Fab_{beva}. Additionally for comparative studies we conjugated two PEG molecules to a Fab′ which was obtained from the $F(ab)_2$ which was obtained from bevacizumab using IdeS as the enzyme for proteolytic digestion. IdeS enzyme was found to be a very efficient enzyme to digest bevacizumab in much shorter time (30 min) with a high yield (86 %) of purified $F(ab)_2$. Since $F(ab)_2$ has 4 interchain disulfide bonds, it was initially hoped that selective reduction could also be conducted of one of interchain disulfides either in the Fab or the hinge regions it would be possible to generate PEG-$F(ab)_2$. While different reducing agents (TCEP, DTT) at different concentrations were examined, no selective reduction between these interchain disulfides could be achieved. It was straightforward to reduce all of these 4 interchain disulfides with DTT and then to conjugate two molecules of PEG mono-sulfone **2** to produce PEG_2-Fab_{beva}′. The PEG_{2x20}-Fab_{beva}′ and PEG_{2x30}-Fab_{beva}′ were prepared. The binding properties between the PEG_{2x20}-Fab_{beva}′ conjugate and mono PEG_{40}-Fab_{beva} conjugate was then compared to investigate how the effect of size, site and number of PEG molecules conjugated to the Fab would influence its binding affinity.

Ion exchange was found to be sufficient to purify the mono PEG-Fab conjugates, PEG_{2x20}-Fab_{beva}′ and PEG_{2x30}-Fab_{beva}′. These purified PEGylated fragments were then evaluated by SDS-PAGE and MALDI-TOF mass spectrometry. A 68 kDa molecular weight was determined for the PEG_{20}-Fab_{beva} using MALDI-

TOF mass spectral analysis. Silver stain detection of the purified PEG-Fab conjugates only showed the presence of the conjugates. There was no impurity from the starting Fab. It was important to ensure the PEGylated products were pure, because if any unPEGylated Fabs were present in the purified PEG-Fab conjugates it would have interfered with the binding studies. The concentrations of the purified PEGylated Fab conjugates were then determined by micro BCA assay and UV spectroscopy (280 nm). It was found that the PEG linker in the PEG-Fab conjugates contributes to the UV absorbance at 280 nm. No interference of the PEG linker is observed when micro BCA is conducted (determined at PolyTherics Ltd). Therefore, concentration of all the PEGylated conjugates were determined by micro BCA assay throughout this PhD. An average yield of about 65% was obtained for the purified, isolated PEG-Fab conjugates. The purified di PEG-Fab_{beva}' conjugate was obtained in about 36% yield.

Since the parent antibodies were being used as controls to compare binding with the PEGylated conjugates, it seemed appropriate to also examine the PEGylation of the antibodies. Since the PEGylation of Fab′ was facile, there was the chance that conjugation at the hinge would not bridge the two heavy chains. While PEGylation at the hinge and at the Fab interchain, we also wanted to PEGylate the antibody to determine how the proteolytic digestion might change. It was expected that the proteolysis rate would decrease, but if the PEGylation were predominantly to occur on the Fab interchain, then digestion would give PEG-Fab directed. It is possible that such an approach would have allowed us to avoid the need to use a protein A column for purification and just use ion exchange chromatography. Likewise if the IdeS enzyme was capable of digesting the PEGylated antibody, this might be a strategy to prepare PEG-$F(ab)_2$.

Several reduction conditions were examined for the partial reduction of bevacizumab and it was found that the interchain disulfide in the Fab region was slightly more susceptible to reduction than the hinge disulfides when reduction was conducted at low conversion. Unfortunately in the experiments that were conducted it was not possible to control the reduction to only one disulfide either at Fab or hinge region when the reductions were conducted at longer incubation times in an effort to achieve a suitable conversion.

Multi isomer PEGylated bevacizumab was therefore produced as a consequence of conjugation of PEG reagent **2** (10 kDa) to the cysteine from the 4 interchain disulfides. No effort was made to identify the positional isomers, but it was

possible to purify what appeared to be mono PEG-bevacizumab from other higher PEGylated isomers. Two purification steps were required and the isolated yield of the PEG-bevacizumab was only about 15%. This material was then incubated with immobilized papain and by SDS-PAGE there appeared to be a mixture of Fab_{beva} and PEG-Fab_{beva}. The mono PEG-bevacizumab was also incubated with the IdeS enzyme. No digestion of the PEG-bevacizumab was observed. More work is required to develop a strategy to prepare PEG-$F(ab)_2$ using our bis-alkylation reagents. Fortunately the homodimer Fab-PEG-Fab conjugates may be a substitute for PEG-$F(ab)_2$ conjugates.

A 3 month stability study was conducted to evaluate the stability of the PEG conjugation and to investigate whether PEGylation was helpful to decrease Fab aggregation. The Fab_{beva} and PEG_{20}-Fab_{beva} were stored at 4 ^{0}C for three month and one sample of PEG-Fab_{beva} was stored for 8 months at 4 ^{0}C. It was found that Fab_{beva} started to aggregate by SDS-PAGE, DLS and SEC. No aggregation was observed for PEG-Fab_{beva} after three months. Some aggregate observed in PEG-Fab_{beva} sample stored for 8 months storage, but importantly no de-PEGylation was observed by SDS-PAGE. Another stability experiment was conducted with PEG_{2x20}-Fab_{beva}' where the conjugated was subjected heat (80 ^{0}C) in the presence of DTT. No de-PEGylation or disulfide reduction were observed for PEG_{2x20}-Fab_{beva}' (Figure 3.28). It was thought that the conjugation of the PEG mono-sulfone **2** to the Fab_{beva} was stable and that the conjugation sites were at the Fab and hinge interchain disulfide bonds.

Once the PEG conjugates were prepared and purified, effort was made to evaluate the binding properties, predominantly by BIAcore. Initial binding experiments focused on the PEGylated conjugates of Fab_{beva} and then moved onto Fab_{rani} and Fab_{trast}. Much effort was made to prepare the immobilised sensor chips with a low loading of the ligand to avoid crosslinking and mass transfer artifacts. Once there was confidence that the BIAcore experiment was reproducible and reflective of the relative binding properties of the molecules being evaluated. It was observed that the binding affinity of PEG-Fab conjugates decreased about two fold compare to the native Fabs. This is much less of a decrease than has been reported in the literature PEGylated Fabs [114].

The BIAcore kinetic assays demonstrated that this decrease in binding affinity of the PEG-Fabs was due to change in association rate constant while the dissociation rate constant remained un-changed from the unPEGylated Fab. The kinetic study of

PEG_{10}-bevacizumab also displayed no change in the dissociation rate constant compared to the unPEGylated antibody (Table 4.2). The association rate constant changes because of the steric shielding of the PEG [114]. The better binding affinity of the PEG-Fabs prepared in this work could be due to the stable 3-carbon bridge conjugation between PEG reagent **2** and the Fab.

The molecular weights of the PEG molecule used to conjugate Fab_{beva} was varied from 20-40 kDa to give the three conjugates: PEG_{20}-Fab_{beva}, PEG_{30}-Fab_{beva} and PEG_{40}-Fab_{beva}. The association rate constant of each of these constructs was very similar (Table 4.2). This observation has been made elsewhere where *in vitro* assay results can be broadly independent of PEG molecular weight when the PEG is conjugated to the same site in the protein [117]. The site of PEG conjugation is important for the level of activity, but as important is that activity or in this case, binding affinity can remain essentially the same at different molecular weights. This allows variations in pK properties to be made while not changing the biological activity, which could be important for optimising dosing. There is some evidence in the literature that activity and clearance rates are inversely related for some proteins [305]. The observation that activity can be maintained independent of PEG molecular weight also suggests that at a given site of conjugation, once the PEG reaches a threshold molecular weight, then its steric shielding effects that influence binding to its target do not continue change. An important parameter to know may be what is the minimum, or threshold, molecular weight of PEG at a given site of conjugation where activity remains independent. It would be interesting to map different sites of conjugation on a protein of interest to determine the threshold molecular weight where activity becomes independent of increasing PEG molecular weight.

Interestingly the conjugation of two PEG molecules to Fab'_{beva} in PEG_{2x20}-Fab'_{beva} construct also did not change the association rate constant from the other PEG-Fab_{beva} constructs. These results allowed us to suggest that the steric sheilding effect of the PEG that influence the association rate constant was not varied by the size of the PEG molecule above 20 kDa. With the Fabs and PEGylation that are described herein, it appears that either one or two PEG molecules independently conjugated did not increase this steric sheilding effect in terms of the association rate constant (Table 4.2).

The affinity value of the PEG_{20}-Fab_{beva}, PEG_{30}-Fab_{beva} and PEG_{40}-Fab_{beva} appeared to be similar, however, better than PEG_{2x20}-Fab'_{beva} as a result of a faster

dissociation rate constant in PEG_{2x20}-Fab'_{beva}. It has been reported [38] that random PEGylation of a Fab′ with larger PEG molecules resulted in a greater loss of binding activity that was observed with smaller PEG molecules. Also it has been suggested that random conjugation of a limited number of the larger PEG cause less loss in binding activity of the PEGylated Fab′ than conjugated with a greater number of shorter PEG molecule [38]. Using one molecule of a longer PEG (40 kDa) probably would be a better approach than conjugation of 2 molecules of 20 kDa PEG reagent **2** since the dissociation rate constant increased with 2 molecules of PEG being conjugated. This could be due to a possible interferance of the second PEG with strength of binding between antibody and ligand.

The conjugates derived from Fab_{beva}, Fab_{rani} and Fab_{trast} and PEG reagent **4** to give the Fab-PEG-Fab constructs were important molecules for study. Activation of the reagent followed by conjugation was potentially going to be burdened by competing hydrolysis, or end capping reactions. Compared to the PEG mono-sulfone **2**, the PEG di(mono sulfone) **4** did display evidence of hydrolysis at its both activated end groups during storage at -20 ^{0}C. It is possible that there were end group associations in reagent **4**.

The PEGylation conversion using PEG di(mono-sulfone) **4** to give the Fab-PEG-Fab homodimers was not as high as the conversions observed with PEG mono-sulfone **2**. The purification of the Fab_{beva}-PEG-Fab_{beva} and Fab_{rani}-PEG-Fab_{rani} homodimers were achieved by ion exchange followed by size exclusion chromatography. The range of yields was 5-22 % for Fab-PEG-Fab homodimers (beva, rani, trast). Silver stain was again used to evaluate the purity of the Fab-PEG-Fab conjugates, and no trace of free Fab or PEG-Fabs were observed. To evaluate the stability of the conjugation link, the purified Fab_{beva}-PEG-Fab_{beva} was treated with excess DTT at ambient temperature and there was no evidence by SDS-PAGE of the formation of a protein band at 25 kDa. This implied that the cysteines of the two Fabs were covalently bound in the homodimer conjugate. This should be compared to what happens to an IgG molecule in these conditions, where all the interchain disulfides are reduced. When another sample of the homodimer (20 kDa PEG) was heated up to 80 ^{0}C in the presence of excess DTT, the conjugate underwent the reverse conjugation reaction as evidenced by the formation of a 25 kDa band in SDS PAGE (Figure 3.60). A second sample of this Fab_{beva}-PEG-Fab_{beva} conjugate was then first subjected to treatment with $NaBH_4$ followed by exposure of excess DTT at 80 ^{0}C. In this case only

the band for the conjugate was observed by SDS-PAGE. Compared to PEG-Fab where no evidence of the reverse conjugation was observed in these harsh conditions, the Fab-PEG-Fab conjugate underwent the reverse conjugation reaction. It is possible that self-association of the two Fabs at the PEG termini in Fab-PEG-Fab cause some degree of conformational stress in the linking moieties that is not present in the PEG-Fab conjugates.

The average size of the Fab-PEG-Fab in the solution was compared with bevacizumab using DLS. An average size of 12.7 nm was measured for the Fab_{beva}-PEG_{20}-Fab_{beva} which was similar to the size of bevacizumab (11.37 nm). The average sizes of 9.0 nm and 21 nm were observed for Fab_{beva} and PEG_{20}-Fab_{beva} respectively. The association of the PEG end groups allowed for the association of the Fab moieties probably help to explain why the homodimer size was 12-13 nm rather than twice the size of PEG-Fab_{beva}. The similarity in size of bevacizumab and Fab_{beva}-PEG_{20}-Fab_{beva} homodimer gave us some hope that the binding properties of these two molecules would be similar.

Using BIAcore and ELISA, the binding affinity of the Fab_{beva}-PEG-Fab_{beva} constructs was evaluated and preserved to VEGF. It was found that binding affinity of the homodimer conjugates became better than the parent Fab and mono PEG-Fab. Using BIAcore, the dissociation rate constant of Fab_{beva}-PEG-Fab_{beva} was found to be slower than both Fab and PEG-Fab indicating that there were stronger interactions of the Fab_{beva}-PEG-Fab_{beva} with the immobilised ligand (Table 4.7). These tighter interactions were thought to be a result of the bivalent character of Fab_{beva}-PEG-Fab_{beva}.

Interestingly, all of the prepared Fab-PEG-Fab constructs such as Fab_{beva}-PEG-Fab_{beva}, Fab_{trast}-PEG-Fab_{trast} and Fab_{rani}-PEG-Fab_{rani} displayed the similar binding affinity as full IgG using ELISA and BIAcore methods. The 6, 10 and 20 kDa Fab_{beva}-PEG-Fab_{beva} conjugates displayed even slower dissociation rate constant than bevacizumab studied in BIAcore. There was also a difference in dissociation rate constant of different molecular weight of PEG in Fab_{beva}-PEG-Fab_{beva}. The Fab_{beva}-PEG_{20}-Fab_{beva} displayed slower dissociation rate constant than Fab_{beva}-PEG_6-Fab_{beva} and Fab_{beva}-PEG_{10}-Fab_{beva}. While BIAcore kinetic assay was conducted once for Fab_{beva}-PEG_{20}-Fab_{beva} and twice for Fab_{beva}-PEG_6-Fab_{beva} and Fab_{beva}-PEG_{10}-Fab_{beva}, the effect of the PEG length on binding activity of the homodimer conjugates was further studied using in-vitro angiogenesis assay.

A co-culture angiogenesis study was then conducted to determine if the binding data correlated with biological activity. While the initial work with HUVECs proliferation assay was performed, using co-culture angiogenesis assay was thought to be more relevant assay to study the anti-angiogenesis properties of the conjugates. This assay was selected because it realistically reflected many of the biological functions of angiogenesis [303], such as proliferation, tubular formation and anastomosing function. The results indicated that the 6 and 20 kDa Fab_{beva}-PEG-Fab_{beva} and Fab_{rani}-PEG-Fab_{rani} inhibited angiogenesis even better than bevacizumab, whereas Fab_{beva}-PEG_{20}-Fab_{beva} and Fab_{rani}-PEG_{20}-Fab_{rani} stopped angiogenesis better than 6 kDa homodimer constructs. In the case of homodimer derived from Fab_{rani}, the angiogenesis was completely stopped when VEGF was incubated with the Fab_{rani}-PEG_{20}-Fab_{rani}. It was expected to observe better functional activity in homodimer made from Fab_{rani} rather than Fab_{beva} as the binding affinity of Fab_{rani} was better than Fab_{beva} [193]. Since the PEG is a random coil, it may be the case that two Fabs are brought towards the homodimer VEGF in a manner that is more efficient than for a native IgG, resulting in a stronger binding interaction and hence enhanced functional activity. Longer PEG in the Fab-PEG-Fab homodimer appeared to display better functional activity than smaller PEG. The effect of length and flexibility of the linker used in homodimer molecules on binding affinity and effective concentration of bivalent molecule have been studied by many researchers [150, 158, 160, 162]. It has been shown that flexible linker with longer length resulted in greater binding affinity and higher effective molarities for bivalent molecule.

To establish an *ex-vivo* experiment to allow study of the binding VEGF with anti-VEGF conjugates in the solution with a much faster readout (less than a day), preliminarily work was conducted to study the anti-vasodilation functional activity of bevacizumab. It was hoped that after optimisation of conditions with bevacizumab, the activity of other anti-VEGF molecules such as Fab-PEG-Fab could be examined in this model and compared with the results obtained from the angiogenesis assay.

Making bispecific antibody fragments has been a focus of research during the last 2-3 decades [168-170]. Different methods have been described in the literature to make dimeric proteins of many different types including bispecific antibodies that able to bind to two different ligands simultaneously. The PEG reagent **4** was used to conjugate two different Fabs and to generate a bispecific Fab-PEG-Fab* construct.

The Fab-PEG-Fab* construct was made from Fab_{beva} and Fab_{trast} since the HER-2 and VEGF signalling pathways are related [182-184]. This bispecific construct was selected because combination therapy involving trastuzumab and bevacizumab has been suggested [177, 182, 180]. While Fab_{beva}-PEG-Fab^*_{trast} was prepared, the amount of purified product was just enough to determine that each Fab maintain its binding to its specific target (i.e. VEGF and HER-2). First conjugation, purification and then second conjugation could be followed by SDS-PAGE (Figure 3.63). A new immobilisation method using the two ligands (HER-2 and VEGF) was developed and used to study of the simultaneous binding of the Fab_{beva}-PEG_{20}-Fab^*_{trast} to HER-2 and VEGF. The chip was immobilised with both ligands at very low RU. Immobilising the chip with two ligands in this way may allow for binding/kinetic studies to evaluate bispecific constructs during preclinical development. In addition, it was thought that using this chip it would be possible to compare the association and dissociation rate constants of Fab_{beva}-PEG-Fab^*_{trast} to the monomeric conjugates, PEG-Fab_{beva} and PEG-Fab_{trast}. This would allow the study of how one Fab may influence the binding of the other, but different Fab*. It would be important to study if similar trends exist for the association and dissociation rate constants as was observed for PEG-Fab_{beva} interacting with chip with VEGF only and a chip with both immobilised VEGF and HER-2 ligands.

While further effort is required to fully understand the conjugation properties of PEG di(mono-sulfone) **4**, this reagent was useful to conjugate two Fabs. It appeared to be a valid way to make Fab-PEG-Fab homodimers that could mimic the binding of a full IgG. It was thought that this was most probably due to binding cooperativity that essentially mimicked the cooperativity of the Fabs in an IgG. The results for the homodimer Fab-PEG-Fab constructs appeared to be better than the full IgG. Since recombinant processes can efficiently produce Fabs, a chemical fusion process to use PEG as a linking molecule as described here could have utility to develop bivalent molecules. In this way other protein scaffolds instead of Fab might be useful.

There are now over 25 monoclonal antibodies in the clinic with many more (240) in development [1]. Clearly it seemed that if homodimers such as Fab-PEG-Fab could be easily prepared and if their binding properties could be maintained, there could be future opportunities to develop chemically fused molecules that have binding properties comparable to monoclonal antibodies.

Overall, utilising thiol specific PEGylation reagents that are capable of bis-alkylation is a viable strategy for the PEGylation of Fabs. Using PEG reagents with the bis-alkylation functionality at each terminus of the PEG so that PEG is used as a scaffold, makes it possible to chemically fuse two proteins to make homo or heterodimeric conjugates. This approach may have potential for the chemical fusion of proteins, which could be an alternative for recombinant strategies for protein fusion.

Appendix I

A; NMR of the activated PEG mono-sulfone reagent **2**.

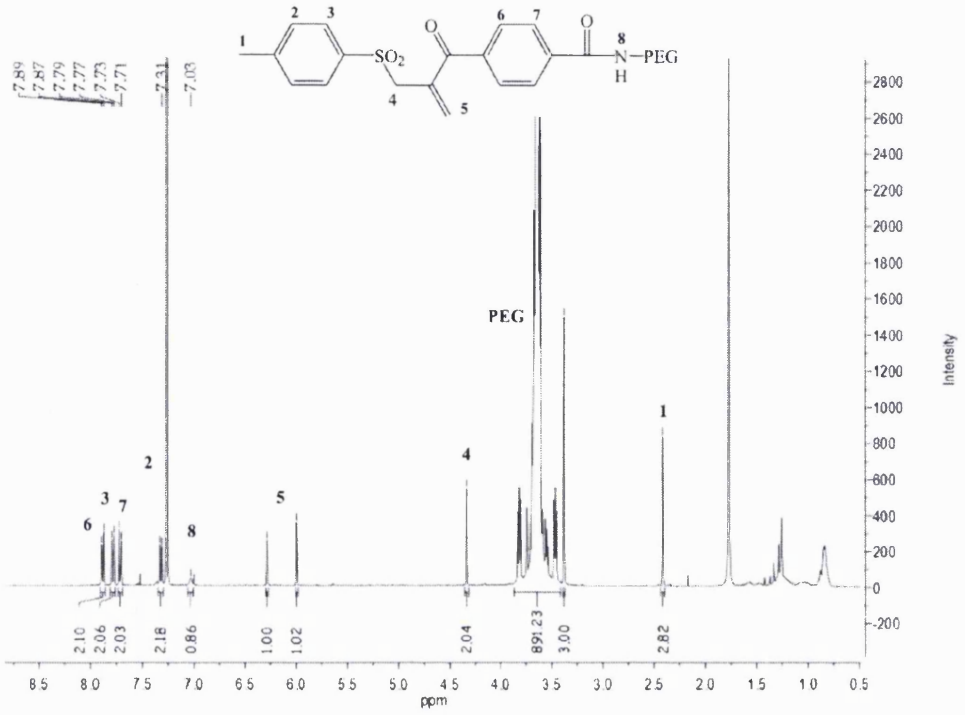

B; NMR of the activated PEG di(mono-sulfone) reagent **4**.

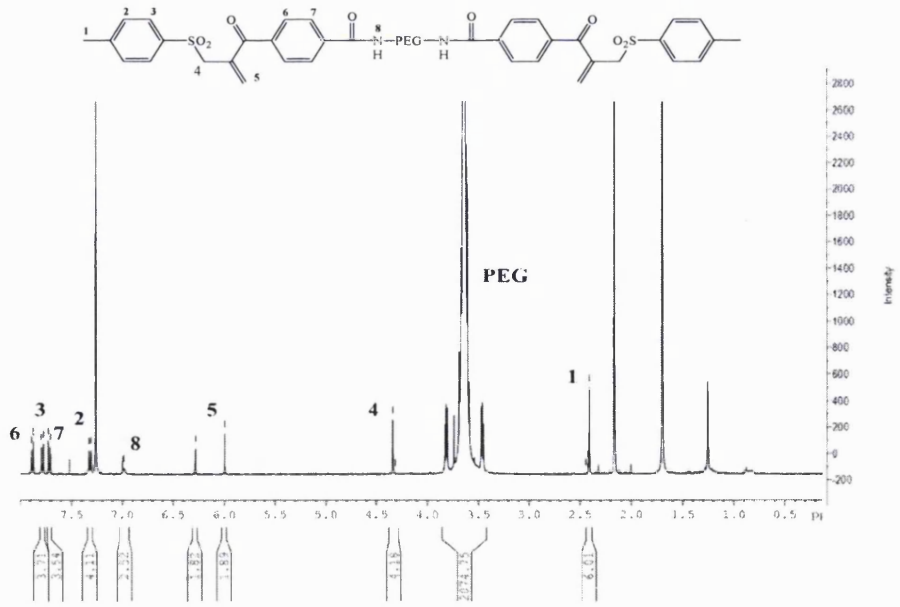

Figure A1.1 NMR of the activated PEG reagent **2 (A)** and **4 (B)**.

Appendix II

Stability study of bevacizumab stored in luer-lock syringes

Ranibizumab (Fab_{rani}) is a FDA approved medicine for treatment of AMD, but it is very expensive, cost of each treatment is 1026 £ in the U.K. [242]. Bevacizumab is used off-lable for AMD with much lower cost, average of 26 £ a dose in the U.K [242]. The most commonly used dose of bevacizumb solution for intravitreal injection is currently 1.25 mg (0.05 mL). Since a very small amount (0.05 mL) of bevacizumab solution needs to be aliquated from the vial for ocular use, it is appropriate to consider if it is possible to transfer the bevacizumab solution from a vial to individual syringes to be stored for future use. This would provide a ready to use syringe filled dosage form of bevacizumab solution for ocular use. Wastage of bevacizumab solution could be avoided if the syringe filled solutions of bevacizumab remain the same as the bevacizumab solution in the vials over an extended storage period. Conditions such as temperature, light and type of syringes can cause instability and aggregation of bevacizumab in the syringe. Pharmaceutical companies have been working on fractionating of bevacizumab into a syringe considering the type of syringe and storage condition.

A collaborative project between Moorfields Pharmaceuticals and our group in the School of Pharmacy was undertaken for a comparative study of the physicochemical characteristics of bevacizumab solution that had been transferred from vials to luer-lock syringes for injection. Two 16 mL vials of bevacizumab solution were fractionated into 1.0 mL syringes. The volume of the bevacizumab solution transferred to each syringe was 0.13 mL, to deliver 0.05 mL for intravitreal injection. The syringe used was a 1.0 mL Becton Dickinson luer-lock syringe, the barrel of which is manufactured from polycarbonate whilst the stopper is a latex free elastomer. The syringe is sealed with a HDPE, latex free cap sourced from B. Braun Medical Inc. The filled syringes were placed on stability storage at $5^{o}C \pm 3^{o}C$, with the temperature being monitored and recorded on a continual basis in Moorfield Pharmaceuticals. The bevacizumab solution in the syringes was then evaluated over a 9-month period at monthly time points in comparison to bevacizumab solution obtained from freshly opened vials. The techniques used were SDS-PAGE, DLS, SEC and BIAcore concentration assay. Samples were evaluated on the day the syringes

were filled (T0) and then at monthly intervals up to 9-months (T1 to T9). Simultaneously, bevacizumab from a freshly opened vial was also evaluated.

SDS-PAGE analysis

SDS-PAGE analysis was conducted by taking the bevacizumab solution from a syringe (1.25 mg/mL, 0.05 mL) and the same volume of bevacizumab solution from the vial (0.05 mL) and adding each to 1.0 mL PBS. Samples were loaded onto a gel and after migration the gels were stained with colloidal blue (Figure A2.1). Three individual samples each from the syringe and the vial were evaluated. Figure A2.1 shows the SDS-PAGE at T0 (A) compared with SDS-PAGE analysis at T9 (D).

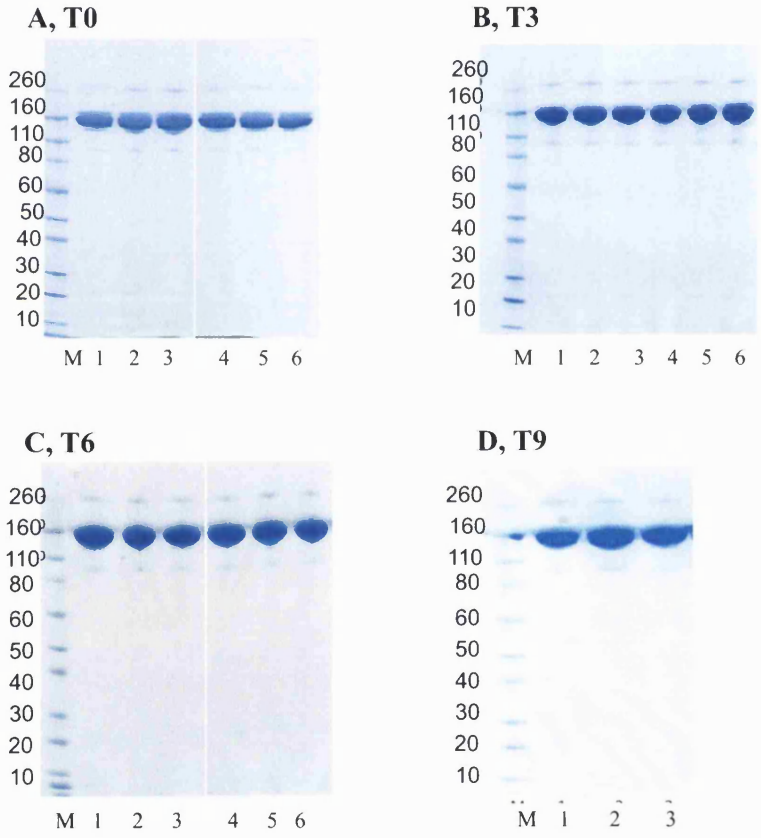

Figure A2.1 SDS-PAGE analysis of bevacizumab solution from both the syringe and vial, at **(A)** T0, **(B)** T3, **(C)** T6, **(D)** T9. Novex Bis-Tris 4-12% gels were stained with colloidal blue. **A, B, C;** *Lane M*: Protein standards. *Lanes 1, 2, 3;* bevacizumab (1.25 mg/ml) from 3 different syringes. *Lanes 4, 5, 6;* bevacizumab (1.25 mg/ml) from a single vial, D; *Lanes 1 and 2*; bevacizumab (1.25 mg/ml) from different syringes, *Lane 3*; bevacizumab (1.25 mg/ml) from vial.

The band at about 150 kDa in each SDS-PAGE gel (Lanes 1-6, Figure A2.1) is bevacizumab and the lighter band at higher molecular weight shows an aggregate, presumably from bevacizumab, but this cannot be ascertained from these experiments. An aggregate was also observed by SEC (Figure A2.2, 58 min). Visually, the amount of this band in the SDS-PAGE gels does not appear to have changed from T0 to T9 for any of the samples.

Size exclusion chromatography (SEC)

For SEC analysis the bevacizumab solution from a freshly open vial (1.25 mg/mL) and the stored syringe samples were transferred to sample vials in an autosampler which then loaded 950 µL of each sample onto a SEC column for separation. SECs were conducted in triplicate for each time point for both syringe and vial samples. Shown in Figure are the SECs for T0 and T9.

The peak at 58 minutes was thought to be from an aggregated species so fractions were also collected from 58-59 min. Analysis of these fractions using SDS-PAGE (Figure A2.3) was accomplished using silver-stain as detection. Silver stain is much more sensitive compared to colloidal blue staining. Fractions were also collected at the main peak (71-72 min; Figure A2.3, Lanes 5-6). The higher molecular weight band was not observed (Figure A2.3, Lanes 5-6) suggesting that this species did not originate from the bevacizumab. Table 1 shows the area under curve (AUC) that was calculated at T0, T3, T6 and T9 for the peak at 58 min. There appeared to be no significant change in the AUC (Table A2.1) of this higher molecular weight species over the 9-month period for the syringe stored samples.

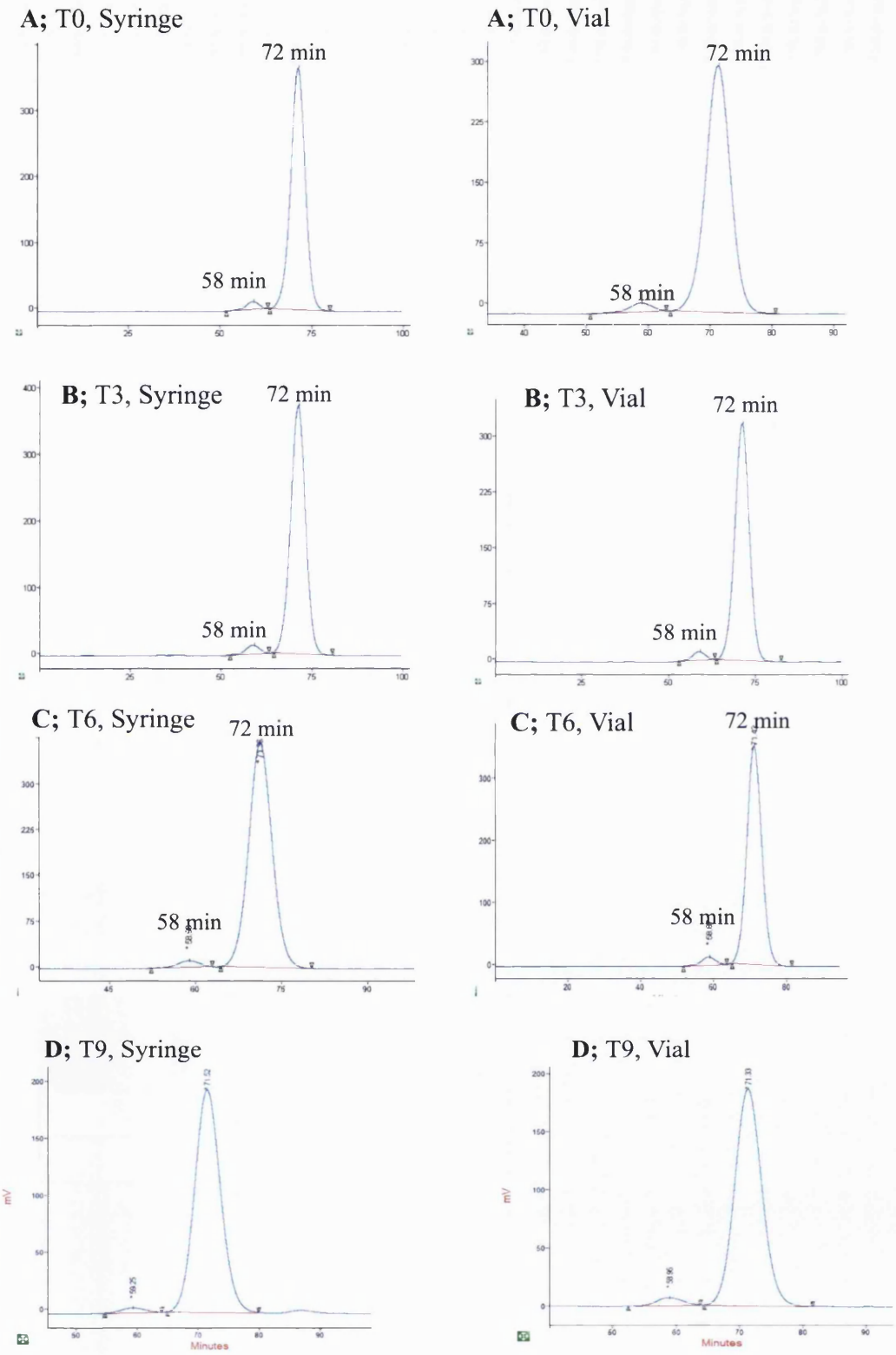

Figure A2.2 SEC chromatograms of bevacizumab solution (1.25 mg/ml) from the syringe and vial at T0 **(A)**, T3 **(B)**, T6 **(C)** and at T9 **(D)**.

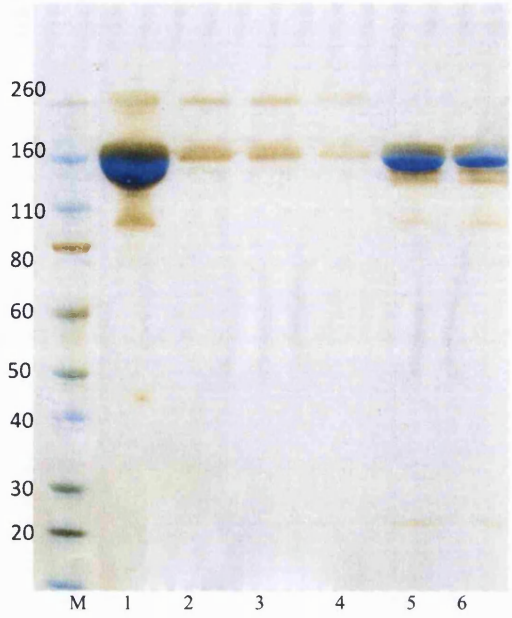

Figure A2.3 SDS PAGE analysis of fractions collected from the SEC of bevacizumab aloquated from a freshly opened vial. Silver stain detection was used. *Lane M:* Protein standard. *Lane 1;* bevacizumab (1.25 mg/ml) before loading to SEC, at T0. *Lane 2;* bevacizumab SEC fraction at 57 min, *Lane 3;* bevacizumab SEC fraction at 58 min, *Lane 4;* bevacizumab SEC fraction at 59 min, *Lane 5;* bevacizumab SEC fraction at 71 min, *Lane 6;* bevacizumab SEC fraction at 72 min.

Table A2.1 Average percentage AUC (100% AUC) at the eluded SEC peak at 58-59 minutes for bevacizumab solution in the syringe and from the vial at T0, T3, T6 and T9.

Bevacizumab 1.25 mg/ml	T0	T3	T6	T9
Syringe	2.84	2.75	2.93	3.00
Vial	3.00	3.05	3.52	3.07

Dynamic light scattering (DLS)

DLS analysis was performed at each time point for the bevacizumab solution (1.25 mg/mL) obtained from a freshly opened vial and from the syringe at each time point (Figure A2.4). Replicates of three (N=3) samples were evaluated; hence 3 separate syringe samples were evaluated at each time point. The DLS analysis suggested that there was no difference of the solution size of the bevacizumab in the syringe and in the vial over the 9-month period (Table A2.2). Figure A2.5 shows an example of the two superpositioned DLS spectra as a representative example of sample reproducibility indicating that there is no evidence of a population of larger species emerging from the syringe samples.

Table A2.2 DLS measurements of bevacizumab at T0, T3, T6 and T9.

Bevacizumab (1.25 mg/ml)	Z-Average size (d.Nm)	PdI
Bevacizumab T0, from syringe	11.16	0.018
Bevacizumab T0, from vial	11.19	0.016
Bevacizumab T3, from syringe	11.37	0.089
Bevacizumab T3, from vial	11.33	0.077
Bevacizumab T6, from syringe	11.57	0.104
Bevacizumab T6, from vial	11.52	0.104
Bevacizumab T9, from syringe	11.86	0.05
Bevacizumab T9, from vial	11.83	0.07

A. T0. Syringe

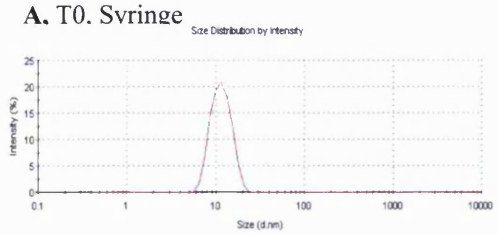

A, T0, Vial

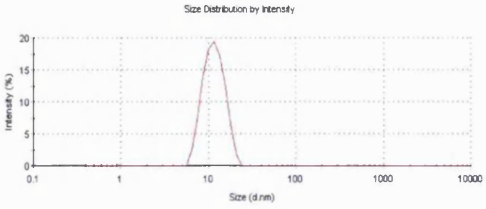

B, T3, Syringe

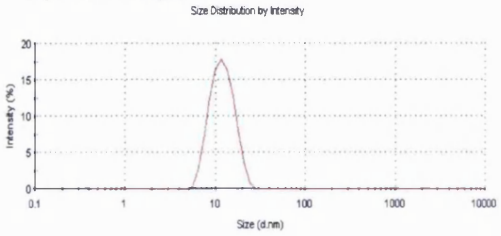

B, T3, Vial

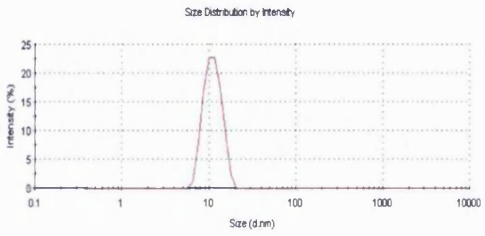

C, T6, Syringe

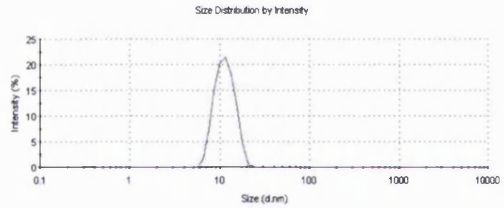

C, T6, Vial

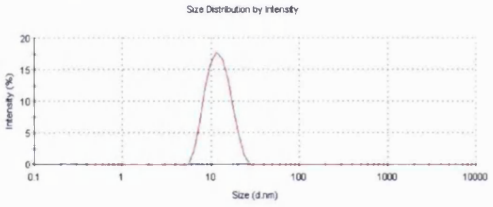

D, T9, Syringe

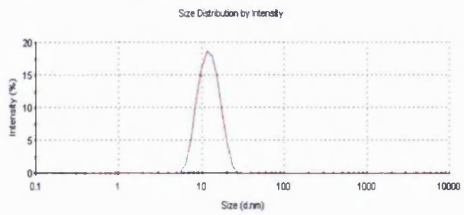

D, T9, Vial

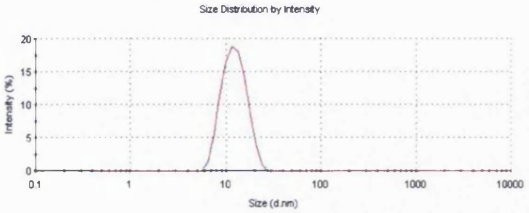

Figure A2.4 DLS analysis of bevacizumab solution in vial and syringe at T0 **(A)**, T3 **(B)**, T6 **(C)** and T9 **(D)**.

A, Superimpose of syringe and vial at T9

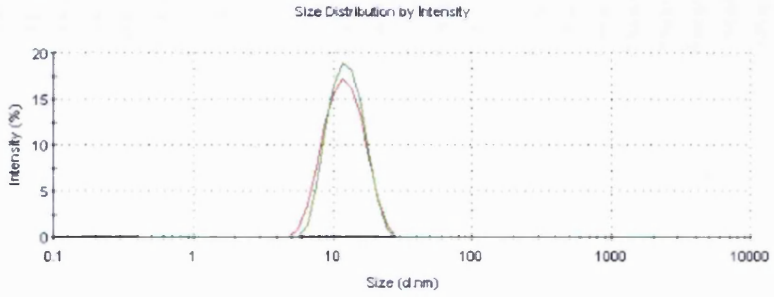

B, Superimpose of syringe at T0 and T9

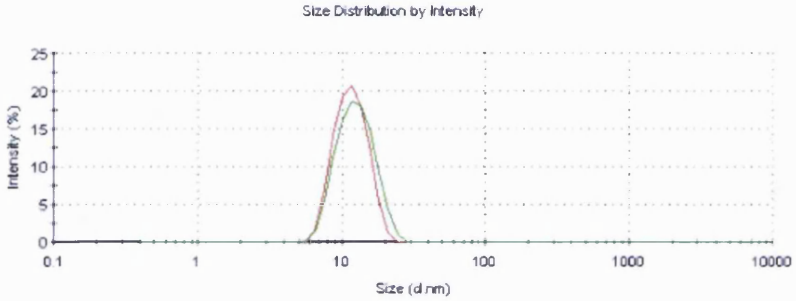

Figure A2.5 Superimposed of DLS of bevacizumab in syringe and vial at T9 **(A)**, and syringe at T0 and T9 **(B)**.

Biacore concentration and binding assay (T0-T6)

A functionalized CM5 with the binding level of 534.0 RU was prepared with VEGF. Chip immobilisation is shown in Figure A2.6. A and the regeneration conditions are in Figure A2.6. B. The manual test run was performed on the prepared chip with bevacizumab (1.25 mg/mL) (Figure A2.6. C) and glycine pH 1.5. Using glycine pH 2.0, it was appeared that baseline could not be regenerated. Glycine pH 1.5 was found to be suitable regeneration buffer when high amount of VEGF was immobilised on CM5 chip.

A; Immobilization of CM5 chip with 534.0 RU.

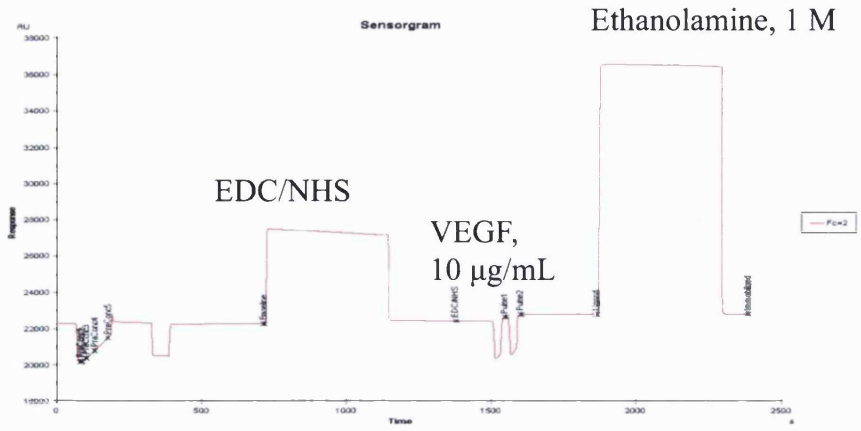

B; Regeneration buffer, Glycine pH 1.5 and 2.0.

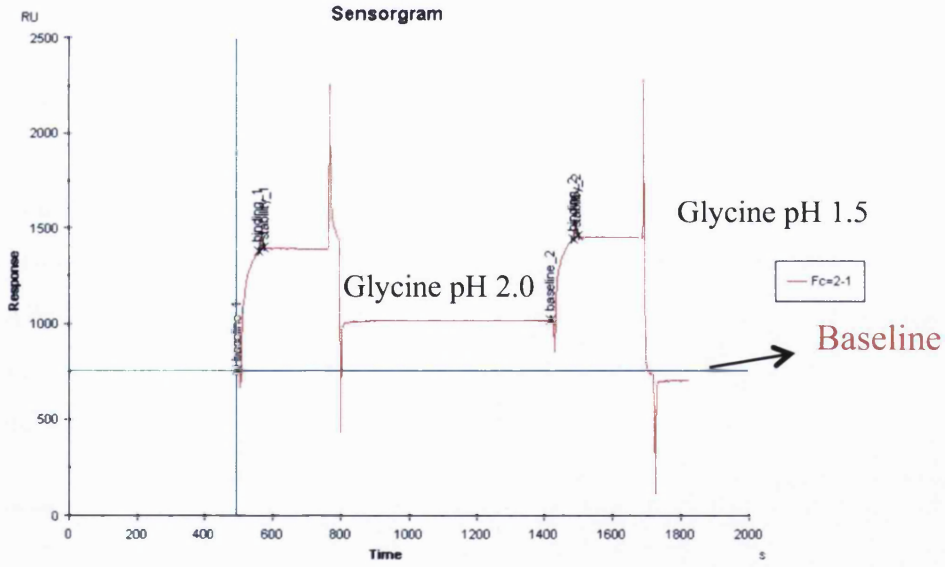

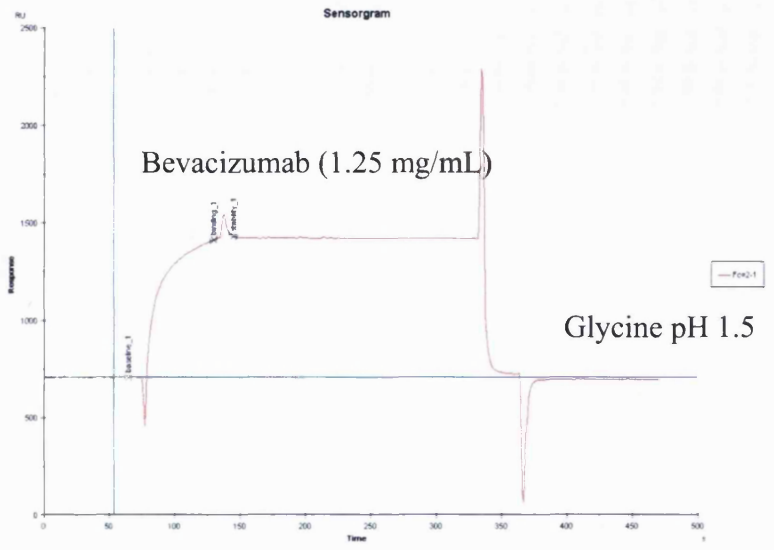

Figure A2.6 Immobilisation of a CM5 chip with VEGF (534 RU) using the Biacore amine coupling method **(A)**, Regeneration buffers with glycine pH 2.0 and 1.5 **(B)**, The manual test run using bevacizuma (1.25 mg/mL) and an optimised regeneration buffer (glycine pH 1.5) **(C)**.

After preparation of the VEGF functionalised chips, a calibration curve for protein concentration was determined using bevacizumab solution obtained from a freshly opened vial (Figure A2.7). Two chips were used at about the same loading of VEGF (534 and 527 RU). Chip 1 (534 RU) was used at T0 and T1 and chip 2 (527 RU) was used for all subsequent time points. The calibration responses (Table A2.3) were then used to calculate the active concentration of bevacizumab in the syringe and vial (Table A2.4). The amount of bevacizumab in the syringe did not change significantly compared to that observed for the vial and no difference was observed at T6 compared with T0.

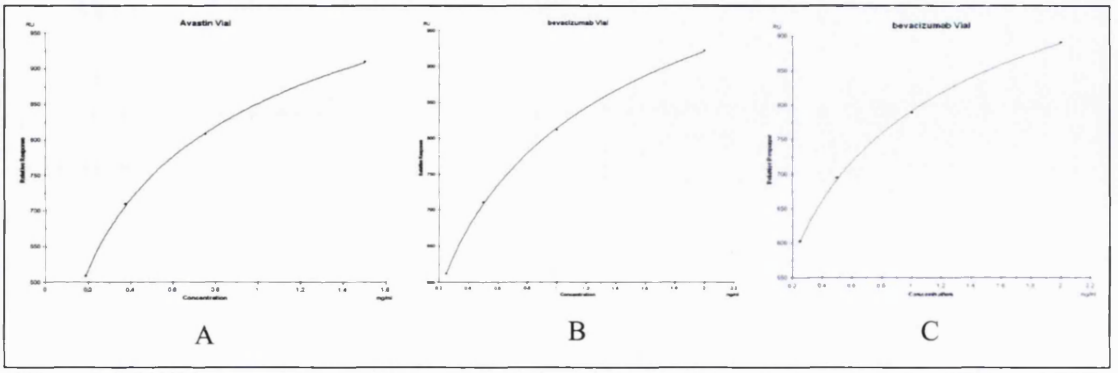

Figure A2.7 Biacore concentration curves using the VEGF functionalised chips (534 and 527 RU). Bevacizumab from a freshly opened vial was used at each time point: **(A)**, T0 (534 RU), **(B)**, T3 (527 RU); and **(C)**, T6 (527 RU).

Table A2.3 Biacore responses with bevacizumab diluted from the solution provided in the vial.

Timepoint	Conc (mg/mL)	Response (RU)	Calc. Conc (mg/mL)
T0 Chip 1 534 RU	0.18	608.4	0.18
	0.37	709.4	0.38
	0.75	807.6	0.74
	1.50	909.4	1.50
T3 Chip 2 527 RU	0.25	611.8	0.25
	0.50	710.6	0.51
	1.00	811.6	0.98
	2.00	922.1	2.02
T6 Chip 2 527 RU	0.25	601.6	0.25
	0.50	694.6	0.51
	1.00	789.0	0.98
	2.00	890.7	2.02

Table A2.4 Biacore calculation of the active protein concentrations bevacizumab obtained from 3 syringes and the vial at T0 and T6.

Time point	Sample Id	Response (RU)	Calc. Conc. (mg/ml)
T0 Chip 1 534 RU	Syringe 1	906.0	1.46
	Syringe 2	895.7	1.37
	Syringe 3	879.3	1.38
	Vial (n=1)	893.9	1.35
	Vial (n=2)	903.0	1.44
	Vial (n=3)	897.3	1.38
T6 Chip 2 527 RU	Syringe 1	829.5	1.30
	Syringe 2	824.7	1.26
	Syringe 3	847	1.47
	Vial (n=1)	818	1.20
	Vial (n=2)	806.1	1.11

A binding assay was performed on bevacizumab (Figure A2.8) that was aliquoted from a freshly opened vial and from the syringe at each time point using the CM5 chips shown in Table A2.3. There did not appear to be any significant difference in the binding response of bevacizumab from the syringe at the different time points compared to the bevacizumab from a freshly opened vial (Figure A2.8). For reference, a superposition is shown in Figure A2.9 of the sensograms for the bevacizumab from both the vial and the syringe (T6).

A; Binding chart at T0.

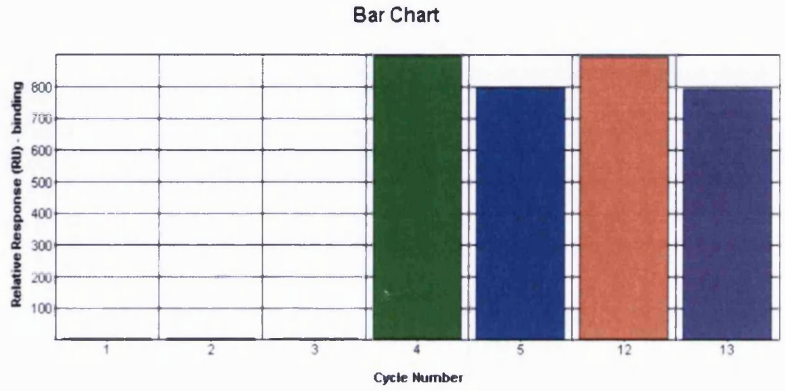

B; Binding chart at T3.

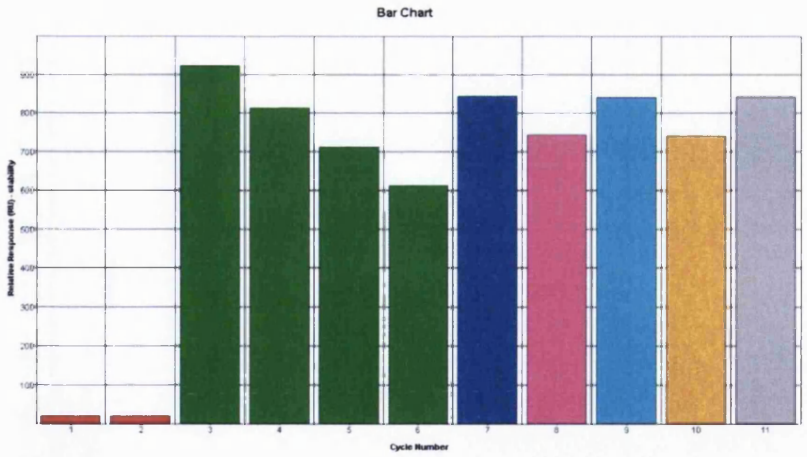

C; Binding chart at T6.

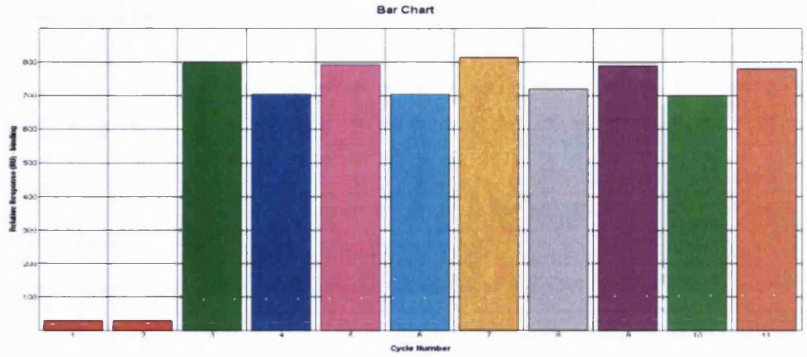

Figure A2.8 The binding chart for bevacizumab in syringe and vial at T0, T3 and T6. **(A)** T0, Cycles 1,2, 3: Buffer (startup), Cycle 4: bevacizumab in the syringe 1.25 mg/mL, Cycle 5: bevacizumab in the syringe 0.625 mg/ml, Cycle 12: bevacizumab from the vial 1.25 mg/ml, Cycle 13: bevacizumab in the vial 0.625 mg/ml, **(B)** T3, Cycles 1, 2: Buffer, Cycles 3-6: calibration concentrations of bevacizumab from vial, Cycle 7: bevacizumab in the syringe 1.25 mg/ml, Cycle 8: bevacizumab in the syringe 0.625 mg/ml, Cycle 9: bevacizumab from the vial 1.25 mg/ml, Cycle 10: bevacizumab from the vial 0.625 mg/ml, Cycle 11: bevacizumab from the vial, **(C)** T6, Cycles 1-2: Buffer, Cycle 3: bevacizumab from the syringe 1.25 mg/ml, Cycle 4: bevacizumab from the syringe 0.625 mg/ml, Cycle 5: bevacizumab from the syringe 1.25 mg/ml, Cycle 6: bevacizumab from the syringe 0.625 mg/ml, Cycle 7: bevacizumab from the syringe 1.25 mg/ml, Cycle 8: bevacizumab from the syringe 0.625 mg/ml, Cycle 9: bevacizumab from the vial, 1.25 mg/ml, Cycle 10: bevacizumab from the vial, 0.625 mg/ml, Cycle 11: bevacizumab from the vial, 1.25 mg/ml.

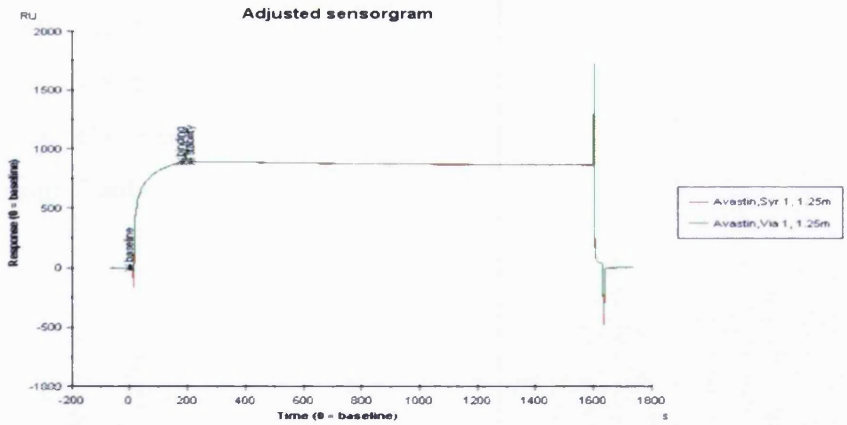

Figure A2.9 Superposition of the sensograms of bevacizumab from the syringe and from the vial (1.25 mg/ml) at T6.

Challenge experiments

A challenge experiment was conducted to determine if a challenge applied to bevacizumab solution could result in observable change. To validate the techniques used in this study, some physical stresses were applied to the bevacizumab solution at 1.25 mg/mL. The stresses applied included heat, UV light and incubation with copper metal (Cu^{+3}).

Bevacizumab solution (1.25 mg/mL) was heated at 74 ^{0}C for 10 min and 1.0 hour. It was also heated for 2.0 h at 62 ^{0}C and left on the bench at ambient temperature overnight. After 1.0 hour at 74 ^{0}C a precipitate was observed (Figure A2.10) in these severe challenge conditions. DSC (differential scanning calorimetry) analysis showed an exothermic peak at 74 ^{0}C (Figure A2.10). This peak was a result of precipitation, which is likely to be a result of denaturation. There was a concentration dependent shift in the precipitation temperature (higher concentration leading to lower precipitation temperature).

No precipitation was observed (62 ^{0}C and RT), but SEC analysis indicated some increase in the %AUC for the peak associated with aggregated species in the bevacizumab formulation (Table A2.5). DLS analysis also indicates an increase in the solution aggregation (Table A2.6). In at least two cases there was not an increase of particle size as determined by DLS, these were when bevacizumab solution was heated for 10 min at 74 ^{0}C and when heated for 120 min at 62 ^{0}C. The increase of particle size after storage overnight at ambient temperature is consistent with the SEC observation (Table A2.5) and suggests that small perturbations can be observed.

A; DSC analysis on bevacizumab

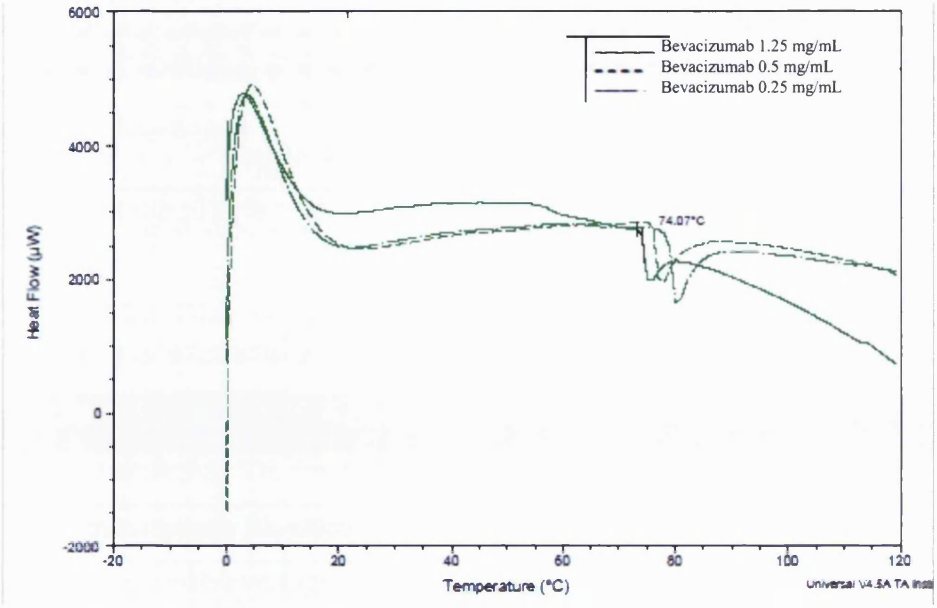

B; Heating of bevacizumab at 74 ^{0}C

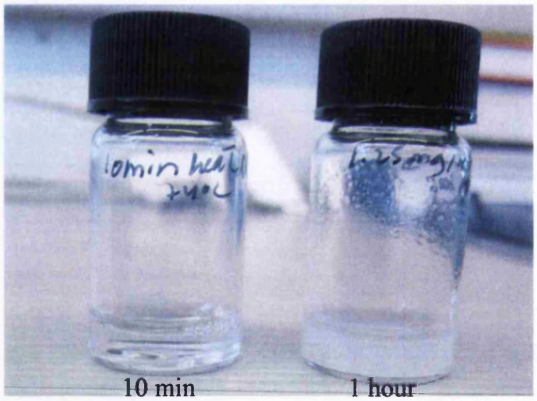

Figure A2.10 (A) Superposition of DSC analysis of bevacizumab at different concentrations, **(B)** A sample of bevacizumab solution aliquoted from the vial precipitated after heating 1.0 h at 74 0C. This admittedly was a severe challenge to the bevacizumab solution, but illustrates the level of challenge necessary to observe a visual indication of loss of protein structure.

Table A2.5 Comparative SEC AUCs of bevacizumab indicating some increase in the AUC for a fresh sample of bevacizumab solution stored at ambient temperature overnight.

Bevacizumab 1.25 mg/ml	Average AUC % 58-59 min; (T6)
Syringe sample	2.93
Vial-fresh sample	3.52
Vial sample after storage overnight at RT	3.80

Table A2.6 DLS measurements of bevacizumab stored in varying conditions to evaluate protein stability.

Bevacizumab (1.25 mg/ml)	Z-Average size (d.Nm)	PdI
Bevacizumab T6, from vial	11.53	0.140
Bevacizumab T1, from vial	11.18	0.053
Bevacizumab overnight at RT	100.5	0.461
Bevacizumab after 10 min at 74 ^{0}C	18.6	0.281
Bevacizumab after 60 min at 74 ^{0}C	5361	0.503
Bevacizumab after 120 min at 62 ^{0}C	13.31	0.181
Bevacizumab treated with 10 µl copper	7956	0.564
Bevacizumab after 2h under UV light	12.21	: 0.196

Based on the analyses conducted, there appears to be no significant change in the physical form of the bevacizumab solution stored in controlled conditions for a 9-month period in the syringes compared to the bevacizumab solution in the vials.

References

1. ElBakri, A. , Nelson, P.N. , and Abu Odeh, R.O. , *The state of antibody therapy.* Hum Immunol, 2010. **71**(12): p. 1243-1250.
2. Beck, A. , Wurch, T. , Bailly, C. , and Corvaia, N. , *Strategies and challenges for the next generation of therapeutic antibodies.* Nature Publishing Group, 2010. **10**(5): p. 345-352.
3. Chan, A.C. and Carter, P.J. , *Therapeutic antibodies for autoimmunity and inflammation.* Nat Rev Immunol, 2010. **10**(5): p. 301-316.
4. Jefferis, R. , *Recombinant antibody therapeutics: the impact of glycosylation on mechanisms of action.* Trends in Pharmacological Sciences, 2009. **30**(7): p. 356-362.
5. Lipman, N.S., Jackson, L.R. , Trudel, L.J., and Weis-Garcia, F. , *Monoclonal versus polyclonal antibodies: distinguishing characteristics, applications and information resources.* ILAR Journal, 2005. **46**(3): p. 258-268.
6. Crommelin, D.J.A. and Sindelar, R.D., eds. *Pharmaceutical Biotechnology* ed. Second. 2002, Taylor & Francis: USA.
7. Kung, P. , Goldstein, G., Reinherz, E.L., and Schlossman, S.F., *Monoclonal antibodies defining distinctive human T cell surface antigens.* Science, 1979. **206**(4416): p. 347-349.
8. Hooks, M.A. , Wade, C.S. , and Millikan, W.J. , *Muromonab CD-3: a review of its pharmacology, pharmacokinetics, and clinical use in transplantation.* Pharmacotherapy, 1991. **11**(1): p. 26-37.
9. Kuus-Reichel, K. , Grauer, L.S. , and Karavodin, L.M. , *Will immunogenecity limit the use, efficacy, and future development of therapeutic monoclonal antibodies ?.* Clin Diag Lab Immunol, 1994. **1**(4): p. 365-372.
10. Anand, B. , Deng, R. , Theil, F.P., Li, J. , Jumbe, S. , Gelzleichter, T. , Fielder, P. , Joshi, A. , and Kenkare-Mitra, S., *Monoclonal Antibodies: From structure to therapeutic application*, in *Pharmaceutical Biotechnology; Fundamentals and Applications*, D.J.A. Crommelin, R.D. Sindelar, and B. Meilbohn, Editors. 2008, informa healthcare: New York. p. 309-363.
11. Khazaeli, M.B. , Conry, R.M. , and LoBuglio, A.F., *Human Immune Response to Monoclonal Antibodies.* Journal of Immunotherapy, 1994. **15**: p. 42-52.
12. Carter, P. , *Improving the efficacy of antibody-based cancer therapies.* Nature review, 2001. **1**(118): p. 1-12.
13. Liu, X.Y., Pop, L.M. , and Vitetta, E. S., *Engineering therapeutic monoclonal antibodies.* Immunological Reviews, 2008. **222**: p. 9-27.
14. Baert, F. , Noman, M. , and Vermiere, S. , *Influence of Immunogenicity on the long-term efficacy of infliximab in Crohn's disease* N Engl I Med, 2003. **348**(7): p. 601-608.
15. Jones, P.T. , Dear, P.H. , Foote, J. , Nueberger, M.S., and Winter, G. , *Replacing the complementarity-determining regions in a human antibody with those from a mouse.* Nature, 1986. **321**: p. 522-525.
16. Filpula, D. , *Antibody engineering and modification technologies.* Biomolecular Engineering, 2007. **24**: p. 201-215.
17. Lobo, E.D. , Hansen, R.J. , and Balthasar, J.P. , *Antibody pharmacokinetics and pharmacodynamics.* J. Pharm. Sci., 2004. **93**(11): p. 2645-2668.

18. Rogers Brambell, F.W. , *The Transmission of Immunity From Mother to Young and The Catabolism of Immunoglobulins.* Lancet, 1966: p. 1088-1093.
19. Wang, W. , Singh, S. , Zeng, D.L., King, K. , and Nema, S. , *Antibody structure, instability, and formulation.* J. Pharm. Sci., 2007. **96**(1): p. 1-26.
20. Jazayeri, J.A. and Carroll, G.J. , *Fc-based cytokines : prospects for engineering superior therapeutics.* Biodrugs, 2008. **22**(1): p. 11-26.
21. Kim, H. , Robinson, S.B. , and Csaky, K.G., *FcRn receptor-mediated pharmacokinetics of therapeutic IgG in the eye.* Mol. Vis., 2009. **15**: p. 2803-2812.
22. Kim, J. , Firan, M. , Radu, C.G. , Hong, C. , Ghetie, K.V. , and Ward, E.S. , *Mapping the site on human IgG for binding of the MHC class I-related receptor, FcRn.* Eur. J. Immunol, 1999: p. 2819-2825.
23. Beck, A. , Bussat, M.C., Zorn, N. , Robillard, V. , Klinguer-Hamour, C. , and Chenu, S. , *Characterization by liquid chromatography combined with mass spectrometry of monoclonal anti-IGF-1 receptor antibodies produced in CHO and NS0 cells.* Journal of Chromatography B, 2005. **819**: p. 203-218.
24. Saphire, E.O. , Stanfield, R.L., Crispin, M. , Parren, P.W.H.I, Rudd, P. M., Dwek, R.A., Burton, D.R., and Wilson, I.A., *Contrasting IgG Structures Reveal Extreme Asymmetry and Flexibility.* Journal of Molecular Biology, 2002. **319**(1): p. 9-18.
25. Zhang, W. and Czupryn, M.J. , *Free Sulfhydryl in Recombinant Monoclonal Antibodies.* Biotechnol Prog, 2002. **18**(3): p. 509-513.
26. Das, S. , Nikolaidis, N. , Klei, J. , and Nei, M. , *Evolutionary redefinition of immunoglobulin light chain isotypes in tetrapods using molecular markers.* PNAS, 2008. **105**(43): p. 16647-16652.
27. Correia, I.R. , *Stability of IgG isotopes in serum.* Mabs, 2010. **2**: p. 221-232.
28. Shields, R.L., *High Resolution Mapping of the Binding Site on Human IgG1 for Fcgamma RI, Fcgamma RII, Fcgamma RIII, and FcRn and Design of IgG1 Variants with Improved Binding to the Fcgamma R.* J Biol Chem, 2000. **276**(9): p. 6591-6604.
29. Idusogie, E.E. , Wong, P.Y. , Presta, L.G. , Gazzano-Santoro, H. , Totpal, K. , Ultsch, M., and Mulkerrin, M.G. , *Engineered Antibodies with Increased Activity to Recruit Complement.* The Journal of Immunology, 2001. **16**: p. 2571-2575.
30. Holliger, P. and Hudson, P.J. , *Engineered antibody fragments and the rise of single domains.* Nat Biotechnol, 2005. **23**(9): p. 1126-1136.
31. Nelson, A.L. and Reichert, J.M. , *Development trends for therapeutic antibody fragments.* Nat Biotechnol, 2009. **27** (4): p. 1-7.
32. Walker, J. M., ed. *The Protein Protocols Handbook.* ed. S. edition. 2002, Humana press.
33. Zhao, Y., Gutshall, L., Jiang, H., Baker, A., Beil, E., G., Obmolva., Carton, J., Taudte, S., and Amegadzie, B., *Two routes for production and purification of Fab fragments in biopharmaceutical discovery research: Papain digestion of mAb and transient expression in mammalian cells.* Protein Expression and Purification, 2009. **67**(2): p. 182-189.
34. Humphreys, D.P., Carrington, B., Bowering, L.C., Ganesh, R., Sehdev, M., Smith, B. J, Reeks, D.G., Lawson, A., and Popplewell, A. G., *A plasmid system for optimization of Fab' production in Escherichia coli: importnace of balance of heavy chain and light chain synthesis.* Protein Expression and Purification, 2002. **26**(2): p. 309-320.

35. Humphreys, D.P. and Glover, D. J., *Therapeutic antibody production technologies: molecules, applications, expression, and purification* Curr. Opin. Drug Disc., 2001. **4**: p. 172-185.
36. Fujimori, K. , Covell, D.G., Fletcher, J.E., and Weinstein, J.N. , *A Modeling Analysis of Monoclonal Antibody Percolation Through Tumors A Binding-Site Barrier.* The Journal of Nuclear Medicine, 1990. **31**(7): p. 1191.
37. Thali, M. , Moore, J., Furman, C. , Charles, M. , Ho, D.D., Robinson, J. , and Sodroski, J. , *Characterization of Conserved Human Immunodeficiency Virus Typel gpl20 Neutralization Epitopes Exposed upon gpl20-CD4 Binding.* Journal of Virology, 1993. **67**(7): p. 3978.
38. Chapman, A.P., *PEGylated antibodies and antibody fragments for improved therapy: a review.* Adv. Drug Del. Rev., 2002. **54**: p. 531-545.
39. Nelson, A.L., *Antibody fragments; Hope and hype.* Mabs, 2010. **2**(1): p. 77-83.
40. Labrijn, A.F. , Aalberse, R.C. , and Schuurman, J. , *When binding is enough: nonactivating antibody formats.* Current Opinion in Immunology, 2008. **20**: p. 479-485.
41. Tracey, D. , Klereskog, L. , Sasso, E.H. , Salfeld, J.G. , and Tak, P.P. , *Tumor necrosis factor antagonist mechanisms of action: A comprehensive review.* Pharmacology and Therapeutics, 2008. **117**: p. 244-279.
42. Smookler, D. S. , Mohammed, F.F. , Kassiri, Z. , Duncan, G.S. , Mak, T.W. , and Khokha, R. , *Cutting Edge: Tissue Inhibitor of Metalloproteinase 3 Regulates TNF-Dependent Systemic Inflammation.* The Journal of Immunology, 2006. **176**: p. 721-725.
43. Shih, T. and Lindley, C. , *Bevacizumab: An Angiogenesis Inhibitor for the Treatment of Solid Malignancies.* Clinical Therapeutics, 2006. **28**(11): p. 1779-1802.
44. Burri, P.H. , Djonov, V. , Hlushchuk, R. , and Djonov, V. , *Intussusceptive angiogenesis: Its emergence, its characteristics, and its significance.* Dev. Dyn., 2004. **231**(3): p. 474-488.
45. Folkman, J. , *Tumor Angiogenesis: Therapeutic Implications.* New England Journal of Medicine, 1971. **285**(21): p. 1182-1186.
46. Fuh, G. , Wei-Ching, P.W. , Mark, L. , Chingwei, U. , Moffat, V.L. , and Wiesmann, C. , *Structure-Function Studies of Two Synthetic Anti-vascular Endothelial Growth Factor Fabs and Comparison with the Avastin Fab.* Journal of Biological Chemistry, 2006. **281**(10): p. 6625-6631.
47. Burri, P.H. and Djonov, V., *Intussusceptive angiogenesis—the alternative to capillary sprouting.* Molecular Aspects of Medicine, 2002. **23**: p. S1–S27.
48. Ferrara, N. , Hillan, K.J., Gerber, H.P., and Novotny, W. , *Discovery and development of bevacizumab, an anti-VEGF antibody for treating cancer.* Nat Rev Drug Discov, 2004. **3**(5): p. 391-400.
49. Penn, J.S. , Madan, A. , Caldwell, R.B. , Bartoli, M. , Caldwell, R.W. , and Hartnett, M.E., *Vascular endothelial growth factor in eye disease.* Progress in Retinal and Eye Research, 2008. **27**: p. 331-371.
50. Prior, B.M. , Yamg, H.T. , and Terjung, R.L., *What makes vessels grow with exercise training?* Journal of Applied Physiology, 2004. **97**(3): p. 1119-1128.
51. Terman, B.I. , Vermazen, M. , Carrion, M.E., Dimitrov, D. , Armellino, D.C. , Gospodarowiczs, D. , and Ghlen, P.B. , *Identification of the KDR tyrosine kinase as a receptor for vascular endothelial cell growth factor.* Biochemical and Biophysical Research Communications, 1992. **187**(3): p. 1579-1586.

52. Liu, M.H. , Jin, H. , Floten, H.S., Ren, Z., Yim, A.P.C. , and He, G.W. , *Vascular Endothelial Growth Factor-Mediated, Endothelium-Dependent Relaxation in Human Internal Mammary Artery.* The Society of Thoracic Surgeons, 2002. **73**(3): p. T819-24.
53. Yang, R. , Ogasawara, A.K. , Zioncheck, T.F., Ren, Z., He, G.W. , DeGuzman, G.G. , Pelletier, N., Shen, B.Q., Bunting, S., and Jin, H., *Exaggerated Hypotensive Effect of Vascular Endothelial Growth Factor in Spontaneously Hypertensive Rats.* Hypertension, 2002: p. 815-820.
54. EMEA, *Avastin 'SCIENTIFIC DISCUSSION'.* http://www.ema.europa.eu/docs/en_GB/document_library/EPAR_-_Scientific_Discussion/human/000715/WC500043550.pdf, . 2005: p. 1-61.
55. Rugo, H. S., *Bevacizumab in the treatment of breast cancer: Rationale and Current data.* The Oncologist, 2004. **9**: p. 43-49.
56. Bakri, S.J. , Snyder, M.R., Reid, J.M., Pulido, J.S., and Singh, R.J., *Pharmacokinetics of Intravitreal Bevacizumab (Avastin).* Ophthalmology, 2007. **114**(5): p. 855-859.
57. Grisanti, S. , *The role of vascular endothelial growth factor and other endogenous interplayers in age-related macular degeneration.* Progress in Retinal and Eye Research, 2008: p. 1-19.
58. EMEA., *Lucentis 'SCIENTIFIC DISCUSSION'.* http://www.ema.europa.eu/docs/en_GB/document_library/EPAR_-_Scientific_Discussion/human/000715/WC500043550.pdf, 2007.
59. Colombo, M. , Corsi, F. , Foschi, D. , Mazzantini, E. , Mazzucchelli, S. , Morasso, C. , Occhipinti, E. , Polito, L., Prosperi, D. , Ronchi, S. , and Verderio, P. , *HER2 targeting as a two-sided strategy for breast cancer diagnosis and treatment: Outlook and recent implications in nanomedical approaches.* Pharmacological Research, 2010. **62**(2): p. 150-165.
60. Cho, H.S. , Mason, K. , Ramyar, K.X. , Stanley, A.M., Gabelli, S.B. , Denney Jr, D.W. , and Leahy, D. J. , *Structure of the extracellular region of HER2 alone and in complex with the Herceptin Fab.* Nature, 2003. **421**(6924): p. 753-756.
61. Molina, M.A. , Codony-Servat, J. , and Albanell, J. , *Trastuzumab (Herceptin), a Humanized Anti-HER2 Receptor Monoclonal Antibody, Inhibits Basal and Activated HER2 Ectodomain Cleavage in Breast Cancer Cells.* Cancer Res, 2001. **61**: p. 4744-4749.
62. Herceptin package label, *Herceptin package label,*.
63. Lofgren, J.A. , Dhandapani, S. , Pennucci, J J. , Abbott, C.M. , Swanson, S.J. , and Mullenix, M.C., *Comparing ELISA and Surface Plasmon Resonance for Assessing Clinical Immunogenicity of Panitumumab.* J Immunol, 2007. **178**: p. 7467-7472.
64. Pollaro, L. and Heinis, C. , *Strategies to prolong the plasma residence time of peptide drugs.* MedChemComm, 2010. **1**(5): p. 319.
65. Andersen, J.T. , Terje, J. , and Sandlie, I. , *The Versatile MHC Class I-related FcRn Protects IgG and Albumin from Degradation: Implications for Development of New Diagnostics and Therapeutics.* Drug Metabol. Pharmacokinetics, 2009. **24**(4): p. 318-332.
66. Dennis, M.S., Zhang, M., Meng, Y. , Kadkhodayan, M. , Kirchhofer, D. , Combs, D., and Damico, LA *Albumin binding as a general strategy for improving the pharmacokinetics of proteins.* J. Biol. Chem., 2002. **277**(38): p. 35035-35043.

67. Halpern, W. , Riccobene, T.A. , Agostini, H. , Baker, K. , Stolow, D.D. , Gu, M.L. , Hirsch, J. , Mahoney, A. , Carrell, J. , and Boyd, E. , *Albugranin TM, a Recombinant Human Granulocyte Colony Stimulating Factor (G-CSF) Genetically Fused to Recombinant Human Albumin Induces Prolonged Myelopoietic Effects in Mice and Monkeys.* Pharm. Res., 2002. **19**(11): p. 1720-1729.
68. Otagiri, M. and Chuang, V.T.G., *Pharmaceutically Important Pre-and Posttranslational Modifications on Human Serum Albumin.* Bio. Pharm. Bull., 2009. **32**(4): p. 527-534.
69. Stork, R. , Campigna, E. , Robert, B. , Muller, D. , and Kontermann, R.E., *Biodistribution of a Bispecific Single-chain Diabody and Its Half-life Extended Derivatives.* J. Biol. Chem., 2009. **284**(38): p. 25612-25619.
70. Subramanian, G.M. , Fiscella, M. , Lamousé-Smith, A. , Zeuzem, S. , and Mchutchison, J.G., *Albinterferon α-2b: a genetic fusion protein for the treatment of chronic hepatitis C.* Nat Biotechnol, 2007. **25**(12): p. 1411-1419.
71. Sung, C. , Nardelli, B. , LaFleur, D.W. , Blatter, E., Corcoran, M., Olsen, H.S. , Birse, C.E. , Pickeral, O.K. , Zhang, J., and Shah, D., *An IFN-β-albumin fusion protein that displays improved pharmacokinetic and pharmacodynamic properties in nonhuman primates.* J. Interferon Cytokine Res., 2003. **23**(1): p. 25-36.
72. Trussel, S. , Dumelin, C. , Frey, K. , Villa, A. , Buller, F. , and Neri, D. , *New Strategy for the Extension of the Serum Half-Life of Antibody Fragments.* Bioconjugate Chem., 2009. **20**: p. 2286-2292.
73. Bailon, P. and Won, C. , *PEG-modified biopharmaceuticals.* Expert Opin. Drug Deliv., 2009. **6**(1): p. 1-16.
74. Hamidi, M. , Rafiei, P. , and Azadi, A. , *Designing PEGylated therapeutic molecules: advantages in ADMET properties.* Expert Opin. Drug Discov., 2008. **3**(11): p. 1293-1307.
75. Jevsevar, S. , Kunstelj, M. , and Porekar, V.G. , *PEGylation of therapeutic proteins.* Biotechnol. J., 2010. **5**(1): p. 113-128.
76. Kang, J.S. , DeLuca, P.P., and Lee, K.C., *Emerging PEGylated drugs.* Expert Opin. Emerg. Drugs, 2009. **14**(2): p. 363-380.
77. Payne, R.W., Murphy, B.M. , and Manning, M.C. , *Product development issues for PEGylated proteins.* Pharmaceutical Development and Technology, 2010: p. 1-18.
78. Pisal, D.S. , Kosloski, M.P. , and Balu-Iyer, S.V. , *Delivery of therapeutic proteins.* J. Pharm. Sci., 2010. **99**(6): p. 2557-2575.
79. Veronese, F. , *Peptide and protein PEGylation a review of problems and solutions.* Biomaterials, 2001. **22**(5): p. 405-417.
80. Elliott, S. , Lorenzini, T., Asher, S. , Aoki, K. , Brankow, D. , Buck, L. , Busse, L. , Chang, D. , Fuller, J. , and Grant, J. , *Enhancement of therapeutic protein in vivo activities through glycoengineering.* Nat Biotechnol, 2003. **21**(4): p. 414-421.
81. Marshall, S.A. , Lazar, G.A., Chirino, A.J. , and Desjarlais, J. R., *Rational design and engineering of therapeutic proteins.* Drug Discov. Today, 2003. **8**(5): p. 212-221.
82. Sola, R.J. and Grievenow, K. , *Glycosylation of therapeutic proteins an effective strategy to optimize efficacy.* Biodrugs, 2010. **24**(1): p. 9-21.
83. Huang, C. , *Receptor-Fc fusion therapeutics, traps, and MIMETIBODY technology.* Current Opinion in Biotechnology, 2009. **20**: p. 692-699.

84. Nguyen, A. , Reyes, A.E. , Z.hang, M. , McDonald, P. , Wong, W.L.T. , Damico, L.A. , and Dennis, M.S., *The pharmacokinetics of an albumin-binding Fab (AB.Fab) can be modulated as a function of affinity for albumin.* Protein Eng. Des. Sel., 2006. **19**(7): p. 291-297.
85. Mueller, D. , Karle, A. , Meissburger, B. , Hoefig, I. , Stork, R. , and Kontermann, R.E. , *Improved pharmacokinetics of recombinant bispecific antibody molecules by fusion to human serum albumin.* J Biol Chem, 2007. **282**(17): p. 12650-12660.
86. Schellenberger, V. , Wang, C.W. , Geething, N.C. , Spink, B.J. , Campbell, A. , To, W. , Scholle, M.D. , Yin, Y., Yao, Y., Bogin, O., Cleland, J.L., Silverman, J., and Stemmer, W.P.C., *A recombinant polypeptide extends the in vivo half-life of peptides and proteins in a tunable manner.* Nature biotechnology, 2009: p. 1-7.
87. Schlapschy, M. , Theobald, I. , Mack, H. , Schottelius, M. , Wester, H.J. , and Skerra, A. , *Fusion of a recombinant antibody fragment with a homo-amino-acid polymer: effects on biophysical properties and prolonged plasma half-life.* Protein Engineering Design and Selection, 2007. **20**(6): p. 273.
88. Davis, F.F. , *The orgin of pegnology.* Adv. Drug Del. Rev., 2002. **54**: p. 457-458.
89. Abuchowski, A. , Es, T. , Palczuk, N.C. , and Davis, F.F. , *Alteration of immunlogical properties of bovine serum albumin by covalent attachment of polyethylene glycol.* J. Biol. Chem., 1977. **252**(11): p. 3578-3581.
90. Gauthier, M. and Klok, H. , *Peptide/protein-polymer conjugates:synthetic strategies and design concepts.* Chem. Comm., 2008: p. 2591-2611.
91. Greenwald, R.B. , Choe, Y.H. , McGuire, J. , and Conover, C.D., *Effective drug delivery by PEGylated drug conjugates.* Adv. Drug Del. Rev., 2003. **55**: p. 217-250.
92. Harris, J.M. and Chess, R.B. , *Effect of Pegylation on pharmaceuticals.* Nat. Rev. Drug Dis., 2003. **2**(3): p. 214-221.
93. Heredia, K.L. and Maynard, M.H.D. , *Synthesis of protein-polymer conjugates.* Org. Biomol. Chem., 2007. **5**(1): p. 45-53.
94. Kochendoerfer, G.G. , *Site-specific polymer modification of therapeutic proteins.* Curr. Opin. Chem. Biol., 2005. **9**: p. 555-560.
95. Pasut, G. , Guiotto, A. , and Veronese, F.M., *Protein, peptide and non-peptide drug PEGylation for therapeutic application.* Expert Opin. Ther. Pat., 2004. **14**(5): p. 1-36.
96. Lutz, J.F. and Borner, H.G. , *Modern trends in polymer bioconjugates design.* Prog. Polym. Sci., 2008. **33**: p. 1-39.
97. Zalipsky, S. , *Chemistry of poly(ethylene glycol) conjugates with biologically active molecules.* Adv. Drug Del. Rev., 1995. **16**: p. 157-182.
98. Caliceti, P. and Veronese, F. , *Pharmacokinetic and biodistribution properties of poly (ethylene glycol)–protein conjugates.* Adv Drug Deliv Rev, 2003. **55**(10): p. 1261-1277.
99. Webster, R., Didier, E. , Harris, P. , Siegel, N. , Stadler, J., Tilbury, L., and Smith, D., *PEGylated proteins:evaluation of their safety in the absence of definitive metabolism studies.* Durg Metabol. Dispos., 2007. **35**(1): p. 9-16.
100. Fuertges, F. and Abuchowski, A., *The clinical efficacy of poly(ethylene glycol) modified proteins.* J. Cont. Rel, 1990. **11**: p. 139-148.
101. Fried, M.W., Shiffman, M.L. , Reddy, K.R. , Smith, C. , Marinos, G. , Goncales, F.L. , Haussinger, D. , Diago, M. , Carosi, G. , Dhumeaux, D. ,

Craxi, A. , Lin, A. , Hoffman, J. , and Yu, J., *Peginterferon alfa-2a plus ribavirin for chronic hepatitis C virus infection.* N. Engl. J. Med., 2002. **34**: p. 975-982.
102. Sherman, M.R. , Saifer, M.G.P., and Ruiz, F.P., *PEG-uricase in the management of treatment-resistant gout and hyperuricemia.* . Adv. Drug Del. Rev., 2008. **60**: p. 59-68.
103. Birerdinc, A. and Younossi, Z.M., *Emerging therapies for hepatitis C virus.* Expert Opin. Emerg. Drugs, 2010(0): p. 1-10.
104. Foster, G.R. , *Pegylated Interferons for the Treatment of Chronic Hepatitis C: Pharmacological and Clinical Differences between Peginterferon--2a and Peginterferon--2b.* Drugs, 2010. **70**(2): p. 147-165.
105. Munir, S. , Saleem, S. , Idrees, M. , Tariq, A. , Butt, S. , Rauff, B., Hussain, A., Badar, S., Naudhani, M., Fatima, Z., Ali, M., Ali, L., Akram, M., Aftab, M., Khubaib, B., and Awan, Z., *Hepatitis C Treatment: current and future perspectives.* Virology Journal, 2010. **7**(1): p. 296-301.
106. Petta, S. and Craxì, A. , *Optimal therapy in hepatitis C virus genotypes 2 and 3 patients.* Liver International, 2011. **31**: p. 36-44.
107. Vezali, E. , Aghemo, A. , and Colombo, M. , *Interferon in the treatment of chronic hepatitis C: a drug caught between past and future.* Expert Opin. on Biol.Thera., 2011(0): p. 1-13.
108. Young, M.A. , Malavalli, A., Winslow, N., Candegriff, K.D. , and Winslow, R.M., *Toxicity and hemodynamic effects after single dose administration of MalPEG-hemoglobin (MP4) in rhesus monkeys.* Translational Res., 2007. **149**(6): p. 333-342.
109. Parkinson, C. , Scarlett, J.A. , and Trainer, P.J. , *Pegvisomant in the treatment of acromegaly.* Adv. Drug Del. Rev., 2003. **2003**: p. 1303-1314.
110. Yin, D. , Vreeland, F. , Schaaf, L.J. , Millham, R. , Duncan, B.A. , and Sharma, A., *Clinical pharmacodynamic effects of the growth hormone receptor antagonish Pegvisomant: implications for cancer therapy.* . Clin. Cancer Res., 2007. **13**(3): p. 1000-1009.
111. Sandborn, W.J. , Feagan, B.G. , Stoinov, S. , Honiball, P.J. , Rutgeerts, P. , Mason, D. , Bloomfield, R. , and Schreiber, S. , *Certolizumab Pegol for the treatment of Crohn's disease.* N. Engl. J. Med., 2007. **357**(3): p. 228-238.
112. Fishburn, C.S. , *The pharmacology of PEGylation: Balancing PD with PK to generate novel therapeutics.* J. Pharm. Sci., 2008. **97**(10): p. 4167-4183.
113. Talal, A. and al., et, *Pharmacodynamics of PEG-IFN alpha differentiate HIV/HCV coinfected sustained virological responders from nonresponders.* Hepatology, 2006. **43**: p. 943-953.
114. Kubetzko, S. , Sarkar, C.A., and Plückthun, A. , *Protein PEGylation decreases observed target association rates via a dual blocking mechanism.* Molecular Pharmacology, 2005. **68**(5): p. 1439-1454.
115. Fee, C., *Size comparison between protein PEGylation with branched and linear poly(ethylene glycol) molecules.* Biotechnol. Bioeng., 2007. **98**(4): p. 725-731.
116. Veronese, F.M. , ed. *PEGylated Protein Drugs: Basic Science and Clinical Applications.* Milestones in Drug Therapy, ed. M.J. Parnham and J. Bruinvels. 2009, Birkhauser: Basel.
117. Brocchini, S. , Godwin, A. , Balan, S., Choi, J.W., Zloh, M., and Shaunak, S., *Disulfide bridge based PEGylation of proteins.* Advanced Drug Delivery Reviews, 2007: p. 1-10.

118. Veronese, F.M. and Pasut, G., *PEGylation, successful approach to drug delivery.* Drug Discov. Today, 2005. **10**(21): p. 1451-1458.
119. Rosendahl, M.S. , Doherty, D.H., Smith, S.J., Carlson, S.J., Chlipala, E.A., and Cox, G.N. , *A long-acting, highly potent interferon a-2 conjugate created using site-specific PEGylation.* Bioconjugate Chem., 2005. **16**: p. 200-207.
120. Roberts, M.J. , Bentley, M.D. , and Harris, J. M. , *Chemistry for peptide and protein PEGylation.* Adv. Drug Del. Rev., 2002. **54**: p. 459-476.
121. Doherty, D.H. , Rosendahl, M.S., Smith, D.J., Hughes, J.M., Chlipala, E.A. , and Cox, G.N. , *Site-specific PEGylation of engineered cysteine analogues of recombinant human granulocyte-macrophage colony-stimulating factor.* Bioconjugate Chem., 2005. **16**(5): p. 1291-1298.
122. Mei, B. , Pan, C. , Jiang, H. , Tjandra, H. , Strauss, J. , Chen, Y. , Liu, T. , Zhang, X., Severs, J. , Newgren, J., Chen, J., Gu, J.M., Subramanyam, B., Fournel, M.A., Pierce, G.F., and Murphy, J.E., *Rational design of a fully active, long-acting PEGylated factor VIII for hemophilia A treatment.* Blood, 2010. **116**(2): p. 270-279.
123. Yang, K. , Basu, A. , Wang, M. , Chintala, R. , Hsieh, M. , Liu, S., Hua, J., Zhang, Z., Zhou, J., Li, M., Phyu, H., Petti, G., Mendez, M., Janjua, H., Peng, P., Longley, C., Borowski, V., Mehlig, M., and Filpula, D., *Tailoring structure-function and pharmacokinetic properties of single-chain Fv proteins by site-specific PEGylation.* Protein Eng., 2003. **16**(10): p. 761-770.
124. Schumacher, F.F. , Nobles, M. , Ryan, C.P., Smith, M.E.B. , Tinker, A. , Caddick, S. , and Baker, J.R. , *In Situ Maleimide Bridging of Disulfides and a New Approach to Protein PEGylation.* Bioconjugate Chem, 2011: p. 1-5.
125. Pfisterer, A. , Eisele, K. , Chen, X. , Wagner, M. , Müllen, K. , and Weil, T. , *Bioactive Unnatural Somatostatin Analogues through Bioorthogonal Iodo and EthynylDisulfide Intercalators.* Chem. Eur. J, 2011. **17**: p. 9697-9707.
126. Gauthier, M.A. and Klok, H.A., *Arginine-Specific Modification of Proteins with Polyethylene Glycol.* Biomacromolecules, 2010. **12**: p. 482-493.
127. Maullu, C. , Raimondo, D. , Caboi, F. , Giorgetti, A. , Sergi, M. , Valentini, M. , Tonon, G. , and Tramontano, A. , *Site-directed enzymatic PEGylation of the human granulocyte colony-stimulating factor.* FEBS Journal, 2009. **276**(22): p. 6741-6750.
128. Rabuka, D. , *Chemoenzymatic methods for site-specific protein modification.* Curr. Opin. Chem. Biol., 2010. **14**: p. 790-796.
129. Sato, H. , *Enzymatic procedure for site-specific pegylation of proteins.* Adv. Drug Del. Rev., 2002. **54**: p. 487-504.
130. Defrees, S. , Wang, Z.G. , Xing, R. , Scott, A.E. , Wang, J., Zopf, D., Gouty, D.L., Sjoberg, E.R., Panneerselvam, K., and Brinkman-Van der Linden, E., *GlycoPEGylation of recombinant therapeutic proteins produced in Escherichia coli.* Glycobiology, 2006. **16**(9): p. 833-843.
131. Henderson, G.E. , Isett, K.D., and Gerngross, T.U. , *Site-Specific Modification of Recombinant Proteins: A Novel Platform for Modifying Glycoproteins Expressed in E. coli.* BIOCONJUGATE CHEMISTRY, 2011. **22**(5): p. 903-912.
132. Plesner, B. , Westh, P. , and Nielsen, A. , *Biophysical characterisation of GlycoPEGylated recombinant human factor VIIa.* Int. J. Pharm., 2011. **406**: p. 62-68.
133. Stennicke, H.R., Ostergaard, H. , Bayer, R.J. , Kalo, M.S. , Kinealy, K. , Holm, P.K., Sørensen, B.B. , Zopf, D. , and Bjørn, S.E. , *Generation and*

biochemical characterization of glycoPEGylated factor VIIa derivatives. Tierärztliche Praxis Großtiere, 2008. **36**(3): p. 163-169.
134. Alley, S.C. , Benjamin, D.R., Jeffrey, S.C. , Okeley, N.M. , Meyer, D.L. , Sanderson, R.J. , and Senter, P.D. , *Contribution of linker stability to the activities of anticancer immunoconjugates.* Bioconjugate Chem., 2008. **19**: p. 759-765.
135. Bloom, L. and Calabro, V. , *FN3: a new protein scaffold reaches the clinic.* Drug Discov. Today, 2009. **14**: p. 949-955.
136. Lipovsek, D. , *Adnectins: engineered target-binding protein therapeutics.* Protein Eng., 2011. **24**(1-2): p. 3-9.
137. Brocchini, S. , Balan, S., Godwin, A. , Choi, J.W., Zloh, M. , and Shaunaik, S., *PEGylation of native disulfide bonds in proteins.* Nat. Protocols, 2006. **1**(5): p. 2241-2252.
138. Balan, S. , Choi , J.W. , Godwin, A. , Teo, I. , Laborde, C.M., Heidelberger, S. , Zloh, M. , Shaunak, S. , and Brocchini, S. , *Site-specific PEGylation of protein disulfide bonds using a three-carbon bridge.* Bioconjugate Chem., 2007. **18**(1): p. 61-76.
139. Shaunak, S. , Godwin, A. , Choi, J.W., Balan, S. , Pedone, E., Vijayarangam, D. , Heidelberger, S. , Teo, I., Zloh, M. , and Brocchini, S. , *Site-specific PEGylation of native disulfide bonds in therapeutic proteins.* Nat. Chem. Bio., 2006: p. 312-313.
140. Brocchini, S. , Bryant, P. , Cong, Y. , Choi, J. , Godwin, A. , and Powell, K. , *Novel conjugated proteins and peptides.*, in *WO/2009/047500.* 2009.
141. Woestenenk, E.A. , Hammarström, M. , Van den Berg, S. , Härd, T. , and Berglund, H. , *His tag effect on solubility of human proteins produced in Escherichia coli: a comparison between four expression vectors.* J Struct. Func. Genomics, 2004. **5**(3): p. 217-229.
142. Li, M. and Huang, D. , *On-column refolding purification and characterization of recombinant human interferon-λ1 produced in Escherichia coli.* Protein Expression and Purification, 2007. **53**(1): p. 119-123.
143. Porekar, G. and Menart, V. , *Potential for Using Histidine Tags in Purification of Proteins at Large Scale.* Chem. Eng. Technol., 2005. **28**(11): p. 1306-1314.
144. Tolner, B. , Smith, L. , Hillyer, T. , Bhatia, J. , Beckett, P. , Robson, L. , Sharma, S.K. , Griffin, N. , Vervecken, W. , and Contreras, R. , *From laboratory to Phase I/II cancer trials with recombinant biotherapeutics.* Eur. J. Cancer, 2007. **43**(17): p. 2515-2522.
145. Kaslow, D.C. and Shiloach, J. , *Production, purification and immunogenicity of a malaria transmission-blocking vaccine candidate: TBV25H expressed in yeast and purified using nickel-NTA agarose.* Nat. Biotechnol., 1994. **12**(5): p. 494-499.
146. Mayer, A.R.J. , Francis, R.J. , Sharma, S.K. , Tolner, B. , Springer, C.J. , Martin, J. , Boxer, G.M. , Bell, J. , Green, A.J. , Hartley, J.A. , Cruickshank, C. , Wren, J. , Chester, K.A., and Begent, R.H.J., *A Phase I Study of Single Administration of Antibody-Directed Enzyme Prodrug Therapy with the Recombinant Anti-Carcinoembryonic Antigen Antibody-Enzyme Fusion Protein MFECP1 and a Bis-Iodo Phenol Mustard Prodrug.* Clin. Cancer Res., 2006. **12**(21): p. 6509-6516.
147. Murphy, R. , Green, S. , Ritter, G. , Cohen, L. , Ryan, D. , Woods, W. , Rubira, M. , Cebon, J. , Davis, I., Sjolander, A., Kypridis, A., Kalnins, H.,

McNamara, M., Moloney, M., Ackland, J., Cartwright, G., Rood, J., Dumsday, G., Healey, K., Maher, D., Maraskovsky, E., Chen, Y., Hoffman, E., Old, L., and Scott, A., *Recombinant NY-ESO-1 cancer antigen: production and purification under cGMP conditions.* Prep. Biochem. Biotech., 2005. **35**(2): p. 119-134.

148. Mammen, M. , Choi, S. , and Whitesides, G.M. , *Polyvalent interactions in biological systems: implications for design and use of multivalent ligands and inhibitors.* Angew. Chem., Int. Ed., 1998. **37**: p. 2754-2794.
149. Badjic, J.D. , Nelson, A., Cantrill, Turnbull, S.J., and Stoddart, W.B. , *Multivalency and Cooperativity in Supramolecular Chemistry.* ChemInform, 2005. **38**(50): p. 723-732.
150. Kane, R. S., *Thermodynamics of Multivalent Interactions: Influence of the Linker.* Langmuir, 2010. **26**(11): p. 8636-8640.
151. Mammen, M. , Helmerson, K. , Kishore, R. , Choil, S.K. , Phillips, W.D. , and Whitesides, G.M. , *Optically controlled collisions of biological objects to evaluate potent polyvalent inhibitors of virus-cell adhesion.* Chemistry & Biology, 1996. **13**(9).
152. Sigal, G.B. , Mammen, M. , Dahmann, G. , and Whitesides, G.M. , *Polyacrylamides Bearing Pendant R-Sialoside Groups Strongly Inhibit Agglutination of Erythrocytes by Influenza Virus: The Strong Inhibition Reflects Enhanced Binding through Cooperative Polyvalent Interactions.* J. Am. Chem. Soc., 1996. **118**(16): p. 1-12.
153. Basha, S., Rai, P., Poon, V., Saraph, A., Gujraty, K., Go, M. Y., Sadacharan, S., Frost, M., Mogridge, J., and Kane, R., *Polyvalent inhibitors of anthrax toxin that target host receptors.* PNAS, 2006. **103**(36): p. 13509-13513.
154. Gao, X. , Cui, Y. , Levenson, R.M. , W K Chung, L. , and Nie, S. , *In vivo cancer targeting and imaging with semiconductor quantum dots.* Nat Biotechnol, 2004. **22**(8): p. 969-976.
155. Madhankumar, A.B., Slagle-Webb, B. , Mintz, A. , Sheehan, J.M. , and Connor, J.R. , *Interleukin-13 receptor-targeted nanovesicles are a potential therapy for glioblastoma multiforme.* Molecular Cancer Therapeutics, 2006. **5**(12): p. 3162-3169.
156. Caplan, M.R. and Rosca, E.V., *Targeting Drugs to Combinations of Receptors: A Modeling Analysis of Potential Specificity.* Ann Biomed Eng, 2005. **33**(8): p. 1113-1124.
157. Shewmake, T.A., Solis, F.J., Gillies, R.J., and Caplan, M.R., *Effects of Linker Length and Flexibility on Multivalent Targeting.* Biomacromolecules, 2008. **9**(11): p. 3057-3064.
158. Rosca, E.V. , Stukel, J.M. , Gillies, R.J. , Vagner, J. , and Caplan, M.R. , *Specificity and Mobility of Biomacromolecular, Multivalent Constructs for Cellular Targeting.* Biomacromolecules, 2007. **8**(12): p. 3830-3835.
159. Valen, D.V., Haataja, M., and Philips, R., *Biochemistry on a leash: The Roles of Tether Length and Geometry in Signal Integration Proteins.* Biophysical Journal, 2009. **94**(4): p. 1275-1292.
160. Reeves, D. , Cheveralls, K. , and Kondev, J. , *Regulation of biochemical reaction rates by flexible tethers.* Phys. Rev. E, 2011. **84**(2).
161. Mack, E.T. , Snyder, P.W. , Perez-Castillejos, R. , and Whitesides, G.M. , *Using Covalent Dimers of Human Carbonic Anhydrase II To Model Bivalency in Immunoglobulins.* Journal of the American Chemical Society, 2011. **133**(30): p. 11701-11715.

162. Krishnamurthy, V.M., Semetey, V. , Bracher, P.J., Shen, N. , and Whitesides, G.M. , *Dependence of Effective Molarity on Linker Length for an Intramolecular Protein–Ligand System.* Journal of the American Chemical Society, 2007. **129**(5): p. 1312-1320.
163. Damle, N.K., *Antibody-drug conjugates ace the tolerability test.* Nat Biotechnol, 2008. **26**(8): p. 884-885.
164. Burke, P. J., Toki, B.E., Meyer, D.W., Miyamoto, J.B., Kissler, K.M., Anderson, M. , Senter, P.D., and Jeffrey, S.C. , *Novel immunoconjugates comprised of streptonigrin and 17-amino-geldanamycin attached via a dipeptide-p-aminobenzyl-amine linker system.* Bioorganic and Medicinal Chemistry Letters, 2009. **19**(10): p. 2650-2653.
165. Junutula, J.R. , Raab, H. , Clark, S. , Bhakta, S. , Leipold, D.D. , Weir, S., Chen, Y., Simpson, M., Tsai, S.P., Dennis, M.S., Lu, Y., Meng, Y.G., Ng, C., Yang, J., Lee, C.C., Duenas, E., Gorrell, J., Katta, V., Kim, A., Mcdorman, K., Flagella, K., Venook, R., Ross, S., Spencer, S.D., Lee Wong, W., Lowman, H.B., Vandlen, R., Sliwkowski, M.X., Scheller, R.H., Polakis, P., and Mallet, W., *Site-specific conjugation of a cytotoxic drug to an antibody improves the therapeutic index.* Nat Biotechnol, 2008. **26**(8): p. 925-932.
166. Shen, B.Q., Xu, K., Liu, L., Raab, H., Bhakta, S., Kenrick, M., Parsons-Reponte1, K. L., Tien, J., Yu, SF., Mai, E., Li, D., Tibbitts, J., Baudys, J., Saad, O. M., Scales, S. J., McDonald, P. J., Hass, P. E., Eigenbrot, C., Nguyen, T., Solis, W. A., Fuji, R. N., Flagella, K. M., Patell, D., Spencer, S. D., Khawli, L. A., Ebens, A., Wong, W. L., Vandlen, R., Kaurl, S.., Sliwkowskil, S. X., Scheller, R. H., Polakis, P., and Junutulal, J. R., *Conjugation site modulates the in vivo stability and therapeutic activity of antibody-drug conjugates.* Nature biotechnology, 2012: p. 1-7.
167. Barok, M. , Tanner, M. , Köninki, K. , and Isola, J. , *Trastuzumab-DM1 is highly effective in preclinical models of HER2-positive gastric cancer.* Cancer Lett, 2011. **306**(2): p. 171-179.
168. Spriel, A. B., Ojik, H. H., and Winkel, J. G.J., *Immunotherapeutic perspective for bispecific antibodies.* Review Immunology, 2000. **21**(8): p. 391-396.
169. Holmes, D., *Buy buy bispecific antibodies.* Nature Review, 2011. **10**: p. 798-800.
170. Brennen, M., *Preparation of Bispecific Antibodies by chemical recombinant of monoclonal immunoglobulin G1 fragments.* Scienec, 1985. **229**(4708): p. 81-83.
171. Nisonoff, A. and Rivers, MM. , *Recombination of a mixture of Univalent antibody fragmnets of different specificity.* Arch Biochem Biophys., 1961. **93**(2): p. 460.
172. Doppalapudi, V.R. , Huang, J., Liu, D. , Jin, P. , Liu, B. , Li, L., Desharnais, J. , Hagen, C., Levin, N.J., Shields, M.J., Parish, M., Murphy, R.E., Del Rosario, J., Oates, B.D., Lai, J.Y., Matin, M.J., Ainekulu, Z., Bhat, A., Bradshaw, C.W., Woodnutt, G., Lerner, R.A., and Lappe, R.W., *Chemical generation of bispecific antibodies.* P Natl Acad Sci Usa, 2010. **107**(52): p. 22611-22616.
173. Greco, F. and Vicent, M. J., *Combination therapy: Opportunities and challenges for polymer-drug conjugates as anticancer nanomedicines.* Advanced Drug Delivery Reviews, 2009. **61**(13): p. 1203-1213.
174. Fischer, N. and Eacute Ger, O.L., *Bispecific Antibodies: Molecules That Enable Novel Therapeutic Strategies.* Pathobiology, 2007. **74**(1): p. 3-14.

175. Kufer, P. , Lutterbuse, R. , and Baeuerle, P.A. , *A revival of bispecific antibodies.* TRENDS in Biotechnology, 2004. **22**(5): p. 238-244.
176. Davis, J. H., Aperlo, C., Li, Y., Kurosawa, E., Lan, Y., Lo, KM., and Huston, J. S., *SEEDodies: fusion proteins based on strand-exchange engineered domain (SEED) CH3 heterodimers in an Fc analogue platform for asymmetric binders or immunofusions and bispecific antibodies.* Protein Eng Des Sel, 2010. **23**(4): p. 195-202.
177. Valladares, I.G. and Espinoza, L.R. , *Designing two-in-one antibodies.* Immunotherapy, 2009. **1**(5): p. 749-751.
178. Ciardiello, F. , Bianco, R. , Damiano, V. , Fontanini, G. , Caputo, R. , Pomatico, G. , De Placido, S. , Bianco, A.R. , Mendelsohn, J. , and Tortora, G. , *Antiangiogenic and antitumor activity of anti-epidermal growth factor receptor C225 monoclonal antibody in combination with vascular endothelial growth factor antisense oligonucleotide in human GEO colon cancer cells.* Clin. Cancer Res., 2000. **6**(9): p. 3739-3747.
179. Gerber, H.P. , Kowalski, J. , Sherman, D. , Eberhard, D.A., and Ferrara, N. , *Complete inhibition of rhabdomyosarcoma xenograft growth and neovascularization requires blockade of both tumor and host vascular endothelial growth factor.* Cancer Res, 2000. **60**(22): p. 6253-6258.
180. Foy, K.C. , Liu, Z. , Philips, G. , Miller, M. , and Kaumaya, P.T. P. , *Combination Treatment with HER-2 and VEGF Peptide Mimics Induces Potent Anti-tumor and Anti-angiogenic Responses in Vitro and in Vivo.* Journal of Biological Chemistry, 2011. **286**(15): p. 13626-13637.
181. Vallböhmer, D. , Zhang, W. , Gordon, M. , Yang, D.Y. , Yun, J., Press, O.A., Rhodes, E.K., Sherrod, K.E., Iqbal, S., Danenberg, K.D., Groshen, S., and Lenz, H.J., *Molecular determinants of cetuximab efficacy.* J. Clin. Oncol., 2005. **23**(15): p. 3536-3544.
182. Bernard-Mart, C., Lebrun, F., Awada, A., and Piccart, M. J, *Monoclonal Antibody-based targeted therapy in breast cancer: current status and future directions.* Drugs, 2006. **66**(12): p. 1577-1591.
183. Tabernero, J. , *The Role of VEGF and EGFR Inhibition: Implications for Combining Anti-VEGF and Anti-EGFR Agents.* Molecular Cancer Research, 2007. **5**(3): p. 203-220.
184. Naumov, G.N. , Nilsson, M.B. , Cascone, T. , Briggs, A. , Straume, O. , Akslen, L.A. , Lifshits, E. , Byers, L.A., Xu, L., Wu, H.K., Janne, P., Kobayashi, S., Halmos, B., Tenen, D., Tang, X.M., Engelman, J., Yeap, B., Folkman, J., Johnson, B.E., and Heymach, J.V., *Combined Vascular Endothelial Growth Factor Receptor and Epidermal Growth Factor Receptor (EGFR) Blockade Inhibits Tumor Growth in Xenograft Models of EGFR Inhibitor Resistance.* Clinical Cancer Research, 2009. **15**(10): p. 3484-3494.
185. Kurfurst, M.M. , *Detection and Molecular Weight Determinationof Polyethylene Glycol-Modified Hirudin by Staining after Sodium Dodecyl Sulfate-Polyacrylamide Gel Electrophoresis.* Analytical Biochemistry, 1992. **200**: p. 244-248.
186. Vincents, B. , von Pawel-Rammingen, U. , Bjo¨rck, L. , and Abrahamson, M. , *Enzymatic Characterization of the Streptococcal Endopeptidase, IdeS, Reveals That It Is a Cysteine Protease with Strict Specificity for IgG Cleavage Due to Exosite Binding.* Biochemistry, 2004. **43**: p. 15540-15549.
187. Scollard, Deborah A, Chan, Conrad, Holloway, Claire M B, and Reilly, Raymond M, *A kit to prepare 111In-DTPA-trastuzumab (Herceptin) Fab*

fragments injection under GMP conditions for imaging or radioimmunoguided surgery of HER2-positive breast cancer. Nuclear Medicine and Biology, 2011. **38**(1): p. 129-136.
188. Myszka, D.G. , *Improving biosensor analysis.* J Mol Recognit, 1999. **12**: p. 279-284.
189. Mulvany, MJ. and Halpern, W., *Contractile properties of small arterial vessels in spontaneously hypertensive and normatensive rats.* Circulation Research, 1977. **41**: p. 19-26.
190. Harlow, E. and Lane, D. , *Antibodies: A Laboratory Manual.* Cold Spring Harbor Laboratory 1988: Cold Spring Harbor, NY.
191. Mage, M.G., *Preparation of Fab Fragments from IgGs of Different Animal Species.* Methods in Enzymology, 1978. **70**: p. 142-150.
192. Rousseaux, J., Rousseaux-Prevost, R. , and Bazin, H. , *Optimal Conditions for the Preparation of Fab and F(ab)2 Fragments from Monoclonal IgG of Different Rat IgG Subclasses.* Journal of lmmunological Methods,, 1983. **64**(1-2): p. 141-146.
193. Meyer, C.H. and Holz, F.G. , *Preclinical aspects of anti-VEGF agents for the treatment of wet AMD: ranibizumab and bevacizumab.* Eye, 2011. **25**(6): p. 661-672.
194. Cresswell, C. , Newcombe, A.P. , Davies, S. , Macpherson, I. , Nelson, P. , Apos, K.O. , Donovan, and Francis, R. , *Optimal conditions for the papain digestion of polyclonal ovine IgG for the production of biotherapeutic Fab fragments.* Biotechnol. Appl. Biochem., 2005. **42**(2): p. 163.
195. Mitchel, R.E., Chaiken, I.M. , and Smith, E.L., *The complete Amino Acid Sequence of Papain.* The journal of biological chemistry, 1970. **245**(14): p. 3485-3492.
196. Dainiak, M. B., Muronetz, V. I, Izumrudov, V. A., Yu, I., and Mattiasson, B., *Production of Fab Fragments of Monoclonal Antibodies Using Polyelectrolyte Complexes.* Analytical Biochemistry, 2000. **277**: p. 58-66.
197. Sjoquist, A. and Forsgren, J. , *Protein A from S. Aureus : I. Pseudo-Immune Reaction with Human γ-Globulin.* J Immunol, 1966. **97**: p. 822-827.
198. Sjoquist, J. , Meloun, B. , and Hjelm, H. , *Protein A Isolated from Staphylococcus aureus after Digestion with Lysostaphin.* Eur. J.Biochem, 1972. **29**: p. 572-578.
199. Bjork, I. , *Some Physicochemical Properties of Protein A from Staphylococcus aureus.* Eur. J. Biochm., 1972. **29**: p. 579-584.
200. Shapiro, A. L., Vinuela, E., and Maizel, J. V., *Molecular weight estimation of polypeptide chain by electrophoresis in SDS-polyacrylamide gels.* Biochemical and Biophysical Research Communications, 1967. **28**(5): p. 815-820.
201. Manufacturer protocol, *Vivaspin 6 and 20 mL.* sartorius stedim.
202. Whitaker, J. R. and Grahum, P.E. , *An Absolute Method for Protein Determination Based on Difference in Absorbance at 235 and 280 nm.* Analytical Biochemistry, 1980. **109**: p. 156-159.
203. Gill, S.C. and Hippel, V.P.H., *Calculation of Protein Extinction Coefficients from Amino Acid Sequence Data.* Anlytical Biochemistry, 1989. **182**: p. 319-326.
204. Pace, C.N. , Vajdos, F., Fee, L. , Grimsley, G. , and Gray, T. , *How to measure and predict the molar absorption coefficient of a protein.* Protein Science, 1995. **4**: p. 2411-2423.

205. Barbas, C.F. , Crowe, J.E. , Cababa, J.R.D. , Suzanne, T.M.J. , Zebedeei, L., Murphy, B.R. , Chanock, R.M. , and Burton, D.R. , *Human monoclonal Fab fragments derived from a combinatorial library bind to respiratory syncytial virus F glycoprotein and neutralizeinfectivity.* Proc.Natl.Acad.Sci, 1992. **89**: p. 10164-10168.
206. Minor, L.K. , *Handbook of assay development in drug discovery.* Drug discovery series, Edited by; A. Carmen. CRC Press, Talor & Francis group, 2006: p. 423.
207. Nikolayenko, I.V. , Galkin, O.Y. , Grabchenko, N.I. , and Spivak, M.Y. , *Preparation of highly purified human IgG, IgM, and IgA for immunization and immunoanalysis.* Ukrainica Bioorganica Acta 2, 2005: p. 3-11.
208. Thermo Scientific, *Extinction Coefficients guidline.* TR0006.3, 2008.
209. Papain instructions, *Immobilised papain.* Thermo Scientific. **20341**.
210. Johnstone, A. and Thorpe, R., *Immunochemistry in Practice.* 1988: Blackwell Scientific Publications.
211. Smith, P.K., Krohn, R.I., Hermanson, G.T. , Mallia, A.K., Gartner, F.H. , Provenzano, M.D., Fujimoto, E.K., Goeke, N.M., Olson, B.J., and Klenk, D.C., *Measurement of protein using bicinchoninic acid.* Anal Biochem., 1985. **150**(1): p. 76-85.
212. Vlckova, M., Kalmanb, F. , and Schwarz, M.A. , *Pharmaceutical applications of isoelectric focusing on microchip with imaged UV detection.* Journal of Chromatography A, 2008. **1181** p. 145–152.
213. Huo, F.J., Sun, Y.Q. , Su, J. , Chao, J.B., Zhi, H.J., and Yin, C.X., *Colorimetric Detection of Thiols Using a Chromene Molecule.* Org. Lett., 2009. **11**(21): p. 4918-4921.
214. Riener, C. K., Kada, G., and Gruber, H., *Quick measurement of protein sulfhydryls with Ellman's reagent and with 4,4-dithiodipyridine.* Anal Bioanal Chem, 2002. p. 266-276.
215. Yi, Long, Li, Heyang, Sun, Lu, Liu, Liangliang, Zhang, Caihong, and Xi, Zhen, *A Highly Sensitive Fluorescence Probe for Fast Thiol-Quantification Assay of Glutathione Reductase.* Angewandte Chemie International Edition, 2009. **48**(22): p. 4034-4037.
216. Ellman, G. L., *Tissue Sulfhydryl Groups.* Archieve of Biochemistry and Biophysics, 1959. **82**: p. 70-77.
217. Riddles, P.W., Blakeley, R.L., and Zerner, B., *Ellman's reagent: 5,5'-dithiobis(2-nitrobenzoic acid)--a reexamination.* Anal Biochem, 1979. **94**(1): p. 75-81.
218. Sedlak, J. and Lindsay, R.H., *Estimation of Total, Protein-Bound, and Nonprotein Sulfhydryl Groups in Tissue with Ellman's Reagent.* Analytical Biochemistry, 1968. **25**: p. 192-205.
219. Manufacturer protocol, *Ellma's Reagent.* Pierce. **22582**.
220. Begg, G.E. and Speicher, D.W. , *Mass spectrometry detection and reduction of disulfide adducts between reducing agents and recombinant proteins with highly reactive cysteines.* J. Biomol.Tech, 1999. **10**: p. 17-20.
221. Humphreys, D.P., Heywood, S.P., Henry, A. , Ait-Lhadj, L. , Antoniw, P. , Palframan, R. , Greenslade, K.J., Carrington, B., Reeks, D.G., Bowering, L.C., West, S., and Brand, H.A., *Alternative antibody Fab' fragment PEGylation strategies: combination of strong reducing agents, disruption of the interchain disulphide bond and disulphide engineering.* Protein Eng Des Sel, 2007. **20**(5): p. 227-234.

222. Netto, L.E.S. and Stadtman, E.R., *The Iron-Catalyzed Oxidation of Dithiothreitol Is a Biphasic Process: Hydrogen Peroxide Is Involved in the Initiation of a Free Radical Chain of Reactions.* Archives of Biochemistry and Biophysics, 1996. **330**(1): p. 233-242.
223. Han, J.C. and Han, G.Y. , *A Procedure for Quantitative Determination of Tris(2-carboxyethyl)phosphine, an Odorless Reducing Agent more Stable and Effective Than Dithiothreitol.* Analytical Biochemistry, 1994. **220**: p. 5-10.
224. Getz, E.B. , Xiao, M. , Chakrabarty, T., Cooke, R. , and Selvin, P.R., *A Comparison between the Sulfhydryl Reductants Tris(2-carboxyethyl)phosphine and Dithiothreitol for Use in Protein Biochemistry.* Analytical Biochemistry, 1999. **273**: p. 73-80.
225. Humphreys, D.P. , Vetterlein, O.M. , Chapman, A.P. , King, D.J. , Antoniw, P. , Suitters, A.J. , Reeks, D.G. , Parton, T.A.H. , King, L.M. , Smith, B.J. , L.ang, V. , and Stephens, P.E. , *F(ab)2 molecules made from Escherichia coli produced fab' with hinge sequences conferring increased serum survival in an animal model.* Journal Of Immunological Methods, 1998. **217**: p. 1-10.
226. Alessi, M.L. , Norman, A.I., Knowlton, S.E. , Ho, D.L. , and Greer, S.C., *Helical and Coil Conformations of Poly(ethylene glycol) in Isobutyric Acid and Water.* Macromolecules, 2005. **38**(22): p. 9333-9340.
227. Zheng, C. Y., Ma, G., and Su, Z., *Native PAGE eliminate the problem of PEG-SDS interaction in SDS-PAGE and procides an alternative to HPLC in characterization of protein PEGylation.* Electrophoresis, 2007. **28**(2801-2807).
228. Lu, Y. , Harding, S.E. , Turner, A. , Smith, B. , and Athwal, D.S. , *Effect of PEGylation on the solution conformation of antibody fragments.* J. Pharm. Sci., 2008. **97**(6): p. 2062-2079.
229. Bjellqvist, B., Pasquali, C., Ravier, F., Sanchez, J., and Hochstrasser, D., *A nonlinear wide-range immobilised pH gradient for two-dimensional electrophoresis and its definition in a relvent pH scale.* Electrophoresis, 1993. **14**: p. 1357-1365.
230. Wang, W., Nema, S., and Teagarden, D., *Protein aggregation-Pathways and influencing factors.* Int. J. Pharm., 2010. **390**(2): p. 89-99.
231. Knappik, A. and Brundiers, R., *Recombinant Antibody Expression and Purification*, in *The Protein Protocol Handbook*, J.M. Walker, Editor. 2009, Springer.
232. Rosenberg, Amy S, *Effects of Protein Aggregates: An Immunologic Perspective.* The AAPS Journal, 2006. **8**(3): p. 1-7.
233. Chen, B. , Bautista, R. , Yu, K. , Zapata, G.A., Mulkerrin, M.G., and Chamow, S.M., *Influence of histidine on the stability and physical properties of a fully human antibody in aqueous and solid forms.* Pharm Res, 2003. **20**(12): p. 1952-1960.
234. Goldburg, W.I., *Dynamic light scattering.* Am. J. Phys, 1999. **67**(12): p. 1152-1160.
235. Carter, P. , Kelley, R.F., Rodrigues, M.L., Snedecor, B. , Covarrubias, M. , Velligan, M.D., Wong, W.L. , Rowland, A.M., Kotts, C.E., and Carver, M.E., *High level Escherichia coli expression and production of a bivalent humanized antibody fragment.* Biotechnology (N.Y.), 1992. **10**(2): p. 163-167.
236. Johansson, B.P., Shannon, O. , and Björck, L. , *IdeS: A Bacterial Proteolytic Enzyme with Therapeutic Potential.* PLoS ONE, 2008. **3**(2): p. e1692.

237. Akesson, P., Moritz, L., Truedsson, M., Christensson, B., and Pawel-Rammingen, U. V., *IdeS, a highly Specific Immunoglobulin G (IgG)-cleaving Enzyme from Streptococcus pyogenes, Is Inhibited by specific IgG Antibodies Generated during Infection.* INFECTION AND IMMUNITY, 2006. **74**(1): p. 497-503.
238. Manufacturer protocol, *FabRICATOR-perfect F(ab)2 fragments in minutes.* Genovis.
239. Singh, R. and Kats, L. , *Catalysis of Reduction of Disulfide by Selenol.* Analytical Biochemistry, 1995. **231**: p. 86-91.
240. Casey, J.L., Pedley, R.B. , King, D.J., Boden, R., Chapman, A.P. , Yarranton, G.T. , and Begent, R.H.J., *Improved tumour targeting of di-Fab' fragments modified with polyethylene glycol.* Tumor Target, 2000. **4**: p. 235-244.
241. Demeule, B. , Palais, C. , Machaidze, G. , Gurny, R. , and Arvinte, T. , *New methods allowing the detection of protein aggregates, A case study on trastuzumab.* Mabs, 2009. **1**(2): p. 142-150.
242. Raftery, J, Clegg, A, Jones, J, Tan, S C, and Lotery, A, *Ranibizumab (Lucentis) versus bevacizumab (Avastin): modelling cost effectiveness.* British Journal of Ophthalmology, 2007. **91**(9): p. 1244-1246.
243. Liu, Hongcheng, Chumsae, Chris, Gaza-Bulseco, Georgeen, Hurkmans, Karen, and Radziejewski, Czeslaw H, *Ranking the Susceptibility of Disulfide Bonds in Human IgG1 Antibodies by Reduction, Differential Alkylation, and LC-MS Analysis.* Anal Chem, 2010: p. 1-8.
244. Manufacturer protocol, *TCEP* Thermo Scientific. **20490**.
245. Manufacturer protocol, *2-Mercaptoethylamine.HCl.* Therno Scientific. **20408**.
246. Solomons, T.W.G. and Fryhle, C. B., *Organic Chemistry.* Eight ed. 2004: John Wiley & son.
247. Herbst, R.S. , *Phase I/II Trial Evaluating the Anti-Vascular Endothelial Growth Factor Monoclonal Antibody Bevacizumab in Combination With the HER-1/Epidermal Growth Factor Receptor Tyrosine Kinase Inhibitor Erlotinib for Patients With Recurrent Non-Small-Cell Lung Cancer.* Journal of Clinical Oncology, 2005. **23**(11): p. 2544-2555.
248. Rudnick, S.I. and Adams, G.P. , *Affinity and Avidity in Antibody-Based Tumor Targeting.* Cancer Biotherapy and Radiopharmaceuticals, 2009. **24**(2): p. 1-8.
249. Lappalainen, M. and Hedman, K. , *Serodiagnosis of toxoplasmosis. The impact of measurement of IgG avidity.* Ann Ist Super Sanità, 2004. **40**(1): p. 81-88.
250. Casasnovas, J.M. and Springer, T.A., *Kinetics and thermodynamic of Virus binding to Receptor.* The journal of biological chemistry, 1995. **270**: p. 13216-13224.
251. Khan, M.N. and Findlay, J.W.A. , eds. *Ligand-Binding Assays* 2010, John Wiley & Sons, Inc: New Jersey.
252. Karlsson, R. , Hakan Roos, R. , Fagerstam, L. , and Persson, B. , *Kinetic and Concentration Analysis Using BIA Technology.* Methods: A companion to methods in enzymology, 1994. **6**: p. 99-110.
253. Myszka, D.G., *Kinetic analysis of macro molecular interactions using surface plasmon resonance biosensors.* Current Opinion in Biotechnology, 1997. **8**: p. 50-57.

254. Karush, F. , *The affinity of antibody: range. variability and the role of multivalence*, in *Comprehensive Immunology: Immunoglobulins*, G.W. Litman, and Good, R. A., Editor. 1987, Plenum: New York. p. 85-116.
255. Ong, G.L. and Mattes, M.J. , *Re-evaluation of the concept of functional affinity as applied to bivalent antibody binding to cell surface antigens.* Molecular Immunology, 1993. **30**(16): p. 1455-1462.
256. Mattes, M. J., *On the Validity of "Functional Affinity" Determination for Antibodies Binding to Cell Surface Antigens or Other Polyvalent Antigens.* Cancer Res, 1995. **55**: p. 5733-5735.
257. Yoon, S. , Macknight, W.J. , and HSU, S.L., *End-Group Effect on Chain Conformation of Poly(propylene glycol) and Poly(ethylene glycol).* Journal of applied polymer science, 1997. **64**(1): p. 197-202.
258. Regenmortel, M.H.V. and Azimzadeh, A. , *Determination of antibody affinity.* J. Immunoassay, 2000. **211**(21): p. 211-234.
259. Schuck, P. , *Reliable determination of binding affinity and kinetics using surface plasmon resonance biosensors.* Curr. Opin. Biotechnol, 1997. **8**: p. 498.
260. Perozzo, R. , Folkers, G. , and Scapozza, L. , *Thermodynamics of Protein–Ligand Interactions: History, Presence, and Future Aspects.* Journal of Receptors and Signal Transduction, 2004. **24**(1-2): p. 1-52.
261. Tetin, S.Y. , Swift, K.M. , and Matayoshi, E.D. , *Measuring antibody affinity and performing immunoassay at the single molecule level.* Anal. Biochem, 2002. **307**(84).
262. Lakey, J.H. and Raggett, E.M. , *Measuring protein-protein interactions.* Current opinion in Structural Biology, 1998. **8**: p. 119-123.
263. Pierce, M.M., Raman, C.S. , and Nall, B.T., *Isothermal Titration Calorimetry of Protein–Protein Interactions.* Methods, 1999. **19**: p. 213–221.
264. Tao, J. , Xiang, J.J., Li, D. , Deng, N. , Wang, H. , and Gong, Y.P., *Selection and characterization of a human neutralizing antibody to human fibroblast growth factor-2.* Biochemical and Biophysical Research Communications, 2010. **394**(3): p. 767-773.
265. Stenberg, E., Persson, B. , Roos, H. , and Urbaniczky, C., *Quantitative Determination of surface concentration of protein with Surface Plasmon Resonance using radiolabeled proteins.* Journal of Colloid and Interface science, 1991. **143**(2): p. 513-526.
266. Jönsson, U. , Fägerstam, L. , Ivarsson, B. , Karlsson, R. , Lundh, K. , Löfås, S. , Persson, B. , Roos, H. , and Rönnberg, I. , *Real-time biospecific interaction analysis using surface plasmon resonance and a sensor chip technology.* BioTechniques, 1991. **11**(5): p. 620-627.
267. Harding, S.E. and Chowdhry, B.Z. , eds. *Surface plasmon resonance. In "Protein-Ligand Interaction: hydrodynamics and calorimetry",*. ed. Oxford University Press. 2001, P. Anton Van Der Merwe. : Oxford.
268. Tanious, F.A. and al., et, *Biosensor-Surface plasmon resonance methods for quantitative analysis of biomolecular interactions.* Methods in cell biology, 2008. **84**: p. 53-77.
269. Myszka, D.G. , He, X. , Dembo, M. , Morton, T.A. , and Goldstein, B. , *Extending the Range of Rate Constants Available from BIACORE: Interpreting Mass Transport-Influenced Binding Data.* Biophysical Journal, 1998. **75**(2): p. 583-594.

270. Fisher, R.J., Fivash, M. , Casas-Finet, H. , Bladen, S. , and Larson, K. , *Real-time BIAcore measurment of Escherichia coli single-stranded DNA binding (SSB) protein to polyeoxythemidylic acid reveal single-state kinetics with steric cooperativity.* Methods: A companion to methods in enzymology, 1994. **6**: p. 121-133.
271. Silin, V. and Plant, A. , *Biotechnological applications of surface plasmon resonance.* Trends biotechnol, 1997. **15**: p. 353-383.
272. GE Healthcare, *BIAcore concentration Analysis Handbook.* 2008, Sewden. 1-100.
273. Bobrovnik, S.A., *Determination of antibody affinity by ELISA. Theory.* Journal of biochemical and biophysical methods, 2003. **57**(3): p. 213-236.
274. Stevens, F.J. and Bobrovnik, S.A. , *Deconvolution of antibody affinities and concentrations by non-linear regression analysis of competitive ELISA data.* J Immunol Methods, 2007. **328**(1-2): p. 53-58.
275. Heinrich, L. , Tissot, N. , Hartmann, D.J. , and Cohen, R. , *Comparison of the results obtained by ELISA and surface plasmon resonance for the determination of antibody affinity.* Journal Of Immunological Methods, 2010. **352**(1-2): p. 13-22.
276. GE Healthcare, *kinetics and affinity analysis.* 2007. p. 1-10.
277. Tiedemann, B.V. and Bilitewski, U. , *Characterization of the vascular endothelial growth factor-receptor interaction and determination of the recombinant protein by an optical receptor sensor.* . Biosensors and Bioelectronics, 2002. **17**: p. 983-991.
278. Muller, Y.A., Chen, Y. , Christinger, H.W. , Li, B., Cunningham, B.C. , Lowman, H.B. , and M de Vos, A. , *VEGF and the Fab fragment of a humanized neutralizing antibody: crystal structure of the complex at 2.4 Å resolution and mutational analysis of the interface.* Structure, 1998. **6**(9): p. 1153-1167.
279. Yu, L, Wu, X, Cheng, Z, Lee, C V, LeCouter, J, Campa, C, Fuh, G, Lowman, H, and Ferrara, N, *Interaction between Bevacizumab and Murine VEGF-A: A Reassessment.* Invest Ophth Vis Sci, 2008. **49**(2): p. 522-527.
280. Anton Van der Merwe, P. , *Surface Plasmon Resonance.* 2003. p. 1-50.
281. Dhalluin, C. , Ross, A. , Huber, W. , Gerber, P. , Brugger, D. , Gsell, B. , and Senn, H., *Structural, kinetic, and thermodynamic analysis of the binding of the 40 kDa PEG-interferon-alpha 2a and its individual positional isomers to the extracellular domain of the receptor IFNAR2.* Bioconjugate Chem., 2005. **16**: p. 518-527.
282. Patel, R. and Andrien Jr, B. A. , *Kinetic analysis of a monoclonal therapeutic antibody and its single-chain homolog by surface plasmon resonance.* Analytical Biochemistry, 2010. **396**(1): p. 59-68.
283. Kou, G. , Shi, J. , Chen, L. , Zhang, D. , Hou, S. , Zhao, L. , Fang, C. , Zheng, L. , Zhang, X. , Liang, P. , Zhang, X. , Li, B. , and Guo, Y. , *A bispecific antibody effectively inhibits tumor growth and metastasis by simultaneous blocking vascular endothelial growth factor A and osteopontin.* Cancer Lett, 2010. **299**(2): p. 130-136.
284. Liang, WC., Wu, X., Peale, F. V., Lee, C. V. , Meng, Y. G., Gutierrez, J. , Fu, L. , Malik, A. K. , Gerber, H. P., Ferrara, N. , and Fuh, G. , *Cross-species Vascular Endothelial Growth Factor (VEGF)-blocking Antibodies Completely Inhibit the Frowth of Human Tumor Xenografts and Measure the Contribution*

of Stormal VEGF. The journal of biological chemistry, 2006. **281**(2): p. 951-961.

285. Chen, Y. , Weismann, C. , Fun, G. , Li, B. , Christinger, H.W. , McKay, P. , M. de Vos, A. , and Lowman, H.B. , *Selection and Analysis of an Optimized Anti-VEGF Antibody: Crystal Structure of an Affinity-matured Fab in Complex with Antigen.* J Mol Biol, 1999. **293**: p. 865-881.
286. Shafir, T., *Personal communication.* 2010, BIAcore GE healthcare specialist: London.
287. Product information, *Vascular Endothelial Growth Factor (VEGF).* Sigma. **V4512**.
288. Chen, C. , Constantinou, A. , and Deonarain, M. , *Modulating antibody pharmacokinetics using hydrophilic polymers.* Expert Opin. Drug Deliv., 2011. **8**(9): p. 1221-1236.
289. Mabry, R. , Rani, M. , Geiger, R. , Hubbard, G.B. , Carrion, R. , Brasky, K. , Patterson, J.L., Georgiou, G. , and Iverson, B.L. , *Passive Protection against Anthrax by Using a High-Affinity Antitoxin Antibody Fragment Lacking an Fc Region.* Infection and Immunity, 2005. **73**(12): p. 8362-8368.
290. Lowe, J. , Araujo, J. , Yang, J. , Reich, M. , Oldendorp, A. , Shiu, V. , Quarmby, V. , Lowman, H., Lien, S. , Gaudreault, J. , and Maia, M. , *Ranibizumab inhibits multiple forms of biologically active vascular endothelial growth factor in vitro and in vivo.* Experimental Eye Research, 2007. **85**(4): p. 425-430.
291. Bostrom, J. , Haber, L. , Koenig, P. , Kelley, R.F., and Fuh, G. , *High Affinity Antigen Recognition of the Dual Specific Variants of Herceptin Is Entropy-Driven in Spite of Structural Plasticity.* PLoS ONE, 2011. **6**(4): p. e17887.
292. Cheng, T.L., Chuang, K.H., Chen, B.M., and Roffler, S.R., *Analytical Measurement of PEGylated Molecules.* Bioconjug. Chem., 2012 Jan.
293. Choy, E.H.S., Hazleman, B. , Smith, M., Moss, K., Lisi, L., Scott, D.G.I., Patel, J., Sopwith, M., and Isenberg, D.A. , *Efficacy of a novel PEGylated humanized anti-TNF fragment (CDP870) in patients with rheumatoid arthritis: a phase II double-blinded, randomized, dose-escalating trial.* Rheumatology, 2002. **41**: p. 1133-1137.
294. Scatchard, G. , *The attraction of proteins for small molecules and ions.* Ann. N. Y. Acad. Sci, 1949. **51**(660).
295. GraphPad PRISM, *Saturation Binding Curves and Scatchard Plots.* 2003. p. 1-13.
296. Kolassa, N. and Turnheim, K. , *Limitations of the direct linear plot in evaluation of drug-protein binding parameters.* Experientia, 1976. **32**(10): p. 1355-1356.
297. Duncan, R. and Gaspar, R., *Nanomedicine(s) under the microscope.* Mol. Pharmaceutics, 2011. **8**(6): p. 2101-2141.
298. Bruce, D. and Tan, P.H. , *Blocking the interaction of vascular endothelial growth factor receptors with their ligands and their effector signaling as a novel therapeutic target for cancer: time for a new look?* Expert Opin. Investig. Drugs, 2011. **20**(10): p. 1413-1434.
299. Marrelli, A. , Cipriani, P. , Liakouli, V. , Carubbi, F. , Perricone, C. , Perricone, R., and Giacomelli, R., *Angiogenesis in rheumatoid arthritis: A disease specific process or a commonresponse to chronic inflammation?* Autoimmunity Reviews, 2011. **10**: p. 595-598.

300. Wang, Y. , Fei, D. , Vanderlaan, M. , and Song, A. , *Biological activity of bevacizumab, a humanized anti-VEGF antibody in vitro.* Angiogenesis, 2004. **7**(4): p. 335-345.
301. Marshall, J.J. and Kontos, H.A., *Endothelium-derived relaxing factors. A perspective from in vivo data.* Hypretension, 1990. **16**: p. 371-371386.
302. Yoon, Y. , Song Seung, J. , Hong, H. , and Kim, J.Q., *Plasma Nitric Oxide Concentrations and Nitric Oxide Synthase Gene Polymorphisms in Coronary Artery Disease.* Clinical Chemistry, 2000. **46**(10): p. 1626-1630.
303. Hoeben, A., Landuyt, B., Highley, M. S., Wildiers, H., Oosterom, A. T. V., and Bruijn, E. A., *Vascular Endothelial Growth Factor and Angiogenesis.* Pharmacological Reviews, 2004. **56**(4): p. 549-580.
304. Chennamsetty, N., Voynov, V., Kayser, V., Helk, B., and Trout, B. L., *Prediction of Aggregation Prone Regions of Therapeutic Proteins.* J. Phys. Chem, 2010. **114**: p. 6614-6624.
305. Kontermann, R. E., *Strategies for extended serum half-life of protein therapeutics.* Current Opinion in Biotechnology, 2011. **22**(6): p. 868-876.